Molecular cloning, expression, purification and characterization of β-mannanase of family 26 glycoside hydrolase and associated family 35 carbohydrate binding module from *Clostridium thermocellum* and its application in manno-oligosaccharides production

A Thesis

Submitted in Partial Fulfilment of the requirements for the Degree of

DOCTOR OF PHILOSOPHY

by

ARABINDA GHOSH

Under the supervision of

Professor Arun Goyal

October 2014

DEPARTMENT OF BIOTECHNOLOGY
INDIAN INSTITUTE OF TECHNOLOGY GUWAHATI
GUWAHATI – 781039, ASSAM, INDIA

INDIAN INSTITUTE OF TECHNOLOGY GUWAHATI

DEPARTMENT OF BIOTECHNOLOGY

STATEMENT

I do hereby declare that the content embodied in this thesis entitled "**Molecular cloning, expression, purification and characterization of β-mannanase of family 26 Glycoside Hydrolase and associated family 35 carbohydrate binding module from *Clostridium thermocellum* and its application in manno-oligosaccharides production**" is the result of investigations carried out by me in the Department of Biotechnology, Indian Institute of Technology Guwahati, Guwahati, Assam, India under the guidance of Professor Arun Goyal.

In keeping with the general practice of reporting scientific observations, due acknowledgements have been made wherever the work described is based on the findings of other investigators.

Arabinda Ghosh

October, 2014

Arabinda Ghosh

09610615

INDIAN INSTITUTE OF TECHNOLOGY GUWAHATI

DEPARTMENT OF BIOTECHNOLOGY

CERTIFICATE

It is certified that the work described in this thesis entitled **"Molecular cloning, expression, purification and characterization of β-mannanase of family 26 Glycoside Hydrolase and associated family 35 carbohydrate binding module from *Clostridium thermocellum* and its application in manno-oligosaccharides production"** by **Arabinda Ghosh** (**Roll No. 09610615**) for the award of degree of Doctor of Philosophy is an authentic record of the results obtained from the research work carried out under my supervision mainly in the Department of Biotechnology, Indian Institute of Technology Guwahati, Guwahati, Assam, India. The work embodied in this thesis has not been submitted elsewhere for a degree.

20/10/14

Dr. Arun Goyal
(FAMI, FBRS, FABAP, FNABS, FNAAS, FIFIB)
Professor
(Thesis Supervisor)
Department of Biotechnology
Indian Institute of Technology Guwahati
Guwahati, 781 039, India

ACKNOWLEDGEMENTS

The findings I have personified in this thesis would never been possible without the support, active guidance, assistance and the encouragement of several individuals. Therefore, I take the pleasant opportunity to express my sincere gratitude and debt towards all the personages who have helped me in this endeavor.

My first and sincere gratitude with a deep sense of veneration goes to my supervisor Professor Arun Goyal, Department of Biotechnology, IIT Guwahati, for his excellent guidance, caring, patience and providing me with an excellent atmosphere for doing research. I am indebted to him for introducing me into the realm of this interesting work, training me with the techniques, giving me the freedom in designing and conducting the experiments. As my supervisor, he has constantly encouraged and motivated me to remain focused on achieving my goal. His advices and insight was invaluable to me. He has not only guided me in research, also his invaluable suggestion helped me to become a stronger person in life. I will remain grateful to him for all that he did for me.

I would also like to express my sincere gratitude to all my doctoral committee members Dr.(Mrs.) G.K. Saini, Dr. V. Trivedi and Prof. M. Jawed for their support, encouragement and valuable suggestions during my seminars and progress reviews that has led to the successful completion of my thesis. I extended my heartfelt gratitude to Prof. Nikhil K. Chrungoo of Department of Botany, North Eastern Hill University, Shillong, Meghalaya, Prof. Munishwar Nath Gupta of Department of Chemistry, Indian Institute of Technology Delhi and Prof. Carlos M.G.A Fontes, CIISA, Faculty of Veterinary Medicine, Lisbon, Portugal, for their help in materialization of some of my experimental endeavors.

I owe my profound gratitude to the present and previous Heads of the Department of Biotechnology, IIT Guwahati, Prof. V. V. Dasu and Prof. Arun Goyal for providing me with the necessary facilities. My sincere thanks are due to other

faculty members of the department for their help, encouragement and providing facility for carrying out the experiments.

I am thankful to the Indian Institute of Technology Guwahati for providing me with the state of the art infrastructure for advance level of research. The financial support for scholarship from Ministry of Human Resource Development (MHRD), India is duly acknowledged. I take this opportunity to sincerely acknowledge the University Grants Commission (UGC), New Delhi, India for providing financial assistance in the form of both Junior as well as Senior Research Fellowship which buttressed my stay and work comfortably.

I remain thankful to my seniors and colleagues Dr. Seema Patel, Dr. Deepmoni Deka and Dr. Shadab Ahmed, Dr. Saprativ Das, Dr. Jaganmohan Rao, Dr. Rishikesh Shukla, Dr. Shraddha Shukla for their guidance and training. My completion of this study could not have been accomplished without the support of my research group members and I am immensely thankful to all of them. I am grateful to all my lab members and the staff of Department of Biotechnology for their support and cooperation.

My greatest appreciation and friendship goes to my closest friends, Subrata Sinha, Anupa, and Ashutosh who were always a great support in all my struggle and frustration during my stay in IIT Guwahati. They always cheered me up and stood by me through the good times and bad times. I heartily thank my Hostel friends Dr. Saprativ, Dr. Jagan and Soumyadeep, Vikky for the humour we shared and the love they showered on me.

At the fag-end I am thankful to my family members whose continuous encouragement, support and blessings helped me in successful completion of my research work. I owe my achievements to my parents, elder brother Dr. Amalendu Ghosh and sister-in-law for their motivation.

Arabinda Ghosh
October, 2014

SYNOPSIS

Plant cell wall is predominantly composed of complex structural polysaccharides such as celluloses and hemicelluloses. Polysaccharides of the primary cell wall components of plant are cellulose, hemicelluloses such as xyloglucans, mannans, galactomannans, glucomannans, laminarin, glucuronoarabinoxylans, arabinoxylan etc. Mannans are the polysaccharides with a backbone chain of β-(1→4)-linked mannose units. They constitute a major portion of hemicelluloses in hardwoods. The major distribution of mannan polysaccharides substituted with galactose and glucose units in plant hemicellulose reservoir is abundant in nature. Carob galactomannan from *Ceratonia siliqua* plant contains β-(1→4)-D-mannan backbone (78%) and α-(1→6)-linked galactose (22%) single units, whereas guar gum (from endosperm of guar seeds) backbone is a linear chain of β-(1→4)-linked mannose residues to which galactose residues are (1→6)-linked at every second mannose forming short side-branches. Glucomannan from *Amorphophallus konjac* is a water-soluble polysaccharide that is considered as a dietary fiber. The component sugars units in konjac glucomannan are β-(1→4)-linked D-mannose and D-glucose residues in a molar ratio of 1.6:1. β-D-mannanase (endo β-(1→4)-mannan mannohydrolase, E.C. 3.2.1.78) hydrolyzes β-(1→4)-D-mannopyranosyl linkages within the main chain of mannans, glucomannans, galactomannans and galactoglucomannans. Mannanases have been listed within glycoside hydrolase (GH) families *viz.* GH26, GH5 and GH113 in carbohydrate active enzyme database (http://www.cazy.org/Glycoside-Hydrolases.html) based on sequence similarity (Henrissat, 1991; Davis and Henrissat, 2002). β-D-mannanases belong to family GH5,

GH26, GH113 display a $(\beta/\alpha)_8$ barrel shaped protein folding pattern and the acid-base-assisted catalysis via a double displacement mechanism involving a covalent glycosyl-enzyme intermediate. The mechanism of glycosidic bond cleavage is found conserved within these families. These are the characteristic patterns of clan GH-A protein families and helped β-D-mannanases of family GH5, GH26 and GH113 to group into this clan. Due to the retaining double displacement mechanism, these enzymes can perform transglycosylation. Transglycosylation may leads to the synthesis of new glycosides or oligosaccharides longer than the original substrate. GH5 and GH113 mannanases have been described as able to catalyse transglycosylation reactions while to date no evidence of transglycosylation has been reported for GH26 mannanases. The non-catalytic polysaccharides recognizing modules were initially named cellulose binding domain. Later on the term CBM (carbohydrate binding module) evolved reflecting the diversity in ligand specificity of these proteins. Currently, CBMs have been classified into 67 distinct families based on sequence similarity (http://www.cazy.org/Carbohydrate-Binding-Module) and they display substantial diversity in terms of ligand specificity. The CBMs append to the glycoside hydrolases that degrade the soluble or insoluble polysaccharides. Family 35 carbohydrate binding module is often appended to glycoside hydrolase family 26 (GH26) and GH5 mannanases, xylanases (GH30) which significantly alter the polysaccharide specificity for plant cell wall polysaccharides such as galactomannan, glucomannan, mannan and glucouronoxylan. Out of 67 distinct families, CBMs are also included within 7 different fold families. The majority of the folded families are comprised of β-sandwich fold. Refinement of the CBM classification was improvised recently where Type A CBMs are those which can recognize the surface of the

crystalline polysaccharides and Type B CBMs are classified according to their endo acting mode of action internally to glycan chains. Type C CBMs are attributed by their exo-type binding either at the side chain or at the polysaccharide termini. Usually Type B CBMs are abundant in cellulases, xylanases and mannanases that bind to cellulose, xylan and mannan, respectively. Thus CBMs maintain the target substrate within the close proximity of their complete protein structures. In general, most family 35 carbohydrate binding module (CBM35) acquired a type B conformation in nature.

Present work

The present investigations are carried out on the "**Molecular cloning, expression, purification and biochemical characterization of β-mannanase (*Ct*Manf) of family 26 Glycoside Hydrolase and its truncated derivative (*Ct*ManT) and associated family 35 carbohydrate binding module (*Ct*CBM35) from *Clostridium thermocellum***". In the present study molecular characterization of endo-β-mannanae (*Ct*Manf) of family 26 glycoside hydrolase (GH26) and the associated carbohydrate binding module of family 35 (*Ct*CBM35) were carried out. The recombinant protein *Ct*Manf and its truncated derivatives *Ct*ManT, *Ct*CBM35 were cloned, expressed, purified and functionally characterized. The influence of CBMs on catalytic module and their binding affinities towards soluble and insoluble polysaccharides were explored. Reports of Type A having mannanse (Man26A and Man5A) activity are already available but to our knowledge this is the first report of any Type B (Man26B) having the ability to hydrolyze both mannan polysaccharides and cellulosic polysaccharides. The thesis work is comprised of 5 Chapters.

Chapter 1 is the General Introduction which embodies the brief review of literature dedicated to the importance of cellulose and hemicelluloses and their structural features. It mainly focuses on the enzymes having the capability to hydrolyze plant cell-wall cellulose and hemicellulose. It illustrates sequence-similarity based classification of cellulases and hemicellulases belonging to different glycoside hydrolase (GH) families. It also describes different GHs categorized in to various 'clans' based on fold of proteins or core structural features. This chapter elaborately reviewed family 26 glycoside hydrolases and associated non-catalytic carbohydrate binding module (CBM), especially, CBM35. The chapter reviews about the type of core architecture seen in various family 26 GHs, their enzyme activities, substrate specificity, active site and active site residues. The various type of endo-β-mannanases belonging to family 26 GH, have been discussed and their biochemical properties have been highlighted. The various types of binding clefts or binding sites possible in CBM35 have also been elaborated. Previous literatures highlighting their ligand or polysaccharide binding capabilities have also been demonstrated. Previously characterized recombinant family 26 GHs and CBM35 from different bacteria have been illustrated. The chapter also reviews the potential applications of endo-β-mannanases.

Chapter 2 describes the full length gene *Ct*Manf and its truncated derivatives *Ct*ManT and *Ct*CBM35 were extracted from the genomic library of *Clostridium thermocellum* ATCC 27405 (nucleotide accession: CP000568.1). The molecular architecture revealed an N-terminal non catalytic family 35 carbohydrate binding module (*Ct*CBM35, 420 bp) followed by glycoside hydrolase module (*Ct*ManT, 1029

bp) at the C-terminus. PCR amplified fragment of full length gene *Ct*Manf showed a band of 1449 bp, whereas, the truncated catalytic module *Ct*ManT displayed a PCR amplified fragment of 1029 bp and *Ct*CBM35 420 bp, respectively. The above amplified products were purified from the agarose gel by gel extraction kit (Qiagen). *Ct*Manf and its truncated derivatives *Ct*ManT and *Ct*CBM35 were digested with *Nhe*I-*Xho*I restriction enzymes and the digested fragments extracted from gel and purified using gel extraction kit. Similarly, the pET-28a(+) vector was also digested with *Nhe*I-*Xho*I restriction enzymes and the digested fragment of each was purified by gel extraction kit and followed by ligation.

E. coli (DH5α) competent cells were transformed with ligated samples of each derivative mentioned above. The transformed cells were spread on LB agar plates with kanamycin and grown at 37°C, which resulted in many colonies after 12h incubation. The plasmid DNA of each recombinant derivative was isolated from the colonies after growing in 5 ml LB medium supplemented with appropriate antibiotics at 37°C and at 180 rpm. The cloning of *Ct*Manf and its truncated derivatives *Ct*ManT and *Ct*CBM35 in pET-28a(+) vector was confirmed by restriction digestion analysis of the recombinant plasmid DNA. The *E. coli* BL-21 competent cells were transformed with recombinant plasmid DNA of full length *Ct*Manf as well as its truncated derivatives *Ct*ManT and *Ct*CBM35 for expression of recombinant proteins. Over expression of recombinant proteins was achieved by using IPTG as inducer at a final concentration of 1 mM. The hyperexpression of the recombinant proteins were checked and confirmed by SDS-PAGE gel analysis.

After confirming the successful expression, the recombinant proteins were purified from their respective cell free extracts by immobilized metal ion

chromatography (IMAC) using HiTrap chelating columns. The degree of purification obtained after this purification step was higher than 90%, and therefore these proteins were considered as suitable for further biochemical analysis. The catalytic enzymes purified by IMAC displayed molecular sizes of 53 kDa (*Ct*Manf), 38 kDa (*Ct*ManT) on SDS-PAGE. The non-catalytic carbohydrate binding modules *Ct*CBM35 showed molecular sizes of 15 kDa on SDS-PAGE. The amount of protein obtained from 100 ml of cultures *Ct*Manf and its truncated derivatives *Ct*ManT, *Ct*CBM35 after IMAC purification were 0.16 mg/ml (*Ct*Manf), 0.15 mg/ml (*Ct*ManT), 0.12 mg/ml (*Ct*CBM35). These purified proteins were used for further biochemical and functional characterization.

Chapter 3 elaborates the substrate specificity and kinetic properties of catalytic modules *viz.* *Ct*Manf and *Ct*ManT from *C. thermocellum*. The catalytic modules *Ct*Manf and *Ct*ManT showed maximum enzyme activities at optimum pH 6.9 and 6.5, respectively. The optimal temperatures for *Ct*Manf and *Ct*ManT were 60°C and 50°C, respectively. *Ct*Manf and *Ct*ManT displayed more or less similar pH and thermal stability profile. Both *Ct*Manf and *Ct*ManT were stable over a pH range 5.0-7.5. The enzymes displayed significant loss of activity at 70°C or higher temperature. *Ct*Manf and *Ct*ManT showed maximum activity of 97.0±5.0 U/mg and 91.0±4.0 U/mg, respectively, with carob galactomannan. The catalytic enzymes *Ct*Manf and *Ct*ManT also displayed noticeable activities with soluble locust bean galactomannan (85.4±6.0 U/mg and 83.1±5.0 U/mg), konjac glucomannan (81.0±3.0 U/mg and 79.8±4.0 U/mg) and insoluble ivory nut mannan (50.0±2.0 U/mg and 26.5± 0.9 U/mg). Interestingly, both *Ct*Manf and *Ct*ManT displayed low but observable activity against barley β-

glucan, lichenan, carboxymethyl cellulose, hydroxyethyl cellulose, avicel and xyloglucan signifying multi-substrate specificty. The catalytic modules were unable to act upon synthetic substrates such as *p*NP-β-D-mannopyranoside and with *p*NP-α-D-mannopyranoside that ruling out any exo-enzyme activity. Therefore, both *Ct*Manf and *Ct*ManT can be considered as endo-β-mannanases. In addition the zymogram study of against both recombinant enzymes carob galactomannan confirmed their endo acting nature.

The enzyme activity of *Ct*Manf and *Ct*ManT increased significantly by approximately, 1.5 fold in presence of Ca^{2+} and Mg^{2+} salts, implying that these ions are needed as cofactors. Significant enzyme activities of both *Ct*Manf and *Ct*ManT were observed considerably at moderate concentrations of Mn^{2+}, Co^{2+} and Zn^{2+} ions. However, the enzyme activity was inhibited significantly in presence of Cu^{2+}, Al^{3+} and Ni^{2+} ions and cationic detergent SDS at their low concentrations. The enzyme activity of *Ct*Manf and *Ct*ManT, when assayed in the presence of Ca^{2+} ions, increased by two-fold, but in presence of EGTA and EDTA sharply decreased. This implied that Ca^{2+} ions might be involved in the catalysis and imparting stability to the *Ct*Manf and *Ct*ManT structures. Chaotropic agents, urea and GnHCl at higher concentrations also inactivated significantly the enzyme activity of recombinant enzymes.

Media composition played a significant role in production of recombinant *Ct*Manf and *Ct*ManT. The recombinant *Ct*Manf and *Ct*ManT showed highest cell density and concentration of protein in TY medium as compared with TB, 5xLB and LB medium. In LB medium moderate cell density was achieved with low protein concentration. The 5x LB medium did not support the growth due to higher

concentrations of yeast extract, tryptone and sodium chloride and as a result lowest protein concentration was achieved. The rich source of tryptone, yeast extract and phosphate salts facilitated to achieve highest cell densities in TY media as compared to other chemically defined media used. Higher concentration of phosphate is important for attaining high cell densities of *E. coli* harbouring *Ct*Manf and *Ct*ManT, as the lower concentrations of phosphate limits the growth. The low cell densities and lower production of recombinant proteins in LB and 5x LB medium were due to lack of buffering capacity

Protein-melting curves of full length protein *Ct*Manf showed that the catalytic module, *Ct*ManT and carbohydrate binding module, CBM35 melt independent of each other. The protein-melting peaks of *Ct*ManT and CBM35 shifted to higher temperature in the presence of Ca^{2+} ions. However, the addition of equimolar concentration of EDTA to the Ca^{2+} ion containing *Ct*Manf and *Ct*ManT, shifted back the melting temperature peaks to the original positions. This further corroborated the fact that Ca^{2+} ions impart thermal stability to the protein structures.

The structure and functional aspects of *Ct*ManT was examined by generating a model by homology modelling and validated successfully. The modelled *Ct*ManT displayed $(\beta/\alpha)_8$"TIM" barrel fold with extended loops around the active center that constructed the broader saddle-shaped, open active site cavity. The structure analysis showed that *Ct*ManT is structurally closer to the fungal mannanase as compared wth other structurally characterized bacterial mannanase available in PDB database. *Ct*ManT involved in retention mechanism where amino acid residue Glu181 acted as a catalytic acid/base, while Glu288 act as a catalytic nucleophile. Molecular docking

study with manno-configured ligands suggested wide binding site pocket accommodating larger oligosaccharides with higher affinity. 3D-structure superimposition of modeled *Ct*ManT with the template protein showed six potential subsite having two subsite towards aglycone whereas four subsite to glycon side for galactomannan.

Chapter 4 illustrates the binding analysis of *Ct*CBM35 from *Clostridium thermocellum*. The cloned family 35 Carbohydrate binding module (*Ct*CBM35) from *Clostridium thermocellum* preferred binding with manno-configured polysaccharides. *Ct*CBM35 discriminated during carbohydrate selection showing its affinity only with manno-configured ligands among the manno-, cello- and xylo-configured polysaccharides. The binding analysis of *Ct*CBM35 to soluble polysaccharides was evaluated using affinity gel electrophoresis. The equilibrium binding constant (K_a) of the *Ct*CBM35 was determined for mannotriose, konjac glucomannan, carob galactomannan and locust bean galactomannan by measuring the relative migration distance of proteins on native PAGE gels in the presence of above ligands. Both *Ct*CBM35 showed lesser affinity for carob galactomannan (for which the catalytic modules showed maximum activity) as compared to konjac glucomannan which was clear from greater retardation of *Ct*CBM35 at lower concentration of konjac glucomannan during affinity electrophoresis. Oligosaccharide and polysaccharide binding studies were also corroborated the findings of affinity electrophoresis where ligand binding was observed higher with mannotriose and konjac glucomannan as compared with carob and locust bean galactomannan. Ligand binding with *Ct*CBM35 was evidenced from the fluorescence

peack shift of 21 nm. In dynamic light scattering, the larger particle size of *Ct*CBM35 is due to the polysaccharide binding. The cationic interaction of aromatic residues with carob galactomannan and konjac glucomannan insists *Ct*CBM35 domain alteration to more compact form reducing the random diffusion of the particles between polysaccharide and amino acid residues. Due to simpler structure of oligosaccharide (mannotriose) and the polysaccharide ligand konjac glucomannan, the interaction with aromatic residues in the binding pocket of *Ct*CBM35 uphold strong binding as compared to carob galactomannan with substituted galactose side chain.

Instances of Ca^{2+} ion induced stability of *Ct*CBM35 was evident from protein melting study where the low melting temperature of the protein was shifted to higher temperature. The metal ion (Ca^{2+}) chelation by EDTA revealed the protein stability lost at very low temperature but the structure could be repaired while Ca^{2+} was added to minimize the effects of EDTA. Therefore, divalent metal cation Ca^{2+} plays significant role in holding the structure that is sensitive against temperature.

Higher temperature invoked lesser stability to *Ct*CBM35 and was evidenced from fluorescence spectrum at different temperatures. The loss in structural stability attributed to higher temperature was also hampered the ligand binding capacity of *Ct*CBM35 and isothermal titration calorimetry revealed that at the melting temperature *Ct*CBM35 lost its 100 fold ligand binding capacity. The highly substituted α-(1→6)-galactose on β-(1→4)-mannose backbone in locust bean galactomannan might be the another reason for lower binding by *Ct*CBM35. *Ct*CBM35 is sensitive towards thermal exposure and shows weak binding ability of

ligands at its melting temperature. Titrations against polysaccharides at 55°C, *Ct*CBM35 exhibited ~100 fold lower binding affinity against konjac glucomannan, locust bean galactomannan and carob galactomannan as compared to binding at 25°C. The interpretation of unfolding transition in presence of GnHCl and urea revealed that *Ct*CBM35 holds a significant structural stability and can resist denaturation at higher concentrations of these denaturants.

The 3-dimensional model of *Ct*CBM35 from *Clostridium thermocellum* generated by Modeller9v8 displayed predominance of β-sheets arranged as β-jelly-roll fold. The secondary structure of*Ct*CBM35 by PredictProtein showed presence of two α-helices (3%), twelve β-sheets (45%) and fifteen random coils (52%). Secondary structural element analysis of cloned, expressed and purified recombinant *Ct*CBM35 by Circular dichroism also corroborated the *in-silico* predicted secondary structure. Multiple sequence alignment of *Ct*CBM35 showed conserved residues (Tyr123, Gly124 and Phe125), which are commonly observed in mannan specific CBMs. The docking analysis of *Ct*CBM35 with manno-oligosaccharide displayed the involvement of Tyr26, Gln29, Asn43, Trp66, Tyr68, Leu69, Arg76 and Leu127 residues, making polar contact with the ligand molecules. Ligand docking analysis of *Ct*CBM35 exhibited higher binding affinity with mannotriose and galactomannan (Man-Gal-Man, moiety) substantiated the affinity binding and fluorescence results, displaying similar values of K_a.

Chapter 5 describes the TLC and HPAEC analysis of *Ct*Manf (full length endo-β-(1→4)-mannanase) hydrolyzed products of natural substrates. It was apparent from TLC that *Ct*Manf released mannotriose, mannobiose and mannose in prolonged

hydrolysis of carob galactomannan. But, at the earlier stages, the amount of mannobiose was less as compared to mannotriose and mannose. After complete hydrolysis of carob galactomannan *Ct*Manf was able to release mannose, mannobiose and mannotriose. The salient feature of *Ct*Manf catalysis involved only β-(1→4)-bond cleavage when mannobiose and mannotriose were used as substrate and liberated prominently mannose as main product. The release of large amount of mannose at early stage of enzymatic reaction by *Ct*Manf was seen against carob galactomannan and manno-oligosaccharides. HPAEC analysis corroborated the results of TLC analysis of hydrolysis of carob galactomannan products released by *Ct*Manf. The results of HPAEC showed that *Ct*Manf exclusively cleaves carob galactomannan into mannotriose, mannobiose and mannose. It was apparent from TLC and HPAEC analyses *Ct*Manf was able to hydrolyze only β-(1→4) bond cleavage and had potential to produce manno-oligosaccharides from carob galactomannan. The structure analysis of the pretreated copra meal revealed the efficiency of the pretreatment process resulting in significant structural deformity. FT-IR analysis showed the easy accessibility of the major functional groups of the abundant galactomannan for catalysis by *Ct*Manf. Both ^{1}H and ^{13}C NMR revealed that the polysaccharide content of the copra meal majorly galactomannan with α-(1→6)-linked galactose substituted in the β-(1→4)-linked mannose main chain. Time dependent *Ct*Manf catalyzed hydrolysis of the galactomannan of copra meal confirmed the presence of mannose, mannobiose and mannotriose using TLC, HPAEC and mass spectrum. The released manno-oligosaccharides were successfully purified using size exclusion chromatography with significant yield. The mixed treatment of mannobiose and mannotriose supported the enhanced growth of prebiotic

bacteria holding their potential as good prebiotic agent as compared to commercial inulin. The mixed manno-oligosaccharides are highly resistant against simulated gastric juice, intestinal fluid and α-amylase proving a stable prebiotic over inulin. *In vitro* cytotoxicity assay of MOS (500 μg mL^{-1}) on human epithelial colorectal adenocarcinoma cell line (HT-29) demonstrated 60% decreased viability of cells after 48h displaying anti-tumorigenic property.

CONTENTS

Chapter 4. *In vitro* and *in silico* analysis of ligand binding and stability of *Ct*CBM35 from *Clostridium thermocellum* ATCC 27405

Chapter 1

General Introduction

1. Carbohydrates

Carbohydrates are the most abundant biomolecules found on the surface of earth (Bayer *et al.*, 1998). The synthesis of organic carbon as carbohydrate is a major biological process and carbohydrate is the primary source of energy for life. Through photosynthesis plants convert solar energy into organic carbon that can be further utilized by heterotrophic organisms. In plants, cell wall polysaccharides, primarily cellulose and hemicellulose, are the major reservoirs of carbon and energy. However, only a restricted number of microorganisms have acquired the capacity to deconstruct these structural carbohydrates. They are present everywhere in nature as they are found in plant biomass, exoskeleton of insects, bacterial cell surfaces, bio-films and also on mammalian cell surfaces. The utility of carbohydrates is dependent on their overall structural arrangement *viz.* length of the carbohydrate, its sugar composition, the position of the anomeric carbon and the type of glycosidic linkages between sugar monomers (Fontes and Gilbert, 2010). These structural features provide millions of different possible combinations of carbohydrate structures, and each structure is suited for serving its function in nature.

1.1 Structural polysaccharides in plants

Structural polysaccharides act as protective walls for plant cells (Gilbert, 2010). Cellulose, chondroitin sulphates, hyaluronic acids and chitin are some examples of structural polysaccharides. The terrestrial biomass contributed by plants is mainly composed of plant cell-wall materials *viz.* cellulose and hemicellulose (Bayer *et al.*, 2007). These are the most abundant naturally occurring substances found on the earth. They account for more than 60% of all global carbon bound to organic matter according to Ramamurthy *et al.* (1992). Polysaccharides are macromolecular carbohydrates comprising chain of monosaccharides linked together by glycosidic bonds, formed as a result of condensation reaction (Berg, 2007). The bulk of plant cell wall material is cellulose, a homopolymer of β-(1→4)-glucose which takes on an overall linear shape (Bayer *et al.*, 2000). Cellulose is hypothesized to exist in two forms, crystalline and amorphous. In the crystalline form cellulose chains self associate via intra- and intermolecular hydrogen bonds and van der Waals forces to form cellulose fibrils and micro-fibrils, which are insoluble and provide the majority of tensile strength to the plant cell wall (Moon *et al.*, 2011). Amorphous cellulose lacks this higher order structure and more susceptible to degradation. Plant cell walls also contain a number of other sugar polymers termed hemicellulose which includes xylan (β-1→4-linked xylose), laminarin (β-1→3-linked glucose), mannan (β-1→4-linked mannose) and lichenan (mixed 1→3 and 1→4-β-D-glucan) (Scheller and Ulvskov, 2010). Structural polysaccharides are either fibrous-polysaccharides e.g. cellulose in higher plants and some algae or matrix-polysaccharides e.g. arabinoxylans, galactomannans or pectins in plants (Cosgrove, 1999). The other main structural polysaccharide found within the plant cell wall are pectins and substituted

heteropolysaccharides composed of a α-(1→4)-D-galacturonic acid backbone with rhamnose, galactose and arabinose substituents (Bayer *et al.*, 1998).

1.1.1 Cellulose

Cellulose is the polysaccharide that provides structural integrity to plants and is one of the most important substances occurring in nature. About 40% of the plant carbon is composed of cellulose (Demain *et al.*, 2005). However, the percentage of cellulose in plant varies depending on the origin. Its occurrence is widespread, from higher plants to primitive organism such as sea-weeds, flagellates and bacteria. Other cellulose-containing materials include agriculture residues, water plants, grasses etc. The cellulose are linear homopolymer of consisting of regio and enantiopure D-glucopyranose (also known as anhydroglucose units) chains linked together by β-(1→4)-glycosidic linkages (Fig. 1.1).

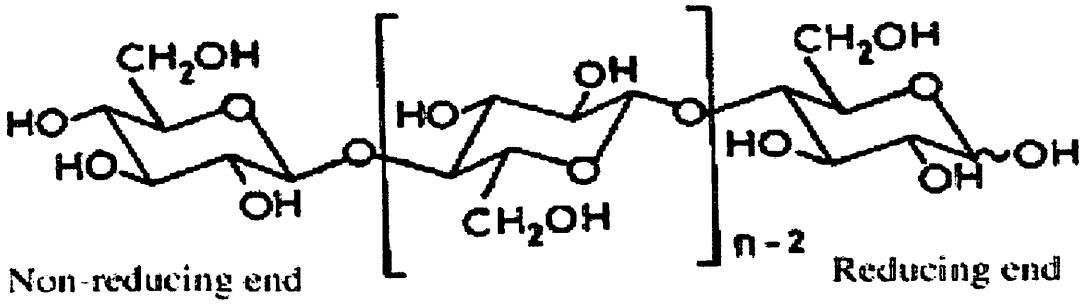

Fig. 1.1 Chemical structure of cellulose showing glycosidic linkages, reducing end and non-reducing end (Somerville, 2006).

1.1.2 Hemicellulose

Hemicelluloses are usually hetero-polysaccharides present in plant cell walls containing β-(1→4)-linked backbones of glucose, mannose or xylose (Scheller and Ulvskov, 2010). They commonly occur in nature as xyloglucans, xylans, arabinoxylans, arabinogalactans, mannans, glucomannans, β-(1→3, 1→4)-glucans and pectins (Schadel *et al.*, 2009). Hemicelluloses are known to be synthesized in Golgi apparatus (membranes) by various glycosyltransferases. Many glycosyltransferases involved in the process of biosynthesis of xyloglucans and mannans are known (Schadel *et al.*, 2009). In contrast, the biosynthesis of xylans and β-(1→3,1→4)-glucans remains elusive and recent studies have led to more questions than answers (Scheller and Ulvskov, 2010). The predominant hemicellulose in many primary cell walls is xyloglucan. Other hemicelluloses found in primary and secondary walls include glucuronoxylan, arabinoxylan, glucomannan, and galactomannan (Schadel *et al.*, 2009).

1.1.2.1 Mannans

Mannans are heteropolymers and contain β-(1→4)-D-mannopyranose backbone and often substituted with galactose or glucose moieties through β-(1→6) and β-(1→4) linkages (Mizutani *et al.*, 2012). It is a form of storage polysaccharide. Ivory nut is a source of mannan. Mannan may also refer to a cell wall polysaccharide found in yeasts. This type of mannan has α-(1→6)-linked backbone and α-(1→2) and α-(1→3) linked branches.

1.1.2.1.1 Galactomannans

Glucomannan is a water-soluble polysaccharide that is considered a dietary fiber. It is a hemicellulose component in the cell walls of some plant species such as *Ceratonia siliqua* (Cui *et al.*, 2009). Galactomannan is composed of a β-(1→4)-D-mannopyranose backbone to which single D-galactosyl units are attached to C-6 of some of the D-mannosyl residues as shown in Fig. 1.2 (Cui *et al.*, 2009). The extent of galactopyranose substitution invariably affects the solubility, viscosity and interaction with other polysaccharides (Cui *et al.*, 2009). The order of increasing number of mannose-to-galactose ratio the abundant galactomannans are *viz.* fenugreek gum, mannose:galactose ~1:1, guar gum, mannose:galactose ~2:1, tara gum, mannose:galactose ~3:1, locust bean gum or carob gum, mannose:galactose ~4:1.

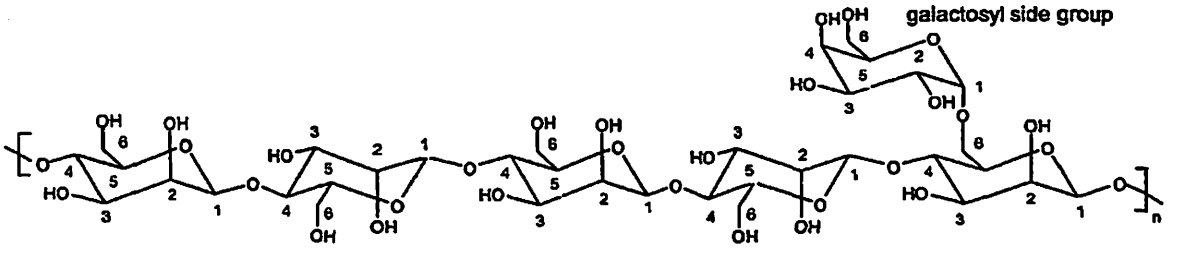

Fig. 1.2 Chemical structure of galactomannan (Cui *et al.*, 2009).

1.1.2.1.2 Glucomannan

Konjac glucomannan is a high molecular polysaccharide, is formed when the residues of glucose and mannose are bound together by β-(1→4)-linkages, the molar ratio of glucose and mannose is 1:1.6. (Fig. 1.3). They are generally found in the secondary walls of softwood (Maeda *et al.*, 1980).

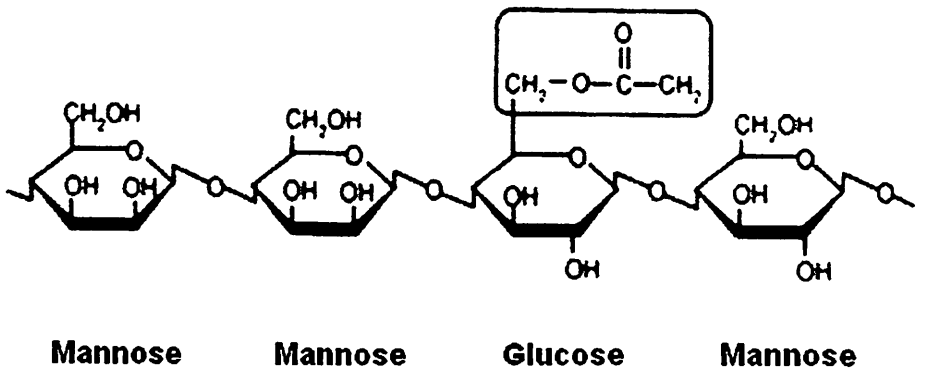

Fig. 1.3 Chemical structure of glucomannan (Maeda *et al.*, 1980).

1.1.2.1.3 Ivory nut Mannan

Crystalline linear β-(1→4) D-mannan is found in the cell walls of ivory nuts and in the algae *Acetabularia crenulata* and *Codium fragile* (Meier, 1958) (Fig. 1.4). Two polymorphs – mannans I and II – have been observed in these cell walls. The morphologies of mannan I and mannan II are granular and fibrillar, respectively (Chanzy *et al.*, 1984). Crystalline glucomannan from wood can be obtained, but only after partial degradation or modification (Timell, 1965).

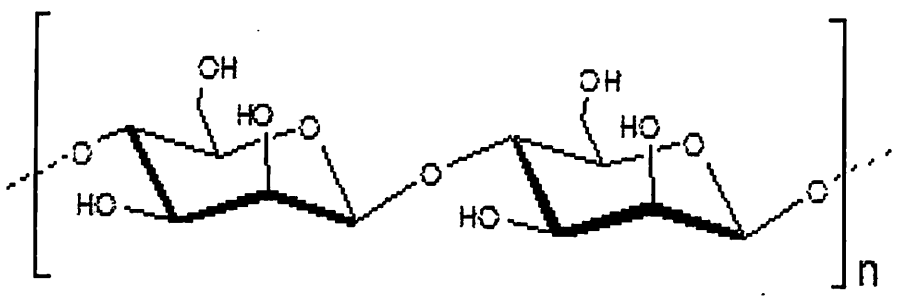

Fig. 1.4 Chemical structure of ivory nut mannan (Meier, 1958).

1.1.2.2 *Xylans*

Xylans are the most abundantly found hemicellulose in plants, which has a backbone of β-(1→4)-linked xylose residues. The linear xylan backbone is generally substituted with a variety of sugars and other moieties. Xylans are substituted with α-

(1→2)-linked glucuronosyl and 4-O-methyl glucuronosyl residues in the secondary wall of dicots (Scheller and Ulvskov, 2010). Often, xylans are hetero-polysaccharides with 1,4-linked-β-D-xylopyranose backbone chains substituted with arabinose, glucuronic acid, or its 4-O-methyl ether, acetic, ferulic, and *p*-coumaric acids side chains depending mainly on the source of xylans (Numan and Bhosle, 2006). Most hemicellulases are anchored in a β-(1→4)-linkage and the main backbone is branched, whereas, the individual sugars may be acetylated or methylated (Numan and Bhosle, 2006; Saha, 2003). The L-arabinosyl residues are often found in hemicelluloses, such as arabinan, arabinoxylan, gum arabic and arabinogalactan.

1.1.2.2.1 Glucouronoxylans

Glucuronoxylans are composed of β-(1→4)-xylose backbone with 4-O-methylglucuronic acid side-chains. Sometimes arabinose and O-acetyl side-chains may also be found attached to the main chain (Fig. 1.5). Glucouronoxylans are the major polysaccharide of secondary walls of dicot plants (Urbanowicz *et al.*, 2012).

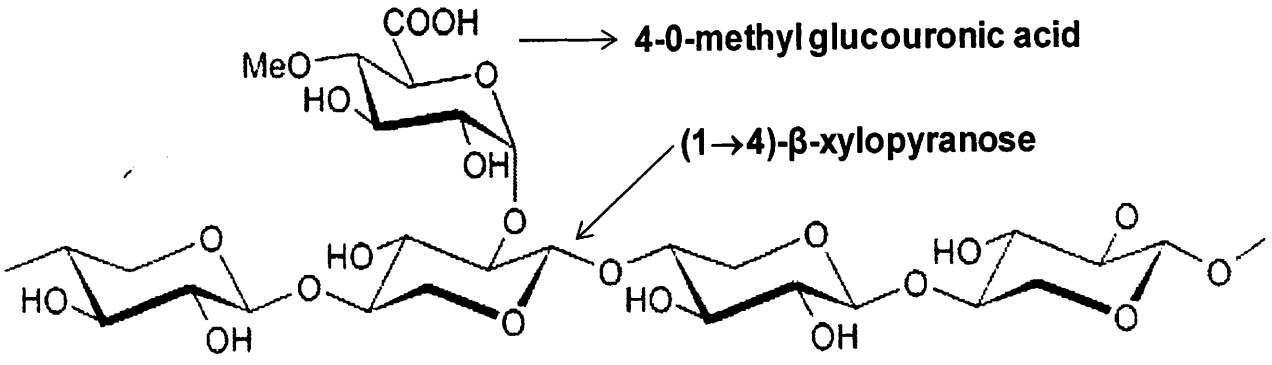

Fig. 1.5 Chemical structure of glucouronoxylan (4-O-methyl-D-glucourono-D-xylan) adapted from Nishitani and Nevins (1991).

1.1.2.2.2 Arabinoxylans

Arabinoxylans are composed of a β-(1→4)-D-xylopyranosyl backbone, with one or more- L-arabinofuranosyl residues substituted at position 2 or 3 (Fig. 1.6). On the other hand, in many cases, hexoses and hexuronic acids are also present, but as minor constituents (Izydorczyk *et al.*, 1995).

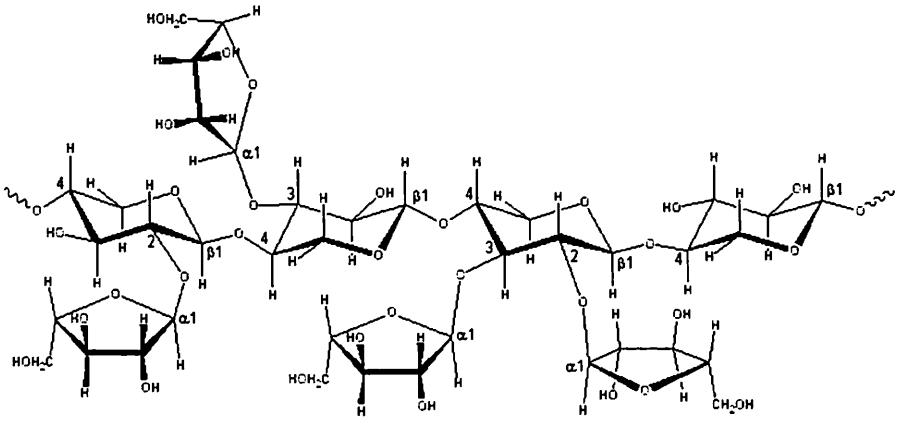

Fig. 1.6 Chemical structure of arabinoxylan (Izydorczyk *et al.*, 1995)

1.1.2.2.3 Xyloglucans

Xyloglucans are composed of β-(1→4)-glucose units in the main chain, substituted with (1→6)-D-xylose side chains (Fig. 1.7) (Lang *et al.*, 1993). Xyloglucan makes up to 20-25% (dry weight) of the type I primary cell walls abundant in dicots. The monocots such as grasses and legumes contain type II primary cell wall where xyloglucan exists in lesser amounts, 2-5% (Fry, 1989; Brennan and Harris, 2010).

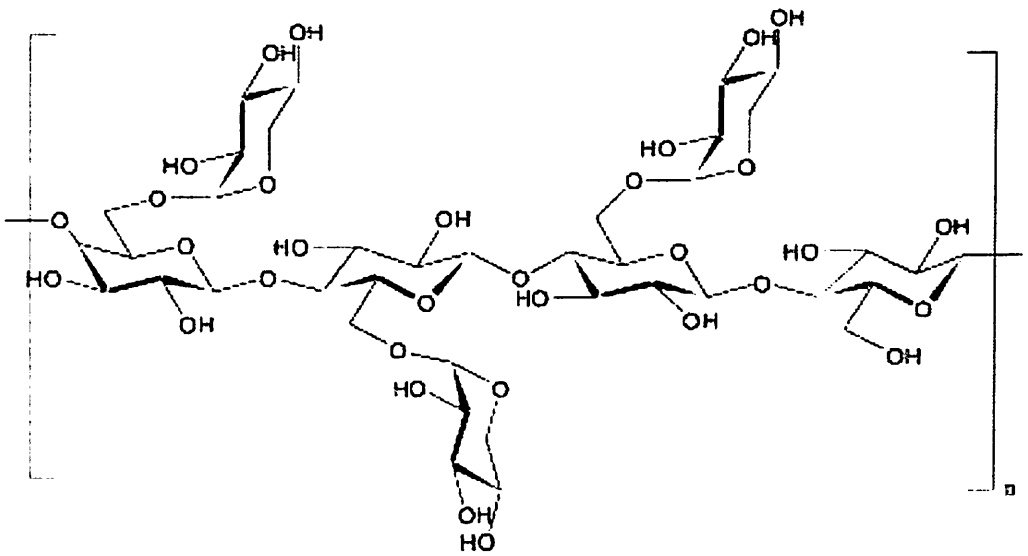

Fig. 1.7 Chemical structure of xyloglucan (Lang *et al.*, 1993)

1.1.2.3 *Arabinans*

Arabinans, of cell-wall pectic-substances, comprise (1→5)-α-linked-L-arabinofuranosyl main chain residues to which other L-arabinofuranosyl residues are linked by (1→3)-α and (1→2)-α in either a comb-like or a ramified arrangement (http://polysac3db.cermav.cnrs.fr/discover_pectins.html). The branched arabinan display a main chain of 1,5-α-linked-L-arabinofuranose substituted with L-arabinofuranosyl residues at 1→3 or 1→2 position as depicted in Fig. 1.6. Arabinan is composed of a linear main chain of (1→5)-α-linked-L-arabinofuranose (Fig. 1.8).

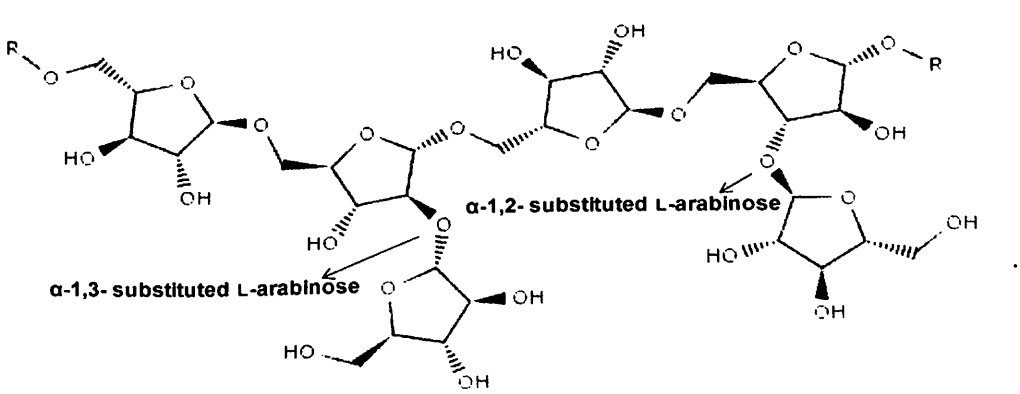

Fig. 1.8 Chemical structure of branched arabinan (http://www.brenda-enzymes.org, Technische Universitat Braunschweig).

1.1.2.4 *Galactans*

Galactans are polymers of β-D-galactopyranose. They are sometimes included in the hemicellulose group, but a recent review by Scheller and Ulvskov (2010) suggested that they should not be included in the heterogeneous group of hemicelluloses. However, at present they are classified as a hemicellulose. Scheller and Ulvskov gave reason that since galactans appear to be part of pectin molecules, at least in the initial synthesis stage. The galactans are also found to be substituted with arabinosyl resides in arabinogalactans. These are of two types, Type I which is rich in (1→4)-linkages and type II, contains terminal (1→3→5)-linked arabinose or (3→5)-linked arabinose substituted to main chain of galatan (e.g larchwood arabinogalatan) (Fig. 1.9).

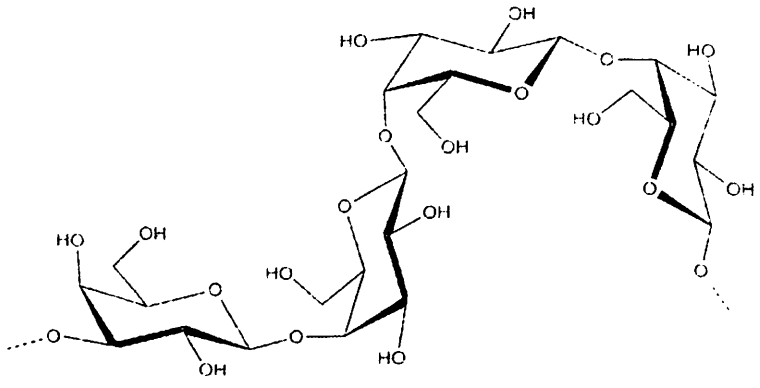

Fig. 1.9 Arabinogalactan structure from Larchwood (Heinze *et al.*, 2005).

1.1.3 Lignin

The main building blocks of lignin are the hydroxycinnamyl alcohols (or monolignols) coniferyl alcohol and sinapyl alcohol, with typically minor amounts of *p*-coumaryl alcohol (Fig. 1.10). Lignins are large group of aromatic polymers that result from the oxidative combinatorial coupling of 4-hydroxyphenylpropanoids as shown in Fig. 1.10 (Boerjan *et al.*, 2003; Ralph *et al.*, 2004). Lignin is found in all

vascular plants, mostly between the cells and also within the cells and in the cell walls. It usually occurs as complex structure bound to the hemicelluloses in wood.

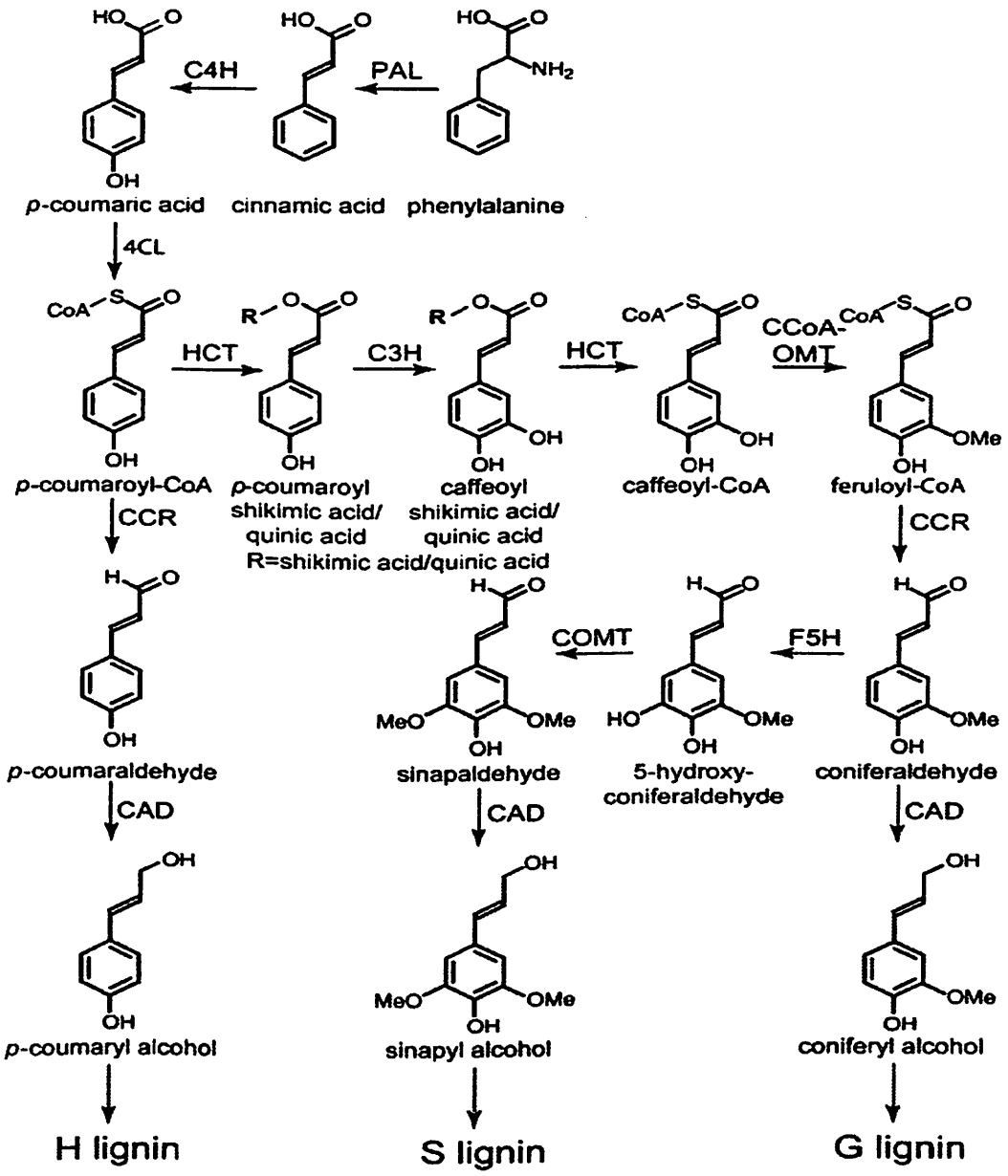

Fig. 1.10 The main biosynthetic pathway for synthesis of the monolignols p-coumaryl, coniferyl, and sinapyl alcohol (Boerjan *et al.*, 2003). Phenylalanine ammonia-lyase (PAL); Cinnamate-4-hydrolyase (C4H); 4-coumarate:CoA ligase (4CL); p-coumarate-3-hydrolyase (HCT), p-hydroxycinnamoyl-CoA:Quinate/Shikmate-p-hydroxycinnamoyltranferase (CCoAOMT), Caffeoyl-CoA-O-methyltransfersae (CCR), Cinnamoyl CoA reductase ferrulate-5-hydroxylyase (F5H), Caffeic acid-O-methyltransferase (COMT); Cinnamoyl alcohol dehydrogenase (CAD) (Adapted from Borjan *et al.*, 2003 and Ralph *et al.*, 2004).

1.1.4 Pectin

Pectins are a family of complex polysaccharides that contain (1→4)-linked α-D-galactosyluronic residues. Three pectic polysaccharides, homogalacturonan, rhamnogalacturonan-I and substituted galacturonans have been isolated from primary plant cell walls (Ridley *et al.*, 2001). Homogalacturonan is a linear chain of 1,4-linked α-D-galactosyluronic residues, in which some of the carboxyl groups are methyl esterified (Fig. 1.11). Homogalacturonan may also be O-acetylated at the C-2 and C-3 positions. Rhamnogalacturonan-I is a family of pectic polysaccharides containing a backbone of the repeating disaccharide [→4)-α-D-GalpA-(1→2)-α-L-Rhap-(1→] as shown in Fig. 1.11 (Ridley *et al.*, 2001). The minor component of the pectin backbone is rhamnogalacturonan-II. This is not structurally related to rhamnogalacturonan-I since its backbone is composed of (1→4)-linked α-D-galactosyluronic units (dimers) like homogalacturonan (Fig. 1.12). Rhamnogalacturonan-II is present in primary walls predominantly as a dimer of (1→4)-linked α-D-galactosyluronate that is cross-linked by a 1:2 borate-diol ester as shown in Fig. 1.12 (Kobayashi *et al.*, 1996; Ishii *et al.*, 1999). This cross-link is formed between OH-2 and OH-3 of the apifuranosyl residues (βApi*f*) in each monomeric rhamnogalactoronan-II subunit (Fig. 1.12). Rhamnogalactoronan-II is of interest as it occurs in relatively high amounts in wine and other fruit juices and it has been demonstrated that it binds heavy metals and has immunomodulating activities (Ridley *et al.*, 2001).

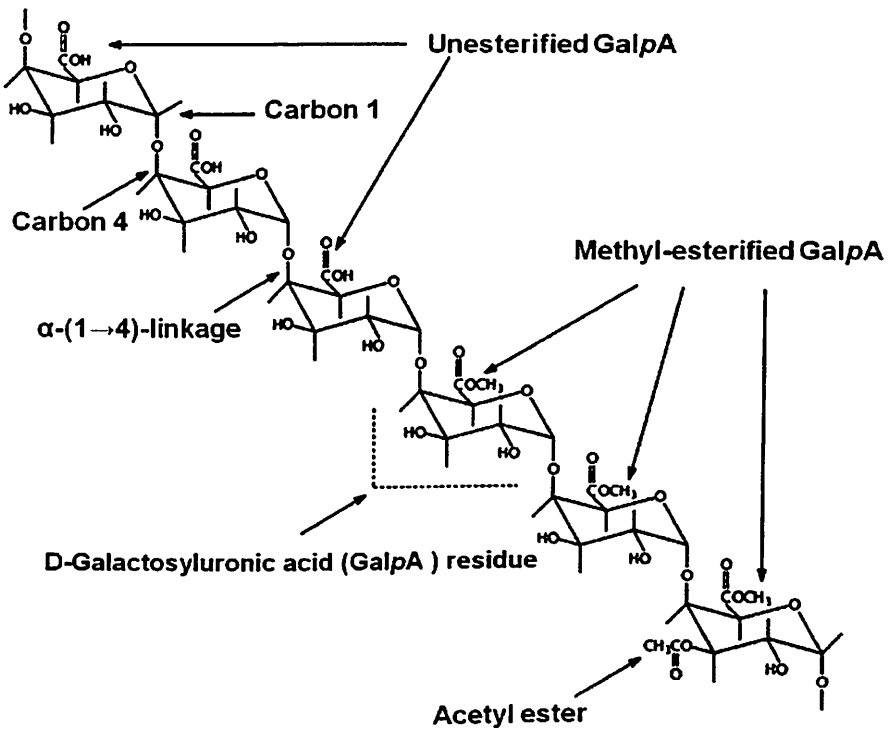

Fig. 1.11 Chemical structure of homogalacturonan showing 1,4-linked α-D-galactopyranosyluronic acid residues (GalpA). The carboxyl groups of the GalpA residues are often methyl-esterified. Some of the hydroxyl groups may be O-acetylated (Ridley *et al.*, 2001).

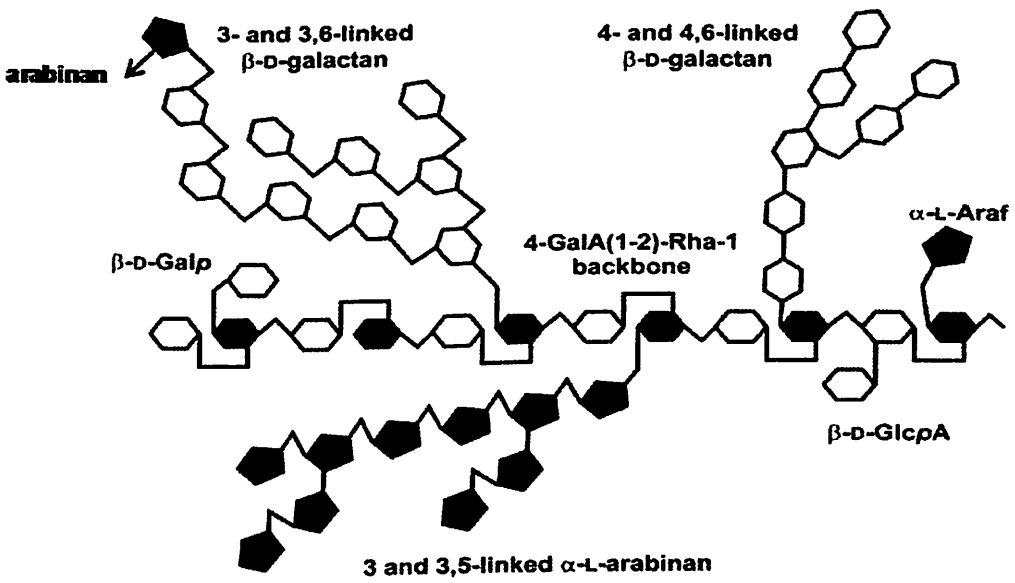

Fig. 1.12 A schematic presentation showing the major structural features of Rhamnogalacturonan II. The backbone is composed of the disaccharide repeating unit [1→4- α-D-galactopyranoseA-(→2)-α-L-rhamnopyranose-(1→]. Branched and linear oligosaccharides composed predominantly of α-L-arabinofuranose and β- D -galactopyranose residues are linked to C4 of some of the rhamnopyranose residues. Some of the rhamnopyranose residue may also be O-acetylated at C2 and/or C3 (Ridley *et al.*, 2001).

1.2 Carbohydrate-active enzymes

Carbohydrates are dynamic molecules that are constantly synthesized and broken down. There are varieties of enzymes involved in the synthesis as well as breakdown of carbohydrates. The glycosyltransferases (GTs) are mainly involved in the formation of the glycosidic bond or biosynthesis of carbohydrates. The polysaccharide lyases (PLs), carbohydrate esterase (CEs) and glycoside hydrolases (GHs) are concerned with the breakdown of polysaccharides. In summary, the carbohydrate-active enzymes are grouped into 347 families based on amino acid sequence similarity and are listed in the continually updated carbohydrate-active enzyme (CAZy) database (www.cazy.org). Out of 347 carbohydrate-active enzymes, about 133 families belong to GHs (Henrissat, 1991). These enzymes belonging to 133 GH families have been reported from nearly 1884 species of bacteria, 130 species of archaea and 65 species of eukaryote (www.cazy.org). A close inspection of the genomes listed within the database reveals the fact that 1-3% of the genome of most organisms is devoted to encoding glycosyltransferases (GTs) and glycoside hydrolases (GHs) (www.cazy.org). The information available at CAZy database provide a wealth of gene sequences (many yet to be characterized) to study the structure and function of carbohydrate-active enzymes (Henrissat and Davies 1997; Cantarel *et al.*, 2009).

1.2.1 Glycosyltransferases

Glycosyltransferases (GTs) are enzymes that catalyse the transfer of any sugar moiety from activated donor molecules to a specific acceptor molecule, forming glycosidic bonds (Sinnot, 1990). These enzymes utilize 'activated' sugar phosphates as glycosyl donors and catalyze glycosyl group transfer to a nucleophilic group, usually

an alcohol (Campbell *et al.*, 1997). The product of glycosyl transfer may be an O-, N-, S-, or C-glycoside; the glycoside may be part of a monosaccharide, oligosaccharide or polysaccharide (Lairson *et al.*, 2008). As of now, nearly 94 families of GTs have been recognized and are listed in the CAZy database (http://www.cazy.org/GlycosylTransferases.html). There are almost over 8000 gene sequences in GenBank and the crystal structure of 36 GTs has been solved to date (http://www.cazy.org/GlycosylTransferases.html). Many GTs have been reported from a wide range of bacterial population *viz. Acidophilium, Actinoplanes, Bacillus, Clostridium, Gloeobacter, Lactobacillus,* etc (Coutinho *et al.*, 2008).

1.2.2 Polysaccharide lyases

Polysaccharide lyases (PLs) are group of enzymes that break the uronic acid-containing polysaccharide chains following a β-elimination mechanism to liberate an unsaturated hexenuronic acid residue and a new reducing end (http://www.cazy.org/Polysaccharide-Lyases.html). The CAZy database contains 22 families of these enzymes classified, based on amino acid sequence similarities, which also reflect their structural features (Lombard *et al.*, 2010). As of now, more than a thousand gene sequences of PLs have been deposited in the GenBank and out of them 546 sequences are from bacteria. Nearly 98 PLs have been characterized to date and the crystal structures of only 12 PLs have been solved (http://www.cazy.org/Polysaccharide-Lyases.html).

1.2.3 Carbohydrate esterase

The carbohydrate esterase (CEs) catalyzes the de-O or N-deacylation of substituted saccharides. Two types of substrates have been considered for

carbohydrate esterases: i) those in which the sugar plays the role of the "acid", such as pectin methyl esters for 4-O-methyl-glucuronoyl methylesterase from *Schizophyllum commune* (Li *et al.*, 2007) and ii) those in which the sugar behaves as the alcohol, such as acetylated xylan for acetyl xylan esterase (family 1 and 2 CEs) from *Clostridium thermocellum* ATCC 27405 (Montanier *et al.*, 2009).

1.2.4 Glycoside hydrolase

The glycoside hydrolases are a group of enzymes that exists in most living organism (Cantarel *et al.*, 2009). Glycoside hydrolases (GHs) are enzymes that catalyze the hydrolysis of the glycosidic linkage of glycosides, leading to the formation of a sugar hemiacetal or hemiketal and the corresponding free aglycone (Henrissat, 1991). Glycoside hydrolases are also referred to as glycosidases, and sometimes also as glycosyl hydrolases. Glycoside hydrolases can catalyze the hydrolysis of O-, N- and S-linked glycosides. They hydrolyze the glycosidic linkages between two or more carbohydrates or between a carbohydrate and a non-carbohydrate moiety (http://www.cazy.org/Glycoside-Hydrolases.html). The carbohydrate-active enzymes database (CAZy) provides a continuous updated list of the glycoside hydrolase families. They are classified into different families based on homology of their primary sequence (Henrissat, 1991). As of now, the GHs are grouped into 133 families based on amino acid sequence with more than 30,000 entries in the CAZy database (www.cazy.org). GHs are also grouped into 14 clans based on the fold of proteins as it was found to be better conserved than their amino acid sequence (Cantarel *et al.*, 2009). Even the closely related catalytic GHs are very often found to differ in substrate specificity (http://www.cazy.org/), while enzymes with very different enzyme activities are found among glycoside hydrolase homologs

(Coutinho *et al.*, 2003). Small changes in the primary structure of glycoside hydrolases are able to change their substrate specificity (Andrews *et al.*, 2000). Unlike other CAZymes (GTs, CLs, and CEs), GHs has clearly displayed several different folds, such as $(\alpha/\alpha)_6$, β-helix, β-propeller, β-jelly roll and the $(\alpha/\beta)_8$ TIM barrel motif. The $(\alpha/\beta)_8$ TIM barrel is found in the majority of GHs listed in CAZy database (Cantarel *et al.*, 2009).

GHs are important plant cell wall degrading enzymes and thus cell wall degradation by microbial enzymes is pivotal to many biological and industrial processes (Gilbert *et al.*, 2010). The polysaccharides of plant cell walls are relatively recalcitrant to enzymatic degradation and due to this the microbes, with time, have evolved and developed a complex enzymatic systems in order to counter this problem. For example, *Clostridium thermocellum* and *Clostridium cellulolyticum* secrete a mega-dalton multi-modular enzyme complex called the "cellulosome" (Bayer *et al.*, 2007; Fontes and Gilbert, 2010). The cellulosome is a macromolecular complex, whose components interact in a synergistic manner to catalyze the efficient degradation of cellulose. The cellulosome complex is composed of numerous kinds of cellulases and related enzyme subunits, which are assembled into the complex by virtue of a unique type of scaffolding subunit (Bayer *et al.*, 1998; Bayer *et al.*, 2004).

1.2.4.1 Glycoside hydrolases and their modular nature

A module is defined as a contiguous amino acid sequence within a larger sequence that folds independently and has an individual function but together increase the overall efficiency of the enzyme (Doi and Kosugi, 2004). The glycoside hydrolases are often found to exhibit a modular architecture comprising a catalytic module fused or attached with one or more ancillary modules via linker peptides. The

ancillary modules are usually the carbohydrate binding modules (CBMs). The first indication that these enzymes contained distinct independent functioning modules was reported by Davies and Henrissat (1991, 2004) and later many researchers reported the same (Bayer *et al.*, 2004).

1.2.4.2 Cellulosome structure

The cellulosome is a macromolecular complex, whose components interact in a synergistic manner to catalyze the efficient degradation of cellulose (Bayer *et al.*, 2007). The cellulosome complex comprises numerous kinds of cellulases and related enzyme subunits, which are assembled into the complex by virtue of a unique type of scaffolding subunit known as scaffoldin (Bayer *et al.*, 2004). The cellulosomal enzymes from *Clostridium thermocellum* range in molecular size from about 40 to 180 kDa (Fontes and Gilbert, 2010). The realization about the discovery of the multienzyme complex (cellulosome) occurred gradually with discoveries of different catalytic and binding domains, dockerins and scaffoldins, first in clostridial species and then subsequently in other bacteria (Doi *et al.*, 1994; Belaich *et al.*, 1997; Doi and Kosugi, 2004). Each of the cellulosomal subunits consists of a multiple set of modules, two classes of which (dockerin domains on the enzymes and cohesin domains on scaffoldin) govern the incorporation of the enzymatic subunits into the cellulosome complex (Bayer *et al.*, 1998). The cellulosomal enzymes are usually members of the glycosyl hydrolase families of enzymes, which hydrolyze oligosaccharides and polysaccharides (Henrissat, 1991; Fontes and Gilbert, 2010).

1.2.4.3 Glycoside hydrolases and their activity

The glycosidic bond linking two carbohydrates together or a carbohydrate to another non-sugar (aglycone) compound is generally a very stable bond with an estimated half life of 5 million years (Wolfenden *et al.* 1998). The GHs act to hydrolyze these glycosidic bonds and thereby increase bond cleavage efficiency up to ~ 10^{17} fold (Wolfenden *et al.* 1998). The substrates degraded by GHs include plant cell wall polysaccharides such as cellulose, hemicellulose and lignin.

1.2.4.4 Mechanism of action of Glycoside hydrolase

Glycoside hydrolases usually hydrolyze glycosidic bonds by adding water across the glycosidic bond. Asp or Glu are the most commonly found catalytically active residues, although a few exceptions do exist (Davies *et al.*, 2002; Rajan *et al.*, 2003). There are two fundamental mechanisms of action by which these enzymes hydrolyze the substrates (www.cazy.org). These include i) Retaining mechanism and ii) Inverting mechanism and are explained in the sub sections 1.2.4.4.1 and 1.2.4.4.2.

1.2.4.4.1 Retaining mechanism

Glycoside hydrolase involves in retaining mechanism generally have a nucleophile and catalytic acid/base residues approximately, 6Å apart (Zechel and Withers, 2000). This reaction proceeds *via* a double displacement mechanism (Fig 1.17A). In the first step, the nucleophilic attack occurs at the anomeric centre with immediate protonation of the glycosidic oxygen by the general acid (Fig 1.17A). This occurs through a transition state that has oxocarbenium ion character and results in the formation of a glycosyl-enzyme intermediate and results in retention of stereochemistry at the anomeric carbon as shown in Fig. 1.17A (Zechel and Withers,

2000). Hydrolysis of the intermediate occurs and simultaneously, the general base deprotonates an incoming water molecule, which further attacks the anomeric centre causing hydrolysis of the glycosyl-enzyme intermediate (Fig 1.17A).

1.2.4.4.2 Inverting mechanism

Inverting glycoside hydrolases require a larger distance between general base and general acid residues in order to accommodate the direct attack of a water molecule and the substrate (Zechel and Withers, 2000). This reaction proceeds *via* a single displacement mechanism (Fig. 1.17B). Water is deprotonated by the general base and attacks the anomeric centre while the general acid concomitantly protonates the leaving group (Fig. 1.17B). The inverting mechanisms proceed via an oxacarbenium ion-like transition state and results in overall inversion of the stereochemistry at the anomeric carbon (Zechel and Withers, 2000).

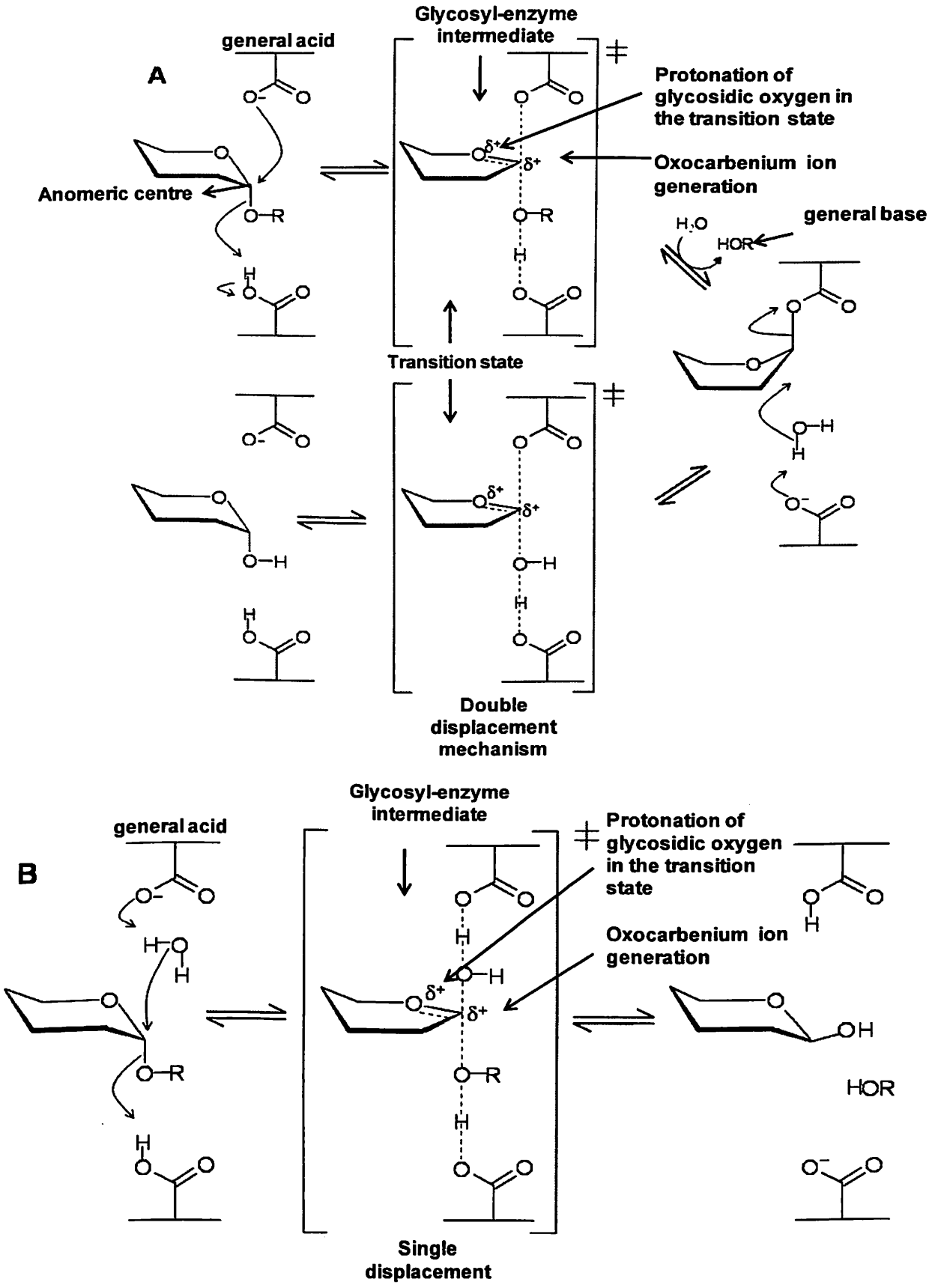

Fig. 1.17 Mechanisms of action of hydrolysis by glycoside hydrolases. A) Retaining mechanism, B) Inverting mechanism.

1.3 Family 26 glycoside hydrolase

Glycoside hydrolases of family 26 are primarily endo-β-(1→4)-mannanases, although an exo-acting β-mannanase has also been reported (Cartmell *et al.*, 2008). The major enzymes within family 26 are β-mannanase (EC 3.2.1.78); β-(1→3)-xylanase (EC 3.2.1.32); lichenase / endo-β-(1→3, 1→4)-glucanase (EC 3.2.1.73); mannobiose-producing exo-β-mannanase (EC 3.2.1.-). The family also contains enzymes that display β-(1→3), (1→4)-glucanase (Taylor *et al.*, 2005) and β-(1→3)-xylanase activities (Araki *et al.*, 2000). The catalytic residues were first identified in the endo-β-(1→4)-mannanase *Cj*Man26A from *Cellvibrio japonicus*. The general acid/base residue is the glutamate Glu320, which is separated in protein sequence by ~100 residues from the catalytic nucleophile, Glu212. The catalytic nucleophile was identified by site-directed mutagenesis in combination with the kinetics of 2,4-dintrophenyl-β-mannobioside hydrolysis which, although very slow was associated with a dramatic decrease in K_m. The identity of the catalytic nucleophile (glutamic acid) was also revealed by site-directed mutagenesis (Bolam *et al.*, 1996) and its function was confirmed by X-ray crystallography where the glycosyl enzyme intermediate bound to 2-deoxy-2-fluoromannose (Ducros *et al.*, 2002). In Clan GHA, of which GH26 is a member, the residue immediately preceding the general acid/base residue in sequence is an asparagine that makes pivotal interactions with the 2-hydroxyl of the substrate (Ducros *et al.*, 2002). In GH26 the equivalent amino acid is a histidine, His211 in *Cj*Man26A, although its function is conserved; it also makes important interactions with the 2-hydroxyl of the substrate (Ducros *et al.*, 2002).

1.3.1 Endo-β-(1→4)-mannanase

β-D-mannanase (endo β-(1→4)-mannan mannohydrolase, E.C. 3.2.1.78) hydrolyzes β-(1→4)-D-mannopyranosyl linkages within the main chain of mannans, glucomannans, galactomannan, and galactoglucomannans. Mannanases have been listed within glycoside hydrolase (GH) families *viz.* GH26, GH5 and GH113 in carbohydrate active enzyme database (http://www.cazy.org/Glycoside-Hydrolases.html) based on sequence similarity. The mechanism of glycosidic bond cleavage is found conserved within these families. These are the characteristic patterns of clan GH-A protein families which led β-D-mannanases of family GH5, GH26 and GH113 to group into this clan. There are currently around 50 β-mannanase gene sequences in families 5 and 26 GHs from various microbial origins. The family 26 Glycoside Hydrolase (GH26) mannanase has narrow substrate specificity hydrolyzing (1→4)-β-D-linkages in mannans, galacto-mannans, glucomannans and galactoglucomannans but does not show activity against β-glycan chain of soluble cellulose derivatives (Halstead *et al.*, 1999). Studies exhibited the presence of distinct types of mannanases (GH5A, GH5B, GH5C, GH26A, GH26B, GH26C) expressed on the cell surface of *Cellvibrio japonicas* having different substrate specificity (Hogg *et al.*, 2001). GH5 mannanase exhibits some activity for cellulosic substrates (Cartmell *et al.*, 2008). There are distinct differences between mannanase 26A (Man26A) and Man26B pertaining to sequence similarity and functional attributes. Man26B displays endo-mannanase enzyme activity which linked to the cell membrane of *Cellvibrio japonicas* via ~70 residue linker sequence (Hogg *et al.*, 2001). The endo mannanase activity by Man26A from *Clostridium thermocellum* was reported earlier by Halstead

et al., (1999) but the cloning and expression of Man26B in a heterologous host has not been reported from *Clostridium thermocellum*.

1.3.2 Applications of mannanases

Mannanases have immense commercial applications. Mannanases are used mainly for improving the quality of food, feed and aiding in enzymatic bleaching of softwood pulp in the paper industries (Talbot and Sygusch, 1990; Wong and Saddler, 1993; Ademark *et al.*, 1998). Different mannanase preparations are used for the hydrolysis of coffee mannan, thus reducing significantly the viscosity of coffee extracts (Araujo and Ward, 1990; Sachslehner *et al.*, 2000). Mannan is the main polysaccharide component of these extracts and is responsible for their high viscosity, which negatively affects the technological processing of instant coffee (Sachslehner *et al.*, 2000). Mannanase is also be used for hydrolyzing galactomannan present in a liquid coffee extract, preferably in order to inhibit gel formation during freeze drying of the (instant) coffee (Sachslehner *et al.*, 2000). Alkaline mannanases are the stable constituents of detergents used in certain laundry segments and act as stain removal booster (Schafer *et al.*, 2002). Mannanases present in detergents hydrolyze mannan containing materials like gums (galactomannans, glucomannans and guar gum) that are present in sauce, jam etc (Schafer *et al.*, 2002).

β-mannanase lowers the gum content of poultry feed in the intestine and therefore facilitates easy digestion and control the weight of poultry bird (Wu *et al.*, 2005). Mannanases can also be used to enhance the flow of oil or gas in drilling operations by forcing out open crevices in the surrounding bedrock, which is done by flooding the well with a natural polymer (guar gum) solution and sand particles, capping the well and then pressurizing the bedrock until it fractures (Adams *et al.*,

1995). The viscous polymer solution carries the sand through the fractures, propping open cracks for oil and gas flow (Adams *et al.*, 1995). Mannanases can be used in enzymatic oil extraction of coconut (Saittagaroon. *et al.*, 1983; Chen and Diosady, 2003).

The mannanase can be used for preparation of fibers or for cleaning of fibers in combination with detergents in the textile and cellulosic processing industry. Mannanases also contribute to the human health as they degrade mannans, which otherwise are resistant to mammalian digestive enzymes in the small intestine but are readily fermented in the large intestine, particularly by probiotic bacteria belonging to the genera *Bifidobacterium* and *Lactobacillus* (Kobayashi *et al.*, 1987). Prebiotic oligosaccharides including manno-oligosaccharides i.e. hydrolysis products of mannan degradation, are believed to promote the selective growth and proliferation of human beneficial intestinal microflora (Kobayashi *et al.*, 1987). Mannanases only recently attracted increased scientific and commercial attention due to its potential applications in various industries.

1.4 Carbohydrate binding modules

The carbohydrate binding modules (CBMs) were earlier known as cellulose-binding domains (CBDs), as previously only cellulose binding domains were discovered. As more diverse carbohydrate binding ligands were identified for new CBMs, the term CBD was changed to CBM. The first identification of a cellulose binding domain was illustrated in 1986 by the proteolytic degradation of a cellulase produced from the fungus *Trichoderma reesei* (Saha, 2003). It was observed that one domain retained the cellulase activity and the other domain had cellulose-binding capacity (Saha, 2003). Carbohydrate binding modules (CBMs) may be defined as

independently folding modules, occurring alongside the carbohydrate-active enzymes (Boraston *et al.*, 2004). The CBMs are the non-catalytic modules known to help or bring the catalytic modules in close proximity to its substrates or stabilize the structure of catalytic modules and increase their thermal stability (Boraston *et al.*, 2004; Henshaw *et al.*, 2006; Dvortsov *et al.*, 2009). The CBMs may contain up to 200 amino acids and are found attached as single, double or triple domain in one protein, located at C- or N-terminal within the parental protein (Shoseyov *et al.*, 2006). Similar to the catalytic modules of glycoside hydrolases, the sequence based classification of carbohydrate binding module (CBM) families have been grouped into 69 families based upon amino acid sequence according to the carbohydrate active enzymes (CAZy) database, similarity (http://www.cazy.org/Carbohydrate-Binding-Modules.html).

1.4.1 Binding site architecture of carbohydrate binding modules

The sequence-based carbohydrate binding module (CBM) families have been further subdivided into three types based on mechanism of ligand binding and binding site topology (Fig. 1.19). The type A, CBMs bind to insoluble crystalline cellulose or chitin and have flat platform-like binding sites (Boraston *et al.*, 2004; Abbott *et al.*, 2009; Abbott *et al.*, 2012,). The planar arrangement of aromatic residues of CBMs within the binding site, allows it to rest on the flat hydrophobic surface of a crystalline ligand (Fig. 1.19A). The type B, CBMs have a binding site that exists as an extended groove, within the groove there are multiple sugar sub sites (Fig. 1.19B). These CBMs bind chains of soluble polysaccharides and both polar and nonpolar interactions drive specificity of the binding. The type C, CBMs, considered lectin-like, have a shallow binding pocket ideal for binding mono-, di- or tri-saccharides

specificity; however, the hydrogen bonding interactions are more dominant in type C CBMs (Boraston *et al.* 2004).

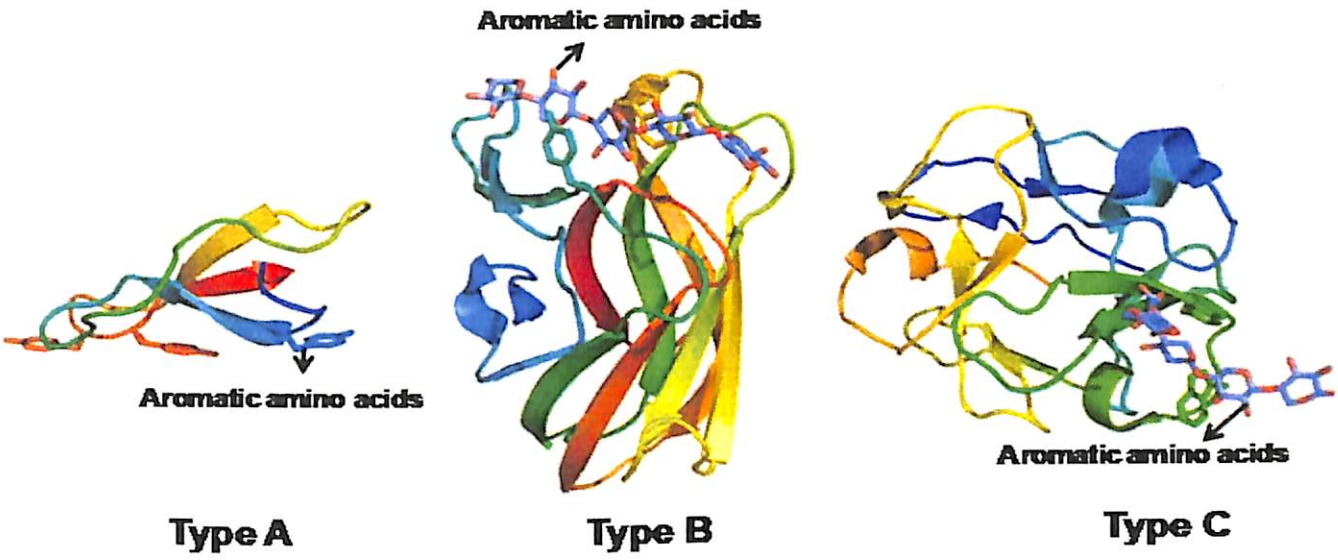

Fig. 1.19 Three types of binding site architecture and ligand binding in CBMs. Aromatic amino acids involved in binding are shown in stick-Type A, cellulose binding *Hj*CBM1 from *Hypocrea jecorina* (PDB code 1CBH), Type B, *Ct*CBM6 from *Clostridium thermocellum* in complex with xylopentaose (PDB code 1UXX), Type C, *Sl*CBM13 from *Streptococcus lividans* in complex with xylopentaose (PDB code 1MC9).

1.4.2 Carbohydrate binding module clans based on fold of their 3-dimensional structure

Currently seven families of folds are reported for CBMs in the CAZy database (Cantarel *et al.* 2008). The seven different folds include the β-sandwich fold, the β-trefoil fold, the oligonucleotide-carbohydrate binding fold (OB), the knottin fold, the hevein fold, the hevein-like fold and a unique fold (http://www.cazy.org/CBM6.html). The second most common fold is the β-trefoil fold reported in CBM6s from *Clostridium cellulolyticum* and *Clostridium thermocellum* by Abbott *et al.* (2009) and Czjzek *et al.* (2001), respectively.

1.4.3 Functions of carbohydrate binding modules

Carbohydrate binding modules (CBMs) increase the ability of glycoside hydrolases to efficiently degrade the polysaccharide substrates. This occurs through three different roles that CBMs play in polysaccharide breakdown, i) they localize the soluble enzyme to its target substrate (Shallom and Shoham, 2003), ii) they are associated with a catalytic domain and contain multiple clefts to attach with substrate, thereby enhancing the catalytic activity (Henshaw *et al.*, 2004; Hashimoto *et al.*, 2006) iii) they can act as fusion proteins capable of binding to a cellulose matrix and consequently used in a protein purification (Shpigel *et al.*, 1998).

The proximity effect describes the binding of the CBM that brings the catalytic module in close proximity (or association) to the substrate and maintains it for a prolonged period. This effect is seen primarily on insoluble substrates such as cellulose and xylan (Tomme *et al.* 1988; Boraston *et al.* 2004). The CBMs bring about the close proximity of catalytic enzyme to its target substrates by two effects as described in sub sections 1.4.3.1 and 1.4.3.2.

1.4.3.1 Targeting effect of carbohydrate binding modules

The targeting effect is observed where CBMs (associated with catalytic module) specifically bind to a substrate thereby bringing the substrate in close proximity of the enzyme (Shallom and Shoham, 2003). For example, there are many cellulose specific CBMs, however, type A cellulose binding CBMs bind crystalline cellulose, whereas, type B cellulose binding CBMs bind non-crystalline components of cellulose. Thus, two different binding mechanisms drive the recognition of different components of cellulose substructure. This targeting effect would drive the

hydrolysis in specific regions of cellulose, rather than just bringing the catalytic modules into proximity as described by Boraston *et al.* 2004.

1.4.3.2 Disruptive effect of carbohydrate binding modules

The disruptive effect may arise due to disruption of the polysaccharide fibres due to CBM permeation within the fibres. It was suggested that the CBMs bind and disrupt the crystalline cellulose (Din *et al.* 1994) or chitin (Vaaje-Kolstad *et al.* 2005) allowing the release of any non-covalently attached fibres thereby exposing the sites for polysaccharide hydrolysis.

1.4.4 Carbohydrate binding modules and multi-valency

Sometimes, more than one CBM may be found within a glycoside hydrolase. CBMs can occur side by side with one another within the enzyme though this is not always the case as the CBMs may also be separated by other modules. More than one CBM from the same family may occur in an enzyme, however, CBMs from different families may also occur within the same enzyme. CBM present side by side may show increased affinity for ligand over that of the individual CBMs though this is not always true (Tomme *et al.* 1998; Boraston *et al.* 2004; Abbott *et al.* 2009). Multivalent binding (two side by side CBMs binding to substrate) can help maintain the CBMs proximity to the carbohydrate surface or fine tune targeting.

1.4.4.1 Family 35 carobhydrate binding module

CBM35 modules are generally composed of ~130 residues. The CBM35 is conserved in xylan-degrading enzymes from three *Cellvibrio* species that binds to xylan and the binding is calcium dependent. CBM35 from *Cellvibrio japonicus* mannanase also binds to decorated soluble mannans and manno-oligosaccharides

(www.cazy.org/CBM35). A CBM35 from *Phanerochaete chrysosporium* galactan (1→3)-β-galactosidase binds to β-galactan. Overall 737 sequences of CBM35 are available in CAZy (www.cazy.org/CBM35). The family 35 carbohydrate binding module has been found appended to family 26 glycoside hydrolase (GH26) and GH5 mannanases and xylanases (GH30) and are involved in binding diverse nature of polysaccharides such as galactomannan, glucomannan, mannan and glucuronoxylan (Taylor *et al.*, 2005; Sunna, 2010; Valenzuela *et al.*, 2012). Three dimensional structure of CBM35 generally has the dominance of secondary structure β-sheet with a jelly roll topology (Valenzuela *et al.*, 2012). CBM35 usually accommodates the polysaccharides utilizing a planer surface of aromatic side chains which interact with the flat chains of manno-configured carbohydrate residues. This form of conformation is known as type B module (Valenzuela *et al.*, 2012). Polysaccharide binding significantly alters the conformation of CBM35 by changing the loop orientation containing amino acid residues which facilitate to create a suitable binding space (Tunnicliffe *et al.*, 2005). The binding specificity of CBM35 depends on the polysaccharide complexity, orientation of monosaccharide moieties of the main chain and the side chain residues (Tunnicliffe *et al.*, 2005).

1.4.5 Applications of carbohydrate binding modules

Three basic features have led to CBMs being perfect candidates for many applications: (i) CBMs are usually independently folding units and therefore can function autonomously in chimeric proteins (Shosheyov *et al.*, 2006) (ii) their ability to attach cellulose matrices which can give an inexpensive way of purifying recombinant proteins (Greenwood *et al.*, 1992) (iii) their binding specificities can be

controlled by modifying the structure using site-directed mutagenesis (Shosheyov *et al.*, 2006).

1.4.5.1 Bioprocessing

Bio-specific affinity purification (affinity chromatography) has become one of the most rapidly developing divisions of immobilized affinity ligand technology. Many protein entities have been expressed when fused to CBMs, establishing CBMs as high-capacity purification tags for the isolation of biologically active target peptides at relatively low cost (Bolam *et al.*, 2004; Shosheyov *et al.*, 2006; Abbott *et al.*, 2009). A high-level production of a cellulose binding domain (CBD_{Cex}) of cellulase (Cex) from *Cellulomonas fimi* expressed in *E. coil*, served as affinity tag in a novel secretion-affinity fusion system for purification of recombinant exoglucanase (Hasenwinkle *et al.*, 1997). Also, a strategy for selecting and characterizing linker peptides for CBM9-tagged fusion proteins expressed in *Escherichia coli* was developed for purification of recombinant proteins (Kavoosi *et al.*, 2007).

1.4.5.2 Cell immobilization using carbohydrate binding modules

Surface-exposed CBMs can be an efficient means of whole-cell immobilization. Whole-cell immobilization by cellulosic material was first demonstrated when an *E. coli* surface anchored CBM, derived from *Cellulomonas fimi*, was attached to cellulose (Saha, 2000). The cells bound tightly to cellulose over a wide range of pH and the extent of immobilization was dependent on the surface of exposed CBM (Saha, 2000; Numan and Bhosle, 2006).

1.4.5.3 Bio-engineering of carbohydrate binding modules for different applications

The potential of carbohydrate binding modules (CBMs) for modifying the characteristics of several enzymes has been reported. The basic approach in CBM engineering was to replace or add a CBM in order to improve hydrolytic activity. Addition of a CBM derived from cellobiohydrolase II of *Trichoderma reesei* to *Trichoderma harzianum* chitinase resulted in increased hydrolytic activity of insoluble substrates (Shoseyov *et al.*, 2006). The replacement of the CBM of endo-1,4-β-glucanase from *Bacillus subtilis* with the CBM of exoglucanase I (Texl) from *Trichoderma viride* conferred higher binding with enhanced hydrolytic activity on the microcrystalline cellulose (Shoseyov *et al.*, 2006). In addition, the hybrid enzyme was more resistant to the tryptic digestion (Shoseyov *et al.*, 2006).

1.5 The microorganism

Clostridium thermocellum is an anaerobic, thermophilic, cellulolytic and ethanologenic, Gram-positive bacterium capable of directly converting cellulose biomass into ethanol (Tachaapaikoon *et al.*, 2012). The general cellular structure of *C. thermocellum* is similar to most rod-shaped bacteria as shown in Scanning Electron Microscopic images in Fig. 1.21 (Lamed *et al.*, 1987).

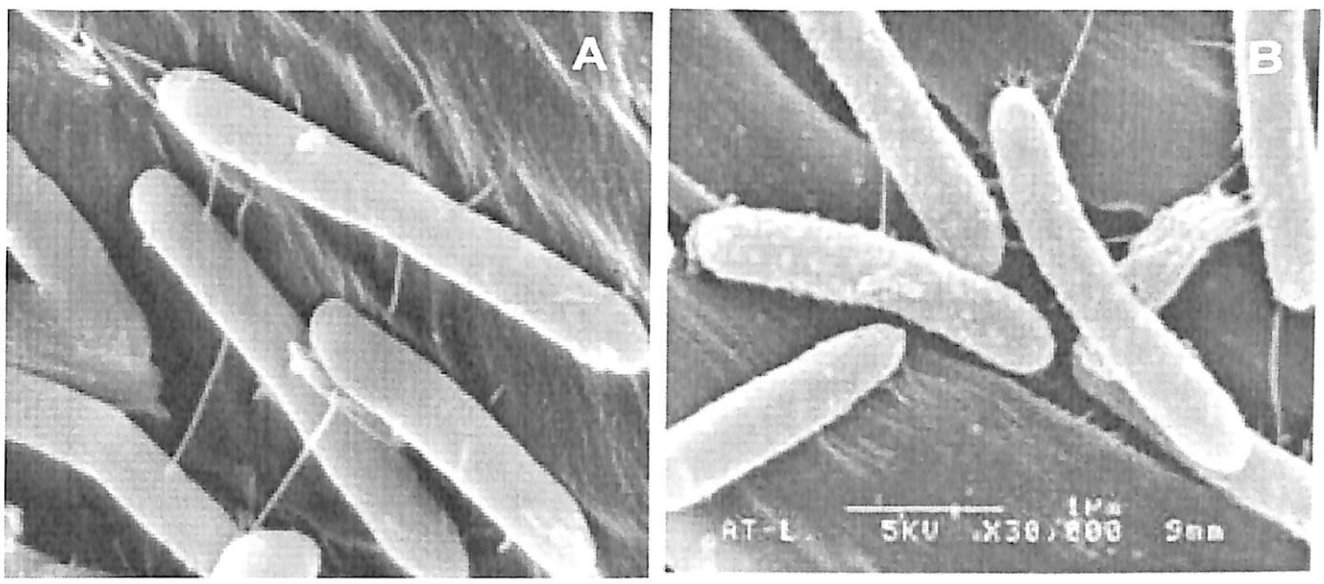

Fig. 1.20 Scanning electron micrographs (SEMs) of (A) *C. thermocellum* S14 and (B) *C. thermocellum* ATCC 27405 (Tachaapaikoon *et al.*, 2012)

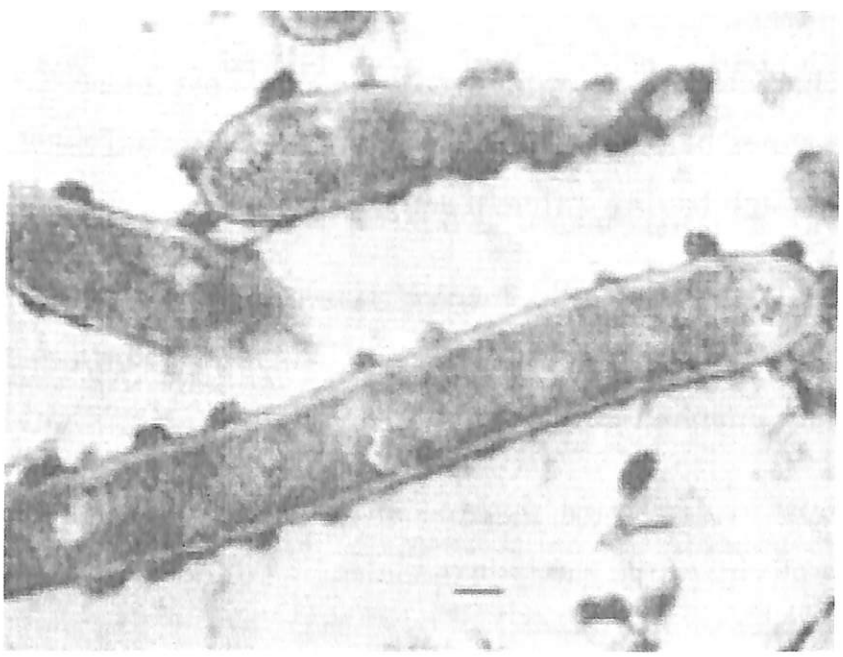

Fig. 1.21 Transmission electron microscope (TEM) image of cationized ferritin (CF) stained *C. thermocellum* YS grown on cellobiose. (adapted from Lamed *et al.*, 1987)

1.6 Objectives of the present study

1.6.1 Why study family 26 GHs and associated family 35 CBMs from Clostridium thermocellum

The reason for selecting the family 26 glycoside hydrolase (GH43) and associated family 35 carbohydrate binding modules (CBM6s) from *Clostridium thermocellum* are summarized as given below:

1. *Clostridium thermocellum* genome contains a complex cellulosome that contains a large number of enzymes, capable of degrading cellulose and hemicellulose.
2. *Clostridium thermocellum* cellulosomal enzyme complex is 50 times more efficient in degrading polysaccharides as reported by Fontes and Gilbert (2010).
3. Functional characterization of family 26 glycoside hydrolase (GH26) is important as all the enzymes belonging to family 26 GH may have the retaining mechanism of catalysis though having different activites.
4. Family 26 GHs are generally hemicellulases which are essential for complete degradation of carob galactomannan, kojac glucomannan, locust bean galactomannan, mannan into respective sugars and oligosaccharides.
5. It is important to determine the role of CBMs in substrate binding if they are altering the activity of the catalytic modules.

In the present study the full length family 26 glycoside hydrolase designated as *Ct*Manf and its truncated derivatives *Ct*ManT, *Ct*CBM35 are proposed to investigated and functionally characterized. The full length family 26 glycoside hydrolase (*Ct*Manf) molecular architecture of the primary sequence showed that it consisted of an C-terminal glycoside hydrolase catalytic module (1029bp, *Ct*ManT) and *Ct*CBM35 (420 bp) at the N-terminus. The influence of CBMs on catalytic modules and its binding affinities towards soluble and insoluble polysaccharides are proposed to be

studied. Biochemical and functional characterization of *Ct*Manf and *Ct*ManT becomes essential as all the family 26 glycoside hydrolases may have the same retaining mechanism of catalysis, but their enzyme activity or substrate specificity are different (http://www.cazy.org/GH26html). The following specific objectives were defined for the thesis work:

1.6.2 Specific Objectives

1. PCR amplification, cloning of full length family 26 glycoside hydrolase (*Ct*Manf) and its truncated derivatives *Ct*ManT, *Ct*CBM35 from *Clostridium thermocellum.*
2. Cloning, expression and purification of family 26 glycoside hydrolase (*Ct*Manf) and its truncated derivatives *Ct*ManT and *Ct*CBM35 from *Clostridium thermocellum* ATCC 27405.
3. Biochemical, functional and structural characterization of catalytic modules *Ct*Manf and *Ct*ManT from *Clostridium thermocellum* ATCC 27405.
4. *In silico* and *in vitro* analysis of ligand binding and stability of *Ct*CBM35 from *Clostridium thermocellum* ATCC 27405.
5. Recovery, purification and characterization of manno-oligosaccharides produced from agro-waste copra meal by *Ct*Manf and to study their potentials as prebiotics and effect on colon cancer cell line.

References

Abbott, D.W. and Boraston, A.B. (2012) Quantitative approaches to the analysis of carbohydrate-binding module function. Methods. Enzymol. 510:211-231.

Abbott, D.W., Ficko-Blean, E., van Bueren, A.L., Rogowski, A., Cartmell, A., Coutinho, P.M., Henrissat, B., Gilbert, H.J. and Boraston, A.B. (2009) Analysis of the structural and functional diversity of plant cell wall specific family 6 carbohydrate binding modules. Biochemistry. 48:10395-10404.

Adams, M.W.W., Perler, F.B. and Kelly, R.M. (1995) Extremozymes: expanding the limits of biocatalysis. Biotechnology. 13:662-668.

Ademark, P., Varga, A., Medve, J., Harjunpa, A. V., Drakenberg, T. and Tjerneld, F. (1998) Softwood hemicellulose-degrading enzymes from *Aspergillus niger*: purification and properties of a β-mannanase. J. Biotechnol. 63:199-210.

Ademark, P., Varga, A., Medve, J., Harjunpa, A. V., Drakenberg, T. and Tjerneld, F. (1998). Softwood hemicellulose-degrading enzymes from Aspergillus niger: purification and properties of a β-mannanase. J. Biotechnol. 63:199-210.

Andrews, S.R., Charnock, S.J., Lakey, J.H., Davies, G.J., Claeyssens, M., Nerinckx, W., Underwood, M., Sinnott, M.L., Warren, R.A. and Gilbert, H.J. (2000) Substrate specificity in glycoside hydrolase family 10. Tyrosine 87 and leucine 314 play a pivotal role in discriminating between glucose and xylose binding in the proximal active site of Pseudomonas cellulosa xylanase 10A. J. Biol. Chem. 275:23027-23033.

Araujo, A. and Ward, O. W. (1990) Purification and some properties of the mannanases from Thielavia terrestris. J. Ind. Microbiol. 6:269-274.

Bayer, E.A., Belaich, J.P., Shoham, Y. and Lamed, R. (2004) The cellulosomes: multi-enzyme machines for degradation of plant cell wall polysaccharides. Annu. Rev. Microbiol. 58:521-554.

Bayer, E.A., Chanzy, H., Lamed, R. and Shoham, Y. (1998) Cellulose, cellulases and cellulosomes. Curr. Opin. Struct. Biol. 8:548-557.

Bayer, E.A., Lamed, R. and Himmel, M.E. (2007) The potential of cellulases and cellulosomes for cellulosic waste management. Curr. Opin. Biotechnol. 18:237-245.

Bayer, E.A., Shoham, Y. and Lamed, R., (2000) Cellulose-decomposing prokaryotes and their enzyme systems. (3rd ed.) Dworkin, M., Falkow, S., Rosenberg, E., Schleifer, K.H., and Stackebrandt, E. (ed.), In *The Prokaryotes: An Evolving Electronic Resource for the Microbiological Community*. 2:578-617.

Belaich, J.P., Tardif, C., Belaich, A. and Gaudin, C. (1997) The cellulolytic system of *Clostridium cellulolyticum,* J. Biotechnol. 57:3–14.

Berg, J.M. (2007) In *Biochemistry,* (6th ed). New York: W.H. Freeman. 310-323.

Boerjan, W., Ralph, J. and Baucher, M. (2003) Lignin biosynthesis. Annu. Rev. Plant Biol. 54: 519-546.

Bolam, D.N., Hughes, N., Virden, R., Lakey, J.H., Hazlewood, G.P., Henrissat, B., Braithwaite, K.L. and Gilbert, H.J. (1996) Mannanase A from Pseudomonas fluorescens ssp. cellulosa is a retaining glycosyl hydrolase in which E212 and E320 are the putative catalytic residues. Biochemistry, 35(50):16195-16204.

Bolam, D.N., Xie, H., Pell, G., Hogg, D., Galbraith, G., Henrissat, B. and Gilbert, H.J. (2004) X4 modules represent a new family of carbohydrate-binding modules that display novel properties. J. Biol. Chem. 279:22953-22963.

Boraston, A.B., Notenboom, V., Warren, R.A., Kilburn, D.G., Rose, D.R. and Davies, G. (2003) Structure and ligand binding of carbohydrate-binding module CsCBM6-3 reveals similarities with fucose-specific lectins and galactose-binding" domains. J. Mol. Biol. 327:659-669.

Brennan, M. and Harris, P.J. (2011) Distribution of fucosylated xyloglucans among the walls of different cell types in monocotyledons determined by immunofluorescence microscopy. Mol. Plant. 4:144-56.

Cantarel, B.L., Coutinho, P.M., Rancurel, C., Bernard, T., Lombard, V. and Henrissat, B. (2009) The Carbohydrate-Active EnZymes database (CAZy): an expert resource for Glycogenomics. Nucleic Acids Res. 37:233-238.

Cartmell, A., McKee, L.S., Peña, M.J., Larsbrink, J., Brumer, H., Kaneko, S., Ichinose, H., Lewis, R.J., Nielsen, A.V., Gilbert, H.J. and Wright, J.M. (2011) The structure and function of an arabinan-specific α-1,2-arabinofuranosidase identified from screening the activities of bacterial GH43 glycoside hydrolases. J. Biol. Chem. 286: 15483-15495.

Cartmell, A., Topakas, E., Ducros, M.A.V., Suits, M.D.L., Davis, G.J. and Gilbert, H.J. (2008) The Cellvibrio japonicus mannanase CjMan26C displays a unique exo-mode of action that is conferred by subtle changes to the distal region of the active site. J. Biol. Chem. 283:34403-34413.

Chanzy, H.D.A., Grosrenaud, R. and Mackie, W. (1984) The crystalline polymorphism of mannan in plant cell walls and after recrystallization. Planta. 161(4):320-329.

Chen, B. K., and Diosady, L. L. (2003) Enzymatic aqueous processing of coconuts. Int. J. Appl. Sci. Engg. 1(1):55-61.

Cosgrove, D.J. (1999) Enzymes and other agents that enhance cell wall extensibility. Annu. Rev. Plant Physiol. Plant Mol. Biol. 50:391-417.

Coutinho, P.M., Stam, M., Blanc, E. and Henrissat, B. (2008) Why are there so many carbohydrate-active enzyme-related genes in plants? Trends Plant Sci. 8:563-565.

Cui, S.W. and Wang, Q. (2009) Cell wall polysaccharides in cereals: chemical structures and functional properties. Struct. Chem. 20:291-297.

Czjzek, M., Bolam, D.N., Mosbah, A., Allouch, J., Fontes, C.M., Ferreira, L.M., Bornet, O., Zamboni, V., Pires, V.M., Henshaw, J.L., Prates, J.A., Bolam, D.N., Ferreira, L.M., Fontes, C.M., Henrissat, B., Planas, A., Czjzek, M. and Gilbert, H.J. (2004) The crystal structure of the family 6 carbohydrate binding module from *Cellvibrio mixtus* endoglucanase 5a in complex with oligosaccharides reveals two distinct binding sites with different ligand specificities. J. Biol. Chem. 279:21560-21568.

Davies, G.J. and Henrissat, B. (2002) Structural enzymology of carbohydrate-active enzymes: implications for the post-genomic era. Biochem. Soc. Trans. 30:291-297.

Demain, A.L., Newcomb, M. and Wu, J.H. (2005) Cellulose, clostridia and ethanol. Microbiol. Mol. Biol. Rev. 69:124-154.

Din, N., Forsythe, I.J., Burtnick, L.D., Gilkes, N.R., Miller, R.C.Jr., Warren, R.A. and Kilburn, D.G. (1994) The cellulose-binding domain of endoglucanase A (CenA) from *Cellulomonas fimi*: evidence for the involvement of tryptophan residues in binding. Mol. Microbiol. 11:747-55.

Doi, R.H. and Kosugi, A. (2004) Cellulosome: plant-cell-wall degrading enzyme complexes. Nat. Rev. Microbiol. 2:541-551.

Doi, R.H., Goldstein, M., Hashida, S., Park, J.S. and Takagi, M. (1994) The *Clostridium cellulovorans* cellulosome. Crit. Rev. Microbiol. 20:87-93.

Ducros, V.M., Zechel, D.L., Murshudov, G.N., Gilbert, H.J., Szabó, L., Stoll, D., Withers, S.G., and Davies, G.J. (2002) Substrate distortion by a beta-mannanase: snapshots of the Michaelis and covalent-intermediate complexes suggest a B(2,5) conformation for the transition state. Angew. Chem. Int. Ed. Engl. 41(15):2824-2827.

Dvortsov, I.A., Lunina, N.A., Chekanovskaya, L.A., Schwarz, W.H., Zverlov, V.V. and Velikodvorskaya, G.A. (2009) Carbohydrate-binding properties of a separately folding protein module from beta-1,3-glucanase Lic16A of *Clostridium thermocellum*. Microbiology, 155:2442-2449.

Fontes, C.M.G.A. and Gilbert, H.J. (2010) Cellulosomes: highly efficient nanomachines designed to deconstruct plant cell wall complex carbohydrates. Annu. Rev. Biochem. 79:655-681.

Frei, E. and. Preston, R.D. (1968) Noncellulosic structural polysaccharides in algal cell walls. III. Mannan in siphoneous green algae. Proc. Royal Soc. B. 169(1015):127-145.

Fry, S.C. (1989) The structure and functions of xyloglucan. J. Exp. Bot. 40:1-11.

Gilbert, H.J. (2010) The biochemistry and structural biology of plant cell wall deconstruction. Plant Physiol. 153:444-455.

Halstead, J.R., Vercoe, P.E., Gilbert, H.J., Davidson, K. and Hazlewood, G.P. (1999) A family 26 mannanase produced by Clostridium thermocellum as a component of the cellulosome contains a domain which is conserved in mannanases from anaerobic fungi. Microbiology, 145:3101-3108.

Heinze, T., Schwikal, K. and Barthel, S. (2005) Ionic liquids as reaction medium in cellulose functionalization. Macromol. Biosci. 5:520-525.

Henrissat, B. (1991) A classification of glycosyl hydrolases based on amino-acid sequence similarities. Biochem. J. 280:309-316.

Henrissat, B. and Davies, G. J. (1997) Structural and sequence-based classification of glycoside hydrolases. Curr. Opin. Struct. Biol. 7:637-644.

Henshaw, J.L., Bolam, D.N., Pires, V.M., Czjzek, M., Henrissat, B., Ferreira, L.M., Fontes, C.M.G.A. and Gilbert, H.J. (2004) The family 6 carbohydrate binding module *Cm*CBM6-2 contains two ligand-binding sites with distinct specificities. J. Biol. Chem. 279:21552-21559.

Henshaw, J.L., Bolam, D.N., Pires, V.M., Czjzek, M., Henrissat, B., Ferreira, L.M., Fontes, C.M.G.A. and Gilbert, H.J. (2004) The family 6 carbohydrate binding module CmCBM6-2 contains two ligand-binding sites with distinct specificities. J. Biol. Chem. 279:21552-21559.

Hogg, D., Woo, E.J., Bolam, D.N., McKie, V.A., Gilbert, H.J. and Pickersgill, R.W. (2001) Crystal structure of mannanase 26A from *Pseudomonas cellulosa* and analysis of residues involved in substrate binding. J. Biol. Chem. 276:31186-31192.

Ishii, T. and Ono, H. (1999) NMR spectroscopic analysis of the borate diol esters of methyl apiofuranoside. Carbohydr. Res. 321:257-260.

Izydorczyk, M. S. and Biliaderis, C. G. (1995) Cereal arabinoxylans: Advances in structure and physicochemical properties, Carbohydr. Polym. 28:33-48.

Kavoosi, M., Creagh, A.L., Kilburn, D.G. and Haynes, C.A. (2007) Strategy for selecting and characterizing linker peptides for CBM9-tagged fusion proteins expressed in *Escherichia coli*. Biotechnol. Bioeng. 98:599-610.

Kobayashi, Y., Echigen, R., Mada, M. and Mutai, M. (1987) Effects of hydrolysates of konjac mannan and soybean oligosaccharides on intestinal flora in man and rats. Intestin. flora. Food. Fact. 79-87.

Kobayashi, M., Matoh, T. and Azuma, J. (1996) Two chains of rhamnogalacturonan II are cross linked by borate-diol ester bonds in higher plant cell walls. Plant Physiol. 110: 1017–1020.

Lamed, R., Naimark, J., Morgenstern, E. and Bayer, E.A. (1987) Specialized cell surface structures in cellulolytic bacteria. J. Bacteriol. 169:3792-3800.

Lang, P., Kajiwara, K.. and Burchard, W. (1993) Investigations on the solution architecture of carboxylated tamarind seed polysaccharide by static and dynamic light scattering. Macromolecules, 26:3992-3998.

Li, X.L., Spániková, S., de Vries, R.P. and Biely, P. (2007) Identification of genes encoding microbial glucuronoyl esterases. FEBS Lett. 581:4029-4035.

Lombard, V., Bernard, T., Rancurel, C., Brumer, H., Coutinho, P.M. and Henrissat, B. (2010) A hierarchical classification of polysaccharide lyases for glycogenomics. Biochem. J. 432:437-444.

Meier, H. (1958) On the structure of cell walls and cell wall mannans from ivory nuts and from dates. Biochim. Biophys. Acta. 28:229-240.

Montanier, C., Money, V.A., Pires, V.M.R., Flint, J.E., Pinheiro, B.A., Goyal, A., Prates, J.A.M., Izumi, A., Stalbrand, H., Morland, C., Cartmell, A., Kolenova, K., Topakas, E., Dodson, E.J., Bolam, D.N., Davies, G.J., Fontes, C.M.G.A. and Gilbert, H.J. (2009) The active site of a carbohydrate esterase displays divergent catalytic and noncatalytic binding functions. PLoS Biol. 31, e71.

Moon, R. J., Martini, A., Nairn, J., Simonsen, J. and Youngblood, J. (2011) Cellulose nanomaterials review: structure, properties and nanocomposites. Chem. Soc. Rev. 40: 3941–3994

Numan, M.T. and Bhosle, N.B. (2006) Alpha-L-arabinofuranosidases: the potential applications in biotechnology. J. Ind. Microbiol. Biotechnol. 33:247-260.

Rajan, S.S., Yang, X., Collart, F., Yip, V.L., Withers, S.G., Varrot, A., Thompson, J., Davies, G.J. and Anderson, W.F. (2004) Novel catalytic mechanism of glycoside hydrolysis based on the structure of an NAD^{+}/Mn^{2+} -dependent phospho-alpha-glucosidase from *Bacillus subtilis*. Structure, 12:1619-1629.

Ralph, J., Lapierre, C., Marita, J.M., Kim, H., Lu, F., Hatfield, R.D., Ralph, S., Chapple, C., Franke, R., Hemm, M.R., Van Doorsselaere, J., Sederoff, R.R., O'Malley, D.M., Scott, J.T., MacKay, J.J., Yahiaoui, N., Boudet, A., Pean, M., Pilate, G., Jouanin, L. and Boerjan, W. (2004) Elucidation of new

structures in lignins of CAD- and COMT-deficient plants by NMR. Phytochemistry, 57:993-1003.

Ramamurthy, V., Thacker, S.P. and Kothari, R.M. (1992) Optimised protocol for the pilot-scale preparation of fungal cellulase. J. Ind. Microbiol. 9:121-125.

Ridley, B.L., O'Neill, M.A. and Mohnen, D. (2001) Pectins: structure, biosynthesis, and oligogalacturonide-related signaling. Phytochemistry, 57:929–967.

Sachslehner, A., Foildl, G., Foidl, N., Gübitz, G. and Haltrich, D. (2000) Hydrolysis of isolated coffee mannan and coffee extract by mannanases of *Sclerotium rolfsii*. J. Biotechnol. 80:127-134

Saha, B.C. (2003) Hemicellulose bioconversion. J. Ind. Microbiol. Biotechnol. 30, 279-291.

Saittagaroon, S., Kawakishi, S., and Namiki, M. (1983) Characterisation of polysaccharides of copra meal. J. Sci. Food. Agric. 34:855-860.

Schafer, T., Kirk, O., Borchert, T. V, Fuglsang, C.C., Pedersen, S., Salmon, S., Olsen, H. S, Deinhammer, R. and Lund, H. (2002) Enzymes for technical applications. Biopolymers, 5:377-437.

Scheller, H.V. and Ulvskov, P. (2010) Hemicellulose. Annu. Rev. Plant. Biol. 61:263-289.

Schladel, C., Blochl, A., Richter, A. and Hoch, G. (2009) Short-term dynamics of nonstructural carbohydrates and hemicelluloses in young branches of temperate forest trees during bud break. Tree Physiol. 29:901–911.

Shoseyov, O., Shani, Z. and Levy I. (2006) Carbohydrate binding modules: biochemical properties and novel applications. Microbiol. Mol. Biol. Rev. 70:283-295.

Shpigel, E., Elias, D., Cohen, I. R. and Shoseyov, O. (1998) Production and purification of a recombinant human hsp60 epitope using the cellulose-binding domain in *Escherichia coli*. Protein Expr. Purif. 14:185-191.

Sinnott, M.L. (1990) Catalytic mechanisms of enzymatic glycosyl transfer. Chem. Rev. 90: 1171-1202.

Sunna, A. (2010) Modular organisation and functional analysis of dissected modular β-mannanase *Cs*Man26 from *Caldicellulosiruptor* Rt8B.4. Appl. Microbiol. Biotechnol. 86(1):189-200.

Tachaapaikoon, C., Kosugi, A., Pason, P., Waeonukul, R., Ratanakhanokchai, K., Kyu, K..L. Arai, T., Murata, Y. and Mori, Y. (2012) Isolation and characterization of a new cellulosome-producing *Clostridium thermocellum* strain. Biodegradation, 23:57-68.

Talbot, G. and Sygusch, J. (1990) Purification and characterization of thermostable β-mannanase and α-galactosidase from *Bacillus stearothermophilus*. Appl. Env. Microbiol. 56:3505-3510.

Taylor, E.J., Goyal, A., Guerreiro, C.I.P.D., Prates, J.A.M., Money, V.A., Ferry, N., Morland, C., Planas, A., Macdonald, J.A., Stick, R.V., Gilbert, H.J., Fontes, C.M. and Davies, G.J.. (2005) How family 26 glycoside hydrolases orchestrate catalysis on different polysaccharides structure and activity of a *Clostridium thermocellum* lichenase? J. Biol. Chem. 280(38):32761-3276.

Timell, T. E. (1965) Wood Hemicelluloses: Part II. Adv. Carbohydr. Chem. 20:409-483.

Tomme, P., Boraston, A., McLean, B., Kormos, J., Creagh, A.L., Sturch, K., Gilkes, N.R., Haynes, C.A., Warren, R.A. and Kilburn, D.G. (1998) Characterization and affinity applications of cellulose-binding domains. J. Chromatogr. B. 715:283–96.

Tunnicliffe, R.B., Bolam, D.N., Pell, G., Gilbert, H.J. and Williamson, M.P. (2005) Structure of a mannan-specific family 35 carbohydrate-binding module: evidence for significant conformational changes upon ligand binding. J. Mol. Biol. 347:287-296.

Urbanowicz, B.R., Peña, M.J., Ratnaparkhe, S., Avci, U., Backe, J., Steet, H.F., Foston, M., Li, H., O'Neill, M.A., Ragauskas, A.J., Darvill, A.G., Wyman, C., Gilbert, H.J. and York, W.S. (2012) 4-O-methylation of glucuronic acid in Arabidopsis glucuronoxylan is catalyzed by a domain of unknown function family 579 protein. Proc. Natl. Acad. Sci. (USA). 109:14253-14258.

Vaaje-Kolstad, G., Horn, S.J., van Aalten, D.M., Synstad, B. and Eijsink, V.G. (2005) The non-catalytic chitin-binding protein CBP21 from *Serratia marcescens* is essential for chitin degradation. J. Biol. Chem. 280:28492-28497.

Valenzuela, S.V., Diaz, P., Pastor, F.I. (2012) Modular glucuronoxylan-specific xylanase with a family CBM35 carbohydrate-binding module. Appl. Environ. Microbiol. 78(11):3923-31.

Wolfenden, R., Lu, X. and Young, G. (1998). Spontaneous hydrolysis of glycosides. J. Am. Chem. Soc. 120:6814-6815.

Wong, K.K.Y. and Saddler, J.N. (1993) Applications of hemicellulases in the food, feed and pulp and paper industries. In Hemicellulose and Hemicellulases, Coughlan, M.P. and Hazlewood, G.P. (Ed). London: Portland Press, pp127-143.

Wu, G., Bryant, M. M., Voitle, R. A. and Roland, D. A. (2005) Effects of β-mannanase in corn-soy diets on commercial leghorns in second cycle hens. Poult. Sci. 84:894-897.

Zechel, D.L. and Withers, S.G. (2000) Glycosidase mechanisms: anatomy of a finely tuned catalyst. Acc. Chem. Res. 33:8-11.

Chapter 2

Cloning, expression and purification of family 26 glycoside hydrolase (*Ct*Manf) and its truncated derivatives *Ct*ManT and *Ct*CBM35 from *Clostridium thermocellum* ATCC 27405

2.1 Introduction

Plant cell wall is predominantly composed of complex structural polysaccharides such as celluloses and hemicelluloses. Polysaccharides of the primary cell wall components of plant are cellulose, hemicelluloses such as xyloglucans, mannans, galactomannans, glucomannans, laminarin, glucuronoarabinoxylans, arabinoxylan etc. Mannans are the polysaccharides with a backbone chain of β-(1→4)-linked mannose units. They constitute a major portion of hemicelluloses in hardwoods. The major distribution of mannan polysaccharides substituted with galactose and glucose units in plant hemicellulose is abundant in nature. Carob galactomannan from *Ceratonia siliqua* plant contains β-(1→4)-D-mannan backbone (78%) and α-(1→6)-linked galactose (22%) single units, whereas guar gum (from endosperm of guar seeds) contains a linear chain of β-(1→4)-linked mannose residues to which galactose residues are (1→6)-linked at every second mannose forming short side-branches (Hirst and Jones, 1948). Glucomannan from *Amorphophallus konjac* is a water-soluble polysaccharide that is considered as a dietary fiber. The sugar

component in konjac glucomannan are β-(1→4)-linked D-mannose and D-glucose residues in a molar ratio of 1.6:1 (Katsuraya *et al.*, 2003).

β-D-mannanase (endo β-(1→4)-mannan mannohydrolase, E.C. 3.2.1.78) hydrolyzes β-(1→4)-D-mannopyranosyl linkages within the main chain of mannans, glucomannans, galactomannans and galactoglucomannans (Dumitriu, 2010). Mannanases have been listed within glycoside hydrolase (GH) families *viz.* GH26, GH5 and GH113 in carbohydrate active enzyme database (http://www.cazy.org/Glycoside-Hydrolases.html) based on sequence similarity (Henrissat, 1991; Davis and Henrissat, 2002). β-D-mannanases belong to family GH5, GH26, GH113 display a $(\beta/\alpha)_8$ barrel shaped protein folding pattern and the acid-base-assisted catalysis via a double displacement mechanism involving a covalent glycosyl-enzyme intermediate (Henrissat *et al.*, 1991; Zhang *et al.*, 2008). The mechanism of glycosidic bond cleavage is found conserved within these families. These are the characteristic patterns of clan GH-A protein families and helped β-D-mannanases of family GH5, GH26 and GH113 to group into this clan (Henrissat *et al.*, 1991; Zhang *et al.*, 2008). Due to the retaining double displacement mechanism, these enzymes can perform transglycosylation. Transglycosylation may leads to the synthesis of new glycosides or oligosaccharides longer than the original substrate. GH5 and GH113 mannanases have been described as able to catalyse transglycosylation reactions (Henrissat *et al.*, 1991; Zhang *et al.*, 2008) while to date no evidence of transglycosylation has been reported for GH26 mannanases

The non-catalytic polysaccharides recognizing modules were initially named cellulose binding domain (Bayer, 2000). Later on the term CBM (carbohydrate binding module) evolved reflecting the diversity in ligand specificity of these proteins

(Boraston *et al.*, 2004; Shoseyov *et al.*, 2006). Currently, CBMs have been classified into 67 distinct families based on sequence similarity (http://www.cazy.org/Carbohydrate-Binding-Module) and they display substantial diversity in terms of ligand specificity. The CBMs append to the glycoside hydrolases that degrade the soluble or insoluble polysaccharides (Bolam *et al.*, 2004). Family 35 carbohydrate binding module is often appended to glycoside hydrolase family 26 (GH26) and GH5 mannanases (Taylor *et al.*, 2005; Suna, 2010; Bolam *et al.*, 2004), xylanases (GH30) (Valenzuela *et al.*, 2012) which significantly alter the polysaccharide specificity for plant cell wall polysaccharides such as galactomannan, glucomannan, mannan and glucouronoxylan. Out of 67 distinct families, CBMs are also included within 7 different fold families. The majority of the folded families are comprised of β-sandwich fold (Boraston *et al.*, 2004). Refinement of the CBM classification was improvised recently where Type A CBMs are those which can recognize the surface of the crystalline polysaccharides and Type B CBMs are classified according to their endo acting mode of action internally to glycan chains (Gilbert et al. 2013). Type C CBMs are attributed by their exo-type binding either at the side chain or at the polysaccharide termini (Gilbert *et al.*, 2013). Usually Type B CBMs are abundant in cellulases, xylanases and mannanases that bind to cellulose, xylan and mannan, respectively. Thus CBMs maintain the target substrate within the close proximity of their complete protein structures (Boraston *et al.*, 2004). In general, most family 35 carbohydrate binding module (CBM35) acquired a type B conformation in nature (Valenzuela *et al.*, 2012).

In the present study the gene encoding *Ct*Manf and its truncated derivatives *Ct*ManT and *Ct*CBM35 from *Clostridium thermocellum* ATCC 27405 were cloned,

expressed in *Escherichia coli* and purified by immobilized metal ion affinity chromatography (IMAC) in a single step.

2.2 Materials and Methods

2.2.1 Chemicals, reagents and kits

Taq DNA polymerase for PCR amplification, dNTPs and $MgCl_2$ were acquired from Bioline, USA. PCR tubes (0.2 ml) used were from Axygen, Germany. Restriction enzymes *Nhe*I, *Bgl*II and *Xho*I were purchased from Fermentas, Germany. The oligonucleotide primers of *Ct*Manf, *Ct*ManT *and Ct*CBM35 were procured from Stabvida, Portugal. The genomic DNA of *Clostridium thermocellum* ATCC 27405 was gift from Professor Carlos M.G.A Fontes, Faculdade de Medicina Veterinaria, Avenida da Universidade Técnica, Lisbon, Portugal. The expression vector pET-28a(+) was purchased from Novagen, EMD4 BioScience, Germany. T_4 DNA ligase, 10x ligase buffer were purchased from Promega, USA. RNAse solution (20 mg/ml), glacial acetic acid (99.9 % pure) Trizma base (Tris free base), ethidium bromide, Bradford reagent, DNAse-RNAse free water (pH 8.0) and components of polyacrylamide gel electrophoresis were obtained from Sigma-Aldrich Co. LLC, USA., Coomassie Brilliant Blue R250, for protein staining was acquired from Himedia, whereas, methanol was supplied by Merck, India. The miniprep plasmid isolation kit was purchased from Sigma-Aldrich Co. LLC, USA. The gel extraction kit was purchased from Qiagen, Germany. The DNA was detected using SeaKem® LE agarose (Cambrex Bio Science, USA). The DNA marker *viz.* Hyperladder I was purchased from Bioline, USA. The Page Ruler protein marker was procured from Fermentas, Germany. Disodium ethylenediamine tetra acetate salts (EDTA), glucose, sodium hydroxide, sodium dodecyl sulphate (SDS), LB and SOC medium components *viz.* tryptone, yeast extract, sodium chloride, potassium chloride, magnesium chloride and glucose were supplied by HiMedia Laboratories Pvt. Ltd.,

India. The antibiotics kanamycin was procured from Sigma-Aldrich Co. LLC, USA. Coomassie Brilliant Blue G-250 was purchased from Amresco LLC, USA.

2.2.2 Microorganisms

E. coli (DH5α) cells were procured from Invitrogen (USA). *E. coli* BL-21 (DE3) cell for expression of recombinant proteins was obtained from Novagen, EMD4 BioScience, Germany.

2.2.3 PCR amplification of full length *Ct*Manf and truncated derivative *Ct*ManT

The ORF region encoding full length *Ct*Manf (CBM35-*Ct*ManT) containing family 35 carbohydrate binding module (nucleotide accession: CP000568.1) at N-terminal and the C-terminal family 26 glycoside hydrolase (GH26), a mannanase B (Man26B) catalytic module, named *Ct*ManT (nucleotide accession: CP000568.1) were amplified from the genomic DNA of *Clostridium thermocellum* ATCC 27405 using two oligonucleotide primers for each (Table 2.2.1). The forward primer contained *Nhe*I and reverse primer contained *Xho*I restriction sites. The details of PCR reaction mixture (50 µl) and PCR cycles for amplification are shown in Tables 2.2.2 and 2.2.3, respectively. The PCR amplification was performed using a thermal cycler (Applied Biosystems, GeneAmp® PCR System 9700). The amplified PCR fragments were run on 0.8 (%, w/v) agarose gel as mentioned in Section 2.2.5.

Table 2.2.1 Oligonucleotide primer sequences used for cloning full length *Ct*Manf and truncated derivative *Ct*ManT from *Clostridium thermocellum*.

Construct	Primer sequence
***Ct*Manf**	Forward: 5'-CAC**GCTAGC**GCATATTCCCTTCCTG-3'
	Reverse: 5'-CAC**CTCGAG**TTAAAGTTCATCCAAGCTGC-3'
***Ct*ManT**	Forward: 5'-CAC**GCTAGC**GCATATTCCCTTCCTG-3'
	Reverse: 5'-CAC**CTCGAG**TTAGCTAAAGTATATTTTG-3'

Table 2.2.2 PCR mixture for amplification of full length *Ct*Manf and truncated derivative *Ct*ManT from *Clostridium thermocellum.*

PCR components	Volume (µl)	Final concentration
10x reaction buffer	5.0	1x
100 mM dNTP mix	0.1	0.2 mM
Forward primer (15 µM)	1.5	0.45 µM
Reverse primer (15 µM)	1.5	0.45 µM
Sigma water, pH 8.0	40.4	--
Genomic DNA (20.0 µg/ml)	0.5	10.0.ng
Taq DNA polymerase (1 U/µl)	1.0	0.02 U
Total	50.0	--

Table 2.2.3 PCR cycles for amplification of full length *Ct*Manf and truncated derivative *Ct*ManT from *Clostridium thermocellum.*

Steps		Time
I. Denaturation at 94°C		4 min
II. 30 cycles of	i) Denaturation at 94°C	30s
	ii) Annealing at 55°C	60s
	iii) Extension at 72°C	2 min
III. Final extension at 72°C		10 min

2.2.4 PCR amplification of family 35 carbohydrate binding module *Ct*CBM35

*Ct*CBM35 gene was amplified from the genomic DNA of *Clostridium thermocellum* ATCC 27405 (nucleotide accession number: CP000568) using a forward primer containing *Nhe*I and the reverse primer having *Xho*I restriction site. The primer details are given in Table 2.2.4. The PCR amplification was carried out similarly in 50 µl reaction mixture, as mentioned in Table 2.2.2. The PCR cycles used for amplification of *Ct*CBM35 are mentioned in Table 2.2.3. The amplified products were run on a 0.8% agarose gel and purified gel as described in Section 2.2.5.

Table 2.2.4 Oligonucleotide sequences (primers) used for cloning *Ct*CBM35 from *Clostridium thermocellum*. The underlined sequences signify the sites for *Nhe*I (forward) and XhoI (reverse), respectively.

Construct	Primer sequence
***Ct*CBM35**	Forward: 5'- CAC**GCTAGC**GCATATTCCCTTCCTG -3'
	Reverse: 5'- CAC**CTCGAG**TTAAAGTTCATCCAAGCTG -3'

2.2.5 Agarose gel electrophoresis of PCR amplified and other DNA

The PCR amplified products were checked on a 0.8% agarose gel prepared in 1x TAE buffer. A stock solution of 10x TAE buffer was prepared using 400 mM Tris-acetate, 10 mM EDTA pH 8.0, according to Sambrook and Russell (2001). 0.8% agarose gel was prepared by dissolving 400 mg agarose (500 mg for 1.0% gel) in 50 ml of 1x TAE buffer by heating in a microwave oven for 5-6 min to get a clear transparent solution. Then 5.0 µl of ethidium bromide (5.0 mg/ml) was added when the solution temperature was around 50°C. The solution was mixed and poured on the casting apparatus, combs were placed and the gel was allowed to set for 30 min. The DNA sample and DNA loading dye were mixed in 4:1 ratio and The PCR amplified DNA was separated under the constant electric field (80 Volts) for 1h in 1x TAE (Tris-acetate-EDTA) running buffer which was used for the preparation of agarose gel (Sambrook and Russel, 2001). The bands were then visualized under UV illumination in a gel documentation system (Kodak, Gel Logic 1500).

2.2.5.1 Preparation of DNA loading dye

The DNA or sample loading dye was prepared by mixing the components mentioned below in Table 2.2.6. A 5x stock solution of DNA loading dye was prepared and was mixed with 4 volumes of DNA sample to make it final 1x before loading on to the agarose gel. The final pH of the DNA loading dye was adjusted to pH 8.0.

Table 2.2.6 Composition of 5x DNA loading dye.

Components	Final concentration (5x)
Tris-HCl	50 mM
Glycerol	25% (w/v)
EDTA	5.0 mM
Bromophenol blue	0.2% (w/v)
Xylene cyanol	0.2% (w/v)

2.2.6 Extraction of DNA from agarose gel

The PCR amplified DNA or other plasmid DNA was purified from agarose gel using a kit (Qiagen, QIAquick® Gel Extraction Kit), following the protocol provided by the manufacturer as described in Section 2.2.6.1. The extracted DNA was eluted in 50 µl DNase free water (Sigma-Aldrich Co. LLC, USA.).

2.2.6.1 DNA gel extraction protocol

1. 1.5 ml sterile, empty microcentrifuge tube was weighed and the weight of the tube was noted.
2. The PCR or plasmid DNA band was were excised from gel using sharp sterile scalpel and transferred to an empty microcentrifuge tube. The tube was weighed again and the weight of excised gel was determined by subtracting the empty tube weight (noted above).
3. Three volumes of buffer QG was added to every 1 volume of gel (100 mg ~ 100 µl) in the microcentrifuge tube.
4. The microcentrifuge tube containing excised gel were incubated at 50°C for 10 min (or until the gel slice has completely dissolved). When the gel slice dissolved completely, the colour of the solution became yellow (similar to Buffer QG without dissolved agarose).

5. QIAquick spin column (DNA binding column) was placed in 2 ml collection tube provided with the kit. The above solution containing PCR-amplified or plasmid DNA (750 µl) was added to DNA binding columns and centrifuged at 17,900*g* for 1 min at room temperature and the flow through was discarded. If the volume was more than 750 µl, the remaining solution was centrifuged similarly and again the flow through was discarded.
6. 500 µl of buffer QG was added to each QIAquick spin column and the mixtures was centrifuged again at 17,900*g* for 1 min at room temperature, and the flow through was discarded.
7. Now, 750 µl of buffer PE was added to each column containing PCR DNA or recombinant plasmid DNA and the mixture was centrifuged at 17,900*g* for 1 min at room temperature. The flow through was discarded and the column was given an additional spin of 1 min at 17,900*g*, to completely remove the residual ethanol.
8. Now the column containing bound DNA was placed in a fresh 1.5 ml sterile microcentrifuge tube. 30 µl of DNAse free water (Sigma-Aldrich Co. LLC, USA) or elution buffer (10 mM Tris-Cl, pH 8.5) was added at the centre of the column. The column was incubated for 2 min at room temperature and centrifuged at 17,900*g* for 1 min.
9. The PCR amplified or plasmid DNA was eluted from QIAquick spin columns was collected in 1.5 ml sterile microcentrifuge tube. The DNA was stored at -20°C for further use.

2.2.7 Restriction enzyme digestion of the PCR amplified DNA

The PCR DNA purified after gel extraction was digested with restriction enzymes (RE) *Nhe*I and *Xho*I as per the set up described in Table 2.2.7. The reaction mixtures were incubated in a water bath (Julabo GmbH, Germany) at 37°C for 90 min. The digested PCR fragments were run on 1.0% agarose gel and the desired fragments were extracted using gel extraction kit as mentioned in Section 2.2.6 and eluted in 25 µl of sterile DNase free water pH 8.0 (Sigma-Aldrich Co. LLC, USA).

Table 2.2.7 Restriction enzyme digestion set up of PCR amplified DNAs of *Ct*Manf and truncated derivatives *Ct*ManT, *Ct*CBM35.

RE digestion set up	1x (µl)
10x reaction buffer	6.0
PCR DNAs	30
DNAse free water	18
*Nhe*I (10 U/µl)	3.0
*Xho*I (10 U/µl)	3.0
Total	60

2.2.8 Restriction digestion of pET expression vector for cloning of *Ct*Manf, *Ct*ManT *Ct*CBM35 amplified PCR fragments

The pET-28a(+) vector of 5.369 Kb was subjected to restriction digestion with *Nhe*I and *Xho*I to prepare it for ligation of PCR amplified and restriction enzymes digested fragments of *Ct*Manf, *Ct*ManT and *Ct*CBM35. The stock solution (100 ng/µl) of pET-28a(+) was prepared from using DNase free water (pH 8.0) and restriction digestion was carried out as described in Table 2.2.8. The digestion mixture was incubated in a water bath at 37°C for 90 min. The *Nhe*I-*Xho*I digested pET-28a(+) vector was run on 1% agarose gel and purified as described in Section 2.2.6.

Table 2.2.8 Restriction enzyme digestion set up of pET-28a(+).

RE digestion set up	1x (µl)
10x reaction buffer	2.0
vector pET-28a (100 ng/µl)	10.0
DNAse free water	6.0
*Nhe*I (10 U/µl)	1.0
*Xho*I (10 U/µl)	1.0
Total	20.0

2.2.9 Ligation of *Nhe*I-*Xho*I digested PCR fragments into pET-28a(+) vector

The *Nhe*I-*Xho*I digested PCR fragments mentioned in Section 2.2.7 were cloned into pET-28a(+) vector, which was also digested with same restriction enzymes as described in Section 2.2.8. The concentration of *Nhe*I-*Xho*I digested pET-28a(+) vector, was adjusted to 100 ng/µl using DNase free Sigma water. The full length gene, *Ct*Manf and the truncated derivatives *Ct*ManT and *Ct*CBM35 were cloned into pET-28a(+) vector. The insert: vector molar ratio was kept at 3:1 for all the fragments. The amounts of *Nhe*I-*Xho*I digested insert DNA of *Ct*Manf, *Ct*ManT and *Ct*CBM35 required for cloning were calculated using the following formula (Engler and Richardson, 1982).

$$\frac{\text{ng of vector} \times \text{kb size of insert}}{\text{kb size of vector}} \times \text{insert : vector molar ratio} = \text{ng of insert}$$

$$\frac{100 \text{ ng} \times 1.449 \text{ kb} \times 3}{5.369 \text{ kb} \quad 1} = 81 \text{ ng of insert (}Ct\text{Manf)}$$

$$\frac{100 \text{ ng} \times 1.029 \text{ kb} \times 3}{5.369 \text{ kb} \quad 1} = 58 \text{ ng of insert (}Ct\text{ManT)}$$

$$\frac{100 \text{ ng} \times 0.420 \text{ kb} \times 3}{5.369 \text{ kb} \quad 1} = 23.46 \text{ ng of insert (}Ct\text{CBM35)}$$

The ligation set up used for digested PCR fragments and pET-28a(+) vector is shown in Table 2.2.9. Each set of ligation reaction was incubated at 16°C, overnight.

Table 2.2.9 Ligation set up of PCR inserts and pET-28a(+).

Ligation set up	1x (µl)
10x buffer	3.0
pET-28a(+) vector (100 ng)	1.0
RE digested PCR DNA insert (ng)	25.0
T4 DNA ligase (3 U/µl)	1.0
Total	30.0

2.2.10 Preparation of *E. coli* (DH5α) competent cells by calcium chloride method

Day 1

1. 50 µl of culture of *E. coli* (DH5α) from glycerol stocks were inoculated into 5.0 ml LB medium (Sambrook *et al.*, 1989), as shown in Section 2.2.11, in test tube grown at 37°C and 180 rpm for overnight.
2. 0.1 M $CaCl_2$ solution was prepared and filter-sterilized via 0.22 µm membrane filter (Pall) in laminar air flow and stored at 4°C.

Day 2

3. 1.0 ml of grown culture from above was taken and inoculated into 100 ml LB medium in 250 ml conical flask. The flask was incubated at 37°C, 180 rpm till cell OD reached 0.5-0.6 at 600 nm.
4. Micro-centrifuge tubes, 50 ml centrifuge tubes (round bottom) and micro tips were autoclaved and kept on ice bath placed in a laminar air flow.
5. 50 ml from 100 ml grown culture was transferred aseptically to the two 50 ml bottom centrifuge tubes (the centrifuge tubes were weighed for balancing before placing on refrigerated centrifuge).
6. The centrifuge tubes were centrifuged at 4°C with 4000***g*** for 10 min.

7. The supernatant was discarded and the cell pellet was gently resuspended in 3-4 ml of sterile, ice-chilled 0.1 M $CaCl_2$ solution and then the remaining solution was added to 10 ml final volume. The resuspended cells in centrifuge tubes were kept on ice for 10 min.
8. The tubes were centrifuged again at 4000*g* at 4°C for 10 min.
9. The supernatant was carefully removed and the pellet was gently resuspended in 3.0 ml of sterile, ice chilled 0.1 M $CaCl_2$ solution.
10. 100 µl of competent cells were aliquoted into sterile 1.5 ml microcentrifuge tube containing 10 (%, v/v) glycerol (final concentration) and kept at -80°C for further use.

2.2.11 Preparation of Luria-Bertani (LB) medium

The composition of LB medium is mentioned in Table 2.2.10. The contents were dissolved in 800 ml of deionized water, the pH was adjusted to 7.2 and the final volume was made up to 1 litre. 100 ml of LB medium was then transferred to each of 250 ml conical flask and the flasks were autoclaved at 121°C at 15 psi for 20 min. It is the most commonly used medium for the growth of recombinant *E. coli* cells. The filter sterilized 50 µg/ml (final concentration) of kanamycin was added to autoclaved and cooled LB medium prior to inoculation.

Table 2.2.10 Composition of Luria-Bertani medium (Sambrook *et al.*, 1989).

Components	Final concentration (%, w/v)
Tryptone	1.0
Yeast extract powder	0.5
Sodium chloride	1.0

2.2.11.1 Preparation of LB-agar medium

LB agar medium was prepared by dissolving the components mentioned in Table 2.2.10 and in addition agar-agar type 1 was also added to a final concentration of 2% (w/v). The medium was autoclaved as described in Section 2.2.11. The medium was allowed to cool around 50-55°C and then antibiotics kanamycin (50 µg/ml, final concentration) was added and mixed. Immediately after mixing 25 ml of medium supplemented with antibiotic was poured in sterile petriplates and the medium was allowed to solidify for 15- 20 min.

2.2.12 Preparation of SOC (super optimal medium with catabolic repression) medium

SOC (super optimal medium with catabolic repression) was prepared using the components as described in Table 2.2.11. It is a modified SOB (super optimal broth) medium with addition of glucose (Hanahan, 1983; Deutscher, 2008; Park *et al.*, 2012). Bactotryptone, yeast extract powder and NaCl were autoclaved separately. 1 M stock solutions of KCl, $MgCl_2$, $MgSO_4$ and glucose were filter-sterilized and the required volume was added to above solution in the laminar hood to finally make SOC medium having desired concentration of each component.

Table 2.2.11 Composition of SOC medium (Sambrook *et al.*, 1989).

Components	Final concentration
Bactotryptone	2.0 (%, w/v)
Yeast extract powder	0.5 (%, w/v)
NaCl	10 mM
KCl	2.5 mM
$MgCl_2.2H_2O$	10 mM
$MgSO_4.7H_2O$	10 mM
Glucose	20 mM

2.2.13 Transformation of ligated DNA using *E. coli* (DH5α) competent cells

The ligated DNAs (recombinant plasmid DNAs) of *Ct*Manf, *Ct*ManT and *Ct*CBM35 were transformed using *E. coli* (DH5α) competent cells. The steps followed in transformation protocol are as follows:

1. The microcentrifuge tube containing competent cell (100 µl) was taken out from -80°C and kept on ice for 5 min, then 10 µl of ligation mixture was added to it (the mixture was given a very short spin prior to use).
2. The tube was gently tapped 4-5 times and kept on ice for 30 min.
3. The cells were given a heat shock at 42°C for 40s.
4. The cells were immediately transferred to ice for 2-3 min.
5. 1.0 ml of SOC (Hanahan, 1983; Sambrook *et al.*, 1989) medium previously incubated at 37°C was added to the transformed cells.
6. The transformed cells were incubated at 37°C in a shaking incubator at 200 rpm for 1h.
7. The cells were harvested by centrifugation at 2000***g*** at 25°C for 3 min.
8. 1.0 ml supernatant was discarded and the cell pellet was then resuspended in remaining 100 µl supernatant.
9. The cells were spread on LB agar plates as described in Section 2.2.11.1 supplemented with kanamycin at a final concentration 50 µg/ml.
10. The LB agar plates were incubated at 37°C for overnight.
11. The transformation efficiency was calculated using the following equation,

$$\text{Transformation efficiency} = \frac{\text{No. of colonies on LB agar plate} \times 1000}{\text{ng of insert DNA}} = \text{cfu/µg}$$

The colonies were picked at random from LB agar plates and inoculated in 5 ml LB medium supplemented with 50 µg/ml kanamycin and incubated at 37°C, 180 rpm for 12h for isolation of plasmid DNA to check for positive clones.

2.2.14 Isolation of recombinant plasmid DNA

The recombinant plasmid DNAs of *Ct*Manf and truncated derivatives *Ct*ManT and *Ct*CBM35 were isolated from *E. coli* (DH5α) cells using alkaline lysis method (Sambrook *et al.*, 1989) and eluted in 30 µl of sterile DNAse free water pH 8.0 (Sigma-Aldrich Co. LLC, USA.). Plasmid DNA was also isolated using plasmid miniprep kit (Sigma-Aldrich Co. LLC, USA) following manufacturer's protocol. The plasmid DNA was isolated by alkaline lysis and with plasmid miniprep kit as described in Sections 2.2.14.1 and 2.2.14.2, respectively.

2.2.14.1 Plasmid miniprep (alkaline lysis) protocol

1. The colonies were randomly picked from LB agar plates and each colony was inoculated into 5.0 ml of LB medium supplemented with 50 µg/ml kanamycin and incubated at 37°C with shaking at 180 rpm for 12h.
2. 1.5 ml culture was taken in micro-centrifuge tubes and centrifuged at 16,000***g*** for 1 min. The supernatant was removed and the above step was repeated twice with fresh 1.5 ml culture so as to process a total of 3.0 ml for plasmid isolation and rest was kept for glycerol stock preparation.
3. The cell pellet was resuspended in 200 µl of GTE solution (50 mM Glucose, 25 mM Tris-HCl, 10 mM EDTA, pH 8.0) containing RNAse at a final concentration of 20 µg/ml.

4. Then 200 µl of lysis solution (0.2 M NaOH, 1% SDS) was added to it and the tubes were inverted gently 5-6 times.
5. 300 µl of ice chilled 5 M potassium acetate solution (pH 4.8) was added immediately and the tubes were gently inverted again 5-6 times. This solution neutralizes NaOH added in the previous lysis step, while precipitating the genomic DNA and SDS in an insoluble white, rubbery precipitate. The tubes were kept on ice for 3-5 min.
6. The mixture was then spun at 16,000***g*** and at 4°C for 5 min.
7. The supernatant was transferred to new tube (2.0 ml micro-centrifuge tube), while taking care not to pick up any white precipitate.
8. The plasmid DNA was extracted with 1 volume of PCI (phenol/chloroform/ isoamyl alcohol; 25:24:1) removing the protein contaminations. The mixture was mixed on vortex for 30s and then centrifuged at 16000***g*** and at 4°C for 10 min. The organic PCI layer stayed at the bottom of tube after the spin.
9. The upper aqueous layer containing the plasmid DNA was carefully transferred to fresh microcentrifuge tube (2.0 ml), avoiding the white precipitated protein layer above the organic PCI layer.
10. The plasmid DNA was precipitated by adding 2 volumes of absolute ethanol at 25°C. The solution was mixed well and kept again at 25°C for 2 min. Thereafter, the plasmid DNA was centrifuged at 16,000***g*** and 4°C for 5 min.
11. Ethanol was removed by micropipette. The plasmid DNA was washed with 700 µl of 70% (v/v) ethanol and DNA pellet was made by spinning at 16,000***g*** and 4°C for 5 min. Ethanol was removed again by micropipette and the microcentrifuge tube containing plasmid DNA was air dried for 5 min.

12. The plasmid DNA was resuspended in 30 µl Tris buffer (10 mM Tris-Cl, pH 8.0) or DNase free Sigma water (pH 8.0). 10 µl of RNase A solution was added (20 µg/ml final concentration) and the plasmid DNA was mixed well and stored at -20°C.

2.2.14.2 Plasmid isolation protocol (Sigma-Aldrich Co. LLC, USA)

1. 1.5 ml from the each of the grown recombinant culture was taken and was transferred to 1.5 ml microcentrifuge tube aseptically.
2. The cells were then centrifuged at 13000***g*** for 1 min and the process was repeated twice with another 1.5 ml of grown culture.
3. The resulting cell pellets of each recombinant derivative were resuspended in 200 µl resuspension solution by vortex. RNAse at final concentration of 20 µg/ml, was added to the re-suspension solution prior to use.
4. 200 µl of lysis solution was added to each tube and the tubes were gently inverted 5-6 times. The tube was allowed to stand for 2-5 min.
5. 350 µl of neutralization solution was added to the mixture and the tubes were inverted again for 4–6 times to mix properly.
6. The mixture was then centrifuged at 16,000***g*** for 10 min.
7. The DNA binding columns were prepared or activated by adding 500 µl of column preparation solution to binding column and centrifuging at 13,000***g*** for 1 min. The flow through accumulated in collection tube was discarded.
8. The clear lysate was then transferred to activated DNA binding column and centrifuged at 13,000***g*** for 1 min and the flow through in the collection tube was discarded again.

9. The plasmid DNA bound to column were washed with wash solution and spun at 13,000*g* for 1 min. The flow through was discarded and the column was given another 1 min spin at 13,000*g* for removing the wash solution completely.
10. The DNA binding column was transferred to a fresh sterile microcentrifuge tube and 30 µl of DNase free water (Sigma-Aldrich Co. LLC, USA) was added at the centre of binding column. The microcentrifuge tube was allowed to stand for 2 min at room temperature and then plasmid DNA was eluted by centrifugation at 13,000*g* for 1 min. The plasmid DNA then got collected in the sterile microcentrifuge tube.
11. The eluted plasmid DNA in sterile microcentrifuge tube was stored at -20°C.

2.2.15 Screening of recombinant plasmid DNA for identification of positive clones

10 µl of each recombinant plasmid DNA of all the derivatives *viz.* *Ct*Manf and truncated *Ct*ManT and *Ct*CBM35, isolated by alkaline lysis method as described in Section 2.2.14, were taken separately, in a fresh sterile microcentrifuge tube for restriction enzyme digestion analysis. The recombinant DNA of each of the above mentioned derivatives was digested with restriction enzymes, *Nhe*I and *Xho*I, to check for positive clones following the reaction set up as given in the Table 2.2.12. The reaction mixtures for each recombinant derivative were incubated at 37°C in a water bath (Julabo, GmbH) for 90 min. The digested products were run on 1% agarose gel as described in Section 2.2.5. The digested fragments *viz.* pET-28a(+) vector and the insert DNA of above mentioned recombinant derivatives were visualized under UV transilluminator. The digested fragments (insert and vector) were analyzed to check whether the size of insert DNA and vector pET-28a(+), were same as determined

earlier in Sections 2.2.7 and 2.2.8. Based on this observation, the positive clones for the respective recombinant derivatives were identified. Glycerol stocks of *E. coli* (DH5α) cells harbouring the recombinant plasmids of each of the above mentioned derivatives were prepared by keeping final concentration of glycerol to 20-25% (v/v). The glycerol stocks in cryo vials of 2 ml were stored at -80°C. The positive clones for each of the recombinant derivatives *viz.* *Ct*Manf, *Ct*ManT and *Ct*CBM35 were identified and were preserved.

Table 2.2.12 Restriction enzyme digestion set up of recombinant DNA.

Digestion set up	**1x (µl)**
10x buffer	2.0
DNAse free water	6.0
Recombinant plasmid DNA (approx. 100 ng)	10.0
*Nhe*I (10 U/µl)	1.0
*Xho*I (10 U/µl)	1.0
Total	20.0

2.2.18 Transformation of recombinant plasmids in *E. coli* BL-21 (DE3) cells for protein expression

10 µl of from each of the recombinant plasmid DNA isolated by Sigma miniprep method, was transformed in *E. coli* BL-21 cells for expression of *Ct*Manf , truncated *Ct*ManT and *Ct*CBM35. 100 µl of *E. coli* BL-21(DE3) competent cells (preparation described in the section 2.2.10). The protocol for transformation followed was same as described in Section 2.2.13. The cells harboring recombinant plasmids were spread on LB agar plates with 50 µg/ml kanamycin and grown at 37°C for 12h. The colonies were randomly picked from LB agar plates recombinant cells after 12h of and inoculated into 5.0 ml LB medium supplemented with 50 µg/ml kanamycin as mentioned in Section 2.2.13. The cells containing recombinant

plasmids were grown at 37°C in shaking incubator at 180 rpm for expression analysis of protein as described in Section 2.2.19.

2.2.19 Hyper-expression of recombinant proteins

The *E. coli* BL-21 (DE3) cells harbouring recombinant plasmids of *Ct*Manf, truncated *Ct*ManT and *Ct*CBM35 as described in Section 2.2.18 were analyzed for protein expression. The protocol for protein expression was followed as described by Taylor *et al.*, (2005). The colonies grown on LB agar plates supplemented with kanamycin were picked and inoculated in 5 ml LB medium as stated in Section 2.2.13 containing kanamycin (50 µg/ml) and incubated in a shaking incubator at 37°C and 180 rpm. The cells were allowed to grow up to mid-exponential phase till cell absorbance at 600 nm (A_{600}) reached ~0.6. 1.0 ml of this grown culture containing uninduced cells were taken out for making glycerol stocks (after expression analysis) and for the sample preparation for analysis by SDS-PAGE. The remaining 4.0 ml culture was then induced with isopropyl-1-thio-β-D-galactopyranoside (IPTG) at 1.0 mM final concentration for hyper-expression of recombinant proteins and further incubated at 24°C (for all recombinant derivatives *viz.* *Ct*Manf, truncated *Ct*ManT and *Ct*CBM35) with shaking at 200 rpm for 24h. The expression of recombinant protein was checked by loading respective uninduced and induced cell samples on polyacrylamide gel (SDS-PAGE) as described in the Section 2.2.20. These *E. coli* BL-21 containing recombinant proteins *viz.* *Ct*Manf, *Ct*ManT and *Ct*CBM35 were preserved at -80°C as glycerol stocks by keeping the final glycerol concentration 20-25% (v/v) as described in Section 2.2.15.

2.2.20 Sodium dodecyl sulphate-Polyacrylamide gel electrophoresis (SDS-PAGE) analysis of recombinant proteins

2.2.20.1 Preparation of SDS-PAGE gel

The components of a SDS-PAGE gel are acrylamide 30% (w/v), resolving gel (Tris-HCl, pH 8.8), a stacking gel (Tris-HCl, pH 6.8), SDS 10 % (w/v), APS 10% (w/v), TEMED, sample loading buffer (pH 6.8) and electrophoretic running or tank buffer (pH 8.3-8.5). The composition of each component of SDS-PAGE gels and buffers are described below in Sections 2.2.20.2 to 2.2.20.5.

2.2.20.2 Preparation of acrylamide 30% (w/v) solution

0.8 g of bis-acrylamide was weighed and transferred into an amber colour bottle and dissolved in 50 ml of ultra-pure deionized water collected at 18 MΩcm (Millipore, Milli-Q water purification system) using a magnetic stirrer (IKA, C-MAG HS7). After completely dissolving bis-acrylamide, 29.2 g of acrylamide was added to and stirred on a magnetic stirrer till the solution was clear. The final volume was adjusted to 100 ml with ultra-pure water by keeping the measuring cylinder (100 ml) wrapped in aluminium foil as acrylamide is light sensitive. The acrylamide solution was then filtered (Whatman No. 1) under dark condition and stored at 4°C.

2.2.20.3 Polymerization of SDS-PAGE gel

The resolving gel and stacking gels were prepared by following the protocols from Sambrook *et al.* (1989) using the composition as described in Tables 2.2.13 and 2.2.14. The resolving gel was prepared by adding the all the components in the order as mentioned in Table 2.2.13, in a 25 ml beaker, by keeping acrylamide concentration at 13% (w/v). Similarly, the stacking gel (4%, w/v) was prepared by dissolving all the components mentioned in Table 2.2.13.

Table 2.2.13 Composition of SDS-PAGE for preparation of resolving gel.

Components	13% gel volume (ml)
Acrylamide solution (30%, w/v)	4.33
Deionized water	0.36
SDS (10%, w/v)	1.0
Glycerol (50%, v/v)	1.0
1.5 M Tris-HCl (pH 8.8)	3.3
Amonium per sulphate (10%, w/v)	0.1
TEMED	0.01

Table 2.2.14 Composition of SDS-PAGE components for preparation of stacking gel.

Components	4% gel volume (ml)
Acrylamide solution (30%, w/v)	0.7
Deionized water	2.8
SDS (10%,w/v)	0.5
0.5 M Tris-HCl (pH 6.8)	1.0
Amonium per sulphate (10%, w/v)	0.05
TEMED	0.005

2.2.20.4 Preparation of SDS-PAGE running buffer

The SDS-PAGE gels were run using a 1x running or tank buffer prepared from the 5x stock solution as described in Table 2.2.15. 15.14 g of Tris free base and 94 g of glycine were dissolved in 800 ml of deionized water. To this 50 ml of 10% (w/v) SDS was added and the final volume was adjusted to 1 litre. The final pH of the buffer was adjusted to 8.3. The 5x buffer was filtered (Whatman, Filter No. 1) and stored at 4°C.

Table 2.2.15 Composition of 5x Tris-Glycine, running or tank buffer.

Components	Final concentration (5x buffer)
Tris base	0.125 M
Glycine	1.25 M
SDS	0.5 % (w/v)

2.2.20.5 Preparation of sample buffer

5x sample loading buffer was prepared by dissolving the components while keeping the concentration of components as described in Table 2.2.16 and the pH of the buffer was adjusted to 6.8. The components were dissolved in the order as mentioned in Table 2.2.16 to make 5x sample buffer. However, the final concentration while loading to a SDS-PAGE gel was always kept to 1x by mixing 4 volumes of sample (protein) with 1 volume of 5x sample buffer.

Table 2.2.16 Composition of 5x sample loading buffer (Laemmli, 1970).

Components	Final concentration (5x buffer)
Tris-HCl (pH 6.8)	62.5 mM
Glycerol	20.0 (%, v/v)
SDS	2.0 (%, w/v)
Bromophenol Blue	0.025 (%, w/v)
β-mercaptoethanol	5.0 (%, w/v)

2.2.20.6 Preparation of staining and destaining solutions

The staining solution (100 ml) was prepared by dissolving 250 mg or 0.25% (w/v), of Coomassie Brilliant Blue (CBB R-250) dye in 50 ml of deionized water in an amber colour bottle by keeping on a magnetic stirrer for overnight. The solution was filtered (Whatman, Filter No. 1), then 40 ml of methanol and 10 ml of glacial acetic acid were added to finally make the ratio 5:4:1 (deionized water:methanol:glacial acetic acid). The destaining solution was prepared by dissolving deionized water: methanol: glacial acetic in 5:4:1 ratio. The gels were destained by immersing it in destaining solution under gentle shaking condition with change of destaining solution every 30 min, until the protein bands were clear.

2.2.21 Purification of recombinant proteins

The *E. coli* BL-21(DE3) cells harbouring recombinant plasmids were grown in 100 ml LB medium in 250 ml flask with kanamycin as mentioned in Section 2.2.10.2. The recombinant proteins contained a His_6 tag at N-terminal in pET-28a(+) vector. A single step purification method based on immobilized metal-ion affinity chromatography (IMAC) for His_6-tag containing proteins was employed using 1.0 ml sepharose columns (GE Healthcare, HiTrap chelating HP). The compositions of binding as well as elution buffers used for affinity column purification of recombinant proteins are mentioned Table 2.2.16. All the buffers (binding, elution and cleaning buffer), 0.1M $NiSO_4$ solution and water was filtered through 0.45 μm filter and degassed to avoid back pressure due to clogging of column.

Table 2.2.17 Composition of buffers required for purification recombinant proteins by immobilized metal ion affinity chromatography (IMAC).

Buffers	Composition
Equilibration buffer	20 mM sodium phosphate, pH 7.4 500 mM NaCl, 60 mM Imidazole
Elution buffer	20 mM sodium phosphate, pH 7.4 500 mM NaCl, 300 mM Imidazole
Cleaning buffer	20 mM sodium phosphate, pH 7.4 500 mM NaCl, 50 mM EDTA

The bacterial cells (100 ml culture) were harvested by centrifugation at 9,000***g*** using a centrifuge (Sigma, 4K15) and the resulting cell pellets were re-suspended in 5 ml of 20 mM sodium phosphate buffer pH 7.4 containing 1 mM phenylmethanesulfonyl fluoride (PMSF). The cells were sonicated (Sonics, Vibra cell) on ice for 16 min (9s on/off pulse; 30% amplitude) and again centrifuged at 19,000***g*** at 4°C for 20 min to get the crude cell free extract. The cell free extract was

passed through a 0.45 µm filter membrane before loading on HiTrap chelating HP column (GE Healthcare, USA). Initially the column was washed with 5 volumes of filtered and degassed water to remove the alcohol. The column was activated using 2-3 ml of 0.1 M $NiSO_4$ solution and the unbound nickel was washed away with 5 volumes of water. Then the column was equilibrated with 5 volumes of equilibration buffer (Table 2.2.17). The filtered cell free extract (4-4.5) ml of recombinant protein was loaded on to the column using a peristaltic pump (P1, GE Healthcare) at a flow rate of 1 ml/min. The column was then washed with 50-60 column volumes of equilibration buffer to remove the unbound proteins. The retained proteins were then eluted with elution buffer and 1 ml fractions were collected (Carvalho *et al.*, 2004; Taylor *et al.*, 2005). The column was cleaned using cleaning buffer as mentioned in Table 2.2.17, washed with 2-5 volumes of water and incubated in 1N NaOH at 4°C for 2h. The column was then washed with 20 volumes of water to remove NaOH, and finally stored in 20% (v/v) ethanol at 4°C. The collected fractions were analyzed for protein content by taking 20 µl of purified protein and 80 µl of Bradford's reagent in a microcentrifuge tube. Development of blue colour complex indicated the presence of protein and usually the purified protein was eluted in third fraction as 1 ml HiTrap column was used. The purified recombinant proteins *Ct*Manf, *Ct*ManT and *Ct*CBM35 were dialyzed (14 kDa Mol wt cut off membrane) against 50 mM sodium phosphate buffer pH 7.0. The purity and molecular mass of recombinant proteins were verified by SDS-PAGE as described in Section 2.2.14. The purified clostridial recombinant proteins were quantified using Bradford reagent (Bradford, 1976) as described in Section 2.2.22.

2.2.22 Protein estimation by Bradford method

The concentrations of the recombinant proteins were determined using the Bradford's method of estimating proteins at a wavelength of 595 nm (Bradford, 1976). Bovine serum albumin (BSA) purchased from Sigma-Aldrich Co. LLC, USA. was used as standard protein. A standard plot of OD at 595 nm versus different concentration of BSA in 10-100 µg/ml was prepared.

2.2.22.1 Preparation of Bradford's reagent

The Bradford assay estimates the amount of protein in a solution by using the spectral properties of Coomassie Brilliant Blue G-250 (Bradford, 1976). 100 mg 0.01% (w/v) Coomassie Brilliant Blue G-250 was weighed and dissolved in 50 ml 95% ethanol (in an amber colour bottle). 100 ml 85% (w/v) phosphoric acid was added to it. A magnetic bead was placed inside the bottle and the contents were mixed properly by keeping on magnetic stirrer until the dye completely dissolved. The dye was finally diluted to 1 liter with deionized water, filtered (Whatman, No. 1 paper) under dark conditions and stored at 4°C.

Commercial Bradford reagent (Sigma-Aldrich Co. LLC, USA) was also used for protein content determination. The amount of recombinant protein was estimated using the following equation,

$$[\text{Protein}] = \frac{\Delta A_{595} \times V \times C}{v}$$

Where,

A_{595} = change in absorbance of the sample
V = volume of the protein-buffer mixture (ml)
C = 1 OD equivalent of BSA from standard plot (mg/ml)
v = volume of the enzyme used for assay (ml)

2.3 Results and Discussion

2.3.1 PCR amplification of full length family 26 glycoside hydrolase (*Ct*Manf) and its truncated derivatives *Ct*ManT and *Ct*CBM35

The molecular architecture of full length family 26 glycoside hydrolase mannanase *Ct*Manf (1449 bp) displayed a family 35 carbohydrate binding module (*Ct*CBM35) (420 bp) at its N-terminal and the truncated derivative the catalytic *Ct*ManT (1029 bp) at its C terminal (Fig. 2.3.1). Two mannanase genes (locus name: Cthe_0032 and Cthe_2811) (http://www.cazy.org/GH26_bacteria.html) belonging to family 26 glycoside hydrolase (GH26), are available in the native host *Clostridium thermocellum* ATCC 27405 (16S rDNA sequence ID: CP000568). In the present study mannanase encoding ORF region was identified using the protein sequence (gene bank protein accession ABN51273.1, locus name: Cthe_0032) of *Clostridium thermocellum* ATCC 27405 in tBLASTn (http://blast.ncbi.nlm.nih.gov/Blast.cgi) tool. This sequence was used to design the desired oligonucleotide primers for PCR amplification and cloning of full length *Ct*Manf (*Ct*CBM35-*Ct*ManT), truncated catalytic module *Ct*ManT and family 35 carbohydrate binding module *Ct*CBM35 (nucleotide accession: CP000568.1).

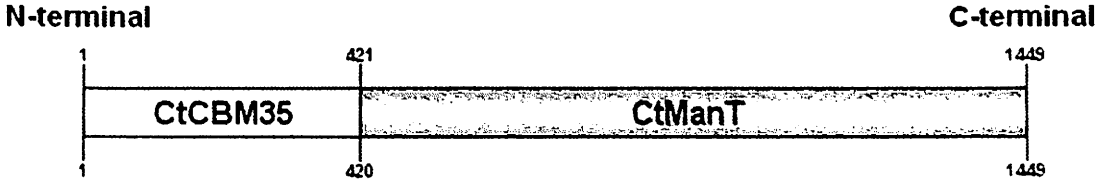

Fig. 2.3.1 Molecular architecture of family 26 glycoside hydrolase (*Ct*Manf) from *Clostridium thermocellum.*

The DNA sequences for *Ct*Manf, *Ct*ManT and *Ct*CBM35 of 1449 bp, 1029 bp and 420 bp, respectively, were PCR amplified from genomic DNA of *Clostridium thermocellum* using the conditions as mentioned in Section 2.2.3. The PCR fragments detected on 0.8% agarose gel were *Ct*Manf (Fig. 2.3.2, lane 2), *Ct*ManT (Fig. 2.3.3, lane 2) and *Ct*CBM35 (Fig. 2.3.4, lane 2). The PCR products were purified from gel using gel extraction kit (Qiagen) as mentioned in Section 2.2.6 and were stored at -20°C for subsequent cloning experiments.

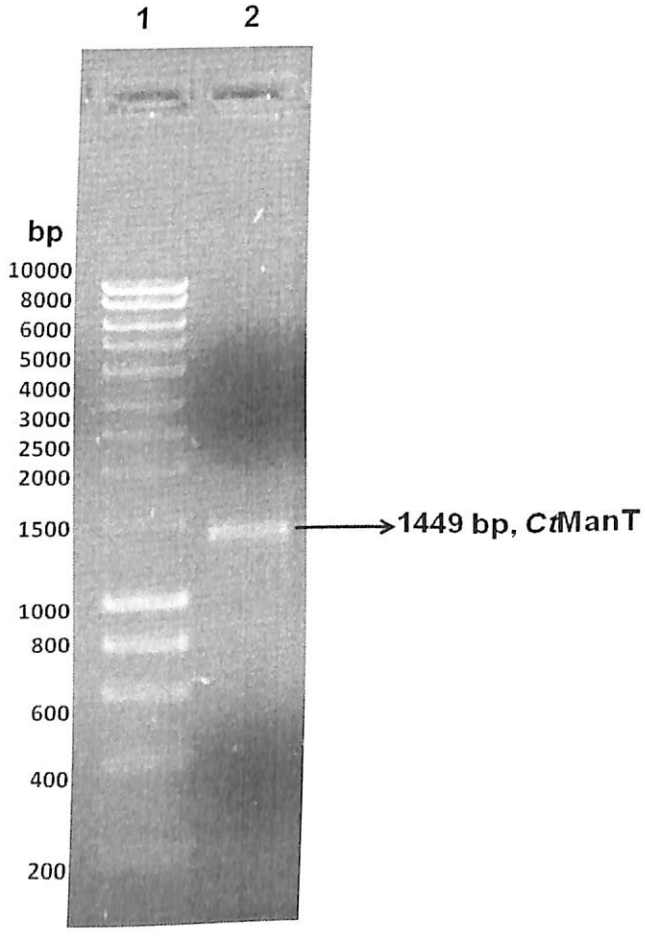

Fig. 2.3.2 Agarose gel (0.8%) showing amplified fragment of *Ct*Manf. Lane 1: DNA marker (Hyperladder I, Bioline), Lane 2: *Ct*Manf (1449 bp).

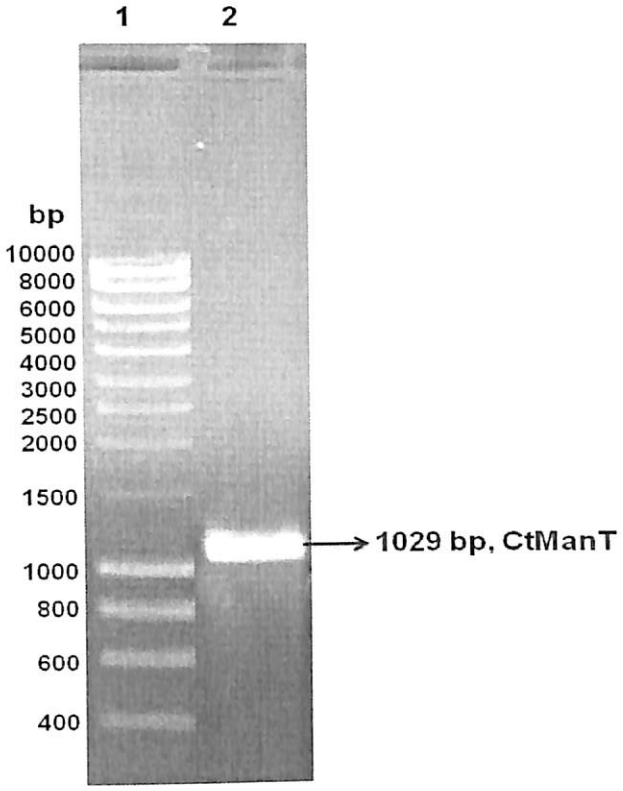

Fig. 2.3.3 Agarose gel (0.8%) showing amplified fragment of *Ct*ManT. Lane 1: DNA marker (Hyperladder I, Bioline), Lane 2: *Ct*ManT (1029 bp).

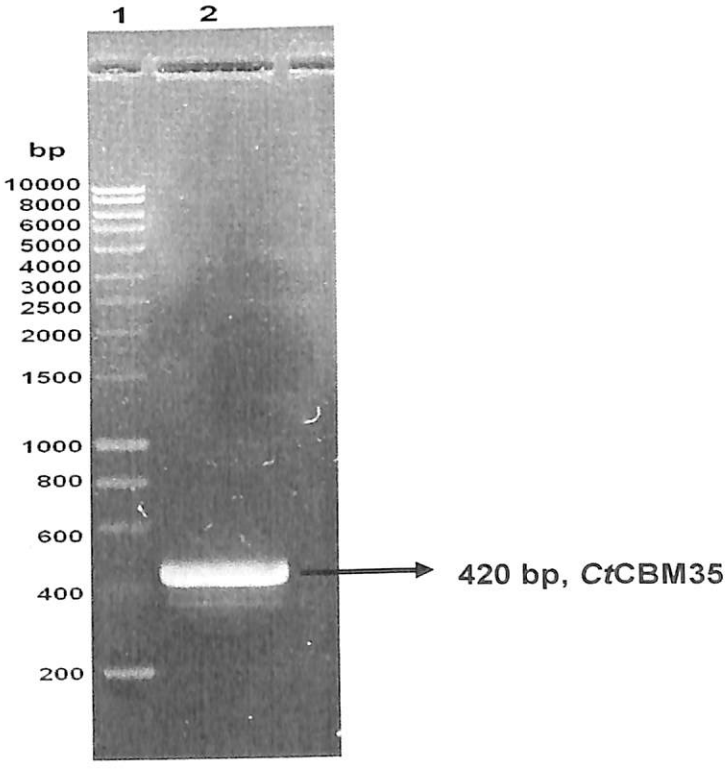

Fig. 2.3.4 Agarose gel (0.8%) showing amplified fragment of *Ct*CBM35. Lane 1: DNA marker (Hyperladder I, Bioline), Lane 2: *Ct*CBM35 (420 bp).

2.3.2 Restriction enzyme digestion of PCR amplified fragments

The amplified fragments of *Ct*Manf, *Ct*ManT and *Ct*CBM35 were digested with *Nhe*I and *Xho*I restriction enzymes to prepare them for cloning into pET-28a(+) expression vector. Simultaneously, pET-28a(+) vector was also digested using the same restriction enzymes. *Nhe*I-*Xho*I digested *Ct*Manf (Fig. 2.3.5, lane 2), *Ct*ManT (Fig. 2.3.5, lane 3) and *Ct*CBM35 (Fig. 2.3.5, lane 4) fragments were visualized on 1.0 % agarose gel. The restriction enzyme digested fragments of *Ct*Manf, *Ct*ManT and *Ct*CBM35 were further used for cloning into pET-28a(+) vector. The *Nhe*I-*Xho*I digested pET-28a(+) depicted. The displayed digested pET-28a(+) (5.369 kb) vector in 1.0 % agarose gel (Fig. 2.3.6, lane 2).

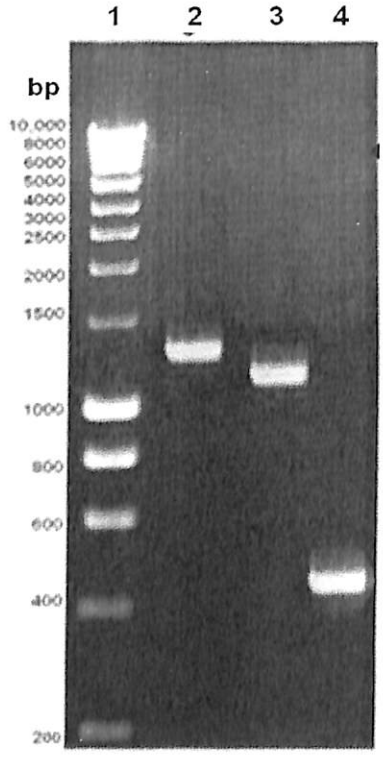

Fig. 2.3.5 Agarose gel (1.0%) showing *Nhe*I-*Xho*I digested PCR fragments of *Ct*Manf and *Ct*ManT and *Ct*CBM35. Lane 1: DNA marker (Hyperladder I, Bioline), Lane 2: digested *Ct*Manf, Lane 3: *Ct*ManT and Lane 4: *Ct*CBM35

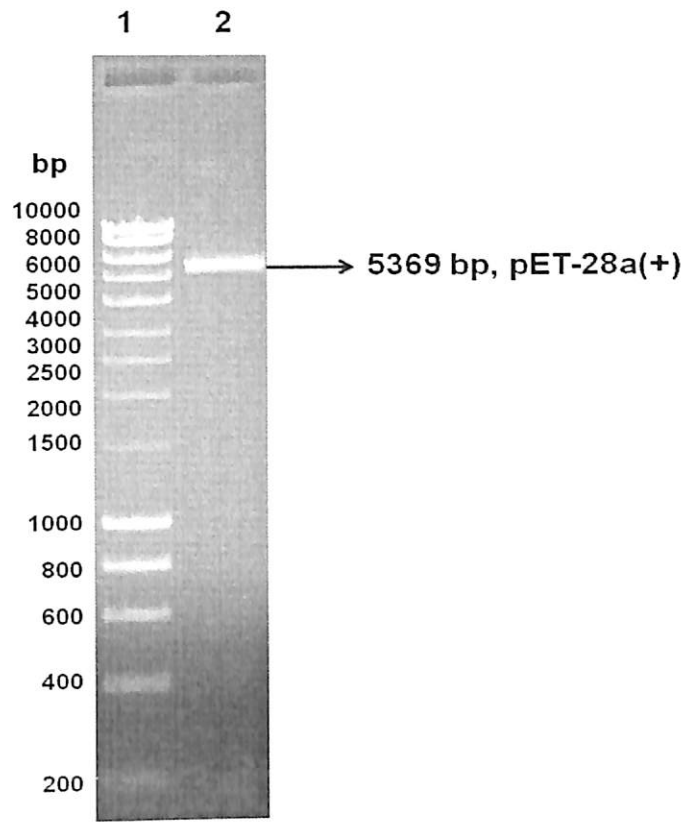

Fig. 2.3.6 Agarose gel (1.0%) showing *Nhe*I-*Xho*I-digested pET-28a(+) vector. Lane 1: DNA marker (Hyper ladder I, Bioline), Lane 2: 5.369 kb, digested pET-28a(+) vector.

2.3.3 Cloning, expression and purification of recombinant proteins *Ct*Manf, *Ct*ManT and *Ct*CBM35

2.3.3.1 Ligation of NheI-XhoI digested fragments to pET-28a(+) expression vector

The ligation of *Ct*Manf, *Ct*ManT and *Ct*CBM35 into the pET-28a(+) vector resulted recombinant plasmids and were confirmed after transformation and digestion with *Nhe*I and *Xho*I restriction enzymes.

2.3.3.2 Transformation of E. coli (DH5α) competent cells with recombinant plasmid DNA

E. coli (DH5α) competent cells were transformed with recombinant plasmid DNA of each derivative *viz.* *Ct*Manf, *Ct*ManT and *Ct*CBM35 as described in Section 2.2.13. The transformed cells were grown on LB agar plates incubated at 37°C for 12-16h. The number of colonies observed on LB agar plates was counted and the transformation efficiency was calculated using the formula described in Section 2.2.13 and the results are displayed in Table 2.3.1.

Table 2.3.1 Transformation efficiency of *E. coli* (DH5α) cells.

Clone	insert DNA (ng)	No. of colonies	Transformation Efficiency (cfu/µg)
Positive Control (pUC18)	1.0	279	2.8×10^5
*Ct*Manf	1.5	175	1.1×10^5
*Ct*ManT	1.9	273	1.4×10^5
*Ct*CBM35	2.0	150	7.5×10^4

2.3.3.3 Isolation of plasmid DNA

The plasmid DNA of each recombinant derivative was isolated from 5.0 ml LB medium supplemented with kanamycin, using the plasmid miniprep kit as described in Section 2.2.14.2. The isolated plasmid DNA for each of the above mentioned recombinant derivatives *viz.* *Ct*Manf, *Ct*ManT and *Ct*CBM35 shown in Fig 2.3.7. The figures displayed recombinant plasmids of *Ct*Manf (Fig. 2.3.7, lane 2), *Ct*CBM35 (Fig. 2.3.7, lane 3) and *Ct*ManT (Fig. 2.3.7, lane 4) as analyzed by 1.0% agarose gel.

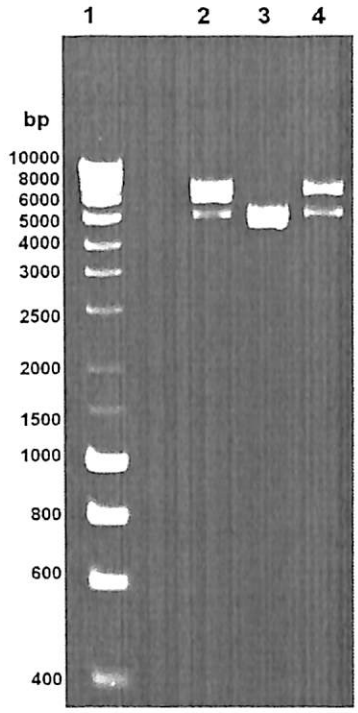

Fig. 2.3.7 Agarose gel (0.8%) showing recombinant plasmids *Ct*Manf, *Ct*CBM35 and *Ct*ManT. Lane 1: DNA marker (Hyperladder I, Bioline), Lane 2: recombinant plasmid of *Ct*Manf, Lane 3: recombinant plasmid of *Ct*CBM35, Lane 4: recombinant plasmid of *Ct*ManT.

2.3.3.4 Screening of recombinant plasmid DNA for identification of positive clones

The positive clones were identified by restriction digestion analysis of the recombinant plasmids as shown Fig. 2.3.8A-C. The confirmation of recombinant plasmid containing *Ct*Manf by *Nhe*I-*Xho*I restriction enzymes digestion is displayed in Fig 2.3.8A, lane 2. The *Nhe*I-*Xho*I digested plasmid DNA of *Ct*Manf showed two distinct bands of the 5.369 kb pET-28a (+) vector and 1.449 kb insert (*Ct*Manf). It was concluded from the result that the clone harbours the desired recombinant plasmid (*Ct*Manf). Similarly, the recombinant plasmid of *Ct*ManT was also digested using *Nhe*I-*Xho*I, which resulted in two fragments (Fig. 2.3.8B, lane 2) detected on 1.0 % agarose gel. The fragments obtained were 5.369 kb pET-28a (+) vector and 1029 bp insert of *Ct*ManT. Similarly, *Nhe*I-*Xho*I digestion of *Ct*CBM35 resulted in

two fragments, one was 5.369 kb pET-28a(+) vector and the others was insert of *Ct*CBM35 (420 bp) (Fig. 2.3.8C, lane 2). The positive clones of *Ct*Manf and *Ct*ManT and *Ct*CBM35 were further confirmed by sequencing from Eurofin India (Bangalore, India) and the results are incorporated in Annexure I.

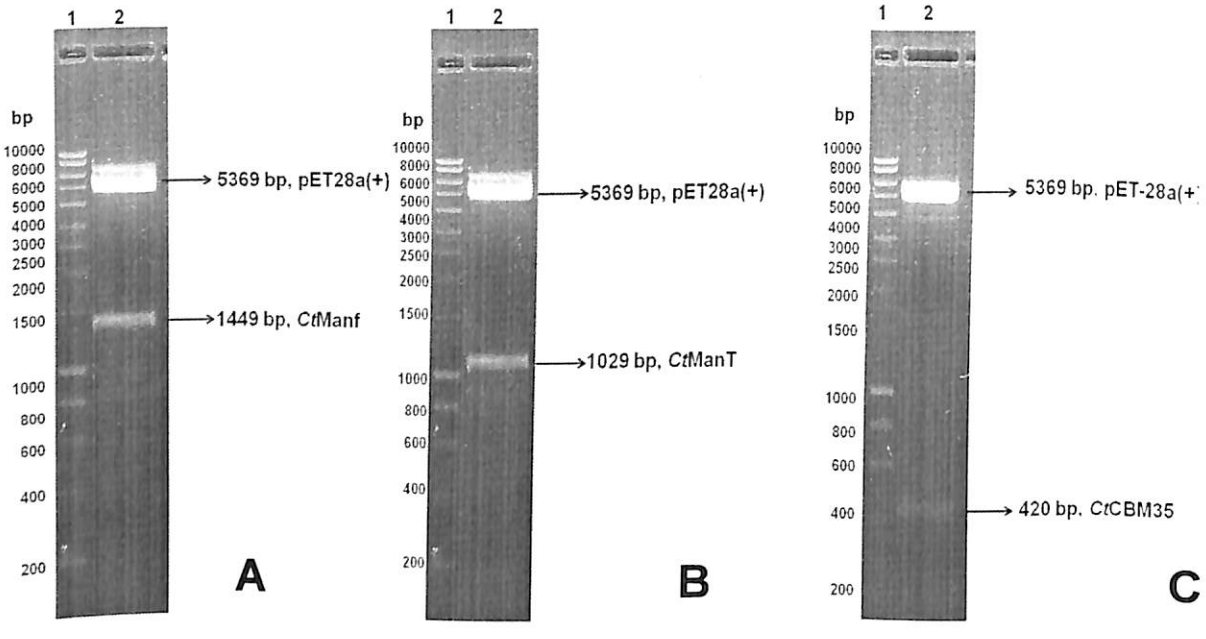

Fig. 2.3.8 Agarose gel (1.0%) showing *Nhe*I-*Xho*I digested recombinant plasmids containing *Ct*Manf and *Ct*ManT and *Ct*CBM35 fragment. (A) Lane 1: Hyper ladder I (Bioline), Lane 2: digested 1.449 kb fragment of *Ct*Manf (insert) and vector (5.369 kb, pET-28a). (B) Lane 1: Hyper ladder I (Bioline), Lane 2: digested 1.029 kb fragment of *Ct*ManT (insert) and vector (5.369 kb, pET-28a). (C) Lane 1: Hyper ladder I (Bioline), Lane 2: digested 420 bp fragment of *Ct*CBM35 (insert) and vector (5.369 kb, pET-28a).

2.3.3.5 Hyper-expression analysis and purification of recombinant proteins

Hyper-expression of recombinant *Ct*Manf, *Ct*ManT and *Ct*CBM35 was analyzed on SDS-PAGE, by loading uninduced as well as the induced cells of recombinant protein on adjacent wells, as depicted in Fig. 2.3.9 to Fig. 2.3.11. The hyper-expression of *Ct*Manf is shown in Fig. 2.3.9, *Ct*ManT in Fig. 2.3.10 and the expression of is displayed in *Ct*CBM35 in Fig. 2.3.11.

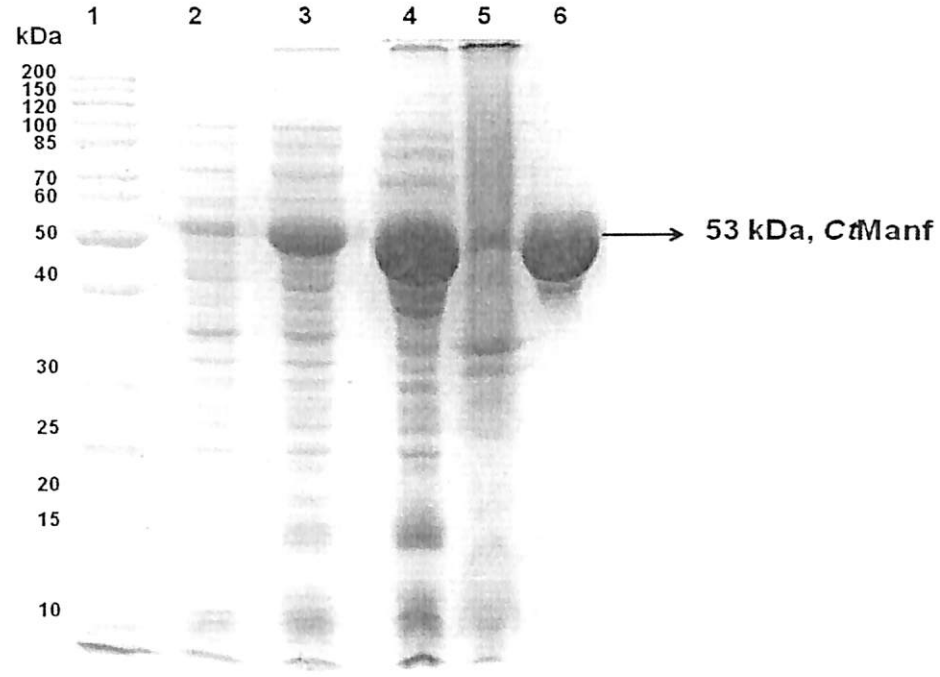

Fig. 2.3.9 SDS-PAGE (13.0%) gel showing expression and purification of recombinant *Ct*Manf in *E. coli* BL-21(DE3) cells. Lane 1: Page Ruler protein marker (Fermentas), Lane 2: Uninduced *Ct*Manf cells, Lane 3: Induced *Ct*Manf cells, Lane 4: Cell free extract (*Ct*Manf), Lane 5: cell pellet of *Ct*Manf after sonication, Lane 6: *Ct*Manf affinity column purified (53 kDa).

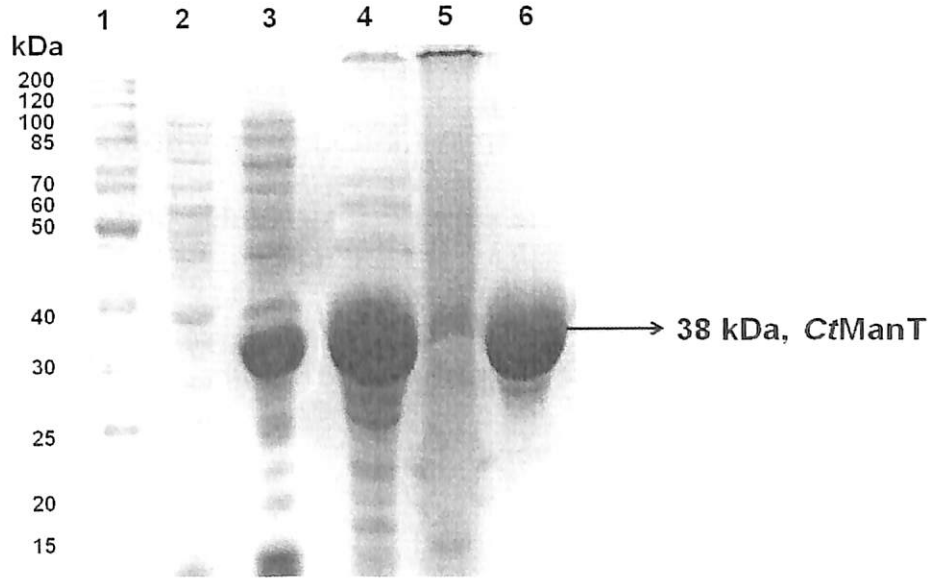

Fig. 2.3.10 SDS-PAGE (13.0%) gel showing expression and purification of recombinant *Ct*ManT in *E. coli* BL-21(DE3) cells. Lane 1: Page Ruler protein marker (Fermentas), Lane 2: Uninduced *Ct*ManT cells, Lane 3: Induced *Ct*ManT cells, Lane 4: Cell free extract (*Ct*ManT), Lane 5: cell pellet of *Ct*ManT after sonication, Lane 6: *Ct*ManT affinity column purified (53 kDa).

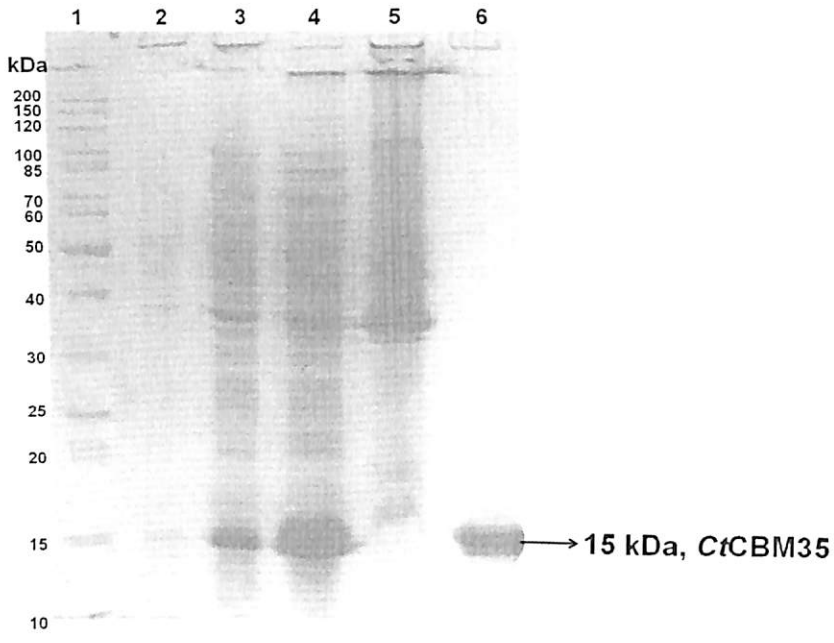

Fig. 2.3.11 SDS-PAGE (13.0%) gel showing expression and purification of recombinant *Ct*CBM35 in *E. coli* BL-21(DE3) cells. Lane 1: Page Ruler protein marker (Fermentas), Lane 2: Uninduced *Ct*CBM35 cells, Lane 3: Induced *Ct*CBM35 cells, Lane 4: Cell free extract (*Ct*CBM35), Lane 5: cell pellet of *Ct*CBM35 after sonication, Lane 6: *Ct*CBM35 affinity column purified (15 kDa).

The hyper-expressed recombinant proteins were purified by immobilized metal ion affinity chromatography as described in Section 2.2.21 and then dialyzed against 50 mM sodium phosphate buffer overnight for the removal of imidazole and NaCl. All the proteins were expressed as soluble proteins, as can be seen in cell free extracts (Fig. 2.3.9, Fig. 2.3.10 and Fig. 2.3.11). The purified *Ct*Manf, *Ct*ManT and *Ct*CBM35 showed homogenous bands of molecular sizes approximately, 53 kDa, 38 kDa and 15 kDa, respectively.

The proteins of all the three recombinant proteins were eluted in 2x1 ml fractions obtained from 100 ml culture. After dialysis the concentration of *Ct*Manf, *Ct*ManT and *Ct*CBM35 were 0.16 mg/ml, 0.15 mg/ml and 1.2 mg/ml, respectively, as determined by Bradford method (Table 2.3.2).

Table 2.3.2 Amount of purified recombinant proteins obtained from 100 ml cultures.

Recombinant derivative	Protein concentration (mg/ml)	Volume of purified protein (ml)	Total amount of purified protein (mg)
*Ct*Manf	0.16±0.10	2.0	0.32±0.2
*Ct*ManT	0.15±0.12	2.0	0.30±0.2
*Ct*CBM35	1.2±0.05	2.0	2.40± 0.1

2.4 Conclusions

The full length *Ct*Manf and its truncated derivatives *Ct*ManT and *Ct*CBM35 sequences were extracted from the genomic library of *Clostridium thermocellum* ATCC 27405 (nucleotide accession: CP000568.1). Molecular architecture revealed an N-terminus non catalytic family 35 carbohydrate binding module (*Ct*CBM35, 420 bp) followed by glycoside hydrolase module (*Ct*ManT, 1029 bp) at the C-terminus. PCR amplified fragments of full length *Ct*Manf, truncated catalytic module *Ct*ManT and *Ct*CBM35 displayed 1449 bp, 1029 bp and 420 bp, respectively. PCR amplified products were digested with *Nhe*I-*Xho*I enzymes and cloned into pET-28a(+) vector. Each Plasmid DNA of the positive clone was transformed using *E. coli* (DH5α) competent cells. Positive clones of *Ct*Manf and its truncated derivatives *Ct*ManT and *Ct*CBM35 were confirmed by restriction digestion analysis of their recombinant plasmid DNAs. *E. coli* BL-21 competent cells were used for transformation of each of the recombinant plasmid DNA for their expression. Over expression of recombinant proteins was achieved by using IPTG as inducer at a final concentration of 1 mM. Hyperexpression of the recombinant proteins were checked and confirmed by SDS-PAGE gel analysis. After confirming the successful expression, recombinant proteins were purified from their respective cell free extracts by immobilized metal ion chromatography (IMAC) using HiTrap chelating columns. Degree of purification obtained after this purification step was higher than 90%, and therefore these proteins were considered as suitable for further biochemical analysis. Recombinant proteins purified by IMAC displayed molecular sizes of 53 kDa (*Ct*Manf), 38 kDa (*Ct*ManT) and 15 kDa (*Ct*CBM35) on SDS-PAGE. The amount of protein obtained from 100 ml of cultures *Ct*Manf, *Ct*ManT and *Ct*CBM35 after IMAC purification were 0.16 mg/ml, 0.15 mg/ml and 1.2 mg/ml, respectively. These purified proteins were used for further biochemical and functional characterization.

References

Bayer, E.A., Shoham, Y. and Lamed, R. (2000) Cellulose-decomposing prokaryotes and their enzyme systems. In (3rd ed.) Dworkin, M., Falkow, S., Rosenberg, E., Schleifer, K.H., and Stackebrandt, E. (ed.), *The Prokaryotes: An Evolving Electronic Resource for the Microbiological Community*. 2, 578-617.

Bolam, D.N., Xie, H., Pell, G., Hogg, D., Galbraith, G., Henrissat, B. and Gilbert, H.J. (2004) X4 modules represent a new family of carbohydrate-binding modules that display novel properties. J. Biol. Chem. 279, 22953-22963.

Boraston, A.B., Bolam, D.N., Gilbert, H.J. and Davies G.J. (2004) Carbohydrate-binding modules: fine-tuning polysaccharide recognition. Biochem. J. 382, 769-781.

Bradford, M. (1976) A Rapid and Sensitive Method for the quantitation of microgram quantities of protein utilizing the principle of protein-dye binding. Anal. Biochem. 72, 248-254.

Carvalho, A.L., Goyal, A., Prates, J.A.M., Bolam, D.N., Gilbert, H.J., Pires, V.M.R., Ferreira, L.M.A., Planas, A., Romão, M.J. and Fontes, C.M.G.A. (2004) The family 11 carbohydrate-binding module of *Clostridium thermocellum* Lic26A-Cel5E accommodates β-1,4 and β-1,3-1,4-mixed linked glucans at a single binding site. J. Biol. Chem. 279, 34785-34793.

Chrambach, A. (1985) *The practice of quantitative gel electrophoresis* (1st ed). Deerfield Beach, FL, VCH, John Wiley & Sons. 9-18, 85-99, 101-104.

Couturier, M.; Roussel, A.; Rosengren, A.; Leone, P.; Stålbrand, H.; Berrin, J. G. (2013) Structural and biochemical analyses of glycoside hydrolase families 5 and 26 beta-(1,4)-mannanases from *Podospora anserina* reveal differences upon manno-oligosaccharides catalysis. J. Biol. Chem. 288(20):14624-14635

Davies, G.J. and Henrissat, B. (2002) Structural enzymology of carbohydrate-active enzymes: implications for the post-genomic era. Biochem. Soc. Trans. 30, 291-297.

Deutscher, J. (2008) The mechanisms of carbon catabolite repression in bacteria. Curr. Opinion Microbiol. 11, 87–93.

Dumitriu, S. (2010) In *Polysaccharides: Structural diversity and functional versatility.* 2nd edition, CRC Press, USA, 1020 pp.

Engler, M.J. and Richardson, D.C. (1982) DNA ligases. In P.D. Boyer (ed.), *The Enzymes*. Academic Press, San Diego. 15, 3-30.

Gilbert H. J., Knox J. P. and Boraston A. B. (2013) Advances in understanding the molecular basis of plant cell wall polysaccharide recognition by carbohydrate binding modules. Curr. Opin. Struct. Biol. 23, 669-677.

Hanahan D. (1983) Studies on transformation of *Escherichia coli* with plasmids. J. Mol. Biol. 166, 557-580.

Henrissat, B. (1991) A classification of glycosyl hydrolases based on amino acid sequence similarities. Biochem. J. 280, 309-316.

Henshaw, J.L., Bolam, D.N., Pires, V.M., Czjzek, M., Henrissat, B., Ferreira, L.M., Fontes, C.M.G.A. and Gilbert, H.J. (2004) The family 6 carbohydrate binding module *Cm*CBM6-2 contains two ligand-binding sites with distinct specificities. J. Biol. Chem. 279, 21552-21559.

Henshaw, J., Horne-Bitschy, A., van Bueren, A.L., Money, V.A., Bolam, D.N., Czjzek, M., Ekborg, N.A., Weiner, R.M., Hutcheson, S.W., Davies, G.J., Boraston, A.B. and Gilbert, H.J. (2006) Family 6 carbohydrate binding modules in β-agarases display exquisite selectivity for the non-reducing termini of agarose chains. J. Biol. Chem. 281, 17099-17107.

Hirst, E. L. and Jones, J. K. N. (1948) The galactomannan of carob-seed gum (gum gatto). J. Chem. Soc. 1278-1282.

Katsuraya, K., Okuyamab, K., Hatanakab, K., Oshimab, R., Satoc, T. and Matsuzakic, K. (2003) Constitution of konjac glucomannan: chemical analysis and ^{13}C NMR spectroscopy. Carbohydr. Polym. 53, 183-189.

Laemmli, U.K. (1970) Cleavage of structural proteins during the assembly of the head of bacteriophage T4. Nature, 227, 680-685.

Meyer, T.S., and Lambert, B, L. (1965) Use of coomassie brilliant blue R250 for the electrophoresis of microgram quantities of parotid saliva proteins on acrylamide-gel strips. Biochim. Biophys. Acta, 107, 144-145.

Neuhoff, V., Stamm, R. and Hansjorg, E. (1985) Clear background and highly sensitive protein staining with Coomassie Blue dyes in polyacrylamide gels: a systematic analysis. Electrophoresis, 6, 427-448.

Park, J.M., Vinuselvi, P. and Lee, S.K. (2012) The mechanism of sugar-mediated catabolite repression of the propionate catabolic genes in *Escherichia coli*. Gene, 504, 116-121.

Sambrook, J., Fritsch, E.F. and Maniatis, T. (1989) In (2nd ed.) *Molecular Cloning: A Laboratory Manual*, Vol. 1. Plainview, Cold Spring Harbor Laboratory Press, Woodbury, New York.

Sambrook, J. and Russel, D.W (2001) In (3rd ed.) *Molecular Cloning: A Laboratory Manual*, Vol. 1. Cold Spring Harbor Laboratory Press, Woodbury, New York.

Shoseyov, O., Shani, Z. and Levy I. (2006) Carbohydrate binding modules: biochemical properties and novel applications. Microbiol. Mol. Biol. Rev. 70, 283-295.

Studier, F.W., Rosenberg, A.H., Dunn, J.J. and Dubendorff, JW. (1990) Use of T7 RNA polymerase to direct expression of cloned genes. Methods Enzymol. 185, 60-89.

Studier, F.W. and Moffatt, B.A. (1986) Use of bacteriophage T7 RNA polymerase to direct selective high-level expression of cloned genes. J. Mol. Biol. 189, 113-130.

Sunna, A. (2010) Modular organisation and functional analysis of dissected modular β-mannanase CsMan26 from *Caldicellulosiruptor* Rt8B.4. Appl. Microbiol. Biotechnol. 86(1), 189-200.

Taylor, E., Goyal, A., Guerreiro, C.I.P.D., Prates, J.A.M., Money, A.V., Ferry, N., Morland, C., Planas, A., Macdonald, J.A., Stick, R.V., Gilbert, H.J., Fontes, C.M.G.A. and Davies GJ. (2005) How family 26 glycoside hydrolases orchestrate catalysis on different polysaccharides? Structure and activity of a *Clostridium thermocellum* lichenase, CtLic26A. J. Biol. Chem. 280, 32761-32767.

van Bueren, A.L., Morland, C., Gilbert, H.J. and Boraston, A.B. (2005) Family 6 carbohydrate binding modules recognize the non-reducing end of β-1,3-linked glcans by presenting a unique ligand binding surface. J. Biol. Chem. 280, 530-537.

Valenzuela, S.V., Diaz, P. and Pastor, F.I. (2012) Modular glucuronoxylan-specific xylanase with a family CBM35 carbohydrate-binding module. Appl. Environ. Microbiol. 78(11), 3923-31.

Zhang, Y., Ju, J., Peng, H., Gao, F., Zhou, C., Zeng, Y., Xue, Y., Li, Y., Henrissat, B., Gao, G. F. and Ma, Y. (2008) Biochemical and structural characterization of the intracellular mannanase AaManA of *Alicyclobacillus acidocaldarius* reveals a novel glycoside hydrolase family belonging to clan GH-A. J. Biol. Chem. 14, 31551-31558.

Chapter 3

Biochemical, functional and structure characterization of catalytic modules *Ct*Manf and *Ct*ManT from *Clostridium thermocellum* ATCC 27405

3.1 Introduction

The benefit of employing novel enzymes for specific industrial processes is well recognized with the discovery of β-mannanases. β-Mannanases (EC 3.2.1.78) hydrolyze mannan based hemicelluloses and liberate short β-(1→4)-manno-oligosaccharides, which can be further hydrolyzed to mannose by β-mannosidases (EC 3.2.1.25). There are currently around 50 gene sequences of β-mannanase in families 5 and 26 glycoside hydrolases from various microbial origins. The family 26 Glycoside Hydrolase (GH26) enzymes have narrow substrate specificity hydrolyzing (1→4)-β-D-linkages in mannans, galacto-mannans, glucomannans and galactoglucomannans but do not show activity against β-glycan chain of soluble cellulose derivatives (Halstead *et al.*, 1999). Several studies exhibited the presence of distinct types of mannanases (GH5A, GH5B, GH5C, GH26A, GH26B, GH26C) expressed on the cell surface of *Cellvibrio japonicas* having different substrate specificity (Cartmell *et al.*, 2008). There are distinct differences in the topology of substrate binding cleft and substrate specificity among three mannnases *viz.* Man26A,

Man26B and Man26C within GH26 family (Bolam *et al.*, 1996). Man26A displays a typical endo-β-(1→4)-bond cleavage activity against small manno-oligosaccharides, hydrolyzing mannotriose approximately, 10000 times more efficiently than Man26B (Cartmell *et al.*, 2008). Man26B of *Cellvibrio japonicas* displays endo-mannanase activity and is linked to the cell membrane via a 70 residue linker sequence (Cartmell *et al.*, 2008). Therefore, this linker sequence will facilitate Man26B to get enough space for accommodating the natural substrates galactomannan and glucomannan. Man26B rapidly generates large amounts of mannose even in the early stages of hydrolysis of galactomannan or manno-oligosaccharide.

Clostridium thermocellum expresses a large number of hemicellulases in its multienzyme complex targeting various hemicellulosic components such as mannans and xylans removes the hemicellulosic polysaccharides exposing the cellulose microfibrils uses it as primary carbon and energy source and releases soluble sugars (Fontes and Gilbert, 2010). The carbohydrate binding modules (CBMs) are the non-catalytic modules known to help or bring the catalytic modules in close proximity to its substrates and also some CBMs are known to stabilize the enzyme (catalytic module) structure and increase its thermostability (Boraston *et al.*, 2004; Dvortsov *et al.*, 2009). The majority of *C. thermocellum* cellulosomal enzymes display rather complex multi-modular architectures containing CBMs either at N- or C- terminal domain. These CBMs potentiate the interaction of the multifunctional complex with the diversity of polysaccharides in the plant cell wall by directing the appended catalytic domains to their target substrates (Fierobe *et al.*, 2005). A family 35 carbohydrate binding module (CBM35) often appended with mannanase that binds to the galactose-decorated mannanas and facilitates their efficient hydrolysis (Couturier

et al., 2013). There are few reports of Man26B functions are explored earlier from *Paenibacillus* sp BME14 (Xiaoyu et al., 2010), *Cellvibrio japonicas* (Hogg *et al.*, 2003), *Clostridium thermocellum* strain F1 (Kurokawa *et al.*, 2001), *Bacillus licheniformis* DSM 13 (Songsiriritthigul *et al.*, 2010).

The biochemical characterization of full length *Ct*Manf and truncated *Ct*ManT and the structural characterization of a family 26 glycoside hydrolase (GH26) mannanase B (*Ct*ManT) from *Clostridium thermocellum* ATCC 27405 were studied. In addition to that, the enzyme is studied structurally by homology modelling, docking study for active site prediction and subsite mapping.

3.2 Materials and Methods

3.2.1 Substrates and reagents

Carob galactomannan, konjac glucomannan, locust bean galactomannan, rye arabinoxylan, wheat arabinoxylan (soluble and insoluble), xyloglucan, arabinogalactan, sugar beet arabinan, pectic galactan, lupin galactan, pustulan, curdlan, rhamnogalactouronan, mannobiose and mannotriose were purchased from Megazyme International (Ireland). Oat spelt xylan, birchwood xylan, beechwood xylan; barley β-D-glucan, carboxy methylcellulose (CMC), carboxy ethylcellulose (CEC) and synthetic *p*NP-glycosides like *p*NP-β-D-mannopyranoside and *p*NP- α-D-mannopyranoside, were purchased from Sigma-Aldrich Co. LLC., USA. D-mannose, sodium hydroxide (NaOH) solution (50%, w/v) and Bradford's reagent were procured from Sigma-Aldrich Co. LLC., USA. Coomassie brilliant blue G-250 was purchased from Amresco LLC, USA. Disodium 2-[2-carboxylatomethyl(carboxymethyl)amino]ethyl (carboxymethyl)amino] acetate (disodium EDTA), sodium carbonate, sodium potassium tartarate, sodium bicarbonate, sodium sulphate, sodium phosphate (monobasic), sodium phosphate (dibasic) and salts of metal ions *viz.* Ca^{2+}, Mg^{2+}, Ni^{2+}, Zn^{2+}, Mn^{2+}, Cu^{2+}, Co^{2+} and Al^{3+} were procured from HiMedia Laboratories Pvt. Ltd., India. Sodium arsenate, ammonium molybdate, sulphuric acid, hydrochloric acid, acetone, acetonitrile, acetic acid were purchased from Merck Limited, India. The TLC plate was purchased from Merck KGaA, Darmstadt, Germany.

3.2.2 Enzyme activity assay

Initially, the enzyme assays of *Ct*Manf and *Ct*ManT were carried out in 100 µl of a reaction mixture in 50 mM sodium phosphate buffer pH 7.0 containing 1% (w/v) substrate (described in Section 3.2.3) using 10 µl of purified enzyme (*Ct*Manf 0.16 mg/ml or *Ct*ManT 0.15 mg/ml), and incubating at 50°C for 15 min. However, after the optimization of pH the assays for *Ct*Manf and *Ct*ManT were carried out in 50 mM sodium phosphate buffer pH 6.9 and pH 6.5, respectively. After temperature optimization the assays of *Ct*Manf and *Ct*ManT were carried out at 60°C and 50°C, respectively, for 15 min. The enzyme activity was measured by estimating the liberated reducing sugar by Nelson-Somogyi method as described in Section 3.2.2.4. To 100 µl of reaction mixture containing the reducing sugar, 100 µl of reagent D was added (Section 3.2.2.1). The solution was mixed and heated for 20 min in the boiling water bath. After 20 min of boiling, the solution was ice cooled and 100 µl of reagent C (Section 3.2.2.1) was added. The colour developed rapidly and completed after the evolution of carbon dioxide stopped. The mixture was diluted by adding water to make up the volume to 1 ml and the absorbance at 500 nm (A_{500}) was measured by a UV-Visible spectrophotometer (Varian, Cary 100 Bio). D-Mannose in the range of 10-500 µg/ml was used for generating the standard plot. as described in Section 3.2.2.2.

3.2.2.1 Preparation of reagents for reducing sugar estimation

Reagent A

Sodium carbonate anhydrous	6.25 g
Sodium potassium tatarate	6.25 g
Sodium bicarbonate	5.0 g
Sodium sulphate anhydrous	50.0 g

The above mentioned components were dissolved in 100 ml of deionized water and the final volume was adjusted to 250 ml. The solution was filtered (Whatman No. 1) and stored at 30°C.

Reagent B

Reagent B was prepared by dissolving 15 g of copper sulfate ($CuSO_4$) in 50 ml deionized water and one or two drops of concentrated sulphuric acid was added to it. The final volume was made up to 100 ml with deionized water and the solution was filtered (Whatman No. 1) and stored at 30°C.

Reagent C

Reagent C was prepared in two steps under dark. First, 2.5 g of ammonium molybdate was dissolved in 45 ml of deionized water in 100 ml beaker and 2.1 ml of concentrated sulphuric acid was added to it. In another beaker 0.3 g of sodium arsenate was dissolved in 2.5 ml of deionized water. Now, this solution was added to ammonium molybdate solution and the contents were mixed (total volume was around 50 ml). The solution was filtered (Whatman No. 1) under dark conditions and stored at 37°C. The solution was used after 24h incubation.

Reagent D

Reagent D was prepared by mixing reagent A and reagent B in the ratio 25:1. Reagent D was freshly prepared for the assay.

3.2.2.2 Generation of standard plot of D-mannose

The standard plot using of D-mannose was prepared by varying the concentration from 10-500 µg/ml. 100 µl reaction mixture contained 50 mM sodium phosphate buffer pH 7.0 and in a 1.5 ml microcentrifuge tube D-mannose was incubated at 50°C for 15 min and then 100 µl of solution D (Section 3.2.2.1) was added to it. The reaction mixture was then heated in boiling water bath for 20 min and cooled. 100 µl of solution C (Section 3.2.2.1) was added and the contents were mixed. Then 700 µl of deionized water was added to make the final volume to 1 ml. The absorbance at 500 nm (A_{500}) was measured using UV-Visible spectrophotometer (Varian, Cary 100 Bio) against a buffer blank. A standard plot of A_{500} versus D-mannose concentration (µg/ml) was generated and 1 A_{500} equivalent of D-mannose (µg/ml) was calculated. 1 A_{500} equivalent of D-mannose (µg/ml) was converted into mg/ml for calculation of enzyme activity.

*3.2.2.3 Calculation of enzyme activity of Ct*Manf *and Ct*ManT

The activity of the enzyme was expressed as U/ml and the specific activity as U/mg of protein. One unit (U) of enzyme activity is defined as the amount of enzyme that liberates 1 µmole of reducing sugar per min. The enzyme activities of *Ct*Manf and *Ct*ManT were calculated as described below,

$$\text{Enzyme activity (U/ml)} = \frac{\Delta A_{500} \times C \times V}{180 \times t \times v} = (\mu \text{ mole/min/ml})$$

where,

ΔA_{500} = change in absorbance of the sample at 500 nm

C = 1 OD equivalent L-arabinose concentration from standard plot

V = volume of the reaction mixture (ml)

t = time of reaction (min)

180 = molecular weight of D-mannose

v = volume of the enzyme taken in assay (ml) for reducing sugar estimation.

3.2.3 Substrate specificity of *Ct*Manf and *Ct*ManT

The enzyme activity of *Ct*Manf and *Ct*ManT was determined by using natural substrates such as carob galactomannan, locust bean galactomannan, konjac glucomannan, guar galactomannan, ivory nut mannan, β-(1→4)-mannan, barley β-glucan, lichenan, carboxymethyl cellulose, hydroxyethyl cellulose, avicel, rye arabinoxylan, glucuronoxylan, arabinogalactan and polygalactouronic acid (PGA) at 1% (w/v) in 50 mM sodium phosphate buffer (pH 7.0) and by measuring the reducing sugar released, as described in the Section 3.2.2. The β-(1→4)-mannan (an insoluble polysaccharide prepared from carob galactomannan pretreated with *Aspergillus niger* mannanase and subsequently de branched to a high extent containing mannose (97%) and galactose (3%) according to manufacturer Megazyme International, Ireland). In both cases 100 µl reaction mixture contained 1% (w/v) substrate, 10 µl of enzyme (*Ct*Manf, 0.16 mg/ml and *Ct*ManT, 0.15 mg/ml). 100 µL reaction mixtures were incubated for both the enzymes at 50°C for 10 min separately with polysaccharides. In

the case of avicel the reaction mixture was incubated for 60 min under shaking condition. The assays were carried out in triplicate.

3.2.4 Determination of optimum pH and temperature of *Ct*Manf and *Ct*ManT

The pH profiles of *Ct*Manf and *Ct*ManT were determined by performing enzyme assay in 50 mM sodium phosphate buffer with pH varying between 4.0 and 8.0. The reaction mixtures (100 µl) containing 1% (w/v) carob galactomannan were incubated at 50°C for 15 min. A wide range of pH was chosen ranging from pH 4.0 to pH 8.0 as β-mannanse display optimum range within this range Huang *et al.*, (2012). Sodium phosphate buffer was prepared as per the protocols described by Gomori (2010). The optimum temperature for enzyme activity of *Ct*Manf and *Ct*ManT was determined by incubating the reaction mixture at varying temperatures from 10°C to 100°C, using 50 mM sodium phosphate buffer, pH 6.9 and 6.5, respectively. The enzyme activity was calculated by estimating the liberated sugar as described in Section 3.2.2.

3.2.5 pH stability of *Ct*Manf and *Ct*ManT

100 µl of *Ct*Manf (0.16 mg/ml) or *Ct*ManT (0.15 mg/ml) was taken and lyophilized using a lyophillizer (Christ Griertrocknumgsanlagen GmbH, ALPHA 1-4). The protein was then dissolved in 50 µl of 50 mM sodium phosphate buffer in 1.5 ml microcentrifuge tube and incubated at different pH varying from 4 to 8 for 1h. The lyophilized protein was dissolved in same volume of buffer in order to keep the protein concentration same in all tubes. The enzyme solutions were then centrifuged at 10,000***g*** at 4°C for 5 min. 10 µl of supernatant was taken for determination of the

enzyme activity, which was calculated as described in Section 3.2.2. The assays were carried out in triplicate by taking total 10 µl of enzyme in 100 µl reaction mixture.

3.2.6 Thermal stability of *Ct*Manf and *Ct*ManT

100 µl each of *Ct*Manf (0.16 mg/ml) in 50 mM sodium phosphate buffer pH 6.9 and *Ct*ManT (0.15 mg/ml) in 50 mM sodium acetate buffer pH 6.5 were incubated at various temperatures in the range 10-100°C for 30 min. The enzymes were then centrifuged at 10,000*g* at 4°C for 5 min. 10 µl of supernatant was taken for estimation of the enzyme activity that was calculated as per description given in Section 3.2.2. The assays were carried out in triplicate by taking total 10 µl of enzyme in 100 µl reaction mixture.

3.2.7 Substrate specificity of *Ct*Manf and *Ct*ManT against natural and synthetic polysaccharides

The enzyme activity of *Ct*Manf and *Ct*ManT was determined by using 50 mM sodium phosphate buffer of pH 6.9 and pH 6.5, respectively. The 100 µl reaction mixture contained 1.0% (w/v) substrate, 10 µl of enzyme (*Ct*Manf, 0.16 mg/ml or *Ct*ManT, 0.15 mg/ml). The reaction mixtures of *Ct*Manf and *Ct*ManT were incubated at 60 °C and 50°C, respectively, for 15 min. The assays were performed in triplicate. The concentration of reducing sugar was estimated using a standard curve of mannose (Section 3.2.2.2) as both *Ct*Manf and *Ct*ManT predominantly showed endo-β-D-mannanase activity. 100 µl of reaction mixture was taken for estimation of enzyme activity which was calculated as per the description given in Section 3.2.2. After analysis of substrate specificity the enzyme assays for *Ct*Manf and *Ct*ManT were performed using 50 mM sodium phosphate buffer at their optimum pH and temperature to analyze the kinetic parameters *viz.* K_m, V_{max}, k_{cat} and k_{cat}/K_m. One unit

of enzyme activity was determined as the release of 1 µmole of mannose per minute. The kinetic parameters of *Ct*Manf and *Ct*ManT were determined using various soluble substrates such carob galactomannan, locust bean galactomannan, konjac glucomannan, guar galactomannan, insoluble ivoru nut mannan and mannan under above mentioned reaction conditions.

3.2.8 Substrate specificity of *Ct*Manf and *Ct*ManT against synthetic *p*-nitrophenyl-glycosides (*p*NP-glycosides)

The assays of *Ct*Manf and *Ct*ManT with synthetic substrates *p*-nitrophenyl glycoside (*p*NP-glycosides) *viz.*, *p*-nitrophenyl-β-D-mannopyranoside and *p*-nitrophenyl-α-D-mannopyranoside were carried out by estimating the release of 4-nitrophenol (*p*NP) at 405 nm using a UV-Visible spectrophotometer (Varian, Cary 100 Bio). 2 mM stock solutions were prepared by taking 5.42 mg of *p*-nitrophenyl-β-D-mannopyranoside and *p*-nitrophenyl-α-D-mannopyranoside and by first dissolving in 50-75 µl of dimethyl sulphoxide (DMSO) and then making up the final volume to 10 ml with 50 mM sodium phosphate buffer (pH 6.0) for both *Ct*Manf and *Ct*ManT. The solutions were kept on ice.

1.0 ml reaction mixture containing *p*-nitrophenyl-β-D-mannopyranoside and *p*-nitrophenyl-α-D-mannopyranoside in 50 mM sodium phosphate buffer (pH 6.0), 20 µl of enzyme (*Ct*Manf 0.16 mg/ml or *Ct*ManT 0.15 mg/ml) was incubated at 50°C for 15 min in a peltier temperature controller (Varian, Cary 100 Bio). The kinetic parameters of *Ct*Manf and *Ct*ManT with *p*-nitrophenyl-β-D-mannopyranoside and *p*-nitrophenyl-α-D-mannopyranoside were determined by varying their concentrations from 20 to 500 µM. The reaction was stopped by adding 0.5 M sodium carbonate to make the reaction mixture highly alkaline (~pH 11.0). The assays were performed in triplicate.

The released *p*NP was quantified by using the molar extinction coefficient of 24150 M^{-1} cm^{-1} as reported by Cartmell *et al.* (2011).

3.2.9 Zymogram study and activity staining of *Ct*Manf and *Ct*ManT

Zymogram study of recombinant *Ct*Manf and *Ct*ManT was performed by using 0.5% (w/v) carob galactomannan as substrate incorporated in 12% (w/v) SDS-PAGE. 10 µg of each of purified *Ct*Manf and *Ct*ManT was mixed with 1x sample buffer (62.5 mM Tris-Cl pH 6.8, 20%, v/v glycerol, 2%, w/v SDS, 0.005% w/v bromophenol blue) (Laemmli, 1970), without β-mercaptoethanol (Aboul-Enein *et al.*, 2010) were loaded on the gel. The non denaturing SDS-PAGE was carried out using gel apparatus (Biorad, Mini Protean III cell, Germany) at a constant 20 mA. After the completion of electrophoresis, the gels were incubated in 2.5% (v/v) Triton-X100 at 25°C for 1 h followed by 1 h incubation in 50 mM sodium phosphate buffer, pH 7.0. Then the gels were incubated in preheated 50 mM sodium phosphate buffer (pH 6.5) at 55°C for 30 min and stained with 0.1% (w/v) congo red for 45 min as described by Aboul-Enein *et al.*, (2010). After congo red staining the gels were counter stained with 1N HCl as described elsewhere (Ruijssennars *et al.*, 2001).

3.2.10 Effect of metal ions, chaotropic agents and detergent on enzyme activity of *Ct*Manf and *Ct*ManT

The effects of different metal cations, chaotropic agents and detergent on the activity of *Ct*Manf and *Ct*ManT were determined. Enzyme activity of both *Ct*Manf and *Ct*ManT was determined in the presence of various metal salts such as Ni^{2+} ($NiSO_4.6H_2O$), Zn^{2+} ($ZnSO_4.7H_2O$), Cu^{2+} ($CuSO_4.5H_2O$), Co^{2+} ($CoCl_2.6H_2O$), Mn^{2+} ($MnCl_2.4H_2O$), Al^{3+} ($AlCl_3.6H_2O$) or Ca^{2+} ($CaCl_2.2H_2O$), chelating agent such as disodium EDTA, EGTA and chaotropic agents, urea or guanidine hydrochloride and

detergent such as SDS. The assays of *Ct*Manf and *Ct*ManT were performed at 60°C and 50°C, respectively, using 50 mM sodium phosphate buffer, of pH 6.9 and pH 6.5, respectively. 100 µl reaction mixture containing carob galactomannan 1% (w/v) and metal salt at concentrations (up to 80 mM) or SDS (up to 20 mM) or EDTA (10 mM) or urea (4M) were incubated for 10 min and a control sample in absence of the additive was also run. All these assays were performed in triplicates. Both the enzymes were incubated with EDTA and urea for 1 h before measuring the residual activity. The enzyme activity was determined as per the description given in Section 3.2.2.

3.2.11 Production of *Ct*Manf and *Ct*ManT in different media

Media screening was performed in order to obtain higher production of recombinant *Ct*Manf and *Ct*ManT. Four different medium viz. Luria Bertani (LB), 5xLB, Terrific Broth (TB) and Tryptone Yeast extract (TY) medium were prepared as previously described by Tripathi *et al.*, (2009). The description of the above mentioned media are given in the Table 3.2.1 Initially, the seed culture was prepared by inoculating respective *E. coli* BL21 cells harboring recombinant plasmids *Ct*Manf and *Ct*ManT in 50 mL LB medium supplemented with 50 µg/ml kanamycin and incubated at 37°C and 180 rpm for overnight. 250 ml culture flask of each of four media containing 100 ml medium supplemented with 50 µg/ml kanamycin were inoculated with 1 mL seed culture. The cells were grown at 37°C, 180 rpm till mid exponential phase ($A_{600nm} \approx 0.6$) followed by induction with 1.0 mM isopropyl-1-thio-β-D-galactopyranoside (IPTG) for hyper-expression of recombinant proteins at 24°C with 200 rpm for 24 h. Dry cell weight of bacterial cell was measured as described by Black (1996). The 100 mL broth was centrifuged at 9,000 *g* for 15 min and the

supernatant was discarded. The resulting pellet was washed with distilled water 3 times followed by centrifugation at 9,000*g* for 15 min after each wash. The cell pellet was dried at 60°C for 16 h and the dry cell weight was measured (Black, 1996). The cells were harvested as described in Chapter 2, Section 2.2.20. The recombinant proteins *Ct*Manf and *Ct*ManT were purified as mentioned earlier in Chapter 2, Section 2.2.21.

Table 3.2.1 Preparation of 100 ml LB, 5xLB, TB and TY medium for production of *Ct*Manf and *Ct*ManT.

Medium	Components	Final concentration (%, w/v)
LB	Tryptone	1.0
	Yeast Extract	0.5
	NaCl	1.0
5xLB	Tryptone	5.0
	Yeast Extract	2.5
	NaCl	2.5
	Glycerol	1.0
TB	Pancreatic digest of casein	1.2
	Yeast extract	2.4
	Di-potassium phosphate	0.94
	Mono-potassium phosphate	0.22
	Glycerol	0.4
TY	Tryptone	2.68
	Yeast extract	2.14
	Di-ammonium hydrogen phosphate	0.16
	Mono-potassium phosphate	0.54
	Magnesium sulphate	0.12
	NaCl	0.85
	Glycerol	0.1

3.2.12 Protein-melting study of *Ct*Manf and *Ct*ManT

The protein melting curves were generated by subjecting *Ct*Manf and *Ct*ManT to various temperatures and measuring the change in the absorbance at 280 nm by a UV-Visible spectrophotometer (Varian, Cary 100-Bio) following the method of Dvortsov *et al*,.(2009). The purified *Ct*Manf and *Ct*ManT at protein concentration of

0.3 mg/ml in 50 mM MES [2-(*N*-morpholino) ethanesulfonic acid] buffer, pH 7.0 were used. The absorbance at 280 nm was measured at different temperatures varying from 40 to 115°C using a peltier temperature controller. The protein solutions (1 ml, 0.3 mg/ml) of *Ct*Manf and *Ct*ManT were kept at the particular temperature for 10 min to attain the equilibrium. Similar experiment was carried out with the addition of 10 mM $CaCl_2$ in the 1 ml enzyme (0.3 mg/ml) solution and the temperature was then varied. The experiment was repeated with the addition of $CaCl_2$ and EDTA to 1 ml enzyme solution (0.3 mg /ml) containing equimolar concentrations of 10 mM, and finally the change in absorbance at 280 nm was measured. A curve of relative derivative absorption coefficient (first derivative coefficient) versus temperature was plotted as described earlier by Dvortsov *et al.*, (2009).

3.2.13 Structure and substrate binding analysis of *Ct*ManT by *in silico* prediction

3.2.13.1 Retrieval of protein sequence and phylogenetic analysis of CtManT

The full length derivative protein sequence of *Ct*ManT (*Ct*Manf) was retrieved from the NCBI protein sequence database (accession number ABN51273.1, Uniprot ID: A3DJS9) (http://www.ncbi.nlm.nih.gov/protein). The domain boundary of modular full length protein was assigned by analyzing the result of PSI-Blast (http://blast.ncbi.nlm.nih.gov/) and InterProScan (http://www.ebi.ac.uk/interpro/). The protein sequence of *Ct*ManT was analyzed for the type of enzyme synthesized using multiple sequence alignment and by generating phylogenetic tree. Multiple sequence alignment (MSA) is used to assess sequence conservation of protein domains, tertiary and secondary structures, and even individual amino acids or nucleotides (Thompson *et al.*, (1994). To draw the phylogenetic tree, first multiple sequence alignment was

performed using the mannanase (Man26A and Man26B) sequences of glycoside hydrolase family 26 (GH26) from *Paenibacillus* sp BME14, *Cellvibrio japonicas*, *Clostridium thermocellum* strain F1, *Bacillus licheniformis* DSM13, *Cellulomonas fimi*, *Rhodothermus marinus*, *Bacillus* sp JAMB750 and *Paenibacillus polymyxa* GS01. The protein sequences of the above mentioned representative members of GH26 mannanase saved in FASTA format in a text file and uploaded in CLUSTALX2 (www.clustal.org/clustal2/). The generated alignment file (.aln) from CLUSTALX2 was fed in MEGA 5.1 tool (http://www.megasoftware.net/mega.php) to generate the phylogenetic tree. The alignment file was also used to generate the multiple sequence alignment (MSA) in ESpript (http://espript.ibcp.fr/ESPript/ESPript/). The phylogenetic analysis of above proteins will reveal information about the common ancestors' they have evolved from. The input set of query sequences were assumed to have an evolutionary relationship by which they share a lineage and are descended from a common ancestor.

3.2.13.2 Homology modeling, model refinement and quality assessment of modelled CtManT

A three dimensional model structure was deduced using Modeller 9v8 by homology modeling based on closest structural homologues from *Podospora anserine* (PDB ID: 3ZM8), *Cellvibrio japonicas* (PDB ID: 2VX4) and *Cellulomanas fimi* (PDB ID: 2BVT) with r.m.s.d. of 1.2, 2.3 and 2.6 Å, respectively, over the 300 amino acids of C^{α} main chain. Modeller 9v8 is an *in silico* tool that derives the restraints from the known related structures and their alignment with the target sequence, therefore to find a closest structural homologs templates to modeled the protein was achieved by using 'BLASTp' program against Protein Data Bank (PDB) database

(http://www.ncbi.nlm.nih.gov/blast/Blast.cgi). An alignment file was prepared for having multiple templates along with the query sequence used as an input in modeller. Initial twenty independent models were generated and ranked by molecular probable density functions score (MOLPDF). The loop regions of top model were again refined selectively by using the loopmodel class of moduler as described earlier by Fiser *et al.*, (2000). After each cycle of loop refinement, discrete optimized protein energy (DOPE) score was generated and the best model having reasonable DOPE and MOLPDF scores was chosen for further refinement. Energy minimization of modelled *Ct*ManT was performed in YASARA energy minimization server (www.YASARA.org/minimizationserver), where new and partly knowledge-based all atom force field derived from Amber was used to run the molecular dynamics simulations of protein molecules in explicit solvent as described earlier by Henrissat *et al.*, (1996). The quality of final modeled *Ct*ManT was validated using various parameters available at NIH structural analysis and validation server (http://nihserver.mbi.ucla.edu/SAVES/) as well as PROSA web server (Yan *et al.*, 2008).

3.2.13.3 Multiple sequence alignment and active site prediction of CtManT

The sequence of closest homolog proteins of known structure were retrieved from PDB (http://www.rcsb.org/pdb/), saved in .pdb file and FASTA format. Sequence analysis of *Ct*ManT was performed by multiple sequence alignment to identify the key conserved residues. Alignment was done using Clustal X program and final figure output designed using ESpript (http://espript.ibcp.fr). Subsite mapping and active site residues of *Ct*ManT were determined by structure superimposition

over all known available structures within the family. Structure comparison analysis study was done using PyMOL1.3 tool.

3.2.13.4 Molecular docking study of modelled CtManT

Molecular docking study was carried out using Autodock 4.2.1 to understand the active site and the energy of ligand binding of *Ct*ManT. In Autodock 4.2.1, novel and robust docking methodology of inbuilt Lamarckian Genetic Algorithm (LGA) and empirical free energy scoring function were used to reproduce the docking results for ligands (Le-Nours *et al.*, 2005). All the ligand molecules (as mentioned in the Section 3.3.9, Table 3.3.8) were retrieved either from PDB files or PubChem (https://pubchem.ncbi.nlm.nih.gov). Input files of ligand were prepared by adding hydrogen atoms and assigning Gasteiger-Marsili charges followed by removing all non-polar hydrogens and merging their charges to the carbon atoms. Grid maps were assigned to each atom type present in protein as well as ligand molecule accompanied by electrostatic and desolvation maps using the AutoGrid (Huey *et al.*, 2007). Grid box was set at 66, 60, 58 (x,y,z) coordinate points with 0.375 Å grid spacing which covered the entire active site pocket of modelled *Ct*ManT. Docking simulations were performed with an initial population size of 300 and 30 independent LGA runs. Best docked confirmation from the largest cluster having a minimum lowest free energy of binding (ΔG), were saved. Results were analyzed using PyMOLfor possible polar and hydrophobic interaction.

3.3 Results and Discussion

3.3.1 Substrate specificity of *Ct*Manf and *Ct*ManT with natural polysaccharides

The enzyme assays with natural substrates were carried out using the optimized assay conditions as described in Section 3.2.7. The substrate specificities of *Ct*Manf and *Ct*ManT with natural substrates were determined at optimized pH and temperature. The enzyme activities with natural substrates are displayed in Table 3.3.1. It is evident from the Table 3.3.1 that both *Ct*Manf and *Ct*ManT have specificity for galactomannan and the highest enzyme activity was achieved with carob galactomannan 97.0 ± 5.0 U/mg and 91.0 ± 4.0 U/mg, respectively. Both *Ct*Manf and *Ct*ManT, respectively, the displayed activity in decreasing order with locust bean galactomannan (85.4 ± 6.0 and 83.1 ± 5.0 U/mg), konjac glucomannan (81.0 ± 3.0 and 79.8 ± 4.0 U/mg) and guar galactomannan (47.6 ± 3.0 and 38.7 ± 4.0 U/mg). *Ct*Manf and *Ct*ManT a biphasic hydrolysis pattern against insoluble polysaccharide ivory nut mannan displayed, where rapid hydrolysis of the substrate occurred till 15 min of incubation followed by slower hydrolysis (Fig. 3.3.1). These enzymes perhaps acted on the amorphous sites (hydrolysable region) of the substrate during rapid hydrolysis (in first phase) and then accessed the crystalline sites (tougher region) in the second phase. Similar results were reported by Mizutani *et al.*, (2012). The enzyme activities of both the enzymes with insoluble ivory nut mannan and β-(1→4)-mannan from the first phase was calculated (Table 3.3.1). *Ct*Manf displayed approximately, two folds higher activity than *Ct*ManT against both the substrates (Table 3.3.1). The specific activity of *Ct*Manf was 50.0 U/mg, whereas, of *Ct*ManT was 26.5 U/mg with ivory nut mannan and with β-(1→4)-mannan the enzyme activities were 40.0 U/mg and 21.2 U/mg, respectively (Table 3.3.1).

Table 3.3.1 Substrate specificity of *Ct*Manf and *Ct*ManT from *Clostridium thermocellum* ATCC 27405.

Substrates (1%, w/v)	Specific Activity [a]*Ct*Manf (U/mg)*	Specific Activity [b]*Ct*ManT (U/mg)*
Carob galactomannan	97.0±5.0	91.0±4.0
Locust bean galactomannan	85.4±6.0	83.1±5.0
Konjac glucomannan	81.0±3.0	79.8±4.0
Guar galactomannan	47.6±3.0	38.7±4.0
Ivory nut mannan	50.0±2.0	26.5± 0.9
Mannan	40.0±1.0	21.2±2.0
Barley-β-glucan	2.94±0.2	1.74±0.1
Lichnan	1.92±0.8	1.22±0.2
Carboxymethyl cellulose	1.09±0.5	0.9±0.05
Hydroxyethyl cellulose	0.87±0.03	0.47±0.03
Avicel	0.39±0.02	0.26±0.03
Xyloglucan	1.5 ± 0.5	1.0 ± 0.3
Rye arabinoxylan	NA	NA
Glucuronoxylan	NA	NA
Arabinogalactan	NA	NA
Polygalactouronic acid	NA	NA

**Values are in Mean ± SD (n=3)*

NA = No Activity.

All the assays were performed at 50°C using 50 mM sodium phosphate (pH 6.9) buffer for [a]CtManf and 50 mM sodium acetate (pH 6.5) buffer for [b]CtManT.

The assays were performed in triplicates. The incubation time and other conditions for reducing sugar estimation were same as described in the Section 3.2.7.

Therefore, the above results indicated that *Ct*CBM35 plays role in potentiating the enzyme activity of the full length enzyme *Ct*Manf in hydrolyzing the insoluble substrates. Similar comment was stated earlier by Mizutani *et al.*, (2012) for CBM32 appended to GH5 mannanase from *Clostridium thermocellum.* Both *Ct*Manf and *Ct*ManT displayed significantly low but observable activity against barley β-glucan, lichenan, carboxymethyl cellulose, hydroxyethyl cellulose, avicel and xyloglucan,

whereas, no activity was observed with arabinogalactan, rye arabinoxylan, glucuronoxylan and polygalactouronic acid (Table 3.3.1).

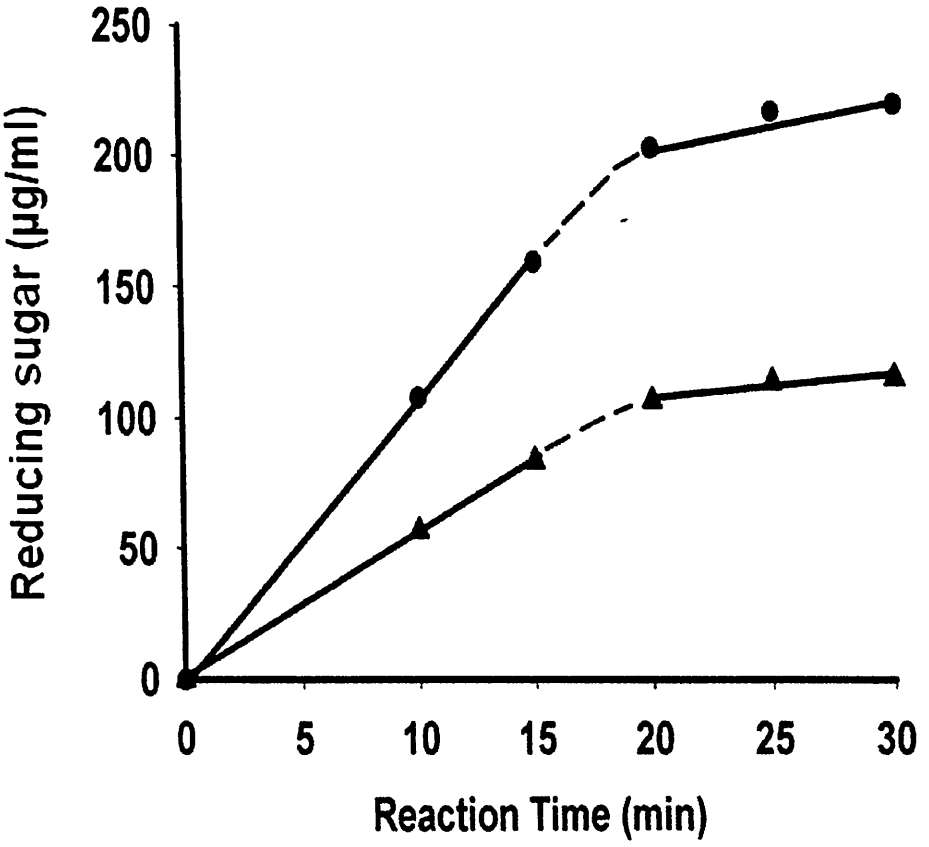

Fig. 3.3.1 Biphasic hydrolysis pattern of insoluble ivory nut mannan by (●) *Ct*Man*f* and (▲) *Ct*ManT. *Ct*Manf and *Ct*ManT (0.16 mg/ml and 0.15 mg/ml) was incubated with carob galactomannan (1%, w/v) at 50°C for 30 min and the liberated sugar was estimated using Nelson and Somogyi's method as described in Section 3.2.7.

3.3.2 Substrate specificity and kinetic parameters of *Ct*Manf and *Ct*ManT with natural and synthetic substrates

The kinetic properties and catalytic efficiency of both the enzymes were determined with the natural substrates (Table 3.3.2). *Ct*Manf and *Ct*ManT displayed turnover number (k_{cat}) 698 min^{-1} and 684 min^{-1}, respectively and the catalytic efficiency (k_{cat}/K_m) 4.1×10^2 and 3.9×10^2 ml/min/mg respectively, with carob galactomannan. The enzymes *Ct*Manf and *Ct*ManT acted on insoluble ivory nut

mannan and showed catalytic efficiencies (k_{cat}/K_m) 3.4 x 10^2 and 2.4 x 10^2 ml/min/mg, respectively and with β-(1→4)-mannan 3.1 x 10^2 and 2.2 x 10^2 ml/min/mg respectively (Table 3.3.2).

The present results showed that *Ct*Manf gave approximately, 1.1 fold higher activity against carob galactomannan and approximately, 2 fold higher activity against insoluble ivory nut mannan and β-(1→4)-mannan than the catalytic *Ct*ManT. Similar results were reported earlier where enhanced activity in presence of a carbohydrate binding domain (CBD) in Man26A (Mannanase A from family GH26) was observed by Halstead *et al.*, (1999). The presence of CBD at the N-terminal of Man26A enhanced turnover of carob galactomannan by 1.1 fold and 2 fold against insoluble ivory nut mannan (Halstead *et al.*, 1999).

Both *Ct*Manf and *Ct*ManT did not show any activity against *p*NP-β-D-mannopyranoside and with *p*NP-α-D-mannopyranoside. Based on the enzyme activity of *Ct*Manf and *Ct*ManT against natural as well as synthetic substrates, it was evident that both these enzymes are predominantly endo-β-D-mannanase. The enzymes specifically cleaved the β-(1→4)-glycosidic linkages between mannopyranosyl residues.

Table 3.3.2. Kinetic properties and catalytic efficiencies of *Ct*Manf and *Ct*ManT from *Clostridium thermocellum* ATCC 27405

Substrate	K_m (mg/ml)*		k_{cat} (min^{-1})*		k_{cat}/K_m ($min^{-1}mg^{-1}ml$)*	
	*Ct*Manf	*Ct*ManT	*Ct*Manf	*Ct*ManT	*Ct*Manf	*Ct*ManT
[a]Natural substrates						
Carob galactromannan	1.8±0.2	1.6±0.2	737±8	634±7	4.1 x 10^2±40	3.9 x 10^2±35
Locust bean galactomannan	1.5±0.1	1.4±0.4	590±6	520±10	3.9 x 10^2±60	3.7 x 10^2±25
Konjac glucomannan	1.5±0.3	1.4±0.2	510±10	462±6	3.4 x 10^2±33	3.3 x 10^2±30
Guar galactomannan	1.2±0.2	1.1± 0.2	320±7	283±8	2.6 x 10^2±35	2.5 x 10^2±40
Ivory nut mannan	0.9±0.1	0.8±0.2	310±4	199±5	3.4 x 10^2±40	2.4 x 10^2±25
Mannanan	0.9±0.2	0.7±0.1	283±6	159±3	3.1 x 10^2±30	2.2 x 10^2±30
[b]Synthetic substrates						
*p*NP-β-D-manno-pyranoside	NA	NA	NA	NA	NA	NA
*p*NP-α-D-manno-pyranoside	NA	NA	NA	NA	NA	NA

**Values are in Mean ± SD (n=3)*

NA = No Activity.

All the assays were performed at 50°C using 50 mM sodium phosphate (pH 6.9) buffer for [a]CtManf and 50 mM sodium acetate (pH 6.5) buffer for [b]CtManT.

The assays were performed in triplicate. The incubation time and other conditions for reducing sugar estimation were same as described in the Section 3.2.7.

[c]Assays with synthetic pNP-glycosides were carried out in 50 mM sodium phosphate buffer pH 6.0.

3.3.3 Effect of pH on the enzyme activity of *Ct*Manf and *Ct*ManT

The enzyme activity of *Ct*Manf and *Ct*ManT displayed significant dependence on the pH of the buffer and the temperature at which the enzyme-substrate mixture was incubated. Initially, with rising pH, the specific activity of *Ct*Manf and *Ct*ManT increased to a maximum pH 6.9 and 6.5, respectively and then dropped to almost 10%

activity in the alkaline pH region (pH 8.0).Both *Ct*Manf and *Ct*ManT displayed bell-shaped pH profile (Fig. 3.3.2). The full length catalytic module *Ct*Manf showed maximum enzyme activity at pH 6.9 (91.0±2.0U/mg) where as truncated module *Ct*ManT showed maximum enzyme activity at pH 6.5 (78.0±4.0U/mg) (Fig. 3.2.2)

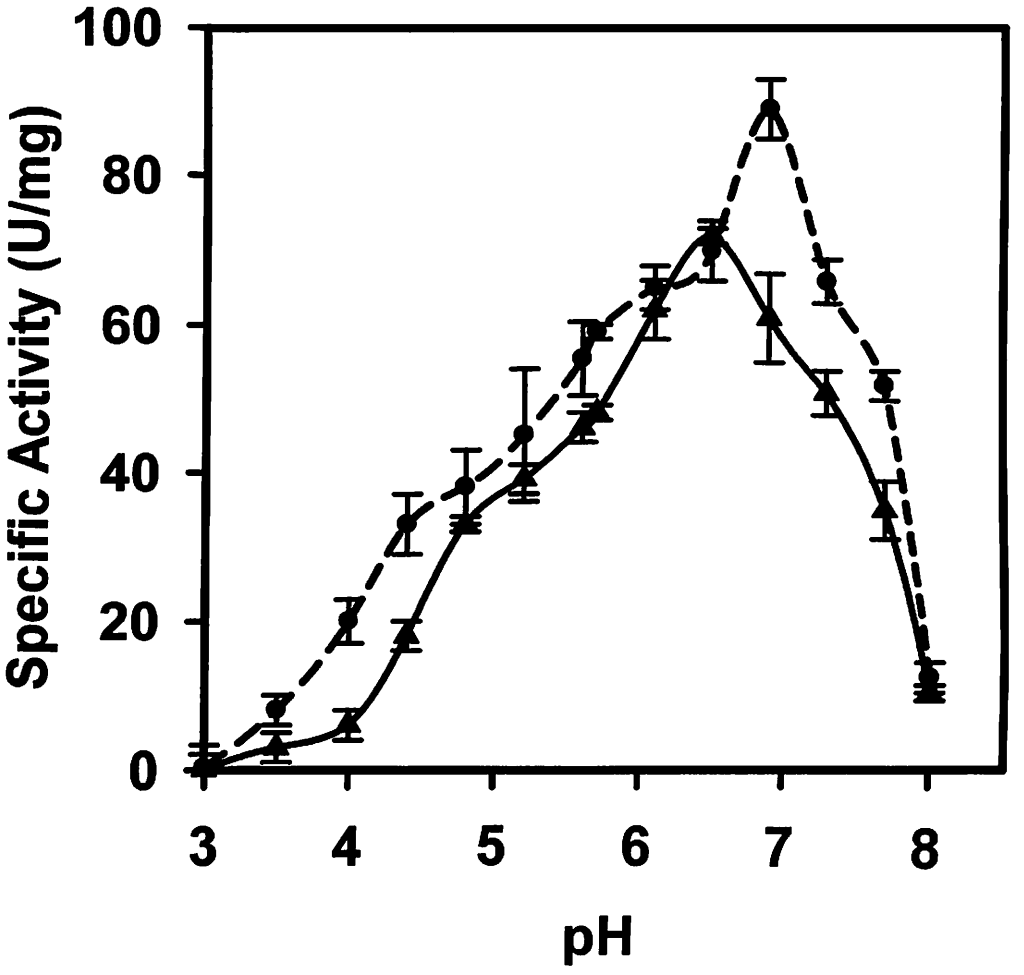

Fig. 3.3.2 Effect of pH on (--●--) *Ct*Manf and (-▲-) *Ct*ManT activity. *Ct*Manf and *Ct*ManT (0.16 mg/ml and 0.15 mg/ml) was incubated with carob galactomannan (1%, w/v) at 50°C for 15 min and the liberated sugar was estimated using Nelson and Somogyi's method as described in Section 3.2.7.

3.3.4 Effect of temperature on the enzyme activity of *Ct*Manf and *Ct*ManT

The enzyme activity of *Ct*Manf and *Ct*ManT displayed significant dependence on the temperature to overcome of activation energy barrier and covert the substrates into reducing sugars. Increase in incubation temperature from 10°C to 100°C, the enzyme activity of *Ct*Manf displayed an elevation profile till 60°C (maximum activity observed 83.1±4.0U/mg) and where as *Ct*ManT showed maximum activity till 50°C (maximum activity observed 79.1±2.0U/mg) (Fig. 3.3.3).

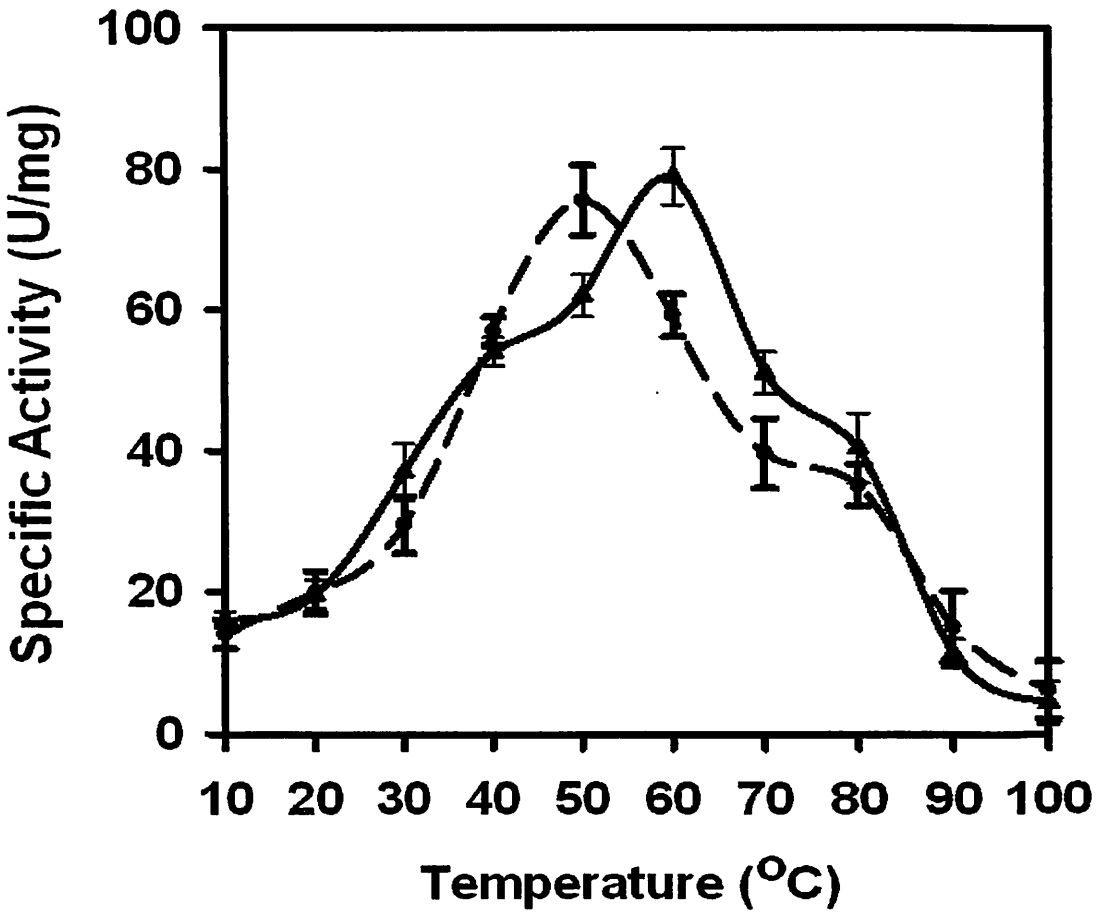

Fig. 3.3.3 Effect of temperature on (-▲-) *Ct*Manf and (--●--) *Ct*ManT activity. *Ct*Manf and *Ct*ManT (0.16 mg/ml and 0.15 mg/ml) was incubated with carob galactomannan (1%, w/v) in 50 mM sodium phosphate buffer, pH 6.9 and 6.5, respectively, for 15 min and the liberated sugar was estimated using Nelson and Somogyi's method as described in Section 3.2.7.

3.3.5 pH stability of *Ct*Manf and *Ct*ManT

Both *Ct*Manf and *Ct*ManT were found to be stable in the pH range of 6.0-7.5 and retained 40% relative activity (Fig. 3.3.4). The pH stability of an enzyme is governed by mainly two factors, i) type of enzyme and direct involvement of ionic groups in the catalytic mechanism and ii) participation of charged groups in the stabilization of the protein structure (Branden and Tooze, 1991). Ionic groups are often involved in enzymatic catalysis, and the state of these groups protonation is essential for the reaction. Deviations from the optimum pH value of *Ct*Manf and *Ct*ManT may alter the state of protonation of the groups involved and perturb their involvement in the catalytic process. Both *Ct*Manf and *Ct*ManT showed almost similar pH stability profile to that of optimum pH profile and this is because in both case, the same charged groups (similar amino acids) may be involved for stabilization of protein structure.

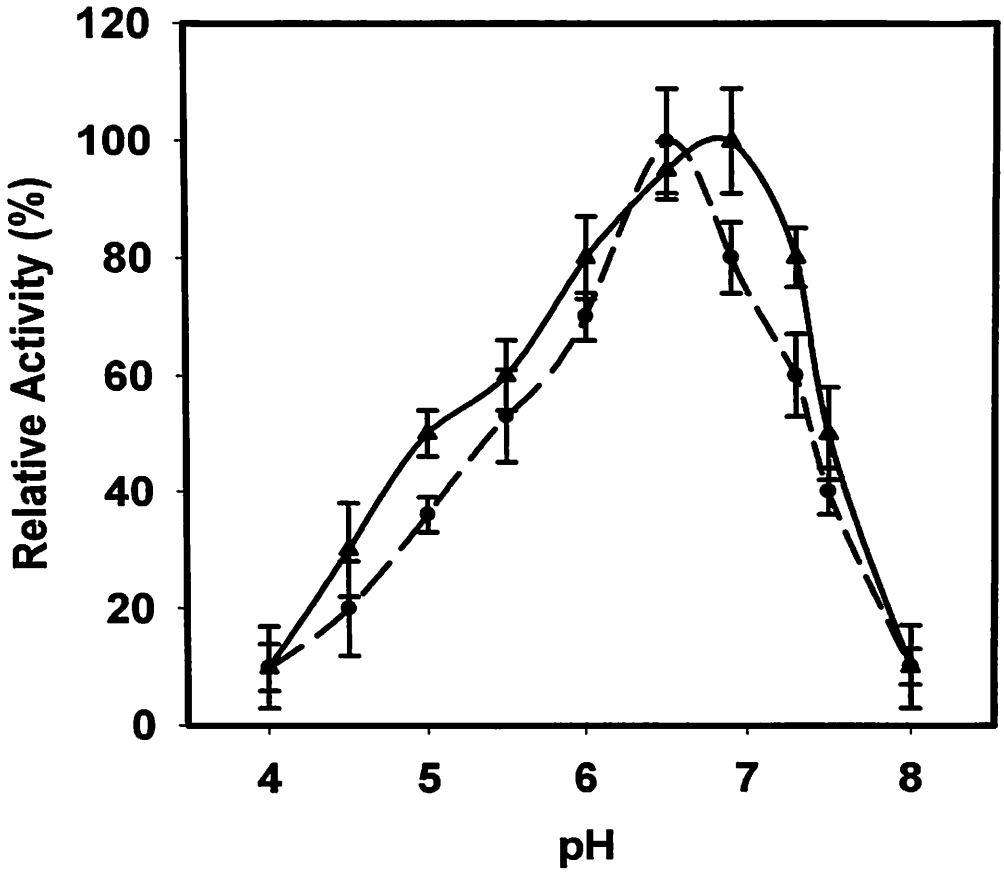

Fig. 3.3.4 pH sability analysis of *Ct*Manf. (▲) and *Ct*ManT (●). 100 µl *Ct*Manf. (0.16 mg/ml) and *Ct*ManT (0.15 mg/ml) was incubated at different pH (4-50°C) for 30 min. After centrifugation, 40 µl aliquot of *Ct*Manf and *Ct*ManT was incubated with carob galactomannan (1%, w/v) in a 100 µl reaction mixture at 50°C for 15 min. The liberated sugar was estimated using Nelson and Somogyi method as described in Section 3.2.7

3.3.6 Thermal stability of *Ct*Manf and *Ct*ManT

*Ct*Manf was stable in temperature range of 10-60°C (Fig. 3.3.5). However, at a temperature higher than 60°C, the enzyme stability decreased to 20% at 100°C (Fig. 3.3.5). *Ct*ManT was thermally stable observed between 10-50°C (Fig. 3.3.5). The enzyme activity significantly lost beyond 50°C and residual activity was 10% at 100°C (Fig. 3.3.5). The most accepted explanation for the loss of enzyme activity at high temperature is the opening or uncoiling of the protein architecture, which results in decreased stability and consequently lower activity (Branden and Tooze, 1991.

Creighton, 1992). The opening of protein tertiary structure changes the conformation of protein architecture that directly affects the velocity of enzyme catalyzed reaction.

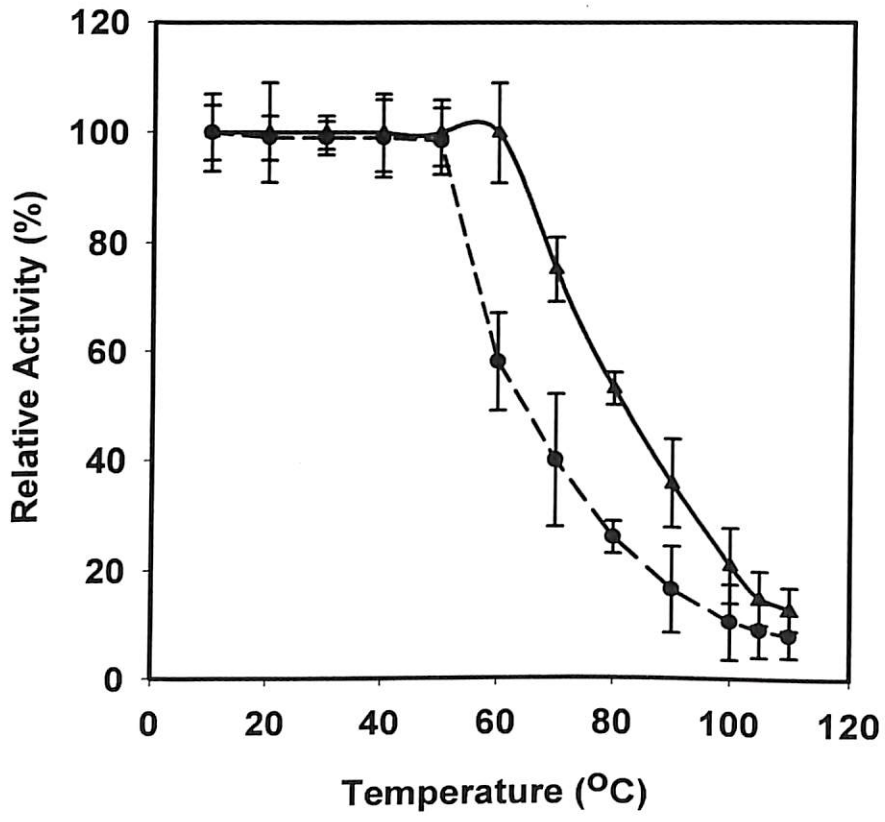

Fig. 3.3.5 Thermal stability analysis of *Ct*Manf. (▲) and *Ct*ManT (●). 100 µl *Ct*Manf. (0.16 mg/ml) and *Ct*ManT (0.15 mg/ml) was incubated at different temperature (10-110°C) for 30 min. After centrifugation, 40 µl aliquot of *Ct*Manf and *Ct*ManT was incubated with carob galactomannan (1%, w/v) in a 100 µl reaction mixture at 50°C for 15 min. The liberated sugar was estimated using Nelson and Somogyi's method as described in Section 3.2.7

Protein stability while functioning at higher temperature is a major concern in industry. Temperature stability study of *Ct*Manf and *Ct*ManT showed that after 1 h of incubation at 60°C and 50°C, respectively retained 100% activity. But they retained around 10% of enzymatic activity at 100°C. Comparing with recombinant ManB from *Bacillus licheniforms* DSM13 which reported no activity within 80-100°C at pH 6.0 (Songsiriritthigul *et al.*, 2010) the recombinant Man26B from *Clostridium thermocellum* ATCC 27405 was thermally more stable at higher temperatures.

3.3.7 Activity staining of *Ct*Manf and *Ct*ManT

Separate SDS-PAGE gels were used in the zymogram study to show the active bands of *Ct*Manf and *Ct*ManT against carob galactomannan (Fig. 3.3.6A and 3.3.6B). *Ct*Manf displayed an activity band around 53 kDa and *Ct*ManT around 38 kDa, after congo red staining and counter staining with 1N HCl (Fig. 3.3.6A and 3.3.6B). Both the enzymes displayed single homogeneous bands and a clear zone of activity with carob galactomannan. Mannan endo-β-(1→4)-mannanase activity was detected as clear zones against red (after staining with congo red) and blue background (after counter stained with 1 N HCl). The results clearly indicated that both of these enzymes have specificity of manno-configured substrates.

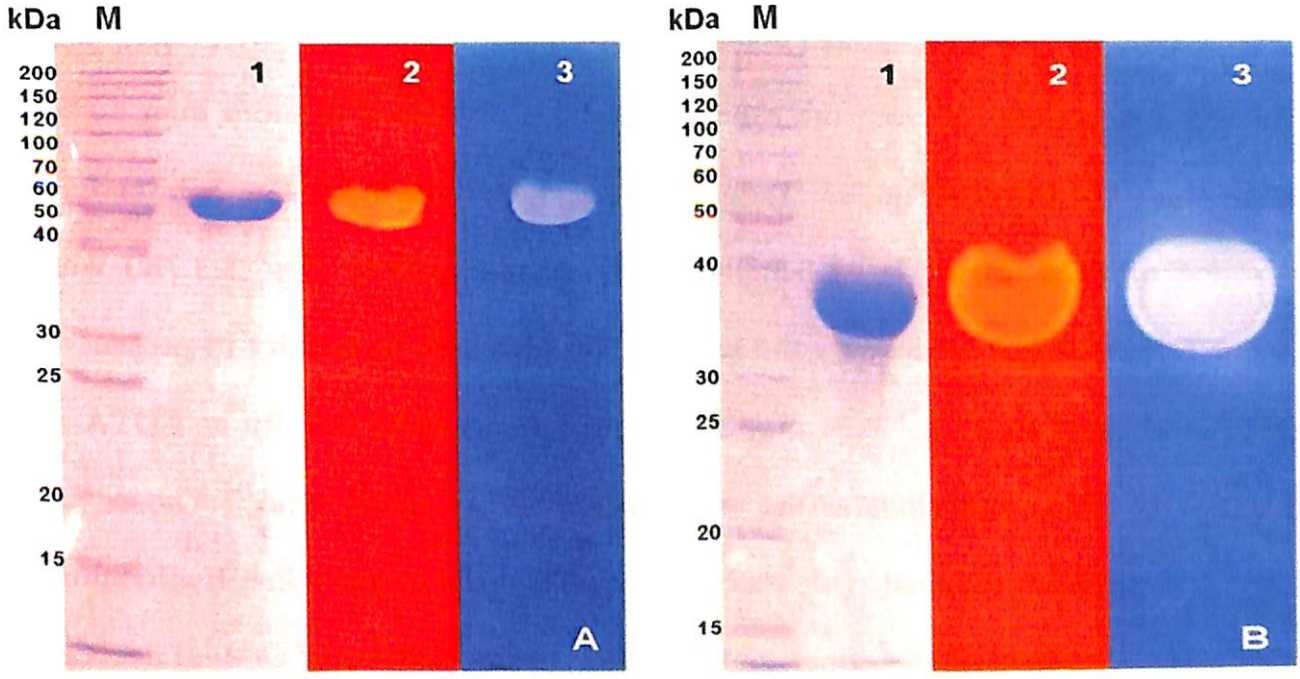

Fig. 3.3.6 Zymogram study using 12% SDS-PAGE (A) *Ct*Manf (panel 1 : purified protein, 2 : congo red staining, 3 : 1 N HCl counter staining, (B) *Ct*ManT (panel 1 : purified protein, 2 : congo red staining, 3 : 1 N HCl counter staining. A clear zone of activity of *Ct*Manf and *Ct*ManT (53 kDa and 38 kDa) bands were observed against 0.5% (w/v) carb galactomannan.

3.3.8 Effects of metal ions and chemical agents on enzyme activity of *Ct*Manf and *Ct*ManT

Effects of metal ions and chemical agents on enzyme activity of *Ct*Manf and *Ct*ManT were shown in Table 3.3.3. The enzyme activity of *Ct*Manf and *Ct*ManT significantly increased by (1.5 fold) in presence of low concentrations of Ca^{2+} (10 mM) (Fig. 3.3.7A) or Mg^{2+} (15 mM) (Table 3.3.3, Fig. 3.3.7B). Both *Ct*Manf and *Ct*ManT retained moderate activities in presence of 10 mM Mn^{2+} (80% and 60%) (Fig. 3.3.7C), 8 mM Ni^{2+} (80% and 80%) (Fig. 3.3.7D), 30 mM Co^{2+} (70% and 70%) (Fig. 3.3.7E), 10 mM Zn^{2+} salts (70% and 60%), respectively (Fig. 3.3.7F). The enzyme activities were adversely affected by low concentrations of Cu^{2+} (5 mM) (Fig. 3.3.7G) and Al^{3+} (6 mM) (Fig. 3.3.7H) salts and *Ct*Manf lost 80% and *Ct*ManT lost 90% of activity at the mentioned concentrations of Cu^{2+} and Al^{3+} salts (Table 3.3.4). The enzyme activity of both the catalytic modules decreased to more than 80% in presence of 8M EDTA (Fig. 3.3.7I) or 10 mM EGTA (Table 3.3.4, Fig. 3.3.7J). In the presence of SDS (10 mM) *Ct*Manf lost 94% enzyme activity (Fig. 3.3.7K) while, *Ct*ManT lost almost completely the activity. The decrease in activity in presence of EDTA indicated that Ca^{2+} ions may be essential for enzyme activity as EDTA and specifically binds and chelates the calcium ions in 1:1 molar ratio.[36] The enzyme activity drastically reduced with chaotropic agents such as guanidine hydrochloride (GnHCl) and urea at higher concentrations. The enzyme activity of *Ct*Manf decreased by 90% at 100 mM GnHCl, whereas, *Ct*ManT lost 95% activity at the same concentration (Fig.3.3.7L). In contrast much higher concentration of urea (4 M) was required for complete diminution (98% - 99%) of enzyme activities of *Ct*Manf and *Ct*ManT (Fig. 3.3.7M).

Table 3.3.4 Effects of metal ions and other agents on *Ct*Manf and *Ct*ManT from *Clostridium thermocellum* ATCC 27405

Ions/ Reagents	Concentration (mM)	Relative activity (%)	
		*Ct*Manf	*Ct*ManT
*Control	--	100	100
Ca^{2+}	10	150	150
Mg^{2+}	15	150	150
Mn^{2+}	10	80	60
Ni^{2+}	8	80	80
Co^{2+}	30	70	70
Zn^{2+}	10	70	60
Cu^{2+}	5	20	10
Al^{3+}	6	20	10
EDTA	8	20	20
EGTA	10	20	20
SDS	8	6	2
Urea	$4x10^3$ (4 M)	10	5
GnHCl	100	2	1

**No additive was added in control and the activity was taken as 100%*

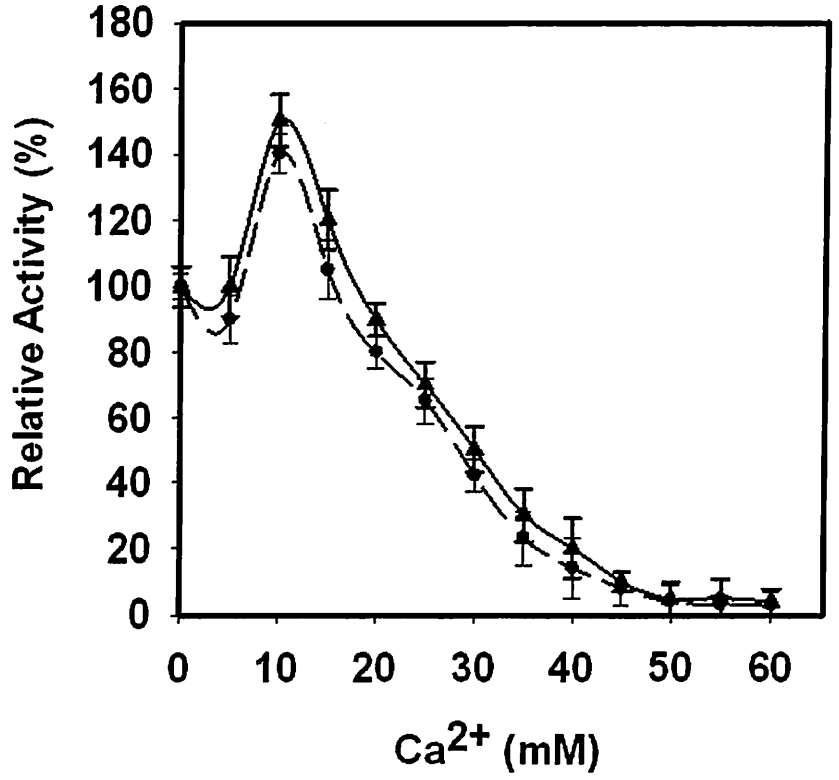

Fig. 3.3.7A Effect of Ca^{2+} ion on enzyme activity of *Ct*Manf (-▲-) and *Ct*ManT (--●--) from *Clostridium thermocellum.*

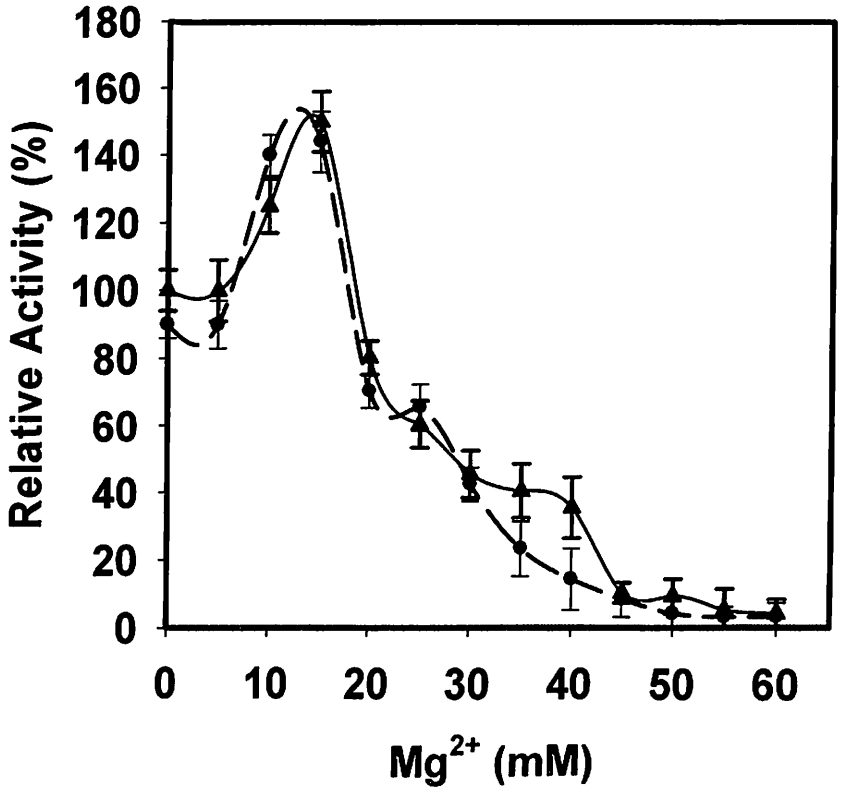

Fig. 3.3.7B Effect of Mg^{2+} ion on enzyme activity of *Ct*Manf (-▲-) and *Ct*ManT (--●--) from *Clostridium thermocellum.*

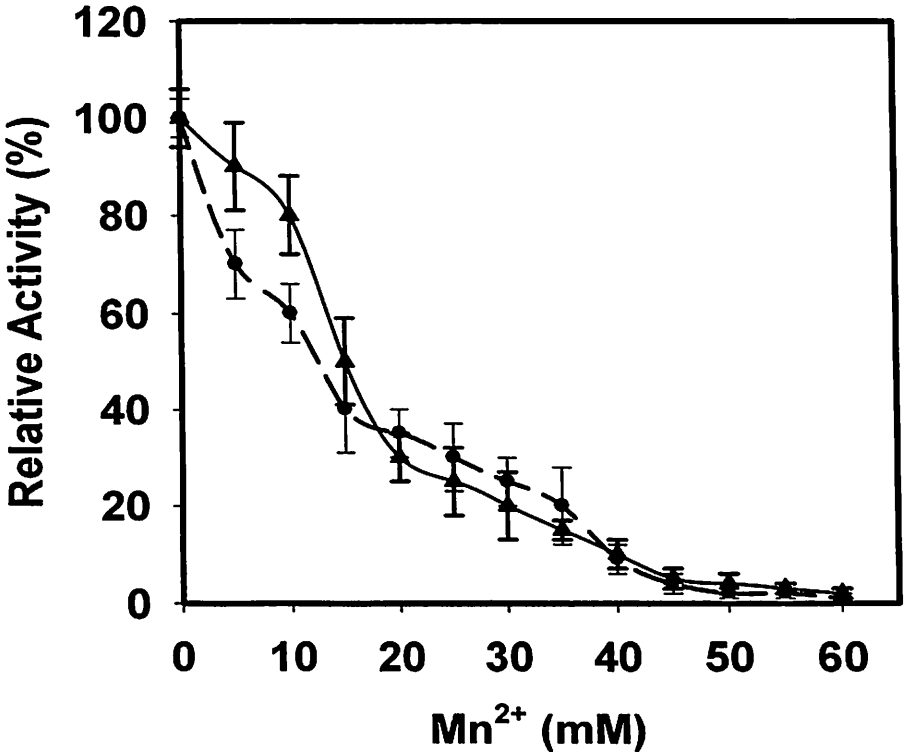

Fig. 3.3.7C Effect of Mn^{2+} ion on enzyme activity of *Ct*Manf (-▲-) and *Ct*ManT (--●--) from *Clostridium thermocellum.*

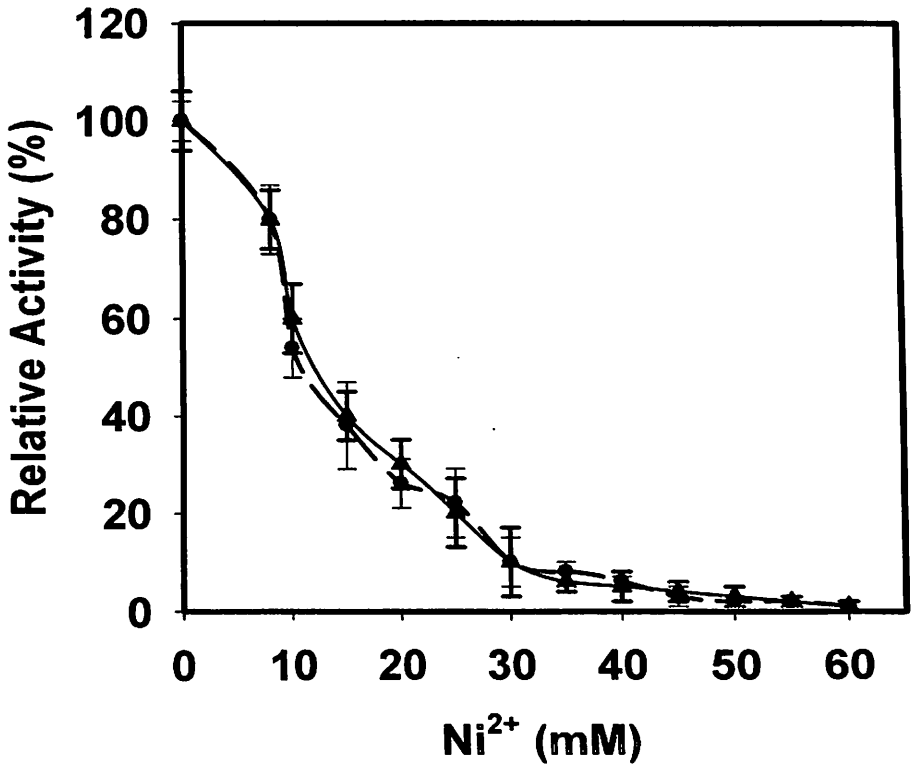

Fig. 3.3.7D Effect of Mn^{2+} ion on enzyme activity of *Ct*Manf (-▲-) and *Ct*ManT (--●--) from *Clostridium thermocellum.*

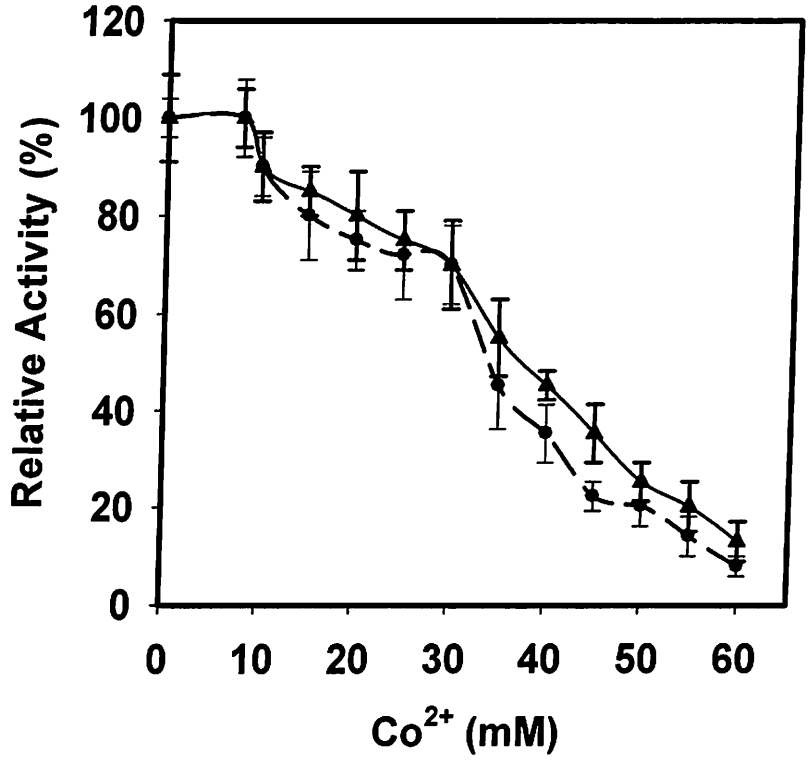

Fig. 3.3.7E Effect of Co^{2+} ion on enzyme activity of *Ct*Manf (-▲-) and *Ct*ManT (--●--) from *Clostridium thermocellum.*

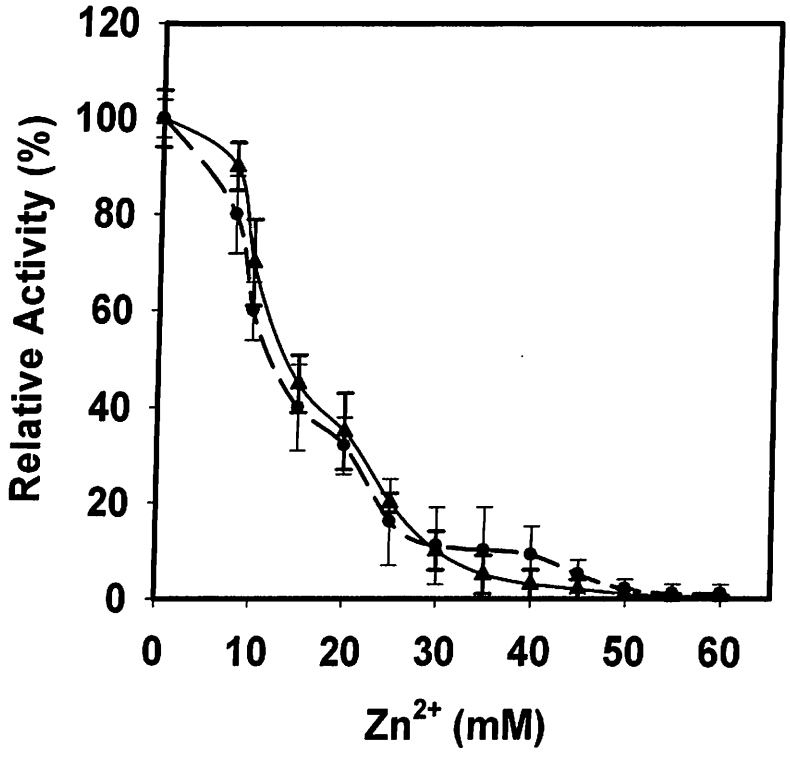

Fig. 3.3.7F Effect of Zn^{2+} ion on enzyme activity of *Ct*Manf (-▲-) and *Ct*ManT (--●--) from *Clostridium thermocellum.*

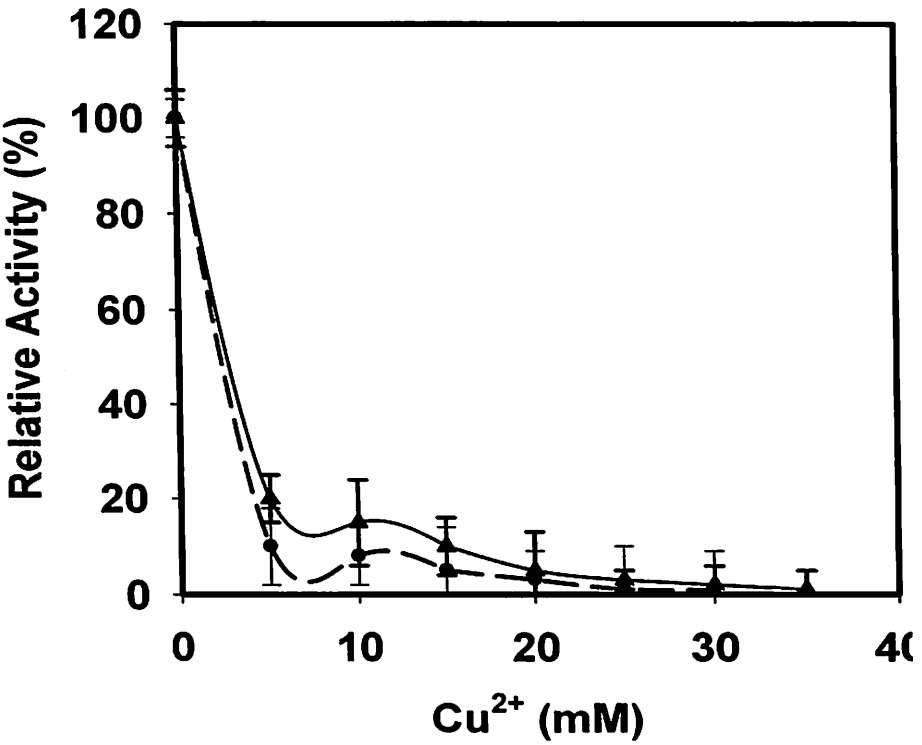

Fig. 3.3.7G Effect of Mn^{2+} ion on enzyme activity of *Ct*Manf (-▲-) and *Ct*ManT (--●--) from *Clostridium thermocellum.*

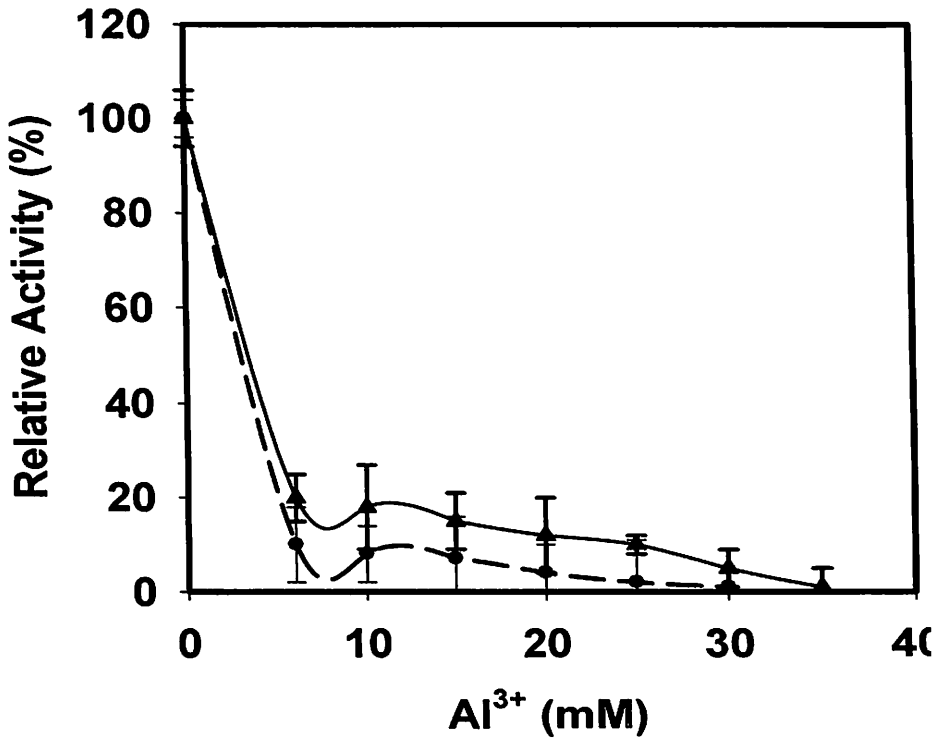

Fig. 3.3.7H Effect of Mn^{2+} ion on enzyme activity of *Ct*Manf (-▲-) and *Ct*ManT (--●--) from *Clostridium thermocellum.*

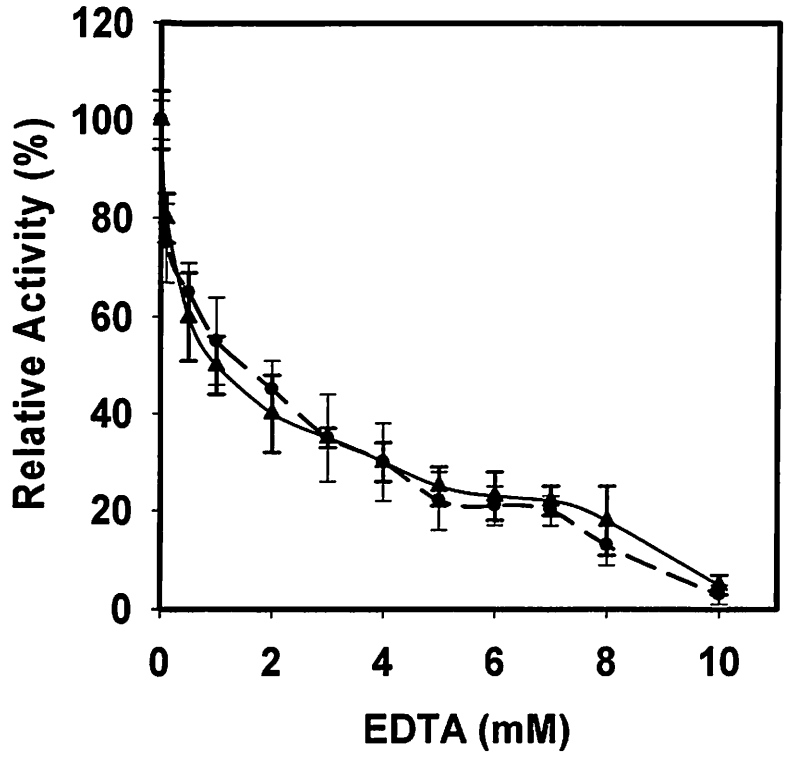

Fig. 3.3.7I Effect of EDTA on enzyme activity of *Ct*Manf (-▲-) and *Ct*ManT (--●--) from *Clostridium thermocellum.*

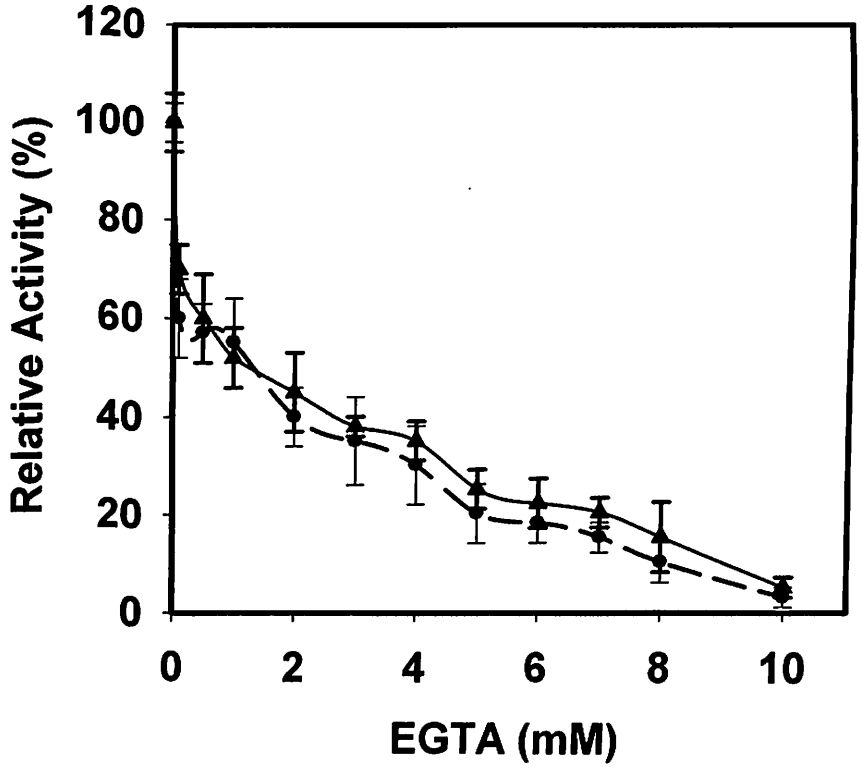

Fig. 3.3.7J Effect of EGTA on enzyme activity of *Ct*Manf (-▲-) and *Ct*ManT (--●--) from *Clostridium thermocellum.*

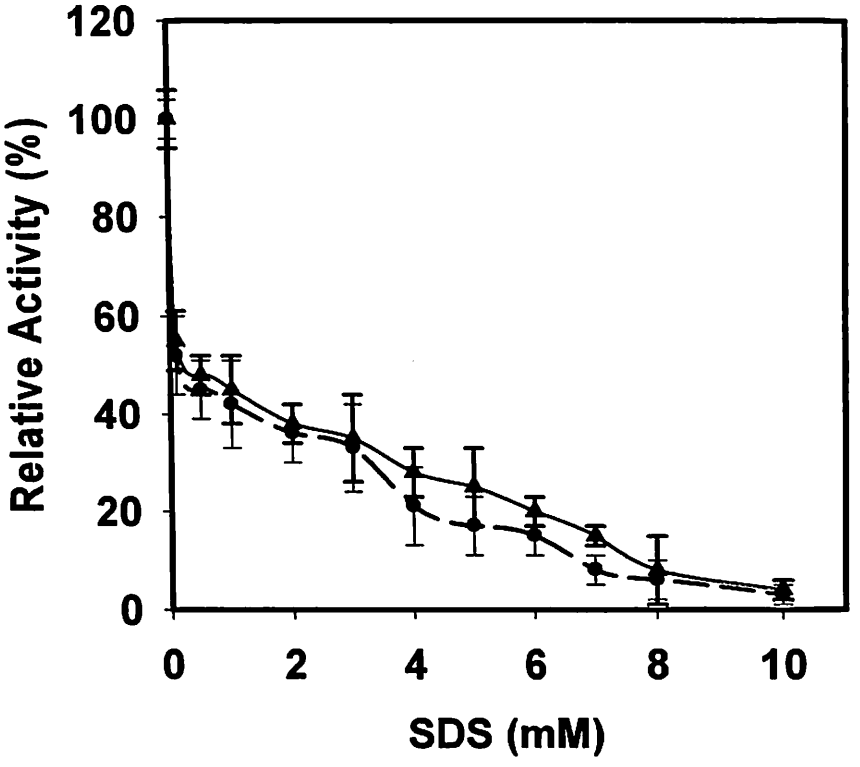

Fig. 3.3.7K Effect of Mn^{2+} ion on enzyme activity of *Ct*Manf (-▲-) and *Ct*ManT (--●--) from *Clostridium thermocellum.*

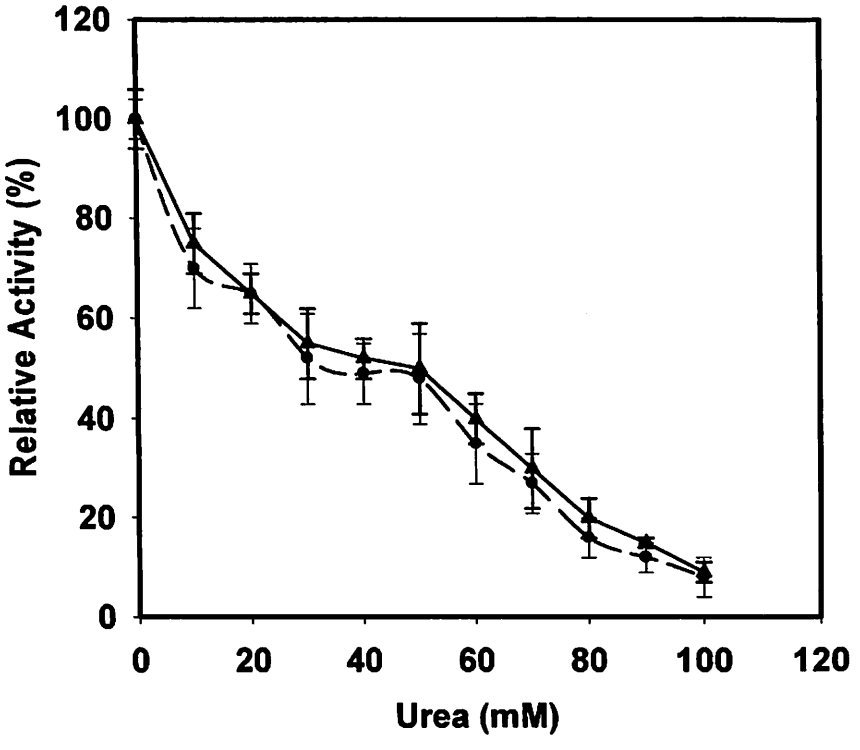

Fig. 3.3.7L Effect of urea on enzyme activity of *Ct*Manf (-▲-) and *Ct*ManT (--●--) from *Clostridium thermocellum.*

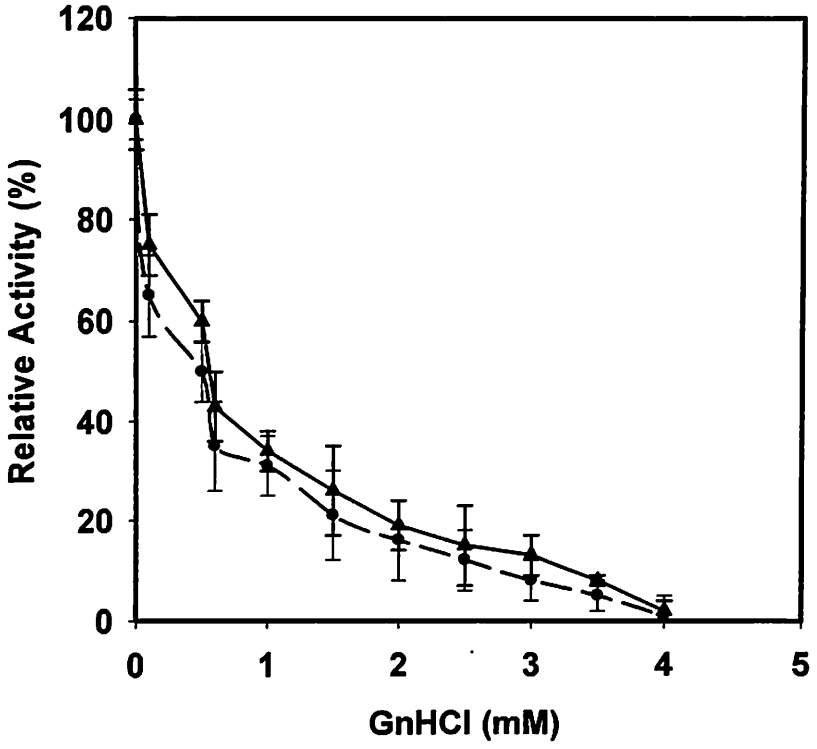

Fig. 3.3.7M Effect of GnHCl on enzyme activity of *Ct*Manf (-▲-) and *Ct*ManT (--●--) from *Clostridium thermocellum.*

Therefore, from the above observations it can be suggested that the enzyme activities of *Ct*Manf and *Ct*ManT increased significantly by 1.5 fold in the presence of Ca^{2+} and Mg^{2+} salts, which suggested that these ions are required as cofactors. However, the enzyme activity was unaffected by lower concentrations of Mn^{2+}, Ni^{2+}, Co^{+}, Zn^{2+} and were able to retain their moderate activities. The enzyme activities of *Ct*Manf and *Ct*ManT were inhibited by lower concentrations of Cu^{2+} and Al^{3+}. Similar observation was reported earlier by Yoshikawa *et al.*, (2009), where a non-competitive type of inhibition was imposed by Cu^{2+} ions by binding at sites other than the α-glucosidase active center. In the presence of low concentration of chelating agents such as EDTA or EGTA, the enzyme activity sharply decreased. The enzyme activity of *Ct*Manf and *Ct*ManT was adversely affected by low concentration of SDS.

The higher concentration of urea and lower concentration of guanidine hydrochloride was required to denature the enzymes.

3.3.9 Production of *Ct*Manf and *Ct*ManT in different media

The highest concentration of recombinant proteins were obtained from 100 mL flask containing TY medium followed by TB, LB and 5xLB media after 24 h of incubation as shown in Table 3.3.5. TY medium achieved highest cell density 31 g/l and 30 g/l dry cell weight, respectively for *Ct*Manf and *Ct*ManT. The protein concentration of *Ct*Manf and *Ct*ManT after sonication and purification by IMAC was 910 mg/l and 880 mg/l, (yield 0.91 and 0.88 mg) respectively. Similarly Tripathi *et al.*, (2009) reported that the TY medium gave the highest cell density of *E. coli* cells 1.12 g/l and expressing the recombinant dengue protein at concentration 10.37 mg/ml (Tripathi *et al.*, 2009). *Ct*Manf and *Ct*ManT gave lesser DCW with TB medium 28 g/l and 26.9 g/l, respectively as compared with TY medium. The purified protein concentrations from TB medium obtained were 500 mg/ml and 410 mg/ml, (yield 0.5 and 0.41 mg) respectively for *Ct*Manf and *Ct*ManT. The dry cell weight (DCW) from 100 mL LB medium obtained 21 g/l and 20 g/l for *Ct*Manf and *Ct*ManT, respectively. The concentrations of purified protein obtained from LB medium were 160 mg/ml for *Ct*Manf and 150 mg/ml for *Ct*ManT (yield 0.16 and 0.15 mg). These results are similar to those of the earlier report of Tripathi *et al.*, (2009). The lowest growth of cell mass of *E. coli* BL21 (DE3) cells were observed for both enzymes in 5xLB medium. The cell densities obtained were 12.0 g/l and 10 g/l, respectively, for *Ct*Manf and *Ct*ManT. The recombinant *Ct*Manf and *Ct*ManT proteins after purification were 300 mg/l and 280 mg/l, (0.3 and 0.28 mg) respectively in 5xLB medium,. Therefore,

it can be suggested that the production of recombinant mannanase and cell biomass can be improved by altering and optimizing medium components.

Table 3.3.5 Effect of different media on production of recombinant *Ct*Manf and *Ct*ManT.

Medium	*E. coli* biomass (g/l)		Protein Concentration (mg/l)		Protein purified (ml)	Yield (mg)	
	*Ct*Manf	*Ct*ManT	*Ct*Manf	*Ct*ManT		*Ct*Manf	*Ct*ManT
LB	21.0	20.0	160	150	1	0.16	0.15
5xLB	12.0	10.0	300	280	1	0.30	0.28
TB	28.0	26.9	500	410	1	0.50	0.41
TY	31.0	30.0	910	880	1	0.91	0.88

The use of chemically defined medium is a common practice in producing recombinant proteins (Lim and Jung, 1998; Cserjan-Puschmann *et al.*, 1999; Zhang, 1999). The recombinant *Ct*Manf and *Ct*ManT showed highest cell biomass and concentration of protein in TY medium. The TB medium showed less cell *E. coli* biomass and *Ct*Manf and *Ct*ManT as compared with TY medium. Although in LB medium moderate cell density was achieved but the lower protein concentrations were depicted as compared with TY and TB medium. The 5×LB medium did not support the growth due to higher concentrations of yeast extract, tryptone and sodium chloride and as a result lowest protein concentration was achieved. Similar effects of media were stated earlier while producing recombinant dengue protein from *E. coli* (Tripathi *et al.*, 2009). The rich source of tryptone, yeast extract and phosphate salts facilitated to achieve highest cell densities in TY media as compared to other chemically defined media used. Yeast extract is a known source of trace components (*viz.* Cd^{2+}, Co^{2+}, Cr^{2+}, Ga^{3+}, Mo^{4+}, Ni^{2+}, Pb^{4+}, Sn^{4+}, Ti^{2+}, and Zn^{2+}) and can relieve cellular stress responses such as the production of proteases during synthesis of recombinant protein

in *E. coli* (Tripathi *et al.*, 2009). Higher concentration of phosphate in TY medium is important for attaining high cell densities of *E. coli*, as the lower concentrations of phosphate limits the growth (Tripathi *et al.*, 2009). The phosphate salts in the medium perhaps provided the buffering capacity against pH fluctuations which adversely affects the metabolic activity of cells. The low cell densities and lower production of recombinant proteins in LB and 5x LB medium were due to lack of buffering capacity.

3.2.10 Protein-melting study of *Ct*Manf and *Ct*ManT

The melting phenomenon of recombinant *Ct*Manf and *Ct*ManT was studied to analyze their thermostability. The full-length *Ct*Manf showed two separate melting peaks at 50°C and 80°C (Fig. 3.3.8A), whereas, *Ct*ManT displayed a single melting peak at 80°C (Fig. 3.3.8B). This suggested that the peak at 50°C corresponds to non-catalytic *Ct*CBM35 and the peak at 80°C to the catalytic module *Ct*ManT and that the two modules are melting independently (Fig. 3.3.8B). The presence of Ca^{2+} ions (10 mM) caused significant changes in *Ct*Manf as well as in *Ct*ManT protein-melting profiles. The peak for *Ct*ManT shifted towards higher temperature i.e. from 80°C to 100°C, but the peak corresponding to *Ct*CBM35 in *Ct*Manf was masked in the presence of Ca^{2+} ions (Fig. 3.3.8A and 3.3.8B). On addition of EDTA (10 mM) to the enzyme-substrate reaction mixture containing Ca^{2+} (10 mM), the melting peaks shifted back to the original temperature of 80°C of catalytic *Ct*ManT and to 50°C, of *Ct*CBM35 (Fig. 3.3.8A and 3.3.8B, small dotted lines).

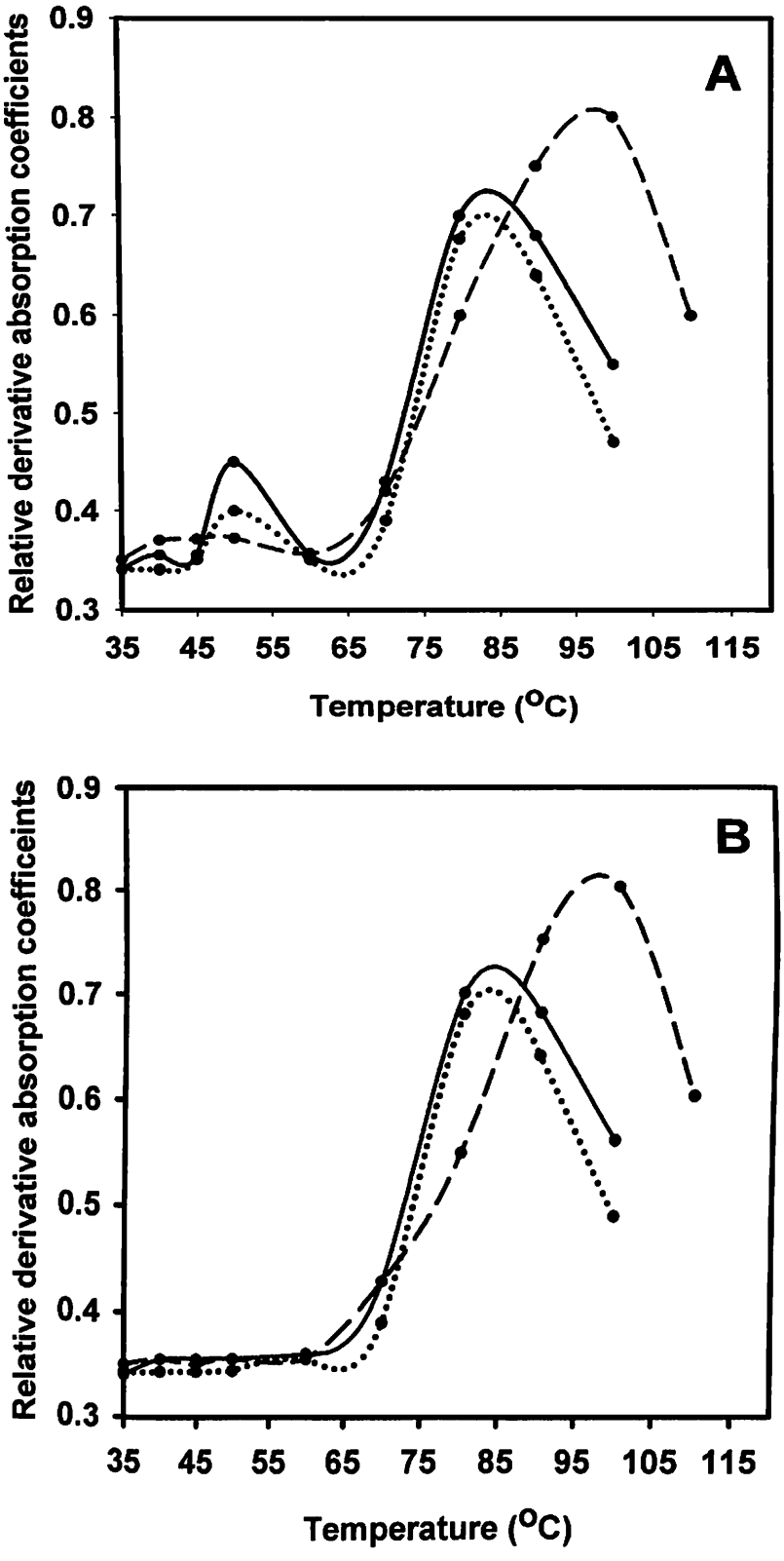

Fig. 3.3.8 Protein-melting analysis of displaying normal melting curve (—●—), melting curve in presence of 10 mM Ca^{2+} ions (--●--), and melting curve in presence of 10 mM Ca^{2+} ions and 10 mM EDTA (···●···). Melting-profile (A) *Ct*Manf and (B) *Ct*ManT.

Protein-melting curves of full length *Ct*Manf showed that the catalytic module *Ct*ManT and carbohydrate binding module *Ct*CBM35 melt independently of each other. The protein-melting peaks of *Ct*ManT and *Ct*CBM35 shifted to higher temperature in the presence of Ca^{2+} ions. However, on addition of equimolar concentration of EDTA to the solutions of *Ct*Manf and *Ct*ManT, the melting temperature peaks shifted back to the original positions. The shift of peak to a higher temperature in the presence of Ca^{2+} ions might be due to the reason that they are providing stability to the protein structure by inducing electrostatic interactions with amino acids, as reported by Noorbatcha *et al.*, (2012). The electrostatic interactions imparted by Ca^{2+} ions in bound protein resulted in less hydrogen bonds and higher number of salt bridges as compared to non bonded proteins (Noorbatcha *et al.*, 2012). Because of the higher fluctuations in the backbone of protein at higher temperature the number of hydrogen bonds will be destabilized which will allow the residues that are in close proximity to calcium ions to form more numbers of salt bridges in Ca^{2+} ion bound state as compared with Ca^{2+} ion-free state (Noorbatcha *et al.*, 2012). Thus the binding by Ca^{2+} ion makes protein more conformationally stable at higher temperature (Zhang *et al.*, 1999). The shifting back of melting peaks in the presence of EDTA was due to chelation of calcium ions making them not available for the enzyme. Therefore, from both thermostability (described in the Section 3.3.6) and protein melting study of *Ct*Manf and *Ct*ManT, it could be concluded that both these enzymes are thermostable and Ca^{2+} ions provided significant thermal stability.

3.3.11 *In silco* structure prediction of *Ct*ManT

3.3.11.1 Protein sequence and phylogenetic analysis of *Ct*ManT

The molecular architecture of full length derivative *Ct*Manf displayed a family 35 carbohydrate binding module (*Ct*CBM35) at N-terminal associated to the catalytic module *Ct*ManT (Man26B) at C-terminal. Amino acid sequence analysis using InterProScan revealed that *Ct*Manf has two distinct modules from region 1 to 134 a non catalytic carbohydrate binding module family 35 (CBM35) and from 135 to 478, a catalytic module belonging to family 26 glycoside hydrolase (GH26). *Ct*ManT showed 50% sequence homology with GH26B mannanase of *Clostridium thermocellum* strain F1 (*CtF1*Man26B) (UniProt ID: Q9F1T9), 33% with *Bacillus licheniformis* DSM13 (*Bl*Man26B) (UniProt id: Q65MP4), 37% with *Paenibacillus* sp. BME-14 (*Ps*Man26B) (UniProt ID: C6KL35), 35% with *Cellvibrio japonicas* (*Cj*Man26B) (UniProt ID: Q840B9), 28% with GH26A mannanase of *Cellulomonas fimi* (*Cf*Man26A) (UniProt id: Q9XCV5) and 26% with *Bacillus* sp. JAMB750 (*Bs*Man26A) (UniProt id: Q2ACI1). Phylogenetic tree analysis showed that *Ct*ManT was found closely related to Man26B of *Clostridium thermocellum* strain F1 (Fig. 3.3.9). Multiple sequence alignment of *Ct*ManT displayed a unique identifier sequence that was highly conserved aromatic amino-acid-rich region with the consensus sequence WFWWG within all the ManGH26 family (Fig. 3.3.10, highlighted in a black box), as also similarly stated by Xiaoyu *et al.*, (2010).

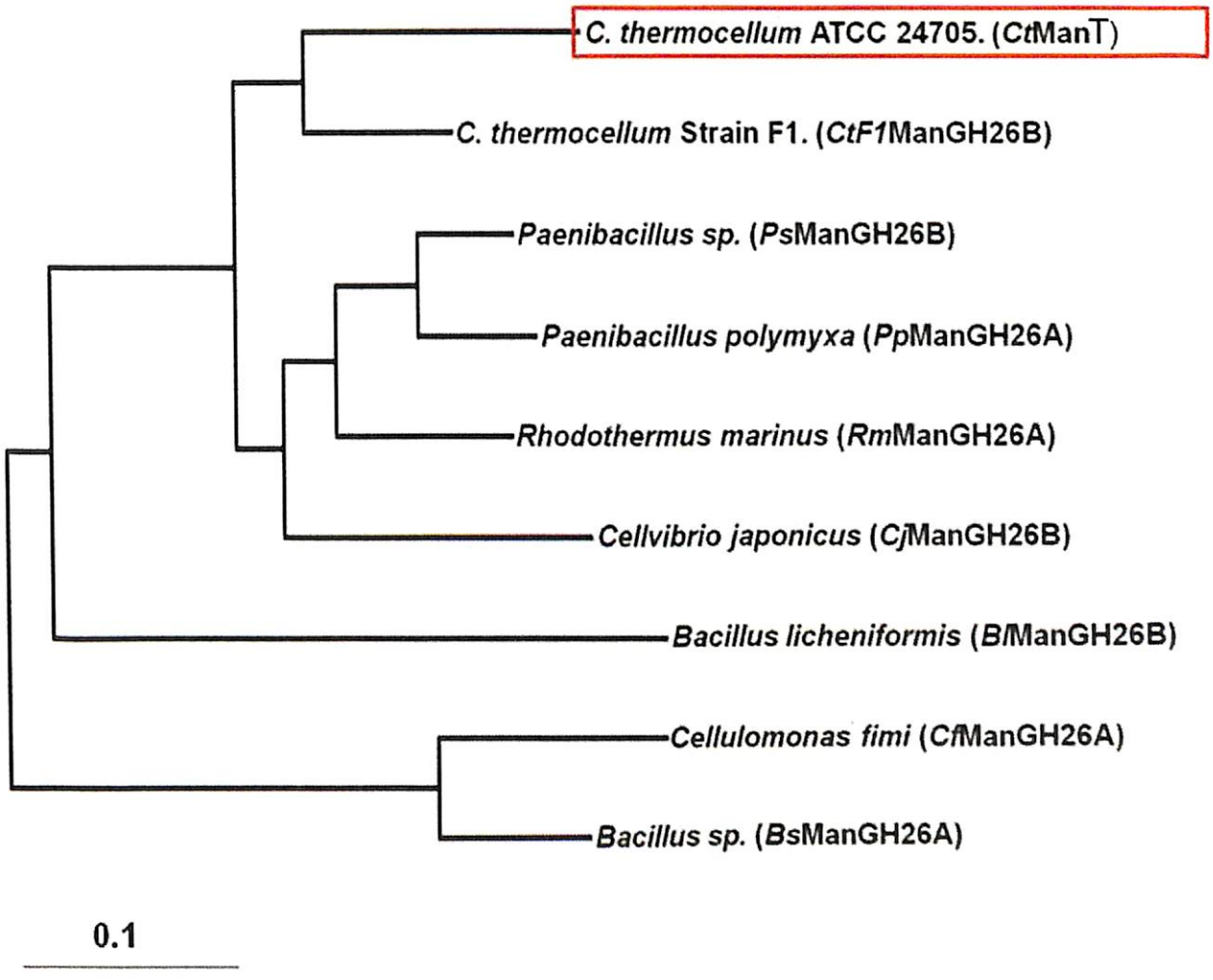

Fig. 3.3.9 Phylogenetic tree showing the comparative study of *Ct*ManT (highlighted in red box) with two different types of GH26 mannanase (Man26A and Man26B) of representative members *Clostridium thermocellum* strain F1 (*CtF1*Man26B), *Bacillus licheniformis* DSM13 (*Bl*Man26B), *Paenibacillus* sp. BME-14 (*Ps*Man26B), *Cellvibrio japonicas* (*Cj*Man26B), *Cellulomonas fimi* (*Cf*Man26A) and *Bacillus* sp. JAMB750 (*Bs*Man26A) and their appearance during evolution based on sequence similarity.

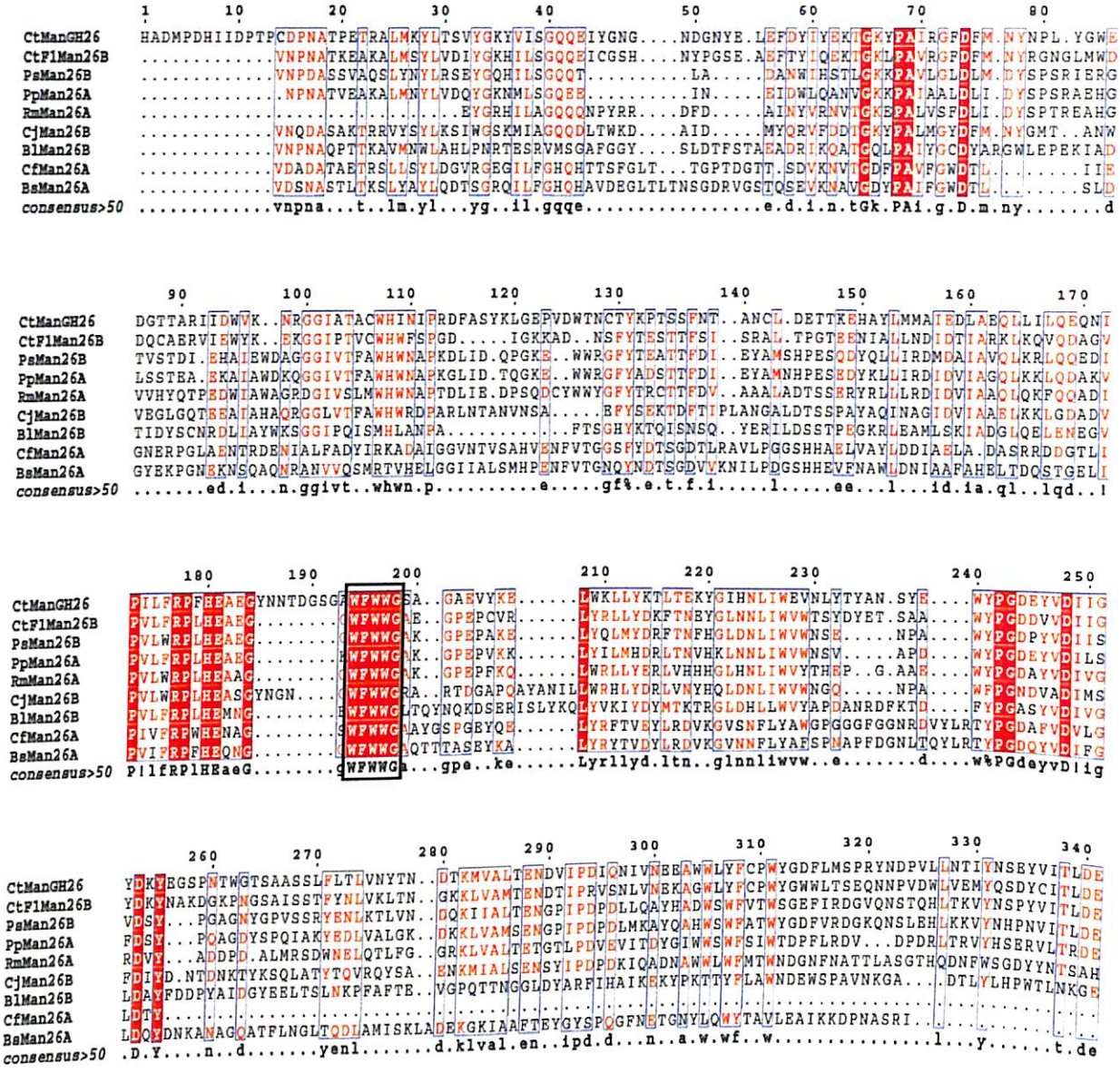

Fig. 3.3.10 Multiple sequence alignment of *Ct*ManT with the representative members having mannanase activity such as Man26A from *Cellulomonas fimi* (*Cf*Man26A) (UniProt ID: Q9XCV5) and *Bacillus* sp. JAMB750 (*Bs*Man26A) (UniProt ID: Q2ACI1), Paenibacillus polymyxa (*Pp*ManGH26A) (UniProt ID Q1A2D0), *Rhodothermus marinus* (*Rm*ManGH26A) (UniProt ID: P49425) and Man26B from *Clostridium thermocellum* strain F1 (*CtF1*Man26B) (UniProt ID: Q9F1T9), *Bacillus licheniformis* DSM13 (BlMan26B) (UniProt ID: Q65MP4), *Paenibacillus* sp. BME-14 (*Ps*Man26B) (UniProt ID: C6KL35) and *Cellvibrio japonicas* (*Cj*Man26B) (UniProt ID: Q840B9). The highlighted sequence displayed in the black box represents the signature sequence (WFWWG) of GH26 family.

3.3.11.2 Homology modeling and structure validation of CtManT

The top of closest structural hit of homolog protein was obtained from BLASTp (http://blast.ncbi.nlm.nih.gov/)against the PDB database. The total query coverage and maximum identity recommended a crystal structure of *Podospora anserina* (PDB ID: 3ZM8) (99% query coverage, 36% identity) was the best template for homology modelling. Structure similarity search in DALI server (http://ekhidna.biocenter.helsinki.fi/dali_server/start) displayed that the model structure of *Ct*ManT is close to *Podospora anserine* (PDB ID: 3ZM8), *Cellvibrio japonicas* (PDB ID:2VX4) and *Cellulomanas fimi* (PDB ID: 2BVT) with root mean square deviation (R.M.S.D) of 1.2, 2.3 and 2.6 Å, respectively, over the 300 amino acids of C^{α} main chain. The structural validation of final modelled *Ct*ManT using Ramachandran plot (Fig. 3.3.11A) displayed 84.3% amino acid residues lying in the most favourable region, 13.7% in additionally allowed, 1.7% in generously allowed and single amino acid residue in disallowed regions. This implies that the structure-backbone dihedral angles, phi (φ) and psi (ψ) were occupied in the acceptable region. PROSA web indicated that the modelled *Ct*ManT was error free and inhabited within the acceptable NMR zone with Z-score of -6.17 (Fig. 3.3.11B). Errat plot analysis showed most of the residues lie below 95% and overall structure quality factor was more than 96% (Fig. 3.3.11C). Furthermore, native protein fold evaluation of modelled *Ct*ManT using the knowledge-based energy profile of PROSAII program showed all the residues came below the zero baseline of energy profile (Fig. 3.3.12A). Verify3D result depicted that more than 90% amino acid residues have average 3D-1D profile score greater than 0.22 assuring the good quality of modeled structure (Fig. 3.3.12B).

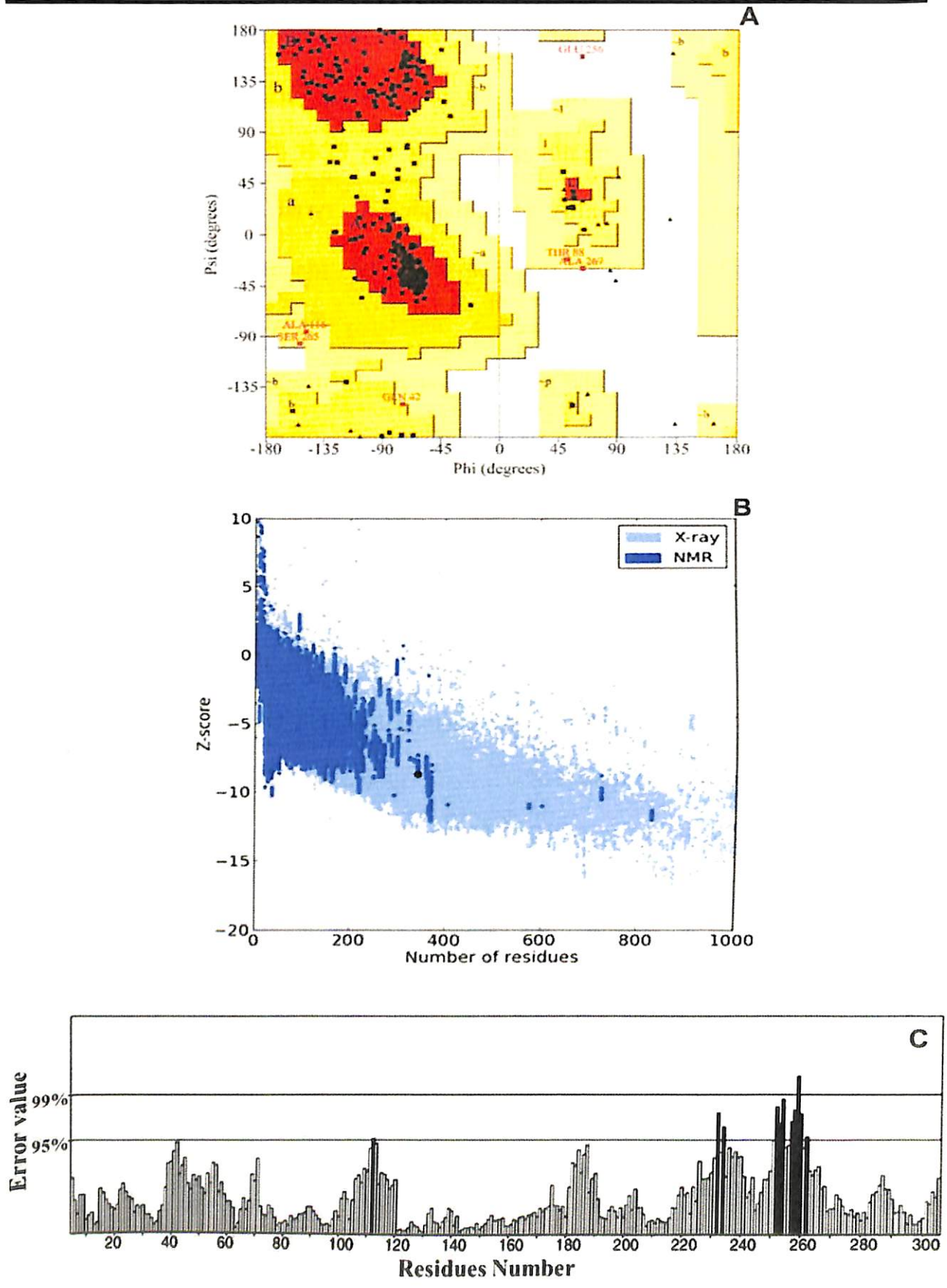

Fig. 3.3.11 Structure validation and quality assessment of *Ct*Man26A by (A) Ramachandran plot (B) ProSA web server (C) Errat plot.

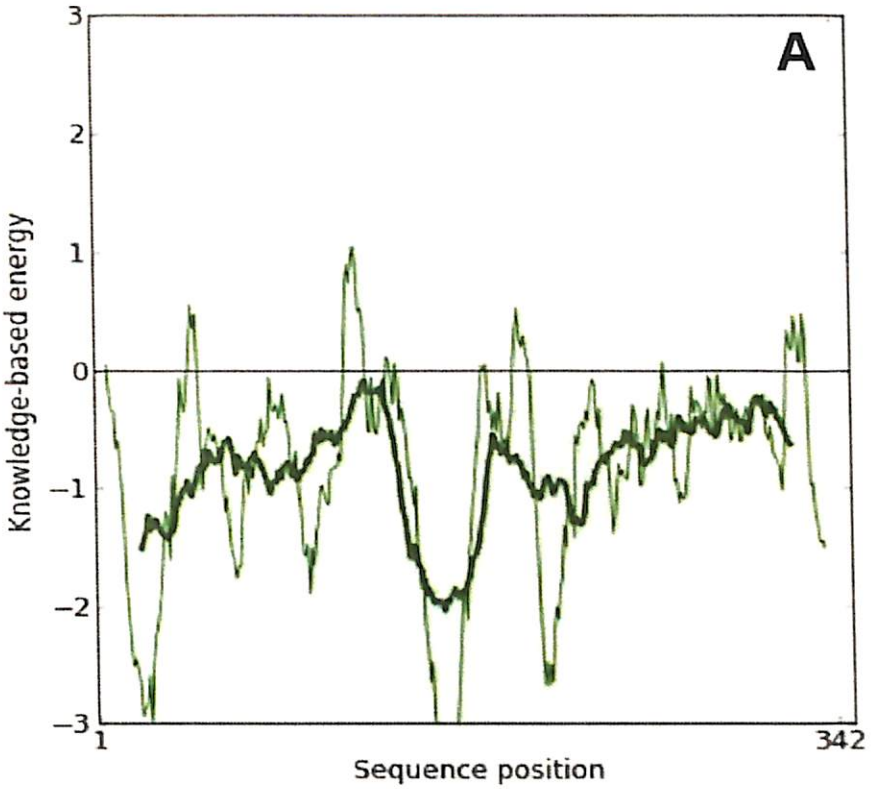

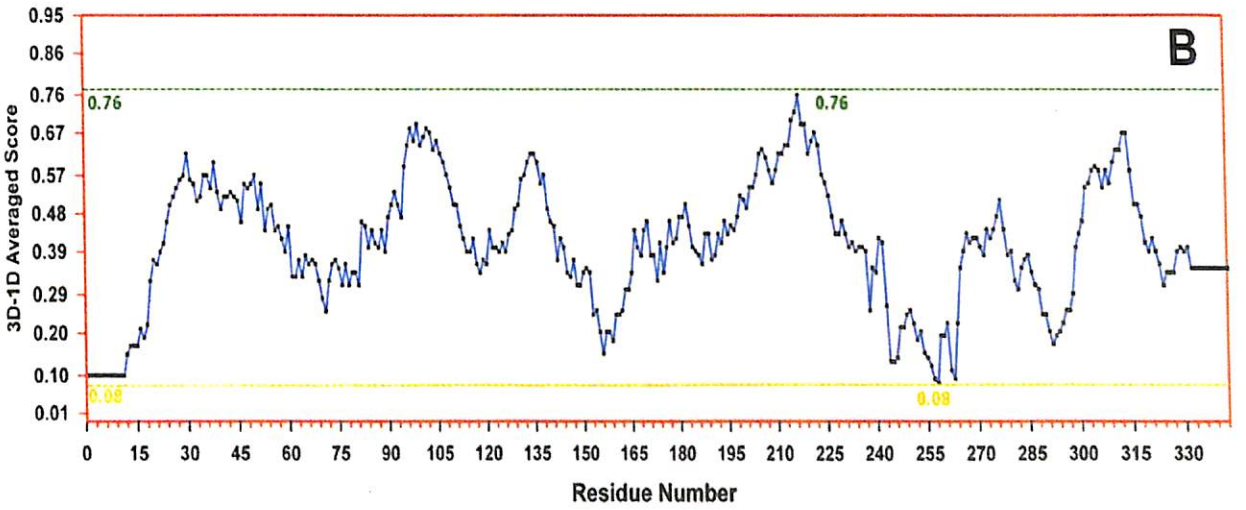

Fig. 3.3.12 (A) PROSAII energy profile showing the amino acid residues of the predicted *Ct*ManT lying predominantly under zero base line. (B) *Ct*ManT was verified using verify 3D server showed more than 90% amino acid residues have average 3D-1D profile score greater than 0.22 indicating that the residues are reasonably folded.

3.3.11.3 Substrate binding pocket and active site residues of CtManT

Three dimensional structure of *Ct*ManT showed the common $(\beta/\alpha)_8$ "TIM" barrel folding motif characteristic of GH-A clan of glycoside hydrolase families. The modelled structure of *Ct*ManT contained 8 encircled β-stands (β_1-β_8) surrounded by 8 α-helixes (Fig. 3.3.13A). Topology diagram displayed the overall 2D arrangement of secondary structure of *Ct*ManT which comprised of 8 loops assigned as loop1 (Ile44-Glu54), loop2 (Met76-Gly87), loop3 (His108-Asn138), loop4 (Pro178-Trp197), loop5 (Ile226-Try232), loop6 (Asp253-Ala266), loop7 (Lys286-Ile292) and loop8 (Lys306-Tyr321) (Fig. 3.3.13B). *Ct*ManT clearly showed remarkable structural differences from the other structurally characterized bacterial origin GH26 mannanase. It showed more similarity towards the fungal mannanase in terms of structure and folds. The structure showed the loops connecting a side of active site of binding pocket (loop 2,3,4 and 5) were relatively longer (especially loop3) as compared with loops present on the other site (loop 1, 6, 7 and 8) of binding cavity. These prolonged loops certainly provide flexibility and subtleties to the active site binding pocket which might influence the function and helps enzyme to accommodate polymeric substrate of variable degrees of polymerization and length. The available sequences of mannanases of GH26 from PDB database such as *Podospora anserine* (PDB ID: 3ZM8), *B. subtilis*, (PDB ID: 2WHK), *B. subtilis* (PDB ID: 2QHA), *C. fimi* (PDB ID: 2BVT), *C. japonicus* (PDB ID: 1GVY) and *C. japonicus* (PDB ID: 2VX4) were aligned with *Ct*ManT sequence using multiple sequence alignment (MSA). The MSA of β-mannanase and exo-β-mannanase of GH26 showed that the acid/base catalytic residues Ala and Glu (marked as star) were conserved (except in *C. japonicus*), while the catalytic nucleophiles were not conserved within the family, and

the catalytic nucleophiles were not conserved within the family, and were located at different places (Fig. 3.3.14). The MSA showed a signature sequence WFWWG conserved within GH26 mannanase. *Ct*ManT contains 8 α-helices and 8 β-sheets and 8 small incomplete helix like structures (η1- η8) which might be involved in the loop formation (Fig. 3.3.14).

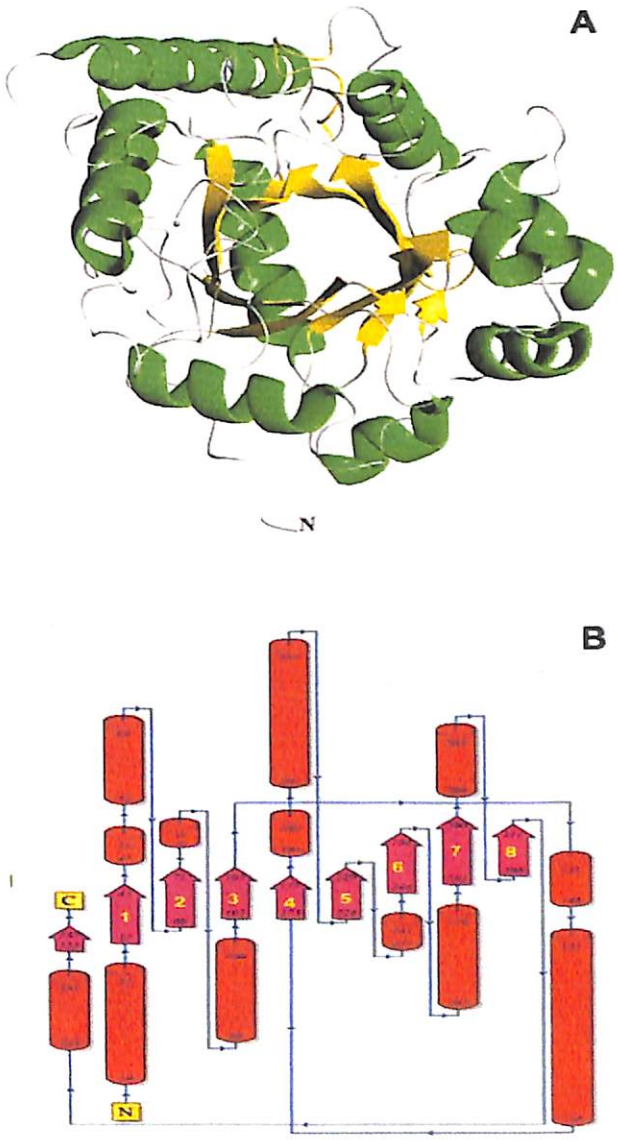

Fig. 3.3.13 The overall structural representation of *Ct*ManT by **(A)** Cartoon representation of 3-D modeled *Ct*ManT shows "TIM barrel" $(\beta/\alpha)_8$ barrel fold structure with encircled β-sheets (yellow color) surrounded by α-helix (green color). **(B)** Topology diagram of *Ct*ManT depicting the organization of secondary structure elements.

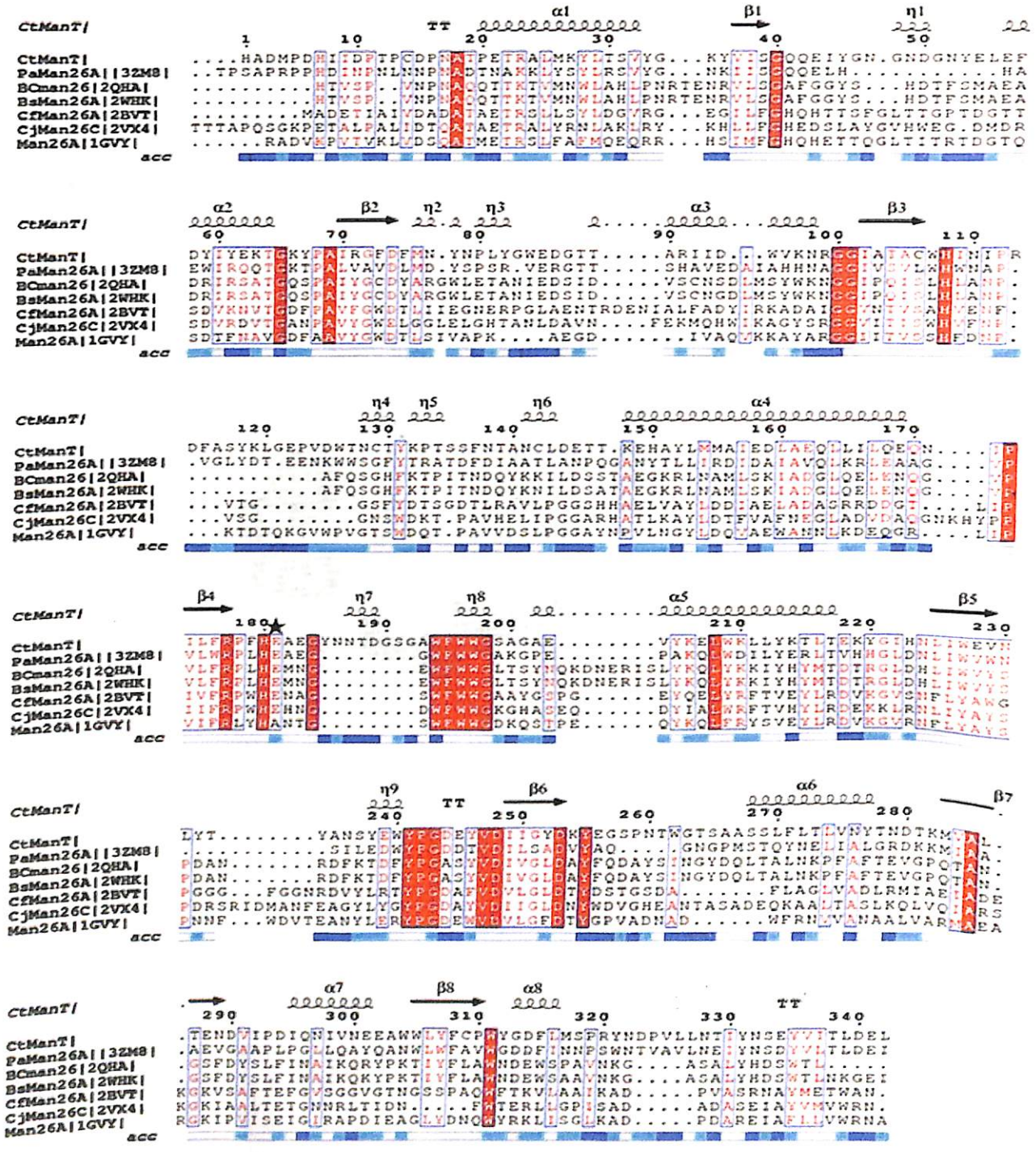

Fig. 3.3.14 Multiple sequence alignment of target (*Ct*ManT with representative member of family GH26 mannanase *viz. Pa*Man26A (PDB id: 3ZM8), *Bs*Man26 (PDB id: 2QHA), *Bs*Man26 (PDB ID: 2WHK), *Cf*Man26 (PDB ID: 2BVT), Man26 (PDB ID: 1GVY) and *Cj*Man26C (PDB ID: 2VX4). The relative surface accessibility at the bottom of sequence alignment displayed with white, cyan and blue colour bands are for buried, intermediate and accessible amino acid residues, respectively. This figure was produced using ESPript3. The catalytic residues are marked with star symbol.

To identify the key active site residues, *Ct*ManT was superimposed with closely related structure of *Pa*Man26A (PDB ID 3ZM8). The results showed that the active site residue Glu181 of *Ct*ManT act as acid/base and corresponds to Glu300 of *Pa*Man26A. The residue Glu288 of *Ct*ManT matched with Glu390 of *Pa*Man26A which acts as a nucleophile (Fig. 3.3.15A and 3.3.15B). The catalytic residue Glu181 situated at the center core in the middle of loop 4 whereas, Glu288 is positioned in the catalytic core, loop 7, and both these residues were 5.8 Å apart (Fig. 3.3.15B). The overall reaction mechanism of *Ct*ManT follows the retention of anomeric configuration through a covalent glycosyl intermediate (Fig. 3.3.15C).

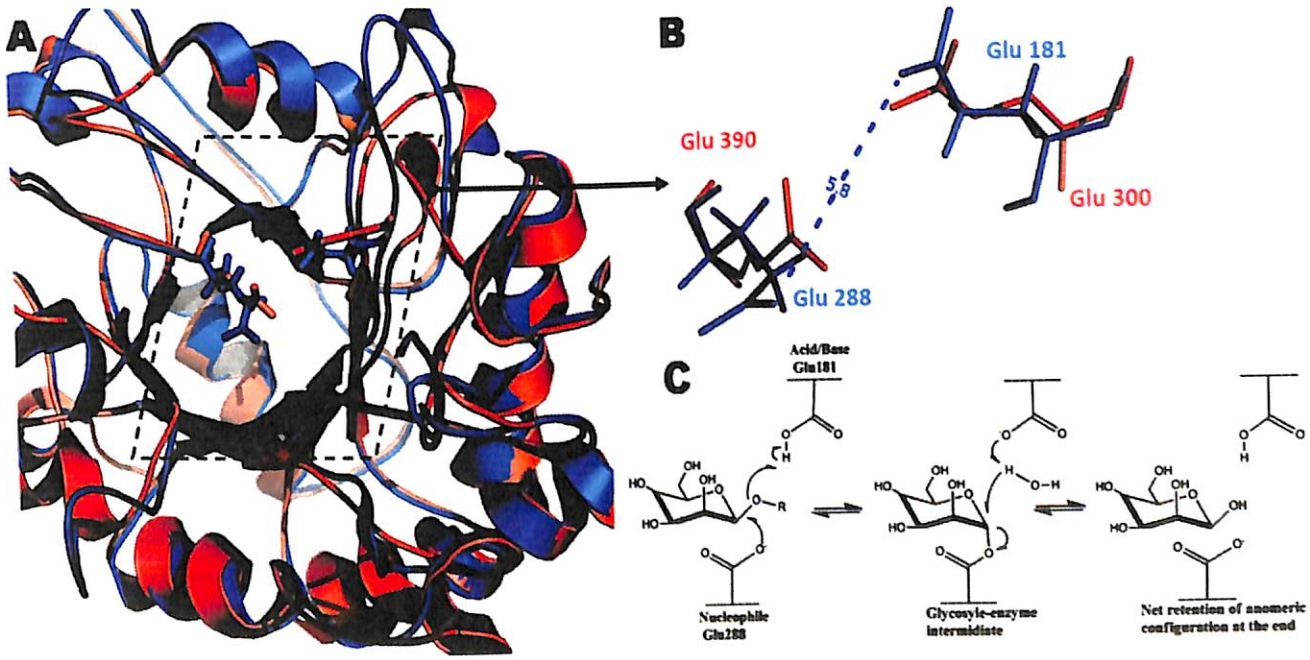

Fig. 3.3.15 (A) Superimposed 3-D structure of *Ct*ManT (purple) with *Pa*Man26A of *Podospora anserine*, PDB id: 3ZM8 (blue) proteins showing the similarity and differences in the structure and folds along with the position of active site residues at the catalytic core. (B) Enlarged view of overlayed catalytic residues (stick view) Glu181 (catalytic acid/base) corresponding to Glu300 and Glu288 (catalytic nucleophile) to Glu390 of *Pa*Man26A. (C) Schematic depiction of proposed catalytic mechanism for *Ct*ManT which follows net retention of anomeric configuration of active site residues through covalent glycosyl-enzyme intermediate.

3.3.11.4 Docking analysis with manno-configured ligands and subsite mapping of CtManT

Molecular docking of different manno-configured ligands (from mannobiose to mannohexose as well as galactomannan) into the active site of *Ct*ManT was carried out in order to understand the role of aromatic and hydrophobic residues in the binding site cavity. The results of docking are summarized in Table 3.3.6. The results showed that free energy of binding (-ΔG) increased concomitantly with the increase in molecular size of ligand (mannobiose to mannopentose). This represented the stable nature of substrate binding subsites present across the active site region of *Ct*ManT. The ability to accommodate larger ligand molecule in the active site of *Ct*ManT is probably due to the long loops enclosing the active site and providing the depth to the cavity. The solvent accessible surface view of *Ct*ManT complex with ligand mannopentaose showed broad saddle-shaped, open active center core (Fig. 3.3.16A). This allows the interaction with internal region of sugar rings of oligosaccharides (endo-acting), reported also for other endo-β-mannanases from family 26 GH (Le *et al.*, 2005; Cartmell *et al.*, 2008). In contrast, *Bc*Man displayed shallow-disc shaped binding pocket (Yan *et al.*, 2008). *Ct*ManT in association with ligand mannopentaose displayed significant polar and hydrophobic interactions with active site residues along with aromatic and hydrophobic residues (Fig. 3.3.16B). The aromatic residues created the overall binding site cavity as well as stabilizing the mannopyranose ring of oligosaccharides.

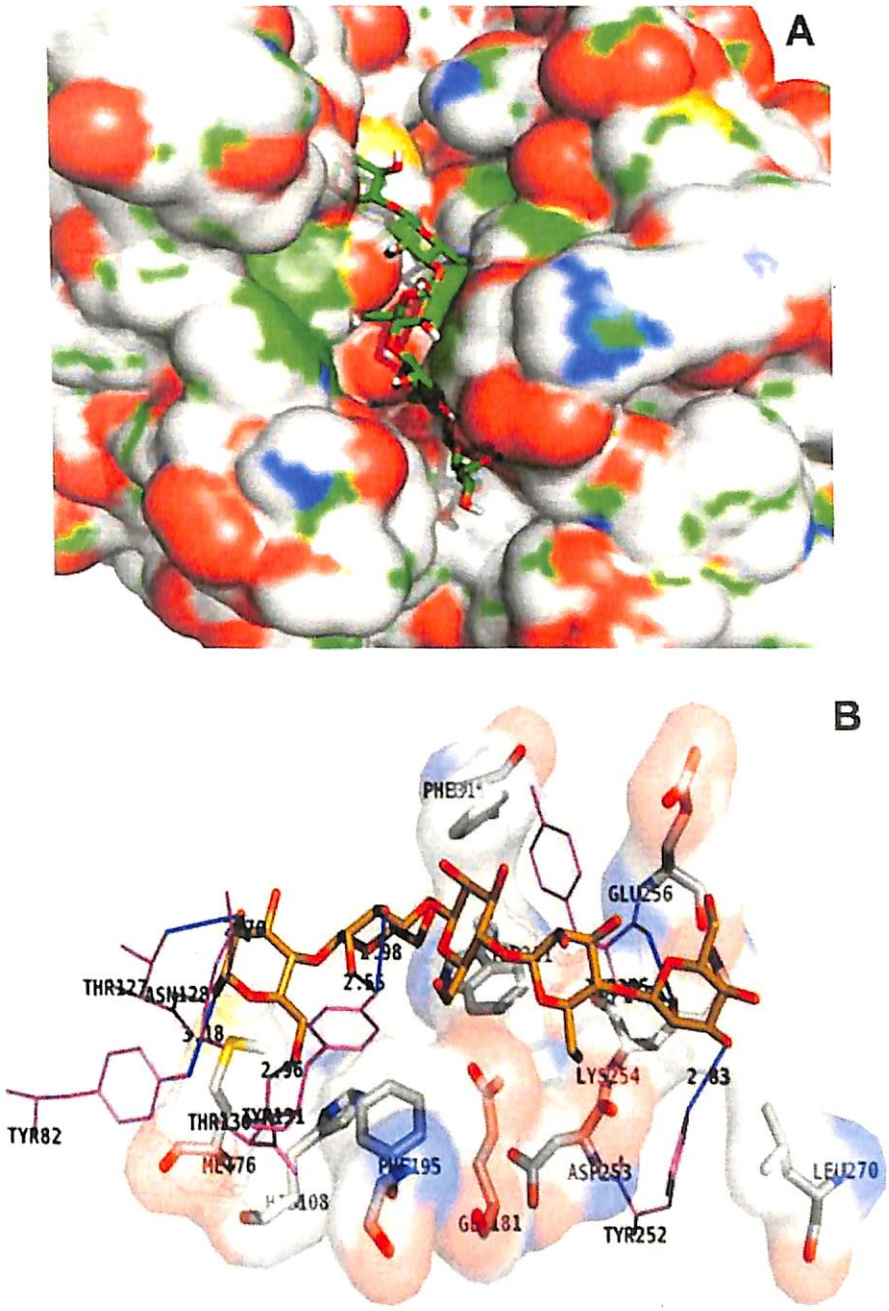

Fig. 3.3.16 (A) Top view of solvent-accessible surface of the substrate binding region of *Ct*ManT showing broad saddle-shaped, open active site cavity along with ligand mannopentaose (B) Docked view of ligand mannopentaose interacting with active site amino acid residues of *Ct*ManT. Residues present at the active site of *Ct*ManT are making hydrophobic interaction (surface view) with mannopentaose and residues involved in hydrogen bonding are represented in magenta colour.

Table 3.3.6 Amino acid residue interactions of *Ct*ManT with manno-configured ligands.

Ligand	(ΔG) (kcal/mol)	Polar interactions	Residue within 4Å region
Mannobiose	-6.84	Tyr312,Trp311, Tyr131, Glu181, Thr130, Asn128, Thr127,Tyr82, His108.	Asp74, Glu288, His180, Phe195, Met76.
Mannotriose	-3.17	Tyr312, Glu181, Trp311, Thr130, Tyr131, Thr127.	Phe315, Tyr255, Phe195, Asn128, Met76, His108, Tyr82.
Mannotetraose	-7.97	Trp311,Tyr255, Asp253,Tyr185, Glu181, Tyr131, Thr130, His108.	Tyr312, Phe315, Lys254, Tyr252, Glu183, Gly184, Phe195, Met76.
Mannopentaose	-8.68	Tyr252, Tyr131, Thr130, Glu256, Tyr255.	Tyr82, Met76, Tyr312, Trp311, Phe315, His108, Asp253, Lys254, Leu270, Tyr185, Glu181, Trp197, Phe195, Asn128, Thr127, Tyr255
Mannohexaose	-8.60	Tyr252, Tyr312, Asp253,His108, Tyr185, Asn128, Thr127.	Trp311, Phe315, Met76, Lys254, Glu183, Gly184, Glu181, Trp194, Phe195, Thr130, Tyr131.
Galactomannan	-3.85	Tyr255, Glu288, Trp311, Glu181, His108.	Trp185, Gly184, Trp194, Phe315, Tyr131, Tyr312, Phe315, His180.

The analysis of ligand bound complex of *Ct*ManT obtained from the docking and the structure superimposition with the ligand bound homolog protein are shown in Fig. 3.3.17A. The products obtained from the hydrolysis of galactomannan are shown in Fig. 3.3.17B. *Ct*ManT contains six galactomannan binding subsite that comprises two aglycone site (reducing end, +1 and +2) and four glycone site (-1 to -4) with binding energy -3.85 kcal/mol. The structure superimposition of galactomannan (Gal2Man4) bound *Ct*ManT with galactomannan (Gal2Man4) bound *Cj*Man26C (PDB ID: 2VX6) were used to map the subsite positions and nearby key residues.

Subsite mapping displayed many hydrophobic and aromatic residues along with acid residues at the catalytic core of *Ct*ManT (in purple) *viz.* Trp311, His108, Glu228, His180, Phe195, Glu181, Tyr255, Trp194 occupied the invariant position which corresponded with Trp373, His156, Glu338, His220, Phe227, Glu221, Tyr297 and Trp226, respectively of *Cj*Man26C (in blue) (Fig. 3.3.17A).

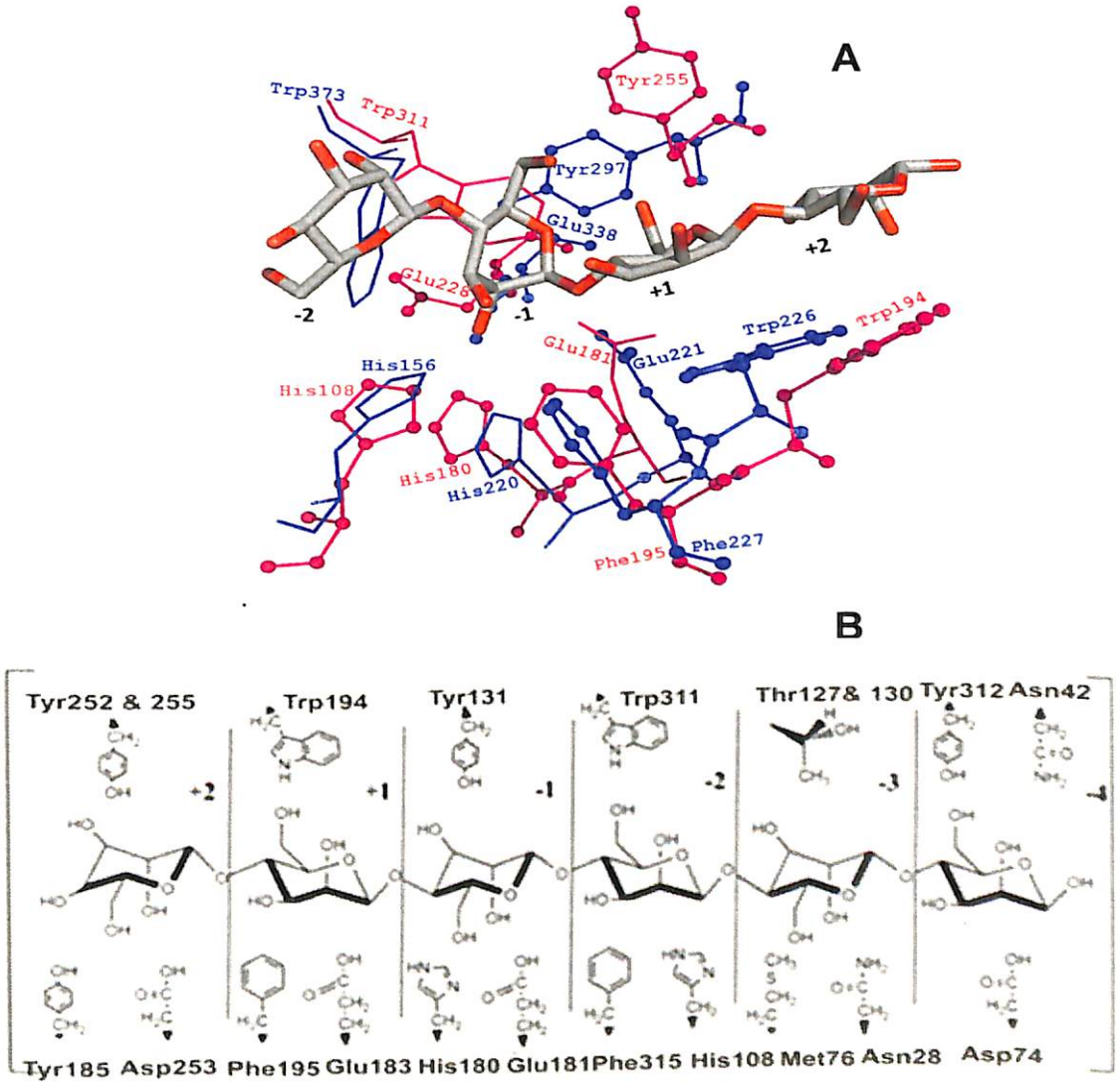

Fig. 3.3.17 (A) Superimposed structure of galactomannan bound *Ct*ManT with galactomannan bound *Cj*Man26C (PDB ID: 2VX6) showing sub-sites. Ligand in stick view (gray-red) occupied +2 to -2 sub-sites of *Ct*ManT and *Cj*Man26C. The key conserved residues of *Ct*ManT (magenta colour) and *Cj*Man26C (blue colour), are forming the sub-site and showing significant interaction with galactomannan. (B) Schematic presentation of amino acid residues of *Ct*ManT involved in formation of substrate binding sub-sites.

The proposed key residues which constitute a different subsite of *Ct*ManT are shown in the Fig. 3.3.17B. Furthermore, all these residues were found to be involved in hydrogen bonding or in the hydrophobic interaction during the docking analysis. Molecular docking study with manno-configured ligands suggested wide binding site pocket accommodating larger oligosaccharides with higher affinity. This might be facilitating in the release of oligosaccharides after the cleavage of β-(1→4)-linkage of galactomannan.

3.4 Conclusions

The modules *Ct*Manf and *Ct*ManT showed mannan specific substrate specificity. Both displayed maximum activity against carob galactomannan followed by locust bean galactomannan, guar galactomannan, ivory nut mannan and mannan. Interestingly, both *Ct*Manf and *Ct*ManT displayed low but observable activity against barley β-glucan, lichenan, carboxymethyl cellulose, hydroxyethyl cellulose, avicel and xyloglucan signifying their multisubstrate specificity. The catalytic modules were unable to act upon synthetic substrates such as *p*NP-β-D-mannopyranoside and *p*NP-α-D-mannopyranoside which ruled out any exo-activity. Therefore, it was concluded that both *Ct*Manf and *Ct*ManT act as endo-β-mannanases. In addition the zymogram study of both the recombinant enzymes against carob galactomannan confirmed their endo acting nature. *Ct*Manf and *Ct*ManT exhibited maximum activity at pH 6.9 and 6.5 and at 60°C and 50°C, respectively. *Ct*Manf and *Ct*ManT displayed similar pH and thermal stability profiles. Both *Ct*Manf and *Ct*ManT were stable over a pH range 5.0-7.5 and 50-60°C.

The enzyme activity of *Ct*Manf and *Ct*ManT increased significantly by 1.5 fold by Ca^{2+} and Mg^{2+} ions. *Ct*Manf and *Ct*ManT retained observable activity at moderate concentrations of Mn^{2+}, Co^{2+} and Zn^{2+} ions. However, the enzyme activity was inhibited significantly by Cu^{2+}, Al^{3+} and Ni^{2+} ions and SDS at lower concentrations. The enzyme activity of *Ct*Manf and *Ct*ManT was sharply decreased by EGTA and EDTA. Urea and GnHCl at higher concentrations also inactivated significantly the enzyme activity of both enzymes.

Media composition played a significant role in production of recombinant *Ct*Manf and *Ct*ManT. Both *Ct*Manf and *Ct*ManT containing *E. coli* cells showed

maximum cell density and maximum protein concentration in TY medium as compared with TB, 5x LB and LB media. The rich source of tryptone, yeast extract and phosphate salts might have facilitated to achieve high cell densities in TY medium.

The protein-melting curves of full length protein *Ct*Manf showed that the catalytic module *Ct*ManT and carbohydrate binding module, CBM35 melt independently. The protein-melting peaks of *Ct*ManT and CBM35 shifted to higher temperature in the presence of Ca^{2+} ions. However, the addition of equimolar concentration of EDTA to the Ca^{2+} ion containing *Ct*Manf and *Ct*ManT, shifted back the melting temperature peaks to the original positions. This displayed that Ca^{2+} ions impart thermal stability to the protein structure.

The structure and functional aspects of *Ct*ManT was examined by generating a model by homology modelling and validated. The modelled *Ct*ManT displayed $(\beta/\alpha)_8$"TIM" barrel fold with extended loops around the active center that constructed the broader saddle-shaped, open active site cavity. The structure analysis showed that structure of *Ct*ManT is closer to the fungal mannanase as against other bacterial mannanases. *Ct*ManT is involved in retention mechanism where amino acid residue Glu181 act as a catalytic acid/base, while Glu288 act as a catalytic nucleophile. Molecular docking study with manno-configured ligands suggested a wide binding site pocket accommodating larger oligosaccharides with higher affinity. 3-D structure superimposition of modelled *Ct*ManT with *Cj*Man26A mannanase showed six potential subsite having two subsite towards a glycone whereas four subsite to glycon side for galactomannan.

References

Aboul-Enein, A., Abouelalla, F., Serour, E. and Hussien, T. (2010) Purification and characterization of a novel thermoactive cellulase from thermophilic actinomycetes isolated from soil sample of Egypt. J. Int. Acad. Res. 2:81-86.

Black, J.G. (1996) Microbiology: Principles and Applications. (3rd ed.), Prentice Hall, Upper Saddle River, New Jersey. 140-144 pp.

Bolam, D.N., Hughes, N., Virden, R., Lakey, J.H., Hazlewood, G.P., Henrissat, B., Braithwaite, K.L. and Gilbert, H.J. (1996) Mannanase A from *Pseudomonas fluorescens* ssp. *cellulosa* is a retaining glycosyl hydrolase in which E212 and E320 are the putative catalytic residues. Biochemistry. 35:16195-16204.

Boraston, A.B., Bolam, D.N., Gilbert, H.J. and Davies, G.J. (2004) Carbohydrate-binding modules: fine-tuning polysaccharide recognition. Biochem. J. 382:769-781.

Branden, C. and Tooze, J. (1991) In *Introduction to Protein Structure*, (2nd ed.), Garland publishing, Taylor and Francis Group, Ney York, NY.

Cartmell, A., Topakas, E., Ducros, V.M., Suits, M.D, Davies, G.J. and Gilbert, H.J. (2008) The *Cellvibrio japonicus* mannanase CjMan26C displays a unique exo-mode of action that is conferred by subtle changes to the distal region of the active site. J Biol Chem. 283(49): 34403-34413.

Cartmell, A., McKee, L.S., Peña, M.J., Larsbrink, J., Brumer, H., Kaneko, S., Ichinose, H., Lewis, R.J., Nielsen, A.V., Gilbert, H.J. and Wright, J.M. (2011) The structure and function of an arabinan-specific α-1,2-arabinofuranosidase identified from screening the activities of bacterial GH43 glycoside hydrolases. J. Biol. Chem. 286:15483-15495.

Couturier, M., Roussel, A., Rosengren. A., Leone, P., Stålbrand, H. and Berrin, J.G. (2013) Glycoside hydrolase families 5 and 26 β-(1,4)-mannanases from *Podospora anserina* reveal differences upon manno-oligosaccharide catalysis. J. Biol. Chem. 288:14624-14635.

Cserjan-Puschmann, M., Kramer, W., Duerrschmid, E., Striedner, G. and Bayer, K. (1999) Metabolic approaches for the optimisation of recombinant fermentation processes. Appl. Microbiol. Biotechnol. 53:43-50.

Creighton, T.E. (1992) In *Proteins: Structures and Molecular Properties*, (2nd ed.), Freeman, W. H. & Company, Macmillan Higher Education, Ney York, NY.

Dvortsov, I.A., Lunina, N.A., Chekanovskaya, L.A., Schwarz, W.H., Zverlov, V.V. and Velikodvorskaya, G.A. (2009) Carbohydrate-binding properties of a separately folding protein module from beta-1,3-glucanase Lic16A of *Clostridium thermocellum.* Microbiology. 155:2442-2449.

Fierobe, H.P., Mingardon, F., Mechaly, A., Belaich, A., Rincon, M. T., Pagès, S., Lamed, R., Tardif, C., Bélaïch, J.P. and Bayer, E.A. (2005) Action of designer cellulosomes on homogeneous versus complex substrates: controlled incorporation of three distinct enzymes into a defined trifunctional scaffoldin. J. Biol. Chem. 280:1625-1634.

Fiser, A., Do, R.K. and Sali, A. (2000) Modeling of loops in protein structures. Prot. Sci. 9(9):1753-73.

Gomori, G. (2010) Handbook of Biochemistry and Molecular Biology. In Preparation of Buffers for Use in Enzyme Studies (eds. Lundblad, R.L. and MacDonald, F.M.), CRC Press, Taylor and Francis Group, LLC, USA, pp721–724.

Halstead, J.R., Vercoe, P.E., Gilbert, H.J., Davidson, K. and Hazlewood, G.P.A. (1999) family 26 mannanase produced by *Clostridium thermocellum* as a component of the cellulosome contains a domain which is conserved in mannanases from anaerobic fungi. Microbiology. 145:3101-3108.

Hogg, D., Pell, G., Dupree, P., Goubet, F., Martin-Oru, S.M., Armand, S. and Gilbert H.J. (2003) The modular architecture of *Cellvibrio japonicus* mannanases in glycoside hydrolase families 5 and 26 points to differences in their role in mannan degradation. Biochem. J. 371:1027-1043.

Huang, J.L., Bao, L.X., Zou, H.Y., Che, S.G. and Wang, G.X. (2012) High-level production of a cold-active β-mannanase from *Bacillus subtilis* BS5 and its molecular cloning and expression. Mol. Gen. Mikrobiol. Virusol. 4:14-27.

Holm, L. and Rosenstrom, P. (2010) Dali server: conservation mapping in 3D. Nucleic Acids Res. 38: 545-549.

Huey R, Morris, G.M, Olson, A.J, Goodsell, D.S (2007) A semiempirical free energy force field with charge-based desolvation. J. Comput. Chem. 28(6): 1145-1152.

Kurokawa, J., Hemjinda, E., Arai, T., Karita, S., Kimura, T., Sakka, K. and Ohmiya, K. (2001) Sequence of the *Clostridium thermocellum* mannanase gene man26B and characterization of the translated product. Biosci. Biotechnol. Biochem. 65:548-554.

Laemmli, U.K. (1970) Cleavage of structural proteins during the assembly of the head of Bacteriophage T4. Nature. 227:680-685.

Le, N.J, Anderson, L., Stoll, D., Stålbrand, H. and Lo-Leggio, L. (2005) The structure and characterization of a modular endo-beta-1,4-mannanase from *Cellulomonas fimi*. Biochemistry. 44(38): 12700-12708.

Lim, H.K. and Jung, K.H. (1998) Improvement of heterologous protein productivity by controlling post induction specific growth rate in recombinant *Escherichia coli* under control of the PL promoter. Biotechnol. Prog. 14:548-553.

Mizutani, K., Fernandes, V.O., Karita, S., Luís, A. S., Sakka, M., Kimura, T., Jackson, A., Zhang, X., Fontes, C.M., Gilbert, H.J. and Sakka, K. (2012) Influence of a mannan binding family 32 carbohydrate binding module on the activity of the appended mannanase. Appl. Environ. Microbiol. 78:4781-4787.

Noorbatcha, I.A., Sultan, A.M., Azura, A. and Salleh, H.M. (2012) Molecular dynamics study of the effect of calcium ions on the thermostability of *Bacillus Amyloliquefaciens* phytase. Aust. J. Basic. App. Sci. 6:109-116.

Ruijssennars, H.J. and Hartmans, S. (2001) Plate screening method for the detection of polysaccharide- producing microorganisms. Appl. Microbiol. Biotechnol. 55:143-149.

Shoseyov, O., Shani, Z. and Levy, I. (2006) Carbohydrate binding modules: biochemical properties and novel applications. Microbiol. Mol. Biol. Rev. 70:283-295.

Songsiriritthigul, C., Buranabanyat, B., Haltrich, D. and Yamabhai, M. (2010) Efficient recombinant expression and secretion of a thermostable GH26 mannan endo-1,4-β-mannosidase from *Bacillus licheniformis* in *Escherichia coli*. Microb. Cell. Fact. 9(20):1-13.

Tailford, L.E., Ducros, V.M., Flint, J.E., Roberts, S.M, Morland, C., Zechel, D.L, Smith, N., Bjørnvad, M.E., Borchert, T.V., Wilson, K.S., Davies, G.J. and Gilbert, H.J. (209) Understanding how diverse beta-mannanases recognize heterogeneous substrates. Biochemistry, 48(29):7009-7018.

Thomsen, R. and Christensen, M.H. (2006) MolDock: a new technique for high-accuracy molecular docking. J. Med. Chem. 49:3315-3321.

Tripathi, N.K., Shrivastva, A., Biswal, K. C. and Rao, P.V.L. (2009) Optimization of culture medium for production of recombinant dengue protein in *Escherichia coli.* Ind. Biotechnol. 5:179-183.

Xiaoyu, F., Huang, X., Liu, P., Lin, L., Wu, G., Li, C., Feng, C. and Hong, Y. (2010) Cloning and characterization of a novel mannanase from *Paenibacillus sp.*BME-14. J. Microbiol. Biotechnol. 20:518-524.

Yoshikawa,Y., Hirata, R,, Yasui, H,, Hattorib, M. and Sakurai, H. (2009) Inhibitory effect of $CuSO_4$ on a-glucosidase activity in ddY mice. Metalomics. 2:67-73.

Yan, X.X, An, X.M, Gui, L.L. and Liang, D.C (2008) From structure to function: insights into the catalytic substrate specificity and thermostability displayed by *Bacillus subtilis* mannanase BCman. J. Mol. Biol. 379(3):535-544.

Zhang, J. and Greasham, R. (1999) Chemically defined media for commercial fermentations. Appl. Microbiol. Biotechnol. 51:407-421.

Chapter 4

In vitro and *in silico* analysis of ligand binding and stability of *Ct*CBM35 from *Clostridium thermocellum* ATCC 27405

4.1 Introduction

A major portion of plant carbohydrates is composed of hemicelluloses such as the polymer and oligomer of xylose, mannose, arabinose etc. apart from celluloses. Polysaccharide recognition, binding and enhanced catalysis of hydrolytic enzymes are truly facilitated by non catalytic modular carbohydrate binding modules (Mizutani *et al.*, 2012). The non catalytic carbohydrate binding module appended to a catalytic module either at their N- or C- terminals often are involved in enhancing the activity of the catalytic module and often have the same specificity for substrate as that of the catalytic module. Carbohydrate binding modules (CBMs) are classified into 67 distinguish families based on sequence similarity (http://www.cazy.org/Carbohydrate-Binding-Module). Family 35 carbohydrate binding module is often appended to glycoside hydrolase family 26 (GH26) and GH5 mannanases (Taylor *et al.*, 2011; Sunna, 2011; Bolam *et al.*, 2004), xylanases (GH30) (Valenzuela *et al.*, 2012) which significantly alter the polysaccharide specificity for plant cell wall polysaccharides such as galactomannan, glucomannan, mannan and glucouronoxylan. Three

dimensional structures of CBM35 family generally have the dominance of β-sheet secondary structures with a jelly roll topology (Valenzuela *et al.*, 2012). CBM35 usually accommodates the polysaccharides utilizing a planer surface of aromatic side chains which interact with the flat chains of manno-configured carbohydrate residues. This form of conformation is known as type B module (Valenzuela *et al.*, 2012). Polysaccharide binding significantly alters the conformation of CBM35 by changing the loop orientation containing amino acid residues which facilitate to create a suitable binding space for polysaccharide accommodation (Tunnicliffe *et al.*, 2005) Refinement of the CBM classification was improvised recently where Type A CBMs are those which can recognize the surface of the crystalline polysaccharides and Type B CBMs are classified according to their endo acting mode of action internally to glycan chains (Gilbert *et al.*, 2013). Type C CBMs are attributed by their exo-type binding either at the side chain or at the polysaccharide termini (Gilbert *et al.* 2013). Usually Type B CBMs are abundant in cellulases, xylanases and mannanases that bind to cellulose, xylan and mannan, respectively. Thus CBMs maintain the target substrate within the close proximity of their complete protein structures (Boraston *et al.*, 2004). Since the binding specificity depends on the polysaccharide complexity and side chain interactions of monosaccharide a variety of diverted binding may be observed. Thus the polysaccharide specificity varies due to chain substitution and orientation of monosaccharides (Mizutani *et al.*, 2012). In earlier study, it was attributed to role of divalent cations in alteration of the domain conformation of CBMs that enhance the higher polysaccharide specificity and thermostability (Hachem *et al.*, 2002). Thermostability one of the major concern of most of the enzyme stability and activity during industrial process and thus this binding module

may restore the potentialities of the hydrolytic enzymes. Moreover, carbohydrate binding modules are used in various analytical processes. Thermostable CBMs were explored to separate cello- and xylo-oligosaccharides based on their affinity towards these carbohydrates (Johansson *et al.*, 2006). CBM microarray technique is more effective which replaced the conventional DNA microarray (Ofir *et al.*, 2005). CBM microarrays were developed due to the limitations of using DNA microarrays for determining gene expression levels in proteomics. The quantity of mRNA in the cell often doesn't reflect the expression levels of the proteins they correspond to. Since it is usually the protein, rather than the mRNA, that has the functional role in cell response, a novel approach was needed. Additionally post-translational modifications, which are often critical for determining protein function, are not visible on DNA microarrays (Ofir *et al.*, 2005). This method is simple, effective and an alternative to various conventional microarray technologies (Ofir *et al.*, 2005). Moreover, substantial rise in effective enzyme catalysis process may induce by this carbohydrate binding module will meet the requirement for carbohydrate fermentation to most demanding biofuel (Jorgensen *et al.*, 2010).

The present study involves the functional and conformational properties of CBM35 from *Clostridium thermocellum* ATCC 27405 termed as *Ct*CBM35. *Ct*CBM35 usually displays the specificity towards manno-configured polysaccharides. The affinity electrophoresis, fluorescence measurements and dynamic light scattering were employed to analyze both qualitative and quantitative binding of *Ct*BM35 with manno-configured polysaccharides. The structural characterization of *Ct*CBM35 by model prediction and ligand binding by docking analysis were also studied.

4.2 Materials and Methods

4.2.1 Reagents, chemicals and substrates

The ingredients for polyacrylamide gel electrophoresis *viz.* acrylamide, bisacrylamide, tris free base, glycine, bromophenol blue, β-mercaptoethanol and Coomassie Brilliant Blue R250 were obtained from Sigma-Aldrich Co. LLC, USA. Glycerol, methanol, concentrated hydrochloric acid and glacial acetic acid were supplied by Merck, India. Bradford reagent was purchased from Sigma-Aldrich Co. LLC, USA. Tween 20 and $CaCl_2$ were procured from Merck Limited, India. Oat spelt xylan was purchased from Sigma-Aldrich Co. LLC, USA. Carob galactomannan, konjac glucomannan, locust bean galactomannan, oligosaccharide mannotriose, , rye arabinoxylan, birchwood xylan, oatspelt xylan and glucouronoxylan, birchwood xylan and arabinan were obtained from Megazyme International, Ireland.

4.2.2 Expression and purification of recombinant *Ct*CBM35

The recombinant *Ct*CBM35 production was initiated by inoculating 50 µl of the *E. coli* BL21 (DE3) culture from glycerol stock into 5 ml of LB medium (pH 7.2) supplemented with 50 µg/ml kanamycin and incubated at 37°C and 180 rpm for 12 h. The expression and purification of *Ct*CBM35 was carried out as described in Chapter 2, Section 2.2.21.

4.2.3 Quantitative binding analysis of *Ct*CBM35 against soluble polysaccharides

4.2.3.1 Binding assay of family 35 Carbohydrate Binding Module (CtCBM35)

The polysaccharide binding capability of non-catalytic *Ct*CBM35 was determined by visualizing the retardation of migration of protein in soluble polysaccharides containing native polyacrylamide gels against no retardation of protein in the gel without the polysaccharide (Takeo, 1984). The purified *Ct*CBM35

(18 µg) was run with 1% (w/v) soluble polysaccharides such as carob galactomannan, konjac glucomannan, carboxymethyl cellulose, rye arabinoxylan, birchwood xylan, oatspelt xylan, glucuronoxylan and oligosaccharide mannotriose in the native gels for qualitative binding analysis. The polysaccharide samples were prepared as described in the following Section 4.2.3.2. Binding study of *Ct*CBM35 with carob galactomannan and konjac glucomannan was carried out in absence and presence of Ca^{2+} ions. 10 mM Ca^{2+} ion was incorporated in 7.5% native polyacrylamide gel before *Ct*CBM35 electrophoresis. In absence of Ca^{2+} ions 7.5% native gels were prepared as control and the relative mobilities of *Ct*CBM35 were calculated.

4.2.3.2 Preparation and running of native-PAGE with soluble polysaccharides

Binding of *Ct*CBM35 to soluble polysaccharides was evaluated by affinity electrophoresis following the protocol of Takeo, (1984) on native-PAGE in absence and presence of varying amount of polysaccharide. The native gel was prepared using stock solutions *viz.* 30% (w/v) acrylamide solution, 1.0 % (w/v) polysaccharide, 1M Tris-HCl (pH 8.8), 50% (v/v) glycerol, 10% (w/v) ammonium per sulfate and TEMED as described for SDS-PAGE in Chapter 2, Section 2.2.20. The only difference in native-PAGE was the absence of SDS in resolving gel and running buffer. So, 7.5% resolving (native) gel was prepared by following the protocol described in Chapter 2, Section 2.2.20 without SDS. 1.0% (w/v) stock solution of polysaccharides was made by dissolving in sterile deionized water by slightly warming until a clear solution was obtained. Thereafter, necessary aliquot of ligand solution (from 1.0 %, w/v stock) was added to the resolving gel prior to the polymerization to make gels containing varying concentration of polysaccharides. The remaining components of native-PAGE, described above were added and the gel

was polymerized. Bovine serum albumin (BSA) (10 µg) was loaded on the gels as an internal standard for reference. Electrophoresis was carried out for 2-4h at 4°C in a Mini PROTEAN Tetra pack (Bio-Rad, USA) at a constant current of 20 mA. The gels were stained with Coomassie Brilliant Blue R250 (Sigma) and destained as described in Chapter 2, Section 2.2.20.6 to detect the protein. Qualitative binding of the *Ct*CBM35 was assessed visually on 7.5% native-PAGE. Quantitative analysis of polysaccharide binding was assessed by measuring the migration distance of *Ct*CBM35 for calculating the equilibrium association constant (K_a) as described in Section 4.2.3.5. Relative mobility for *Ct*CBM35 was calculated as the migration distance of native protein divided by the migration distance of bromophenol blue dye front as described earlier by Takeo, (1984).

4.2.3.3 Preparation of native-PAGE running buffer

The native-PAGE buffer was prepared using components as described in Table 4.2.1. The native-PAGE running buffer did not contain SDS as a component unlike SDS-PAGE running buffer but the final pH was same (pH 8.3). A 5x stock of running buffer was prepared and diluted to 1x before use (Table 4.2.1).

Table 4.2.1 Composition of 5x native-PAGE running buffer.

Components	Final concentration (5x buffer)
Tris base	0.125 M
Glycine	1.25 M

4.2.3.4 Preparation of sample buffer

A 5x sample loading buffer was prepared by dissolving the components maintaining the concentration of components as described in Table 4.2.2 and pH of the buffer was adjusted to 6.8. The components were dissolved in the order as

mentioned in Table 4.2.2 to make 5x sample buffer. However, the final concentration while loading to a native-PAGE gel was always kept to 1x by mixing 4 volumes of sample (protein) with 1 volume of 5x sample buffer.

Table 4.2.2 Composition of 5x sample loading buffer (Laemmli, 1970).

Components	Final concentration (5x buffer)
Tris-HCl (pH 6.8)	62.5 mM
Glycerol	20.0 (%,v/v)
Bromophenol Blue	0.025 (%, w/v)

4.2.3.5 Calculation of equilibrium association constant from affinity electrophoresis

The equilibrium association constant values were calculated by method described earlier by Tomme *et al.* (2000). The interaction of CBM with a polysaccharide can be expressed in Eq. (1) and (2):

$$P + L \leftrightarrow PL \quad (1)$$

$$K_a = [PL]/[P][L] \quad (2)$$

where, P and L are free CBM and polysaccharide (ligand), respectively, PL is the complex and [P], [L], and [PL] are their respective concentrations. K_a is the equilibrium association constant for the interaction. The expressions for the mole fractions of the *Ct*CBM35 in the free (X_P) and complexed form (X_{PL}) are given as:

$$X_{PL} = K_a [L]/[Q] \quad (3)$$

Where, [Q] is the partition function, given as

$$Q = 1 + K_a [Q] \quad (4)$$

The mobility of a *Ct*CBM35 relative to the standard can be expressed as:

$$R = X_P R_P + X_{PL} R_{PL} \quad (5)$$

where, R is the relative mobility of *Ct*CBM35 at a given concentration of polysaccharide (R= mobility of the polypeptide (mm)/mobility of the reference (mm), R_P is the relative mobility of *Ct*CBM35 in the absence of the polysaccharide, and R_{PL} is the relative mobility of *Ct*CBM35 in the presence of polysaccharide. Substitution of Eq. (3a), (3b), and (4) into Eq. (5) gives:

$$R = (R_P + R_{PL} K_a [L]/(1 + K_a[L] \quad (6)$$

Eq. (6) can be used to regression analysis K_a and R_{PL} from affinity data plotted as the relative mobility of *Ct*CBM35 vs. the polysaccharide concentration. R_P is set as a constant equal to the relative mobility of *Ct*CBM35 in the absence of polysaccharide. Normalizing the initial relative mobility in the absence of polysaccharide to 1.0, changes the Eq. (6) to

$$R = (1 + R_M K_a [L]) / (1 + K_a [L]) \quad (7)$$

where, R_R ($R_R = R/R_P$) is the relative mobility normalized to the initial relative mobility in the absence of polysaccharide. R_M ($R_M = R_{PL}/R_P$) is the relative mobility of *Ct*CBM35 fully complexed with polysaccharide normalized to the relative mobility in the absence of polysaccharide. Eq. 7 can be used for regression analysis using K_a and R_M from affinity data plotted as R_R of *Ct*CBM35 against the polysaccharide concentration.

4.2.4 Binding analysis of *Ct*CBM35 with insoluble polysaccharide

Qualitative binding analysis of *Ct*CBM35 with insoluble polysaccharide was carried out by taking 30.0 µg of protein in 50 mM Tris-HCl buffer (pH 7.5) containing 0.05% (v/v) Tween 20 and 5.0 mM $CaCl_2$ and mixed with 1.0 mg of insoluble mannan or ivory nut mannan and keeping the final reaction volume 200 µl

(Carvalho *et al.*, 2004). This reaction mixture was shaken on a vortex (Vibrax VXR B, IKA) continuously at 4°C for 2h. The mixture was centrifuged at 13000***g*** and at 4°C for 5 min. The supernatant containing the unbound fraction was removed and its protein content was determined by Bradford method as described in Chapter 2, Section 2.2.22 (Bradford, 1976). The pellet comprising precipitated insoluble polysaccharide and the bound protein was washed three times with 200 µl of buffer (50.0 mM Tris-HCl, pH 7.5). It was re-suspended in 200 µl of 10% (w/v) SDS containing 10% (w/v) β-mercaptoethanol and boiled for 10 min. The protein samples were dissolved in denaturing 1x sample buffer (Chapter 2, Section 2.2.20.5) and boiled the samples in a water bath for 5 min before loading into the SDS-PAGE gel. The bound protein fractions from the pellet and unbound protein in supernatant were analyzed by SDS-PAGE on 13.0% acrylamide gel using the protocol as described in Chapter 2, Section 2.2.20. The controls containing recombinant *Ct*CBM35 without insoluble polysaccharide were also run in parallel to ensure that no protein precipitation occurred during reaction. A BSA (1 mg/ml) with the polysaccharide control was run in parallel to check for any non-specific binding.

The quantitative analysis of ligand binding by adsorption isotherm was carried out by incubating 5 mg/ml of insoluble ivory nut mannan or mannan with varying protein concentrations 1, 2, 4, 6, 8, 12 and 18 µM and. Two hundred microliters of *Ct*CBM35 and polysaccharide mixtures were prepared in 50 mM sodium phosphate buffer pH 7.0 and incubated at 4°C for 2 h. The protein at the same concentration without any polysaccharide was also kept as control for each set of reaction mixture. The experiment was carried out in triplicate. The reaction mixture was centrifuged at 13000*g* and 4°C for 10 min. The supernatant containing

the unbound protein was removed and analysed for protein content by Bradford method (Bradford, 1976). The concentration of bound protein was estimated by subtracting the unbound protein concentration from supernatant from initial protein concentration and the binding isotherm was generated as described in Section 4.2.4.1.

4.2.4.1 Binding isotherm of CtCBM35 with insoluble polysaccharides

When a ligand (polysaccharide) interacts with a protein, the binding follows the law of mass action and at equilibrium the rate of forward reaction is equal to rate of backward reaction Gilkes *et al.* (1992). Based on this, equilibrium association constants (K_a) were obtained from the depletion isotherms (plot of [B] versus [F]) after fitting (nonlinear regression) of the raw data to a equilibrium binding type or adsorption model. The equation 1 for adsorption reaction given below was modified from Din *et al.* (1994) as described by Gilkes *et al.* (1992) and represented as,

$$K_a = \frac{[B]}{[N][F]} \qquad (1)$$

where, N is the concentration of available binding sites on the ligand (the number of polysaccharide lattice units) [moles/g of *Ct*CBM35], [B] is the concentration of bound *Ct*CBM35 (mol/g of ligand), [F] is the molar concentration of free CBM and K_a is the equilibrium association constant [M^{-1}]. Now, when a single CBM interacts with only one lattice unit of polysaccharide and there are no positive or negative co-operative effects,

$$[N] = [N_0] - [B] \qquad (2)$$

where, N_0 is the total concentration of binding sites of ligand in the absence of CBM. Substitution of Equation 2 into Equation 1 and rearrangement gives Langmuir equation (Gilkes *et al.*, 1992),

$$[B] = \frac{[N_0]\, K_a\, [F]}{(1+K_a\, [F])} \qquad (3)$$

Equation 4 is the widely used for non-linear regression analysis of one binding site model, following the previous reports of Gilkes *et al.* (1992) and Creagh *et al.* (1996). However, if binding involves CBM occupying several lattice units of ligands, then the surface is considered as an array of overlapping potential binding sites. Under these conditions N_0 is considered as a probability function which depends on bound protein [B] and its configuration (Pilz *et al.*, 1990; Shen *et al.*, 1991). Under these conditions Equation 2 can be expressed as,

$$[N] = [N_0] - a[B] \qquad (4)$$

where, a is the number of lattice unit occupied by a single CBM molecule. Substituting Equation 4 into Equation 1 gives,

$$[B] = \frac{[N_0]\, K_a\, [F]}{(1 + aK_a\, [F])} \qquad (5)$$

Rearragement of Equation 5 yields Euation 6,

$$\frac{1}{[B]} = \frac{1}{K_a\, [N_0]} \times \frac{1}{[F]} + \frac{a}{[N_0]} \qquad (6)$$

The slope ($1/K_a[N_0]$) and intercept ($a/[N_0]$) of a plot of 1/[B] versus 1/[F] were calculated by fitting the straight line for low values of [B]. Now the relative equilibrium association constant, K_r (litres/g of ligand) was calculated as,

$$K_r = K_a [N_0] \quad (7)$$

The equation 7 can be used for comparing affinities of *Ct*CBM35 for a given ligand. GraphPad Prism 5.0 software was used for calculating binding constants, binding capacity and generating graphs using single binding site model (McLean *et al.*, 2000).

4.2.5 Polysaccharide binding study of *Ct*CBM35 by fluorescence spectroscopy

On binding to polysaccharides, carbohydrate binding modules undergo conformational changes and behave differently than in its unbound native form (Royer, 2006). To compare the results with affinity electrophoresis, 160 µM of *Ct*CBM35 was incubated with polysaccharides *viz.*, carob galactomannan and konjac glucomannan of varying concentrations. Polysaccharide concentrations (0.01%, 0.04%, 0.06%, 0.08%, 0.15% and 0.2%, w/v) from 0.5% (w/v) stock solution in 100 µl reaction mixture were prepared in 50 mM sodium phosphate buffer, pH 7.0. The samples were incubated at 4°C for 2 h. The fluorescence intensity measurement was carried out using a fluorimeter (Fluoromax 3, Horiba Scientific, USA). Emission and excitation slits were kept at 3.00 and 1.00, respectively, with 0.5 s integration time. Three scans were taken per sample along with a control to reduce the noise created by buffer and polysaccharide. All the samples were excited at λ_{max} = 295 nm (to selectively excite Tryptophan residues) and the emission spectra were recorded between wavelength 320-400 nm. Tryptophan having the indole ring with intrinsic fluorescence property with higher quantum yield, displays fluorescence emission between 320-400 nm (Royer, 2006). The emission spectra of all the solutions were corrected against buffer and polysaccharide solution without *Ct*CBM35 before setting

the interaction study. Relative fluorescence intensities (F_o/F, where F_o is initial fluorescence intensity of *Ct*CBM35 and F is final fluorescence intensity of polysaccharide *Ct*CBM35 conjugate) were plotted against polysaccharide concentration. The association constants K_a (M^{-1}) of *Ct*CBM35 complex with carob galactomannan and konjac glucomannan were derived using modified Stern Volmer equation (Belatik *et al.*, 2012) as follows

$$\text{Log } (F_o\text{-}F)/F = \log K_a + n \log [\text{Polysaccharide}]$$

4.2.6 Study of size of *Ct*CBM35 on binding with polysaccharide and Ca^{2+} by dynamic light scattering

Polysaccharide binding greatly influences the protein conformational changes. These changes may lead to more dispersion in the dynamic environment leading to higher hydrodynamic area. The binding of polysaccharide with *Ct*CBM35 was studied by dynamic light scattering (DLS). In a dynamic environment, the particles of ligand and protein molecules diffuse randomly. DLS essentially measures fluctuation in scattered light intensity due to diffusion of particles, the diffusion coefficient of the particles can be determined. The diffusion coefficient D is then related to the radius R of the particles by means of the Stokes-Einstein Equation [19]:

$$D = kT/6\pi R\eta$$

where, k = Boltzmann-constant, T = temperature and η = viscosity.

The hydrodynamic diameters (R_H) of *Ct*CBM35 in presence of 0.1% (w/v) polysaccharides such as carob galactomannan and konjac glucomannan were measured using spectrophotometer (Malvern, Zetasizer Nano ZS, UK) spectrophotometer. Refractive index and viscosity of 50 mM sodium phosphate buffer (pH 7.0) were adjusted to 1.3206 and 8.945×10^{-3} g/(cm.s), respectively by

using SEDNTERP tool package (http://www.jphilo.mailway.com). The hydrodynamic radius of *Ct*CBM35 was also studied in presence and absence of 10 mM Ca^{2+} ions. *Ct*CBM35 was incubated at 25 °C for 2 h and the extra unbound Ca^{2+} was removed by dialysis against water. The hydrodynamic radius of *Ct*CBM35 bound with Ca^{2+} conjugate was measured and compared against Ca^{2+} free *Ct*CBM35. The instrument was set to measure the absorbance at a fixed angle ($\theta = 90°$). All the measurements were derived by deconvolution of intensity and sample autocorrelation function. Deconvolution of measured intensity was obtained using non negative least square analysis (NNLS) (Morrison *et al.*, 1992; Provencher *et al.*, 1979) algorithm e.g. CONTIN (Ostrowsky *et al.*, 1981), Regularization and Multiple Narrow Mode algorithms (Provencher *et al*, 1982; Shiba *et al.*, 2010). These algorithms of fitting the data were included as inbuilt functions of Zetasizer Nano software package..

4.2.7 Protein melting and stability study of *Ct*CBM35

The stability of *Ct*CBM35 was studied by protein melting curves using UV-absorption spectrophotometer (Varian, Cary 100-Bio) at 280 nm following the method of Dvortsov *et al.* (2009). The temperature was varied from 40 to 100°C using the peltier temperature controller (Varian, Cary 100-Bio) and the solutions were kept at the particular temperature for sufficient time (10 min) to attain equilibrium. *Ct*CBM35 was incubated in 50 mM sodium phosphate buffer (pH 7.0) with and without 10 mM $CaCl_2$ at 25°C for 2 h. The mixture containing Ca^{2+} ions was dialyzed against water to remove additional Ca^{2+} ions. The melting curve analysis of both *Ct*CBM35 with and without Ca^{2+} ions was generated by UV spectroscopy. Equimolar concentration of chelating agent EDTA (10 mM) was added to *Ct*CBM35 and

*Ct*CBM35-Ca^{2+} solutions to investigate the structural stability of *Ct*CBM35 at higher temperatures.

4.2.8 Effect of thermal denaturation on *Ct*CBM35 ligand binding with polysaccharide

Ligand binding ability of *Ct*CBM35 was investigated under melting temperatures as described earlier Dvortsov *et al.* (2009). Fluorescence spectroscopy was employed to understand the ligand binding of *Ct*CBM35 at higher temperatures. 18 µg of *Ct*CBM35 was incubated with 0.3% (w/v, 1.8 mM) carob galactomannan, locust bean galactomannan and konjac glucomannan separately at 45°C, 50°C and 55° for 1h. The fluorescence intensity measurements were carried out using a fluorimeter (Horiba Scientific, Fluoromax 3) as described in the Section 4.2.5.

4.2.9 Isothermal titration calorimetry of *Ct*CBM35 binding to soluble polysaccharides

Isothermal titration calorimetry (ITC) was employed to study the thermodynamic parameters *viz.* Gibb's free energy (ΔG), enthalpy (ΔH), entropy (ΔS), and stoichiometry (n) of *Ct*CBM35 upon ligand binding and carried out as described previously (Carvalho *et al.*, 2007; Pinheiro *et al*, 2008). The titrations were carried out at 55°C where total melting of *Ct*CBM35 was observed (Ghosh *et al.*, 2013) to understand the ligand binding ability at higher temperature. The samples for ITC study contained *Ct*CBM35 in 50 mM Na-HEPES buffer, pH 7.5, 2 mM $CaCl_2$. During titration *Ct*CBM35 (60 µM) was stirred at 300 rev/min in the reaction cell, which was injected with 28 successive 2 µl aliquots of ligands at (1.8 mM) at 180 s intervals. Integrated heat effects, after correction for heats of dilution, were analysed by non-linear regression using a single site-binding model (Microcal ORIGIN.

Version 5.0; Microcal Software). The fitted data yielded the association constant (Ka) and the enthalpy of binding (ΔH). Other thermodynamic parameters were calculated by using the standard thermodynamic equation, $-RT\ln K_a = \Delta G = \Delta H - T\Delta S$ (Luis *et al.*, 2013). N_0 is the number of binding sites. ITC analysis of *Ct*CBM35 carried out with carob galactomannan, locust bean galactomannan and konjac glucomannan.

4.2.10 Unfolding transition of *Ct*CBM35 in guanidine hydrochloride and urea

The structural stability of recombinant *Ct*CBM35 in guanidine hydrochloride and urea was studied at 25°C. Initially 30 µg of *Ct*CBM35 was incubated with varying concentrations of guanidine hydrochloride (GnHCl) or urea at 25°C for 24 h. One milliliter of reaction mixture was prepared by the addition of 50 µl *Ct*CBM35 (0.6 mg/ml) and varying concentrations of GnHCl or urea (1-8 M) prepared in 50 mM TrisHCl buffer, pH 7.0. The unfolding transition of *Ct*CBM35 was monitored by the change in fluorescence intensity of tryptophan (Trp) by recording the emission spectra between wavelengths 320-400 nm by exciting the samples at 295 nm using a fluorimeter (Horiba Scientific, Fluoromax 3). A sample without *Ct*CBM35 was kept as control (buffer and denaturant).

The free energy of denaturation (ΔG) of *Ct*CBM35 in presence of GnHCl and urea was determined at A_{280} using a spectrophotometer (Varian, Cary Bio-100). 30 µg of *Ct*CBM35 was incubated with varying concentrations of guanidine hydrochloride (GnHCl) or urea at 25°C for 24 h. One milliliter of reaction mixture was prepared by the addition of 50 µl *Ct*CBM35 (0.6 mg/ml) and varying concentrations of GnHCl or urea (1-8 M) prepared in 50 mM TrisHCl buffer, pH 7.0. The free energy of denaturation (ΔG) of *Ct*CBM35 was deduced as described by Ahmad *et al.* (1992).

$$K_{eq} = f_d / (1-f_d)$$

Where, K_{eq} = equilibrium constant, f_d = A_{280} of *Ct*CBM35 in presence of varying concentrations of GnHCl and urea

$$\Delta G = - RT \ln [f_d / (1-f_d)]$$

Where, ΔG = Gibb's free energy of denaturation, R = gas constant kJ/mole, T = temperature in Kelvin.

4.2.11 Secondary structure analysis of *Ct*CBM35 by circular dichroism

Far-UV Circular dichroism (CD) spectra of *Ct*CBM35 at 25°C was recorded on a spectropolarimeter (JASCO, J-815, Jasco Corporation, Tokyo, Japan), equipped with a peltier system for temperature control using a cell with a path length of 0.1 cm. Typical spectral accumulation parameters were set: a scanning rate of 50 nm min^{-1} with a 1 nm bandwidth over the wavelength range 195 to 250 nm with six scans averaged for each far-UV spectrum. The CD data are presented in terms of mean residue ellipticity (MRE, expressed as deg cm^2 $dmol^{-1}$) as a function of wavelength, calculated according to the procedure described earlier (Kelly *et al.*, 2005) using a protein concentration of 10-15 μM in 10 mM Tris-HCl, pH 7.5. All CD spectra were corrected for buffer contributions and secondary structures were calculated by using web based K2d neural network software package (kal-el.ugr.es/k2d/spectra.html) (Andrade *et al.*, 1993).

4.2.11.1 Circular dichroism data evaluation

The CD data are recorded either as differences in the absorbance of left (ΔL) or right (ΔR) handed polarized light gives molar extinction coefficient ($\Delta\varepsilon$) as given earlier by Andrade *et al.*, (1993).

$$\Delta\varepsilon = \Delta_L - \Delta_R \qquad (1)$$

or they can be expressed in terms of molar ellipticity $[\theta]$,

$$[\theta] = 3300 \times \Delta\varepsilon. \qquad (2)$$

Applying Beer-Lambert law to equation 1 yields,

$$\Delta\varepsilon = \varepsilon_L - \varepsilon_R = \frac{\Delta_L - \Delta_R}{c \times l} \qquad (3)$$

where, c is the concentration of protein in moles/litre and l is the path length in cm. Molar extinction coefficient of *Ct*CBM35 in left hand polarized light (ε_L) and right hand light (ε_R).

So, $[\theta]$ can be calculated as

$$[\theta] = \frac{\theta \times 100 \times M_r}{c \times l} \qquad (4)$$

where, M_r is the protein molecular weight.

Now if the protein concentration is in mg/ml, the concentration of amino acids can be calculated by assuming a mean residue weight (MRW) of 118 amino acid residue (Creighton, 1997).

The mean molar ellipticity $[\theta]_{MRE}$ can be calculated as,

$$[\theta]_{MRE} = \frac{\Theta \times 100 \times M_r}{c \times l \times N_A} \qquad (5)$$

where, N_A is the number of amino acids per protein. The molar ellipticity was expressed in terms of deg cm^2 $dmol^{-1}$ (Greenfield *et al.*, 2006). The factor 100 is added in the above equations for converting the molar concentration to $dmol/cm^2$ concentration units.

4.2.12 *In silico* structure prediction and ligand binding of *Ct*CBM35

4.2.12.1 Molecular modeling of family 35 carbohydrate binding module

The protein sequence of family 35 carbohydrate binding module (*Ct*CBM35) was retrieved from the NCBI protein sequence database with accession number ABN51273 (nucleotide accession number: CP000568) and uniprot ID A3DBE4. The molecular architecture deduced from amino acid sequence showed that *Ct*CBM35 (134 aa) is located at the N-terminal, sandwiched between a 32 amino acid signal peptide and catalytic module *Ct*ManT (373 aa) at C-terminus followed by a dockerin type 1 module. Modeller9v8 was used to build the 3-D model of *Ct*CBM35. Modeller is a computer program used for comparative protein structure modeling by satisfaction of the spatial restraints (http://salilab.org/modeller/). In the first step target query sequence was aligned with template sequences and this alignment file was used as an input to generate models of *Ct*CBM35. Loop refinement was performed using the loop model class program in Modeller. The model with the lowest discrete optimized protein energy (DOPE) was chosen for further refinements.

4.2.12.2 Structure refinement and quality assessment

The structure of *Ct*CBM35 with the least DOPE score, obtained from the modeller was further improved by energy minimization at YASARA Energy Minimization Server (www.YASARA.org/minimizationserver), in which molecular dynamics simulations of models were carried out in explicit solvent. It uses a new partly knowledge-based all atom force field derived from Amber (Krieger *et al.*, 2009). Final structure after energy minimization was subjected to structure validation using verification server (SAVES) at NIH-MBI (http://nihserver.mbi.ucla.edu). Protein secondary structure prediction tool (PredictProtein) from ExPasy SIB tool site

at Columbia University server (http://cubic.bioc.columbia.edu/predictprotein/) was used to calculate the presence of α-helix, β-sheet, turns and coils.

4.2.12.3 Multiple Sequence Analysis

Generally the amino acid residues involved in ligand binding are conserved within the family CBM35. To investigate these conserved amino acid residues, multiple sequence alignment was performed with representative members of CBM35 having different substrate specificities whose X-ray crystal or NMR structures were known. The protein sequence was retrieved from PDB (http://www.rcsb.org/pdb/), saved in FASTA format. Alignment was performed using CLUSTALW program (Thompson *et al.*, 1994) and final alignment was generated by ESpript (http://espript.ibcp.fr), for better understanding of conserved residues and structure.

4.2.12.4 Docking study of modelled CtCBM35

Docking study was carried out with the help of Autodock version 4.2.1. Ligands (mannotriose and galactomannan) for docking study were obtained from pubchem (http://pubchem.ncbi.nlm.nih.gov) in 3D SDF format, which were converted and saved in Mol2 format using OpenBabel 2.2.3 (O'Boyle *et al.*, 2011). Galactomannan having a mannan backbone is decorated with α-(1→6)-galactosyl moiety (Man-Gal-Man). Therefore, this tri-saccharide moiety was considered as galactomannan ligand. The two other ligands, mannopentaose and mannohexose in their pdb format were retrieved from the crystal structures of *C. polysaccharolyticus* CBM16 bound to mannopentaose (PDB ID: 3OEB) and CBM29 complex with mannohexaose (PDB ID: 1GWL), respectively for docking study of *Ct*CBM35. Ligand preparation was done by assigning Gastegier partial charges, merging non-polar hydrogens and finally saved as extended PDBQT file format using AutoDock

Tools (ADT) 1.5.4. *Ct*CBM35 modelled protein was also saved as a PDBQT file format after removing non-polar hydrogen atoms and adding their charges with the carbon atoms. Address for ligands where to dock, was fixed in a grid parameter file. The grid map dimensions were set in such a way that it fully covers active site cavity and gives enough space for ligand molecule to rotate freely. For different conformation search of ligand molecule Lamarckian Genetic Algorithm (LGA) was implemented and number of LGA runs was set to 30. Rest all other parameters were set to default values such as initial population size (150), maximum energy evaluation per run (2500000) and maximum number of generation (27000). After 30 independent successful docking runs protein-ligand complex for each ligand having auto generated lowest free energy of binding (ΔG) confirmation were saved. Docking results were analyzed using PyMOL (www.pymol.org) (0.99) for possible polar and hydrophobic interactions and final figure was generated with the help of PyMOL and YASARAView (12.2.22). For better understanding of protein-ligand interaction in 2D, Ligplot were generated (http://www.ebi.ac.uk/pdbsum/).

4.2.12.5 Molecular dynamics study of CtCBM35 in presence of Ca^{2+} ion

To investigate the role of Ca^{2+} ion in altering protein conformations a model of *Ct*CBM35 from *Clostridium thermocellum* was generated in presence of Ca^{2+} ion based on the crystal structure of closest homolog of CBM35 from *Amycolaptosis orientalis* (PDB ID: 2VZPA) by Modeller9v8 program. The homolog was identified using Blast PDB (http://www.ncbi.nlm.nih.gov/blast/Blast.cgi). The structure was energy minimized with GROMACS4.0.7 package (http://www.gromacs.org/) using steepest descent algorithm with GROMOS96 43a1 force field and simple point charge (SPC) water model (Berendsen *et al.*, 1995; Van der Spoel *et al.*, 2005; Hess *et al.*,

2008). Molecular dynamics (MD) simulation on the energy minimized *Ct*CBM35 model was carried out with the periodic boundary conditions applied in three dimensions to analyse the stability of the protein model. The net charge of system was neutralized by the addition of eleven sodium ions by replacing water molecules that are at least 3.50 Å from the protein surface (Saravanan *et al.*, 2012). The stable model was further visualized and analyzed in PyMOL tool.

4.3 Results and Discussion

4.3.1. Binding assay of *Ct*CBM35 with soluble polysaccharides

To investigate the polysaccharide binding specificity of *Ct*CBM35 the protein was expressed and purified to electrophoretic homogeneity (as described in Chapter 2, Section 2.3.3.5). The initial screening with 0.1% (w/v) polysaccharide binding using affinity electrophoresis, *Ct*CBM35 displayed preferential binding with carob galactomannan, konjac glucomannan, locust bean galactomannan and oligosaccharide mannotriose (Table 4.3.3). However, no significant binding of *Ct*CBM35 was observed with carboxymethyl cellulose, hydroxyethyl cellulose, barley β-glucan, rye arabinoxylan, oatspelt xylan, glucuronoxylan, birchwood xylan and arabinan (Table 4.3.3). These results showed that *Ct*CBM35 is mannan specific binding CBM.

Table 4.3.3 Ligand screening using affinity gel electrophoresis of *Ct*CBM35.

Ligand (1%, w/v)	Affinity Binding
Carob galactomannan	++
Konjac glucomannan	++
Locust bean galactomannan	++
Mannotriose	+++
Carboxymethyl cellulose	--
Hydroxyethyl cellulose	--
Barley β-glucan	--
Rye arabinoxylan	--
Oatspelt xylan	--
Glucuronoxylan	--
Birchwood xylan	--
Arabinan	--

+++ = Maximum binding, ++ = Moderate binding, -- = No binding

The relative mobility of *Ct*CBM35 was determined by running the protein in the native PAGE with gel containing varying concentration of carob galactomannan, konjac glucomannan, locust bean galactomannan and oligosaccharide mannotriose

against a reference with no polysaccharide (Fig 4.3.1A, Fig. 4.3.2A, Fig. 4.3.3A and Fig. 4.3.4A, respectively).

The *Ct*CBM35 displayed higher binding affinity with mannotriose and konjac glucomannan as compared to carob galactomannan and locust bean galactomannan. The association constants (K_a) were found to be 3.2×10^5 M^{-1} and 1.43×10^5 M^{-1} with mannotriose and konjac glucomannan, respectively. Whereas association constant (K_a) was 1.24×10^5 M^{-1} with carob galactomannan and 1.23×10^5 M^{-1} with locust bean galactomannan (Table 4.3.2).

To assess the Ca^{2+} induced affinity the binding of *Ct*CBM35 with varying concentrations polysaccharides was carried out by affinity electrophoresis. In the presence of 10 mM Ca^{2+} ions the affinity of *Ct*CBM35 for manno-configured ligand was increased to approximately, 2.5 fold and the equilibrium association constant (K_a) was obtained as 7.21×10^5 M^{-1}, 4.1×10^5 M^{-1}, 3.0×10^5 M^{-1}, 2.9×10^5 M^{-1} with mannotriose, konjac glucomannan, carob galactomannan and locust bean galactomannan (Table 4.3.2, Fig. 4.3.1B, Fig. 4.3.2B, Fig. 4.3.3B and Fig. 4.3.4B, respectively). A linear regression plot was generated between relative migration of *Ct*CBM35 against varying concentrations of carob galactomannan, konjac glucomannan, locust bean galactomannan and mannotriose to calculate the association constant (K_a) (Fig 4.3.1C, Fig. 4.3.2C, Fig. 4.3.3C and Fig. 4.3.4C, respectively).

Table 4.3.2 Binding analysis of *Ct*CBM35 with polysaccharides and oligosaccharide by affinity electrophoresis and in presence of 10 mM Ca^{2+} ions.

Substrates	Without Ca^{2+} ions	With Ca^{2+} ions
	K_a (10^5 M^{-1})	K_a (10^5 M^{-1})
Locust bean galactomannan	1.23	2.91
Carob galactomannan	1.24	3.03
Konjac glucomannan	1.43	4.10
Mannotriose	3.20	7.21

Family 35 CBM from *Clostridium thermocellum* and *Cellvibrio japonicus* showed affinity toward ligands other than manno-configured polysaccharides containing β-(1→4)-mannose chain, such as Δ-4,5-anhydrogalacturonic acid and glucuronic acid (Correia *et al.*, 2010). *Ct*CBM35 showed higher affinity with mannotriose and konjac glucomannanan than carob galactomannan and locust bean galactomannan. The rationale behind this selective affinity is due to the galactose unit in locust bean galactomannan which probably interferes with the *Ct*CBM35 binding. Locust bean galactomannan is composed of a β-(1→4)-linked D-mannan backbone to which single D-galactosyl units are attached to C-6 of D-mannosyl residues. Whereas, mannotriose is a linear trisaccharide comprising β-(1→4)-linked D-mannosyl residues. However, no significant binding of *Ct*CBM35 with carboxymethyl cellulose, rye arabinoxylan, birchwood xylan, oat spelt xylan and glucouronoxylan showed that it is a mannan specific binding CBM. Therefore, the results showed that *Ct*CBM35 was able to distinguish the simpler structural organization of mannotriose and highly galactosylated locust bean galactomannan.

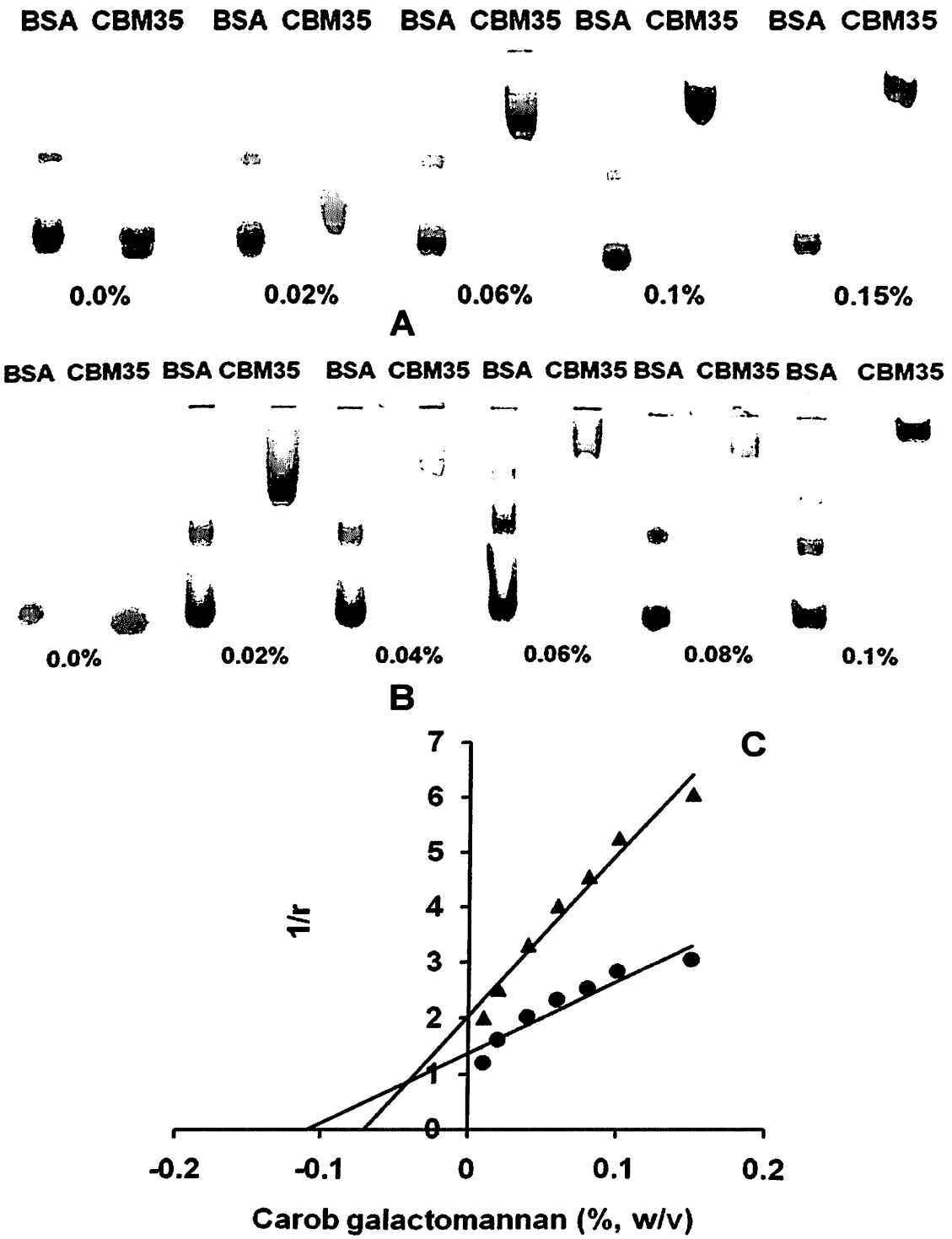

Fig. 4.3.1 Affinity electrophoresis of *Ct*CBM35 using 7.5% native-PAGE gel in presence of varying concentrations of (A) carob galactomannan (B) 10 mM Ca^{2+} incorporated with carob galactomannan (C) A linear regression plot of inverse relative migration of *Ct*CBM35 (1/r) against carob galactomannan concentration (%, w/v).

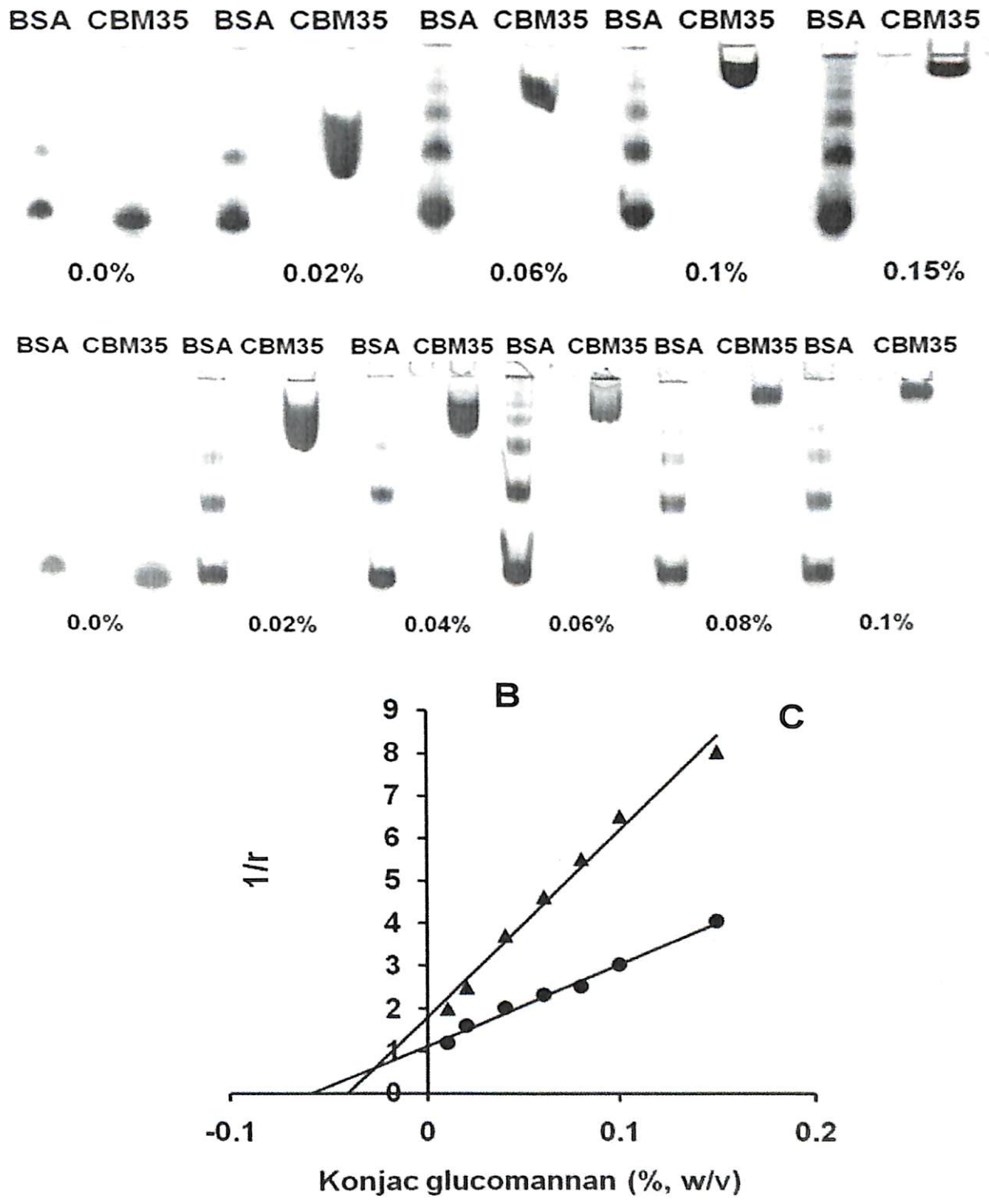

Fig. 4.3.2 Affinity electrophoresis of *Ct*CBM35 using 7.5% native-PAGE gel in presence of varying concentrations of (A) konjac glucomannan (B) 10 mM Ca^{2+} incorporated with konjac glucomannan (C) A linear regression plot of inverse relative migration of *Ct*CBM35 (1/r) against konjac glucomannan concentration (%, w/v).

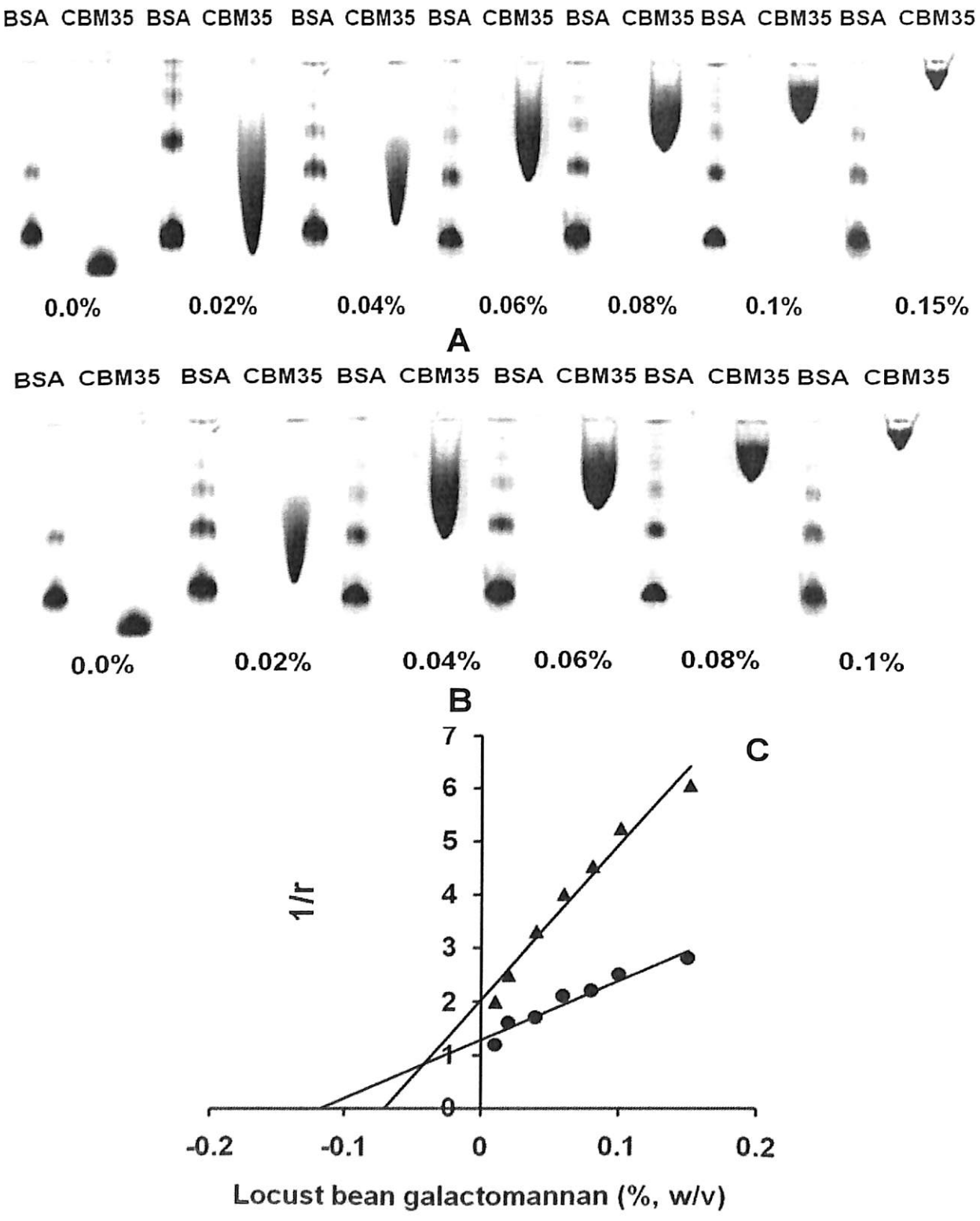

Fig. 4.3.3 Affinity electrophoresis of *Ct*CBM35 using 7.5% native-PAGE gel in presence of varying concentrations of (A) locus bean galactomannan (B) 10 mM Ca^{2+} incorporated with locus bean galactomannan (C) A linear regression plot of inverse relative migration of *Ct*CBM35 (1/r) against locus bean galactomannan concentration (%, w/v).

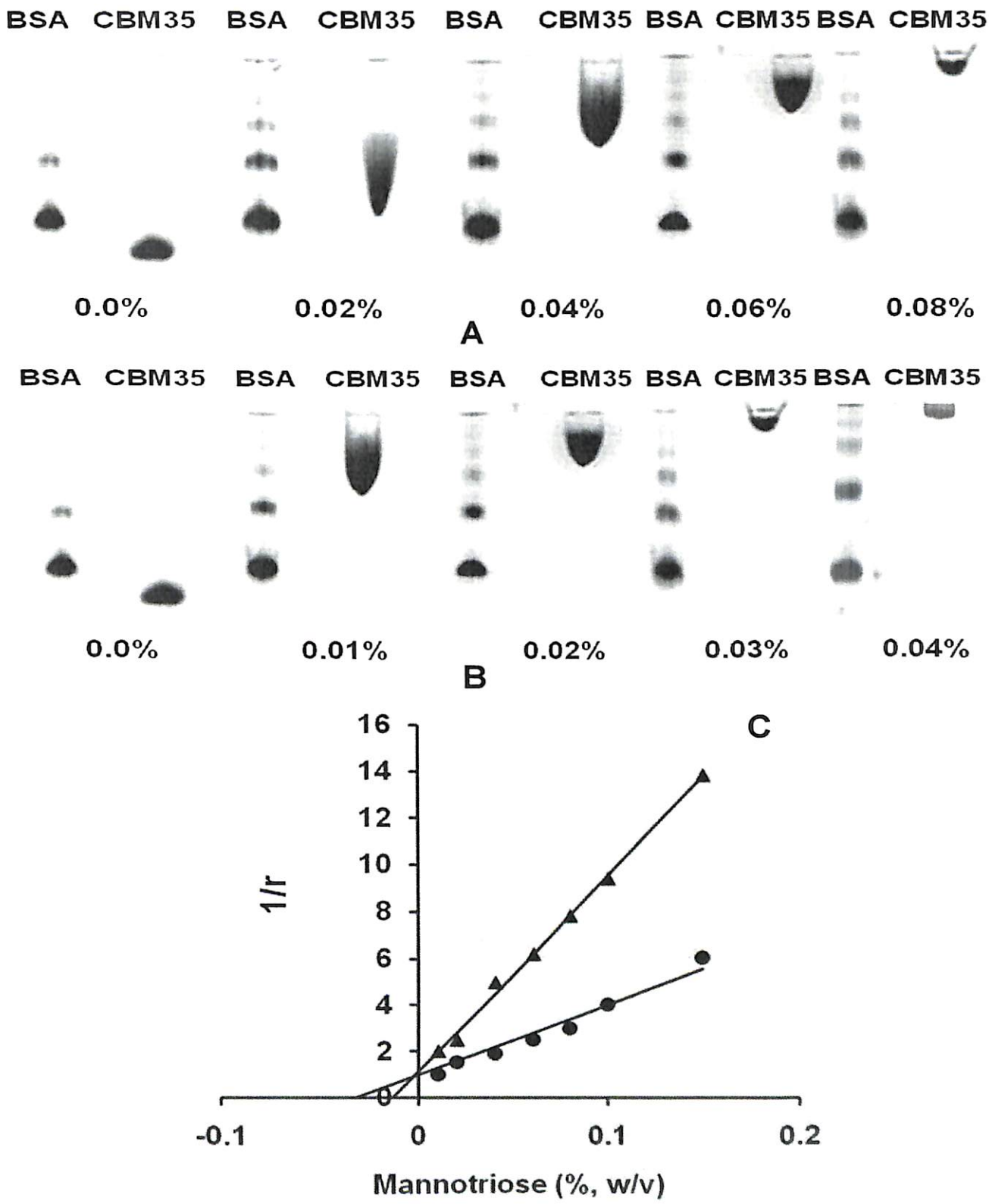

Fig. 4.3.4 Affinity electrophoresis of *Ct*CBM35 using 7.5% native-PAGE gel in presence of varying concentrations of (A) mannotriose (B) 10 mM Ca^{2+} incorporated with mannotriose (C) A linear regression plot of inverse relative migration of *Ct*CBM35 (1/r) against mannotriose concentration (%, w/v).

4.3.2 Binding analysis of *Ct*CBM35 with insoluble polysaccharides

The qualitative and quantitative binding of *Ct*CBM35 with insoluble polysaccharides was assessed by adsorption isotherm analysis. Quantitative binding analysis revealed that *Ct*CBM35 displays low binding with insoluble mannan and ivory nut mannan as analysed by SDS-PAGE when compared with the protein in free (unbound to ligand) form and the total protein (Fig. 4.3.5A and Fig. 4.3.6A, respectively). *Ct*CBM35 displayed no binding with avicel and wheat arabinoxylan. The quantitative binding assessment showed that the equilibrium association constants (K_a) of *Ct*CBM35 with insoluble mannan and ivory nut mannan were, 12 μM^{-1} and 2.5 μM^{-1}, respectively (Table 4.3.3). The relative equilibrium association constant K_r and the concentration of binding sites in mannan surface [N_o] were calculated from a linear regression plot between bound *Ct*CBM35 versus free *Ct*CBM35. The data were analyzed by GraphPad (Prism 2.0.1) software using linear regression analysis (the inset) based on one binding site equation (Fig. 4.3.5B and Fig. 4.3.6B). The estimated values of relative equilibrium constant K_r and concentration of binding sites [N_o] were 0.49 ± 0.2 l/g and 0.04 ± 0.002 μmole/g with mannan and 0.35 ± 0.5 l/g and 0.14 ± 0.004 μmole/g (Table 4.3.3). These results suggested that *Ct*CBM35 bind to insoluble mannan and ivory nut mannan less effectively as the availability of protein binding site on the polysaccharide was less (<1). This may be due to binding of protein to the non reducing end of the polysaccharide.

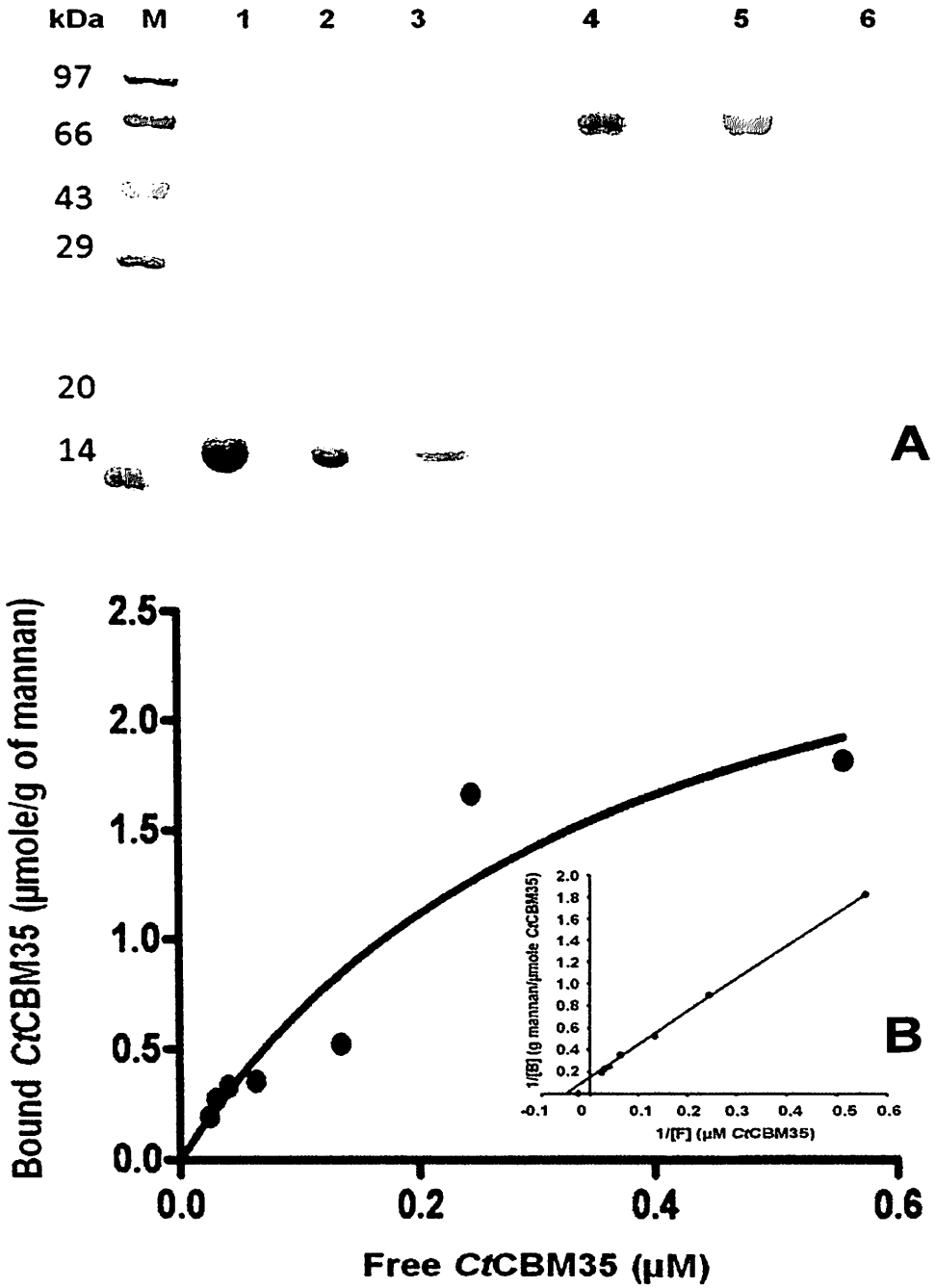

Fig. 4.3.5 (A) Qualitative binding of *Ct*CBM35 with insoluble mannan using 12% SDS-PAGE. Lane M: Mid range unstained molecular weight marker (97 kDa - 14 kDa), lane 1: Purified *Ct*CBM35, lane 2: unbound *Ct*CBM35, lane 3: bound *Ct*CBM35, lane 4: Bovine serum albumin (BSA) as control, lane 5: unbound BSA, lane 7: bound BSA. (B) Quantitative analysis of binding of *Ct*CBM35 to insoluble mannan. The main panel shows the equilibrium adsorption isotherm ([B] versus [F]) for *Ct*CBM35. Adsorption assay was done at 4°C, as described under methods section. Initial protein concentrations of *Ct*CBM35 were 0.2-9 µM. The inset shows the linear regression plot of 1/[B] versus 1/[F] concentrations to derive the association constant (K_a).

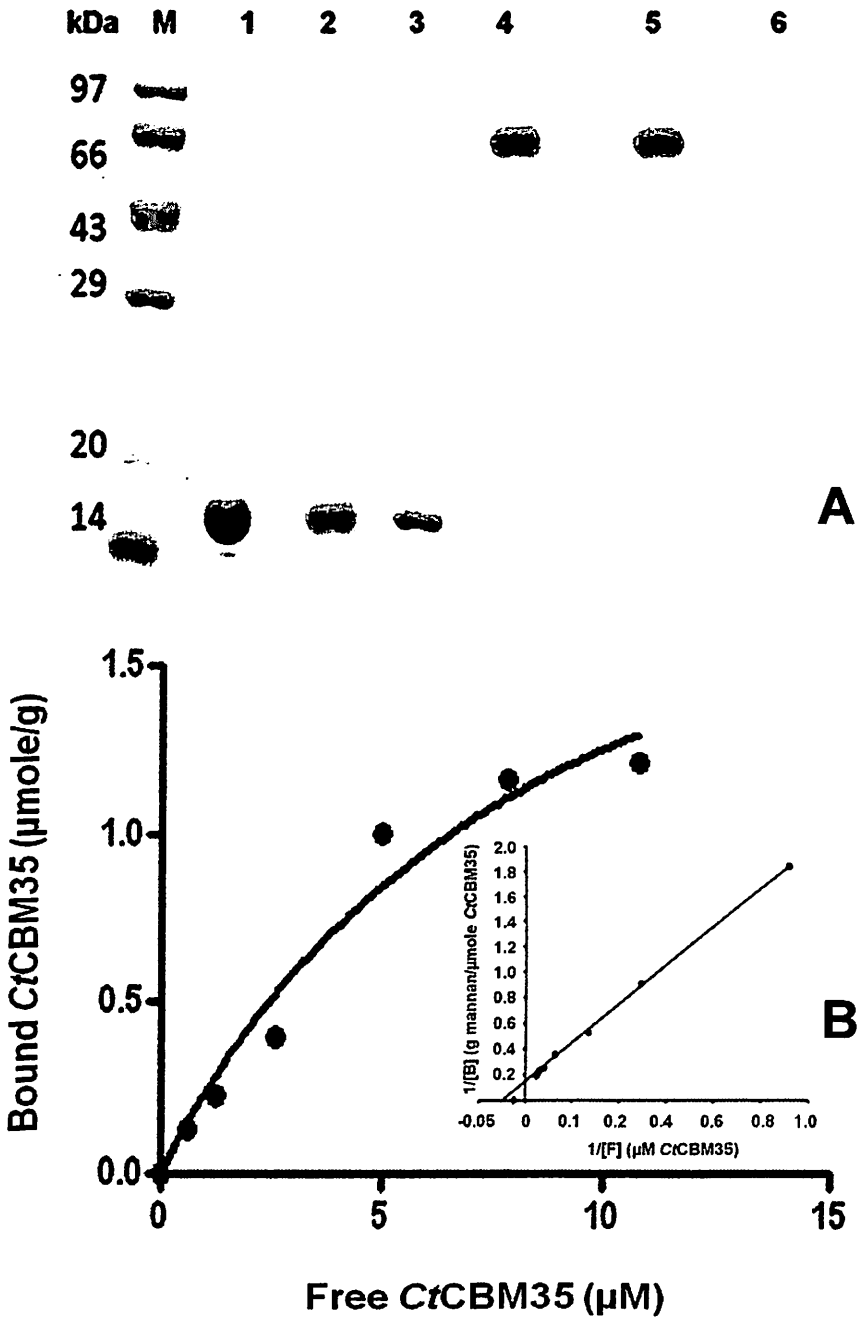

Fig. 4.3.6 (A) Qualitative binding of *Ct*CBM35 with insoluble mannan using 12% SDS-PAGE. Lane M: Mid range unstained molecular weight marker (97 kDa - 14 kDa), lane 1: Purified *Ct*CBM35, lane 2: unbound *Ct*CBM35, lane 3: bound *Ct*CBM35, lane 4: Bovine serum albumin (BSA) as control, lane 5: unbound BSA, lane 7: bound BSA. (B) Quantitative analysis of binding of *Ct*CBM35 to insoluble mannan. The main panel shows the equilibrium adsorption isotherm ([B] versus [F]) for *Ct*CBM35. Adsorption assay was done at 4°C, as described under methods section. Initial protein concentrations of *Ct*CBM35 were 0.2-20 µM. The inset shows the linear regression plot of 1/[B] versus 1/[F] concentrations to derive the association constant (K_a).

Table 4.3.3 Kinetic parameters of *Ct*CBM35 binding with insoluble polysaccharides from adsorption isotherm analysis.

Polysaccharide	K_r (l/g)	K_a (μM^{-1})	N_o (μmole/g)
Mannan	0.49 ± 0.02	12	0.04 ± 0.002
Ivory nut mannan	0.35 ± 0.05	2.5	0.14 ± 0.004
Avicel	*nb*	*nb*	*nb*
Wheat arabinoxylan	*nb*	*nb*	*nb*

values are mean ± SD (n=3)
nb = no binding observed

The recombinant *Ct*CBM35 preferred binding manno-configured polysaccharides. *Ct*CBM35 discriminated during carbohydrate selection showing its affinity only with manno-configured ligands when tested against diverse polysaccharides.

4.3.3 Polysaccharide binding study of *Ct*CBM35 by fluorescence spectroscopy

Among the three aromatic amino acids tryptophan shows highest quantum yield and better stability which facilitates use as a probe for fluorescence detection during polysaccharide binding with protein (Royer, 2006). In presence of polysaccharides such as carob galactomannan, konjac glucomannan, locust bean galactomannan or mannotriose and with their increase in concentrations *Ct*CBM35 displayed significant blue shifts. Binding of carob galactomannan, konjac glucomannan, locust bean galactomannan or mannotriose with *Ct*CBM35 displayed 21 nm peak shift towards shorter wavelength from λ_{max} 350 nm to 329 nm of tryptophan on excitation at 295 nm (Fig. 4.3.7A, Fig. 4.3.8A, Fig. 4.3.9A and Fig. 4.3.10A, respectively). The association constant (K_a) of *Ct*CBM35 with carob galactomannan, konjac glucomannan, locust bean galactomannan and mannotriose were derived from Hill plots (Fig. 4.3.7B, Fig. 4.3.8B, Fig. 4.3.9B and Fig. 4.3.10B, respectively). From Hill plot of polysaccharide or oligosaccharide concentrations and

relative fluorescence intensities, the calculated K_a values of *Ct*CBM35 were 1.14 x 10^5 M^{-1} for carob galactomannan, 1.43 x 10^5 M^{-1} for konjac glucomannan, 1.01 x 10^5 M^{-1} for locust bean galactomannan and 3.1 x 10^5 M^{-1} for mannotriose (Table 4.3.4). The K_a values were similar to those derived from affinity electrophoresis (Table 4.3.2). Therefore, the fluorescence studies of polysaccharide binding of *Ct*CBM35 confirmed the results of affinity electrophoresis. The number of binding site concentrations (n) were derived from Stern Volmer equation and were found n = 0.79 for carob galactomannan, n= 0.80 for konjac glucomannan, n = 0.67 for locust bean galactomannan and n = 0.98 for mannotriose (Table 4.3.4). This shows that *Ct*CBM35 has a single binding site for all the polysaccharides and mannotriose. Since, *Ct*CBM35 displayed significant affinity for mannose derived ligands, from the derived affinity constants the Gibb's free energy of binding was calculated using the equation:

$$\Delta G = -RT\ln K_a$$

where, ΔG = Gibb's free energy, R = gas constant (Joule/K/mole), T = Temperature in Kelvin, K_a = association constant (M^{-1}). The free energy of binding of *Ct*CBM35 was -30.0 kJ/mole with mannotriose, -27.0 kJ/mole with carob galactomannan, -28.0 kJ/mole with konjac glucomannan and -26.53 kJ/mole with locust bean galactomannan (Table 4.3.4). The higher binding affinity and free energy of *Ct*CBM35 binding to small oligosaccharide mannotriose and linear β(1→4) linked konjac glucomannan suggested that their simple molecular structure made an easy accessible platform for *Ct*CBM35 than complex structured carob galactomannan and locust bean galactomannan.

Table 4.3.4 Association constants (K_a) and free energy of binding of *Ct*CBM35 from relative fluorescence intensities.

Ligand	K_a (10^5 M^{-1})	Binding site (n)	Gibb's free energy (ΔG) (kJ $mole^{-1}$)
Carob galactomannan	1.14	0.79	-27.00
Konjac glucomannan	1.43	0.80	-28.00
Locust bean galactomannan	1.01	0.67	-26.53
Mannotriose	3.10	0.98	-30.00

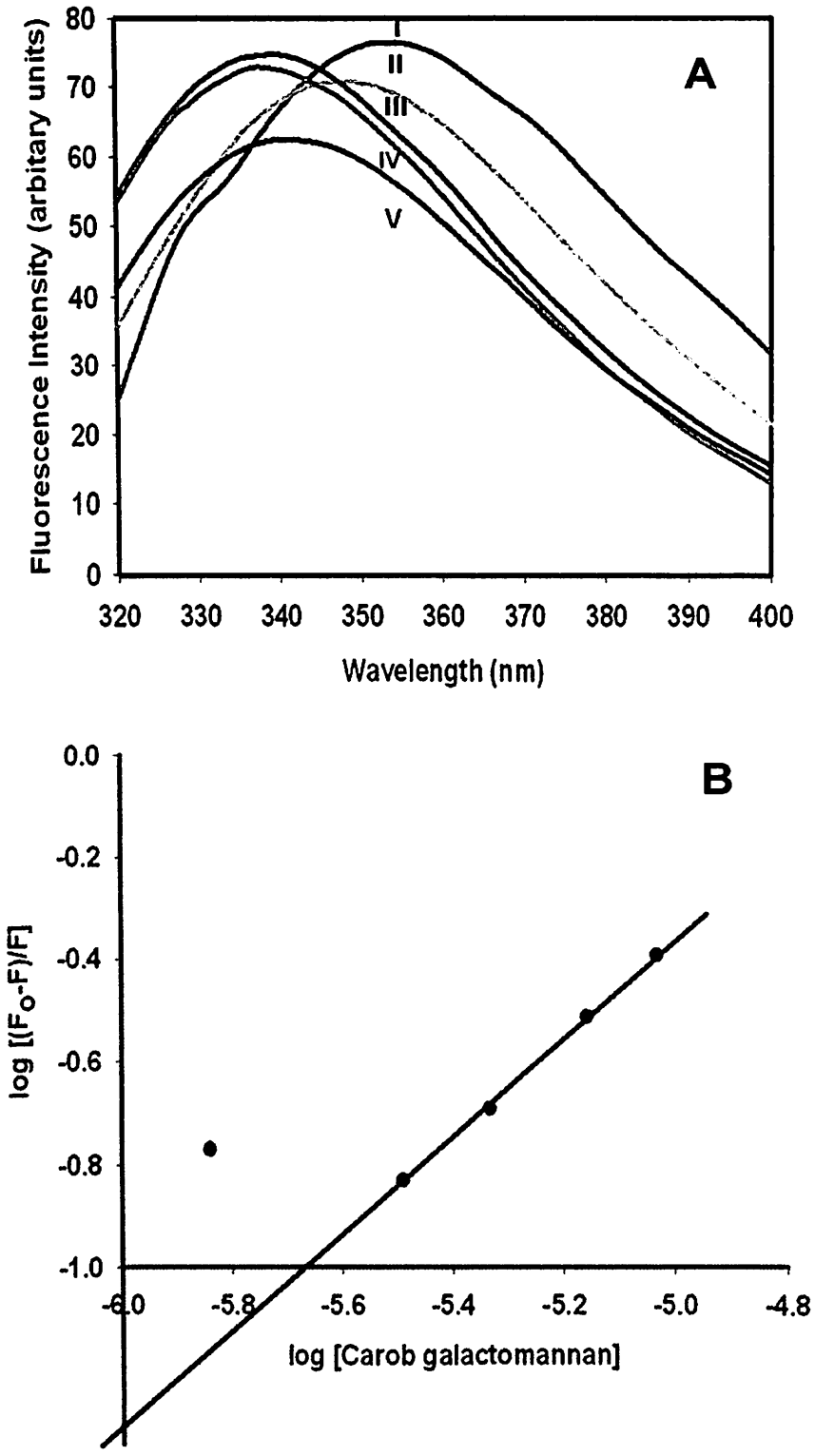

Fig. 4.3.8 Tryptoptophan fluorescence emission spectrum of *Ct*CBM35 in presence of (A) carob galactomannan (%, w/v), represented in lines: (I) without polysaccharide, (II) 0.01, (III) 0.04, (IV) 0.06, (V) 0.08. (B) Hill plot of log $[(F_o\text{-}F)/F]$ vs log [carob galactomannan] used to derive association constant (K_a).

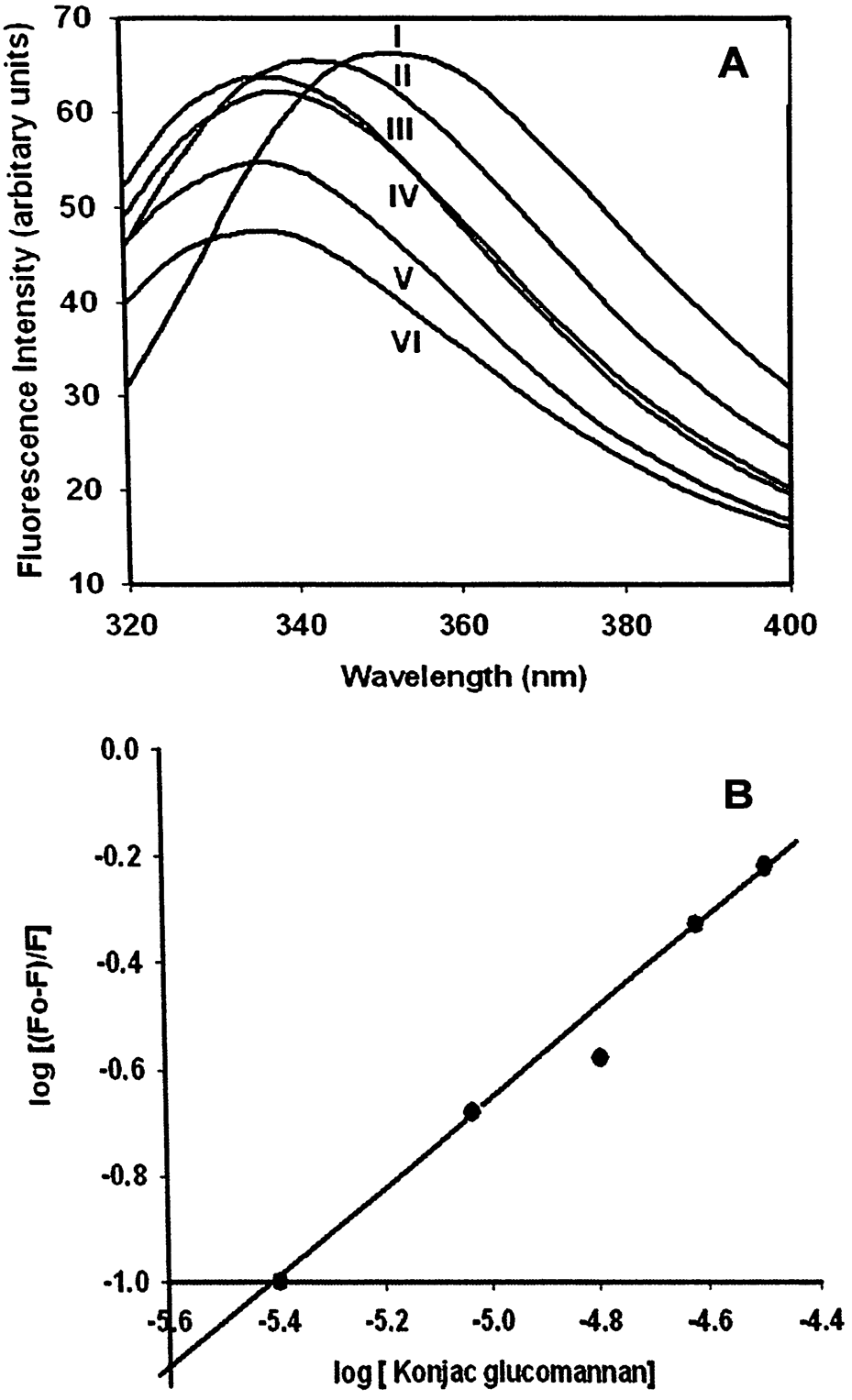

Fig. 4.3.9 Tryptoptophan fluorescence emission spectrum of *Ct*CBM35 in presence of (A) konjac glucomannan (I) without polysaccharide, (II) 0.01, (III) 0.04, (IV) 0.06, (V) 0.08, (VI) 0.1. (B) Hill plot of log [(F_o-F)/F] vs log [konjac glucomannan] used to derive association constant (K_a).

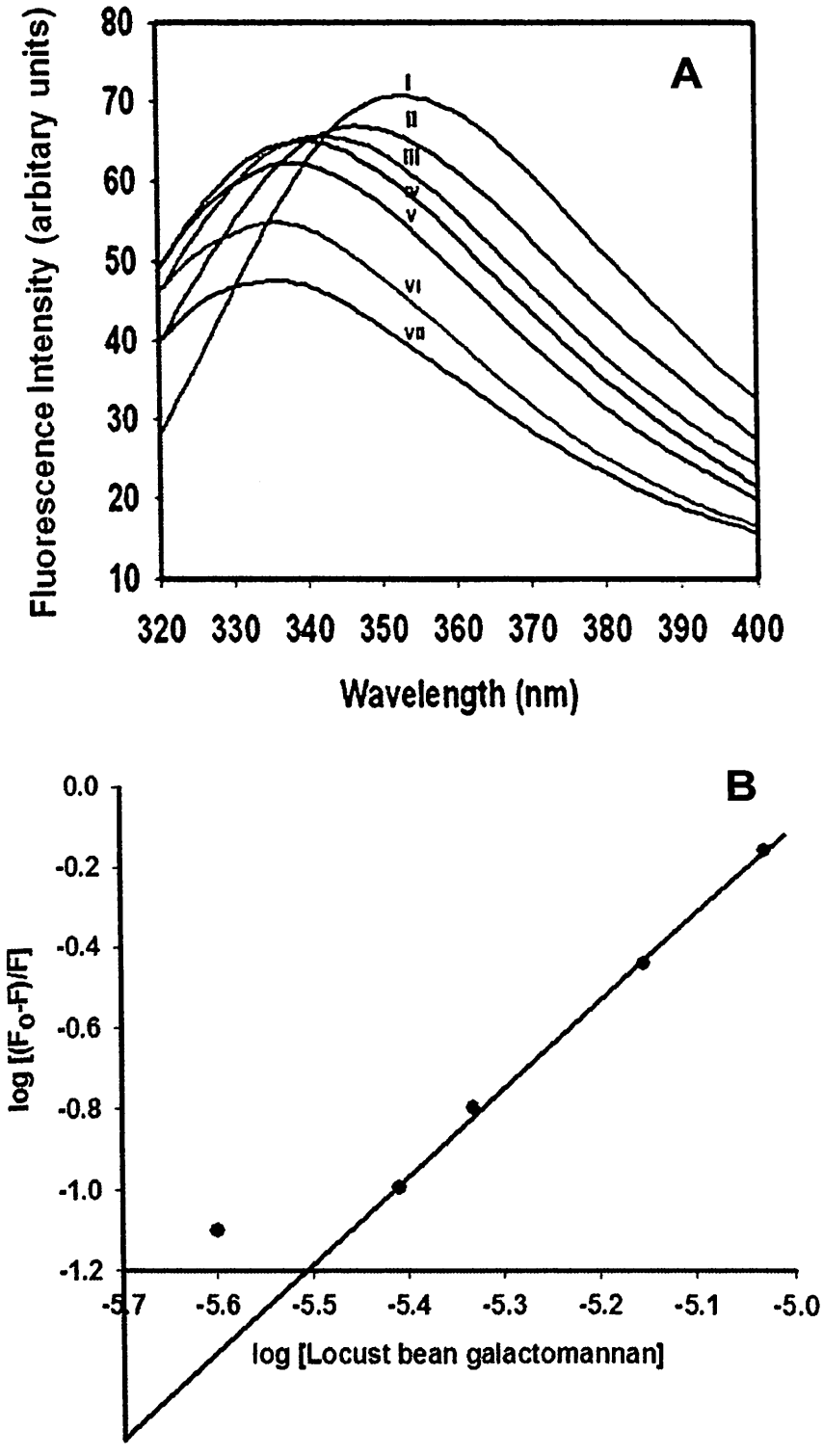

Fig. 4.3.10 Tryptoptophan fluorescence emission spectrum of *Ct*CBM35 in presence of (A) locust bean galactomannan (I) without polysaccharide, (II) 0.01, (III) 0.04, (IV) 0.06, (V) 0.08, (VI) 0.1. (B) Hill plot of log $[(F_o\text{-}F)/F]$ vs log [locust bean galactomannan] used to derive association constant (K_a).

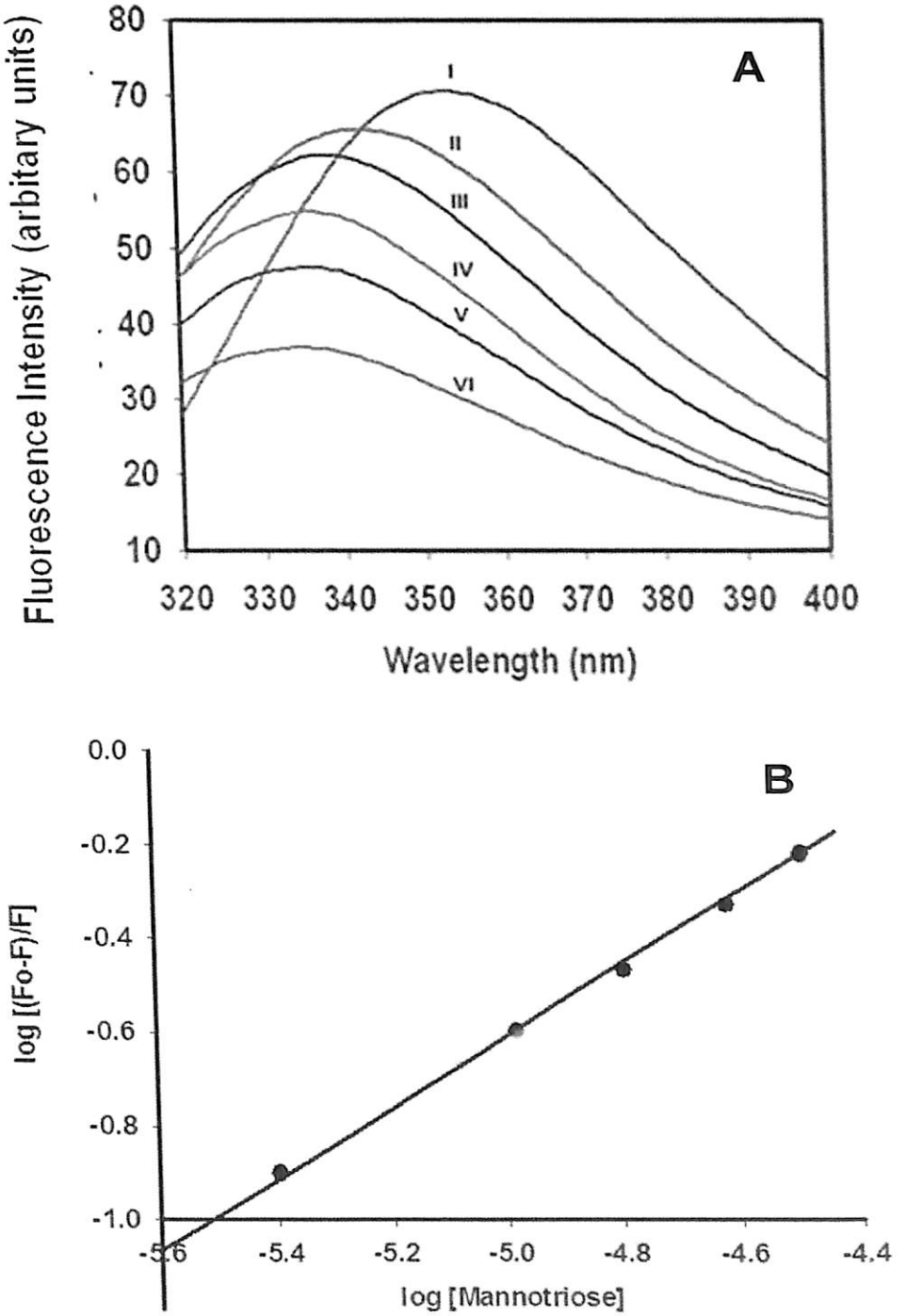

Fig. 4.3.11 Tryptoptophan fluorescence emission spectrum of *Ct*CBM35 in presence of (A) mannotriose (I) without oligosaccharide, (II) 0.01, (III) 0.04, (IV) 0.06, (V) 0.08, (VI) 0.1. (B) Hill plot of log $[(F_o\text{-}F)/F]$ vs log [mannotriose] used to derive association constant (K_a).

4.3.4 Study of size of *Ct*CBM35 on binding with polysaccharide and Ca^{2+} by DLS

Polysaccharide binding greatly influences and causes the alterations in the dynamic environment of a protein. The hydrodynamic radius (R_H) of *Ct*CBM35 as measured from dynamic light scattering (DLS) was 4.25 nm which was in the acceptable range as this value is higher than theoretical R_H, 2 nm for a 15 kDa protein. The R_H value augmentation from 4.25 nm to 6 nm was observed for *Ct*CBM35 in presence of 0.1% (w/v) carob galactomannan (Fig. 4.3.12A). In contrast, konjac glucomannan binding (0.1 %, w/v) exhibited much broader R_H of 8 nm (Fig. 4.3.12B). The augmentation in size was due to strong binding with konjac glucomannan leading to a stiffer structure and low random diffusion of the particles of protein and polysaccharides in the dynamic environment. Random diffusion of the particles measured in terms of random diffusion coefficient and is inversely proportional to R_H. In the presence of 10 mM Ca^{2+} ions, the hydrodynamic radius of *Ct*CBM35 was remarkably increased from 4.25 nm in absence of Ca^{2+} ions to 4.52 nm (Fig. 4.3.12C). In this case Ca^{2+} ions might be binding with the amino acid residues of *Ct*CBM35 and imparting a stiffer structure than usual. Therefore, the random diffusion of the protein system reduced and as a result the dynamic radius of *Ct*CBM35-Ca^{2+} complex increased.

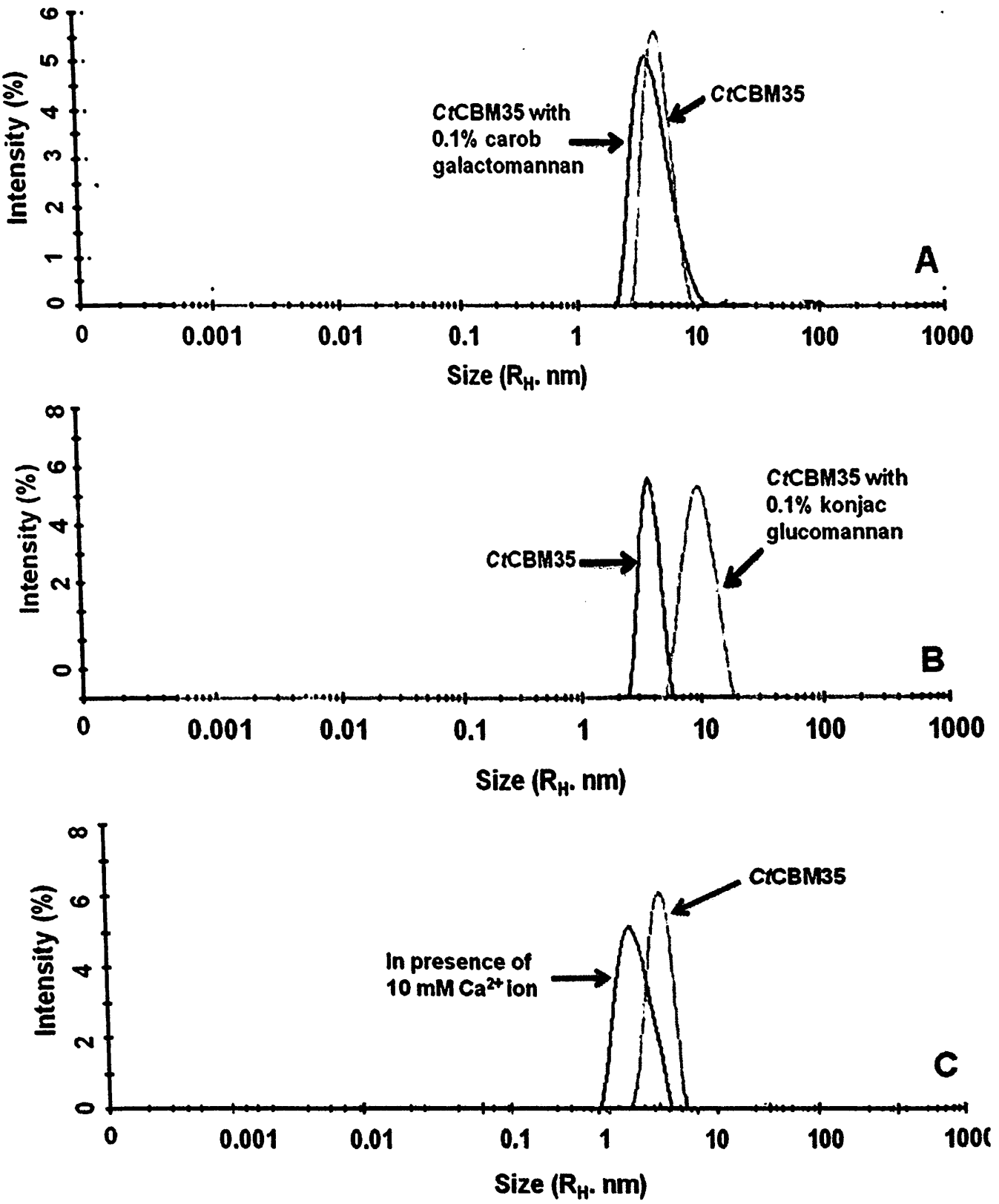

Fig. 4.3.12 Dynamic light scattering of *Ct*CBM35 in conjugation with 0.1% (w/v) (A) carob galactomannan, (B) konjac glucomannan and (C) 10 mM Ca^{2+} ions.

4.3.5 Protein melting and stability study of *Ct*CBM35

The melting of *Ct*CBM35 was studied to investigate the protein stability which perhaps plays a major role in polysaccharide binding at higher temperature and improves the catalytic properties of the appended catalytic module. *Ct*CBM35 displayed a single melting peak at 55°C, which shifted towards higher temperature (75°C) in the presence of 10 mM Ca^{2+} (Fig. 4.3.13). However, when EDTA was added in equimolar concentration as Ca^{2+} (10 mM) to the *Ct*CBM35 and the melting peak shifted back to the original temperature of 55°C (Fig. 4.3.13). The presence of EDTA imparted detrimental effect on thermostability of *Ct*CBM35 as the peak shifted 5° lower to 50°C, coupled with significant loss in peak absorbance (Fig. 4.3.13). Therefore, it could be concluded that Ca^{2+} ions provide thermal stability to the *Ct*CBM35 structure. Similar observations were reported with CBM6 from *C. thermocellum* ATCC 27405 by Ahmed *et al.* (2013).

Protein stability while functioning at higher temperature is a major concern in industry. The protein melting phenomenon of recombinant *Ct*CBM35 was analyzed to study its thermostability. The protein-melting peaks of *Ct*CBM35 shifted to higher temperature in the presence of Ca^{2+} ions. However, on addition of equimolar concentration of EDTA to the solutions of *Ct*CBM35, the melting temperature peaks shifted back to the original positions. EDTA chelates any divalent cation such as Ca^{2+} and thus imparted lower thermostability to *Ct*CBM35.The shift of peak to a higher temperature might be due to the reason that Ca^{2+} ions provided stability to the protein structure assembled either by coordinate bonds or by hydrogen bonds with amino acids, as reported earlier (Henshaw *et al.* 2006, Montanier *et al.* 2009, Ghosh *et al.*

2009, Ghosh *et al.* 2013). The ionic interactions of Ca^{2+} ions in the bound protein resulted in stability of ligand binding Tyr residues (Henshaw et *al.* 2006).

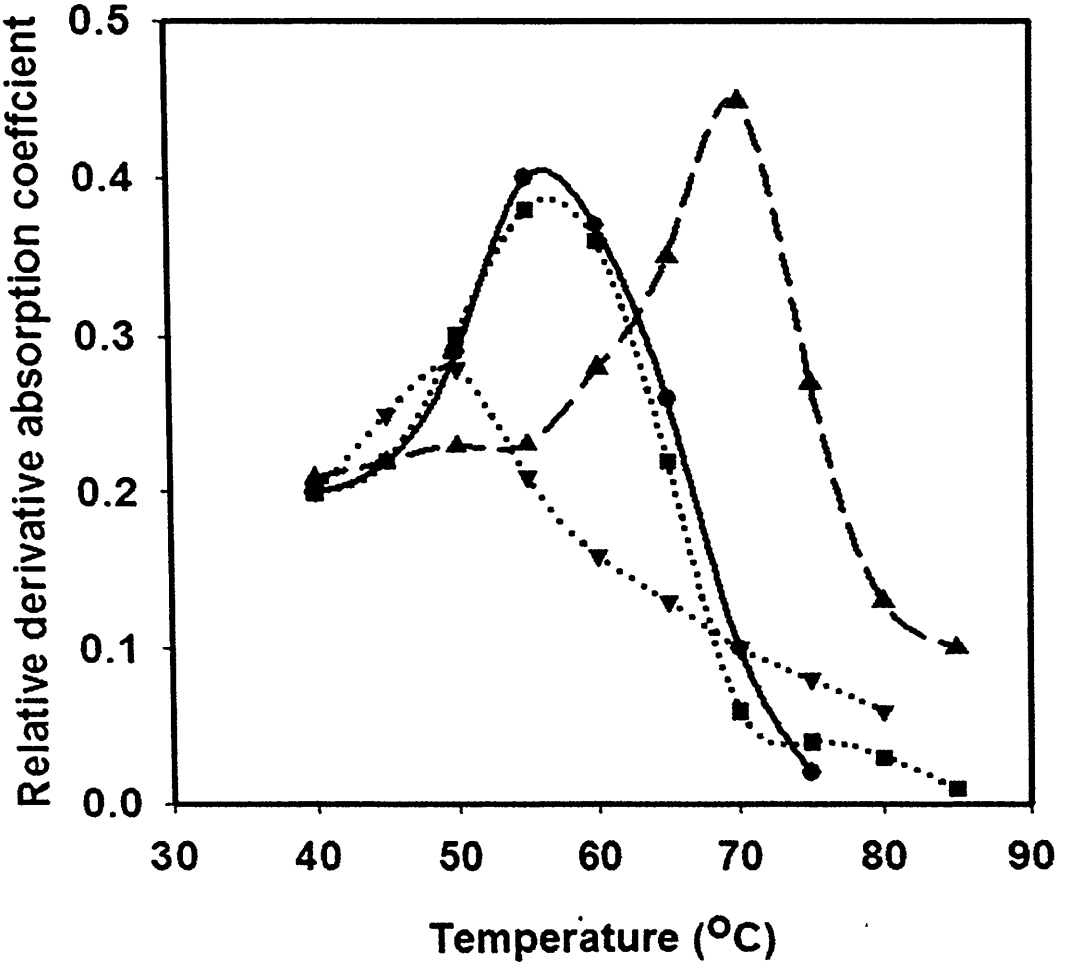

Fig. 4.3.13 Protein melting curves of *Ct*CBM35 with no additive (—●—), in the presence of 10 mM Ca^{2+} (--▲--), in the presence of 10 mM Ca^{2+} and 10 mM EDTA (···■···) and in presence of 10 mM EDTA (··▼··).

4.3.6 Thermal denaturation study of *Ct*CBM35 by fluorescence spectroscopy

*Ct*CBM35 displayed only 2 nm shift (blue shift) of fluorescence peak from its initial peak wavelength 350 nm on increasing the temperature from 45°C to 50°C, in the presence of 0.3% (w/v) konjac glucomannan, locust bean galactomannan and carob galactomannan coupled with significant fall in peak intensity displaying partial denaturation of *Ct*CBM35 in bound state (Fig. 4.3.14). *Ct*CBM35 undergoes thermal denaturation and loses its polysaccharide binding ability at higher temperature. *Ct*CBM35 showed the thermal denaturation in its polysaccharide bound state on increasing the temperature from 45°C to 55°C (Fig. 4.3.14). The complete denaturation of *Ct*CBM35 occurred at 55°C, due to structural deformity and displaying binding affinity in increasing order with polysaccharides, konjac glucomannan < locust bean galactomannan < carob galactomannan. This result corroborates with the protein melting of *Ct*CBM35 displaying complete unfolding at 55°C as described earlier in the Section 4.3.5.

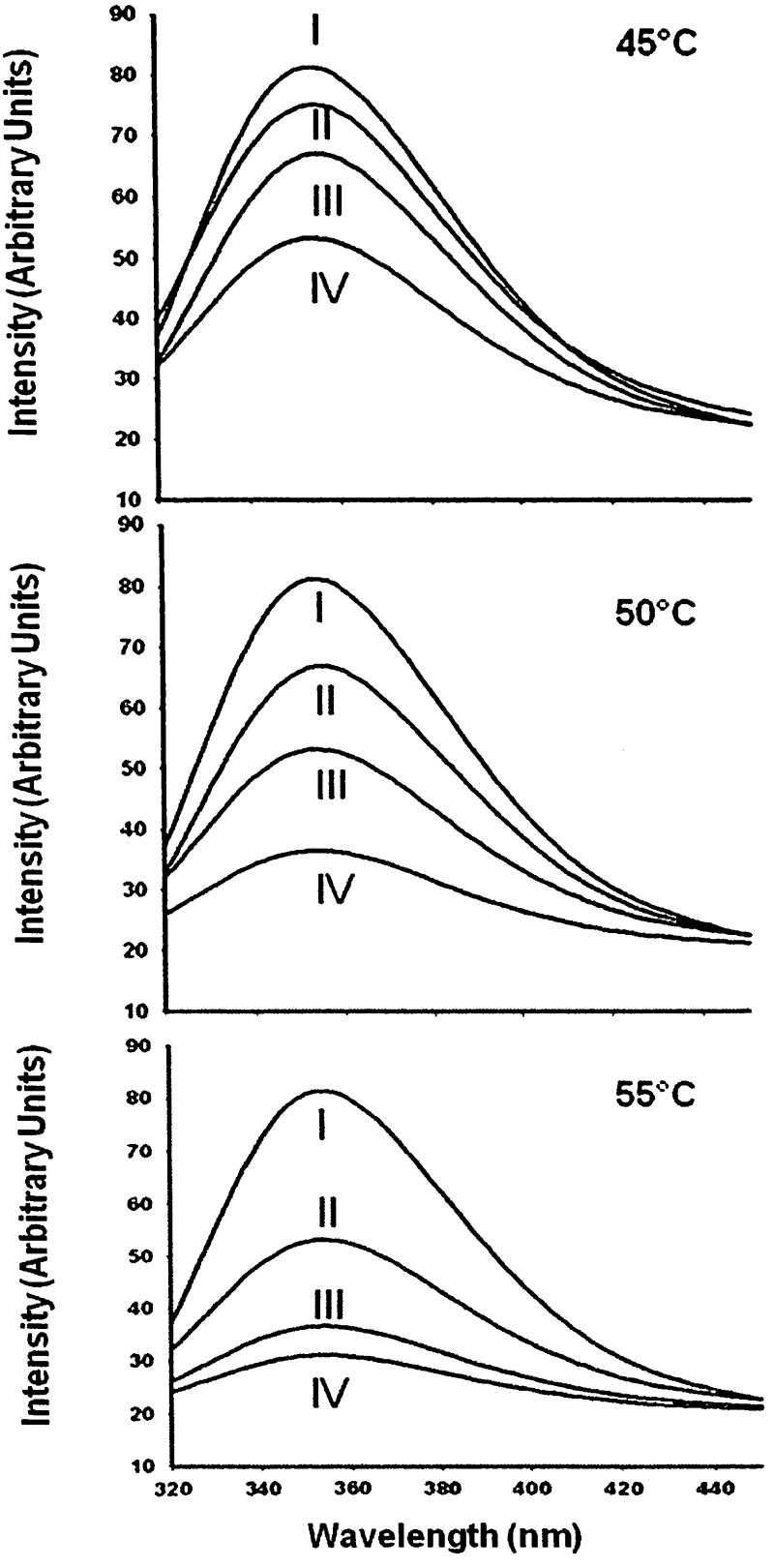

Fig. 4.3.14 Thermal denaturation analysis of *Ct*CBM35 by tryptophan fluorescence emission spectrum at 45, 50 and 55°C. *Ct*CBM35 without polysaccharide (I) and in presence of 0.3% (w/v) carob galactomannan (II), locust bean galactomannan (III) and konjac glucomannan (IV).

4.3.7 Isothermal titration calorimetry of ligand binding at higher temperature

The titrations of *Ct*CBM35 against carob galactomannan, locust bean galactomannan and konjac glucomannan are displayed in Fig. 4.3.15A, Fig. 4.3.15B and Fig. 4.3.15C, respectively. The quantitative assessment and thermodynamics of ligand binding by *Ct*CBM35 were determined by ITC at 55°C and are displayed in Table 4.3.5. *Ct*CBM35 displayed higher binding affinity as association constant (K_a) with carob galactomannan was 1.8 x 10^3±105 M^{-1} followed by locust bean galactomannan, 1.7 x 10^3±144 M^{-1} and konjac glucomannan 1.5 x 10^3±155 M^{-1} in ITC study (Table 4.3.5). The ITC analysis at 55°C displayed 100 fold reduced ligand binding affinity of *Ct*CBM35 as compared to the affinity electrophoresis (Section 4.3.1) where, K_a values of *Ct*CBM35 at 25°C against carob galactomannan and konjac glucomannan were 1.24 x 10^5 M^{-1} and 1.43 x 10^5 M^{-1}, respectively (Ghosh *et al.*, 2013). Similarly, the K_a values of *Ct*CBM35 upon binding with these substrates on analysis by fluorescence spectroscopy (Section 4.3.3) at 25°C were 100 fold higher than those of ITC studied at 55°C. The lowering of affinity for ligands might be due to the reduced entropy (ΔS) at higher temperatures as stated in earlier reports (Kinoshita and Yoshidome, 2009; Luís *et al.*, 2013) The cause of reduced entropy may be due to the decrease in entropy of the polar amino acids residues of disordered *Ct*CBM35 at high temperature. The polar amino acid residues of the disordered protein are able to re-establish the hydration shells in even more disordered environment by lowering the entropy at higher temperatures (Kinoshita and Yoshidome, 2009). The free energy of binding (ΔG) against carob galactomannan, locust bean galactomannan and konjac glucomannan were 4.9 kcal/mole, 4.8 kcal/mole and 4.7 kcal/mole, respectively by ITC (Table 4.3.5). The reduction in ΔG

in ITC was also lower than those as compared with fluorescence spectroscopy (Section 4.3.3) where *Ct*CBM35 displayed higher free energy (ΔG) -6.0 kcal/mole against konjac glucomannan and -5.26 kcal/ mole against carob galactomannan, (Ghosh *et al.*, 2013). Thus, the temperature is an important factor in ligand binding by the carbohydrate binding modules.

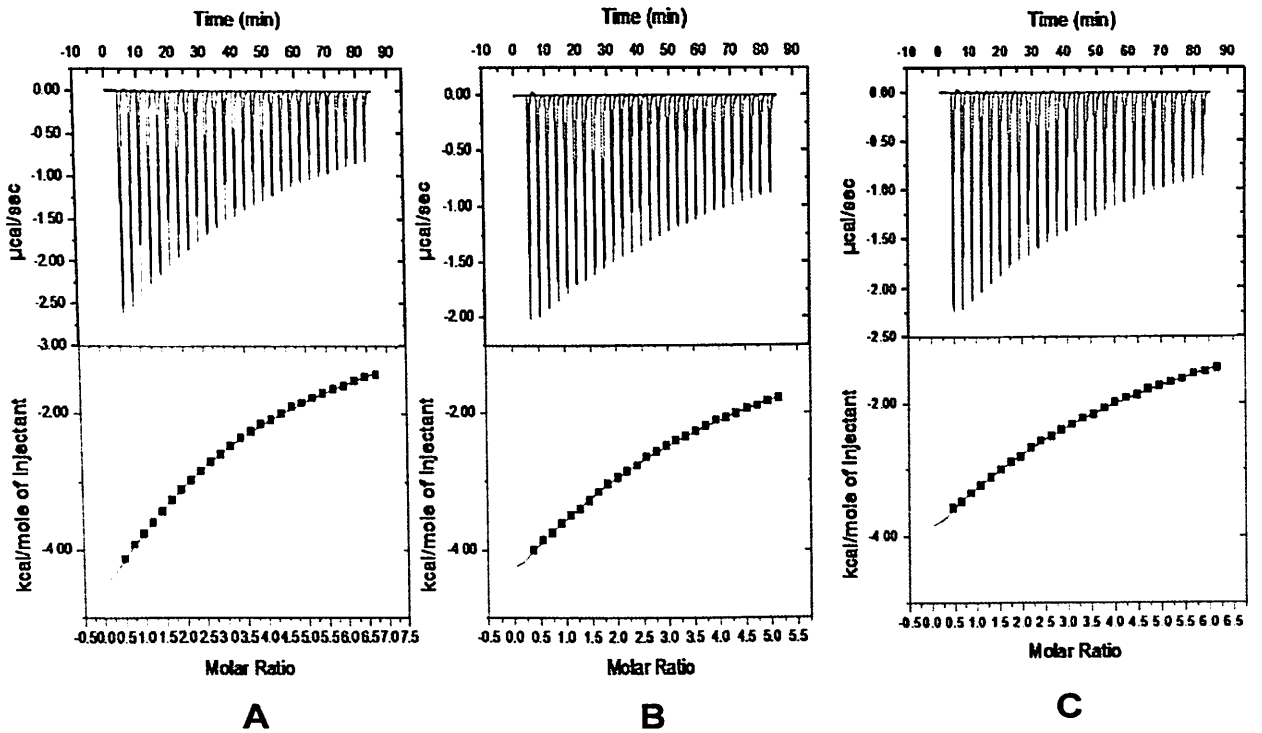

Fig. 4.3.15 Isothermal titration calorimetry of *Ct*CBM35 in presence of 0.3% (w/v) (a) carob galactomannan, (b) locust bean galactomannan and (c) konjacglucomannan at 55°C.

Table 4.3.5 Affinity and thermodynamic binding parameters of *Ct*CBM35 with polysaccharide ligands derived by ITC at 55°C.

Ligand	K_a (M^{-1})	-ΔG (kcal $mole^{-1}$)	-ΔH (cal $mole^{-1}$)	-TΔS (cal $mole^{-1}$)	n
Carob galactomannan	$1.8\times10^3\pm105$	4.9	6.16×10^4	5.67×10^4	0.8±0.3
Locust bean galactomannan	$1.7\times10^3\pm144$	4.8	1.8×10^4	1.32×10^4	1.53±0.4
Konjac glucomannan	$1.5\times10^3\pm155$	4.7	6.96×10^4	6.49×10^4	1.02±0.7

4.3.8 Unfolding transition of *Ct*CBM35 in guanidine hydrochloride and urea

The unfolding transition of *Ct*CBM35 was investigated in presence of GnHCl and urea. The addition of GnHCl (1-6M) and urea (1-7M) to *Ct*CBM35 displayed decrease in the peak intensity as denaturant concentration increased (Fig. 4.3.16A and Fig. 4.3.16B). The maximum fall in fluorescence peak intensity of *Ct*CBM35 was observed at 6M GnHCl and 7M urea (Fig. 4.3.16A and Fig. 4.3.16B, respectively). The lowering of peak intensities was coupled with a bathochromic shift (red shift, shift towards longer wavelength) of the fluorescence maxima from 355 nm (native form) to 370 nm (denatured form) in presence of GnHCl (6M) and from 355 nm to 360 nm in presence of urea (7M). This was perhaps due to the Trp residue, which is otherwise buried in the native form, became exposed on the surface in the denatured *Ct*CBM35. A similar unfolding mechanism of recombinant human interferon γ was described earlier (Christova *et al.*, 2003).

The unfolding curves were obtained by deducing the unfolded fractions (Section 4.2.9) at pH 7.0 for GnHCl and urea, are shown in Fig. 4.3.16C. In both the cases, the curves displayed a sigmoid pattern signifying that the unfolding of *Ct*CBM35 in presence of GnHCl and urea was a two-stage process, where low unfolded fractions of *Ct*CBM35 were obtained till 4 M and 5 M, respectively. The unfolding of *Ct*CBM35 increased up to 5.5 M of GnHCl and 6.5 M of urea thereafter a saturation phase was observed upto 8 M. The results also indicated that the unfolding of *Ct*CBM35 was more effective in presence of GnHCl than urea. It was observed in Fig. 4.3.16C, that the midpoint value of unfolding of *Ct*CBM35 was 5M for GnHCl and 6.25M for urea. The free energies ΔG of *Ct*CBM35 unfolding calculated from these curves by linear extrapolation method at pH 7.0 were ΔG = 2.19

kJ/mole with GnHCl and ΔG = 1.97 kJ/mole with urea. The free energies clearly indicated that higher energy is required by both denaturants to destabilize the electrostatic interactions within *Ct*CBM35. These results are contrary to those with the unfolding phenomenon of human interferon γ in presence of GnHCl and urea which required lower energies to unfold as described by Christova *et al.* (2003).

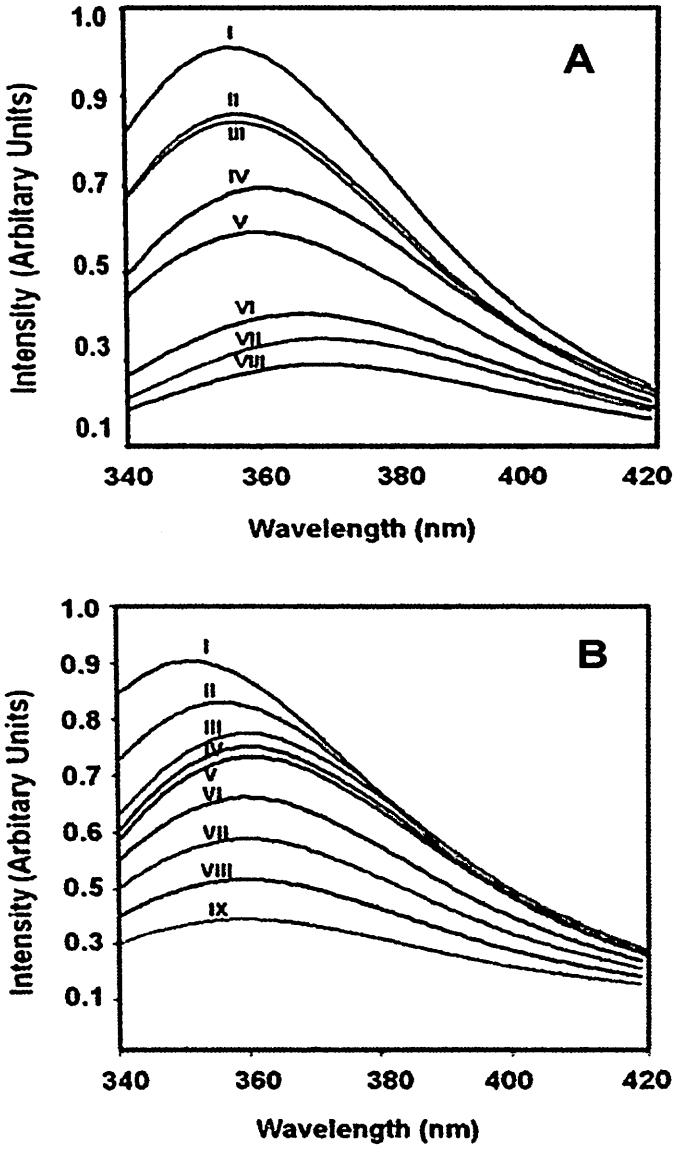

Fig. 4.3.16 Tryptophan fluorescence emission spectrum of *Ct*CBM35 in presence of (A) Guanidium hydrochloride (GnHCl), (I) Control, (II) 1 M, (III) 2 M, (IV) 3 M, (V) 4 M, (VI) 5 M, (VII) 5.5 M, (VIII) 6 M, (B) Urea, (I) Control, (II) 1 M, (III) 2 M, (IV) 3 M, (V) 4 M, (VI) 5 M, (VII) 6 M, (VIII) 6.5 M, (IX) 7 M.

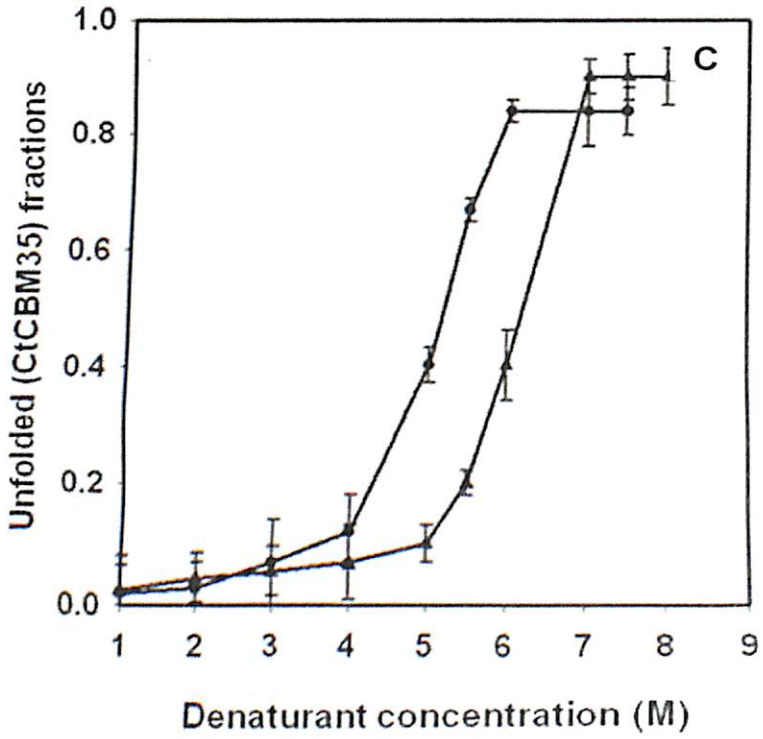

Fig. 4.3.16 Fraction of *Ct*CBM35 unfolded as a function of (●) GnHCl and (▲) Urea concentrations as determined by UV absorbance at A_{280}.

4.3.9 Secondary structure analysis of *Ct*CBM35 by circular dichroism

The protein solution (15 μM) in 10 mM Tris-HCl, pH 7.5 was analyzed on a spectropolarimeter at 25°C and the percentage of α-helices, β-sheets and random coils present in *Ct*CBM35 structure were calculated using K2d software. The analysis of CD spectra of *Ct*CBM35 for detecting the secondary structural elements was based on the previous reports of CD spectra of proteins by Kelly *et al.* (2005). The comparison of CD spectra of *Ct*CBM35 with the reports of Kelly *et al.* (2005) showed that it predominantly contained β-sheets and coils (Fig. 4.3.17). The CD spectra *Ct*CBM35 analyzed K2d as described by Andrade *et al.* (1993) revealed that it contains 45% β-sheets, 52% random coils and only 3% α-helices (Table 4.3.5). Therefore, it could be deduced that the number of secondary structures available in *Ct*CBM35 are 12 β-sheets, 15 random coils and 2 alpha helices (Table 4.3.5)

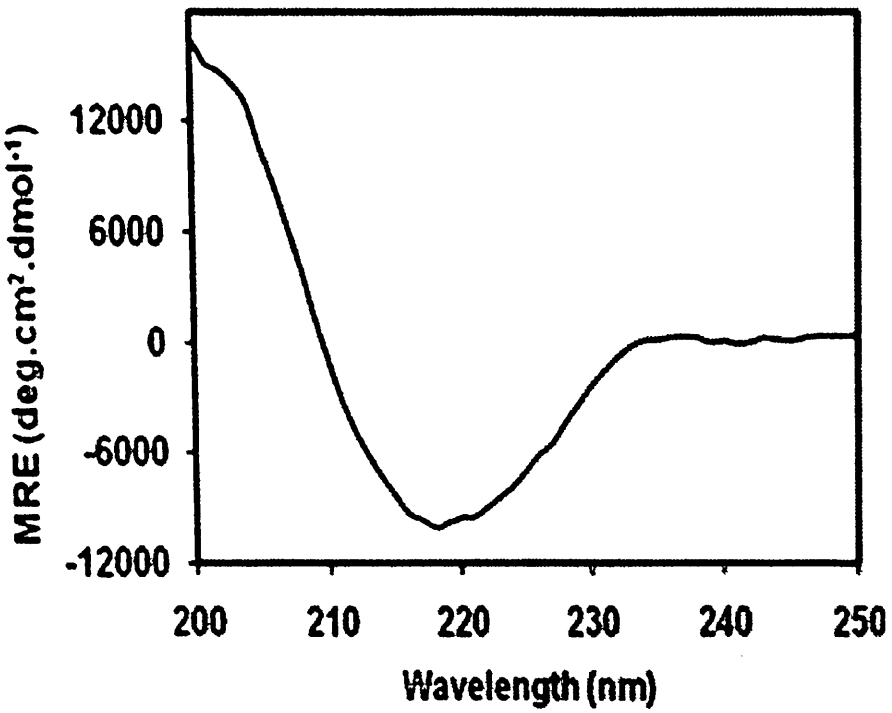

Fig. 4.3.17 Circular dichroism (CD) spectrum of *Ct*CBM35 for the determination of secondary structures.

Table 4.3.5 Secondary structure analysis of *Ct*CBM35 by far-UV CD spectrum.

Secondary structure content	CD Spectra (%)	Numbers of secondary structures (by CD Spectra)
α-helix	03	2
β-sheet	45	12
Random coil	52	15

4.1.10 *In silico* structure prediction and ligand binding of *Ct*CBM35

4.3.10.1 Structure characterization and quality assessment of modelled protein

BLAST (Basic Local Alignment Search Tool) search for sequence similarity with default parameter in NCBI against PDB database retrieved the number of hits of *Ct*CBM35 belongs to the family 35 carbohydrate binding module. Top hit X-ray crystallography structure of CBM35 from *Amycolaptosis orientalis* (PDB ID: 2VZP) which covered full query and displayed 34% similarity (score of 39.7 and Evalue 0.001) was acquired as a template to model the structure of *Ct*CBM35. The overall

3D structure of *Ct*CBM35 showed that it is rich in β–sheets, consisting of a pair of six stranded antiparallel β–sheets having β-jelly-roll fold which is quite common in many CBMs (Fig. 4.3.18A). Topology diagram displayed 12 β-strands (dark grey), only 2 small α-helix (black) and 15 random coil (arrow lines) formed a β-jelly roll topology (Fig. 4.3.18B). Secondary structure prediction by PredictProtein showed a pair of α-helices (<5%) but apart from this, the dominance of a pair of six extended β-sheets (>42%) and fifteen numbers of random coils (<53%) were also observed in the 3-D model *Ct*CBM35 substantiating the the results of CD spectra of *Ct*CBM35. Therefore, CD spectrum analysis validated the prediction of secondary structure of *Ct*CBM35. The presence of high percentage of β-sheets and random coils are in agreement with the *in silico* prediction of *Ct*CBM35 3-D model, which also revealed β-jelly roll architecture.

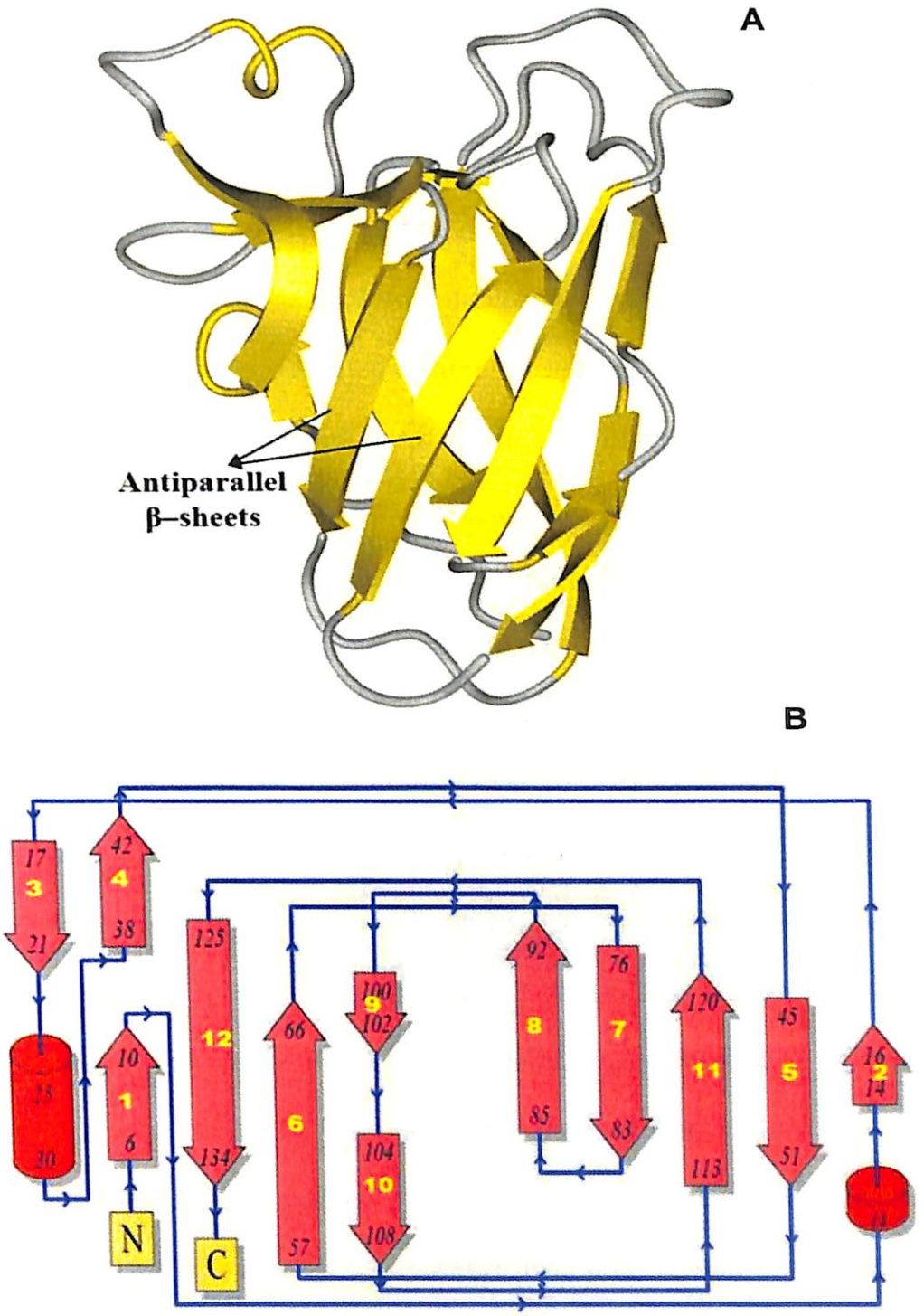

Fig. 4.3.18 (A) Overall 3-D representation of modelled carbohydrate binding module family 35 from *Clostridium thermocellum* showing β-jelly-roll fold (B) Topology diagram of *Ct*CBM35 showing β-jelly roll topology.

Structure similarity search of modelled protein in DaliLite server (www.ebi.ac.uk/Tools/dalilite/) showed similarity with native structure of a family 35 CBM from *C. thermocellum* (2W1W chain B) and CBM35 from *A. orientalis* (2VZP chain B) with RMSD of 1.7Å and 1.8Å, respectively. Modelled *Ct*CBM35 after energy minimization was validated by Ramachandran plot analysis. Out of total of 134 residues, 93% residues lie in most favored regions, 7% residues lie in additional allowed region and there was no residue in generously allowed or disallowed regions (Fig. 4.3.19A). This indicated that amino acid residues in the modelled *Ct*CBM35 occupied favorable phi (φ) and psi (ψ) backbone dihedral angles. Overall quality factor of *Ct*CBM35 was 88% in the ERRAT plot analysis (Fig. 4.3.19B). ERRAT plot displayed the value of the error function *vs* position of a 9-residue sliding window. By comparison with statistics from highly refined structures, the error values have been calibrated to give confidence limits in percentage (http://nihserver.mbi.ucla.edu/ERRATv2/). Merely 12% amino acid residues of modelled *Ct*CBM35 fall over 95% level of significance error rate. This signified the good quality 3-D structure of *Ct*CBM35. Verify 3D score was obtained 95%, i.e. 95% of the residues had an averaged 3D-1D score 0.35 which is > 0.2. It determined a compatibility of an atomic model (3D) with its own amino acid sequence (1D) (Fig. 4.3.19C). First it categorized each residue into structural class based on its location and environment (alpha, beta, loop, polar, non polar etc.) then it generates a score by comparing each residue with a collection of good structures, as a reference (Pace *et al.*, 1989).

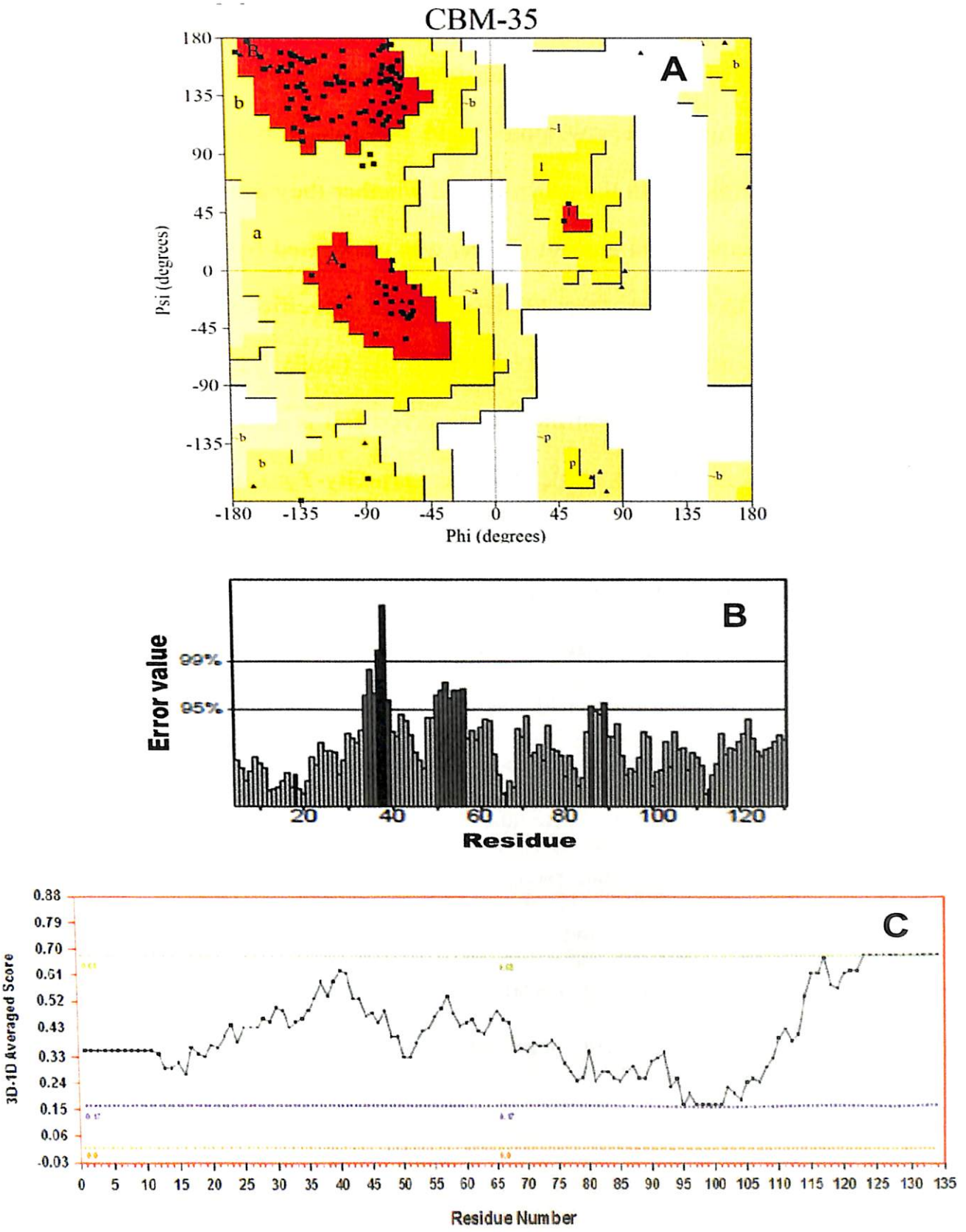

Fig. 4.3.19 Structure validation and quality assessment of *Ct*CBM35 by (A) Ramachandran plot (B) ERRAT Plot (C) Verify 3D.

4.3.10.2 Ligand binding site analysis of CtCBM35

CBMs play a critical role in substrate recognition and binding. It is very important to investigate the key amino acid residues playing significant role in recognition and binding with the substrate and whether they are conserved within the family. Multiple sequence alignment (MSA) was performed by taking representative members of CBM35 family having different substrate specificity. MSA result showed many amino acid residues are conserved within the family 35 CBMs (Fig. 4.3.20). The Trp-Gly-Phe motif was identified as conserved and is also present in *Ct*CBM35 (highlighted in yellow) (Fig. 4.3.20). Moreover, Trp-Gly-Tyr motif which is probably involved in the substrate specificity towards mannans, was conserved within the manann specific CBMs (Pinheiro *et al.*, 2008). It was demonstrated earlier by NMR solution structure of mannan-specific CBM35 from *C. japonicas* that it bound to mannopentose involving amino acid residues Tyr60, Lys63, Trp109, Gly110 and Tyr111 showing maximum chemical shifts on ligand binding (Colovos and Yeates, 1993). While, the involvement of aromatic amino acid residues Tyr22-Tyr53-Tyr129 in β-(1→4) linked glucomannan recognition by CBM11 was reported earlier by Carvalho *et al.* (2004). It was found that the above mentioned key amino acid residues were present in *Ct*CBM35, except Tyr60. The others amino acid residues like Arg76, Trp123, Gly124 and Phe125 were conserved within *Ct*CBM35 (highlighted in yellow, Fig. 4.3.20).

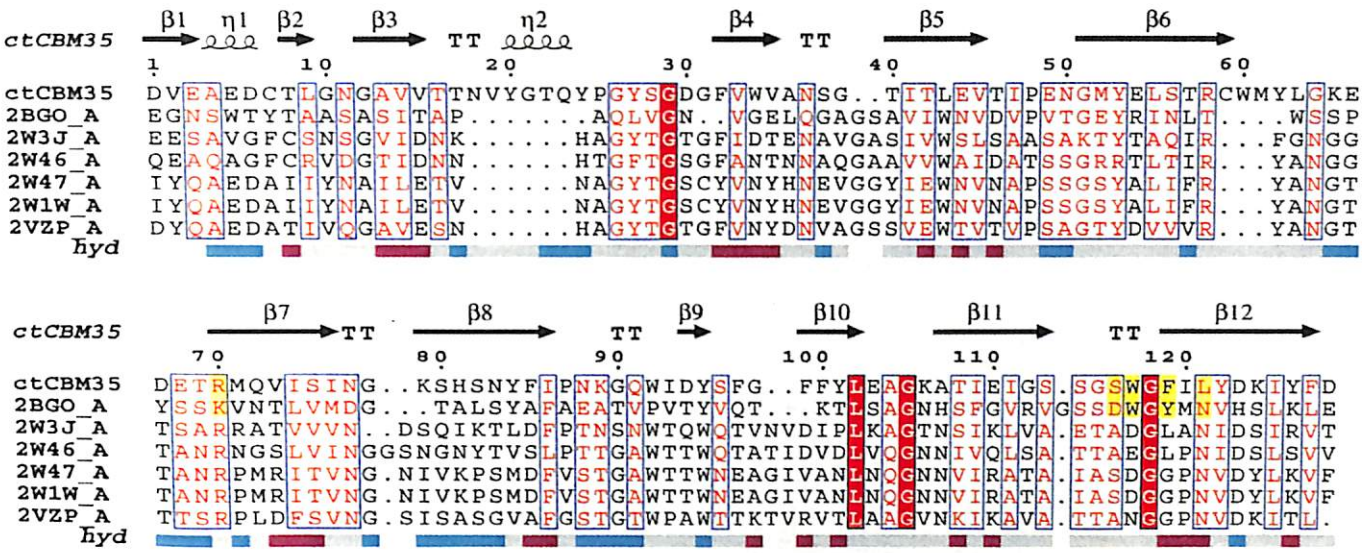

Fig. 4.3.20 Multiple sequence alignment of CBM35 having different substrate specificity with their respective PDB:IDs of *Amycolaptosis orientalis* (2VZP), *Cellvibrio japonicus* Abf62 (2W46), uncultured bacterium from environmental isolate (2W3J), *Clostridium thermocellum* (2W1W), *Clostridium thermocellum* (2W47) and *Cellvibrio japonicus* (2BGO) were aligned with *Ct*CBM35. The residues which are conserved and probably involved in substrate specificity and binding (Man-CBM35) are shown in yellow color. Sequences in red color are fully conserved while amino acids in blue color rectangular box are conserved but not all the residues are identical. Line above the sequence represents secondary structure of *Ct*CBM35. Line below the sequence represents the relative hydrophobicity of the residues, cyan color for hydrophilic, pink for hydrophobic and grey for intermediate.

4.3.11 Docking analysis of ligand binding interaction with *Ct*CBM35

The molecular docking analysis of modelled *Ct*CBM35 with various manno-configured ligands *viz.* oligosaccharides and galactomannan provided a better understanding of the key amino acid residues involved in strong hydrophobic interactions. There are plenty of evidences which show how hydrophobic stacking interactions and hydrogen bonds play an important role in ligand binding in case of family 35 CBMs (Bowie *et al.*, 1991). The docking results of *Ct*CBM35 with mannopentose (Fig. 4.3.21A and Fig. 4.3.21B) and galactomannan (man-gal-man, moiety) (Fig. 4.3.22A and Fig. 4.3.22B) showed that the residues Tyr26, Gln29,

Asn43, Trp66, Tyr68, Leu69, Arg76 and Leu127 are participating in making polar interaction with galactomannan, while residues Tyr30, Trp40, Val41, Ala42, Met67, Trp-123, Phe125 and Ile126 are making a hydrophobic pocket around the binding site cavity.

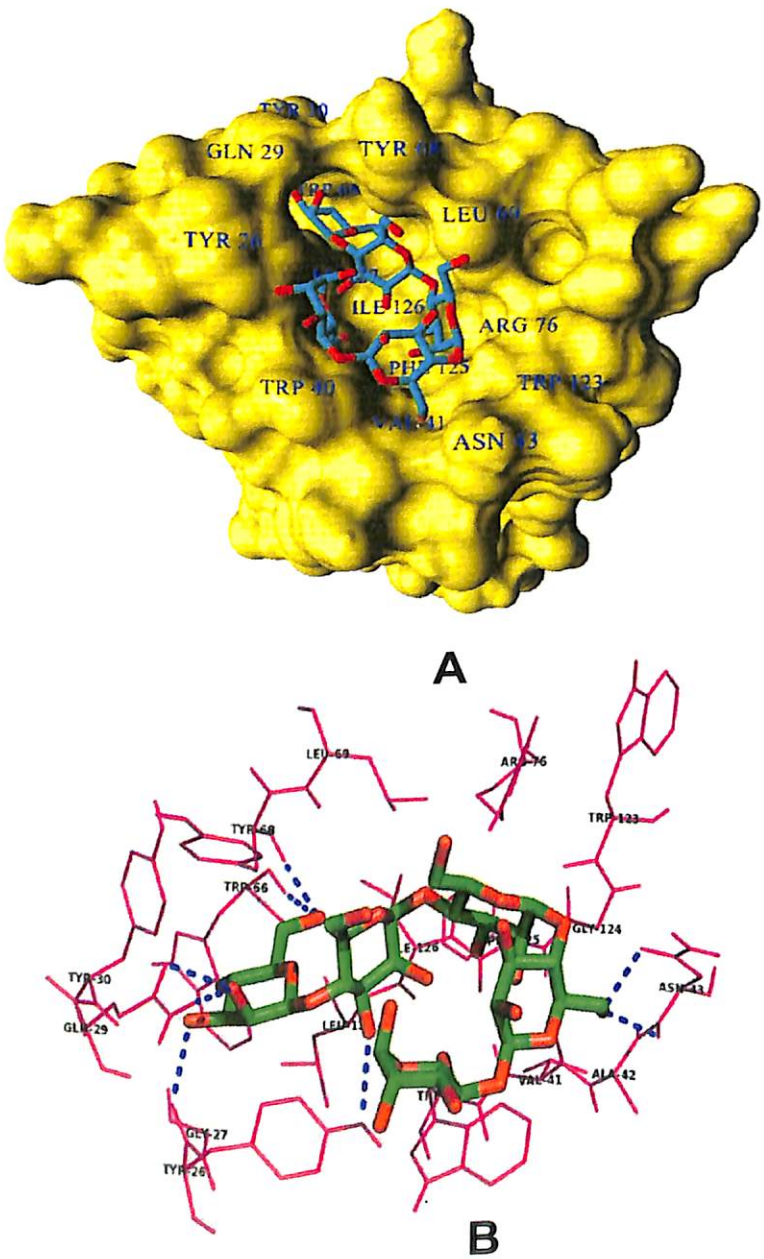

Fig. 4.3.21 (A) Showing binding site surface cavity with labelled residues forming hydrophobic groove to accommodate mannopentose (B) Best pose of docking of *Ct*CBM35 with mannopentose bound conformation shows polar interaction (dash line) and residues probably involve in hydrophobic interaction present within 4 Å.

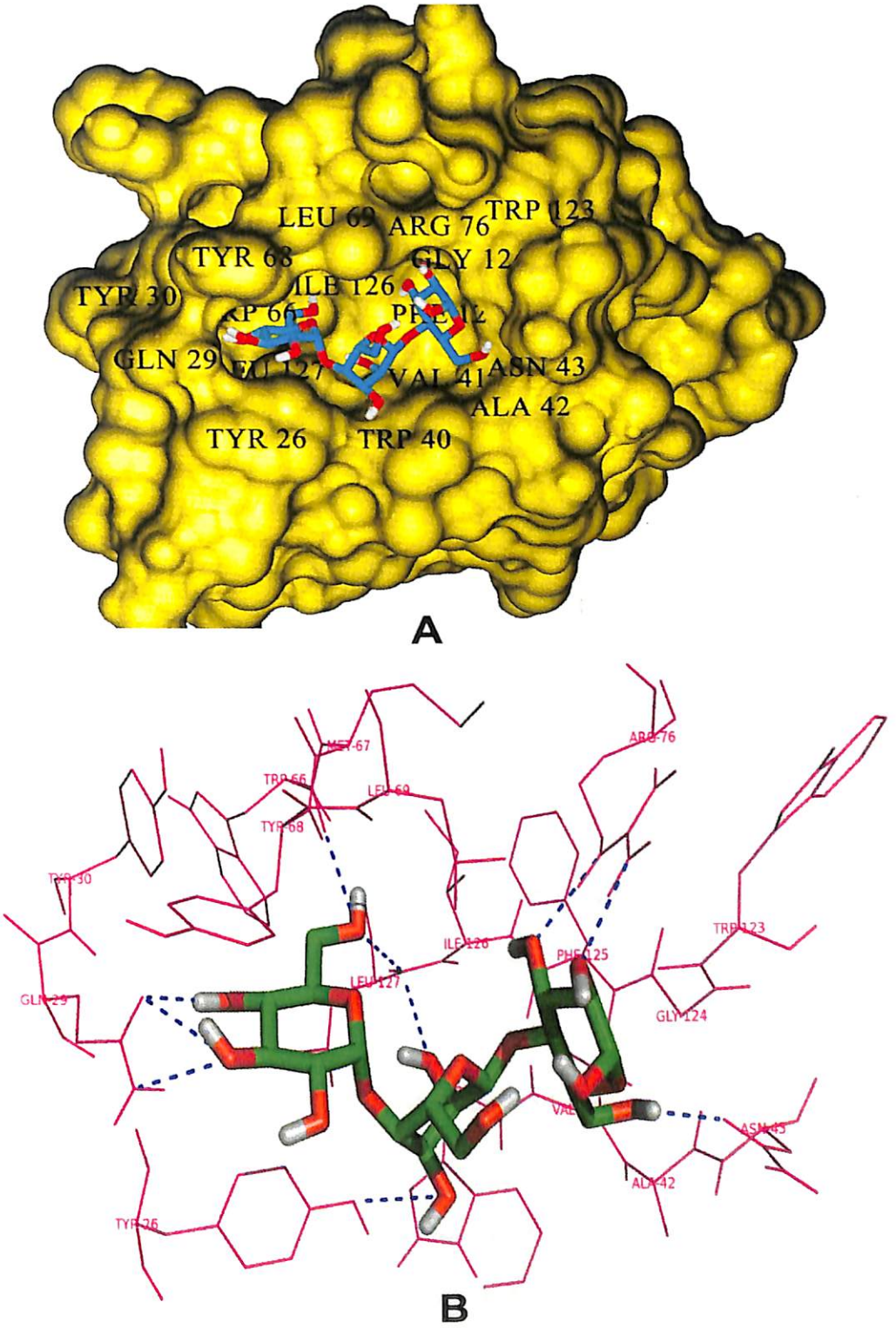

Fig. 4.3.22 (A) Showing binding site surface cavity with labelled residues forming hydrophobic groove to accommodate mannotriose (B) Best pose of docking of *Ct*CBM35 with mannotriose bound conformation shows polar interaction (dash line) and residues probably involve in hydrophobic interaction present within 4 Å.

The docking results of *Ct*CBM35 with oligosaccharides and galactomannan are summarised in Table 4.3.6. Mannotriose showed higher binding affinity for *Ct*CBM35, $K_a = 3.0 \times 10^5\ M^{-1}$ as compared to mannotriose, $K_a = 1.8 \times 10^5\ M^{-1}$ and galactomannan, $K_a = 1.22 \times 10^5\ M^{-1}$ (Table 4.3.6). The free energy of binding (ΔG) of mannotriose was maximum -6.57 kcal/mole, followed by mannopentaose -5.29 kcal/mole galactomannan -4.8 kcal/mole (Table 4.3.6) while mannohexose displayed positive free binding energy on docking with *Ct*CBM35 (not included the data). This was possibly due to the size of binding site pocket, which is not large enough to accommodate bulkier mannohexose as compared to mannotriose. Putative protein-ligand binding site shown by CBMs having β-sandwich fold, is mainly situated on either concave surface made by the anti-parallel β-sheets or at the top cavity made by the loop that connects the two β-sheets (Fanutti *et al.*, 1995). Analysis of binding site topography of the CtCBM35 showed that it was made up by the amino acid residues present in loops connecting anti-parallel β-sheets (Fig. 4.3.23A). First loop started from Ser120 to Phe125 (between 11-12 β-strand) making a base of the cavity, creating a flat hydrophobic platform involving two conserved aromatic amino acids Trp-123 and Phe125. The second loop started from Cys65 to Arg76 (6-7 β-strand) and third loop from Val21 to Tyr33 (3-4 β-sheets) formed the side surface of the cavity and provided the soluble accessible surface for the ligands (Fig. 4.3.23A). Here, amino acid residues Trp66, Tyr68, Leu69 and Arg76 (from loop second) and Tyr26 and Glu29 (from loop third) were also present and made polar contact with the ligand molecule (Fig. 4.3.23B).

Table 4.3.6 Amino acid residue interactions of *Ct*CBM35 with manno-configured ligand

Ligand	Association constant (K_a) (x 10^5 M^{-1})	Free binding energy (ΔG) (kcal/mol)	Polar interactions	Hydrophobic residue in 4Å region
Mannotriose	3.0	-6.57	Tyr26, Glu29, Asn43, Trp66, Arg76, Leu127	Tyr30, Trp40, Val41, Ala42, Met67, Tyr68, Leu69, Phe125, Ile126
Mannopentaose	1.8	-5.29	Tyr26, Gln29, Asn43, Trp66,Tyr68,	Tyr30,Trp40, Val41, Ala42,Leu69 , Arg76,Trp123,Phe125 Ile126, Leu127,
Galactomannan	1.22	-4.80	Asn43, Trp66,Tyr68, Leu69, Arg76	Tyr26, Trp40, Val41, Met67,Ser122, Trp-123, Phe125, Ile126, Leu127,

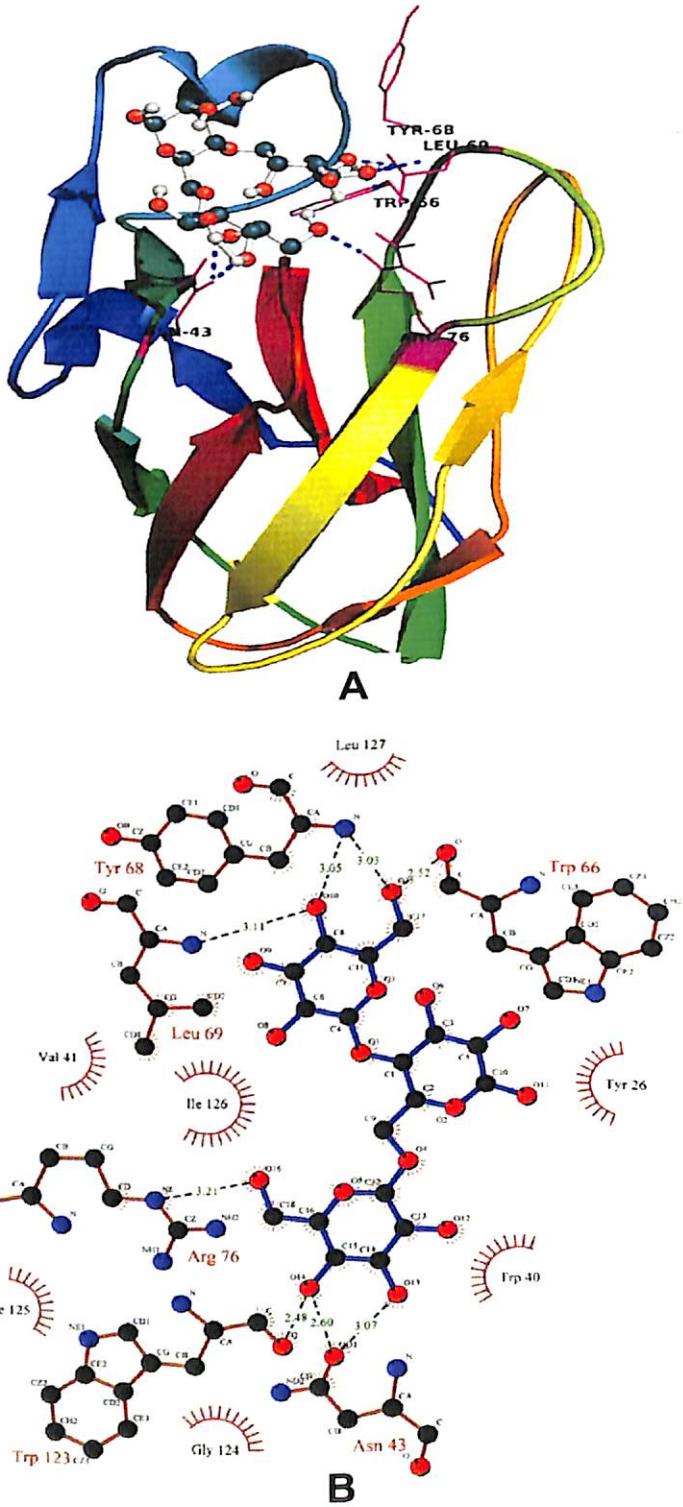

Fig. 4.3.23 (A) Ribbon representation of *Ct*CBM35 using PyMOL complex with galactomannan (ball-stick view) shows position of substrate binding site (shown in circle). Residues making polar contact with galactomannan are positioned mainly in loop region (showed by dashed lines) (B) Schematic 2D depiction of galactomannan binding site residues of *Ct*CBM35. Dashed lines shows hydrogen bonds and connected atoms are shown with spokes radiating back. The amino acid residues displayed in arc with spokes involved in hydrophobic interactions.

4.3.12 Molecular dynamics (MD) study of *Ct*CBM35 in presence of Ca^{2+} ion

The Ca^{2+} ion played a key role in providing higher stability to *Ct*CBM35 at higher melting temperature (described in Section 4.3.5). This analysis was further analyzed using PyMOL tool from the generated model of *Ct*CBM35. In order to check the stability of *Ct*CBM35 model in presence of Ca^{2+} ion, RMSD of backbone atoms from MD production run was plotted as time dependent function in Fig. 4.3.23. The graph clearly indicated that there was little change in RMSD for the initial 1 ns and the system converged with fluctuations less than 0.3 Å. Furthermore, structural comparison of energy minimized structure with structures generated throughout the MD production run indicates that the energy minimized *Ct*CBM35 model represents a stable conformation.

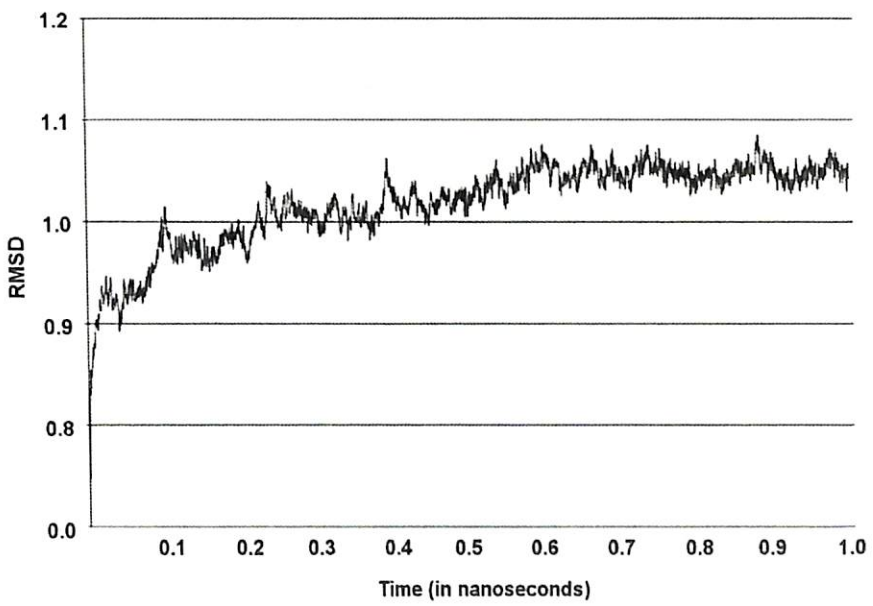

Fig. 4.3.23 MD simulation of modelled *Ct*CBM35 shows that the energy-minimized structure is energetically stable.

There was one Ca^{2+} ion binding pocket interacting with 7 amino acid residues *viz.* Glu 9, Glu 11, Ser 34, Gly 37, Asp 129. It was observed that negatively charged residues were predominant except Ser and Gly which interacted strongly with positively charged Ca^{2+} ions. These amino acid residues made coordinate bonds with Ca^{2+} ion and their orientation was changed remarkably. The comparative study of two *Ct*CBM35 models with unbound and bound Ca^{2+} ion (Fig. 4.3.24A and Fig. 4.3.24B) displayed orientation of amino acid residues within the binding pocket. When both the models were superimposed (Fig. 4.3.24C), it was observed that the residues changed their orientations at their similar positions with Ca^{2+} ion bound state than the unbound structure. The bound state residues have less root mean square deviation (RMSD) value of 1.08 Å as compared to unbound state of 1.8 Å. This reduced RMSD value due to the stiffer binding with Ca^{2+} ion prevented less free movement in their bound state (Noorbatcha *et al.*, 2012).

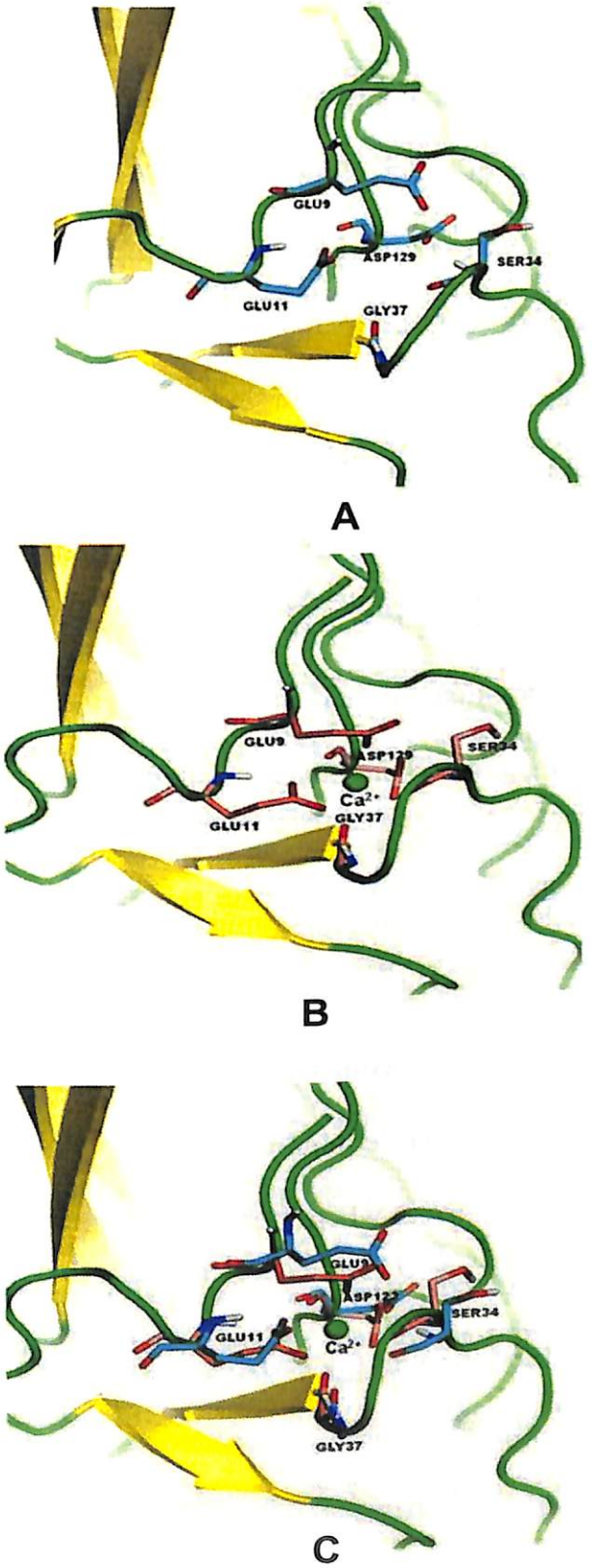

Fig. 4.3.24 Amino acid residues of *Ct*CBM35 in the modelled structure (A) without Ca^{2+} ion (B) with Ca^{2+} ion (C) superimposed structure of both (A) and (B) showing the Ca^{2+} ion binding pocket to compare the altered positions of the amino acid residues in absence and presence of Ca^{2+} ion.

4.4 Conclusions

Polysaccharide binding and structure analyses of *Ct*CBM35 from *Clostridium thermocellum* were carried out. The cloned family 35 Carbohydrate binding module (*Ct*CBM35) from *Clostridium thermocellum* preferred binding with manno-configured polysaccharides. *Ct*CBM35 discriminated during carbohydrate selection showing its affinity only with manno-configured ligands among the manno-, cello- and xylo-configured polysaccharides. The binding analysis of *Ct*CBM35 to soluble polysaccharides was evaluated using affinity gel electrophoresis. The equilibrium association constant (K_a) of the *Ct*CBM35 was determined for mannotriose, konjac glucomannan, carob galactomannan and locust bean galactomannan by measuring the relative migration distance of proteins on native PAGE gels in the presence of above ligands. Both *Ct*CBM35 showed lesser affinity for carob galactomannan (for which the catalytic modules showed maximum activity) as compared to konjac glucomannan which was clear from greater retardation of *Ct*CBM35 at lower concentration of konjac glucomannan during affinity electrophoresis. Oligosaccharide and polysaccharide binding studies were also corroborated the findings of affinity electrophoresis where ligand binding was observed higher with mannotriose and konjac glucomannan as compared with carob and locust bean galactomannan. Ligand binding with *Ct*CBM35 was evidenced from the fluorescence peack shift of 21 nm. In dynamic light scattering, the larger particle size of *Ct*CBM35 is due to the polysaccharide binding. The cationic interaction of aromatic residues with carob galactomannan and konjac glucomannan insists *Ct*CBM35 domain alteration to more compact form reducing the random diffusion of the particles between polysaccharide and amino acid residues. Due to simpler structure

of oligosaccharide (mannotriose) and the polysaccharide ligand konjac glucomannan, the interaction with aromatic residues in the binding pocket of *Ct*CBM35 uphold strong binding as compared to carob galactomannan with substituted galactose side chain.

Instances of Ca^{2+} ion induced stability of *Ct*CBM35 was evident from protein melting study where the low melting temperature of the protein was shifted to higher temperature. The metal ion (Ca^{2+}) chelation by EDTA revealed the protein stability lost at very low temperature but the structure could be restored while Ca^{2+} was added to minimize the effects of EDTA. Therefore, divalent metal cation Ca^{2+} plays significant role in holding the structure that is sensitive against temperature.

Higher temperature invoked lesser stability to *Ct*CBM35 and was evidenced from fluorescence spectrum at different temperatures. The loss in structural stability attributed to higher temperature was also hampered the ligand binding capacity of *Ct*CBM35 and isothermal titration calorimetry revealed that at the melting temperature *Ct*CBM35 lost its 100 fold ligand binding capacity. The highly substituted α-(1→6)-galactose on β-(1→4)-mannose backbone in locust bean galactomannan might be another reason for lower binding by *Ct*CBM35. *Ct*CBM35 is sensitive towards thermal exposure and shows weak binding ability of ligands at its melting temperature. Titrations against polysaccharides at 55°C, *Ct*CBM35 exhibited ~100 fold lower binding affinity against konjac glucomannan, locust bean galactomannan and carob galactomannan as compared to binding at 25°C. The interpretation of unfolding transition in presence of GnHCl and urea revealed that *Ct*CBM35 holds a significant structural stability and can resist denaturation at higher concentrations of these denaturants.

The 3-dimensional model of *Ct*CBM35 from *Clostridium thermocellum* generated by Modeller9v8 displayed predominance of β-sheets arranged as β-jelly-roll fold. The secondary structure of *Ct*CBM35 by PredictProtein showed presence of two α-helices (3%), twelve β-sheets (45%) and fifteen random coils (52%). Secondary structural element analysis of cloned, expressed and purified recombinant *Ct*CBM35 by Circular dichroism also corroborated the *in-silico* predicted secondary structure. Multiple sequence alignment of *Ct*CBM35 showed conserved residues (Tyr123, Gly124 and Phe125), which are commonly observed in mannan specific CBMs. The docking analysis of *Ct*CBM35 with manno-oligosaccharide displayed the involvement of Tyr26, Gln29, Asn43, Trp66, Tyr68, Leu69, Arg76 and Leu127 residues, making polar contact with the ligand molecules. Ligand docking analysis of *Ct*CBM35 exhibited higher binding affinity with mannotriose and galactomannan (Man-Gal-Man, moiety) substantiated the affinity binding and fluorescence results, displaying similar values of K_a.

References

Ahmad, F., Yadav, S. and Taneja, S. (1992) Determining stability of proteins from guanidinium chloride transition curves. Biochem. J. 287:481-485.

Ahmed, S., Luis, A.S., Brás, J.L.A., Fontes, C.M.G.A. and Goyal, A. (2013) Functional and structural characterization of family 6 Carbohydrate Binding Module (*Ct*CBM6A) of *Clostridium thermocellum* α-L-Arabinofuranosidase. Biochemistry (Moscow). 78:1272-1279.

Andrade, M.A., Chacón, P., Merelo, J.J. and Morán, F. (1993) Evaluation of secondary structure of proteins from UV circular dichroism spectra using an unsupervised learning neural network. Protein. Eng. 6:383-390.

Belatik, A., Hotchandani, S., Carpentier, R. and Tajmir-Riahi, H.A. (2012) Locating the binding sites of pb (ii) ion with human and bovine serum albumins. Plos One. 7(5): 1-9.

Berendsen, H.J.C., Van der Spoel, D. and Drunen, R.V. (1995) GROMACS: a message passing parallel molecular dynamics implementation. Comput. Phys. Commun. 91: 43-56.

Bolam, D.N., Xie, H., Pell, G., Hogg, D., Galbraith, G., Henrissat, B. and Gilbert, H.J. (2004) X4 modules represent a new family of carbohydrate-binding modules that display novel properties. J. Biol. Chem. 279:22953-22963.

Boraston, A.B., Bolam, D.N., Gilbert, H J. and Davies G. J. (2004) Carbohydrate-binding modules: fine-tuning polysaccharide recognition. Biochem. J, 382:769781.

Bowie, J.U., Luthy, R. and Eisenberg, D. (1991) A method to identify protein sequences that fold into a known three-dimensional structure. Science. 5019:164-170.

Bradford, M. (1976) A Rapid and Sensitive Method for the quantitation of microgram quantities of protein utilizing the principle of protein-dye binding. Anal. Biochem. 72:248-254.

Carvalho, A. L., Dias, F.M.V., Nagy, T., Prates, J.A.M., Proctor, M.R., Smith, N., Bayer, E.A., Davies, G.J., Ferreira, L.M., Romão, M.J., Fontes, C.M. and Gilbert, H. J. (2007) Evidence for a dual binding mode of dockerin modules to cohesins. Proc. Nat. Acad. Sci. 104(9):3089-3094.

Carvalho, A.L., Goyal, A., Prates, J.A.M., Bolam, D.N., Gilbert, H.J., Pires, V.M.R., Ferreira, L.M.A., Planas, A., Romão, M.J. and Fontes, C.M.G.A. (2004) The family 11 carbohydrate-binding module of *Clostridium thermocellum* Lic26A-Cel5E accommodates β-1,4 and β-1,3-1,4-mixed linked glucans at a single binding site. J. Biol. Chem. 279: 34785-34793.

Christova, P., Todorova, K., Timtcheva, I., Nacheva, G., Karshikoff, A. and Nikolov, P. (2003) Fluorescence studies on denaturation and stability of recombinant human interferon-gamma. Z. Naturforsch. C-a J. Biosci. 58:288-294.

Colovos, C. and Yeates, T. O. (1993) Verification of protein structures: patterns of nonbonded atomic interactions. Prot. Sci., 1993, 2, 1511-1519.

Creagh, A.L., Ong, E., Jervis, E., Kilburn, D.G..and Haynes, C.A. (1996) Binding of the cellulose-binding domain of exoglucanase Cex from *Cellulomonas fimi* to insoluble microcrystalline cellulose is entropically driven. Proc. Natl. Acad. Sci. (USA). 93:12229-12234.

Din, N., Forsythe, I.J., Burtnick, L.D., Gilkes, N.R., Miller, R.C. Jr., Warren, R.A. and Kilburn, D.G. (1994) The cellulose-binding domain of endoglucanase A (CenA) from *Cellulomonas fimi*: evidence for the involvement of tryptophan residues in binding. Mol. Microbiol. 11:747-55.

Dvortsov, I.A., Lunina, N.A., Chekanovskaya, L.A, Schwarz, W.H. (2009) Carbohydrate-binding properties of a separately folding protein module from β-1,3-glucanase Lic16A of *Clostridium thermocellum*. Microbiology. 155: 2442-2449.

Fanutti, C., Ponyi, T., Black, G.W., Hazlewood, G.P. and Gilbert, H.J. (1995) The conserved noncatalytic 40-residue sequence in cellulases and hemicellulases from anaerobic fungi functions as a protein docking domain. J. Biol. Chem. 270:29314-29322.

Ghosh, A., Luís, A.S., Brás, J.L.A., Pathaw, N., Chrungoo, N.K., Fontes, C.M.G.A. and Goyal, A. (2013) Deciphering ligand specificity of a Clostridium thermocellum family 35 carbohydrate binding module (*Ct*CBM35) for gluco- and galacto- substituted mannans and its calcium induced stability. Plos One. 8(12):e80415.

Gilbert, H.J., Knox, J.P. and Boraston, A.B. (2013) Advances in understanding the molecular basis of plant cell wall polysaccharide recognition by carbohydrate binding modules. Curr. Opin. Struct. Biol. 23: 669-677.

Gilkes, N.R., Jervis, E., Henrissat, B., Tekant, B., Miller, R.C.Jr., Warren, R.A. and Kilburn, D.G. (1992). The adsorption of a bacterial cellulase and its two isolated domains to crystalline cellulose. J. Biol. Chem. 267:6743-6749.

Greenfield, N. J. (2006) Using circular dichroism spectra to estimate protein secondary structure. Nat. Protoc. 1:2876-2890.

Hachem, M.A., Karlsson, E.N., Simpson, P.J, Linse, S., Sellers P, Williamson, M.P., Jamieson, S.J., Gilbert, H.J., Bolam, D.N. and Holst, O. (2002) Calcium binding and thermostability of carbohydrate binding module cbm4-2 of xyn10a from *Rhodothermus marinus*. Biochemistry 41: 5720-5729.

Henshaw J., Horne-Bitschy A., van Bueren A. L., Bolam D. N., Czjek M., Ekborg N. A., Weiner R. M., Hutcheson S. W., Davis G. J., Boraston A. B. & Gilbert H. J. (2006) Family6 carbohydrate binding modules in β-agarase display exquisite selectivity for the non-reducing termini of agarose chains. J. Biol. Chem. 281:17099-17107.

Hess, B., Kutzner, C., Van der Spoel, D. and Lindahl, E. (2008) GROMACS 4: algorithms for highly efficient, load-balanced and scalable molecular simulation. J. Chem. Theory. Comput. 4:435-447.

Johansson, R., Gunnarsson, L.C., Ohlin, M. and Ohlson, S. (2006) Thermostable carbohydrate-binding modules in affinity chromatography. J. Mol. Recognit. 19(4):275-281.

Jorgensen, H., Sanadi, A.R., Felby, C., Lange, N.E, Fischer, M. and Ernst, S. (2010) Production of ethanol and feed by high dry matter hydrolysis and fermentation of palm kernel press cake. Appl. Biochem. Biotechnol. 161(1-8):318-332.

Kelly, S.M., Jess, T.J. and Price, N.C. (2005) How to study proteins by circular dichroism. Biochim. Biophys. Acta., 2005, 1751, 119-139.

Kinoshita, M. and Yoshidome, T. (2009) Molecular origin of the negative heat capacity of hydrophilic hydration. J. Chem. Phys. 130(14):doi: 10.1063/1.3112610.

Krieger, E., Joo, K., Lee, J., Raman, S., Thompson, J., Tyka, M., Baker, D.and Karplus, K. (2009) Homology modeling in YASARA. Proteins. 77:114-122.

Luís, AS., Venditto, I., Temple, M.J., Rogowski, A., Baslé, A., Xue, J., Knox, J.P., Prates, J.A.M., Ferreira, L.M.A., Fontes, C.M.G.A., Najmudin, S. and Gilbert, H.J. (2013) Understanding how noncatalytic carbohydrate binding modules can display specificity for xyloglucan. J. Biol. Chem. 288:4799-4809.

McLean, B.W., Bray, M.R., Boraston, A.B., Gilkes, N.R., Haynes, C.A. and Kilburn, D.G. (2000) Analysis of binding of the family 2a carbohydrate-binding module from *Cellulomonas fimi* xylanase 10A to cellulose: specificity and identification of functionally important amino acid residues. Protein. Eng. 13, 801-809.

Mizutani K, Fernandes V.O, Karita S, Luís A.S, Sakka, M., Kimura, T., Jackson, A., Zhang, X., Fontes, C.M., Gilbert, H.J. and Sakka, K. (2012) Influence of a mannan binding family 32 carbohydrate binding module on the activity of the appended mannanase. Appl. Environ. Microbiol. 78(14):4781-4787.

Montanier, C., van Bueren, A.L., Dumon, C., Flint, J.E., Correia, M.A., Prates, J.A., Firbank, S.J., Lewis, R.J., Grondin, G.G., Ghinet, M.G., Gloster, T.M., Herve, C., Knox, J. P., Talbot, B.G., Turkenburg, J.P., Kerovuo, J., Brzezinski, R., Fontes, C.M., Davies, G.J., Boraston, A.B. and Gilbert H. J. (2009) Evidence that family 35 carbohydrate binding modules display conserved specificity but divergent function. Proc. Natl. Acad. Sci. USA. 106: 3065-3070.

Morrison, J.D., Corcoran, J.D. and Lewis, K.E. (1992) The determination of particle size distributions in small-angle scattering using the maximum-entropy method. Appl. Crystallogr. 25:504-513.

Noorbatcha, I.A, Sultan, A.M., Azura, A. and Salleh, H.M. (2012) Molecular dynamics study of the effect of calcium ions on the thermostability of *Bacillus Amyloliquefaciens* phytase. Aust. J. Basic. App. Sci. 6(1):109-116.

O'Boyle, N.M., Banck, M., James, C.A., Morley, C., Vandermeersch, T. and Hutchison, G.R. (2011) Open Babel: An open chemical toolbox. J. Chem. Inf. Model. 3:1-14.

Ofir, K., Berdichevsky, Y., Benhar, I., Azriel-Rosenfeld, R., Lamed, R. (2005) Versatile protein microarray based on carbohydrate-binding modules. Proteomics. 5(7):1806-1814.

Ostrowsky, N., Sornette, D., Parker, P. and Pike, E.R. (1981) Exponential sampling method for light scattering polydispersity analysis. Optica. Acta. 28(8):1059-1070.

Pace, N.C., Shirley, B.A. and Thomson J. A. (1989) in Protein structure: a particular approach, (T. E. Creighton, ed.). IRL Press, Oxford, pp 311-329.

Pilz, I., Schwarz, E., Kilburn, D.G., Miller, R.C. Jr., Warren, R.A. and Gilkes, N.R. (1990) The tertiary structure of a bacterial cellulase determined by small-angle X-ray-scattering analysis. 271:277-280.

Pinheiro, B.A., Proctor, M.R., Martinez-Fleites, C., Prates, J.A.M., Money, V.A., Davies, G.J., Bayer, E.A., Fontesm, C.M., Fierobe, H.P. and Gilbert, H.J. (2008) The *Clostridium cellulolyticum* dockerin displays a dual binding mode for its cohesin partner. *J.* Biol. Chem. 283:18422-18430.

Provencher, S.W. (1979) Inverse problems in polymer characterization: Direct analysis of polydispersity with photon correlation spectroscopy. Macromol. Chem. 180:201-209.

Provencher SW. (1982) Contin: a general purpose constrained regularization program for inverting noisy linear algebraic and integral equations. Comput. Phys. Commun. 27(3):213-227.

Royer, C.A. (2006) Probing protein folding and conformational transitions with fluorescence. Chem. Rev. 106:1769-1784.

Saravanan, P., Avinash, H., Dubey, V.K. and Patra, S. (2012) Targeting essential cell wall lipase Rv3802c for potential therapeutics against tuberculosis. J. Molr. Graph. Mod. 38:235-242.

Shen, H., Schmuck, M., Pilz, I., Gilkes, N.R., Kilburn, D.G., Miller, R.C. Jr. and Warren, R.A. (1991). Deletion of the linker connecting the catalytic and cellulose-binding domains of endoglucanase A (CenA) of *Cellulomonas fimi* alters its conformation and catalytic activity. J. Biol. Chem. 266, 11335-11340.

Shiba, K., Niidome, T., Katoh, E. and Xiang, H. (2010) Polydispersity as a parameter for indicating the thermal stability of proteins by dynamic light scattering. Analyt. Sci. 26:659-663.

Sunna, Anwar. (2010) Modular organisation and functional analysis of dissected modular β-mannanase *Cs*Man26 from *Caldicellulosiruptor* Rt8B.4. Appl. Microbiol. Biotechnol. 86(1):189-200.

Takeo, K. (1984) Affinity electrophoresis: Principles and applications. Electrophoresis 5:187-195.

Taylor, E.J., Goyal, A., Guerreiro, C.I.P.D., Prates, J.A, Money, V.A, Ferry, N., Morland, C., Planas, A., Macdonald, J.A., Stick, R.V., Gilbert, H.J, Fontes, C.M. and Davies, G.J. (2005) How family 26 glycoside hydrolases orchestrate catalysis on different polysaccharides structure and activity of a *Clostridium thermocellum* lichenase. J. Biol. Chem. 280(38):32761-3276.

Thompson, J.D., Higgins, D.G. and Gibson, T.J. (1994) CLUSTAL W: improving the sensitivity of progressive multiple sequence alignment through sequence weighting, position-specific gap penalties and weight matrix choice. Nucleic.. Acids. Res. 22:673-4680.

Tomme, P., Boraston, A., Kormos, J.M., Warren, R.A and Kilburn, D.G. (2000) Affinity electrophoresis for the identification and characterization of soluble sugar binding by carbohydrate-binding modules. Enzyme. Microb. Technol. 27:453-458.

Tunnicliffe, R.B., Bolam, D.N., Pell, G., Gilbert, H.J. and Williamson, M.P. (2005) Structure of a mannan-specific family 35 carbohydrate-binding module: evidence for significant conformational changes upon ligand binding. J. Mol. Biol. 347:287-296.

Valenzuela, S.V., Diaz, P. and Pastor, F.I. (2012) Modular glucuronoxylan-specific xylanase with a family CBM35 carbohydrate-binding module. Appl Environ Microbiol 78(11): 3923-31.

Van der Spoel, D., Lindahl, E., Hess, B., Groenhof, G., Mark, A.E. and. Berendsen, H.J. (2005) GROMACS: fast, flexible, and free. J. Comput. Chem. 26:1701-1718.

Chapter 5

Purification and characterization of manno-oligosaccharides produced from commercial substrates and from agro-waste copra meal by *Ct*Manf and their prebiotic and anticancer properties

5.1 Introduction

Galactomannan is a natural and water-soluble polysaccharide consisting of β-(1→4)-linked D-mannose backbone, randomly substituted with single unit of α-(1→6)-linked D-galactose residues (Ramesh *et al.*, 2001; Cerqueira *et al.*, 2009). The commercially available polysaccharides *viz.* carob galactomannan, locust bean galactomannan and guar galactomannan are rich sources of galactomannan. The functional properties of polysaccharide hydrocolloids are directly related with their structure. Polysaccharides could be depolymerized through various methods, such as γ-irradiation (Prawitwong *et al.*, 2007), ionizing radiation (Al-Assaf *et al.*, 2007), microwave irradiation (Singh and Tiwari, 2007) chemical (Ganter et al., 1995; Cheng *et al.*, 2002) and enzymatic hydrolysis (Lama-Mu˜noz *et al.*, 2012; Mudgil *et al.*, 2012; Shobha *et al.*, 2005). In general, enzymatic hydrolysis can be kinetically controlled to produce desired end products. Degraded galactomannan with reduced molecular weight and viscosity could be applied as soluble dietary fiber in functional foods (Bilgicli *et al.*, 2001).

Copra meal is dry coconut flesh (kernel) generally regarded as agricultural waste without any nutritional value. It is a byproduct, prepared after water decantation and oil extraction. It contains a large amount of hemicellulose viz. mannan and galactomannan (Mulimani and Naganagouda, 2010; Hossain, 1996). Though copra meal is nutritionally poor but it contains a large amount of hemicellulose *viz.* mannan and galactomannan (Mulimani and Naganagouda, 2010). The abundance of galactomannan 65% galactomannan in copra meal thrives its way as a suitable source of manno-oligosaccharides (MOS) (Hossain, 1996). MOSs have potential immune-modulator as reported earlier by Kovacs-Nolan *et al.* (2013), where the of β-(1→4)-mannobiose as one of the components of MOS induces Toll-like receptor (TLR) mediated macrophage activation. More reports on the exploration of MOS as antiallergenic agent was deciphered in Balb/c mice (Yang *et al.*, 2013). The prebiotic effect of MOS was also reported as it beneficially affect on human health by selectively stimulating growth of the intestinal microflora such as *Bifidobacterium* spp. and *Lactobacillus* spp., where in contrast limiting the growth of pathogenic bacteria in the colon (Gibson, 2001). The impaired growth of pathogenic bacteria might be due to production of increased in short-chain fatty acid (SCFA) by probiotic bacteria, resulting in lower pH and inhibition of undesirable microorganisms in the colon (Hongpattarakere, 2013).

The inhibitory effects of oligosaccharides on pathogens are due to the direct interaction with human mucosal receptors and hence blocking of the bacterial binding sites. Therefore, this process improved the elimination of these bacteria during excretion rather than their binding to mucosal receptors (Ishihara *et al.*, 2000; Spring *et al.*, 2000). It has been reported that the fructo-oligosaccharides have potential role

as antitumorigenic agent, for example; fructo-oligosaccharides isolated from apple showed induced apoptosis to colon cancer cells and cell cycle arrest in S phase (Lin and Chen, 2004). Oligosaccharides from apple induced apoptosis in HT29 cells by modulating Bax, Bcl-2 and Bcl-xl protein expression. The cell cycle arrest in the S phase in HT29 cells was due to the inhibition of the formation of the Cdk2-cyclin A1 complex by decreasing Cdk2 expression. There is only one report on MOS having anti-tumorigenic potential (Cole and Jayson, 2008) where sulfonated MOS from Pichia pastoris inhibited angiogenesis resulting in delayed tumor cell invasion and tumorigenesis (Cole and Jayson, 2008). Therefore, several investigations are required to study the effect of MOS from other sources on tumorigenesis.

Endo-β-annanases catalyze the random cleavage of β-(1→4)-mannosidic linkages within the backbones of mannan, galactomannan, glucomannan and galactoglucomannan resulting in production of various manno-oligosaccharides (Naughton *et al.*, 2001). We describe here, the production of manno-oligosaccharides from commercial substrates and defatted copra meal, a by-product from coconut, by a recombinant endo-β-(1→4)-mannanase (*Ct*Manf). The manno-oligosaccharides produced were purified, characterized and their role as prebiotics and as anti-tumorigenic agents was studied.

5.2 Materials and Methods

5.2.1 Reagents, chemicals and ligands

Copra powder was procured from local market in Guwahati, Assam, India. The components for MRS medium, Tryptone Glucose Yeast extract (TGY) medium, the reagents for reducing sugar and total carbohydrate estimation and inulin were purchased from HiMedia Laboratories, India. α-Amylase, trypsin and guar galactomannan were obtained from Sigma Aldrich Co. LLC, USA. Deuterium oxide (D_2O) was procured from Merck, Darmstadt, Germany. Locust bean galactomannan and konjac glucomannan were procured from Megazyme Int., Ireland. The probiotic bacteria *Lactobacillus acidophilus* NRRL B-4495 and *Bifidobacterium infantis* NRRL B-41661 were procured from Agricultural Research Service Culture Collection (Peoria, USA). The enteric pathogen strain *Enterobacter aerogenes* MTCC 3030 was procured from Microbial Type Culture Collection and Gene Bank (MTCC), Institute of Microbial Technology, Chandigarh, India.

5.2.2 Production of oligosaccharides from commercial substrates

5.2.2.1 Thin-layer chromatography of hydrolyzed products by CtManf

The qualitative analysis of hydrolyzed products by the reaction of *Ct*Manf on carob galactomannan was performed by thin-layer chromatography (TLC) on silica gel-coated aluminium foil (TLC Silica gel 60 F_{254} 20×20 cm, Merck) for detecting sugars. The enzyme *Ct*Manf (10 µl and 0.16 mg/ml) with 1% (w/v) carob galactomannan in 100 µl reaction mixtures were incubated at optimized temperature 60°C and optimized pH 6.9, for time intervals of 1 h, 4 h, 8 h, 16 h and 24 h. The reaction products were boiled for 2 min to stop enzymatic hydrolysis and then centrifuged 13,000*g* for 5 min. Then 0.2 µl of sample as well as of standard solutions

(1.0 mg/ml) were loaded on the TLC plate and kept in the developing chamber saturated with the developing solution (mobile phase) which consisted of acetic acid-*n*-propanol-water-acetonitrile (4:10:11:14). Mannose and oligosaccharides (mannobiose and mannotriose) were used as standards. At the end of the run, migrated sugars were visualized by immersing the TLC plate in a visualizing solution (sulphuric acid/methanol 5:95, v v^{-1}; α-napthol 5.0 %, w/v). The TLC plates were then dried at 80°C for 20 min. The migrated reaction products (sugars) appeared as spots on the TLC plate.

5.2.2.2 HPAEC analysis of polysaccharide hydrolysis by CtManf

*Ct*Manf (10 µl and 0.16 mg/ml) with 1% (w/v) carob galactomannan in 100 µl reaction mixtures were incubated, at optimal conditions of 60°C and pH 6.9 for 1 h, 4 h, 8 h 16 h and 24 h. These reaction mixtures were treated with 2 volumes (200 µl) of absolute ethanol to precipitate the remaining non reacted polysaccharides (substrates) and then centrifuged at 13,000***g*** for 10 min at 4°C. The supernatant containing the liberated sugar was transferred to another micro-centrifuge tube and the ethanol was removed by evaporation. The supernatant (50 µl) was diluted to 500 µl by adding ultra-pure (MilliQ, Millipore, USA) water and filtered through syringe filter using 0.2 µm membrane. The liberated sugars were analyzed by high pressure anion exchange chromatography (HPAEC) using ion chromatography system (Dionex, ICS-3000). From the filtered 500 µl, 25 µl of sample (liberated sugars) was run on CARBOPACK™ PA-200 column (150 x 3 mm, Dionex), attached with CarboPac™ PA200 guard column (30 x 3 mm, Dionex) with borate and amino trap columns which removed impurities and provided high resolution. The instrument (Dionex, ICS-3000) was kept at constant temperature, 30°C during the analysis and the flow rate was

maintained at 0.3 ml/min. The elution of liberated sugars released due to enzyme reaction was carried out with 100 mM sodium hydroxide using pulsed amperometric detector (PAD). 10 µg/ml of D-mannose, mannobiose and mannotriose were used as standards. The solutions of standards were also filtered through 0.2 µm membrane before loading to the column. A standard curve was prepared by using mixture of standards (mannose, mannobiose and mannotriose) from 10 mg/ml stock solutions. Quantitative analysis enzyme catalyzed hydrolysis products were determined from the peak intensity of the released products.

5.2.3 Production of oligosaccharides from natural substrate copra meal

5.2.3.1 Pretreatment of copra meal powder

The unprocessed copra powder (100 g) was washed thrice with 500 ml distilled water to remove any suspended particles and dried in hot air oven at 60°C, overnight. The dried copra powder 100 g was finely ground using grinder for 10 min and sieved through 1 mm mesh. The copra powder was designated as CO. The oil content from CO was partially reduced by following the method of Lin *et al.*, (2004). The partially oil free CO was boiled with 2 volumes of distilled water for 2 h. This step was carried out three times and after each step the water containing oil was removed by decantation and then stored at 4°C for overnight to allow the oil for solidification and finally be removed. Then the suspension was dried in oven at 60°C for 12 h. The partially oil free dried copra powder was designated as FCO. After oil removal step and solidification the possibility any leftover oil chunks were finally removed by solvent extraction using n-hexane for 24h. In solvent extraction process FCO was suspended in 1 l of n-hexane, in a beaker and mixed thoroughly and left overnight. The suspension of FCO was filtered through filter paper (Whatman no. 1)

and dried in an oven and sieved through 1 mm mesh for further study. The completely oil free (defatted) copra meal was designated as dFCO. The structural carbohydrates like hemicellulose and ash were estimated by standardized methods of NREL, USA (Sluiter *et al.*, 2008). 0.3g of dry substrate (dFCO) was mixed with 3 ml of 27 N H_2SO_4 and incubated at 30°C for 1h. Then 54 ml of distilled water was added to normalize H_2SO_4 concentration to 1.5N. The sample was autoclaved at 121°C and 15 psi for 1h. The substrate was cooled to 25°C and the treated dFCO was filtered using a vacuum filtration unit. The residue was weighed which was ash content. The filtrate was collected and pH was neutralized by addition of 1M $CaCO_3$. The protein extraction and total protein content was determined by the method described elsewhere (Samson *et al.*, 1971; Bradford, 1976). The component extracted during the preprocessing steps of copra meal was recognized as lipid after hemicellulase, ash and protein estimation.

5.2.3.2 Structural analysis of copra meal powder

5.2.3.2.1 FESEM analysis of untreated CO and pretreated dFCO

Thirty micoliter of each untreated CO or pretreated dFCO (0.04 g L^{-1}) was placed over a glass slide, subsequently dried and coated with gold film using a SC7620 "Mini", Polaron Sputter Coater (Quorum Technologies, Newhaven, England) and analyzed under the field emission scanning electron microscope (FESEM-Carl Zeiss, SIGMA VP instrument). The images were acquired for both CO and dFCO.

5.2.3.2.2 FT-IR spectroscopy analysis of untreated CO and pretreated dFCO

Fourier transform infrared (FT-IR) spectroscopy (Spectrum Two, Perkin Elmer, USA) was used for analysis of available functional groups in untreated CO and

pretreated dFCO, respectively. One mg each of dried CO and dFCO (45°C for 18 h) was ground with 3 mg potassium bromide powder (Sigma, USA) in 1:3 ratio and made into pellet. Three samples of each were prepared to increase the reproducibility of the analysis and 30 scans were recorded per sample at a resolution of 4 cm^{-1} and 0.1 cm^{-1} data interval.

5.2.3.2.3 ^{1}H and ^{13}C NMR of pretreated dFCO

Nuclear magnetic resonance (NMR) of dFCO was performed using a Varian AS400 spectrometer (Agilent Technologies, Palo Alto, CA, USA). The soluble fractions of dFCO were collected after pre-treatment were dissolved in 0.5 ml deuterium oxide D_2O (Merck, Germany). The solution was lyophilized and 30 mg and 50 mg of dFCO dissolved in 0.5 ml of D_2O for ^{1}H NMR analysis ^{13}C NMR, respectively. Tetramethyl silane (TMS) was used as an internal reference.

5.2.3.2.4 Production and purification of recombinant endo-mannanase (CtManf)

Production and purification of recombinant *Ct*Manf was followed as described in Chapter 2, Section 2.2.21.

5.2.3.2.5 Analysis of enzyme hydrolyzed products of dFCO by TLC and HPAEC

The enzyme activity of *Ct*Manf was determined against 2.0% (w/v) commercial natural substrates such as, carob galactomannan, locust bean galactomannan, konjac glucomannan and pretreated copra meal powder (dFCO) dissolved in 50 mM sodium phosphate buffer pH 6.9 as described in Chapter 3, Section 3.2.7. One hundred microliter of reaction mixture contained 2.0% (w/v) substrate, 10 µl of enzyme (*Ct*Manf, 0.16 mg/ml) and the reaction was incubated at 60°C for 10 min. The resulting reducing sugar concentration was measured at 500 nm

using spectrophotometer (Varian, Cary 100-Bio) as described earlier (Ghosh *et al.*, 2013). All these assays were carried out in triplicates. Qualitative analysis of hydrolyzed products of dFCO was performed by thin-layer chromatography (TLC) on silica gel-coated aluminium foil (TLC Silica gel 60 F_{254} 20×20 cm, Merck) to identify the released sugars. Hydrolysis of dFCO by recombinant endo-mannanase (*Ct*Manf) was carried out under optimum conditions (as described in Chapter 3, Section 3.2.7) at different time intervals of 1 h, 4 h, 8 h, 16 h and 24 h. After each incubation period, the reaction mixtures were boiled for 2 min to stop enzymatic hydrolysis and then centrifuged 13,000***g*** for 5 min. Then 0.2 µl of reaction mixture and standard solutions of mannose, mannobiose and mannotriose (1.0 mg/ml) were loaded on the TLC plate and kept in the developing chamber saturated with the developing solution (mobile phase) consisting of acetic acid-*n*-propanol-water-acetonitrile (4:10:11:14). At the end of the run, migrated sugar spots were investigated by immersing the TLC plate in a visualizing solution (sulphuric acid/methanol 5:95, v/v; *α*-naphthol 5.0%, w/v) and followed by drying at 80°C for 20 min. The migrated reaction products (sugars) appeared as spots on the TLC plate.

The samples for high pressure anion exchange chromatography (HPAEC) were prepared from the reaction mixtures after definite time intervals (as mentioned in TLC) were treated with 2 volume (200 µl) of absolute ethanol to precipitate the remaining non reacted polysaccharides and then centrifuged at 13,000***g*** for 10 min at 4°C. The supernatant containing the liberated sugar was transferred to another micro-centrifuge tube and the ethanol was removed by evaporation. The supernatant (50 µl) was diluted to 500 µl by adding ultra-pure (MilliQ, Millipore, USA) water and filtered through syringe filter using 0.2 µm membrane. The liberated sugars were analyzed

using ion chromatography system (Dionex, ICS-3000). From the filtered 500 µl, 25 µl of sample (liberated sugars) was run on CARBOPACK^{TM} PA-200 column (150 x 3 mm, Dionex), attached with CARBOPACK^{TM} PA200 guard column (30 x 3 mm, Dionex) with borate and amino trap columns which removed impurities and provided high resolution. The instrument (Dionex, ICS-3000) was kept at constant temperature of 30°C during the analysis and the flow rate was maintained at 0.3 ml/ min. The liberated sugars were eluted by 300 mM sodium hydroxide using pulsed amperometric detector (PAD). Quantitative analysis of enzyme catalyzed hydrolysis products was carried determined from the peak intensity of the released products.

5.2.3.2.6 Purification of manno-oligosaccharides from enzymatic hydrolyzed products of dFCO

Purification of manno-oligosaccharides from enzymatic hydrolyzed products of dFCO was carried out 25°C temperature by using FPLC system (AKTA Prime, GE Healthcare, USA). The components of hydrolyzed products of dFCO were separated and isolated using polyacrylamide bead matrix Bio-Gel P2 (45-90 µm) packet in 50 ml Econo-Pack column (Bio-Gel, USA). Two ml sample of enzymatic hydrolyzed product of dFCO was injected in 2 ml sample loop of FPLC system and the oligosaccharide samples were eluted with isocratic elution by deionized water at 0.2 ml/min flow rate. Sixty fractions of 1 ml each were collected using a fraction collector. The total carbohydrate content of fractions was estimated by phenol sulfuric acid method (Dubios *et al.*, 1956) and qualitatively analyzed by thin layer chromatography as described in Section 5.2.3.2, Subsection 5.2.3.2.4. The fractions were analyzed using mass a spectrophotometer (Agilent 6550 iFunnel Q-TOF LC/MS system, Agilent 1200 series, USA). Each fraction was diluted to 5 ppm in methanol

and filtered through 0.45 µm membrane. ESI-MS were carried out for specific fractions in positive ionization mode and analyzed by TOF detector.

5.2.4 *In vitro* prebiotic analyses of MOS

5.2.4.1 Effect of artificial human gastric juice hydrolysis on manno-oligo-saccharides

The prebiotic potential of mixed oligosaccharide was examined and compared with inulin, a commercial prebiotic as reference. The dried sample of mixed manno-oligosaccharides was dissolved in autoclaved MilliQ water to produce 1.0% (w/v) solution. Artificial human gastric juice was prepared by using phosphate buffer saline (PBS) containing (in g/l): NaCl, 8; KCl, 0.2; $Na_2HPO_4.2H_2O$, 8.25; $NaHPO_4$, 14.35; $CaCl_2.2H_2O$, 0.1; $MgCl_2.6H_2O$, 0.18 (Korakli *et al.* 2002). The pH of the buffer was adjusted to 1, 2, 3, 4 and 5 using 5 M HCl (Korakli *et al.* 2002). Artificial gastric juice (6 ml) at each pH was added to the 1% (w/v) MOS and the reaction mixture was incubated in a water bath 37 °C for 6 h. Sample (1 ml) was taken periodically at 0, 1, 2, 4, 5 and 6 h. Reducing sugar content of the sample was determined by the method as described earlier in Chapter 3, Section 3.2.2.3 and total sugar was determined by phenol–sulphuric acid method (Dubois *et al.*, 1956). Percentage hydrolysis of MOS was calculated based on reducing sugar liberated and total sugar content of the MOS (Korakli *et al.*, 2002):

$$\text{Hydrolysis (\%)} = \frac{\text{Reducing sugar released} \times 100}{\text{Total sugar content} - \text{Initial sugar content}}$$

5.2.4.2 Effect of intestinal fluid on mixed manno-oligosaccharides

The intestinal fluid was prepared in PBS with 0.5% (w/v) bile salt (Sigma Aldrich, USA) and 1000 U/ml of trypsin solution (Sigma Aldrich Co. LLC, USA). The pH of the buffer was adjusted to 8.0 with 2N NaOH (Fernandez, *et al.*, 2003). 5 mg mixed manno-oligosaccharides or inulin was dissolved in 5 ml of simulated intestinal fluid to produce final concentration of 1.0% (w/v) solution and incubated at for 37°C for 6 h. The reaction mixture (500 µl) was collected at regular time intervals of 0, 1, 2, 3, 4, 5 and 6 h to determine the reducing and total sugar content by phenol-sulphuric acid method (Dubois *et al.*, 1956) for calculating the percentage hydrolysis as described in the previous Section 5.2.4.2.

5.2.4.3 Effect of α-amylase on mixed manno-oligosaccharides

Effect of α-amylase on mixed manno-oligosaccharides was examined by the method as described earlier (Wichienchot *et al.*, 2010). α-Amylase (100 U/ml) was prepared in 50 mM phosphate buffer saline (PBS) and the pH of the buffer was adjusted to 5, 6, 7 or 8 to a final volume of 5 ml. To each of these solutions 1.0% (w/v) of mixed manno-oligosaccharides or inulin was added and the reaction was set in duplicate and incubated at 37°C for 6 h. The reaction mixture (500 µl) was collected at regular time interval of at 0, 1, 2, 3, 4, 5 and 6 h and the reducing and total sugar content were determined for calculating the percentage hydrolysis of MOS as described in previous Section 5.2.4.2.

5.2.5 Effect of MOS on growth of probiotic bacteria

The growth of probiotic bacteria, *Bifidobacterium infantis* NRRL B-41661 and *Lactobacillus acidophilus* NRRL B-4495 as well as non probiotic enteric bacteria *E.*

coli DH5α and *E. aerogenes* MTCC 3030 was mentioned in the presence of mixed manno-oligosaccharides and inulin as standard prebiotic. The manno-oligosaccharides, mannobiose and mannotriose were pooled after purification and subsequently freeze-dried. The growth of probiotic bacteria was evaluated in basal MRS medium (pH 6.4) supplemented with 0.5 g/l cysteine as described earlier by Hongpattarakere *et al.*, (2013). The overnight grown probiotic cultures of *Bifidobacteria* (~1 x 10^7 cells/ml) and *Lactobacillus* (~12 x 10^7 cells/ml) were separately inoculated to 100 ml MRS basal medium containing filter sterilized 1% (w/v) glucose (as positive control), inulin and incubated under anaerobic condition, at 37°C for 24 h. The growth of non probiotic enteric bacteria was estimated in TGY medium (pH 7.0) containing 5 g/l of tryptone, 5 g/l of yeast extract, 1 g/l di-potassium hydrogen phosphate (K_2HPO_4) and 1 g/l glucose. The non probiotic *E. coil* and *E. aerogenes* were separately inoculated in TGY medium supplemented with filter sterilized 1% (w/v) of mixed-oligosaccharides or inulin in place of glucose and also incubated at 37°C for 48 h under anaerobic condition. The growth of the bacterial culture was determined as cells/ml, by counting colonies that appeared after spreading 100 µL of culture following 12 h and 24 h of incubation on an MRS agar plate (20 g/l agar) (in case of probiotic bacteria) and TGY agar plate (20 g/l) (in case of non probiotic bacteria) and the plates were incubated at 37°C for 18 h.

5.2.6 *In vitro* analysis of effect of MOS on mammalian cells

Mixed MOS from copra meal was used for *in vitro* cytotoxicity assay. The effects of manno-oligosaccharides on human colon cancer cell line (HT29) or Human colon normal cells (FHC ATCC CRL-1831) were studied using the colorimetric 3-(4,5-dimethylthiazolyl-2)-2,5-diphenyltetrazolium bromide (MTT) assay as described

earlier (Mosmann, 1983). HT29 carcinoma cell lines and Human colon normal cells (FHC ATCC CRL-1831) were seeded in 96-well plates at density approximately, 1.2 x 10^4 cells/well and 2.1 and x 10^4 cells/well, respectively, incubated at 37°C for 16 h in 5% CO_2 atmosphere for surface attachment. After incubation the media were removed and the manno-oligosaccharides at different concentrations were added. A concentration range (1 µg/ml to 500 µg/ml) of mixed MOS was used. The media without oligosaccharides were used as negative control. The plates were again incubated at 37° C in 5% CO_2 atmosphere for 48h. After 48 h the media were removed and 100 µl MTT (500 µg/ml) was added to each well and further incubated at 37°C for further 4 h. The supernatant was removed and 100 µl dimethylsulfoxide (DMSO) was added to each well. The absorbance at 570 nm was monitored on a 96-well microplate reader (Tecan, Infinite 200 Pro).

5.3 Results and Discussion

5.3.1 Thin-layer chromatography of hydrolyzed products by CtManf

The analysis of recombinant *Ct*Manf hydrolyzed products of carob galactomannan by TLC is displayed in Fig. 5.3.1. Time dependent hydrolysis of carob galactomannan displayed the release of mannose (dp 1) after 10 min, but after 1 h of hydrolysis little release of mannobiose (dp2) and mannotriose (dp3) was observed (Fig. 5.3.1A). Standards of mono and oligosaccharides (M1: mannose, M2: mannobiose and M3: mannotriose) were run in parallel to compare the released sugars (Fig. 5.3.1A). The complete hydrolysis of carob galactomannan was achieved after 24 h of incubation where maximum mannose, mannobiose and mannotriose release could be observed (Fig. 5.3.1A). Apart from the appearance of dp 1, dp 2 and dp 3, there were two other higher oligosaccharides (dp4 and dp5) spots which were observed throughout the hydrolysis (Fig. 5.3.1A). The mannobiose and mannotriose hydrolysis by *Ct*Manf released principally mannose and mannobiose (Fig. 5.3.1B and Fig. 5.3.1C, respectively) displaying its endo-acting nature. *Ct*Manf was unable to hydrolyze mannobiose till 1 h but after 4 h, complete hydrolysis of mannobiose occurred, leaving only the mannose spot on TLC plate (Fig. 5.3.1B). Whereas, the hydrolysis of mannotriose by *Ct*Manf released, predominantly mannose and trace amount of mannobiose after 4 h. The mannobiose spot disappeared completely after 8 h, leaving only the mannose spot (Fig. 5.3.1C). Thus *Ct*Manf cleaved β-(1→4) bonds of these manno-oligosaccharides.

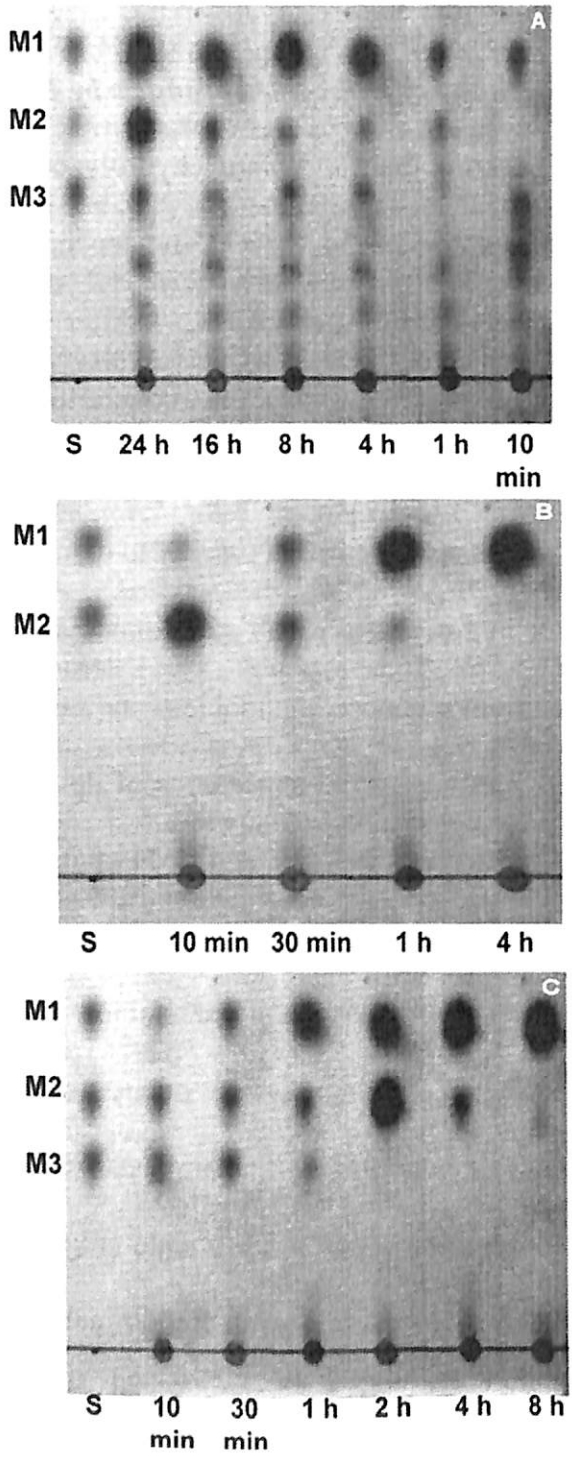

Fig. 5.3.1 Thin layer chromatography analysis of hydrolyis products from (A) carob galactomannan (B) mannobiose and (C) mannotriose by *Ct*Manf. (A) carob galactomannan (1%, w/v) was incubated with *Ct*Manf for 10 min to 24 h, (B) mannobiose (1 mg/ml) was incubated with *Ct*Manf for 10 min to 4 h and (C) mannotriose (1 mg/ml) was incubated with *Ct*Manf for 10 min to 8 h. Samples were taken in intervals and the hydrolysed products analyzed by TLC (standards used M1: mannose, M2: mannobiose M3: mannotriose).

5.3.2 HPAEC analysis of enzyme reaction products

Qualitative and quantitative analysis of *Ct*Manf hydrolyzed products of carob galactomannan were carried out by HPAEC-PAD. Time dependent hydrolysis of carob galactomannan by *Ct*Manf is displayed in (Fig. 5.3.2). The peak intensities of standards are displayed in (Fig. 5.3.2A). After 1 h of *Ct*Manf treatment of carob galactomannan, the prominent peaks of mannose at 3.4 min, mannobiose at 4.06 min and mannotriose at 4.96 min were observed with concentrations 2.12 mg/ml, 0.73 mg/ml, 0.76 mg/ml, respectively (Fig. 5.3.2B). The mannobiose peak was more prominent than mannotriose after 4 h of carob galactomannan hydrolysis while mannose intensity increased continuously with time (Fig. 5.3.2C). The concentrations of mannose were determined as 2.23 mg/ml, mannobiose 1.12 mg/ml and mannotriose 0.80 mg/ml after 4 h of incubation. *Ct*Manf was able to hydrolyze carob galactomannan to a greater extent after 8 h and the products obtained were, mannose (3.16 mg/ml), mannobiose (1.81 mg/ml) and mannotriose (0.90 mg/ml) with much higher peak intensities (Fig. 5.3.2D). After 16 h incubation, the mannobiose and mannotriose concentrations increased to 2.1 mg/ml and 1.1 mg/ml, respectively. This increase was approximately, 1.17 fold and 1.3 fold, respectively, for mannobiose and mannotriose (Fig. 5.3.2E) as compared with that obtained after 8 h hydrolysis of carob galactomannan. The complete hydrolysis of carob galactomannan by *Ct*Manf was observed after 24 h of enzymatic reaction where the concentrations of mannose, mannobiose and mannotriose were 3.6 mg/ml, 2.3 mg/ml and 1.4 mg/ml, respectively (Fig. 5.3.2F). All the concentrations were determined from the regression equation of mannose, mannobiose and mannotriose standard curves. Therefore, *Ct*Manf quite effectively hydrolyzed 10 mg/ml (1%, w/v) carob galactomannan and released

maximum after 24 h yielding 36% mannose, 23% mannobiose and 14% mannotriose. The overall results quite interestingly described the performance of *Ct*Manf in releasing of the manno-oligosaccharides from carob galactomannan which can be scaled up for commercial production.

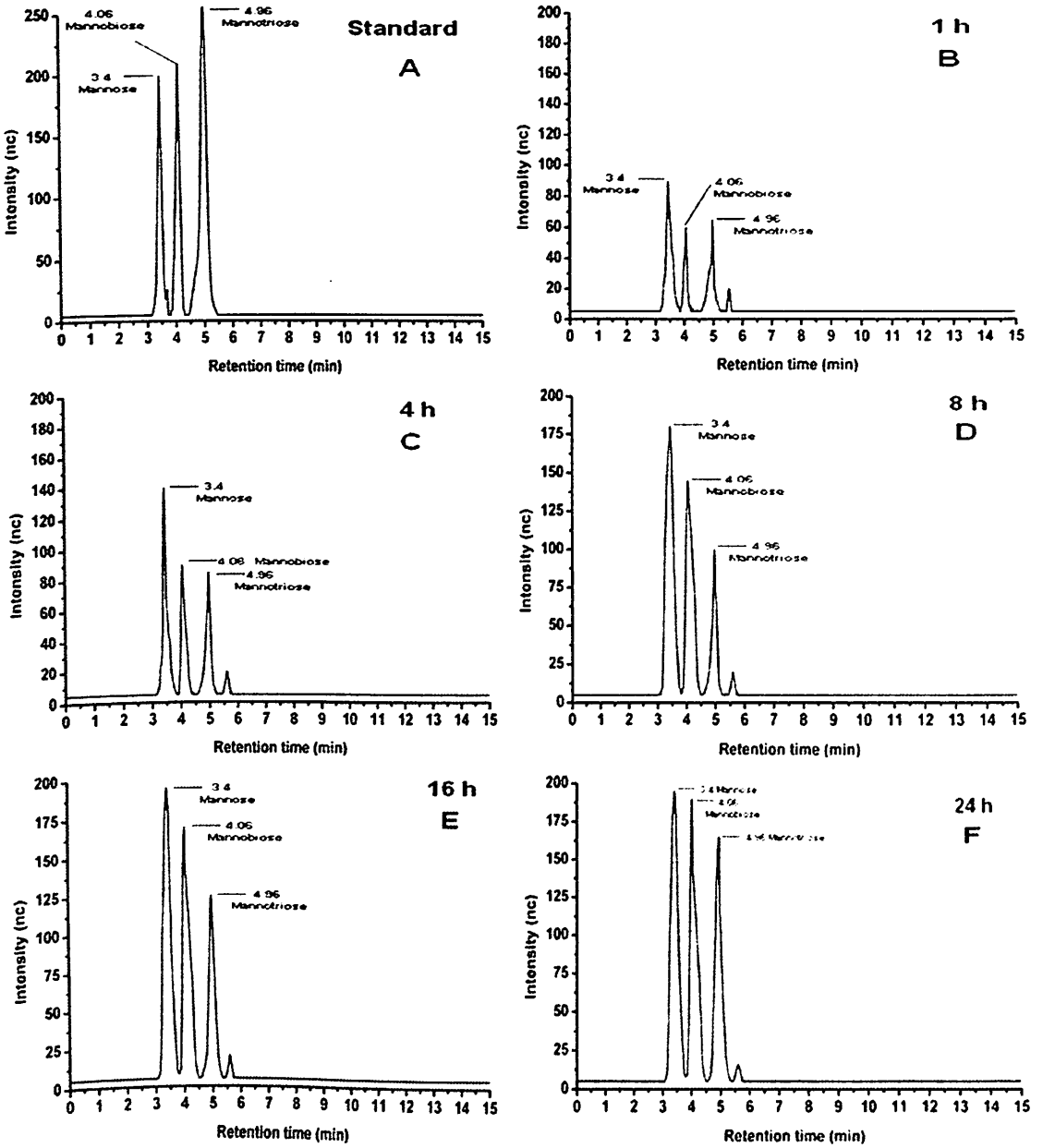

Fig. 5.3.2 HPAEC-PAD analysis of hydrolyzed products of carob galactomannan by *Ct*Manf. (A) Elution patterns of standards used, mannose (3.4 min), mannobiose (4.06 min) and mannotriose (4.96 min). Elution pattern of mannose, mannobiose and mannotriose from *Ct*Manf treated carob galactomannan (1%, w/v) after; 1 h (B), 4h (C), 8h (D), 16h (E) and 24h (F) at 60°C.

5.3.3 Production of oligosaccharides from copra meal

5.3.3.1 Pretreatment of copra meal powder

The pretreatment of defatted copramèal (dFCO) (described in Section 5.2.3.1) resulted in (w/v) 74% hemicellulose, 23.8% protein, 2% ash and 0.2% lipid which were comparable with the previous report of Lin, 2004. The dry matter of copra meal containing 61% galactomannan was reported (Balasubramanium, 1976). Therefore, the pretreatment process was efficient to release the important hemicellulosic materials such as mannan and galactomannan from copra meal for enhanced enzyme accessibility and higher production of mannooligosaccharides.

5.3.3.2 Structural analysis of carbohydrate of defatted copra meal (dFCO)

5.3.3.2.1 FESEM analysis of untreated CO and pretreated dFCO

The FESEM images of pretreated copra meal (dFCO) showed significantly more porous and destabilized structure of the copra meal complex as compared with the untreated copra meal (CO) (Fig. 5.3.3A and Fig. 5.3.3B). Therefore, the structural deformity of the coprameal (dFCO) after the effective pretreatment will pave the way for better enzyme attachment and catalysis which will help the release of mono- and oligosaccharides.

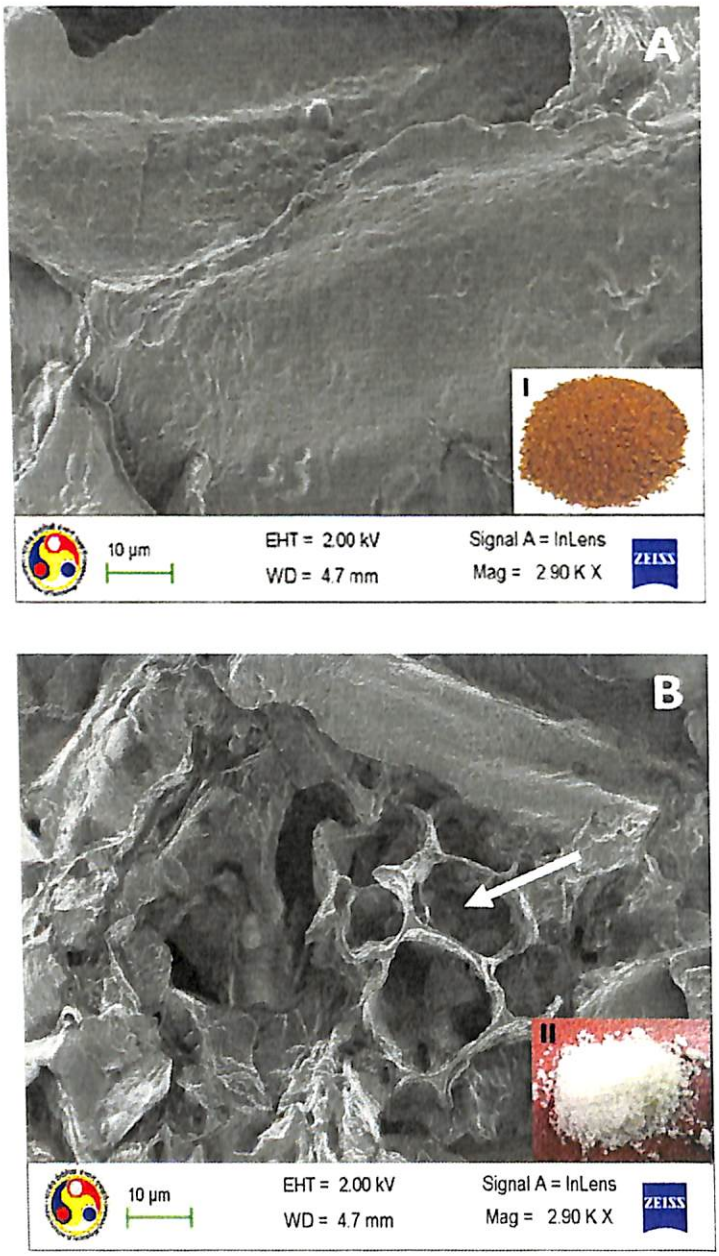

Fig. 5.3.3 FESEM analysis of (A) untreated and (B) pretreated of dried copra meal (dFCO). Topological changes associated with pretreatment are clearly detectable (Arrow). Inset I and II represent the dried copra powder before and after pretreatment, respectively.

5.3.3.2.2 FT-IR spectroscopy analysis of untreated CO and pretreated dFCO

The FT-IR spectral analysis of both untreated and pretreated copra meal samples (dFCO) are illustrated in Fig. 5.3.4. The assignments of functional groups recorded by FT-IR are listed in Table 5.3.1.

Table 5.3.1 FT-IR analysis of pretreated copra meal and assignment of functional groups.

Name of characteristic group	Wavenumber (cm^{-1})
OH	3384
C-H methyl and methylene groups	2930
Aromatic ring stretch of lignin	1642
Aromatic skeletal vibration plus C=O stretch of lignin	1506
C-H (Crystalline cellulose)	1430
Anti-symmetric bridge stretching of C–O–C groups in galactomannan	1152
CH_2 group of mannan	1064
C-O stretch vibration of glucomannan	1030, 870, 810

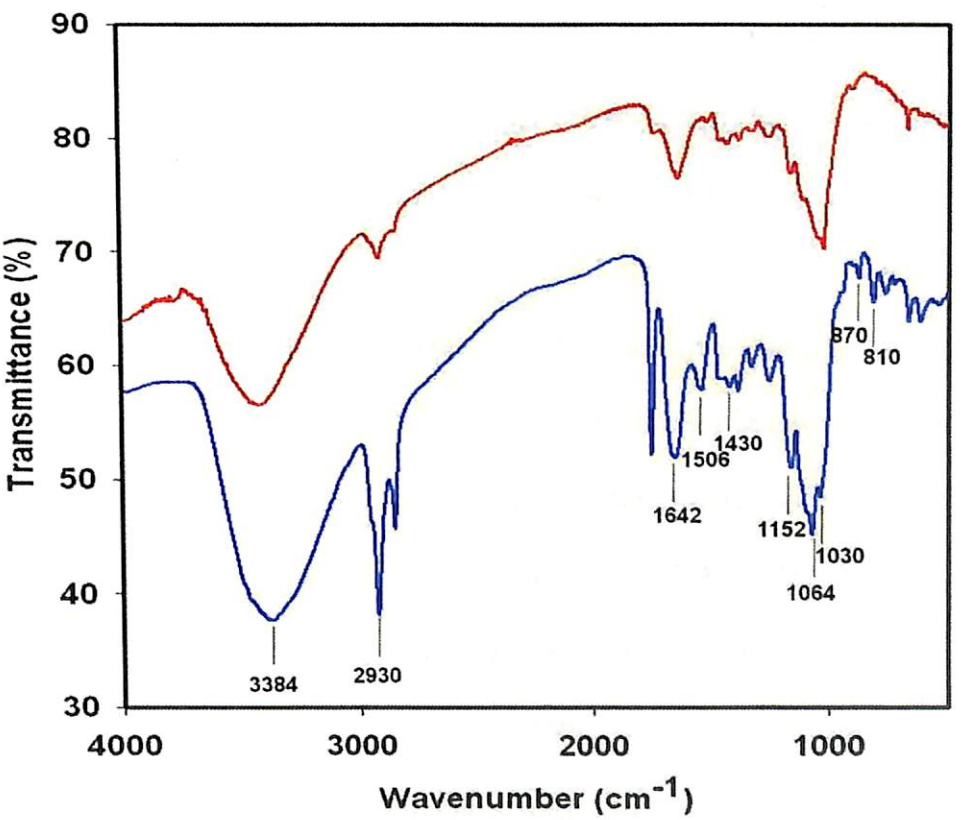

Fig. 5.3.4 FT-IR analysis of untreated copra meal (CO) (red line) and defatted copra meal (dFCO) (blue line) displaying the functional group appeared after pretreatment.

The absorption at 3384 cm^{-1} was attributed to the hydroxyl stretching vibrations, and the band at 2930 cm^{-1} was due to the C-H stretching of methyl groups. Similar identification of hydroxyl stretching vibrations and C-H stretching of methyl

groups of polysaccharide were previously reported (Sun *et al.*, 2012). Small peak shifts and more pronounced peaks at 3384 cm^{-1} and 2930 cm^{-1} was observed in case of treated sample while comparing with untreated copra meal. The band at 1642 cm^{-1} was probably due to the bending mode of water since the hemicelluloses have a strong affinity for water as these macromolecules in the solid state may have disordered structures that could be easily hydrated (Sun *et al.* 2012). The band at 1506 cm^{-1} was due to the aromatic skeletal vibration plus C=C stretch of lignin and the band at 1430 cm^{-1} was due to C-H deformation of crystalline cellulose as also reported earlier (Figueiró *et al.*, 2004). The higher transmittance at 1152 cm^{-1} appeared due to anti-symmetric bridge stretching of C–O–C groups in galactomannan (Figueiró *et al.*, 2004; Prashanth *et al.*, 2006). In addition to a glucose band at 1034 cm^{-1} of glucomannan an extra band at 1064 cm^{-1} appeared due to the mannose units similar to an earlier report on galactomannan (Prashanth *et al.*, 2006). In the anomeric region (950-700 cm^{-1}), pretreated dFCO exhibited the characteristic transmittance at 870 and 810 cm^{-1} suggesting the existence of mannose as reported elsewhere (Kacurakova *et al.*, 2000; Zhang *et al.*, 1995). The absorption peak at 870 cm^{-1} represented the β-glycosidic bond in dFCO as reported in the hemicelluloses from pectic polysaccharides (Kacurakova *et al.*, 2000).

5.3.3.2.3 ^{1}H and ^{13}C NMR spectroscopy analysis of pretreated dFCO

Analysis of the positions and fine structure of correlation peaks in the ^{1}H NMR and ^{13}C spectrum of dFCO are shown in Fig. 5.3.5A and Fig. 5.3.5B, respectively. The two signals at 4.75 ppm and 5.03 ppm observed in the ^{1}H NMR were attributed to the presence of a H-1 protons of β-D-mannopyranose ring [(→4)-β-D-man*p*-(1→)] and branched α-D-galactopyranose ring [α-D-gal*p*-(1→6)],

respectively (Table 5.3.2). Other δH shifts of D-man*p* at 4.16, 3.82, 3.87, 3.59 and 3.95 ppm were attributed to H-2, H-3, H-4, H-5 and H-6 peaks, respectively. Whereas the peaks of D-gal*p* at 3.87, 3.95, 3.93 and 3.79 ppm arose from H-2, H-3, H-4, H-5 and H-6, respectively, (Table 5.3.2). Well resolved ^{13}C NMR peaks were observed in Fig. 5.3.5B, where they corresponded to anomeric carbon of linear β-D-mannopyranose at 103.0 ppm, branched at the 6-HO position of β-D- mannopyranose at 103.3 ppm and branched α-D-galactopyranose at 101.7 ppm. Other chemical shifts are summarized in Table 5.3.2. The deciphered structure of dFCO displayed the resemblance with the structure of mannan and galactomannan from *Delonix regia* (Tamaki *et al.*, 2012) and *Gleditsia delavayi* (Rakhmanberdyeva and Shashkov, 2005).

Table 5.3.2 ^{1}H and ^{13}C NMR chemical shifts of dFCO.

		^{1}H NMR				
Unit	H-1	H-2	H-3	H-4	H-5	H-6
(→4)-β-D-man*p*-(1→)	4.75	4.16	3.82	3.87	3.59	3.95
α-D-gal*p*-(1→6)	5.03	3.87	3.95	3.93	3.90	3.79
		^{13}C NMR				
Unit		C-1	C-2	C-3	C-4	C-5	C-6
Linear (→4)-β-D-man*p*-(1→)		103.0	72.9	72.3	72.2	74.1	64.0
Branch (→4)-β-D-man*p*-(1→)		103.3	72.9	74.3	79.3	77.9	64.4
α-D-gal*p*-(1→6)		101.7	71.3	74.3	79.4	76.3	63.4

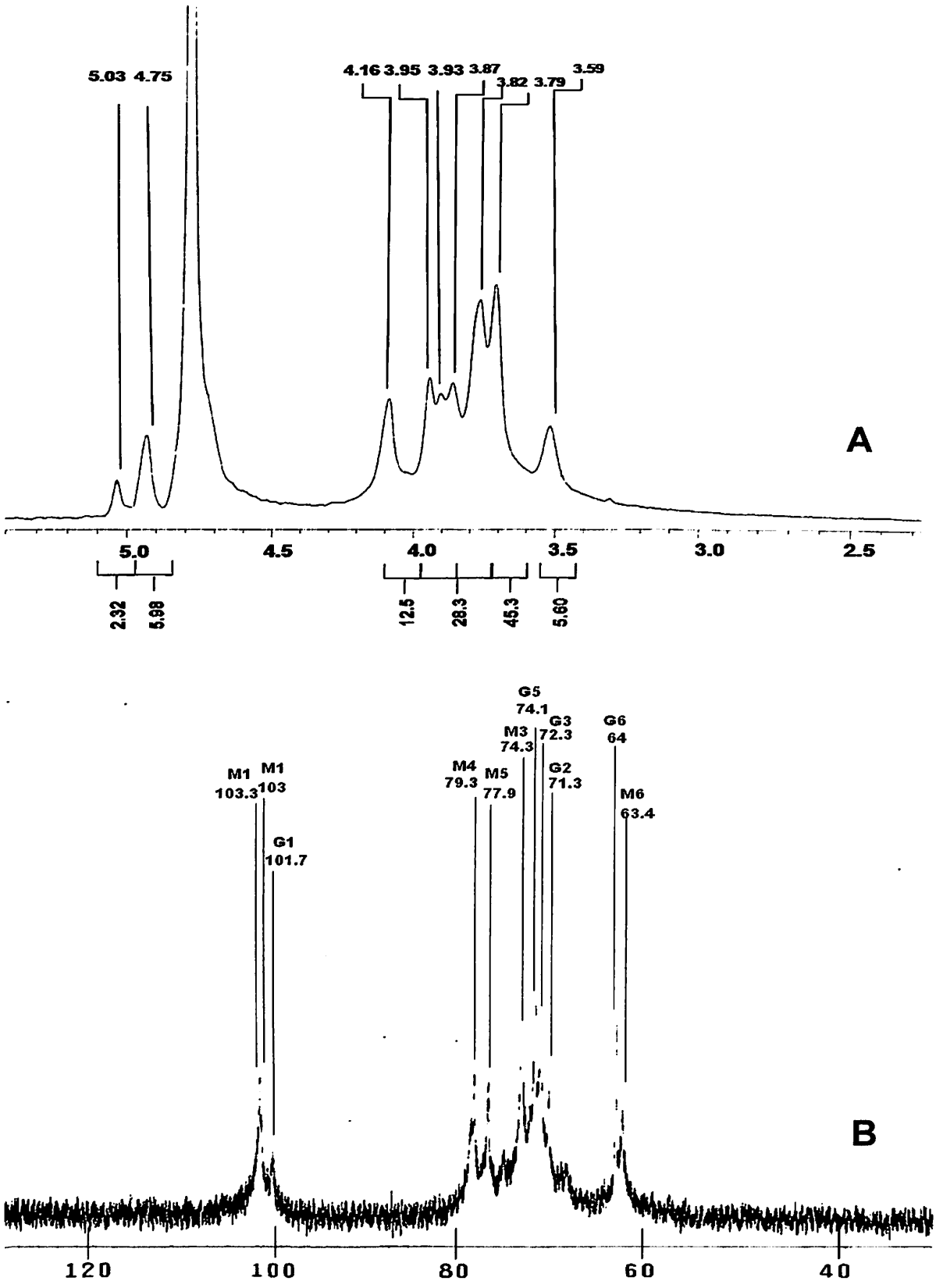

Fig. 5.3.5 NMR spectra of dFCO polysaccharide (A) ^{1}H and (B) ^{13}C, M1/G1, M2/G2, M3/G3, M4/G4, M5/G5, M6/G6 represents C1, C2, C3, C4, C5 and C6, respectively, of D-mannose/D-galactose (M/G).

5.3.4 Production and purification of recombinant endo-mannanase (*Ct*Manf)

The endo-mannanase (*Ct*Manf) that was cloned and expressed in *E. coli* BL21 (DE3) cells as described earlier in Chapter 2, Section 2.2.21. The recombinant *Ct*Manf was purified as described in the Chapter 2, Section 2.3.3.5. The purified endo-β-(1→4)-mannanase (*Ct*Manf) was used for hydrolysis of copra meal to produce mannooligosaccharides (MOS).

5.3.5 Analysis of enzymatic hydrolysis of defatted copra meal by TLC and HPAEC

5.3.5.1 Enzyme assay

The manno-configured substrate specificity of *Ct*Manf was determined as described in the Chapter 3, Section 3.3.2). Under optimal pH and temperature (Chapter 3, Section 3.3.3 and Section 3.3.4), *Ct*Manf displayed highest enzyme activity against commercial soluble substrates *viz.* guar galactomannan (15.20 ± 0.8 U/ml), locust bean galactomannan (27.20 ± 0.5 U/ml) and konjac glucomannan (26.8 ± 0.8 U/ml) (Table 5.3.3). The enzyme activity of *Ct*Manf was determined against untreated copra meal (CO) and pretreated dFCO was 2.12 ± 0.3 U/ml and 26.0 ± 0.2 U/ml, respectively (Table 5.3.3). Earlier reports exhibited similar mannanase activity 27.4 ± 0.6, 26.1 ± 1.3 U/ml from *Aspergillus niger* NCH-189 and *Aspergillus niger*, respectively, against dFCO (Lin, 2004; Naganagouda *et al.*, 2009). In contrast, the mannanase isolated from *Aspergillus niger* NCH-189 and *Aspergillus niger* showed similar activity, 2.6 ± 0.8 and 2.0 ± 0.1 U/ml, respectively, against CO (Lin, 2004; Naganagouda *et al.*, 2009) (Table 5.3.3). Therefore, it was concluded from our study that the recombinant *Ct*Manf was able to effectively access and hydrolyse the pre-

treated defatted copra meal (dFCO) and helped in a subsequent release of higher mannose and MOS.

Table 5.3.3 Comparison of *Clostridium thermocellum* endo-mannanase (*Ct*Manf) with other mannanases.

Substrate (2%, w/v)	Enzyme activity (U/ml)*	Source of mannanase	References
Guar galactomannan	15.2 ± 0.8	*C. thermocellum*	Present study
	11.4 ± 0.7	*Aspergillus niger*	Chen *et al.*, (2003)
	4.3 ± 0.2	*A. niger, A. flavus*	Naganagouda *et al.* (2009)
Locust bean galactomannan	27.2 ± 0.5	*C. thermocellum*	Present study
	7.8 ± 0.8	*Aspergillus niger*	Chen *et al.*, (2003)
	6.0 ± 0.3	*A. niger, A. flavus*	Naganagouda *et al.* (2009)
Konjac glucomannan	26.8 ± 0.8	*C. thermocellum*	In this study
	5.0 ± 0.5	*A. niger, A. flavus*	Chen *et al.*, (2003)
CO	2.1 ± 0.3	*C. thermocellum*	In this study
	2.6 ± 0.8	*Aspergillus niger*	Chen *et al.*, (2003)
	2.0 ± 0.1	*A. niger, A. flavus*	Naganagouda *et al.* (2009)
dFCO	26.0 ± 0.2	*C. thermocellum*	Present study
	27.4 ± 0.6	*Aspergillus niger*	Chen *et al.*, (2003)
	26.1 ± 1.3	*A. niger, A. flavus*	Naganagouda *et al.* (2009)

**Values are in Mean ± SD (n=3)*

5.3.5.2 Analysis of CtManf hydrolyzed products of dFCO by TLC

Time dependent hydrolysis of dFCO by recombinant endo-β-mannanase (*Ct*Manf) using TLC is displayed in Fig. 5.3.6A. The hydrolysis after 10 min and 1 h of reaction displayed the release of mannose (dp1) and mannobiose (dp2) (Figure 3A). Standards of mono- and oligosaccharides (M1: mannose, M2: mannobiose and M3: mannotriose) were run in parallel to compare the released sugars (Fig. 5.3.6A). Till 4 h of incubation with *Ct*Manf, dFCO was not completely hydrolyzed, but during 8-16 h large amounts of mannobiose and significant amounts of mannose and mannotriose were released (Fig. 5.3.6A). Complete hydrolysis of carob galactomannan was achieved after 24 h of incubation where the maximum amount of mannobiose, mannose and mannotriose were produced (Fig. 5.3.6A).

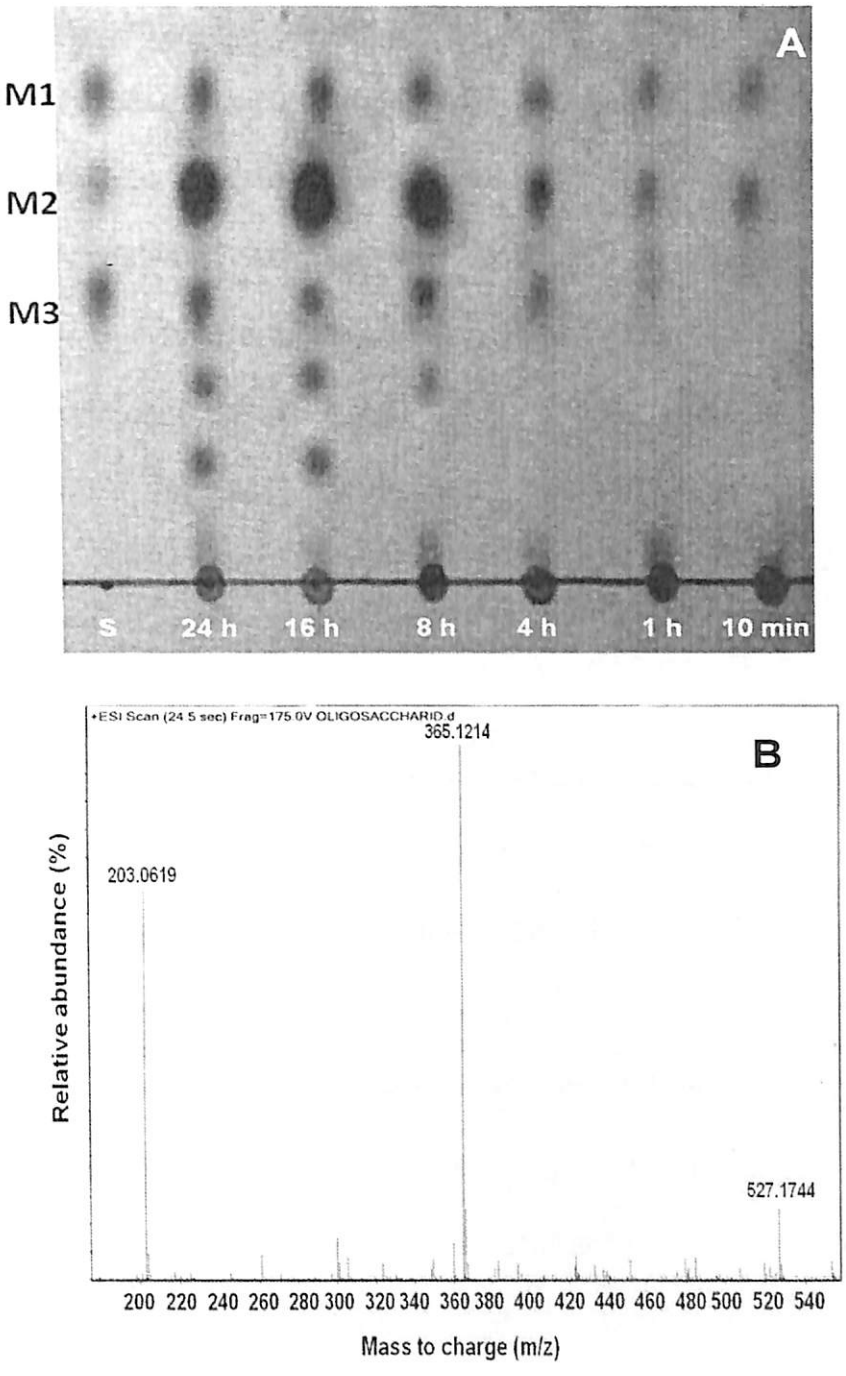

Fig. 5.3.6 Time dependent hydrolysis of copra meal by endo β-mannanase *Ct*Manf (A) TLC analysis displayed the release of mannose (dp1), mannobiose (dp2) and mannotriose (dp3). M1: Mannose, M2: Mannobiose and M3 Mannotriose are standards used. (B) ESI-MOS-TOF of hydrolysis products of copra meal by endo β-mannanase isolated after 24 h. In positive ionization mode the peak displayed mannose (m/z 203.0619), mannobiose (m/z 365.1214) and mannotriose (m/z 527.1744).

However, two other higher dp oligosaccharides (dp4 and dp5) were also observed after 16 h of hydrolysis (Fig. 5.3.6A). The release of mannobiose and mannotriose was attributed to the endo mannanse activity of *Ct*Manf enabling the cleavage of β-(1→4) bond between the mannose residues of dFCO. Mass spectroscopy analysis of dFCO hydrolyzed products by *Ct*Manf was carried out in positive ionization mode (Fig. 5.3.6B). The hydrolyzed fragments appeared as mannose $[M+Na]^+$ (m/z 203, dp1), mannobiose $[2M+Na]^+$ (m/z 365, dp2) and mannotriose $[3M+Na]^+$ (m/z 527, dp3).

5.3.5.3 HPAEC-PAD analysis of hydrolyzed products of dFCO by enzymatic hydrolysis

Qualitative and quantitative analyses of *Ct*Manf hydrolyzed products of dFCO were also monitored by HPAEC-PAD. Time dependent hydrolysis of dFCO by *Ct*Manf is displayed in Fig. 5.3.7. The peak intensities of standards are displayed in Fig. 5.3.7A. After 1 h of *Ct*Manf treatment of dFCO, the prominent peaks of mannose at 3.4 min, mannobiose at 4.06 min and mannotriose at 4.96 min were observed with concentrations 0.9 mg/ml, 1.1 mg/ml and 0.6 mg/ml, respectively (Fig. 5.3.7B). Mannobiose peak was most prominent as compared with mannose and mannotriose peaks after 1, 8 and 24 h of dFCO hydrolysis (Fig. 5.3.7B, C, D). *Ct*Manf was able to hydrolyze dFCO to a greater extent after 8 h and the complete hydrolysis was achieved at 24 h where mannose, mannobiose and mannotriose concentrations obtained were 2.8 mg/ml, 3.4 mg/ml and 1.2 mg/ml, respectively (Fig. 5.3.7D). All the concentrations were determined from the regression equation of mannose, mannobiose and mannotriose standard curves. Therefore, *Ct*Manf effectively hydrolyzed (1.0%, w/v) dFCO yielding 28% mannose, 34% mannobiose and 12%

mannotriose. The overall results interestingly described the performance of *Ct*Manf in releasing manno-oligosaccharides from dFCO which can be scaled up for large scale production.

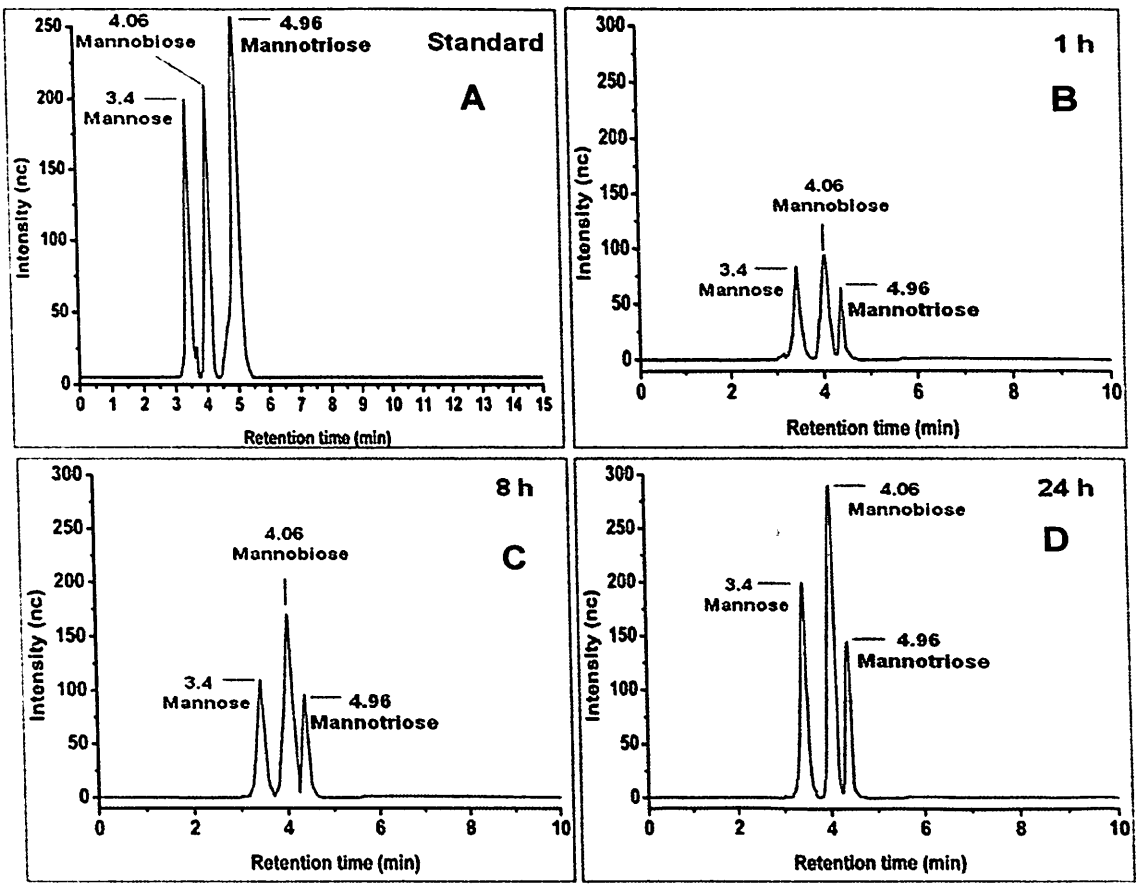

Fig 5.3.7 HPAEC-PAD analysis of hydrolysis products of dFCO by *Ct*Manf. (A) Elution patterns of standards used, mannose (3.4 min), mannobiose (4.06 min) and mannotriose (4.96 min). (B) to (D) elution patterns of mannose, mannobiose and mannotriose from dFCO (1%, w/v) after incubation from 1h to 24 h with *Ct*Manf.

5.3.5.4 Purification of manno-oligosaccharides produced from dFCO by CtManf

The endo-mannanase (*Ct*Manf) hydrolyzed products of dFCO were purified by size exclusion chromatography. The elution profile of oligosaccharides and monosaccharide displayed three individual peaks (Fig. 5.3.8A). Out of 60 fractions (1 ml) collected, the carbohydrate content was found in fractions from 28 to56. These fractions were analyzed by TLC (Fig. 5.3.8B) which showed separation of

carbohydrate components in fractions 52-56, mannose; 42-48, mannobiose and 38-40, mannotriose with a yield of 33%, 40% and 18%, respectively. The overlapping fractions of mannose-mannobiose were also observed in fraction 52 and mannobiose-mannotriose in fraction 34 (Fig. 5.3.8B). The separated fractions were pooled and analyzed by mass spectrometry. In positive ionization mode ESI-MS-TOF analysis of the separated carbohydrate components in fraction 52-56 displayed mannose $[M+Na]^+$ (m/z 203) (Fig. 5.3.8C [I]); 42-48, mannobiose $[2M+Na]^+$ (m/z 365) (Fig. 5.3.8C [II]) and 38-40, mannotriose $[3M+Na]^+$ (m/z 527) (Fig. 5.3.8C [III]). The 41st fraction displayed an overlapping mannobiose and mannotriose peaks at m/z 365 and 527, respectively (Fig. 5.3.8C [IV]). The fractions 50-51, displayed overlapping peaks of mannose and mannobiose at m/z 203 and 365, respectively, (Fig. 5.3.8C [V]). Therefore, it was evident from mass spectral analysis that the individual factions separated by the SEC were effectively purified into mannose, mannobiose and mannotriose.

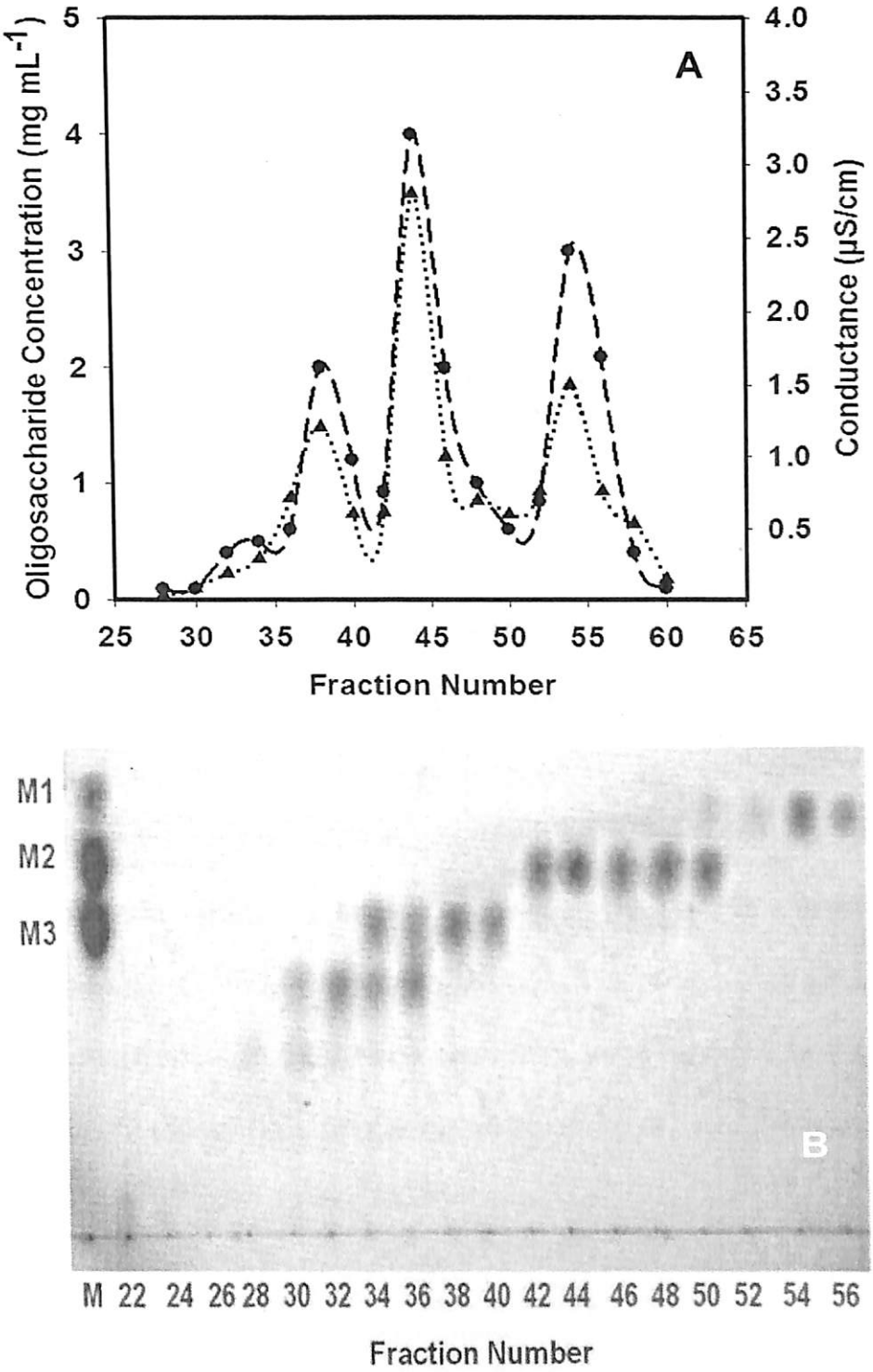

Fig. 5.3.8 Purification of *Ct*Manf hydrolysed products of dFCO. (A) Size exclusion chromatography (Bio Gel P2) showing hydrolyzed products as detected by conductance (··▲··) and by total carbohydrate content (--●--). (B) TLC analysis of fractions under three major peaks with mannose (52-56), mannobiose (42-48) and mannotriose (38-40).

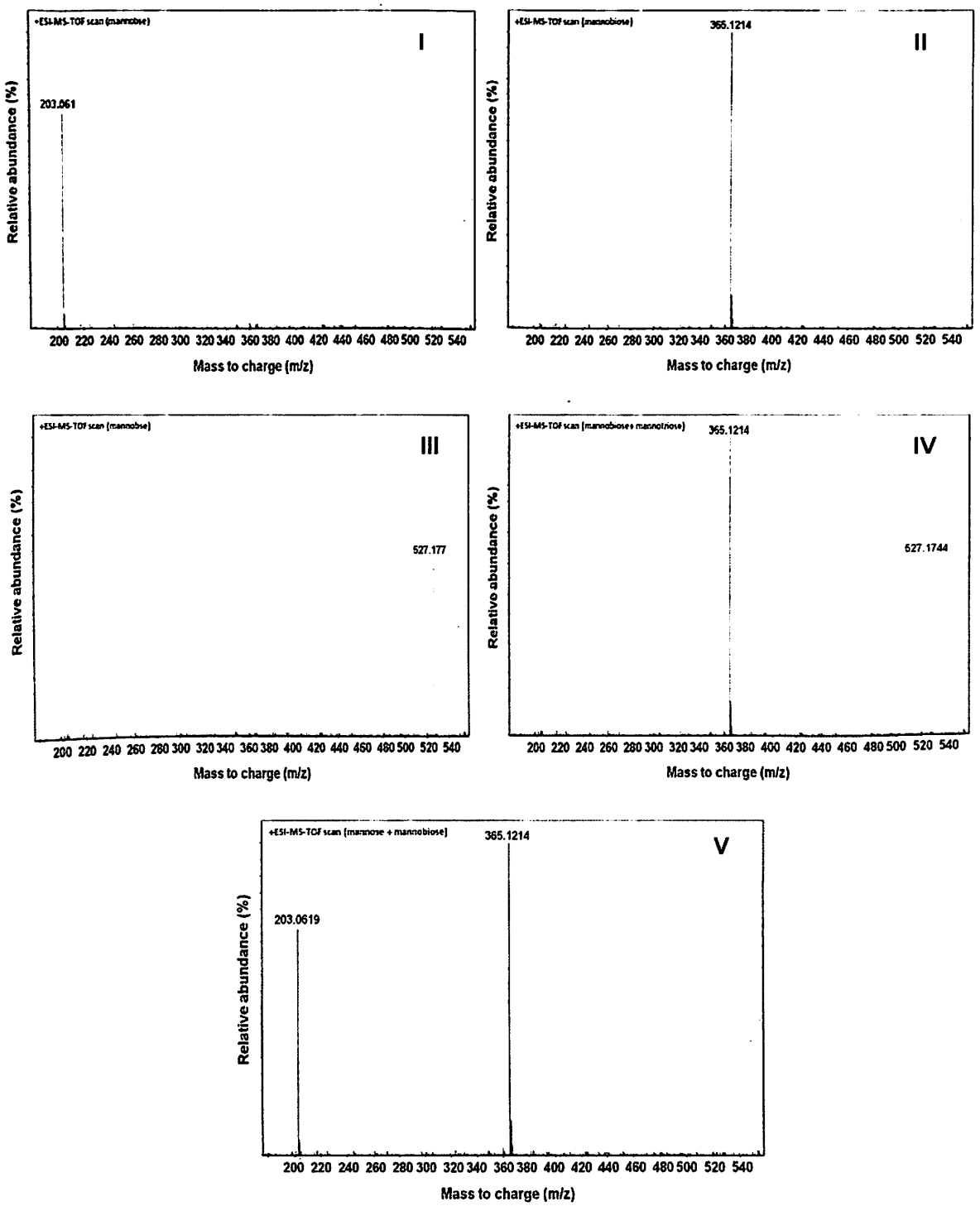

Fig. 5.3.8C ESI-MS-TOF peaks of active fractions (52-56) [I] mannose, (42-48) [II] mannobiose, (38-40) [III] mannotriose, and overlapping fractions (41) [IV] mannobiose-mannotriose, (50-51) [V] mannose-mannobiose eluted from Size exclusion chromatography (BioGel P2).

5.3.6. *In vitro* prebiotic analyses of MOS

5.3.6.1 Effect of artificial human gastric juice on MOS

The mixed MOS obtained from the defatted copra meal (dFCO) showed high resistance towards artificial gastric juice of pH 1-4 after 6 h of incubation at 37°C (Fig. 5.3.9A). The percent hydrolysis of mixed manno-oligosaccharides decreased with increase in the pH of the artificial gastric juice. The hydrolysis at pH 1, 2, 3 and 4 was 2.1%, 1.2%, 0.8% and 0.7%, respectively, after 6 h of incubation (Fig. 5.3.9A). The percent hydrolysis of inulin significantly decreased with increasing the pH as the hydrolysis of inulin at pH 1, 2, 3 and 4 was 30.2%, 24.2%, 14.0% and 8.3%, respectively, after 6 h of incubation (Fig. 5.3.9B). The results showed that the mixed manno-oligosaccharides (MOS) are at least 10 fold higher resistant to hydrolysis by human simulated gastric juice as compared with commercial insulin. The result indicated that the mixed manno-oligosaccharides from dFCO will be easily accessible by probiotic bacteria present in the gastrointestinal tract of human as it was not digested by artificial gastric juice till 6h. The current results are better as compared with the previous findings where oligosaccharides were reported to be resistant to acidic conditions in the artificial human gastric juice for only 2 h (Wichienchot *et al.*, 2010).

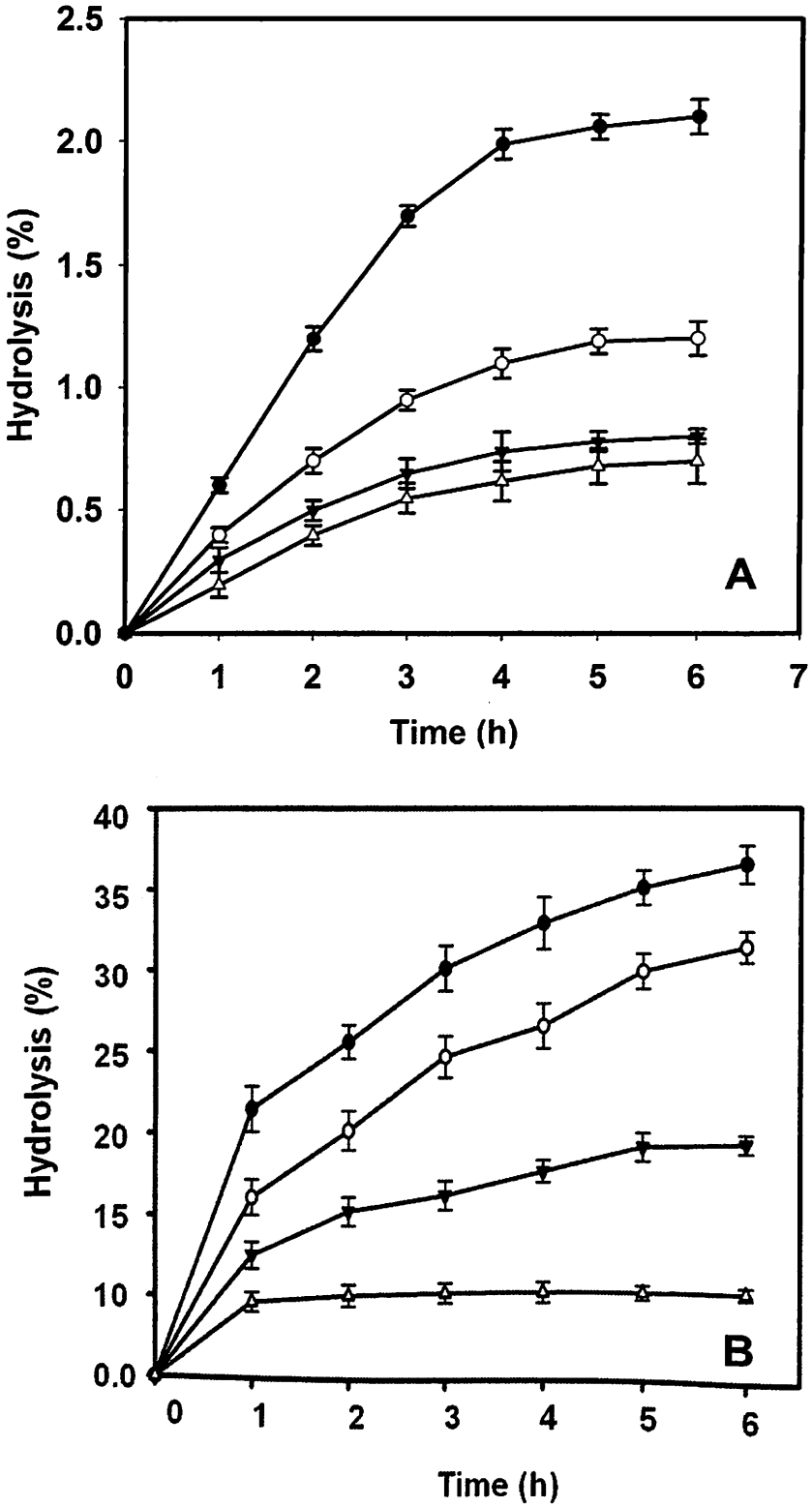

Fig. 5.3.9 Effect of simulated gastric juice on hydrolysis of (A) mixed manno-oligosaccharides and (B) inulin at pH 1 (●), 2 (o), 3 (▼) and 4 (Δ) at 37°C for 6h. The mean value of three independent experiments is presented with ± S.D.

5.3.6.2 Effect of intestinal fluid and α-amylase on mixed manno-oligosaccharides

The mixed MOS from defatted copra meal (dFCO) demonstrated high resistance in intestinal fluid containing 1000 U/ml of trypsin and 0.5% bile salt at pH 8. The maximum hydrolysis was 1.8% as compared with the standard prebiotic inulin, which gave maximum hydrolysis of 6.2% after 6 h of incubation at 37°C (Fig. 5.3.10). These results suggested that 98% of consumed mixed manno-oligosaccharides from defatted copra meal (dFCO) are expected to reach the jejunal portion of small intestine. This finding is more significant as compared with the earlier report, where 60% of oligosaccharides isolated from dragon fruit were able to reach lower portion of small intestine after 2h (Wichienchot *et al.*, 2010).

Hydrolysis of mixed manno-oligosaccharides from defatted copra meal (dFCO) and inulin by α-amylase at pH 5-8 displayed that higher pH resulted in significantly higher degree of hydrolysis. The degree of hydrolysis of mixed manno-oligosaccharides after 6 h of incubation at pH of 5, 6, 7 and 8 was 1.3%, 2.1%, 2.3% and 3.5%, respectively (Fig. 5.3.11A). Whereas, the hydrolysis of inulin by α-amylase showed 9.0%, 14.2%, 16.7% and 21.0% hydrolysis at pH 5, 6, 7 and 8, respectively, yielding higher extent of hydrolysis (Fig. 5.3.11B). The mixed MOS exhibited maximum hydrolysis of 3.5% after 6 h of incubation at 37°C, whereas the standard prebiotic inulin showed maximum hydrolysis of 21.0% at pH 8 after 6 h of incubation at 37°C, suggesting that the mixed manno-oligosaccharides had significantly higher enzymatic resistance as compared with inulin. It has been reported that the 88% of inulin and oligofructose reach the colon (Cummings and Macfarlane, 2002), whereas, the present results suggested that 97% mixed manno-oligosaccharides may reach the colon in intact form. Therefore, the isolated mixed MOS used in present study are

highly resistant to α-amylase hydrolysis. It is evident from this study that the mixed MOS has higher resistance to extreme conditions of the human gastrointestinal tract as compared to the standard inulin. In addition, mixed MOS also served as an alternative carbon source for probiotic bacteria. Thus, prebiotic mixed manno-oligosaccharides, alone or in combination with probiotic bacteria in the form of synbiotics, have the ability to influence and improve the gastrointestinal health of humans.

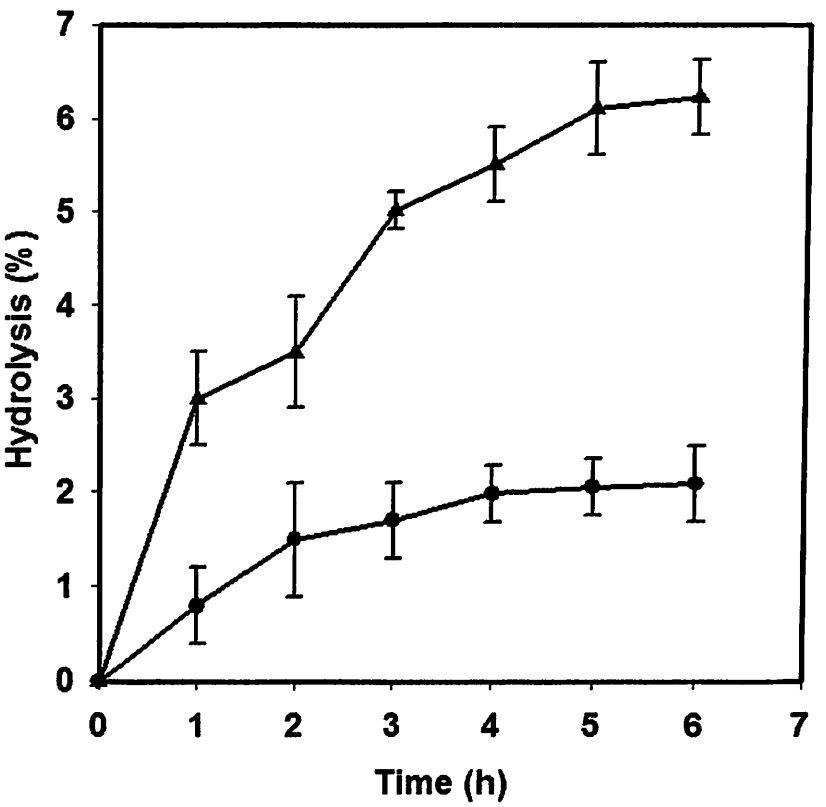

Fig. 5.3.10 Effect of simulated intestinal juice on hydrolysis of mixed manno-oligosaccharides (▲) and reference commercial prebiotic inulin (●) at pH 8 for 6h,

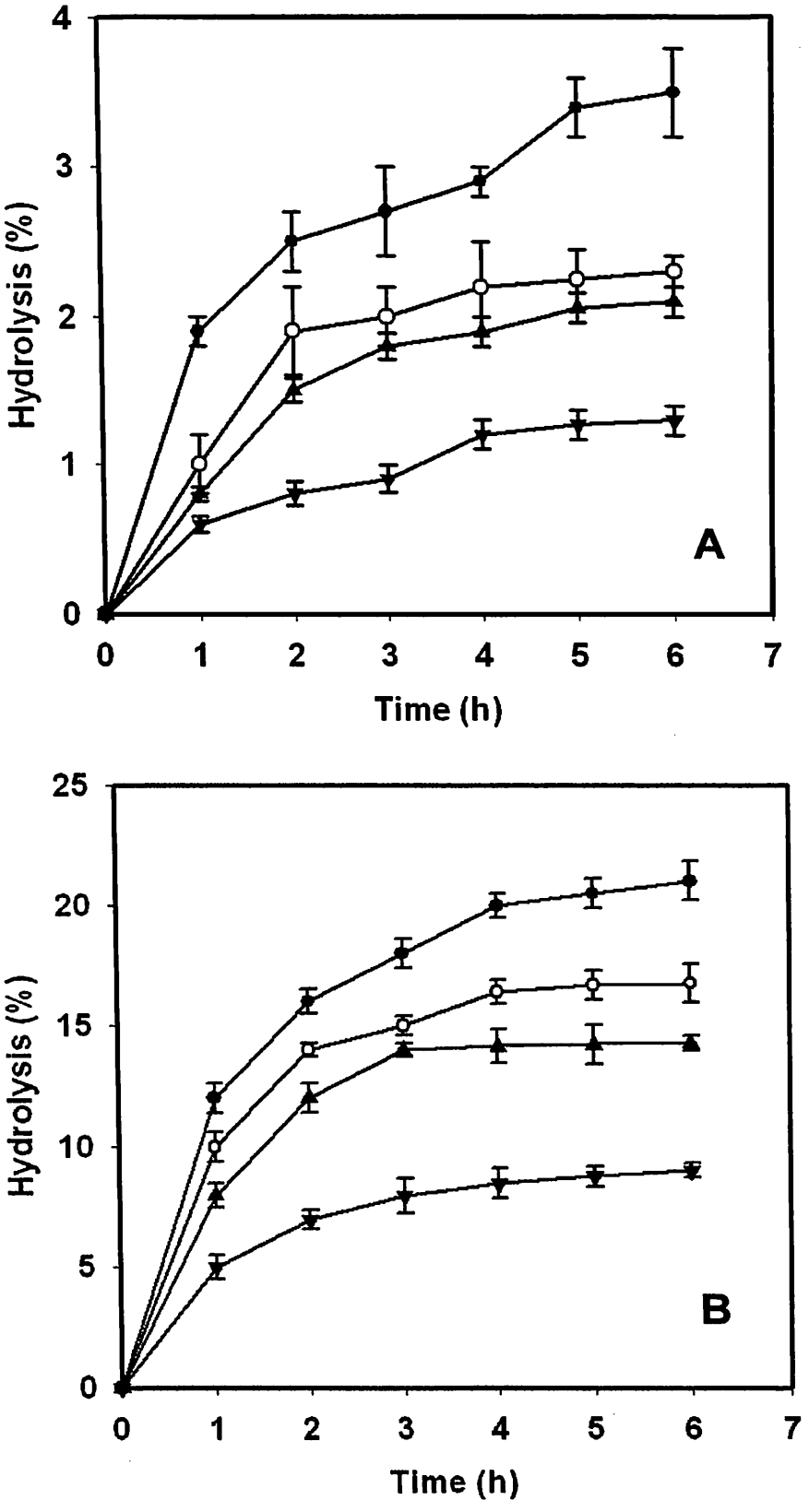

Fig. 5.3.11 Effect of α-amylase (A) on mixed manno-oligosaccharides and (B) on commercial prebiotic inulin at pH 5 (▼), 6 (▲), 7 (O) and 8 (●) at 37°C for 6h.

5.3.7 Effect of MOS on growth of probiotic bacteria

The increment in population of two probiotic bacterial strains *Lactobacillus acidophilus* NRRL B-4496 and *Bifidobacterium infantis* known for colonizing human colon, in the presence of 1% (w/v) mixed mannooligosaccharides (MOS), inulin and glucose are shown in Table 5.3.4. It was found that the mixed MOS stimulated higher growth of *Lactobacillus acidophilus* and *Bifidobacteria infantis* by increasing their number from $1.0x10^7$ to $17x10^7$ cells/ml and from $12x10^7$ to $165x10^7$ cells/ml, respectively, within 24 h (Table 5.3.4). Whereas, inulin promoted to a lesser extent the growth of *Lactobacillus acidophilus* and *Bifidobacteria infantis* from 12×10^7 to $99x10^7$ cells/ml and $1.0x10^7$ to $8.7x10^7$ cells/ml after 24 h, respectively (Table 5.3.4). Therefore, 1.8 fold higher growth of *Lactobacillus* and *Bifidobacteria* were observed in the presence of manno-oligosaccharides as compared with commercial prebiotic inulin. However, MOS did not support the growth of *E. coli* or *E. aerogenes* like commercial prebiotic inulin as shown in Table 5.3.4. The lowering of pH was from 6.4 to 4.1 after 24 h during the growth of both *Lactobacillus acidophilus* and *Bifidobacteria infantis*. It has been reported that both *Lactobacillus* and *Bifidobacteria* can grow at low pH 2.0 till 2 h (Gibson *et al.*, 2000; Pereira and Gibson, 2012). It has been reported earlier that short chain fatty acids (SCFA) and lactate are generated from anaerobic fermentation in the presence of prebiotics which cause the suppression of growth of pathogenic intestinal bacteria and modulation of cholesterol and lipid metabolism (Hongpattarakere, 2013). Therefore, the lowering of pH did not hinder the normal process of cell growth of probiotic bacteria. In contrast, the low growth profiles were observed as in case of *E. coli* and *E. aerogenes* after 24 h which was perhaps due to the pH lowering to 6.4 and 6.1, respectively, and also due

to the exhaustion of carbon source after 24 h. Similar results were reported where lowering of pH inhibited the growth of *E. coli* and this effect was further relieved by addition of methionine which gave tolerance against the acetate formation as well as lowering the pH (Roe *et al.*, 2002).

Table 5.3.4. Effect of mixed manno-oligosaccharides, inulin and glucose on growth of probiotic and non probiotic bacteria.

Bacteria	Mixed manno-oligosaccharides ($x10^7$ cells/ml)			Inulin ($x10^7$ cells/ml)			Glucose ($x10^7$ cells/ml)		
	0 h	12 h	24 h	0 h	12 h	24 h	0 h	12 h	24 h
Lactobacillus acidophilus 4495	12±4.0	95 ±2.0	165±8	12±4.0	62 ±5.0	99±9.0	12±4.0	60 ±2.0	94±7.0
Bifidobacterium infantis 41661	1.0±0.2	9.0±0.2	17±0.5	1.0±0.1	7.0±0.3	8.7±0.6	1.0±0.2	8.2±0.3	9.7±0.5
E. coli DH5α	0.2±0.02	0.8±0.6	1.2±0.3	0.2±0.02	0.7±0.6	1.1±0.3	0.2±0.01	1.0±0.02	1.5±0.6
E. aerogenes 3030	0.7±0.02	1.0±0.4	1.4±0.6	0.7±0.2	0.8±0.3	1.3±0.2	0.7±0.2	0.65±0.2	1.1±0.3

5.3.8 *In vitro* analysis of effect of MOS on mammalian cells

The concentration dependent effects of mixed manno-oligosaccharides on HT29 cell line and on normal human colon cell (FHC ATCC CRL-1831) are displayed in Fig. 5.3.12A and Fig. 5.3.12B, respectively. In the MTT assay, the decrease in viability of HT29 cells was observed when the concentration of mixed MOS increased from 1 to 500 µg/ml (Fig. 5.3.12A). In contrast no cytotoxic effect of MOS on normal cell FHC ATCC CRL-1831 was observed while increasing the concentrations of MOS from 1 to 1000 µg/ml till 48h (Fig. 5.3.12B). At highest concentration of manno-oligosaccharides (500 µg/ml) the percent survival of HT29 cells was only 50.0 ± 3.2% after 24 h of incubation while the percent survival of HT29 cells after 48 h of incubation displayed 40.0 ± 0.9% at 500 µg/ml manno-oligosaccharides concentration (Fig. 5.3.12A). These results showed that the manno-oligosaccharides (MOS) significantly inhibited growth of the human colon carcinoma

cells. The potential effects of oligosaccharides from apple on human colon carcinoma cell line HT29 via cell cycle arrest at S phase resulting in apoptosis was reported (Li *et al.*, 2013). The growth reduction by isolated manno-oligosaccharides from defatted copra meal may open new arena of chemotheraputic agents for colon cancer treatment.

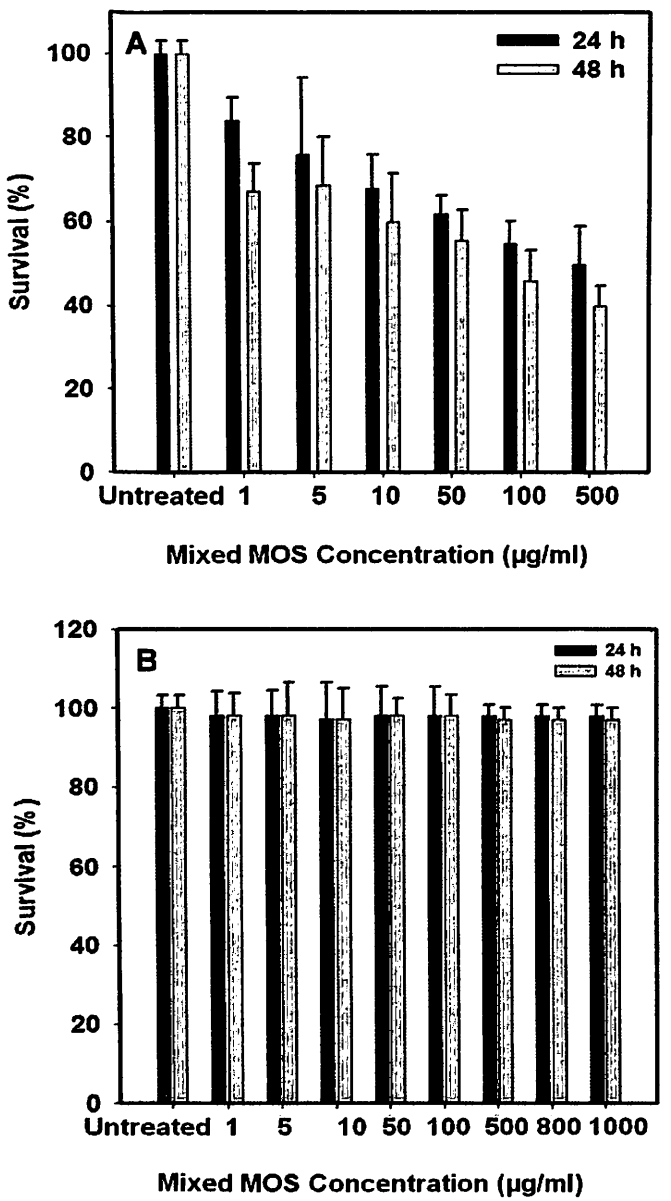

Fig. 5.3.12 Effect of mixed manno-oligosaccharides, (A) 1-500 (µg/ml) on viability of human colon carcinoma HT29 cells and (B) 1-1000 (µg/ml) on viability of human colon normal (FHC ATCC CRL-1831) cells by MTT assay. The data are expressed as mean ± SD of three independent experiments and each analysis was carried out in triplicate.

5.4 Conclusions

*Ct*Manf catalyzed substrate hydrolysis products were analyzed by TLC and HPAEC. It was apparent from TLC that *Ct*Manf released mannotriose, mannobiose and mannose in prolonged hydrolysis of carob galactomannan. After complete hydrolysis of carob galactomannan *Ct*Manf was able to release mannose, mannobiose and mannotriose. The salient feature of *Ct*Manf catalysis involved only β-(1→4)-bond cleavage when mannobiose and mannotriose were used as substrate and liberated mainly mannose as main product. The release of large amount of mannose at early stage of enzymatic reaction by *Ct*Manf was commonly seen against carob galactomannan and manno-oligosaccharides. HPAEC analysis corroborated the results of TLC analysis of hydrolysis of carob galactomannan products released by *Ct*Manf. The results of HPAEC showed that *Ct*Manf exclusively cleaves carob galactomannan into mannotriose, mannobiose and mannose. It was apparent from TLC and HPAEC analyses *Ct*Manf was able to hydrolyze only β-(1→4) bond cleavage and had potential to produce manno-oligosaccharides from carob galactomannan.

The structure analysis of the pretreated copra meal by FESEM revealed the efficiency of the pretreatment process that led to good structural deformity. The FT-IR analysis showed the easy accessibility of the major functional groups of the abundant galactomannan for *Ct*Manf. Both ^{1}H and ^{13}C NMR revealed that the polysaccharide content of the copra meal contains predominantly galactomannan with α-(1→6)-linked galactose substituted in the β-(1→4)-linked mannose main chain. Time dependent *Ct*Manf catalyzed hydrolysis of the galactomannan of copra meal confirmed the presence of mannose, mannobiose and mannotriose on analysis by

TLC, HPAEC and mass spectra. The released manno-oligosaccharides were purified using size exclusion chromatography with significant yield. The mixed manno-oligosaccharides enhanced the growth of probiotic bacteria holding potential as competent prebiotic agent as compared with commercial inulin. The mixed manno-oligosaccharides are highly resistant against hydrolysis by simulated gastric juice, intestinal fluid and α-amylase proving to be a stable prebiotic over inulin. *In vitro* cytotoxicity assay of manno-oligosaccharide (500 µg/ml) on human epithelial colorectal adenocarcinoma cell line (HT-29) demonstrated 60% decreased viability of cells after 48h displaying anti-tumorigenic property. In contrast the MOS did not show any cytotoxic effect on the normal colon cell. Therefore, it can be suggested that MOSs are biocompatible.

References

Al-Assaf, S., Phillips, G.O. and Williams, P.A. (2006) Characterization and properties of Acacia senegal (l.) willd. var. senegal with enhanced properties (acacia (sen) super gum(tm)): part 1--controlled maturation of acacia senegal var. senegal to increase viscoelasticity, produce a hydrogel form and convert a poor into a good emulsifier. Food Hydrocolloids 20:369-377.

Balasubramaniam, K. (1976). Polysaccharides of the kernel of maturing and mature coconuts. J. Food Sci. 41:1370-1373.

Bilgicli, N., Ibanoglu, S. and Herken, E.N. (2007) Effect of dietary fibre addition on the selected nutritional properties of cookies. J. Food. Engg. 78:86-89.

Bradford, M.M . (1976) Rapid and sensitive method for the quantitation of microgram quantities of protein utilizing the principle of protein-dye binding. Anal. Biochem. 72:248-254.

Cerqueira, M.A., Lima, A.M., Teixeira, J.A., Moreira, R.A. and Vicente, A.A. (2009) Suitability of novel galactomannans as edible coatings for tropical fruits. J. Food. Engg. 94(3-4):372-378.

Cheng, Y., Brown, K.M. and Prud'homme, R.K. (2002) Preparation and characterization of molecular weight fractions of guar galactomannans using acid and enzymatic hydrolysis. Int. J. Biol. Macromol. 31:29-35.

Cole, C.L. and Jayson, G.C. (2008) Oligosaccharides as anti-angiogenic agents. Expert. Opin. Biol. Ther. 8: 351-362.

Cummings, J.H. and Macfarlane, G.T. (2002) Gastrointestinal effects of prebiotics. British. J. Nutr. 87:1145-1151.

Dubois, M., Gilles, K.A., Hamilton, J.K., Rebers, P.A. and Smith, F. (1956) Calorimetric method for determination of sugars and related substances. Analyt. Chem. 28:350-356.

Fenandez, M.F., Boris, S. and Barbes, C. (2003) Prebiotic properties of human *Lactobacilli* strains to be used in the grastrointestinal tract. J. Appl. Microbiol. 94:449-455.

Figueiró, S.D., Góes, J.C., Moreira, R.A. and Sombra, A.S.B. (2004) On the physicochemical and dielectric properties of glutaraldehyde crosslinked galactomannan collagen films. Carbohydr. Polym. 56:313-320.

Ganter, J.L.M.S., Heyraud, A., Petkowicz, O., Rinaudo, M. and Reicher, F. (1995) Galactomannans from Brazilian seeds: characterization of the oligosaccharides produced by mild acid hydrolysis. Int. J. Biol. Macromol. 17:13–19.

Gibson, G.R, Ottaway, P.B. and Rastall, R.A. (2000) Prebiotics: new developments in functional foods. Wood head Publishing Limited, Oxford, UK. 108 pp.

Hongpattarakere, T. (2013) Improvement of freeze-dried *Lactobacillus plantarum* survival using water extracts and crude fibers from food crops. Food. Bioprocess. Technol. 6:1885-1896.

Hossain, M.Z, Abe, J. and Hizukuri, S. (1996) Multiple forms of β-mannanase from *Bacillus sp.* KK01. Enzyme. Microb. Technol. 18:95-98.

Ishihara, N., Chu, D.C., Akachi, S. and Juneja, L.R. (2000) Preventive effect of partially hydrolyzed guar gum on infection of *Salmonella enterica* in young and laying hens. Poult. Sci. 79:689-697.

Kacurakova, M., Capeka, P., Sasinkova, V., Wellnerb, N. and Ebringerova, A. (2000) FT-IR study of plant cell wall model compounds: pectic polysaccharides and hemicelluloses. Carbo. Pol. 43:195-203.

Korakli, M., Ganzle, M.G. and Vogel, R.F. (2002) Metabolism by bifidobacteria and lactic acid bacteria of polysaccharides from wheat and rye, and exopolysaccharides produced by *Lactobacillus sanfranciscensis*. J. Appl. Microbiol. 92:958–965.

Kovacs-Nolan, J., Kanatani, H., Nakamura, A., Ibuki, M., Mine, Y. (2013) β-1,4-mannobiose stimulates innate immune responses and induces TLR4-dependent activation of mouse macrophages but reduces severity of inflammation during endotoxemia in mice. J. Nutr. doi: 10.3945/jn.112.167866.

Lama-Mu˜noz, A., Rodríguez-Gutiérrez, G., Rubio-Senent, F. and Fernández-Bola˜nos, J. (2012) Production, characterization and isolation of neutral and pectic oligosaccharides with low molecular weights from olive by-products thermally treated. Food. Hydrocoll. 28: 92-104.

Li, Q., Zhou, S., Jing, J., Yang, T., Duan, S., Wang, Z., Mei, Q and, Liu, L. (2013) Oligosaccharide from apple induces apoptosis and cell cycle arrest in HT29 human colon cancer cells. Int. J. Biol. Macromol. 57: 245-254.

Lin, T.C. and Chen, C. (2004) Enhanced mannanase production by submerged culture of *Aspergillus niger* NCH-189 using defatted copra based media. Proc. Bio. 39:1103-1109.

Mosmann T (1983) Rapid colorimetric assay for cellular growth and survival: application to proliferation and cytotoxicity assays. J Immunol Methods 65: 55-63.

Mudgil, D., Barak, S. and Khatkar, B.S. (2012) Composition, properties and health benefits of indigestible Carbohydrate polymers as dietary fiber: A review. Int. J. Biol. Macromol. 50:1035-1039.

Mulimani, V.H and Naganagouda, K. (2010) Simple laboratory exercise for induction of β-mannanase from *Aspergillus niger*. Res. Food. Sci. Edu. 9:76-79.

Naganagouda, V.K., Patil, A.G.G. and Mulimani, V.H. (2009) Optimization of the production of thermostable endo-β-1,4 mannanases from a newly isolated *Aspergillus niger gr* and *Aspergillus flavus gr*. Appl. Biochem. Biotechnol. 152:213-223.

Naughton, P.J., Mikkelsen, L.L. and Jensen, B.B. (2001) Effects of nondigestible oligosaccharides on *Salmonella enterica* Serovar Typhimurium and nonpathogenic *Escherichia coli* in the pig small intestine *in vitro*. Appl. Environ. Microbiol. 67:3391-3395.

Nelson, N. (1944) A photometric adaptation of the Somogyi method for the determination of glucose. J. Biol. Chem. 153:375-380.

Peng, Y., Zhang, L., Zeng, F., Xu, Y. (2003) Structure and antitumor activity of extracellular polysaccharides from mycelium. Carbo. Pol. 54: 297-303.

Pereira, D.I.A. and Gibson, G.R. (2002) Cholesterol assimilation by lactic acid bacteria and *Bifidobacteria* isolated from the human gut. Appl. Environ. Microbiol. 68:4689-4693.

Prashanth, M.R.S., Parvathy, K.S., Susheelamma, N.S., Prashanth, K.V.H., Tharanathan, R.N., Cha, A. and Anilkumar, G.. (2006) Galactomannan esters a simple, cost-effective method of preparation and characterization. Food. Hydrocoll. 20:1198-1205.

Prawitwong, P., Takigami, S. and Phillips,.G.O. (2007) Effects of γ-irradiation on molar mass and properties of Konjac mannan. Food. Hydrocoll. 21:1362-1367

Rakhmanberdyeva, R.K. and Shashkov, A.S. (2005) Structure of galactomannans from *Gleditsia delavayi* and *G. aquatica* BY 1H and 13C NMR spectroscopy. Chem. Nat. Comp. 41:14-16.

Ramesh, H.P., Yamaki, K., Ono, H. and Tsushida, T. (2001) Two-dimensional NMR spectroscopic studies of fenugreek (*Trigonella foenum-graecum* L.) galactomannan without chemical fragmentation. Carbo. Pol. 45:69-77.

Roe, A.J., O'Byrne, C., McLaggan, D. and Booth, I.R. (2002) Inhibition of *Escherichia coli* growth by acetic acid: a problem with methionine biosynthesis and homocysteine toxicity. Microbiology. 148:2215-2222.

Samson, A.S., Cater, C.M. and Mattil, K.F. (1971) Preparation and characterization of total protein isolates. American. Asso. Cer. Chem. 182-190.

Shobha, M.S., Kumar, A.B.V., Tharanathan, R.N., Koka, R. and Gaonkar, A.K.. (2005) Modification of guar galactomannan with the aid of *Aspergillus niger* pectinase. Carbo. Pol. 62: 267-273.

Singh, V. and Tiwari, A. (2009) Hydrolytic fragmentation of seed gums under microwave irradiation. Int. J. Biol. Macromol. 44:186-189.

Sluiter, A., Hames, B., Ruiz, R., Scarlata, C., Sluiter, J., Templeton, D. and Crocker, D. (2008) Determination of structural carbohydrates and lignin in biomass. In Laboratory Analytical Procedure (LAP). Colorado: Technical Report NREL/ TP-510-42618.

Somogyi, M. (1945) A new reagent for the determination of sugars. J. Biol. Chem. 160:61-68.

Spring, P., Wenk, C., Dawson, K.A. and Newman, K.E. (2000) The effect of dietary mannooligosaccharides on ceca of *Salmonella* challenged broiler chicks. Poult. Sci. 78:205-211.

Sun, S.N., Yuan, T.Q., Li, M.F., Cao, X.F., Xu, F and Liu, Q.Y. (2012) Structural characterization of hemicelluloses from bamboo culms (*Neosinocalamus affinis*). Cell. Chem. Technol. 46:165-176.

Tamaki, Y., Teruya, T. and Tako, M. (2010) The chemical structure of galactomannan isolated from the seeds of *Delonix regia*. Biosci. Biotechnol. Biochem. 74(5):1110-1112.

Wichienchot, S., Jatupornpipat, M. and Rastall, R.A. (2010) Oligosaccharides of pitaya (dragon fruit) flesh and their prebiotic properties. Food. Chem. 120:850-857.

Yang, C., Rupa, P., Kanatani, H., Nakamura, A., Ibuki, M. and Mine, Y. (2013) Therapeutic effects of β-1,4-mannobiose in a Balb/c mouse model of intranasally-induced pollen allergy. Allergol. Int. 62(1):65-76.

Zhang, L., Yang, L., Ding, Q. and Chen, X. (1995) Studies on molecular weights of polysaccharides of *Auricularia auriculajudae*. Carbo. Res. 270:1-10.

LIST OF PUBLICATIONS

Published/accepted

1. **Arabinda Ghosh**, Anil Kumar Verma, Jagan Mohan Rao. T., Rishikesh Shukla and Arun Goyal (**2014**) Recovery and purification of oligosaccharides from coprameal by recombinant endo-β-mannanase and deciphering molecular mechanism involved and its role as potent therapeutic agent. Molecular Biotechnology, DOI: 10.1007/s12033-014-9807-4.
2. Ashutosh Gupta, Saprativ P. Das, **Arabinda Ghosh,** Rajan Choudhary, Debasish Das and Arun Goyal (**2014**) Bioethanol production from *Populus nigra* involving recombinant hemicellulases from *Clostridium thermocellum.* Bioresource Technology, 165, 205-213.
3. **Arabinda Ghosh**, Anil K. Verma, Ana Sofia Luis, Joana L. A. Bras, Carlos M. G. A. Fontes, Arun Goyal (**2014**) Mannan specific family 35 carbohydrate binding module (*Ct*CBM35) of *Clostridium thermocellum*: structure analysis and ligand binding. Biologia, 69(10), DOI: 10.2478/s11756-014-0444-y.
4. **Arabinda Ghosh**, Anil K. Verma, Saurabh Gautam, Munishwar N. Gupta and Arun Goyal (**2014**) Structure and functional investigation of ligand binding by a family 35 carbohydrate binding module (*Ct*CBM35) of β-mannanase of family 26 glycoside hydrolase from *Clostridium thermocellum.* Biochemistry (Moscow), 79(7), 672-686.
5. **Arabinda Ghosh**, Ana S. Luis, Joana L.A. Brás, Neeta Pathaw, N. K. Chrungoo, C. M. G. A. Fontes and Arun Goyal (**2013**) Deciphering ligand specificity of a *Clostridium thermocellum* family 35 carbohydrate binding module (*Ct*CBM35) for gluco- and galacto- substituted mannans and its calcium induced stability. PLoS ONE, 8(12), e80415.
6. **Arabinda Ghosh**, Ana S. Luis, Joana L.A. Brás, C. M.G.A. Fontes and Arun Goyal (**2013**) Thermostable recombinant endo-β-(1→4)-mannanase from *Clostridium thermocellum*: Biochemical characterization and manno-oligosaccharides production. Journal of Agricultural and Food Chemistry, 61 (50), 12333-12344.
7. Shadab Ahmed, Ana Sofia Luis, Joana L. A. Bras, **Arabinda Ghosh**, Saurabh Gautam, Munishwar N. Gupta, Carlos M. G. A. Fontes and Arun Goyal (**2013**) A Novel α-L-arabinofuranosidase of family 43 Glycoside Hydrolase (*Ct*43Araf) from *Clostridium thermocellum*. PLoS ONE, 8(9), e73575.
8. Saprativ P. Das, **Arabinda Ghosh**, Ashutosh Gupta, Arun Goyal and Debasish Das (**2013**) Lignocellulosic fermentation of wild grass employing recombinant hydrolytic enzymes and fermentative microbes with effective bioethanol recovery. BioMed Research International, http://dx.doi.org/10.1155/2013/386063.

9. Saprativ P Das, Deepmoni Deka, **Arabinda Ghosh**, Debasish Das, Mohammad Jawed and Arun Goyal (**2013**) Scale up and efficient bioethanol production involving recombinant cellulase (Glycoside hydrolase family 5) from *Clostridium thermocellum*. Sustainable Chemical Processes, 1(19), 1-11.

10. Saprativ P Das, Rajeev Ravindran, **Arabinda Ghosh**, Deepmoni Deka, Debasish Das, Mohammad Jawed, Carlos M.G.A. Fontes and Arun Goyal (**2013**) Efficient pretreatment for bioethanol production from water hyacinth (*Eichhornia crassipes*) involving naturally isolated and recombinant enzymes and its recovery. Environmental Progress & Sustainable Energy, doi: 10.1002/ep.11885.

11. Shadab Ahmed, Rahul Charan, **Arabinda Ghosh** and Arun Goyal (**2012**) Comparative modelling and ligand binding site prediction of a family 43 Glycoside Hydrolase from *Clostridium thermocellum.* Journal of Proteins and Proteomics, 3(1), 31-38.

LIST OF CONFERENCES

International

1. Vikky Rajulapati, **Arabinda Ghosh**, Carols M.G.A. Fontes, Arun Goyal (**2014**) Cloning, expression of novel multi-substrate specific family 81 glycoside hydrolase (GH81) from *Clostridium thermocellum* ATCC 27405. Association of Microbiologists of India, Coimbatore Unit and Department of Agricultural Microbiology, Nov. 12-14, 2014, Agricultural University, Coimbatore, Tamilnadu, India (*Abstract accepted*).
2. Vivek Gupta, **Arabinda Ghosh** and Arun Goyal (**2014**) Insight into structure prediction, cloning, expression and ligand binding of family 35 carbohydrate binding module (*Ct*CBM35A) of *Clostridium thermocellum.* International Seminar on Harnessing Natural Resources for Sustainable Development Global Trend, Jan. 29-31, Cotton College, Guwahati, Assam.
3. Shraddha Shukla, **Arabinda Ghosh**, Qiao Shi, Ndegwa Maija Tenkanen and Arun Goyal (**2014**) Production of gluco-oligosaccharides from *Weissella confusa* Cab3 and their purification and characterization. 27th International Carbohydrate Symposium, Jan. 12-17, Indian Institute of Science, Bangalore, India.
4. **Arabinda Ghosh**, Anil Kumar Verma, Ana Sofia Luis, Joana L. A. Bras, Carlos M. G. A. Fontes and Arun Goyal (**2013**) 3-Dimensional structure and ligand binding of family 35 carbohydrate binding module (*Ct*CBM35) of *Clostridium thermocellum* by in silico and affinity electrophoresis studies. 10th Convention of Biotech Research Society and International Conference on Advances in Biotechnology and Bioinformatics, Nov. 25-27, D.Y. Patil Institute of Biotechnology and Bioinformatics, Pune, India.
5. **Arabinda Ghosh**, Rishikesh Shukla and Arun Goyal (**2013**) Production of manno-oligosaccharides from copra meal by recombinant endo β-(1→4) mannanase: their potential role as prebiotics and antitumorigenic agent. 10th Convention of Biotech Research Society and International Conference on Advances in Biotechnology and Bioinformatics, Nov. 25-27, D.Y. Patil Institute of Biotechnology and Bioinformatics, Pune, India.
6. Saprativ P. Das, **Arabinda Ghosh**, Ashutosh Gupta, Debasish Das and Arun Goyal (**2013**) Approaches for identification of a combination of hydrolytic enzymes and fermentative microbes for bioethanol production from wild grass. Indraprastha International Conference on Biotechnology, Guru Gobind Singh Indraprastha University, Oct 22-25, New Delhi, India.
7. **Arabinda Ghosh**, Anil K. Verma, Neeta Pathaw, Nikhil K. Chrungoo, Saurabh Gautam, Munishwar N. Gupta and Arun Goyal (**2013**) Conformational change upon ligand binding of a manno-configured substrate specific family 35 Carbohydrate Binding Module (CBM35) from *Clostridium thermocellum.* 10th Carbohydrate Bioengineering Meeting, April 21-24, Institute of Microbiology, Academy of Sciences of the Czech Republic, Prague, Czech Republic.

8. **Arabinda Ghosh**, Anil K. Verma, Carlos M.G.A. Fontes and Arun Goyal (**2012**) Manno-configured substrate specific family 35 carbohydrate binding module (*Ct*CBM35) from *Clostridium thermocellum*. International Conference on Industrial Biotechnology, Nov. 21-23, Punjabi University, Patiala, India.
9. **Arabinda Ghosh**, Anil K. Verma and Arun Goyal (**2012**) 3-D structure prediction and ligand docking analysis of family 35 carbohydrate binding module (*Ct*CBM35) of *Clostridium thermocellum*. International Conference on Industrial Biotechnology, Nov. 21-23, Punjabi University, Patiala, India.
10. **Arabinda Ghosh**, Carlos M.G.A. Fontes and Arun Goyal (**2012**) Cloning and comparative binding of two Carbohydrate Binding Modules of family 35 (Cthe2811 and Cthe0032) from *Clostridium thermocellum*. 18th International Conference (Post ISCBC-2012) on Perspective and Challenges in Chemical and Biological Sciences, Jan. 28-30, Institute of Advanced Study in Science & Technology (IASST), Guwahati, Assam, India.
11. Shadab Ahmed, **Arabinda Ghosh**, Carlos M.G.A. Fontes and Arun Goyal (**2011**) Biochemical characterization of family 43 glycoside hydrolase (GH43F) and its truncated derivative (GH43) from *Clostridium thermocellum*. International Conference on New Horizons in Biotechnology, Nov. 23-26, National Institute of Interdisciplinary Science and Technology (NIIST), Trivandrum, India.
12. **Arabinda Ghosh**, Carlos M.G.A. Fontes and Arun Goyal (**2011**) Comparative biochemical studies of Glycoside Hydrolase Family 26 (GH26) and its derivative (GH26-CBM35) from *Clostridium thermocellum*. International Conference on Microbial Biotechnology for Sustainable Development (52nd Annual Conference of Association of Microbiologists of India), Nov. 3-6, Panjab University, Chandigarh, India.
13. **Arabinda Ghosh**, Shadab Ahmed, Anil Kumar Verma, Carlos M.G.A. Fontes and Arun Goyal (**2011**) Cloning, expression and biochemical characterization of family 26 glycoside hydrolase (GH26-CBM35) and carbohydrate binding module (CBM35) from *Clostridium thermocellum*. 9th Carbohydrate Bioengineering Meeting, May 15-18, Technical University of Lisbon. Portugal.
14. Shadab Ahmed, **Arabinda Ghosh**, Carlos M.G.A. Fontes and Arun Goyal (**2011**) Biochemical characterization of a family 43 glycoside hydrolase (GH43) from *Clostridium thermocellum*. 9th Carbohydrate Bioengineering Meeting, May 15-18, Technical University of Lisbon. Portugal.
15. Anil Kumar Verma, **Arabinda Ghosh** and Arun Goyal (**2011**) In silico structure and substrate binding analyses of family 35 carbohydrate binding module (CBM35) from cellulosome of *Clostridium thermocellum*. World Congress on Biotechnology, March 21-23, Hyderabad, India.
16. Shadab Ahmed, **Arabinda Ghosh** and Arun Goyal (**2010**) Cloning of family 43 glycoside hydrolase (GH43) and its derivative from *Clostridium thermocellum*. 51st Annual Conference of AMI, Dec. 14-17, Birla Institute of Technology, Mesra, Ranchi, India.

17. Seema Patel, **Arabinda Ghosh** and Arun Goyal (**2010**) 16S rRNA based identification of a bioactive dextran producing *Pediococcus pentosaceus* isolated from soil of biodiversity hotspot Assam. International Conference on Environmental Health and Technology, March 15-17, Indian Institute of Technology Kanpur, Kanpur India.
18. Seema Patel, Damini Kothari, **Arabinda Ghosh** and Arun Goyal (**2009**) Optimization of critical medium components using Response Surface Methodology for enhancing the dextran production by the mutant of a new isolate of lactic acid bacteria. 50th Annual Conference of Association of Microbiologists of India, Dec. 15-18, National Chemical Laboratory, Pune, India.

International (Oral Presentation)

1. **Arabinda Ghosh** and Arun Goyal (**2014**) Synthesis and purification of manno-oligosaccharides from coprameal by recombinant endo-β-mannanase and their prebiotic and anticancer properties. International Conference on Biotechnology and Bioengineering, Oct. 29-30, BITS Pilani Dubai Campus, Dubai (*Abstract accepted*).

National (Oral Presentation)

1. **Arabinda Ghosh** and Arun Goyal (**2014**) Novel thermostable recombinant endo-β-mannanase of *Clostridium thermocellum* for manno-oilgosaccharides production. National Seminar On Metabolomics-A new frontier in natural products research, May 23-24, Depatment of Biotechnology, North Eastern Hill University, Shillong, India.

Workshops

1. Participated in International Symposium on "Bioengineering 2012" (ISBE **2012**) organized by Biotech Hub, Centre for the Environment, Indian Institute of Technology Guwahati held on December 10, **2012**.
2. Participated in the workshop on "Genome Annotation 2011" organized by Biotech Hub, Centre for the Environment, Indian Institute of Technology Guwahati held on October 15, **2011**.

VITAE

The author was born on December 21, 1982 in Jorhat, Assam, India. He passed the Secondary School Examination conducted by Board of Secondary Education, Assam, in 1999, and Higher Secondary School Examination conducted by Assam Higher Secondary Education Council, Guwahati, Assam, in 2001. He completed B.Sc. in Zoology and Post Graduate Diploma in Bioinformatics from Dibrugarh University, Dibrugarh, India, in 2005 and 2007, respectively. He did his M.Sc. in Biotechnology from North Eastern Hill University, Shillong, Meghalaya, in 2009.

Arabinda Ghosh joined Ph.D. programme in July 2009 at Department of Biotechnology, Indian Institute of Technology Guwahati, Guwahati 781039, Assam, India. He qualified Graduate Aptitude Test in Engineering (GATE) in 2009 and CSIR-UGC-NET JRF under UGC fellowship scheme in December 2010. He received Junior Research Fellowship from Institute under the scheme run by the Ministry of Human Resource and Development (MHRD), India. He also received Junior Research Fellowship as well as Senior Research Fellowship from University Grants Commission (UGC), New Delhi, India. He successfully completed the course work with 8.0/10 Cumulative Point Index (CPI). He gave the Open (PhD Synopsis) Seminar on July 31st, 2014 and presented his thesis work before the Doctoral Committee and his performance was satisfactory. He submitted the PhD thesis in October, 2014.

The positive clones of recombinant *Ct*Manf, *Ct*ManT and *Ct*CBM35 were sequenced from Eurofin India (Bangalore, India). The sequences are listed below, which were further analyzed using BLAST (www.ncbi.nlm.nih/Blastn).

*Ct*Manf (Glycoside Hydrolase 26 catalytic module from *Clostridium thermocellum* ATCC 27405)

TTACTTTTGTGTAACGGGAAATTTTGTAATTGCTTTCATTATAAATCTTTTTAATATTGTCAAATCGGTTGAATTGAT
TGAACCGTCACCGTTTAAATCTGCTGCTTTTTCAGGGACATTCATTCTTTCAAGAACTTTTAAAATATATTTCTTCA
GTATCATATAATCGGTTGAGTTTATATTTCCGTCATTGTTCAAATCGCCGTAGTTGATATCCGGTATTTCACCATCA
TATTCATAAAGGTTTTCCGGAAGTTCATCCAAGGTGATTACATATTCACTGTTGTAGATAGTGTTCAAAAGTACGG
GGTCGTTGTATCTGGGACTCATAAGGAAATCACCGTACCATGGGCAGAAATACAGCCACCAGGCTTCCTCATTAAC
TATATTTTGAATATCGGGAATAACGTCATTTTCAGTCAATGCAACCATCTTTGTGTCGTTTGTGTAATTTACAAGTG
TAAGGAATAATGATGATGCGGCGCTTGTGCCCCAGGTATTGGGTGAACCTTCATATTTGTCGTATCCGATAATGTC
CACATACTCATCGCCGGGATACCATTCATAAGAATTGGCATATGTATAAAGGTTTACTTCCCATATCAAATTATGA
ATGCCGTATTTTTCGGTAAGAGTTTTATAAAGAAGTTTCCAGAGTTCCTTGTAAACTTCAGCACCTGCAGAACCCC
ACCAGAACCATGCGCCGGAGCCGTCGGTGTTGTTGTAGCCTTCAGCTTCATGGAACGGACGGAAAAGTATAGGAA
TGTTTTGCTCCTGAAGAATTAAAAGCTGCTCTGCAAGGTCTTCAATTGCCATCATCAGGTAAGCATGTTCTTTTGTT
GTTTCATCAAGGCAGTTTGCGGTATTAAAGCTGCTTGTCGGTTTGTATGTACAGTTTGTCCAATCCACCGGCTCACC
GAGTTTATAACTTGCAAAATCCCTGGGAATATTTATATGCCAGCATGCTGTTGCAATACCGCCGCGATTTTTTACCC
AGTCGATTATACGTGCCGTTGTACCGTCTTCCCATCCGTACAGAGGATTGTAGTTCATGAAATCAAAGCCTCTGAT
TGCAGGATATTTGCCTGTCTTCTCATAAATATAATCGAATTCAAGTTCATAATTGCCGTCGTTTCCGTTTCCGTAAA
TCTCCTGCTGGCCGGAAATAACATATTTTCCGTACACGCTGGTAAGGTATTTCATAAGAGCTCTTGTTTCAGGAGTT
GCATTTGGATCACACGGAGTCGGGTCAATTATATGATCGGGCATGTCAGCATGGTCAAAGTATATTTTGTCGTACA
GTATAAAGCCCCAGCTTCCGGAGGAACCTATCTCAATAGTTGCTTTACCGGCCTCAAGATAGAAGAATCCGAAACT
GTAATCAATCCATTGGCCTTTGTTTGGAATAAAATAGTTGCTGTGTGATTTTCCGTTGATGCTTATAACCTGCATTC
TGGTCTCATCTTCTTTGCCAAGATACATCCAGCATCTTGTGGAAAGCTCATACATACCGTTTTCAGGAATGGTGACT
TCCAATGTTATCGTTCCCGAGTTGGCCACCCATACGAATCCGTCGCCGGAATATCCGGGATATTGAGTTCCGTATA
CATTGGTGGTAACAACGGCACCGTTGCCAAGAGTGCAATCTTCTGCTTCAACGTCCACAGGAAGGGAATATGCAG
CATAAGTTGAAACGGGCATGACTAAAAGAACGGAAAACACCATTGCAAATGTTACCAGCAGACTCAGTGTCCTGC
CAAAAATTTTCCCCAT

*Ct*ManT (Glycoside Hydrolase 26 catalytic module from *Clostridium thermocellum* ATCC 27405)

CATGCGGATATGCCGGATCATATTATTGATCCGACCCCGTGCGATCCGAACGCGACCCCGGAAACCCGCGCGCTG
ATGAAATATCTGACCAGCGTGTATGGCAAATATGTGATTAGCGGCCAGCAGGAAATTTATGGCAACGGCAACGAT
GGCAACTATGAACTGGAATTTGATTATATTTATGAAAAAACCGGCAAATATCCGGCGATTCGCGGCTTTGATTTTA
TGAACTATAACCCGCTGTATGGCTGGGAAGATGGCACCACCGCGCGCATTATTGATTGGGTGAAAAACCGCGGCG
GCATTGCGACCGCGTGCTGGCATATTAACATTCCGCGCGATTTTGCGAGCTATAAACTGGGCGAACCGGTGGATTG
GACCAACTGCACCTATAAACCGACCAGCAGCTTTAACACCGCGAACTGCCTGGATGAAACCACCAAAGAACATGC
GTATCTGATGATGGCGATTGAAGATCTGGCGGAACAGCTGCTGATTCTGCAGGAACAGAACATTCCGATTCTGTTT
CGCCCGTTTCATGAAGCGGAAGGCTATAACAACACCGATGGCAGCGGCGCGTGGTTTTGGTGGGGCAGCGCGGGC
GCGGAAGTGTATAAAGAACTGTGGAAACTGCTGTATAAAACCCTGACCGAAAAATATGGCATTCATAACCTGATT
TGGGAAGTGAACCTGTATACCTATGCGAACAGCTATGAATGGTATCCGGGCGATGAATATGTGGATATTATTGGCT
ATGATAAATATGAAGGCAGCCCGAACACCTGGGGCACCAGCGCGGCGAGCAGCCTGTTTCTGACCCTGGTGAACT
ATACCAACGATACCAAAATGGTGGCGCTGACCGAAAACGATGTGATTCCGGATATTCAGAACATTGTGAACGAAG
AAGCGTGGTGGCTGTATTTTTGCCCGTGGTATGGCGATTTTCTGATGAGCCCGCGCTATAACGATCCGGTGCTGCT
GAACACCATTTATAACAGCGAATATGTGATTACCCTGGATGAACTG

*Ct*CBM35 (Carbohydrate Binding Module 35 from *Clostridium thermocellum* ATCC 27405)

GCGTATAGCCTGCCGGTGGATGTGGAAGCGGAAGATTGCACCCTGGGCAACGGCGCGGTGGTGACCACCAACGTG
TATGGCACCCAGTATCCGGGCTATAGCGGCGATGGCTTTGTGTGGGTGGCGAACAGCGGCACCATTACCCTGGAA
GTGACCATTCCGGAAAACGGCATGTATGAACTGAGCACCCGCTGCTGGATGTATCTGGGCAAAGAAGATGAAACC
CGCATGCAGGTGATTAGCATTAACGGCAAAAGCCATAGCAACTATTTTATTCCGAACAAAGGCCAGTGGATTGAT
TATAGCTTTGGCTTTTTTTATCTGGAAGCGGGCAAAGCGACCATTGAAATTGGCAGCCATGGCAGCTGGGGCTTTA
TTCTGTATGATAAAATTTATTTTGAT

Mol Biotechnol
DOI 10.1007/s12033-014-9807-4

RESEARCH

Recovery and Purification of Oligosaccharides from Copra Meal by Recombinant Endo-β-mannanase and Deciphering Molecular Mechanism Involved and Its Role as Potent Therapeutic Agent

Arabinda Ghosh · Anil Kumar Verma · Jaganmohan Rao Tingirikari · Rishikesh Shukla · Arun Goyal

Abstract Production of manno-oligosaccharides (MOSs) from pretreated and defatted copra meal (dFCO) hydrolysis was achieved by endo-mannanase. Structural characterization of dFCO by FT-IR and NMR exhibited resemblance with galactomannan. The time-dependent hydrolysis of dFCO by recombinant endo-β-(1 → 4)-mannanase of *Clostridium thermocellum* by TLC and HPAEC displayed the release of mannose and MOSs mannobiose and mannotriose. Purified MOSs yielded 40 % mannobiose and 18 % mannotriose confirmed by mass spectroscopy which showed mannobiose ($m/z = 365$) and mannotriose ($m/z = 527$). The homology based structural analysis of catalytic endo-mannanase (*Ct*ManT) showed the catalytic core composed of Glu181 and Glu300 acting as acid/base and Glu288 as a nucleophile during galactomannan hydrolysis. Sub-site mapping of *Ct*ManT exhibited two aglycone and four glycone sites at cleavage sites existing on either side of β-(1 → 4)-linkage of galactomannan. Isolated MOSs displayed potential prebiotic characteristics and supported higher growth of probiotic *Lactobacillus acidophilus* and *Bifidobacterium infantis* than with standard inulin. Moreover, MOSs displayed over 97 % tolerance to simulated gastric juice, intestinal fluid, and α-amylase proving its potential as a stable prebiotic over inulin. In vitro cytotoxicity assay of MOSs (500 μg/mL) on human epithelial colorectal adenocarcinoma cell line (HT-29) demonstrated 60 % decreased viability of cells after 48 h displaying anti-tumorigenic property.

Keywords Copra meal · Mass spectrometry · Catalytic core · Sub-site · Prebiotics · Anti-tumor

Introduction

Copra meal is dry coconut flesh (kernel) generally regarded as agricultural waste without any nutritional value. It is a by-product, prepared after water decantation and oil extraction. It contains a large amount of hemicellulose viz. mannan and galactomannan [1, 2]. The abundance of 65 % galactomannan in copra meal is a suitable source of MOSs [2]. The galactomannan is usually composed of repeating β-(1 → 4)-mannose units and a few α-(1 → 6)-galactose units attached to the β-(1 → 4)-mannose backbone [2]. The enzymatic hydrolysis of galactomannan by endo-mannanase releases MOSs [2]. MOSs have been shown to exhibit immune-modulatory effect as one of the components of toll-like receptor (TLR) mediated macrophage activation [3]. More reports on the exploration of MOSs as antiallergenic agent was discovered in Balb/c mice [4]. The prebiotic effect of MOSs was also reported as it beneficially affects human health by selectively stimulating growth of the intestinal microflora such as *Bifidobacterium* spp. and *Lactobacillus* spp., while in contrast limiting the

Arabinda Ghosh and Anil Kumar Verma contributed equally.

A. Ghosh · A. K. Verma · J. R. Tingirikari · R. Shukla · A. Goyal (✉)
Department of Biotechnology, Indian Institute of Technology Guwahati, Guwahati 781 039, Assam, India
e-mail: arungoyl@iitg.ernet.in

A. Ghosh
e-mail: arabinda@iitg.ernet.in

A. K. Verma
e-mail: ak.verma@iitg.ernet.in

J. R. Tingirikari
e-mail: tjmrao@iitg.ernet.in

R. Shukla
e-mail: r.shukla@iitg.ernet.in

Published online: 27 September 2014

growth of pathogenic bacteria in the colon [5]. The impaired growth of pathogenic bacteria might be due to increase production of short-chain fatty acid (SCFA) by probiotic bacteria, resulting in lower pH and inhibition of undesirable microorganisms in the colon [6].

MOSs can also directly inhibit pathogenic microorganisms besides promoting the growth of probiotic microorganisms [7]. The inhibitory effects of oligosaccharides on pathogens are due to the direct interaction with human mucosal receptors and hence blocking of the bacterial binding sites. Therefore, this process improved the elimination of these bacteria during excretion rather than their binding to mucosal receptors [7, 8]. It has been reported that the fructo-oligosaccharides have a potential role as anti-tumorigenic agents; for example, fructo-oligosaccharides isolated from apple showed induced apoptosis in colon cancer cells and cell cycle arrest in S phase [9]. Oligosaccharides from apple induced apoptosis in HT29 cells by modulating Bax, Bcl-2, and Bcl-xl protein expression. The cell cycle arrest in the S phase in HT29 cells was due to the inhibition of the formation of the Cdk2-cyclin A1 complex by decreasing Cdk2 expression. There is only one report on MOSs having anti-tumorigenic potential [10] where sulfonated MOSs from *Pichia pastoris* inhibited angiogenesis resulting in delayed tumor cell invasion and tumorigenesis [10]. Therefore, further investigations are essential to discover the potential of MOSs for delaying tumorigenesis.

In an earlier study, we reported the production of MOSs from carob galactomannan by endo-β-(1 → 4)-mannanase (*Ct*Manf) of *Clostridium thermocellum* and a family 26 glycoside hydrolase (GH26) containing a non-catalytic carbohydrate binding module CBM35 [11]. Endo-β-mannanases catalyze the random cleavage of β-(1 → 4)-mannosidic linkages within the backbones of mannan, galactomannan, glucomannan, and galactoglucomannan resulting in production of various MOSs [12]. We describe here the production of MOSs from defatted copra meal, a by-product from coconut, by the same recombinant endo-β-(1 → 4)-mannanase (*Ct*Manf). The structure of endo-β-(1 → 4)-mannanase was characterized by in silico methods, and subsite mapping for substrate binding was carried out. The molecular mechanism involved in galactomannan hydrolysis was investigated. The MOSs produced were purified and characterized, and their role as prebiotic and anti-tumorigenic agents was studied.

Materials and Methods

Chemicals, Media, and Microorganisms

Copra powder was procured from the local market in Guwahati, Assam, India. The components for MRS medium tryptone glucose yeast extract (TGY) medium and the chemicals for reducing sugar and total carbohydrate estimation and inulin were purchased from Hi-Media Pvt. Ltd, India. α-Amylase, trypsin, and guar galactomannan were obtained from Sigma Aldrich, USA. Deuterium oxide (D_2O) was procured from Merck, Darmstadt, Germany. Locust bean galactomannan and konjac glucomannan were procured from Megazyme Int., Ireland. The recombinant endo-mannanase *Ct*Manf from *C. thermocellum* ATCC 27405 was cloned in pET-28a(+) and expressed in *E. coli* cells [11]. The probiotic bacteria *Lactobacillus acidophilus* NRRL B-4495 and *B. infantis* NRRL B-41661 were procured from Agricultural Research Service Culture Collection (Peoria, USA). The enteric pathogen strain *Enterobacter aerogenes* MTCC 3030 was procured from Microbial Type Culture Collection and Gene Bank (MTCC), Institute of Microbial Technology, Chandigarh, India.

Pretreatment of Copra Meal Powder

The unprocessed copra powder (100 g) was washed three times with 500 mL distilled water to remove any suspended particles and dried in a hot air oven at 60 °C, overnight. The dried copra powder 100 g was finely ground for 10 min and sieved through 1-mm mesh. Initially, this copra powder was designated as CO. The oil content from CO was partially reduced by following the method of by Lin and Chen [9]. The partially oil-free CO was boiled three times with two volumes of distilled water for 2 h and stored at 4 °C overnight to allow the oil to solidify and be finally removed. Then the suspension was dried in oven at 60 °C for 12 h. The partially oil-free dried copra powder was designated as FCO. After solidification and subsequent removal step, any possible left over oil chunks were finally removed by solvent extraction using *n*-hexane for 24 h. In solvent extraction process, FCO was suspended in 1 L of *n*-hexane, in a beaker and mixed thoroughly and left overnight. The suspension of copra powder was filtered through Whatman No. 1 filter paper and dried in an oven and sieved through 1-mm mesh for further study. The completely oil-free (defatted) copra meal was designated as dFCO. The structural carbohydrates like hemicellulose and ash were estimated by standardized methods of NREL, USA [13]. 0.3 g of dry substrate (dFCO) was mixed with 3 mL of 27 N H_2SO_4 and incubated at 30 °C for 1 h. Then 54 mL of distilled water was added to normalize H_2SO_4 concentration to 1.5 N. The sample was autoclaved at 121 °C and 15 psi for 1 h. The substrate was cooled to 25 °C, and the treated biomass was filtered using a vacuum filtration unit. The residue was weighed which gave ash content. The filtrate was collected and pH was neutralized by addition of 1 M $CaCO_3$. The protein extraction and total protein content were determined by the method described elsewhere

[14, 15]. The component extracted during the preprocessing steps of copra meal was recognized as lipid after hemicellulase, ash, and protein estimation.

Structural Analysis of Copra Meal Powder

FESEM Analysis of Untreated and Pretreated dFCO

Thirty microliter of each untreated CO or pretreated dFCO (0.04 g/L) was placed over a glass slide, subsequently dried and coated with gold film using a SC7620 "Mini", Polaron Sputter Coater (Quorum Technologies, Newhaven, England) and analyzed under the field emission scanning electron microscope (FESEM-Carl Zeiss, SIGMA VP instrument). The images were acquired for both CO and dFCO.

FT-IR Spectroscopy Analysis of Untreated CO and Pretreated dFCO

Fourier transform infrared (FT-IR) spectroscopy (Spectrum Two, Perkin Elmer, USA) was used for analysis of available functional groups in untreated CO and pretreated dFCO, respectively. One mg each of dried CO and dFCO (45 °C for 18 h) was ground with 3 mg potassium bromide powder (Sigma, USA) in 1:3 ratio and made into a pellet. Three samples of each were prepared to increase the reproducibility of the analysis, and 30 scans were recorded per sample at a resolution of 4 and 0.1/cm data interval.

^{1}H and ^{13}C NMR of Pretreated dFCO

Nuclear magnetic resonance (NMR) of dFCO was performed using a spectrometer (Varian AS400, Agilent Technologies, Palo Alto, CA, USA). The soluble fractions of dFCO were collected after pretreatment were dissolved in 0.5 mL deuterium oxide D_2O (Merck, Germany). The solution was lyophilized and 30 and 50 mg of dFCO dissolved in 0.5 mL of D_2O for ^{1}H NMR analysis ^{13}C NMR, respectively. Tetramethyl silane (TMS) was used as an internal reference.

Production and Purification of Recombinant Endo-mannanase (*Ct*Manf)

In our earlier study, we cloned, hyper-expressed, and biochemically characterized family 26 glycoside hydrolase endo-mannanase (*Ct*Manf) from *C. thermocellum* ATCC 27405 [11]. The production and purification of recombinant endo-mannanase (*Ct*Manf) were carried out by following the methods described elsewhere [11].

Analysis of Enzyme Hydrolyzed Products of dFCO by TLC and HPAEC

The enzyme activity of *Ct*Manf was determined against 2.0 % (w/v) unprocessed and pretreated copra meal powder (dFCO) dissolved in 50 mM sodium phosphate buffer pH 6.9. One hundred microliter of reaction mixture contained 2.0 % (w/v) substrate and 10 µL of enzyme (*Ct*Manf, 0.16 mg/mL), and the reaction was incubated at 60 °C for 10 min. The resulting reducing sugar concentration was measured at 500 nm using spectrophotometer (Varian, Cary 100 Bio) as described earlier [16, 17]. All these assays were carried out in triplicates.

Qualitative analysis of hydrolyzed products of dFCO was performed by thin-layer chromatography (TLC) on silica gel-coated aluminum foil (TLC Silica gel 60 F_{254} 20 × 20 cm, Merck) to identify the released sugars. Hydrolysis of dFCO by recombinant endo-mannanase (*Ct*Manf) was carried out under optimum conditions as described previously [11] at different time intervals of 1, 4, 8, 16, and 24 h. After each incubation period, the reaction mixtures were boiled for 2 min to stop enzymatic hydrolysis and then centrifuged at 13,000×*g* for 5 min. Then 0.2 µL of reaction mixture and standard solutions of mannose, mannobiose, and mannotriose (1.0 mg/mL) were loaded on the TLC plate and kept in the developing chamber saturated with the developing solution (mobile phase) consisting of acetic acid–*n*-propanol–water–acetonitrile (4:10:11:14). At the end of the run, migrated sugar spots were investigated by immersing the TLC plate in a visualizing solution (sulfuric acid/methanol 5:95, v/v; α-naphthol 5.0 %, w/v) and followed by drying at 80 °C for 20 min. The migrated reaction products (sugars) appeared as spots on the TLC plate.

The samples for high-pressure anion exchange chromatography (HPAEC) prepared from the reaction mixtures after definite time intervals (as mentioned in TLC) were treated with two volume (200 µL) of absolute ethanol to precipitate the remaining non-reacted polysaccharides and then centrifuged at 13,000×*g* for 10 min at 4 °C. The supernatant containing the liberated sugar was transferred to another micro-centrifuge tube, and the ethanol was removed by evaporation. The supernatant (50 µL) was diluted to 500 µL by adding ultra-pure (MilliQ, Millipore, USA) water and filtered through a syringe filter using 0.2 µm membrane. The liberated sugars were analyzed using ion exchange chromatography system (Dionex, ICS-3000). From the filtered 500, 25 µL of sample (liberated sugars) was run on CARBOPACK™ PA-200 column (150 × 3 mm, Dionex), attached with CARBOPACK™ PA200 guard column (30 × 3 mm, Dionex) with borate and amino trap columns which removed impurities and provided high resolution. The instrument (Dionex, ICS-3000)

was kept at constant temperature of 30 °C during the analysis and the flow rate was maintained at 0.3 mL/min. The liberated sugars were eluted by 300 mM sodium hydroxide using pulsed amperometric detector (PAD). Quantitative analysis of enzyme catalyzed hydrolysis products was determined from the peak intensity of the released products as described earlier [11].

Mechanism of Oligosaccharide Synthesis by Endo-β-mannanase

Two approaches were followed to decipher the mechanism of oligosaccharide synthesis from copra meal, first by homology modeling of endo-mannanase since no X-ray crystal structure is available for family 26 glycoside hydrolase (Man26B) catalytic segment (*Ct*ManT) of endo-β-(1 → 4)-mannanase from *C. thermocellum* ATCC 27405 and second by structure superimposition of modeled *Ct*ManT with substrate bound template to understand the mechanism of substrate binding, catalysis, and sub-site mapping. A three dimensional model structure was deduced using Modeller 9v8 by homology modeling based on closest structural homologs having 36 % maximum sequence identity from *Podospora anserine* (pdb id: 3ZM8), *Cellvibrio japonicas* (pdb id: 2VX4) and *Cellulomonas fimi* (pdb id: 2BVT) with r.m.s.d. of 1.2, 2.3, and 2.6 Å, respectively, over the 300 amino acids of C^{α} main chain. The loop regions of best model were refined selectively by using the loop model class of modeler and after each cycle of loop refinement discrete optimized protein energy (DOPE) score was generated [18]. The best model having reasonable DOPE and MOLPDF scores was chosen for further refinement. Energy minimization of modeled *Ct*ManT was performed in YASARA energy minimization server (www.YASARA.org/minimizationserver), where a new and partly knowledge-based all atom force field derived from Amber was used to run the molecular dynamics simulations of protein molecules in explicit solvent [19]. The quality of final modeled *Ct*ManT was validated using various parameters available at NIH structural analysis and validation server (http://nihserver.mbi.ucla.edu/SAVES/) [20], as well as PROSA web server [21]. A molecular docking study was carried out using Autodock 4.2.1 to understand the binding site of the ligands in the protein and sub-site mapping. In Autodock 4.2.1, novel and robust docking methodology of inbuilt Lamarckian Genetic Algorithm (LGA) and empirical free energy scoring function were used to reproduce the docking results for ligands [22]. All the ligand viz. mannobiose, mannotriose, mannotetrose, mannopentose, mannohexose, and galactomannan were retrieved either from PDB files or PubChem (https://pubchem.ncbi.nlm.nih.gov). Input files of ligands were prepared by adding hydrogen atoms and assigning Gasteiger–Marsili charges followed by deleting all non-polar hydrogens and merging their charges on the carbon atoms. Grid maps were assigned to each atom type present in the protein as well as ligand molecule accompanied by electrostatic and desolvation maps using the AutoGrid [23]. Grid boxes were set to be 66, 60, and 58 (x, y, and z) points with 0.375 Å and the grid spacing covering the entire active site pocket of modeled *Ct*ManT. Docking simulations were performed with an initial population size of 300 and 30 independent LGA runs were carried out. Best docked conformations from the largest cluster, having a minimum lowest free energy of binding (ΔG), were saved. Results were analyzed using PyMOL for possible polar and hydrophobic interaction.

Purification of Manno-Oligosaccharides from Enzymatic Hydrolyzed Products of dFCO

Purification of MOSs from enzymatic hydrolyzed products of dFCO was carried out at 25 °C by using FPLC system (AKTA Prime, GE Healthcare, USA). The components of hydrolyzed products of dFCO were separated and isolated using polyacrylamide bead matrix Bio-Gel P2 (45–90 μm) packet in 50 mL Econo-Pack column (Bio-Gel, USA). Two milliliters of crude sample of enzymatic hydrolyzed product of dFCO was injected in the 2 mL sample loop of the FPLC system and the oligosaccharide samples were eluted with isocratic elution by deionized water at 0.2 mL/min flow rate. Sixty fractions of 1 mL each were collected using a fraction collector. The total carbohydrate content of fractions was estimated by phenol sulfuric acid method [24] and qualitatively analyzed by TLC as reported earlier [11]. The fractions were analyzed using a mass spectrophotometer (Agilent 6550 iFunnel Q-TOF LC/MS system, Agilent 1200 series, USA). Each fraction was diluted to 5 ppm in methanol and filtered through a 0.45 μm membrane. ESI–MS were carried out for specific fractions in positive ionization mode and analyzed by TOF detector.

In Vitro Analysis of Mixed Manno-Oligosaccharides as Prebiotics

Growth Profile of Probiotic Bacteria in the Presence of Manno-Oligosaccharides

The growth of probiotic bacteria, *B. infantis* NRRL B-41661 and *L. acidophilus* NRRL B-4495 as well as non-probiotic enteric bacteria *E. coli* DH5α and *E. aerogenes* MTCC 3030 was monitored in the presence of mixed MOSs and inulin as standard prebiotic. The MOSs, mannobiose, and mannotriose were pooled after purification and subsequently freeze-dried. The growth of probiotic

bacteria was evaluated in basal MRS medium (pH-6.4) supplemented with 0.5 g/L cysteine as described earlier by Hongpattarakere [6]. The overnight grown probiotic cultures of *Bifidobacterium* ($\sim 1 \times 10^7$ cells/mL) and *Lactobacillus* ($\sim 12 \times 10^7$ cells/mL) cultures were separately inoculated to 100 mL MRS basal medium containing filter sterilized 1 % (w/v) glucose (as positive control), mixed-oligosaccharides or inulin and incubated under anaerobic conditions, at 37 °C for 24 h. The growth of non-probiotic enteric bacteria was estimated in TGY medium (pH-7.0) containing 5 g/L of tryptone, 5 g/L of yeast extract, 1 g/L di-potassium hydrogen phosphate (K_2HPO_4), and 1 g/L glucose. The non-probiotic *E. coli* and *E. aerogenes* were separately inoculated in TGY medium supplemented with filter sterilized 1 % (w/v) of mixed-oligosaccharides or inulin in place of glucose and also incubated at 37 °C for 48 h under anaerobic condition. The growth of the bacterial culture was determined as cells/mL, by counting colonies that appeared after spreading 100 µL of culture following 12 and 24 h of incubation on an MRS agar plate (20 g/L agar) (in case of probiotic bacteria) and a TGY agar plate (20 g/L) (in case of non-probiotic bacteria) and the plates were incubated at 37 °C for 18 h.

Effect of Artificial Human Gastric Juice Hydrolysis on Manno-Oligosaccharides

The prebiotic potential of mixed oligosaccharide was examined and compared with inulin, a commercial prebiotic as reference. The dried sample of mixed MOSs was dissolved in autoclaved MilliQ water to produce 1.0 % (w/v) solution. Artificial human gastric juice was prepared by using phosphate buffer saline (PBS) containing (in g/L): NaCl, 8; KCl, 0.2; $Na_2HPO_4 \cdot 2H_2O$, 8.25; $NaHPO_4$, 14.35; $CaCl_2 \cdot 2H_2O$, 0.1; and $MgCl_2 \cdot 6H_2O$, 0.18. The pH of the buffer was adjusted to 1, 2, 3, 4, and 5 using 5 M HCl (Korakli et al. [25]). Artificial gastric juice (6 mL) at each pH was added to the sample solution of 1 % (w/v) MOSs, and the reaction mixture was incubated in a water bath at a controlled temperature of 37 °C for 6 h. Samples (1 mL) were taken periodically at 0, 1, 2, 4, 5, and 6 h. Reducing sugar content of the samples was determined by the method as described earlier by [16, 17], and total sugar was determined by phenol–sulfuric acid method [24]. Percentage hydrolysis of MOSs was calculated based on reducing sugar liberated and total sugar content of the MOSs [25]:

$$\text{Hydrolysis}(\%) = \frac{\text{Reducing sugar released} \times 100}{\text{Total sugar content} - \text{initial sugar content}}.$$

Effect of Artificial Human Intestinal Fluid on Mixed Manno-Oligosaccharides

The artificial human intestinal fluid was prepared in PBS with 0.5 % (w/v) bile salt (Sigma Aldrich, USA) and 1,000 U/mL of trypsin solution (Sigma Aldrich, USA). The pH of the buffer was adjusted to 8.0 with 2 N NaOH [26]. The mixed MOSs or inulin was dissolved in simulated intestinal fluid to produce final concentration of 1.0 % (w/v) mixed MOSs and incubated at for 37 °C for 6 h. The reaction mixture (500 µL) was collected at regular time intervals of 0, 1, 2, 3, 4, 5, and 6 h to determine the reducing and total sugar content for calculating the percentage hydrolysis as described in the previous section.

The Effect of α-Amylase on Mixed Manno-Oligosaccharides

Effect of α-amylase on mixed MOSs was examined as described earlier [27]. α-Amylase (100 U/mL) was prepared in PBS, and the pH of the buffer was adjusted to 5, 6, 7, or 8. To each of these solutions 1.0 % (w/v) of mixed MOSs or inulin was added and the reactions were set in duplicate and incubated at 37 °C for 6 h. The reaction mixture (500 µL) was collected at regular time intervals of at 0, 1, 2, 3, 4, 5, and 6 h to determine the reducing and total sugar content for calculating the percentage hydrolysis as described in previous section.

In Vitro Anti-tumorigenic Activity of Mixed Manno-Oligosaccharides

Mixed MOSs from copra meal was used for in vitro anticancer activity assay. The effects of MOSs on human colon cancer cell line (HT29) were studied using the colorimetric 3-(4,5-dimethylthiazolyl-2)-2,5-diphenyltetrazolium bromide (MTT) assay as described earlier [28]. HT29 cell lines were seeded in 96-well plates at density approximately 1.2×10^4 cells/well and incubated at 37 °C for 16 h in 5 % CO_2 atmosphere for surface attachment. After incubation, the media were removed and the MOSs at different concentrations were added. A concentration range (1–500 µg/mL) of mixed MOSs was used. The media without oligosaccharides were used as negative control. The plates were again incubated at 37 °C in 5 % CO_2 atmosphere for 48 h. After 48 h the media were removed and 100 µL MTT (500 µg/mL) was added to each well and further incubated at 37 °C for further 4 h. The supernatant was removed and 100 µL dimethylsulfoxide (DMSO) was added to each well. The absorbance at 570 nm was

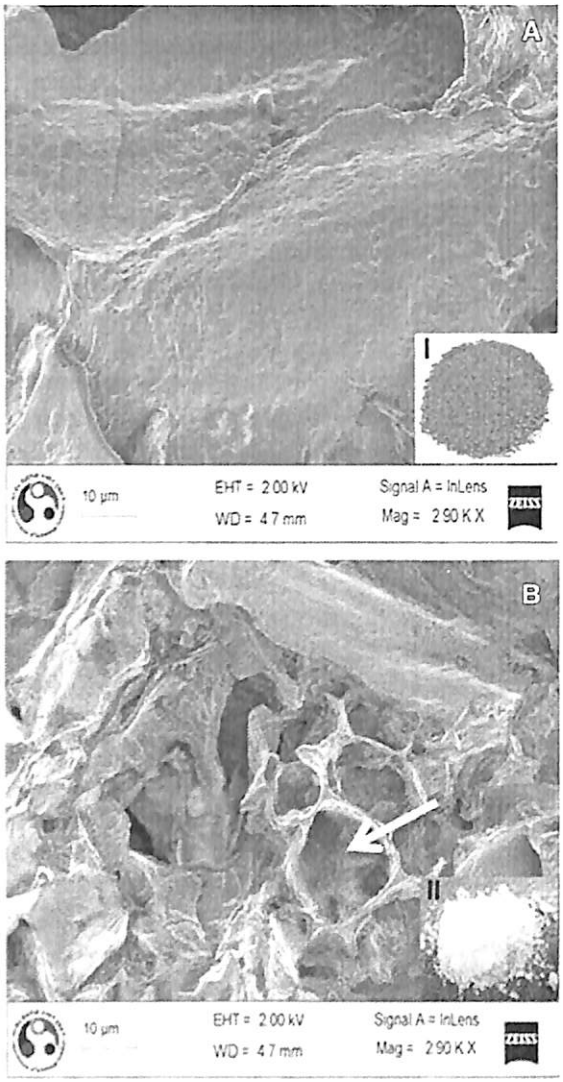

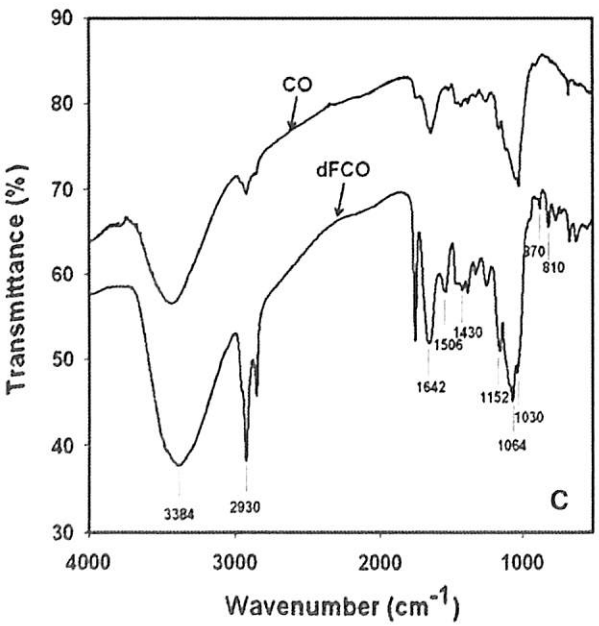

◀**Fig. 1** FESEM analysis of **a** untreated and **b** pretreated of dried coconut (copra meal). Topological changes associated with pretreatment are clearly detectable (*arrow*). *Inset I* and *II* represent the dried copra powder before and after pretreatment, respectively. **c** FT-IR analysis of untreated copra meal (CO) and pretreated defatted copra meal (dFCO)

Table 1 FT-IR analysis of pretreated copra meal and assignment of functional groups

Name of characteristic group	Wavenumber (cm^{-1})
OH	3,384
C–H methyl and methylene groups	2,930
Aromatic ring stretch of lignin	1,642
Aromatic skeletal vibration plus C=O stretch of lignin	1,506
C–H (crystalline cellulose)	1,430
Anti-symmetric bridge stretching of C–O–C groups in galactomannan	1,152
CH_2 group of mannan	1,064
C–O stretch vibration of glucomannan	1033, 870, 810

monitored on a 96-well microplate reader (Tecan, Infinite 200 Pro).

Results and Discussion

Structural Analysis of Carbohydrate of Defatted Copra Meal (dFCO)

The carbohydrate analysis of dFCO after pretreatment exhibited (w/v) 74 % hemicellulose, 23.8 % protein and in addition to that 2 % ash and 0.2 % lipid which were comparable with the previous report [9]. The FESEM images of pretreated copra meal (dFCO) showed significantly more porous and destabilized structure of the copra meal complex as compared to the untreated copra meal (CO) (Fig. 1a, b). The FT-IR spectral analysis of both untreated and pretreated copra meal samples (dFCO) is illustrated in Fig. 1c. The assignments of functional groups recorded by FT-IR are listed in Table 1. The absorption at 3,384 cm^{-1} was attributed to the hydroxyl stretching vibrations, and the band at 2,930 cm^{-1} was due to the C–H stretching of methyl groups. Similar identification of hydroxyl stretching vibrations and C–H stretching of methyl group was reported previously [29]. The small peak shifts and more pronounced peaks at 3,384 and 2,930 cm^{-1} were observed in case of dFCO while comparing with non-treated copra meal. The band at 1,642 cm^{-1} was probably due to the bending mode of water

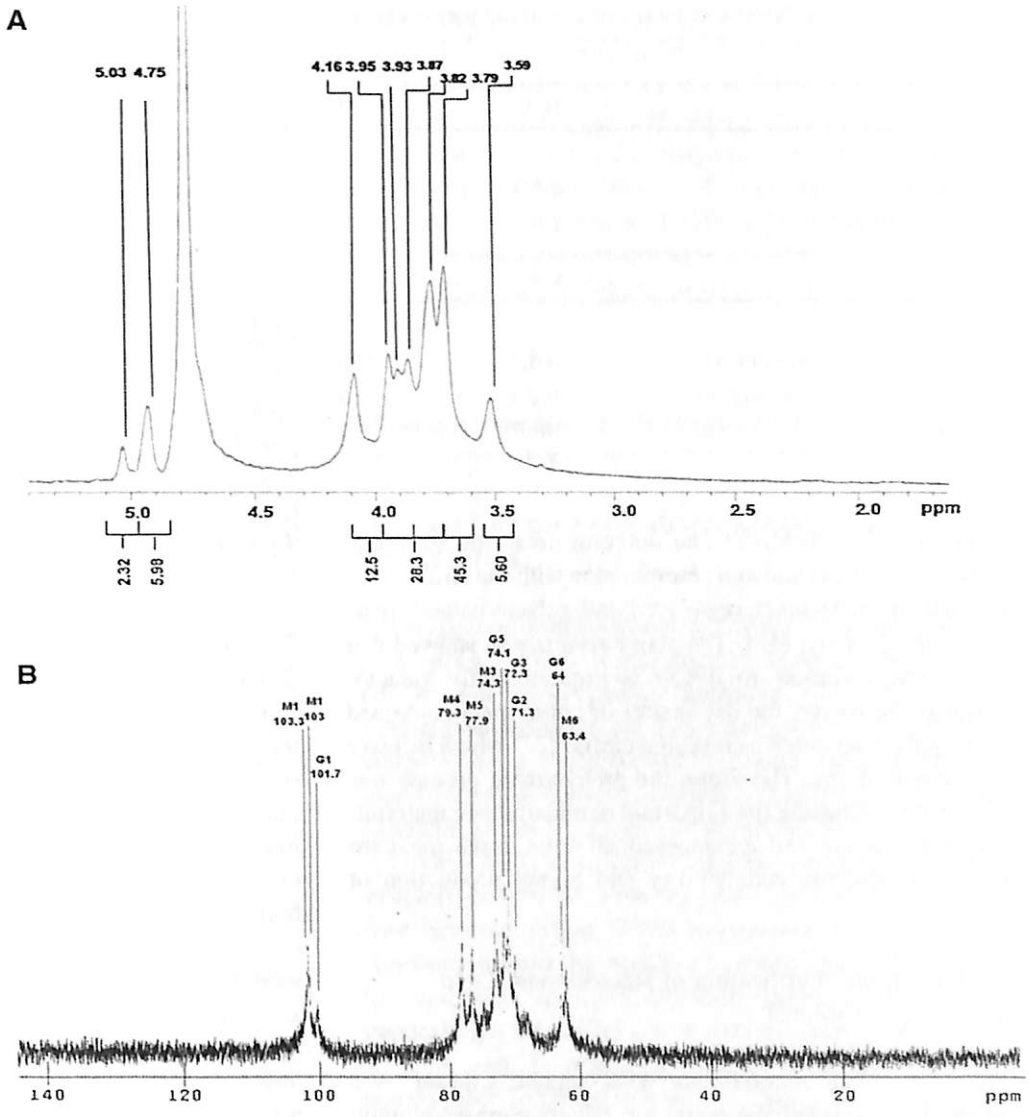

Fig. 2 NMR spectra of dFCO polysaccharide **a** ^{1}H and **b** ^{13}C. *M1/G1*, *M2/G2*, *M3/G3*, *M4/G4*, *M5/G5*, and *M6/G6* represent C1, C2, C3, C4, C5 and C6, respectively, of D-mannose/D-galactose

since the hemicelluloses have a strong affinity for water as these macromolecules in the solid state may have disordered structures that could be easily hydrated as also reported elsewhere [30]. The band at 1,506 cm^{-1} was due to the aromatic skeletal vibration plus C=C stretch of lignin and the band at 1,430 cm^{-1} was due to C–H deformation of crystalline cellulose as also reported earlier [30]. The higher transmittance at 1,152 cm^{-1} appeared due to anti-symmetric bridge stretching of C–O–C groups in galactomannan similar to the earlier reports [30, 31]. In addition to a glucose band at 1,034 cm^{-1} of glucomannan, an extra band at 1,064 cm^{-1} appeared due to the mannose units similarly reported earlier [32]. In the anomeric region (950–700 cm^{-1}), pretreated dFCO exhibited the characteristic transmittance at 870 and 810 cm^{-1} suggesting the existence of mannose as also reported elsewhere [33, 34]. The absorption peak at 870 cm^{-1} represented the β-glycosidic bond in dFCO [33].

Analysis of the positions and fine structure of correlation peaks in the ^{1}H NMR and ^{13}C spectrum of dFCO is shown in Fig. 2a, b, respectively. The two signals at δH 4.75 and 5.03 ppm are observed in the region for resonance of anomeric protons in the ^{1}H NMR are attributed to the presence of a H-1 proton of the β-D-mannopyranose ring [(→ 4)-β-D-man*p*-(1 →)] and branched α-D-galactopyranose ring [α-D-gal*p*-(1 → 6)], respectively (Table 2). Other δH shifts were attributable to H-2, H-3, H-4, H-5, and H-6 peaks from D-man*p* at 4.16, 3.82, 3.87, 3.59, and 3.95 ppm, whereas H-2, H-3, H-4, H-5, and H-6 peaks arose from D-gal*p* at 3.87, 3.95, 3.93, and 3.79 ppm, respectively (Table 2). Well-resolved ^{13}C NMR peaks are observed in Fig. 2b, where they corresponded to anomeric carbon of linear β-D-mannopyranose at 103.0 ppm, branched at the 6-HO position of β-D-mannopyranose at 103.3 ppm and branched α-D-galactopyranose at 101.7 ppm. Other chemical shifts are

Table 2 ^{1}H and ^{13}C NMR Chemical shifts of dFCO polysaccharide

Unit						
	H-1	H-2	H-3	H-4	H-5	H-6
^{1}H NMR						
(→ 4)-β-D-man*p*-(1 →)	4.75	4.16	3.82	3.87	3.59	3.95
α-D-gal*p*-(1 → 6)	5.03	3.87	3.95	3.93	3.90	3.79
	C-1	C-2	C-3	C-4	C-5	C-6
^{13}C NMR						
Linear (→4)-β-D-man*p*-(1→)	103.0	72.9	72.3	72.2	74.1	64.0
Branch (→4)-β-D-man*p*-(1→)	103.3	72.9	74.3	79.3	77.9	64.4
α-D-gal*p*-(1 → 6)	101.7	71.3	74.3	79.4	76.3	63.4

summarized in Table 2. The outcome from the structural analysis of dFCO showed resemblance with the structure of mannan from *Delonix regia* [35] and galactomannan from *Gleditsia delavayi* [36]. The above results also showed that 74 % hemicellulose in dFCO is predominantly galactomannan. However, the dry matter of copra meal contained 61 % galactomannan as reported earlier [37] which is lower than our findings. Therefore, the pretreatment process was efficient in releasing the important hemicellulosic materials such as mannan and galactomannan from copra meal for enhanced enzyme accessibility and higher production of MOSs.

Production and Purification of Recombinant Endo-mannanase (*Ct*Manf)

The clostridial recombinant His_6-tagged *Ct*Manf was purified by immobilized metal ion affinity chromatography (IMAC) from the cell-free extracts to homogeneity. The SDS–PAGE analysis of purified *Ct*Manf displayed molecular size 53 kDa [11]. The recombinant protein was expressed as a soluble protein.

Analysis of Enzymatic Hydrolysis of Defatted Copra Meal by TLC and HPAEC

Enzyme Assay

The manno-configured substrate specificity of *Ct*Manf was determined in our earlier report [11]. The enzyme activity of *Ct*Manf against 2.0 % (w/v) non-processed copra meal (CO) and pretreated dFCO displayed 13.25 and 162.5 U/mg, respectively. Therefore, it can be suggested from our study that the recombinant endo-mannanase was able to access the preprocessed dFCO and helped in a subsequent release of higher reducing sugars.

Analysis of *Ct*Manf Hydrolyzed Products of dFCO by TLC

Time-dependent hydrolysis of dFCO by recombinant endo-β-mannanase (*Ct*Manf) using TLC is displayed in Fig. 3a. The hydrolysis after 10 min and 1 h of reaction displayed the release of mannose (dp1) and mannobiose (dp2) (Fig. 3a). Standards of mono- and oligosaccharides (M1: mannose, M2: mannobiose, and M3: mannotriose) were run in parallel to compare the released sugars (Fig. 3a). Till 4 h of incubation with *Ct*Manf, dFCO was not completely hydrolyzed, but during 8–16 h large amounts of mannobiose and comparable amounts of mannose and mannotriose were released (Fig. 3a). Complete hydrolysis of dFCO was achieved at 24 h of incubation where the maximum amount of mannobiose, mannose, and mannotriose were produced; however, two other higher oligosaccharides (dp4 and dp5) were also observed at 16 and 24 h of hydrolysis (Fig. 3a). Therefore, the release of mannobiose and mannotriose was attributed to the endo-mannanse activity of *Ct*Manf enabling the cleavage of the β-(1 → 4) bond between the mannose residues of dFCO. Mass spectrometry analysis of dFCO hydrolyzed products by *Ct*Manf was carried out in positive ionization mode (Fig. 3b). The hydrolyzed fragments appeared as mannose $[M+Na]^+$ (*m/z* 193, dp1), mannobiose $[2M+Na]^+$ (*m/z* 365, dp2), and mannotriose $[3M+Na]^+$ (*m/z* 527, dp3).

HPAEC–PAD Analysis of Hydrolyzed Products of dFCO by Enzymatic Hydrolysis

Qualitative and quantitative analyses of *Ct*Manf hydrolyzed products of dFCO were also monitored by HPAEC–PAD. Time-dependent hydrolysis of carob galactomannan by *Ct*Manf is displayed in Fig. 4. The peak intensities of standards are displayed in Fig. 4a. After 1 h of *Ct*Manf treatment of carob galactomannan, the prominent peaks of

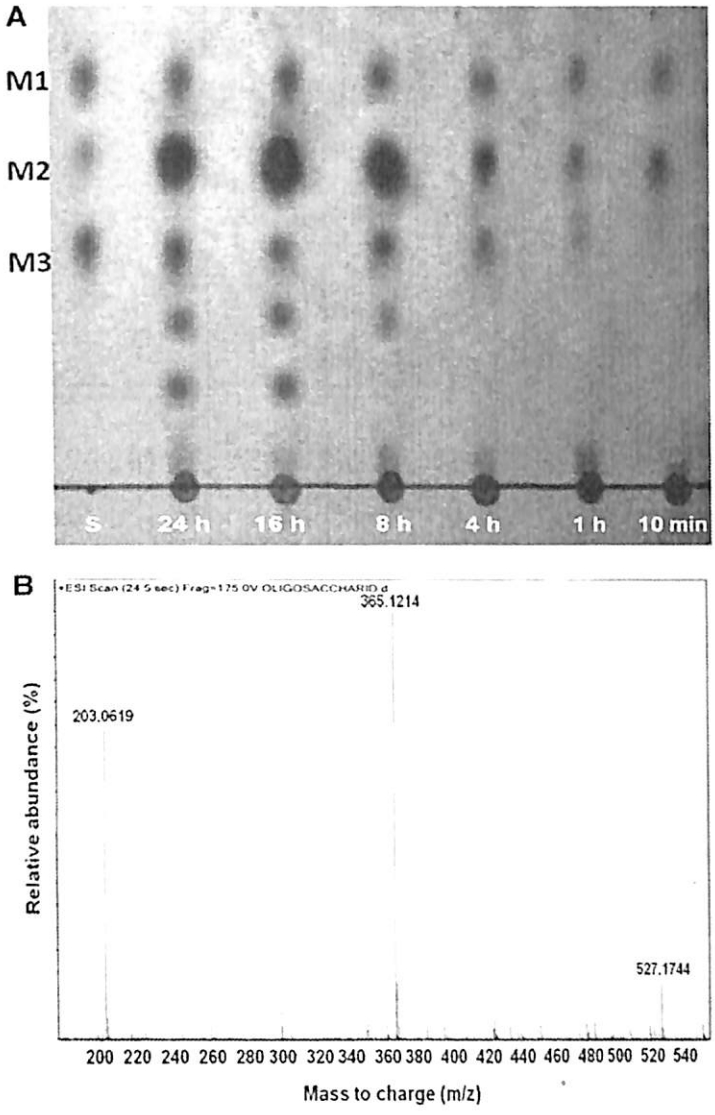

Fig. 3 Time-dependent hydrolysis of copra meal by endo-β-mannanase. **a** TLC analysis displayed the release of mannose (dp1), mannobiose (dp2), and mannotriose (dp3). *M1* Mannose, *M2* Mannobiose, and *M3* Mannotriose are standards used. **b** ESI–MS–TOF of hydrolysis products of copra meal by endo-β-mannanase isolated after 24 h. In positive ionization mode, the peak displayed mannose (*m/z* 203.0619), mannobiose (*m/z* 365.1214), and mannotriose (*m/z* 527.1744)

mannose at 3.4 min, mannobiose at 4.06 min, and mannotriose at 4.96 min were observed with concentrations 0.88, 1.09, and 0.60 mg/mL, respectively (Fig. 4b). The mannobiose peak was more prominent than mannotriose after 8 h of carob galactomannan hydrolysis while mannose intensity increased continuously (Fig. 4c). *Ct*Manf was able to hydrolyze carob galactomannan to a greater extent after 8 h, and the products obtained and the complete hydrolysis of carob galactomannan by *Ct*Manf were observed after 24 h of enzymatic reaction where mannose, mannobiose, and mannotriose concentrations of 2.8, 3.4 , and 1.2 mg/mL, respectively, were obtained (Fig. 4d). All the concentrations were determined from the regression equation of mannose, mannobiose, and mannotriose standard curves. Therefore, *Ct*Manf quite effectively hydrolyzed 10 mg/mL (1.0 %, w/v) carob galactomannan and gave maximum release after 24 h yielding 28 % mannose, 34 % mannobiose, and 12 % mannotriose. The overall results convincingly described the performance of *Ct*Manf in releasing of MOSs from dFCO which can be taken for higher scale production.

Molecular Mechanism of Oligosaccharides Formation by Endo-β-mannanase

Structure Prediction of Endo-β-mannanase Catalytic Core (*Ct*ManT)

Three-dimensional structure of *Ct*ManT showed the common $(\beta/\alpha)_8$ "TIM" barrel folding motif characteristic of GH-A clan of glycoside hydrolase families [18, 19]. *Ct*ManT comprised eight loops assigned as loop1 (Ile44-Glu54), loop2 (Met76-Gly87), loop3 (His108-Asn138), loop4 (Pro178-Trp197), loop5 (Ile226-Try232), loop6 (Asp253-Ala266), loop7 (Lys286-Ile292), and loop8 (Lys306-Tyr321). *Ct*ManT clearly showed remarkable structure differences from the other structurally characterized bacterial origin GH26 mannanase. It showed more similarity toward the fungal mannanase in terms of structure and folds. In depth, structure study showed the loops connecting a side of the active site of binding pocket (loops 2, 3, 4, and 5) relatively longer (especially loop3) as compared to loops present on the other side (loops 1, 8, 7, and 6) of the binding cavity. These prolonged loops certainly provide flexibility and subtleties to the active site binding pocket which might influence the function and help the enzyme to accommodate polymeric substrate of variable degrees of polymerization and length. To identify the key active site residues, *Ct*ManT was superimposed with the closely related structure of *Pa*Man26A (PDB id 3ZM8). The results showed that the active site residue Glu181 of *Ct*ManT acts as acid/base and corresponds to Glu300 of *Pa*Man26A. The residue Glu288 of *Ct*ManT matched with Glu390 of *Pa*Man26A which acts as a nucleophile (Fig. 5a). Catalytic residue Glu181 situated at the center core in the middle of loop4, whereas Glu288 was positioned in the catalytic core, loop7; both the residues were 5.8 Å apart (Fig. 5b) and are in the agreement of the retention type of mechanism as reported for mannanase of family GH26 [38]. The above results support the contention that the mechanism of *Ct*ManT reaction involves the retention of anomeric configuration through a covalent glycosyl intermediate (Fig. 5c).

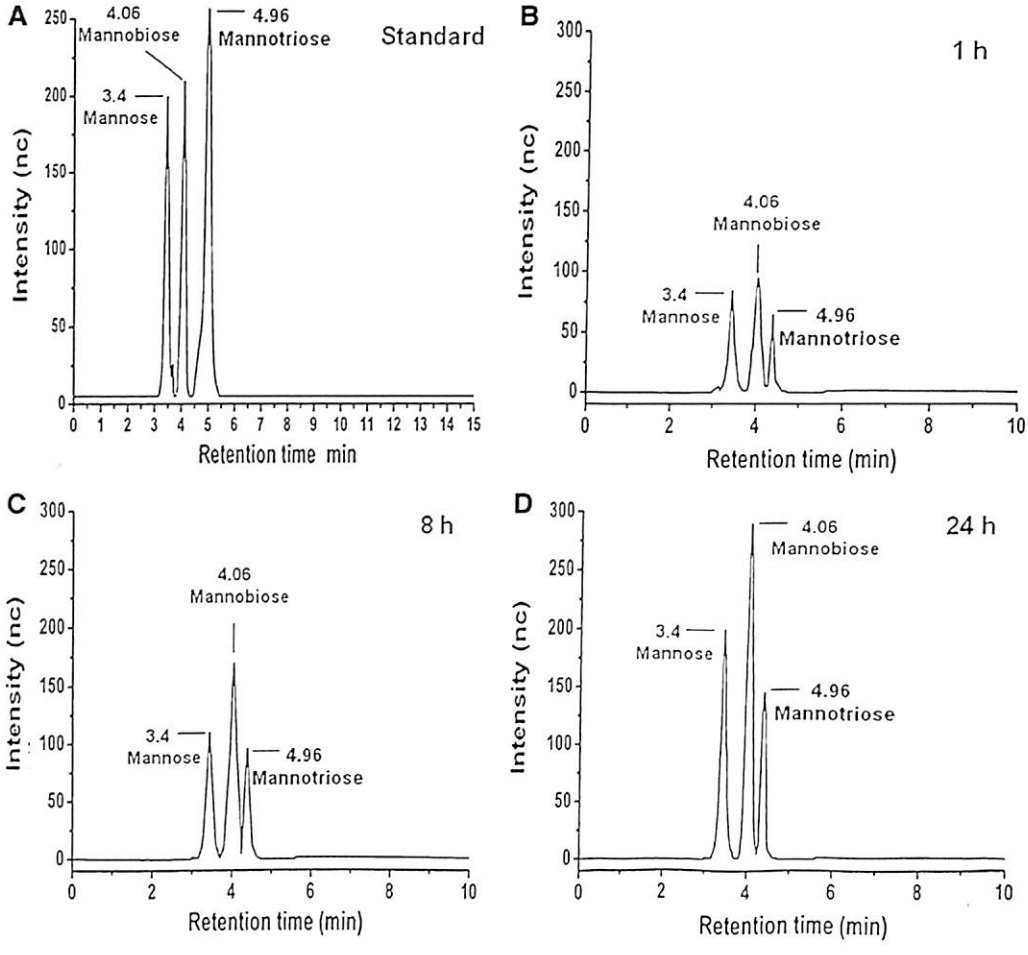

Fig. 4 HPAEC–PAD analysis of hydrolysis products of dFCO by *Ct*Manf. **a** Elution patterns of standards used, mannose (3.4 min), mannobiose (4.06 min), and mannotriose (4.96 min). **b–d** elution patterns of mannose, mannobiose, and mannotriose from dFCO (1 %, w/v) after incubation from 1 to 24 h with *Ct*Manf

Docking Analysis and Sub-site Mapping of *Ct*ManT Involved in Oligosaccharide Synthesis

Molecular docking study of *Ct*ManT with different manno-configured ligands (from mannobiose to mannohexose as well as galactomannan) was carried out in order to understand the role of aromatic and hydrophobic residues present in the ligand binding site. The results of docking are summarized in Table 3. The results showed free energy of binding increased ($-\Delta G$) concomitantly with the increased size of ligands (up to mannopentose from mannobiose) and that represented the stable nature of substrate binding sub-sites' presence across the active site region of *Ct*ManT. The ability to accommodate larger ligand molecules in the active site of *Ct*ManT is probably due to the long loops enclosing the active site that provided the depth of the cavity. The solvent-accessible surface view of *Ct*ManT complex with ligand mannopentose showed broad saddle-shaped, open active center core (Fig. 5d). This allows interaction with internal region of sugar rings of oligosaccharides (endo-acting), reported also for other endo-β-mannanases from family 26 GH [39, 40]. In contrast, *Bc*Man displayed shallow-disk shaped binding pocket [41]. *Ct*ManT in association with ligand mannopentose displayed the significant polar and hydrophobic interactions with active site residues along with

Fig. 5 **a** Superimposed view of *Ct*ManT (*gray*) over *Pa*Man26A of *P. anserine*, pdb id: 3ZM8 (*black*) proteins showing the similarity and differences in the structure and folds along with the position of active site residues at the catalytic core. **b** Enlarged view of overlayed catalytic residues (stick view) Glu181 (catalytic acid/base) corresponding to Glu300 and Glu288 (catalytic nucleophile) to Glu390 of *Pa*Man26A. **c** Schematic 2D depiction of proposed catalytic mechanism for *Ct*ManT which follows net retention of anomeric configuration through covalent glycosyl-enzyme intermediate. **d** Top view of solvent-accessible surface of the substrate binding region of *Ct*ManT showing broad saddle-shaped, open active site cavity along with ligand mannopentose. **e** Docked view of ligand mannopentose interacting with active site amino acid residues of *Ct*ManT. Residues present at the active site of *Ct*ManT making hydrophobic interaction (surface view) with mannopentaose and residues involved in hydrogen bonding are represented in magenta color. **f** Superimposed structures of *Ct*ManT with complex of *Cj*Man26C (pdb id: 2VX6) with galactomannan are used for sub-site mapping. Ligand (in stick view) occupied +2 to −2 sub-sites of *Ct*ManT and *Cj*Man26C. The key conserved residues of *Ct*ManT (Tyr255, Trp311, Glu288, His108, His180, Glu181, Phe195, and Trp194) and *Cj*Man26C (Trp373, Tyr297, Glu338, His156, His220, Phe227, Glu221, and Trp226) forming the sub-site and showing significant interaction with galactomannan. **g** Schematic presentation of amino acid residues of *Ct*ManT involved in formation of substrate binding sub-sites ▶

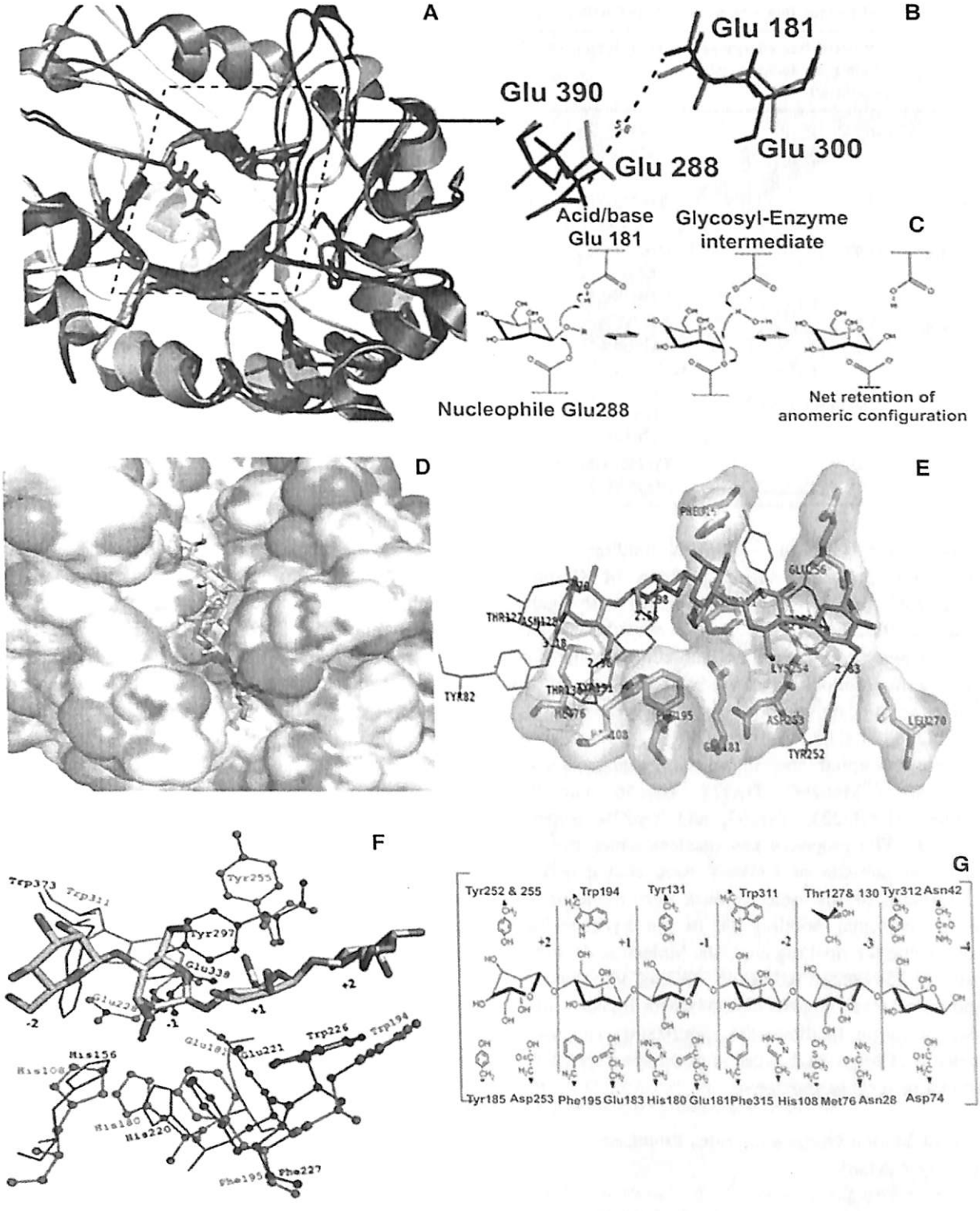

aromatic and hydrophobic residues (Fig. 5e). The aromatic residues created the overall binding site cavity as well as stabilizing the mannopyranose ring of oligosaccharides. Analysis of ligand bound complex obtained from docking and structure superimposition study with ligand bound homolog protein as well as analysis of hydrolysis products obtained from degradation of galactomannan to oligosaccharides as shown in Fig. 3a confirmed that the *Ct*ManT contains six galactomannan binding sub-site that comprise two aglycone site (reducing end, +1 and +2) and

Table 3 Amino acid residue interactions of *Ct*ManT with manno-configured ligands

Ligand	Predicted free energy of binding by docking (ΔG) (kcal/mol)	Polar interactions	Residue within 4 Å region
Mannobiose	−6.84	Tyr312, Trp311, Tyr131, Glu181, Thr130, Asn128, Thr127, Tyr82, His108	Asp74, Glu288, His180, Phe195, Met76
Mannotriose	−3.17	Tyr312, Glu181, Trp311, Thr130, Tyr131, Thr127	Phe315, Tyr255, Phe195, Asn128, Met76, His108, Tyr82
Mannotetraose	−7.97	Trp311,Tyr255, Asp253,Tyr185, Glu181, Tyr131, Thr130, His108	Tyr312, Phe315, Lys254, Tyr252, Glu183, Gly184, Phe195, Met76
Mannopentaose	−8.68	Tyr252, Tyr131, Thr130, Glu256, Tyr255	Tyr82, Met76, Tyr312, Trp311, Phe315, His108, Asp253, Lys254, Leu270, Tyr185, Glu181, Trp197, Phe195, Asn128, Thr127, Tyr255
Mannohexaose	−8.60	Tyr252, Tyr312, Asp253, His108, Tyr185, Asn128, Thr127	Trp311, Phe315, Met76, Lys254, Glu183, Gly184, Glu181, Trp194, Phe195, Thr130, Tyr131
Galactomannan	−3.85	Tyr255, Glu288, Trp311, Glu181, His108	Trp185, Gly184, Trp194, Phe315, Tyr131, Tyr312, Phe315, His180

four glycone site (−1 to −4) with binding energy −3.85 kcal/mol. Structure superimposition of *Ct*ManT with *Cj*Man26C (pdb id: 2VX6) complexes with ligand galactomannan (Gal_2Man_4) was used to map the sub-site positions and nearby key residues. Sub-site mapping displayed many hydrophobic and aromatic residues along with residues at the catalytic core of *Ct*ManT viz. Trp311, His108, Glu228, His180, Phe195, Glu181, Tyr255, and Trp194 were occupied the invariant positions corresponding with *Cj*Man26C Trp373, His156, Glu338, His220, Phe227, Glu221, Tyr297, and Trp226, respectively (Fig. 5f). The proposed key residues which constitute a different sub-site of *Ct*ManT were shown in the Fig. 5g. Furthermore, all these residues were found to be involved in hydrogen bonding or in the hydrophobic interaction during the docking analysis. Molecular docking study with MOSs suggested wide binding site pocket accommodating larger oligosaccharides with higher affinity and which might facilitate the stabilization and subsequent release of oligosaccharides after the cleavage of β-(1 → 4)-linkage of galactomannan.

Purification of Manno-Oligosaccharides Produced from dFCO by *Ct*Manf

The endo-mannanase hydrolyzed products of dFCO were purified by size exclusion chromatography. The elution profile of oligosaccharides and monosaccharide displayed three individual peaks (Fig. 6a). Out of 60 fractions (1 mL) collected, the carbohydrate contents were found in fractions 28–56. These fractions were analyzed by TLC (Fig. 6b) which showed separation of carbohydrate components in fractions 52–56, mannose; 42–48, mannobiose, and 38–40, mannotriose with a yield of 33, 40, and 18 %, respectively. The overlapping fractions of mannose–mannobiose were also observed in fraction 52 and mannobiose–mannotriose in fraction 34 (Fig. 6b). The separated fractions were pooled and analyzed by mass spectrometry. In positive ionization mode ESI–MS–TOF analysis of the separated carbohydrate components in fraction 52–56 displayed mannose $[M+Na]^+$ (*m/z* 193) (Fig. 6c [I]); 42–48, mannobiose $[2M+Na]^+$ (*m/z* 365) (Fig. 6c [II]), and 38–40, mannotriose $[3M+Na]^+$ (*m/z* 527) (Fig. 6c [III]). The 41st fraction displayed overlapping mannobiose and mannotriose peaks at *m/z* 365 and 527, respectively (Fig. 6c [IV]). The fractions 50–51, displayed overlapping peaks of mannose and mannobiose at *m/z* 193 and 365, respectively (Fig. 6c [V]). Therefore, it was evident from mass spectra analysis that the individual factions separated by the SEC were effectively purified into mannose, mannobiose, and mannotriose.

In Vitro Prebiotic Application of Mixed Manno-Oligosaccharides

Growth Profile Probiotic Bacteria in the Presence of Manno-Oligosaccharides

The increment in bacterial population for two probiotic strains which are renowned for their colonization in human colon in the presence of 1 % (w/v) glucose, MOSs, and inulin are shown in Table 4. The growth of probiotic bacteria *L. acidophilus* NRRL B-4496 and *B. infantis* in the presence of mixed MOSs and inulin were comparable with the growth in the presence of glucose at 37 °C at varying

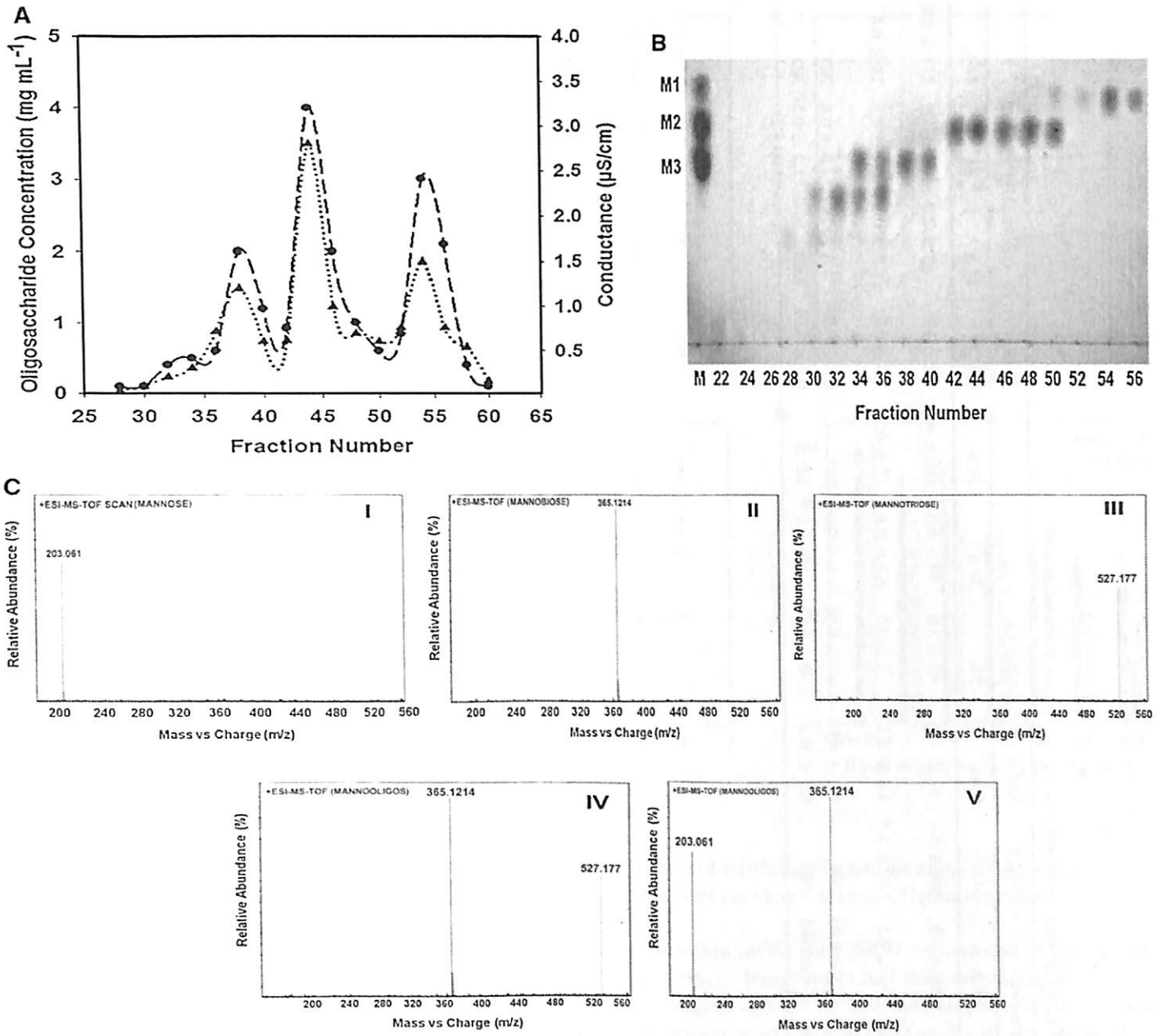

Fig. 6 Purification of *Ct*Manf hydrolyzed products of dFCO. **a** Size exclusion chromatography (Bio-Gel P2) showing abundance of hydrolyzed products as detected by conductance (*black up-pointing triangle*) and by total carbohydrate content (*black circle*). **b** Fractions showing three major peaks with high mannose (52–56), mannobiose (42–48), and mannotriose (38–40) as confirmed by TLC analysis. **c** ESI–MS–TOF peaks of active fractions [I] mannose, [II] mannobiose, [III] mannotriose, and overlapping fractions [III] mannobiose-mannotriose [IV] mannose–mannobiose

time intervals (Table 4). It was found that the mixed MOSs stimulated the higher growth of *B. infantis* and *L. acidophilus* by increasing its number from 1.0×10^7 to 30×10^7 cells/mL and from 12×10^7 to 280×10^7 cells/mL, respectively, within 34 h, whereas inulin promoted the growth of *B. infantis* and *L. acidophilus* from 1.0×10^7 to 17×10^7 cells/mL and 12×10^7 to 160×10^7 cells/mL after 34 h, respectively. Therefore, a ~1.76-fold higher growth of *Bifidobacterium* and *Lactobacillus* were observed in the presence of MOSs as compared with commercial prebiotic inulin. However, MOSs did not support the growth of *E. coli* or *E. aerogenes* like commercial prebiotic inulin as shown in Table 4. It has been reported earlier that SCFAs and lactate are generated from anaerobic fermentation in the presence of prebiotics which are involved in suppression of pathogenic intestinal bacteria and supply energy for colonic epithelium and modulation of cholesterol and lipid metabolism [6]. The lowering of pH was a continuous event

Table 4 Effect of mixed manno-oligosaccharides, inulin, and glucose on growth of probiotic and non-probiotic bacteria

Bacteria	Mixed manno-oligosaccharides ($\times 10^7$ cells/mL)				Inulin ($\times 10^7$ cells/mL)				Glucose ($\times 10^7$ cells/mL)			
	0 h	12 h	24 h	34 h	0 h	12 h	24 h	34 h	0 h	12 h	24 h	34 h
Lactobacillus acidophilus 4495	12 ± 4.0	95 ± 2.0	165 ± 8.0	280 ± 6.0	12 ± 4.0	62 ± 5.0	99 ± 9.0	160 ± 4.0	12 ± 4.0	60 ± 2.0	94 ± 7.0	171 ± 6.0
Bifidobacterium infantis 41661	1.0 ± 0.2	9.0 ± 0.2	17 ± 0.5	30 ± 0.8	1.0 ± 0.1	7 ± 0.3	8.7 ± 0.6	17 ± 0.7	1.0 ± 0.2	8.2 ± 0.3	9.7 ± 0.5	18 ± 0.8
E. coli DH5α	0.2 ± 0.02	0.8 ± 0.06	1.2 ± 0.03	ND	0.2 ± 0.02	0.7 ± 0.06	1.1 ± 0.03	ND	0.2 ± 0.01	1.0 ± 0.02	1.5 ± 0.6	ND
E. aerogenes 3030	0.7 ± 0.02	0.98 ± 0.04	1.4 ± 0.06	ND	0.7 ± 0.2	0.88 ± 0.03	1.3 ± 0.2	ND	0.7 ± 0.02	0.65 ± 0.02	1.1 ± 0.3	ND

Values are in mean ± SD ($n = 3$)

ND no further growth was examined

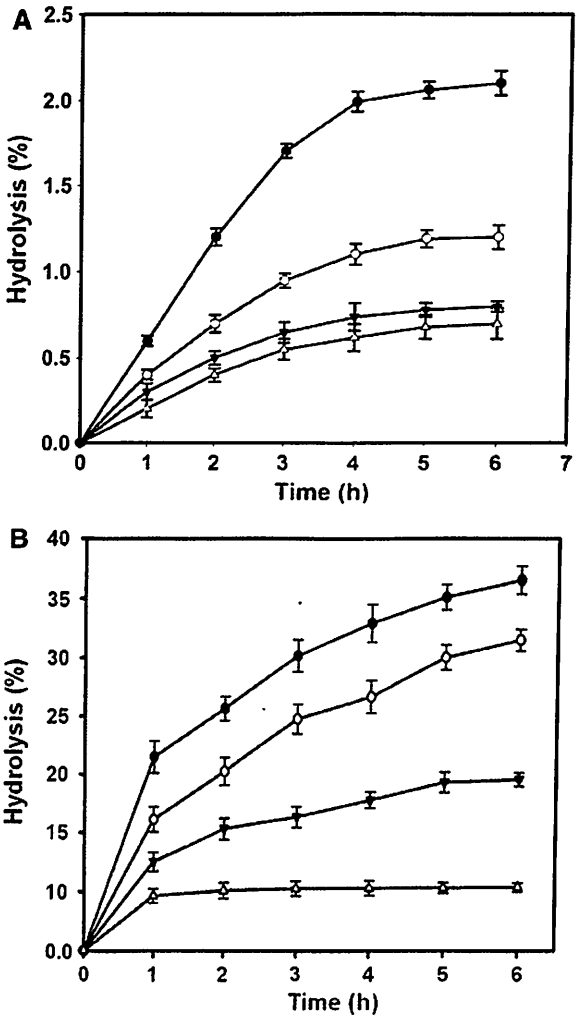

Fig. 7 Effect of simulated gastric juice on hydrolysis of **a** mixed manno-oligosaccharides and **b** inulin at pH 1 (*black circle*), 2 (*white circle*), 3 (*black down-pointing triangle*), and 4 (*white up-pointing triangle*) at 37 °C for 6 h. The mean value of three independent experiments is presented with ± SD

during the assimilation of carbohydrates and growth promotion. During the growth cycle event of *B. infantis*, the gradual decrease of pH from 6.4 to 3.9 after 34 h was observed, while in case of *L. acidophilus*, the pH was found to be 3.7 after 34 h. Earlier Pereira and Gibson reported that both *Bifidobacterium* and *Lactobacillus* can continue their normal growth at low pH 2.0 till 2 h [5, 42]. Therefore, the lowering of pH did not hinder the normal process of cell enumeration of probiotic bacteria, whereas in contrast, low growth profiles were observed as in case of *E. coli* and *E. aerogenes* after 24 h perhaps could be due to the lowering of pH 6.4 and 6.1, respectively, and the exhaustion of carbon source after 24 h. Similar study was reported earlier [43] where lowering of pH inhibited the growth of *E. coli*, and this effect was further relieved by addition of methionine [43].

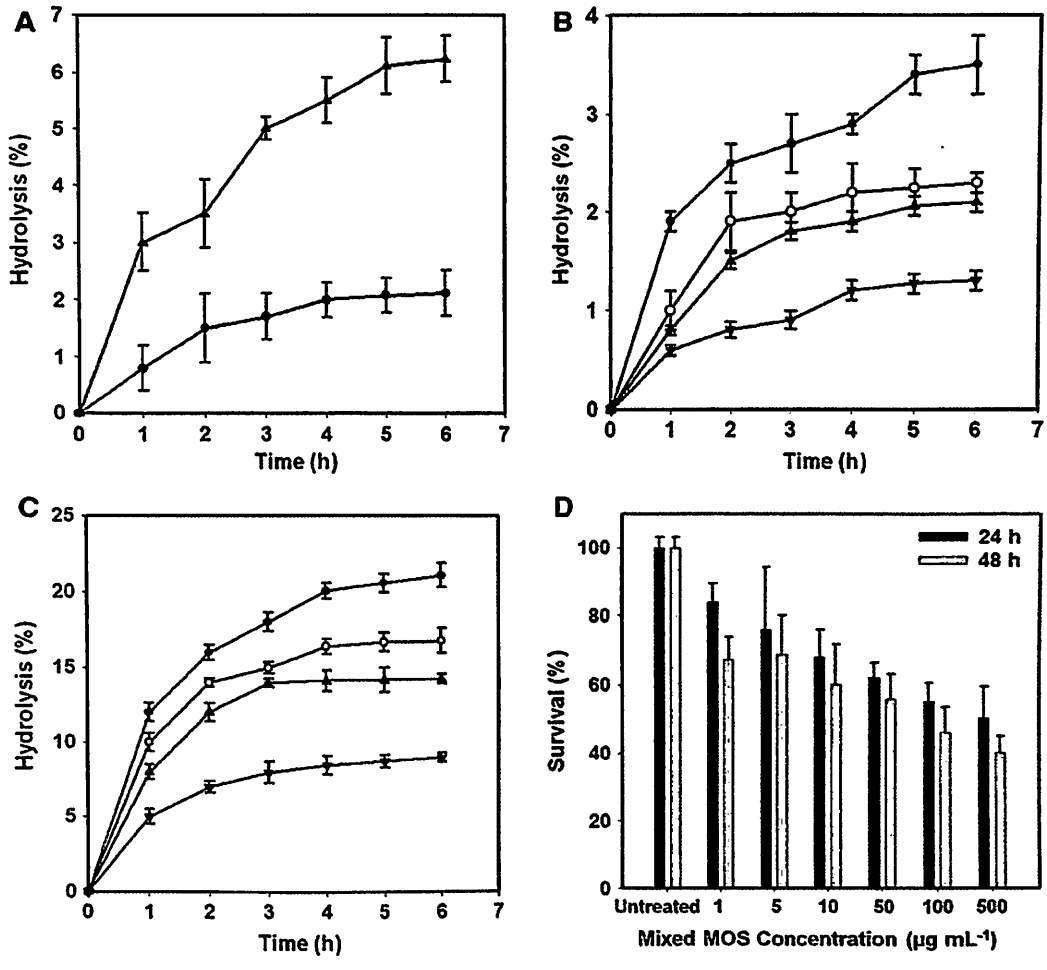

Fig. 8 Effect of a simulated intestinal juice on hydrolysis of mixed manno-oligosaccharides (*black up-pointing triangle*) and reference prebiotic inulin (*black circle*) at pH 8 for 6 h. **b** α-amylase on mixed manno-oligosaccharides. **c** α-amylase on commercial prebiotic inulin at pH 5 (*black down-pointing triangle*), 6 (*black up-pointing triangle*), 7 (*white circle*), and 8 (*black circle*) for 6 h and **d** mixed manno-oligosaccharides (1–500 μg/mL) on cell viability of human colon carcinoma HT29 cell lines by MTT assay. Data are expressed as mean ± SD of three independent experiments and each analysis was carried out in triplicate

Effect of Artificial Human Gastric Juice on Mixed Manno-Oligosaccharides

The mixed MOSs from the dFCO showed elevated resistance toward artificial gastric juice of pH 1–4 after 6 h of incubation at 37 °C (Fig. 7). The percentage of hydrolysis of mixed MOSs decreased with increasing the pH of the artificial gastric juice. The hydrolysis at pH of 1, 2, 3, and 4 was 2.1, 1.2, 0.80, and 0.70 %, respectively, after 6 h of incubation (Fig. 7a). The percentage of hydrolysis of inulin also significantly decreased with increasing the pH as the hydrolysis of inulin at pH of 1, 2, 3, and 4 was 30.21, 24.23, 14.00, and 5.34 %, respectively, after 6 h of incubation (Fig. 7b). The result indicated that the mixed MOSs from dFCO are easily accessible by probiotic bacteria present in the gastrointestinal tract of human as it was unharmed during exposure to artificial gastric juice for 6 h. The current results were better as compared with the previous findings where oligosaccharides were reported to be resistant to acidic conditions in the artificial human gastric juice for only 2 h [27].

Effect of Artificial Human Intestinal Fluid and α-Amylase on Mixed Manno-Oligosaccharides

The mixed MOSs from dFCO demonstrated high resistance in artificial human intestinal fluid containing 1,000 U/mL of trypsin and 0.5 % bile salt at pH 8. The maximum hydrolysis was 1.8 % as compared with the standard prebiotic inulin, which gave maximum hydrolysis of 6.23 % after 6 h of incubation at 37 °C (Fig. 8a). These results signified that 98 % of consumed mixed MOSs from dFCO are expected to reach the jejunal portion of small intestine. This finding is more significant as compared to the earlier report, where 60 % of oligosaccharides isolated from dragon fruit were able to reach lower portion of small intestine after 2 h [27]. Hydrolysis of mixed MOSs from dFCO and inulin by α-amylase at pH 5–8 displayed that higher pH resulted in a significantly higher degree of hydrolysis. The degree of hydrolysis of mixed MOSs after 6 h of incubation at pH of 5, 6, 7, and 8 was 1.3, 2.1, 2.3, and 3.5 %, respectively (Fig. 8b). The hydrolysis of inulin by α-amylase yielded higher extent of hydrolysis as compared

mixed MOSs. It showed 9.0, 14.24, 16.74, and 21.0 % hydrolysis at pH 5, 6, 7, and 8, respectively (Fig. 8c). The mixed MOSs exhibited maximum hydrolysis of 3.5 % after 6 h of incubation at 37 °C, whereas the standard prebiotic inulin showed maximum hydrolysis of 21.0 % at pH 8 after 6 h of incubation at 37 °C, suggesting that the mixed MOSs had significantly higher enzymatic resistance as compared with inulin. It has been reported that 88 % of inulin and oligofructose reach the colon [44], whereas our results displayed that 97 % mixed MOSs can reach the colon in intact form. Therefore, the isolated mixed MOSs used in our study are highly resistant to α-amylase hydrolysis. It is evident from this study that the mixed MOSs has higher resistance to extreme conditions of the human gastrointestinal tract as compared to the standard inulin. In addition, mixed MOSs also served as an alternative carbon source for probiotic bacteria. Thus, prebiotic mixed MOSs, alone or combined with probiotic bacteria in the form of synbiotics, have the ability to influence and improve the gastrointestinal health of humans.

Study of In Vitro Anti-tumorigenic Activity of Mixed Manno-Oligosaccharides

Mixed MOSs isolated from dFCO showed anti-tumorigenic activity against colon cancer (HT29) cell line. The concentration dependent effects of mixed MOSs on HT29 cell line is are displayed in Fig. 8d. At the highest concentration of MOSs (500 µg/mL) the percent survival of HT29 cells was only 50.0 ± 3.2 % after 24 h of incubation while the percent survival of HT29 cells after 48 h of incubation displayed 40.0 ± 0.9 % at 500 µg/mL MOSs concentration (Fig. 8d). These results showed that the MOSs significantly affect the human colon carcinoma cells inhibiting the cell proliferation. The potential effects of fructo-oligosaccharides from apple on human colon carcinoma cell line HT29 via cell cycle arrest at S phase resulting in apoptosis were reported [45]. The growth reduction by isolated MOSs from dFCO may open a new arena of chemotherapeutic agents for colon cancer treatment.

Conclusion

Copra meal is generally considered as agro-waste after oil extraction, but it has mannan hemicelluloses as high as 74 % of its total carbohydrate content. In this study, the production and purification of MOSs from copra meal by recombinant endo-mannanase (*Ct*Manf) is reported first time. The MOSs isolated from copra meal showed potential role as prebiotics resulting in improving the growth of probiotic *Bifidobacterium* and *Lactobacillus*. The purified mixed MOSs from copra meal were highly resistant against gastric juice, intestinal juice, and α-amylase holding properties of a prebiotic molecule. The anti-tumorigenic activity of MOSs paves the way for their potential use as chemotherapeutic agent.

Acknowledgments Arabinda Ghosh is supported by a scholarship from University Grants Commission (UGC), New Delhi, India. The mass spectrometric analysis performed in the Department of Chemistry, IIT Guwahati is gratefully acknowledged. The funder has no role in designing the experiments, preparation of this manuscript and bearing any further publication charges. Moreover, authors declare no conflict of interest.

References

1. Mulimani, V. H., & Naganagouda, K. (2010). Simple laboratory exercise for induction of β-mannanase from *Aspergillus niger*. *Research Journal of Food Science and Education, 9*, 76–79.
2. Hossain, M. Z., Abe, J., & Hizukuri, S. (1996). Multiple forms of β-mannanase from *Bacillus* sp. KK01. *Enzyme Microbial Technology, 18*, 95–98.
3. Kovacs-Nolan, J., Kanatani, H., Nakamura, A., Ibuki, M., & Mine, Y. (2013). β-1,4-mannobiose stimulates innate immune responses and induces TLR4-dependent activation of mouse macrophages but reduces severity of inflammation during endotoxemia in mice. *Journal of Nutrition, 143*, 384–391. doi:10.3945/jn.112.167866.
4. Yang, C., Rupa, P., Kanatani, H., Nakamura, A., Ibuki, M., & Mine, Y. (2013). Therapeutic effects of β1,4 mannobiose in a Balb/c mouse model of intranasally-induced pollen allergy. *Allergology International, 62*, 65–76.
5. Gibson, G. R., Ottaway, P. B., & Rastall, R. A. (2000). *Prebiotics: New developments in functional foods*. Oxford, UK: Wood head. 108 pp.
6. Hongpattarakere, T. (2013). Improvement of freeze-dried *Lactobacillus plantarum* survival using water extracts and crude fibers from food crops. *Food Bioprocess Technology, 6*, 1885–1896.
7. Ishihara, N., Chu, D. C., Akachi, S., & Juneja, L. R. (2000). Preventive effect of partially hydrolyzed guar gum on infection of *Salmonella enterica* in young and laying hens. *Poultry Science, 79*, 689–697.
8. Spring, P., Wenk, C., Dawson, K. A., & Newman, K. E. (2000). The effect of dietary mannooligosaccharides on ceca of *Salmonella* challenged broiler chicks. *Poultry Science, 78*, 205–211.
9. Lin, T. C., & Chen, C. (2004). Enhanced mannanase production by submerged culture of *Aspergillus niger* NCH-189 using defatted copra based media. *Process Biochemistry, 39*, 1103–1109.
10. Cole, C. L., & Jayson, G. C. (2008). Oligosaccharides as anti-angiogenic agents. *Expert Opinion on Biological Therapy, 8*, 351–362.
11. Ghosh, A., Luis, A. S., Brás, J. L. A., Fontes, C. M. G. A., & Goyal, A. (2013). Thermostable recombinant endo-β-(1 → 4)-mannanase from *Clostridium thermocellum*: Biochemical characterization and manno-oligosaccharides production. *Journal of Agricultural and Food Chemistry, 61*, 12333–12344.
12. Naughton, P. J., Mikkelsen, L. L., & Jensen, B. B. (2001). Effects of nondigestible oligosaccharides on *Salmonella enterica* Serovar *Typhimurium* and nonpathogenic *Escherichia coli* in the pig small intestine in vitro. *Applied Environmental Microbiology, 67*, 3391–3395.
13. Sluiter, B., Hames, R., Ruiz, C., Scarlata, J., Sluiter D. Templeton, D. & Crocker, D. (2008). Determination of structural carbohydrates

and lignin in biomass. In Laboratory Analytical Procedure (LAP). Colorado: Technical Report NREL/TP-510-42618.
14. Samson, A. S., Cater, C. M., & Mattil, K. F. (1971). Preparation and characterization of total protein isolates. *American Association for Clinical Chemistry, 77*(8), 182–190.
15. Bradford, M. M. (1976). Rapid and sensitive method for the quantitation of microgram quantities of protein utilizing the principle of protein–dye binding. *Analytical Biochemistry, 72*, 248–254.
16. Nelson, N. (1944). A photometric adaptation of the Somogyi method for the determination of glucose. *Journal of Biological Chemistry, 153*, 375–380.
17. Somogyi, M. (1945). A new reagent for the determination of sugars. *Journal of Biological Chemistry, 160*, 61–68.
18. Fiser, A., Do, R. K., & Sali, A. (2000). Modeling of loops in protein structures. *Protein Science, 9*(9), 1753–1773.
19. Krieger, E., Joo, K., Lee, J., Lee, J., Raman, S., Thompson, J., et al. (2009). Improving physical realism, stereochemistry, and side-chain accuracy in homology modeling: Four approaches that performed well in CASP8. *Proteins, 77*(9), 114–122.
20. Laskowski, R. A., MacArthur, M. W., Moss, D. S., & Thornton, J. M. (1993). Procheck—a program to check the stereochemical quality of protein structures. *Journal of Applied Crystal, 26*, 283–291.
21. Wiederstein, M., & Sippl, M. J. (2007). ProSA-web: Interactive web service for the recognition of errors in three-dimensional structures of proteins. *Nucleic Acids Research, 35*, 407–410.
22. Morris, G. M., Goodsell, D. S., Halliday, R. S., Huey, R., Hart, W. E., Richard, K. B., et al. (1998). Automated docking using a Lamarckian genetic algorithm and an empirical binding free energy function. *Journal of Computational Chemistry, 19*(14), 1639–1662.
23. Huey, R., Morris, G. M., Olson, A. J., & Goodsell, D. S. (2007). A semiempirical free energy force field with charge-based desolvation. *Journal of Computational Chemistry, 28*(6), 1145–1152.
24. Dubois, M., Gilles, K. A., Hamilton, J. K., Rebers, P. A., & Smith, F. (1956). Calorimetric method for determination of sugars and related substances. *Analytical Chemistry, 28*, 350–356.
25. Korakli, M., Ganzle, M. G., & Vogel, R. F. (2002). Metabolism by bifidobacteria and lactic acid bacteria of polysaccharides from wheat and rye, and exopolysaccharides produced by *Lactobacillus sanfranciscensis*. *Journal of Applied Microbiology, 92*, 958–965.
26. Fernandez, M. F., Boris, S., & Barbes, C. (2003). Prebiotic properties of human *Lactobacilli* strains to be used in the gastrointestinal tract. *Journal of Applied Microbiology, 94*, 449–455.
27. Wichienchot, S., Jatupornpipat, M., & Rastall, R. A. (2010). Oligosaccharides of pitaya (dragon fruit) flesh and their prebiotic properties. *Food Chemistry, 120*, 850–857.
28. Mosmann, T. (1983). Rapid colorimetric assay for cellular growth and survival: Application to proliferation and cytotoxicity assays. *Journal of Immunological Methods, 65*, 55–63.
29. Sun, S. N., Yuan, T. Q., Li, M. F., Cao, X. F., Xu, F., & Liu, Q. Y. (2012). Structural characterization of hemicelluloses from bamboo culms (*Neosinocalamus affinis*). *Cellulose Chemistry Technology, 46*, 165–176.
30. Figueiró, S. D., Góes, J. C., Moreira, R. A., & Sombra, A. S. B. (2004). On the physicochemical and dielectric properties of glutaraldehyde crosslinked galactomannan collagen films. *Carbohydrate Polymers, 56*, 313–320.
31. Prashanth, M. R. S., Parvathy, K. S., Susheelamma, N. S., Prashanth, K. V. H., Tharanathan, R. N., Chac, A., et al. (2006). Galactomannan esters a simple, cost-effective method of preparation and characterization. *Food Hydrocolloid, 20*, 1198–1205.
32. Kacurakova, M., Capeka, P., Sasinkova, V., Wellnerb, N., & Ebringerova, A. (2000). FT-IR study of plant cell wall model compounds: Pectic polysaccharides and hemicelluloses. *Carbohydrate Polymers, 43*, 195–203.
33. Peng, Y., Zhang, L., Zeng, F., & Xu, Y. (2003). Structure and antitumor activity of extracellular polysaccharides from mycelium. *Carbohydrate Polymers, 54*, 297–303.
34. Zhang, L., Yang, L., Ding, Q., & Chen, X. (1995). Studies on molecular weights of polysaccharides of *Auricularia auriculajudae*. *Carbohydrate Research, 270*, 1–10.
35. Tamaki, Y., Teruya, T., & Tako, M. (2010). The chemical structure of galactomannan isolated from the seeds of *Delonix regia*. *Bioscience, Biotechnology, and Biochemistry, 74*(5), 1110–1112.
36. Rakhmanberdyeva, R. K., & Shashkov, A. S. (2005). Structure of galactomannans from *Gleditsia delavayi* and *G. aquatica* BY ^{1}H and ^{13}C NMR spectroscopy. *Chemistry of Natural Compounds, 41*, 14–16.
37. Balasubramaniam, K. (1976). Polysaccharides of the kernel of maturing and mature coconuts. *Journal of Food Science, 41*, 1370–1373.
38. Cartmell, A., Topakas, E., Ducros, V. M., Suits, M. D., Davies, G. J., & Gilbert, H. J. (2008). The *Cellvibrio japonicus* mannanase CjMan26C displays a unique exo-mode of action that is conferred by subtle changes to the distal region of the active site. *Journal of Biological Chemistry, 283*(49), 34403–34413.
39. Naganagouda, V. K., Patil, A. G. G., & Mulimani, V. H. (2009). Optimization of the production of thermostable endo-β-1,4 mannanases from a newly isolated *Aspergillus niger* gr and *Aspergillus flavus* gr. *Applied Biochemistry and Biotechnology, 152*, 213–223.
40. Le, N. J., Anderson, L., Stoll, D., Stålbrand, H., & Lo-Leggio, L. (2005). The structure and characterization of a modular endo-beta-1,4-mannanase from *Cellulomonas fimi*. *Biochemistry, 44*(38), 12700–12708.
41. Yan, X. X., An, X. M., Gui, L. L., & Liang, D. C. (2008). From structure to function: Insights into the catalytic substrate specificity and thermostability displayed by *Bacillus subtilis* mannanase BCman. *Journal of Molecular Biology, 379*(3), 535–544.
42. Pereira, D. I. A., & Gibson, G. R. (2002). Cholesterol assimilation by lactic acid bacteria and *Bifidobacteria* isolated from the human gut. *Applied Environmental Microbiology, 68*, 4689–4693.
43. Roe, A. J., O'Byrne, C., McLaggan, D., & Booth, I. R. (2002). Inhibition of *Escherichia coli* growth by acetic acid: A problem with methionine biosynthesis and homocysteine toxicity. *Microbiology, 148*, 2215–2222.
44. Cummings, J. H., & Macfarlane, G. T. (2002). Gastrointestinal effects of prebiotics. *British Journal of Nutrition, 87*, 1145–1151.
45. Li, Q., Zhou, S., Jing, J., Yang, T., Duan, S., Wang, Z., et al. (2013). Oligosaccharide from apple induces apoptosis and cell cycle arrest in HT29 human colon cancer cells. *International Journal of Biological Macromolecules, 57*, 245–254.

ISSN 0006-2979, Biochemistry (Moscow), 2014, Vol. 79, No. 7, pp. 672-686. © Pleiades Publishing, Ltd., 2014.
Published in Russian in Biokhimiya, 2014, Vol. 79, No. 7, pp. 845-863.
Originally published in Biochemistry (Moscow) On-Line Papers in Press, as Manuscript BM13-251, March 15, 2014.

Structure and Functional Investigation of Ligand Binding by a Family 35 Carbohydrate Binding Module (*Ct*CBM35) of β-Mannanase of Family 26 Glycoside Hydrolase from *Clostridium thermocellum*

A. Ghosh[1#], A. K. Verma[1#], S. Gautam[2], M. N. Gupta[2], and A. Goyal[1]*

[1]*Department of Biotechnology, Indian Institute of Technology Guwahati, Guwahati, 781039, Assam, India; fax: 91 (361) 2690762; E-mail: arungoyl@iitg.ernet.in; amalarastar@gmail.com*
[2]*Department of Chemistry, Indian Institute of Technology Delhi, New Delhi, 110016, Delhi, India*

Received August 31, 2013
Revision received February 26, 2014

Abstract—Functional attributes of recombinant *Ct*CBM35 (family 35 carbohydrate binding module) of β-mannanase of family 26 Glycoside Hydrolase from *Clostridium thermocellum* were deduced by biochemical and *in silico* approaches. Ligand-binding analysis of expressed *Ct*CBM35 analyzed by affinity-gel electrophoresis and fluorescence spectroscopy exhibited association constants K_a ~ $1.2 \cdot 10^5$ and $3.0 \cdot 10^5$ M^{-1} with locust bean galactomannan and mannotriose, respectively. However, *Ct*CBM35 showed low ligand-binding affinity with insoluble ivory nut mannan with K_a of $5.0 \cdot 10^{-5}$ M^{-1}. Unfolding transition analysis by fluorescence spectroscopy explained the conformational changes of *Ct*CBM35 in the presence of guanidine hydrochloride (5 M) and urea (6.25 M). This explained that *Ct*CBM35 has good conformational stability and requires higher free energy of denaturation to invoke unfolding. The three-dimensional (3-D) model of *Ct*CBM35 from *C. thermocellum* generated by Modeller9v8 displayed predominance of β-sheets arranged as β-jelly-roll fold. The secondary structure of *Ct*CBM35 by PredictProtein showed the presence of two α-helices (3%), 12 β-sheets (45%), and 15 random coils (52%). Secondary structural element analysis of cloned, expressed, and purified recombinant *Ct*CBM35 by circular dichroism also corroborated the *in silico* predicted secondary structure. Multiple sequence alignment of *Ct*CBM35 showed conserved residues (Tyr123, Gly124, and Phe125), which are commonly observed in mannan specific CBMs. Docking analysis of *Ct*CBM35 with manno-oligosaccharide displayed the involvement of Tyr26, Gln29, Asn43, Trp66, Tyr68, Leu69, Arg76, and Leu127 residues, making polar contact with the ligand molecules. Ligand docking analysis of *Ct*CBM35 exhibiting higher binding affinity with mannotriose and galactomannan (Man-Gal-Man moiety) substantiated the affinity binding and fluorescence results, displaying similar values of K_a.

DOI: 10.1134/S0006297914070098

Key words: *Ct*CBM35, homology modeling, docking, CD spectra, affinity electrophoresis, fluorescence spectra, unfolding transition

Hydrolytic enzymes and their enhanced polysaccharide specificity are often improved by a noncatalytic carbohydrate-binding module appended either at their N- or C-terminals. Polysaccharide recognition, binding, and enhanced catalysis by hydrolytic enzymes are facilitated by noncatalytic modular carbohydrate binding modules. Carbohydrate binding modules (CBMs) have been classified into 67 distinguished families based on sequence similarity (http://www.cazy.org/Carbohydrate-Binding-Module). Usually CBMs are annexed with hydrolytic enzymes such as cellulase, mannanase, and xylanase as scaffoldings and as peptides with noncatalytic functions [1]. Family 35 carbohydrate binding module is often associated with glycoside hydrolase family 26 (GH26) and GH5 mannanases [2-4], xylanases (GH30) [5], and GH39 [6], which significantly alter the polysaccharide specificity for galactomannan, glucomannan, mannan, and glucuronoxylan. The solved 3-D structures of family 35 CBMs have shown a dominance of β-sheet organized as jelly rolls [5]. CBM35 usually accommodates the polysaccharides utilizing a planer surface of aromatic side chains, which interact with the flat chains of manno-configured carbohydrates [5]. This form of conformation is

# These authors contributed equally.
* To whom correspondence should be addressed.

known as type B module [5]. Polysaccharide binding significantly alters the conformation of CBM35, which creates a suitable binding space for polysaccharide accommodation [7]. Generally, it has been observed that bacterial CBMs have affinity towards the same or variable substrates other than their substrate-specific cognate catalytic modules [8]. Affinity gel electrophoresis and fluorescence spectroscopy are effective approaches that are popular for elucidating functional properties of a CBM [9].

It was reported earlier that CBM35 from *Clostridium thermocellum* possesses β-sandwich fold, forming a cavity that specifically accommodates the side chain galactose of galactomannan and Δ-4,5-anhydrogalaturonic acid [10, 11]. The present study describes the ligand binding properties of over-expressed recombinant *Ct*CBM35 by affinity gel electrophoresis and fluorescence spectroscopy and the structural characterization of *Ct*CBM35 by model prediction and its ligand binding by docking analysis. The gene encoding *Ct*CBM35 present at the N-terminal of family GH26 glycoside hydrolase (β-mannanase) was cloned in pET28a(+) vector expressed in *E. coli* BL-21 cells [12]. The recombinant *Ct*CBM35 was purified by immobilized metal ion affinity chromatography (IMAC). Structural stability and the unfolding transition of *Ct*CBM35 were investigated in the presence of guanidine hydrochloride (GnHCl) and urea.

MATERIALS AND METHODS

Bacterial strains, plasmid, and fine chemicals. *Escherichia coli* DH5α cells were used for cloning of *Ct*CBM35, and *E. coli* BL-21(DE3) cells were used as expression host. The plasmid used for cloning and expression was pET28a(+). All the above-mentioned items were procured from Novagen (USA). The chemicals required for polyacrylamide gel electrophoresis (PAGE), Bradford's reagent, oat spelt xylan, birchwood xylan, carboxymethyl cellulose, and Avicel were purchased from Sigma-Aldrich (USA). Glycerol, methanol, concentrated hydrochloric acid, glacial acetic acid, urea, and guanidine hydrochloride were procured from Merck (India). Locust bean galactomannan, rye arabinoxylan and wheat arabinoxylan (insoluble), ivory nut mannan, glucuronoxylan, and mannotriose were purchased from Megazyme International (Ireland).

Production and purification of recombinant *Ct*CBM35. In an earlier study we cloned, hyperexpressed, and biochemically characterized *Ct*CBM35 from *C. thermocellum* ATCC 27405 [12]. For production of *Ct*CBM35, 100 μl of the *E. coli* BL21(DE3) culture from glycerol stock was inoculated into 5 ml of LB medium containing 50 μg/ml kanamycin and incubated at 37°C for 16 h at 180 rpm. A 1% (v/v) inoculum of the culture was transferred to 200 ml of LB medium in a 500 ml flask containing 50 μg/ml kanamycin with incubation at 37°C, 180 rpm till the culture reached mid-exponential phase (A_{600nm} = 0.6). Isopropyl-β-D-thiogalactopyranoside (IPTG) at 1 mM final concentration was added to this mid-exponential phase culture, and it was further incubated at 24°C, 200 rpm, for 24 h for protein induction [12]. The cells were harvested by centrifugation at 9000*g* and 4°C for 15 min, and the resulting pellet was resuspended in 50 mM sodium phosphate buffer, pH 7.0, containing 1 mM phenylmethanesulfonyl fluoride (PMSF). Then the cells were subjected to sonication (Sonics, Vibra cell) on an ice bath for 15 min (9 s on/9 s off pulse, 30% amplitude) and again centrifuged at 19,000*g* at 4°C for 20 min. The cell free supernatant containing the soluble protein was purified by immobilized metal ion chromatography (IMAC). The recombinant *Ct*CBM35 containing His_6 tag was purified by 1 ml HiTrap chelating column (GE Healthcare, USA) following the protocol recommended by the manufacturer. The purity and molecular mass of the recombinant *Ct*CBM35 was verified by SDS-PAGE [12].

Circular dichroism analysis of *Ct*CBM35. The far-UV circular dichroism (CD) spectra of *Ct*CBM35 were recorded on a JASCO J-815 spectropolarimeter (Jasco Corporation, Japan) equipped with a Peltier system for temperature control at 25°C using a cell with a pathlength of 0.1 cm. Typical spectral accumulation parameters were scanning rate of 50 nm/min with a 1 nm bandwidth over the wavelength range 195 to 250 nm with six scans averaged for each far-UV spectrum. The CD data are presented in terms of mean residue ellipticity (MRE, expressed as deg·cm^2·dmol^{-1}) as a function of wavelength, calculated according to the procedure described earlier [13] using a protein concentration of 10-15 μM in 10 mM Tris-HCl, pH 7.5. All CD spectra were corrected for buffer contributions, and secondary structures were calculated by using the web-based K2d neural network software package (kal-el.ugr.es/k2d/spectra.html) [14].

Affinity electrophoresis of *Ct*CBM35 with soluble polysaccharides. Binding of *Ct*CBM35 to soluble polysaccharides was assessed by affinity gel electrophoresis following the protocol of Takeo [15] on 7.5% native polyacrylamide gel in the absence and presence of varying concentration of mannotriose and locust bean galactomannan. Purified *Ct*CBM35 (18 μg) was run on native gels containing soluble polysaccharides such as locust bean galactomannan, carboxymethyl cellulose, rye arabinoxylan, birchwood xylan, oat spelt xylan, and glucuronoxylan and oligosaccharide mannotriose. Native polyacrylamide gels (7.5%) were prepared containing varying polysaccharide concentrations ranging from 0.0 to 1.5% (w/v). A bovine serum albumin (BSA) sample (1.0 mg/ml) was run in native gel for assessment of nonspecific binding interaction.

Binding analysis of *Ct*CBM35 with insoluble polysaccharides. Quantitative and qualitative assessment of *Ct*CBM35 binding was carried out with insoluble polysac-

charides such as ivory nut mannan, Avicel, and wheat arabinoxylan. For qualitative binding analysis, 30 μg of *Ct*CBM35 in 50 mM sodium phosphate buffer, pH 7.0, was mixed with 1 mg of ivory nut mannan or Avicel or wheat arabinoxylan (insoluble) in a final reaction volume of 200 μl. The reaction mixture was incubated for 2 h at 4°C with gentle shaking. After that the insoluble ligand was precipitated by centrifugation at 13,000*g* at 4°C for 5 min. The supernatant, containing the unbound protein, was removed, and the pellet was washed three times with 200 μl of 50 mM sodium phosphate buffer, pH 7.0. The bound protein from the washed pellet was eluted by boiling the polysaccharides in 200 μl of 10% (w/v) SDS containing 10% (v/v) β-mercaptoethanol for 10 min. The pellet of bound protein and the supernatant of unbound protein were analyzed by SDS-PAGE (13%). A BSA (1 mg/ml) control was set in parallel to check for any nonspecific binding. For the quantitative analysis of ligand binding by adsorption isotherm, the protein concentration was varied as 1, 2, 5, 9, and 15 μM and mixed with 5 mg/ml of insoluble ivory nut mannan. Two hundred microliters of *Ct*CBM35–ivory nut mannan mixtures were prepared in 50 mM sodium phosphate buffer, pH 7.0, and incubated at 4°C for 2 h. Different controls (native protein without any polysaccharide) were also kept for each set of reaction mixtures. The experiment was carried out in duplicate. The reaction mixture was centrifuged at 13,000*g* and at 4°C for 10 min. The supernatant containing the unbound fraction was removed, and its protein content was determined by Bradford's method [16]. The adsorption parameters were calculated to determine the binding. If we consider [B] the bound protein concentration, [F] the unbound fraction of protein, [N] the number of binding site concentration, and K_a the association constant, then at equilibrium adsorptions were calculated as described earlier by Gilkes et al. [17].

Polysaccharide binding study of *Ct*CBM35 by fluorescence spectroscopy. On binding to polysaccharide, carbohydrate-binding modules undergo conformational changes and behave differently than in its unbound native form [18]. To compare the results with affinity electrophoresis, 18 μg of *Ct*CBM35 was incubated with polysaccharides *viz.*, locust bean galactomannan and mannotriose at varying concentrations. Polysaccharide concentrations (0.01, 0.04, 0.06, 0.08, 0.15, and 0.2%, w/v) from 0.5% (w/v) stock solution in 100 μl reaction mixture were prepared in 50 mM Tris-HCl buffer, pH 7.0. The samples were incubated at 4°C for 2 h. The fluorescence measurements were carried out using a Fluoromax 3 fluorimeter (Horiba Scientific, USA). Emission and excitation slits were kept at 3.00 and 1.00 nm, respectively, with 0.5 s integration time. Three scans were taken per sample along with a control to reduce the noise created by buffer and polysaccharide. All the samples were excited at λ_{max} = 295 nm with observance of emission spectra between λ_{max} = 320-400 nm. The emission spectra of all tions were corrected against buffer and polysaccharide solution without *Ct*CBM35 before setting the interaction study. The association constants K_a (M^{-1}) of *Ct*CBM35 complex with carob galactomannan and konjac glucomannan were derived using a modified Stern–Volmer equation as described by Belatik et al. [19].

Unfolding transition of *Ct*CBM35 in guanidine hydrochloride and urea. The structural stability of recombinant *Ct*CBM35 in guanidine hydrochloride and urea was studied under isothermal condition. Initially 30 μg of *Ct*CBM35 was incubated with varying concentrations of guanidine hydrochloride (GnHCl) or urea at 25°C for 24 h. One milliliter of reaction mixture was prepared by the addition of 50 μl *Ct*CBM35 (0.6 mg/ml) and varying concentrations of GnHCl or urea (1-8 M) were prepared in 50 mM Tris-HCl buffer, pH 7.0. The unfolding transition of *Ct*CBM35 was monitored by the change in fluorescence intensity of tryptophan (Trp) emission spectra 320-400 nm by exciting the samples at 295 nm using the Fluoromax 3 fluorimeter. A sample without *Ct*CBM35 was kept as control (buffer and denaturant). The free energy of denaturation ΔG was calculated by the method described by Ahmad et al. [20].

Molecular modeling of family 35 carbohydrate-binding module. The protein sequence of family 35 carbohydrate-binding module (*Ct*CBM35) was retrieved from the NCBI protein sequence database with accession number ABN51273 (nucleotide accession number: CP000568) and UniProt ID A3DBE4. The molecular architecture deduced from amino acid sequence showed that *Ct*CBM35 (134 a.a.) is located at the N-terminal, sandwiched between a 32-a.a. signal peptide and catalytic module *Ct*GH26 (373 a.a.) at the C-terminus followed by a dockerin type 1 module. Modeller9v8 was used to build the 3-D model of *Ct*CBM35. Modeller is a computer program used for comparative protein structure modeling by satisfaction of the spatial restraints (http://salilab.org/modeller/). In the first step, target query sequence is aligned with template sequences, and this alignment file was used as an input to generate models of *Ct*CBM35. Loop refinement was done by using the loop model class in Modeller. The model with the lowest discrete optimized protein energy (DOPE) was chosen for further refinements.

Structure refinement and quality assessment. The structure of *Ct*CBM35 with the lowest DOPE score obtained from the modeler was further improved by energy minimization at the YASARA Energy Minimization Server (www.YASARA.org/minimizationserver), in which molecular dynamics simulations of models were carried out in explicit solvent. It uses a new partly knowledge-based all atom force field derived from Amber [21]. The final structure after energy minimization was subjected for structure validation on structure analysis and verification server (SAVES) at NIH-MBI laboratory servers

(http://nihserver.mbi.ucla.edu). Protein secondary structure prediction tool (PredictProtein) from the ExPASy SIB tool site was used to calculate the presence of α-helix, β-sheet, turns, coils, etc. at the Columbia University server (http://cubic.bioc.columbia.edu/predictprotein/).

Multiple sequence analysis. Generally the amino acid residues involved in ligand binding are conserved within the CBM35 family. To investigate these conserved amino acid residues, multiple sequence alignment was performed with representative members of CBM35 having different substrate specificities whose X-ray, crystal, or NMR structures were known. The protein sequence was retrieved from PDB (http://www.rcsb.org/pdb/) saved in FASTA format. Alignment was performed using the ClustalW program [22], and final alignment was generated by ESpript (http://espript.ibcp.fr) for better understanding of conserved residues and structure.

Docking study of modeled *Ct*CBM35. Docking was studied with the help of AutoDock version 4.2.1. Ligands (mannotriose and galactomannan) for the docking study were obtained from PubChem (http://pubchem.ncbi.nlm.nih.gov) in 3D SDF format, which was converted and saved in Mol2 format using OpenBabel 2.2.3 [23]. Galactomannan has a mannan backbone which is decorated with highly substituted α-(1→6)-galactosyl moiety (Man-Gal-Man). Therefore, this trisaccharide moiety was considered as galactomannan ligand. The two other ligands, mannopentaose and mannohexose, were retrieved from PDB, crystal structure of *Caldanaerobius polysaccharolyticus* CBM16 bound to mannopentaose (PDB id: 3OEB), and CBM29 complex with mannohexose (PDB id: 1GWL), respectively. Ligand preparation was done by assigning Gasteiger partial charges, merging nonpolar hydrogens, and finally saved in extended PDBQT file format using AutoDock Tools (ADT) 1.5.4. *Ct*CBM35 modeled protein was also saved as PDBQT file format after removing nonpolar hydrogen atoms and adding their charges with the carbon atoms. Address for ligands where to dock was fixed in a grid parameter file. The grid map dimensions were set in such a way that they fully cover the active site cavity and give enough space for the ligand molecule to rotate freely. For different conformation search of the ligand molecule, the Lamarckian Genetic Algorithm (GA) was implemented and the number of GA runs was set to 30. All other parameters were set to default values such as initial population size (150), maximum energy evaluation per run (2,500,000), and maximum number of generations (27,000). After 30 independent successful docking runs, the protein–ligand complex for each ligand having auto-generated lowest free energy of binding (ΔG) confirmation were saved [24]. Docking results were analyzed using PyMOL (www.PyMOL.org) (0.99) for possible polar and hydrophobic interactions, and the final figure was generated with the help of PyMOL and YASARAView (12.2.22). For better understanding of protein–ligand interaction in 2D, Ligplot was generated (http://www.ebi.ac.uk/pdbsum/).

RESULTS AND DISCUSSION

Cloning, overexpression and purification of recombinant *Ct*CBM6A. The recombinant *Ct*CBM35 was expressed as a soluble protein, and after purification it appeared as a homogenous single band of molecular size 15 kDa on SDS-PAGE [12]. That was close to its theoretical molecular mass of 14.74 kDa as calculated from the amino acid sequence.

Affinity gel electrophoresis of family 35 carbohydrate binding module. The ligand binding of *Ct*CBM35 was investigated by affinity gel electrophoresis, and the degree of association with locust bean galactomannan and mannotriose was determined as described by the method of Takeo [15]. The relative mobilities (r) of *Ct*CBM35 in the presence of varying substrate concentrations were calculated from the polyacrylamide gels (Figs. 1a and 1b). The retardation of *Ct*CBM35 was observed from 0.01% (w/v) with maximum retardation detected at 0.1% (w/v) concentration of locust bean galactomannan (Fig. 1a). In contrast, the retardation was achieved at much lower concentration (0.06%, w/v) of mannotriose (Fig. 1b) owing to simple and small molecular size (dp = 3). Mannotriose accesses the binding sites on *Ct*CBM35 more easily than a galactose-substituted branched polysaccharide like locust bean galactomannan. This was similarly reported earlier by Mizutani et al. [25]. However, no significant binding of *Ct*CBM35 was observed with carboxymethylcellulose, rye arabinoxylan, birchwood xylan, oat spelt xylan, and glucuronoxylan, showing that *Ct*CBM35 is mannan-specific CBM (Table 1). The association constants (K_a) of *Ct*CBM35 with different ligands were derived from linear regression plots between the inverse relative migration ($1/r$) versus substrate concentration (%, w/v) (Fig. 1c). *Ct*CBM35 displayed higher association constant value with mannotriose ($K_a = 3.2 \cdot 10^5$ M^{-1}) than with locust bean galactomannan ($K_a = 1.23 \cdot 10^5$ M^{-1}) (Table 1). The free energy of binding (ΔG) with mannotriose was higher (7.0 kcal/mole) than with locust bean galactomannan (6.2 kcal/mole) (Table 1). While comparing these data with prediction outcome, it was observed that the association constant (K_a) and free energy of binding (ΔG) of *Ct*CBM35 were similar in both cases (Table 1).

The recombinant *Ct*CBM35 preferred binding manno-configured polysaccharides. *Ct*CBM35 discriminated during carbohydrate selection, showing its affinity only with manno-configured ligands among the diverse polysaccharides tested. Family 35 CBMs often show affinity toward ligands other than manno-configured polysaccharides containing β-(1→4)-mannose chains, such as Δ-4,5-anhydrogalacturonic acid and glucuronic acid [26].

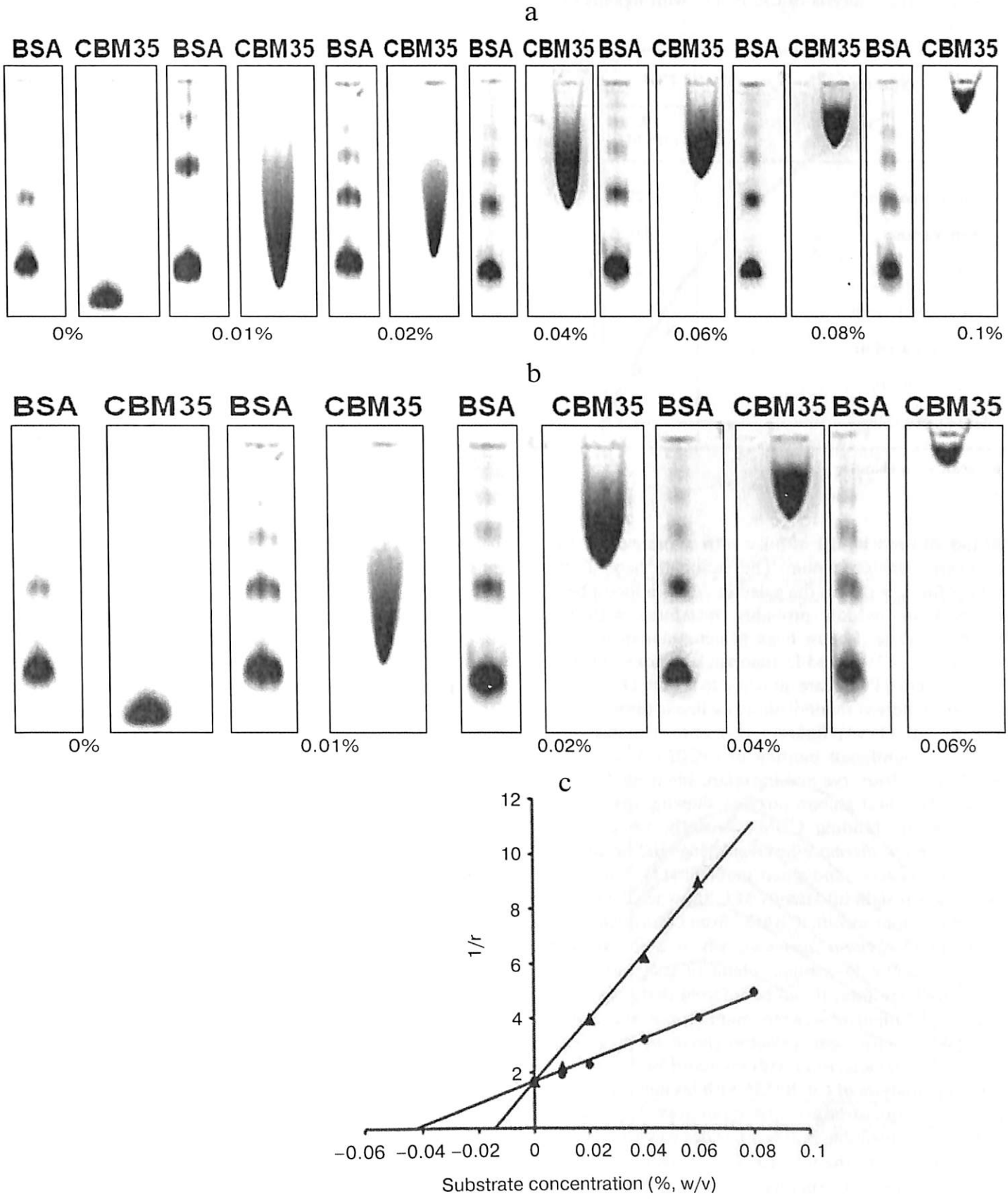

Fig. 1. Affinity gel electrophoresis using native polyacrylamide gel (7.5%) of *Ct*CBM35 against (a) locust bean galactomannan and (b) mannotriose. c) Plot of $1/r$ versus polysaccharide concentration, where r is the relative migration distance of *Ct*CBM35 in the presence of locust bean galactomannan (circles) and mannotriose (triangles) in the gel.

Table 1. Binding analysis of *Ct*CBM35 with ligands by *in silico* prediction, affinity electrophoresis, and fluorescence spectroscopy

Substrates	Prediction outcome		Affinity electrophoresis		Fluorescence spectra	
	K_a (10^5 M^{-1})	$-\Delta G$ (kcal/mole)	K_a (10^5 M^{-1})	$-\Delta G$ (kcal/mole)	K_a (10^5 M^{-1})	$-\Delta G$ (kcal/mole)
Galactomannan[a]	1.22	6.0	1.23	6.2	1.21	6.1
Mannotriose	3.0	6.8	3.2	7.0	3.03	6.9
CMC	–	–	–	–	–	–
Rye arabinoxylan	–	–	–	–	–	–
Birchwood xylan	–	–	–	–	–	–
Oat spelt xylan	–	–	–	–	–	–
Glucuronoxylan	–	–	–	–	–	–

[a] Locust bean; –, no binding observed.

*Ct*CBM35 showed higher affinity with mannotriose than locust bean galactomannan. The rationale behind this selective affinity is due to the galactose unit in locust bean galactomannan, which probably interferes with the *Ct*CBM35 binding. Locust bean galactomannan is composed of a β-(1→4)-linked D-mannan backbone to which single D-galactosyl units are attached to C-6 of D-mannosyl residues, whereas mannotriose is a linear trisaccharide comprising β-(1→4)-linked D-mannosyl residues. However, no significant binding of *Ct*CBM35 with carboxymethylcellulose, rye arabinoxylan, birchwood xylan, oat spelt xylan, and glucuronoxylan showing that it is a mannan specific binding CBM. Recently, we reported *Ct*CBM35 from *C. thermocellum* displaying binding affinity towards both galacto- and gluco-mannan [12]. This finding gives a new insight into family 35 CBM when compared with other mannan specific CBM35 from *Clostridium thermocellum* and *Cellvibrio japonicus*, which were exo and endo acting to the D-mannan chain of galactomannan only [7, 10]. Therefore, it can be inferred that *Ct*CBM35 was able to distinguish between mannotriose and highly galactosylated locust bean galactomannan by displaying better binding characteristics with mannotriose.

Binding analysis of *Ct*CBM35 with insoluble polysaccharides. The quantitative and qualitative binding of *Ct*CBM35 with insoluble polysaccharides was assessed by adsorption isotherm analysis. *Ct*CBM35 displayed lower binding with insoluble mannan as analyzed by SDS-PAGE upon comparison of the bound protein fraction, unbound fraction, and the purified native protein (Fig. 2a). *Ct*CBM35 displayed no binding with Avicel or wheat arabinoxylan (insoluble). The association constant K_a of *Ct*CBM35 with insoluble mannan was observed to be $5.0 \cdot 10^{-5}$ M^{-1} (Table 2). The relative equilibrium association constant K_r and the binding capacity (number of binding site concentration on mannan surface, N_o) were calculated from a nonlinear regression plot between bound *Ct*CBM35 versus free *Ct*CBM35 (Fig. 2b). The data were analyzed by GraphPad (Prism 2.0.1) software using nonlinear regression analysis based on one binding site equation as described by Gilkes et al. [17]. The estimated values of relative equilibrium constant K_r and concentration of binding sites [N_o] were 1.5 ± 0.2 liter/g and 0.45 ± 0.002 μmole/g, respectively. This suggested that *Ct*CBM35 bound less significantly with insoluble ivory nut mannan. The low affinity against insoluble mannan has been reported for the inability of "trans" form (as a separate fold and not appended to a hydrolytic enzyme) of CBM to disrupt the interchain interactions of the polysaccharide [25]. This is in contrast to some CBMs that have the ability to disintegrate the surface of crystalline insoluble polysaccharides displaying higher binding to soluble fractions of insoluble polysaccharides [27, 28].

Table 2. Binding parameters of *Ct*CBM35 with insoluble ligands derived from adsorption isotherm analysis

Polysaccharide	K_r (liter/g)*	K_a ($\times 10^{-5}$ M^{-1})
Ivory nut mannan	0.35 ± 0.02	2.5
Avicel	–	–
Wheat arabinoxylan	–	–

* Values are mean ± SD (n = 3); –, not determined.

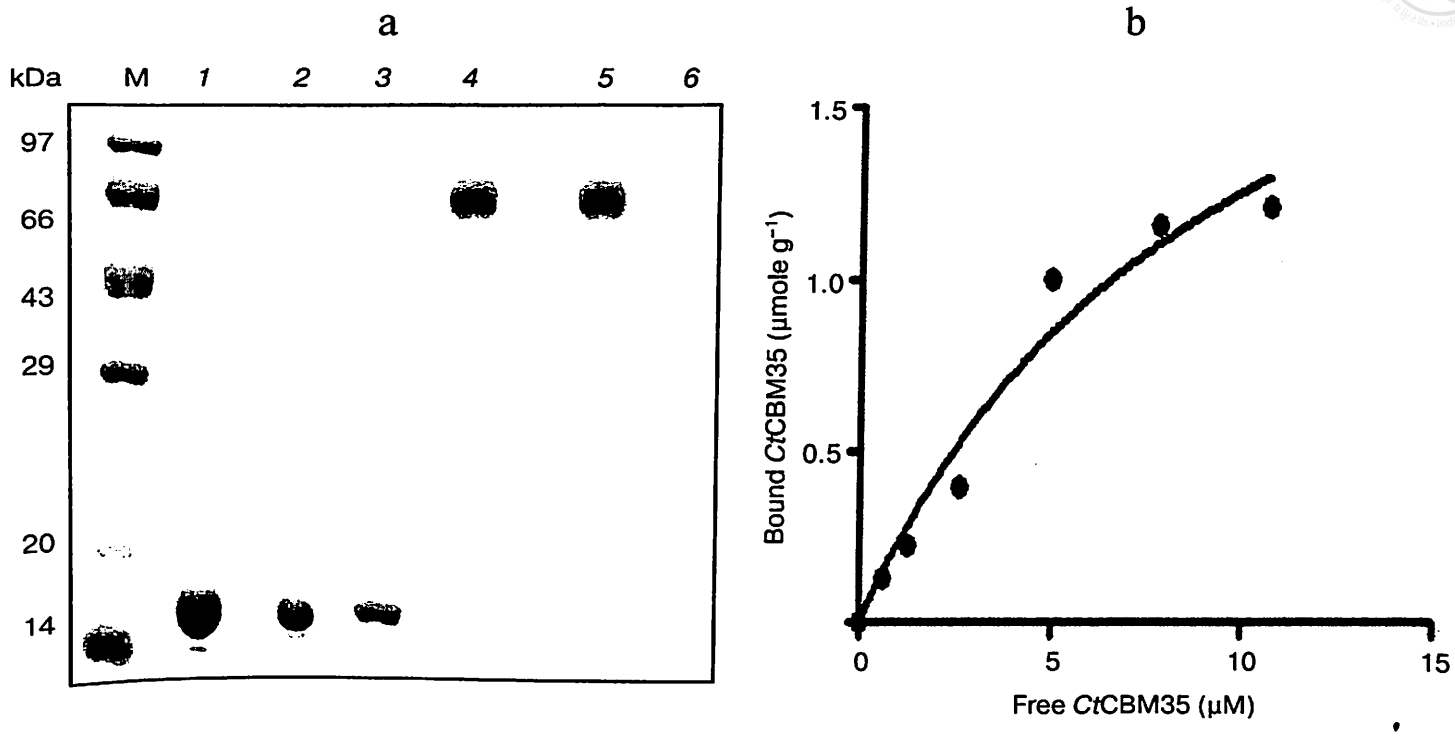

Fig. 2. Binding of *Ct*CBM35 with insoluble ivory nut mannan. a) Qualitative binding analysis using 13% SDS-PAGE. Lanes: M, high range unstained molecular weight marker (14-97 kDa); *1*) purified *Ct*CBM35 as control; *2*) unbound *Ct*CBM35; *3*) bound *Ct*CBM35; *4*) bovine serum albumin (BSA) as negative control; *5*) unbound BSA; *6*) bound BSA. b) Adsorption of *Ct*CBM35 to insoluble ivory nut mannan. The plot shows the equilibrium adsorption isotherm (bound *Ct*CBM35 [B] versus free *Ct*CBM35 [F]). Adsorption assay was done at 4°C as described in "Materials and Methods". Initial protein concentrations of *Ct*CBM35 used were 1-15 μM.

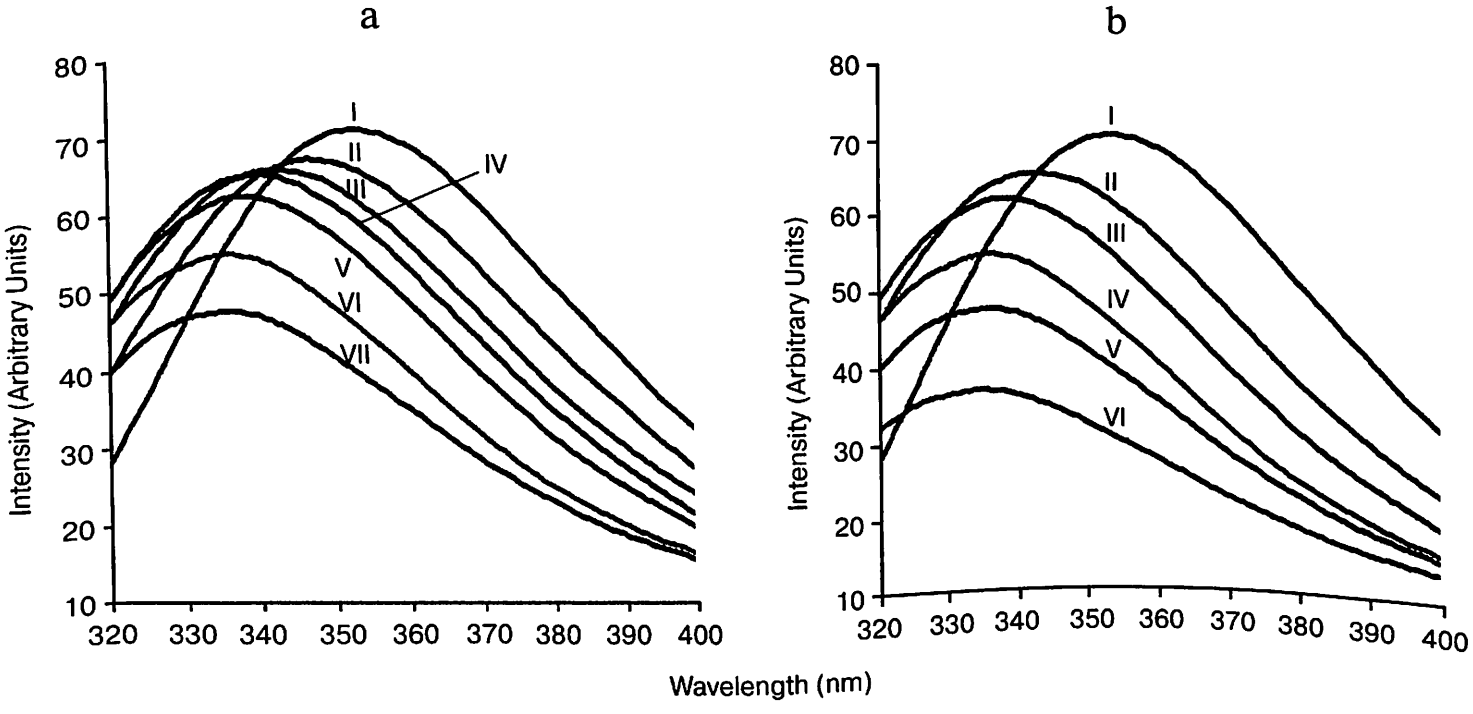

Fig. 3. Tryptophan fluorescence emission spectrum of *Ct*CBM35 in the presence of (a) locust bean galactomannan (% w/v) (0.0 (I), 0.01 (II), 0.02 (III), 0.04 (IV), 0.06 (V), 0.08 (VI), 0.1 (VII)) and (b) mannotriose (0.0 (I), 0.01 (II), 0.02 (III), 0.04 (IV), 0.06 (V), 0.08 (VI)).

Polysaccharide binding study of *Ct*CBM35 by fluorescence spectroscopy. In the presence of polysaccharide such as locust bean galactomannan and oligosaccharide (mannotriose) with their varying concentration from 0.01 to 0.08% (w/v), significant blue shifts were observed. Binding of locust bean galactomannan and mannotriose with *Ct*CBM35 displayed 21-nm peak shifts towards shorter wavelength of tryptophan emission spectra from λ_{max} 355 to 334 nm (Figs. 3a and 3b). Ligand binding changes the microenvironment of tryptophan due to conformational changes in protein [18, 29]. The higher binding affinity of *Ct*CBM35 with mannotriose was due to simpler structure of the trisaccharide composed of β-(1→4) linked mannose moieties resulting in reduced fluorescence peak intensity, whereas the highly substituted α-(1→6)-galactose residues in locust bean galactomannan hindered the main chain of β-(1→4)-linked mannose residues from binding tryptophan of *Ct*CBM35, thus causing comparatively higher fluorescence intensity (Figs. 3a and 3b). The decrease in the fluorescence intensity was also coupled with a peak shift by 21 nm for *Ct*CBM35 binding mannotriose as well as locust bean galactomannan (Figs. 3a and 3b).

From the relative fluorescence intensities, the deduced affinity constant (K_a) of *Ct*CBM35 with locust bean galactomannan was $1.21 \cdot 10^5$ M^{-1} and with mannotriose $3.03 \cdot 10^5$ M^{-1} (Table 1). The K_a values were similar to those determined by affinity electrophoresis. Therefore, the fluorescence studies of polysaccharide binding of *Ct*CBM35 also confirmed the same binding affinity pattern as observed with the affinity electrophoresis experiment. The number of binding site concentration (n) were derived from Stern–Volmer equation, and it was found to be 0.79 ± 0.09 μmol/g with locust bean galactomannan, whereas with mannotriose the binding capacity was observed to be 0.90 ± 0.05 μmole/g. It means both the polysaccharides have a single binding site for *Ct*CBM35. From the derived affinity constants, the Gibb's free energies of binding were calculated using the equation:

$$\Delta G = -RT \cdot \ln K_a,$$

where ΔG is Gibb's free energy, R universal gas constant ($J \cdot K^{-1} \cdot mol^{-1}$), T temperature in Kelvin, K_a association constant (M^{-1}). The free energy of binding of *Ct*CBM35 with locust bean galactomannan was –6.1 kcal/mole and with mannotriose –6.9 kcal/mole (Table 1). The higher binding affinity (K_a) and free energy of binding indicated that mannotriose made an easier platform for *Ct*CBM35 binding than locust bean galactomannan, although *Ct*CBM35 has a similar number of binding site concentration for both of these ligands.

Polysaccharide specificity by members of the *Ct*CBM35 family is probably due to the conserved hydrophobic aromatic residues that play a major role in polysaccharide binding [7]. Tryptophan, beir such residues having an indole ring with intrinsic fluorescence property with higher quantum yield, displays fluorescence emission at 320 to 400 nm [18]. Polysaccharide binding alters the microenvironment of tryptophan due to conformational changes in the protein. Usually in CBMs, the aromatic residues responsible for polysaccharide binding are lying in the hydrophobic core. Due to polysaccharide binding and direct interaction with tryptophan, the fluorescence emission is gradually decreased. Thus, gradual fall in peak intensities were coupled with peak shifts (~21 nm) due to altered conformation of the native *Ct*CBM35.

Unfolding transition of *Ct*CBM35 in guanidine hydrochloride and urea. The unfolding transition of *Ct*CBM35 was investigated in the presence of GnHCl and of urea. The addition of GnHCl (1-6 M) or urea (1-7 M) to *Ct*CBM35 caused a decrease in the peak intensity as the denaturant concentration increased (Figs. 4a and 4b). The maximum fall in peak intensity of *Ct*CBM35 was observed at 6 M GnHCl and 7 M urea (Figs. 4a and 4b). The lowering of peak intensities overlapped with a bathochromic shift (red shift, shift towards longer wavelength) of the fluorescence maxima from 355 nm (native form) to 370 nm (denatured form) in the presence of GnHCl and from 355 to 360 nm in the presence of urea. This was perhaps due to the Trp residue, which is otherwise buried in the native form, being exposed on the surface in the denatured *Ct*CBM35. A similar unfolding mechanism of recombinant human interferon γ was described earlier [30]. The unfolding curves obtained at pH 7.0 for GnHCl and urea are shown in Fig. 4c. In both cases the curves displayed a sigmoid pattern, signifying that the unfolding of *Ct*CBM35 in the presence of GnHCl or urea was a two-stage process, where low unfolded fractions of *Ct*CBM35 were obtained till 4 and 5 M, respectively. The unfolding of *Ct*CBM35 increased up to 5.5 M of GnHCl and 6.5 M of urea with a saturation phase observed till 8 M. The outcomes also indicated that the unfolding of *Ct*CBM35 was more effective in the presence of GnHCl than of urea. As seen in Fig. 4c, the midpoint value of unfolding of *Ct*CBM35 was 5 M for GnHCl and 6.25 M for urea. The free energies ΔG of *Ct*CBM35 unfolding calculated from these curves by a linear extrapolation method at pH 7.0 were 2.19 kJ/mole for GnHCl and 1.97 kJ/mole for urea. The free energies clearly indicated that higher energy is required by both denaturants to destabilize the electrostatic interactions within *Ct*CBM35. These results were similar to those with the unfolding phenomenon of human interferon γ as described by Christova et al. in presence of GnHCl and urea, which required lower energies to unfold [30].

Structure characterization and quality assessment of modeled protein. A BLAST (Basic Local Alignment Search Tool) search for sequence similarity with default parameter in NCBI against PDB database displayed the

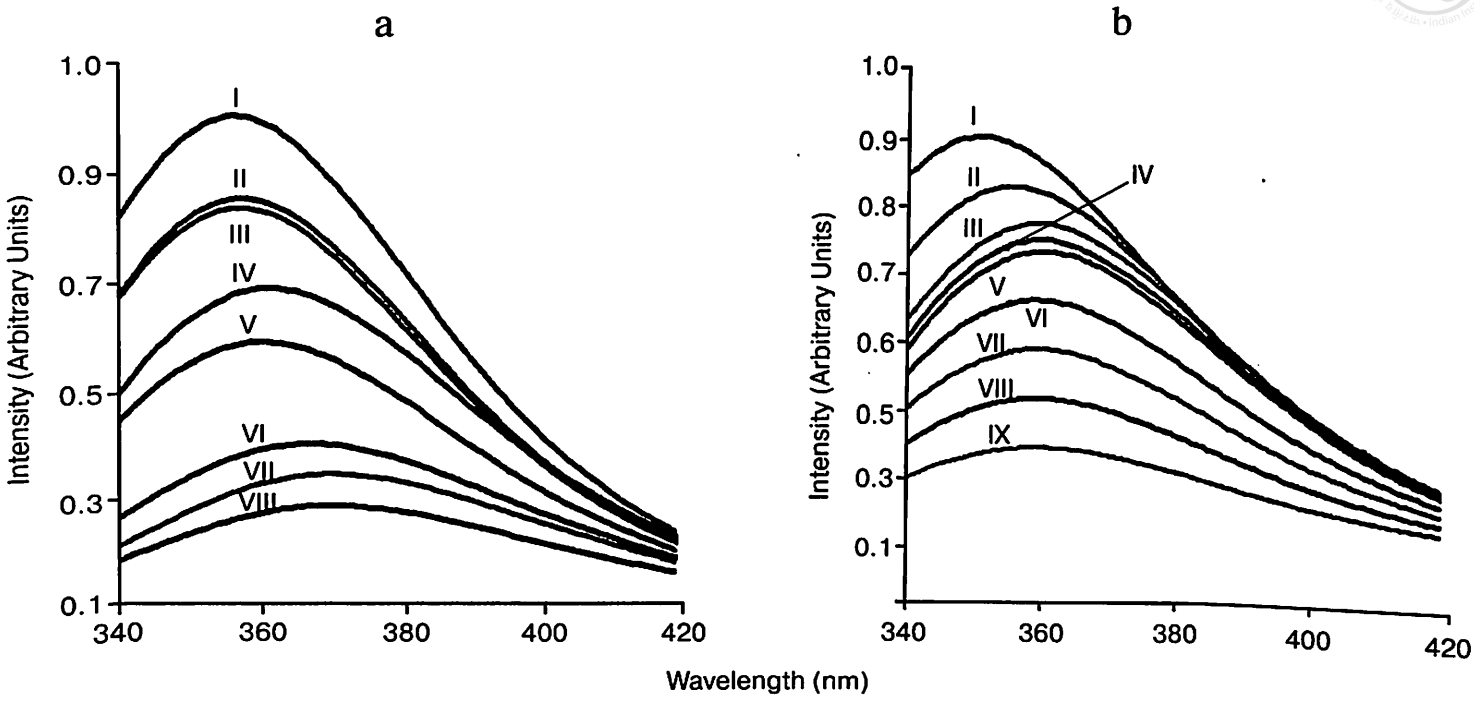

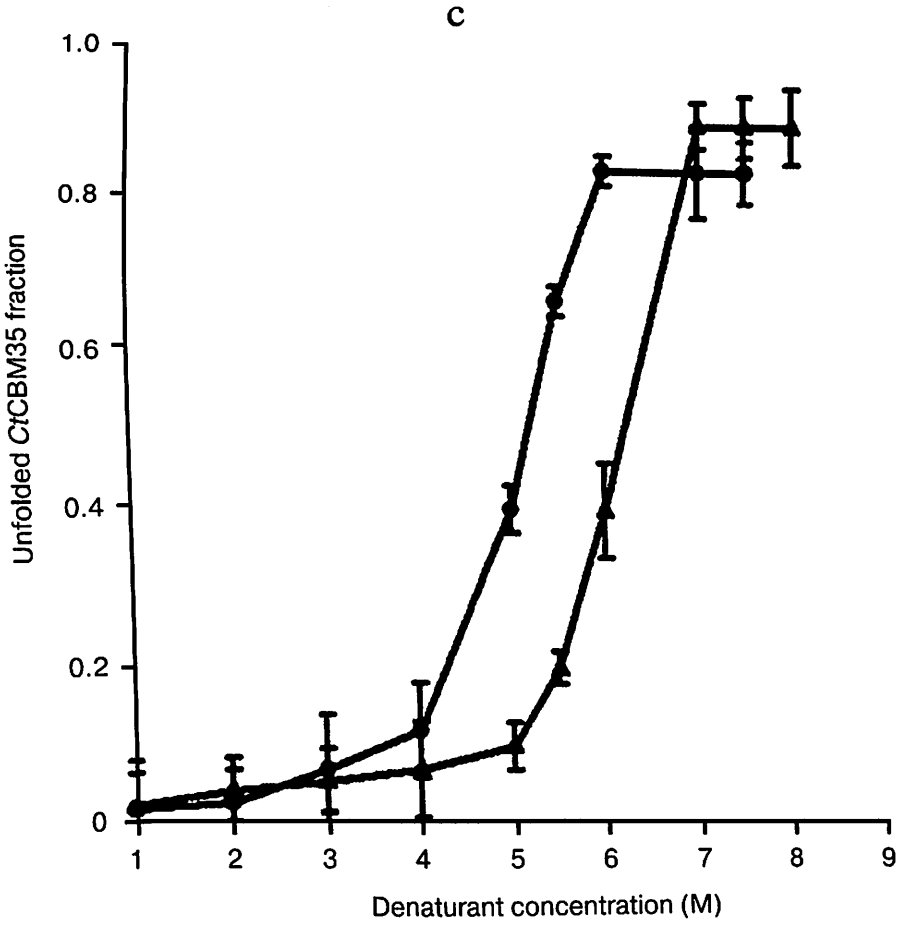

Fig. 4. Tryptophan fluorescence emission spectrum of *Ct*CBM35 in the presence of (a) guanidium hydrochloride (GnHCl) (control (I), 1 M (II), 2 M (III), 3 M (IV), 4 M (V), 5 M (VI), 5.5 M (VII), 6 M (VIII)), (b) urea (control (I), 1 M (II), 2 M (III), 3 M (IV), 4 M (V), 5 M (VI), 6 M (VII), 6.5 M (VIII), 7 M (IX)), (c) fraction of *Ct*CBM35 unfolded as a function of (circles) GnHCl and (triangles) urea concentrations.

number of hits of *Ct*CBM35 belonging to the family 35 carbohydrate-binding module. Top hit X-ray crystallography structure of CBM35 from *Amycolatopsis orientalis* (PDB 2vzp) that covered full query and displayed 34% similarity (score of 39.7 and *E*-value 0.001) was acquired as a template to model the structure. The overall 3-D structure of *Ct*CBM35 showed that it is rich in β-sheets, consisting of a pair of six-stranded antiparallel β-sheets having β-jelly-roll fold, which is quite common in many CBMs (Fig. 5a). The topology diagram displayed 12 β-strands (dark gray), only two small α-helices (black), and 15 random coils (arrow lines) forming a β-jelly roll topology (Fig. 5b). Secondary structure prediction by PredictProtein showed a pair of α-helices (<5%), but apart from this the dominance of a pair of six extended β-sheets (>42%) and 15 random coils (<53%) were also observed (Table 3) in the 3-D model of *Ct*CBM35. The CD spectrum of *Ct*CBM35 (Fig. 5c) was analyzed using the K2d neural network algorithm tool as described by Andrade et al. [14], which revealed that it contains 45% β-sheets (12 in number), 52% random coils (15 in number), and only 3% α-helices (2 in number) (Table 3). Therefore, the CD analysis substantiated that the prediction of secondary structure was acceptable. The presence of a high percentage of β-sheets and random coils are in agreement with the *in silico* prediction of the *Ct*CBM35 3-D model, which also revealed β-jelly roll architecture. Structure similarity search of the modeled protein in the DaliLite server (www.ebi.ac.uk/Tools/dalilite/) showed similarity with the native structure of a family 35 CBM from *C. thermocellum* (2W1W chain B) and CBM35 from *A. orientalis* (2VZP chain B) with RMSD of 1.7 and 1.8 Å, respectively. Modeled *Ct*CBM35 after energy minimization was validated by Ramachandran plot analysis. Out of a total of 134 residues, 93% of the residues lie in most favored regions, 7% of residues lie in additional allowed region, and there was no residue in generously allowed or disallowed regions. This indicated that amino acid residues in the modeled *Ct*CBM35 occupied favorable phi (φ) and psi (ψ) backbone dihedral angles. Overall quality factor of *Ct*CBM35 was 88% in the ERRAT plot analysis (data not shown). Verify 3D score was obtained as 95%, i.e. 95% of the residues had an averaged 3D-1D score >0.2. This determined the compatibility of an atomic model (3D) with its own amino acid sequence (it categorized each residue into structural class based on its location and environment (α, β, loop, polar, nonpolar, etc.), then it generates a score by comparing each residue with a collection of good structures as a reference [31].

Substrate-binding site analysis. CBMs play a critical role in substrate targeting and substrate binding. It is very important to investigate the key residues playing significant roles in recognition and binding with the substrate and whether they are conserved within the family or are substrate-specific. Multiple sequence alignment (MSA) was performed by taking representative members of the CBM35 family having different substrate specificities. The MSA result showed many amino acid residues are conserved within the family 35 CBMs (Fig. 6a). We have identified that a Trp-Gly-Phe motif is conserved and is also present in *Ct*CBM35 (shown in horizontal black box) (Fig. 6a). Moreover, a Trp-Gly-Tyr motif that is probably involved in the substrate specificity towards mannans was conserved within the mannan-specific CBMs [32]. It was demonstrated by NMR solution structure of mannan-specific CBM35 from *C. japonicus* that it bound to mannopentaose, involving amino acid residues Tyr60, Lys63, Trp109, Gly110, and Tyr111 showing maximum chemical shifts on ligand binding [33]. The involvement of aromatic amino acid residues Tyr22-Tyr53-Tyr129 in β-(1→4)-linked glucomannan recognition by CBM11 was reported earlier by Carvalho et al. [34]. We also found that the above-mentioned key amino acid residues were present in *Ct*CBM35, except for Tyr60. The other amino acid residues like Arg76, Trp123, Gly124, and Phe125 were conserved within *Ct*CBM35 (highlighted in black box in Fig. 6a).

Docking analysis of ligand binding interaction with *Ct*CBM35. The molecular docking analysis of modeled *Ct*CBM35 with various manno-oligosaccharides provided a better understanding about the key amino acid residues involved in making strong hydrophobic interactions with the ligand. There is much evidence that shows how hydrophobic stacking interactions and hydrogen bonds play an important role in ligand binding in the case of family 35 CBMs [35]. Our docking results showed that residues Tyr26, Gln29, Asn43, Trp66, Tyr68, Leu69, Arg76, and Leu127 participate in making polar interac-

Table 3. Secondary structure analysis of *Ct*CBM35 by far-UV CD spectrum and the PredictProtein tool

Secondary structure content	CD spectra (%)	PredictProtein (%)	Numbers of secondary structures (by CD spectrum and PredictProtein analysis)
α-Helix	03	<5	2
β-Sheet	45	>42	12
Random coil	52	<53	15

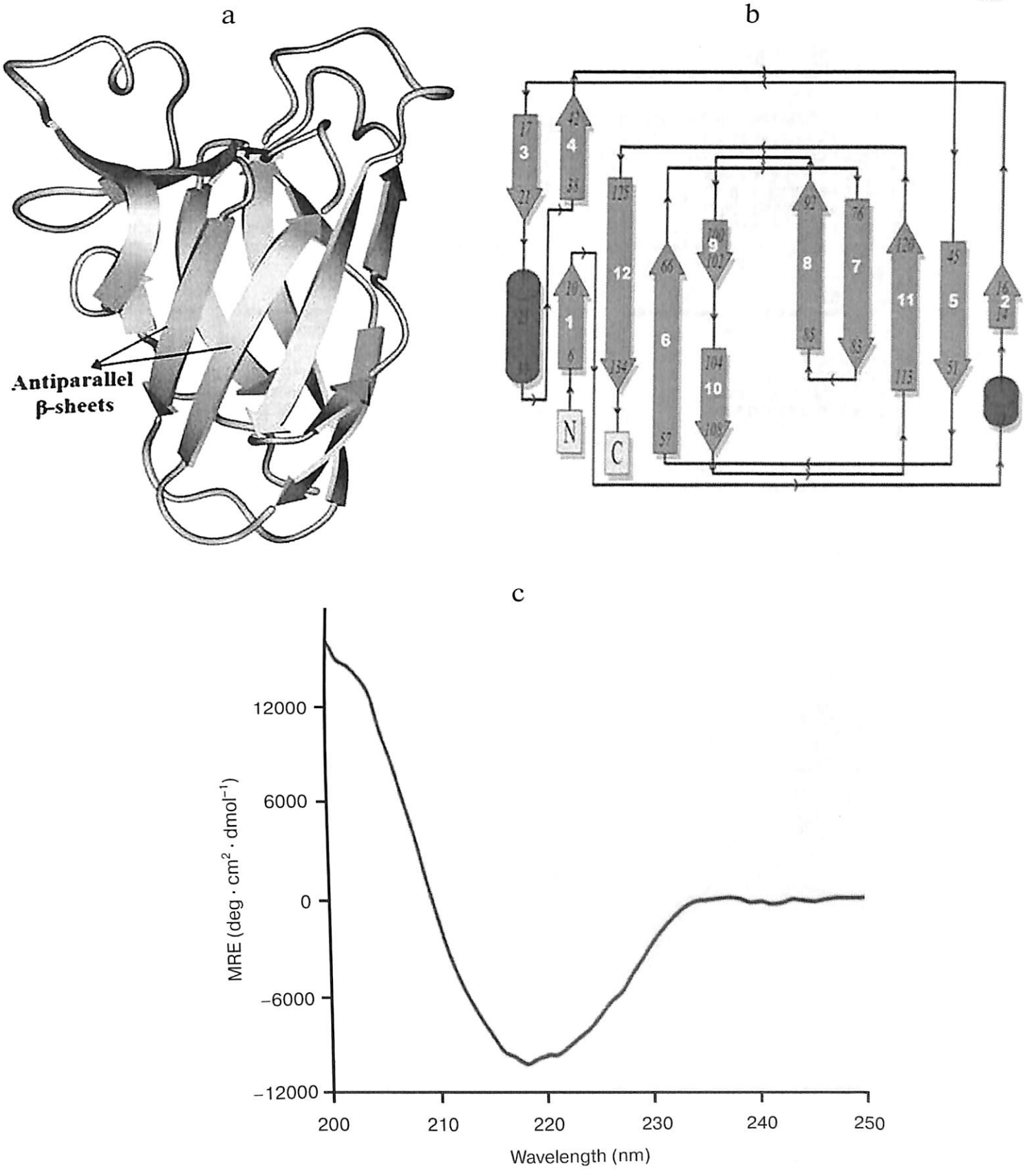

Fig. 5. a) Overall 3-D representation of modeled carbohydrate-binding module family 35 from *Clostridium thermocellum* showing β-jelly-roll fold; b) topology diagram of *Ct*CBM35 showing β-jelly roll topology; c) CD spectrum of *Ct*CBM35 for secondary structure determination.

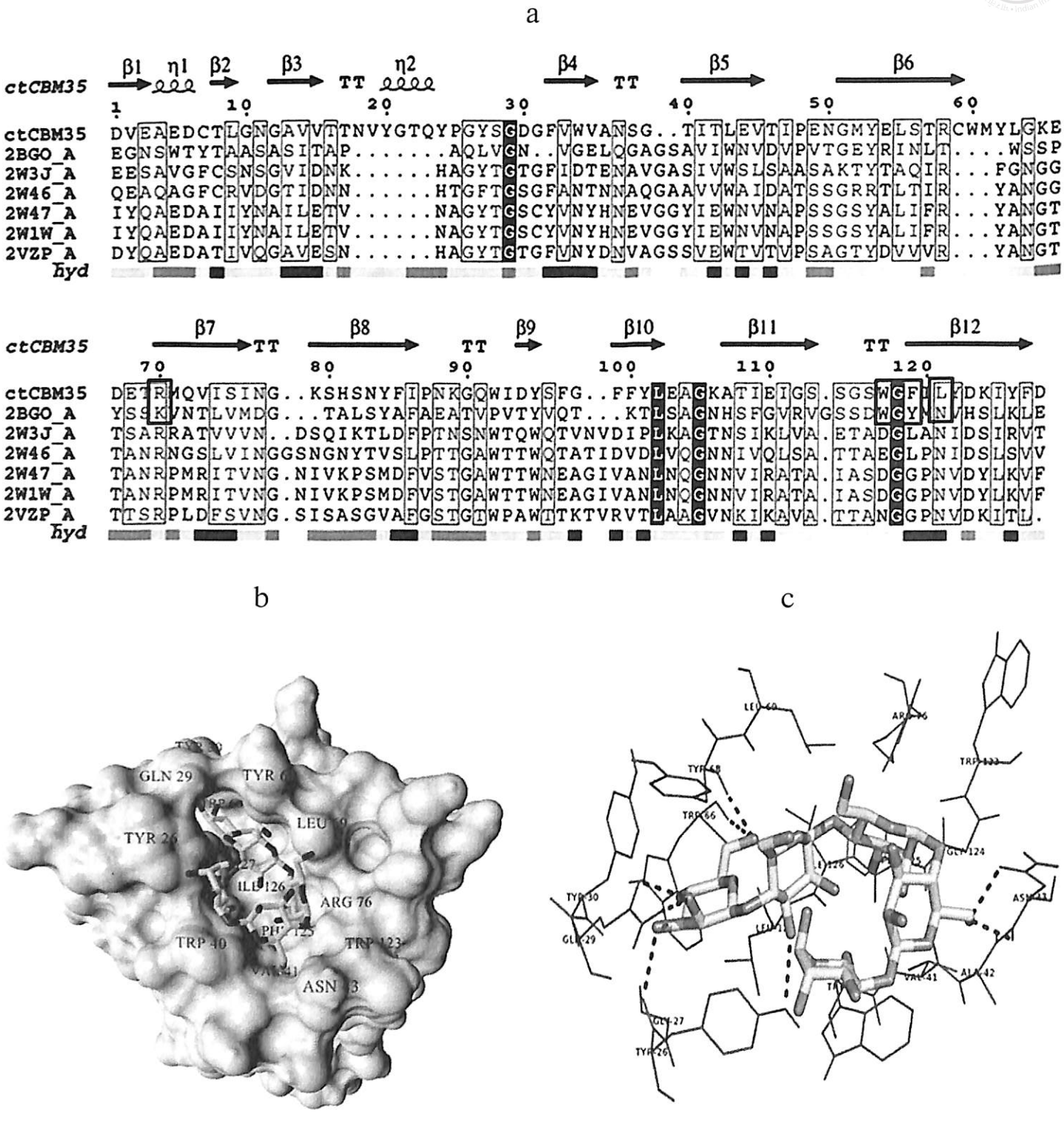

Fig. 6. a) Multiple sequence alignment of CBM35 family members having different substrate specificity with their respective PDB:IDs of *Amycolatopsis orientalis* (2VZP), *Cellvibrio japonicus* Abf62 (2W46), uncultured bacterium from environmental isolate (2W3J), *Clostridium thermocellum* (2W1W), and *Cellvibrio japonicus* (2BGO) were aligned with *Ct*CBM35. The residues that are conserved and probably involved in substrate specificity and binding (Man-CBM35) are shown in rectangular boxes. The line below the sequence represents the relative hydrophobicity of the residues, dark gray for hydrophilic, black for hydrophobic, and light gray for intermediate. b) Model of binding site surface cavity with labeled residues forming a hydrophobic groove to accommodate mannopentaose. c) Best pose of docking of *Ct*CBM35 with mannopentaose bound conformation shows polar interaction (dashed line) and residues probably involve in hydrophobic interaction present within 4 Å.

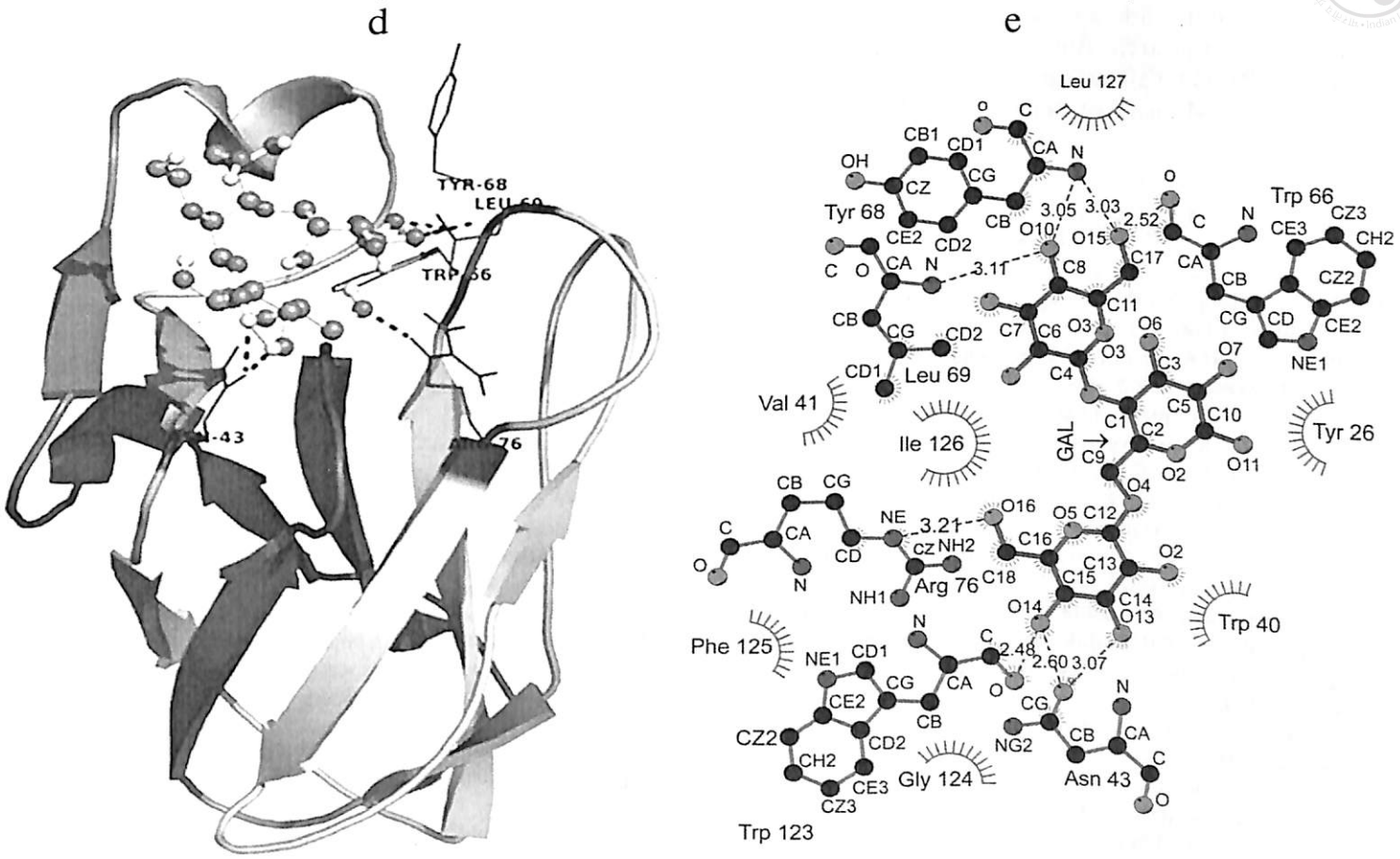

Fig. 6. d) Ribbon representation of *Ct*CBM35 using PyMOL complex with galactomannan (ball-stick view) shows position of substrate binding site (shown in circle). Residues making polar contact with galactomannan are positioned mainly in the loop region (shown by dashed lines). e) Schematic 2-D depiction of galactomannan (GAL) binding site residues of *Ct*CBM35. Dashed lines show hydrogen bonds, and connected atoms are shown with spokes radiating back. The amino acid residues displayed in the arc with spokes are involved in hydrophobic interactions.

tion with mannopentaose, while residues Tyr30, Trp40, Val41, Ala42, Met67, Trp123, Phe125, and Ile126 make a hydrophobic pocket around the binding site cavity (Figs. 6b and 6c). Mannotriose showed higher binding affinity for *Ct*CBM35, $K_a = 3.0 \cdot 10^5$ M^{-1} as compared to galactomannan, $K_a = 1.22 \cdot 10^5$ M^{-1} (Table 2). The free energy of binding (ΔG) of mannotriose was maximum (−6.8 kcal/mole), followed by galactomannan (−6.0 kcal/mole) (Table 1), while mannohexose displayed positive free binding energy on docking with *Ct*CBM35 (data not shown). This is possibly due to the size of the binding site pocket, which is not large enough to accommodate bulkier mannohexose as compared to mannotriose. The putative protein–ligand binding site shown by CBMs having β-sandwich fold is mainly situated on either concave surface made by the antiparallel β-sheets or at the top cavity made by the loop that connects the two β-sheets [36]. Analysis of binding site topography of the *Ct*CBM35 showed that it is made up by the amino acid residues present in loops connecting antiparallel β-sheets (Fig. 6d). The first loop started from Ser120 to Phe125 (between the 11-12 β-strand) making a base of the cavity, creating a flat hydrophobic platform involving two conserved aromatic amino acids Trp123 and Phe125. The second loop started from Cys65 to Arg76 (the 6-7 β-strand), and third loop from Val21 to Tyr33 (the 3-4 β-sheets) formed the side surface of the cavity and provided the solvent accessible surface for the ligands (Fig. 6d). Here, amino acid residues Trp66, Tyr68, Leu69, and Arg76 (from the loop second) and Tyr26 and Glu29 (from the loop third) were also present and made polar contact with the ligand molecule (Fig. 6e).

Therefore, the functional and structural elucidation of mannan specific *Ct*CBM35 from *C. thermocellum* may be useful to enhance activity by appending to a mannanase for higher degree of hydrolysis of complex manno-configured polysaccharides into simple sugars. Moreover, these findings might lead to understanding mannan-specific CBM35 from *C. thermocellum*, which may play a role in prebiotic oligosaccharide production in conjunction with mannanase from mannan rich polysaccharides.

The research work was supported in part by the Cutting-Edge Research Enhancement and Scientific Training (CREST) Fellowship from the Department of Biotechnology, Ministry of Science and Technology, to Arun Goyal.

REFERENCES

1. Cai, S., Zheng, X., and Dong, X. (2011) CBM3d, a novel subfamily of family 3 carbohydrate-binding modules identified in Cel48A exoglucanase of *Cellulosilyticum ruminicola*, *J. Bacteriol.*, **193**, 5199-5206.
2. Taylor, E. J., Goyal, A., Guerreiro, C. I. P. D., Prates, J. A., Money, V. A., Ferry, N., Morland, C., Planas, A., Macdonald, J. A., Stick, R. V., Gilbert, H. J., Fontes, C. M., and Davies, G. J. (2005) How family 26 glycoside hydrolases orchestrate catalysis on different polysaccharides: structure and activity of a *Clostridium thermocellum* lichenase, CtLic26A, *J. Biol. Chem.*, **280**, 32761-32767.
3. Sunna, A. (2010) Modular organization and functional analysis of dissected modular β-mannanase CsMan26 from *Caldicellulo siruptor* Rt8B.4, *Appl. Microbiol. Biotechnol.*, **86**, 189-200.
4. Bolam, D. N., Xie, H., Pell, G., Hogg, D., Galbraith, G., Henrissat, B., and Gilbert, H. J. (2004) X4 modules represent a new family of carbohydrate-binding modules that display novel properties, *J. Biol. Chem.*, **279**, 22953-22963.
5. Valenzuela, S. V., Diaz, P., and Pastor, F. I. (2012) Modular glucuronoxylan-specific xylanase with a family CBM35 carbohydrate-binding module, *Appl. Environ. Microbiol.*, **78**, 3923-3931.
6. Ahmed, S., Saraf, T., and Goyal, A. (2009) Homology modeling of family 39 glycoside hydrolase from *Clostridium thermocellum*, *Curr. Trend. Biotechnol. Pharm.*, **3**, 210-218.
7. Tunnicliffe, R. B., Bolam, D. N., Pell, G., Gilbert, H. J., and Williamson, M. P. (2005) Structure of a mannan-specific family 35 carbohydrate-binding module: evidence for significant conformational changes upon ligand binding, *J. Mol. Biol.*, **347**, 287-296.
8. Johansson, R., Gunnarsson, L. C., Ohlin, M., and Ohlson, S. (2006) Thermostable carbohydrate-binding modules in affinity chromatography, *J. Mol. Recognit.*, **19**, 275-281.
9. Abbott, D. W., and Boraston, A. B. (2012) Quantitative approaches to the analysis of carbohydrate-binding module function, *Methods Enzymol.*, **510**, 211-231.
10. Correia, M. A., Abbott, D. W., Gloster, T. M., Fernandes, V. O., Prates, J. A., Montanier, C., Dumon, C., Williamson, M. P., Tunnicliffe, R. B., Liu, Z., Flint, J. E., Davies, G. J., Henrissat, B., Coutinho, P. M., Fontes, C. M. G. A., and Gilbert, H. J. (2010) Signature active site architectures illuminate the molecular basis for ligand specificity in family 35 carbohydrate binding module, *Biochemistry*, **49**, 6193-6205.
11. Montanier, C., van Bueren, A. L., Dumon, C., Flint, J. E., Correia, M. A., Prates, J. A., Firbank, S. J., Lewis, R. J., Grondin, G. G., Ghinet, M. G., Gloster, T. M., Herve, C., Knox, J. P., Talbot, B. G., Turkenburg, J. P., Kerovuo, J., Brzezinski, R., Fontes, C M., Davies, G. J., Boraston, A. B., and Gilbert, H. J. (2009) Evidence that family 35 carbohydrate binding modules display conserved specificity but divergent function, *Proc. Natl. Acad. Sci.* 3065-3070.
12. Ghosh, A., Luis, A. S., Bras, J. L. A., Pathaw, N., Chrungoo, N. K., Fontes, C. M. G. A., and Goyal, A. (2013) Deciphering ligand specificity of a *Clostridium thermocellum* family 35 carbohydrate binding module (*Ct*CBM35) for gluco- and galacto-substituted mannans and its calcium induced stability, *Plos One*, **8**, e80415.
13. Kelly, S. M., Jess, T. J., and Price, N. C. (2005) How to study proteins by circular dichroism, *Biochim. Biophys. Acta*, **1751**, 119-139.
14. Andrade, M. A., Chacon, P., Merelo, J. J., and Moran, F. (1993) Evaluation of secondary structure of proteins from UV circular dichroism spectra using an unsupervised learning neural network, *Protein Eng.*, **6**, 383-390.
15. Takeo, K. (1984) Affinity electrophoresis: principles and applications, *Electrophoresis*, **5**, 187-195.
16. Bradford, M. M. (1976) Rapid and sensitive method for the quantitation of microgram quantities of protein utilizing the principle of protein–dye binding, *Anal. Biochem.*, **72**, 248-254.
17. Gilkes, N. R., Eric, J. S., Henrissat, B., Tekant, B., Miller, R. C., Jr., Warren, R. A., and Kilburn, D. G. (1992) The adsorption of a bacterial cellulase and its two isolated domains to crystalline cellulose, *J. Biol. Chem.*, **267**, 6743-6749.
18. Royer, C. A. (2006) Probing protein folding and conformational transitions with fluorescence, *Chem. Rev.*, **106**, 1769-1784.
19. Belatik, A., Hotchandani, S., Carpentier, R., and Tajmir-Riahi, H. A. (2012) Locating the binding sites of Pb (II) ion with human and bovine serum albumins, *Plos One*, **7**, 1-9.
20. Ahmad, F., Yadav, S., and Taneja, S. (1992) Determining stability of proteins from guanidinium chloride transition curves, *Biochem. J.*, **287**, 481-485.
21. Krieger, E., Joo, K., Lee, J., Raman, S., Thompson, J., Tyka, M., Baker, D., and Karplus, K. (2009) Homology modeling in YASARA, *Proteins*, **77**, 114-122.
22. Thompson, J. D., Higgins, D. G., and Gibson, T. J. (1994) ClustalW: improving the sensitivity of progressive multiple sequence alignment through sequence weighting, position-specific gap penalties and weight matrix choice, *Nucleic Acids Res.*, **22**, 4673-4680.
23. O'Boyle, N. M., Banck, M., James, C. A., Morley, C., Vandermeersch, T., and Hutchison, G. R (2011) Open babel: an open chemical toolbox, *J. Chem. Inf. Model*, **3**, 1-14.
24. Morris, G. M., Goodsell, D. S., Halliday, R. S., Huey, R., Hart, W. E., Belew, R. K., and Carlson, A. J. (1998) Automated docking using a Lamarckian genetic algorithm and an empirical binding free energy function, *J. Comput. Chem.*, **19**, 1639-1662.
25. Mizutani, K., Fernandes, V. O., Karita, S., Luis, A. S., Sakka, M., Kimura, T., Jackson, A., Zhang, X., Fontes, C. M., Gilbert, H. J., and Sakka, K. (2012) Influence of a mannan binding family 32 carbohydrate binding module on the activity of the appended mannanase, *Appl. Environ. Microbiol.*, **78**, 4781-4787.
26. Montanier, C., van Bueren, A. L., Dumon, C., Flint, J. E., Correia, M. A., Prates, J. A., Firbank, S. J., Lewis, R. J., Grondin, G. G., Ghinet, M. G., Gloster, T. M., Herve, C., Knox, J. P., Talbot, B. G., Turkenburg, J. P., Kerovuo, J., Brzezinski, R., Fontes, C. M., Davies, G. J., Boraston, A.

B., and Gilbert, H. J. (2009) Evidence that family 35 carbohydrate binding modules display conserved specificity but divergent function, *Proc. Natl. Acad. Sci. USA*, **106**, 3065-3070.
27. Din, N., Damude, H. G., Gilkes, N. R., Miller, R. C., Jr., Warren, R. A., and Kilburn, D. G. (1994) C1-Cx revisited: intramolecular synergism in a cellulose, *Proc. Natl. Acad. Sci. USA*, **91**, 11383-11387.
28. Din, N., Gilkes, N. R., Tekant, B., Miller, R. C., Jr., Warren, R. A. J., and Kilburn, D. G. (1991) Non-hydrolytic disruption of cellulose fibers by the binding domain of a bacterial cellulase, *Nat. Biotechnol.*, **9**, 1096-1099.
29. Mohan, S., Thambi Dorai, D., Srimal, S., Bachhawat, B. K., and Das, M. K. (1983) Fluorescence studies on the interaction of some ligands with carcinoscorpin, the sialic acid specific lectin, from the horseshoe crab, *Carcinoscorpius rotundacauda*, *J. Biosci.*, **5**, 155-162.
30. Christova, P., Todorova, K., Timtcheva, I., Nacheva, G., Karshikoff, A., and Nikolov, P. (2003) Fluorescence studies on denaturation and stability of recombinant human interferon-gamma, *Z. Naturforsch. C*, **58**, 288-294.
31. Pace, N. C., Shirley B. A., and Thomson, J. A. (1989) in *Protein Structure: a Particular Approach* (Creighton, T. E., ed.) IRL Press, Oxford, pp. 311-329.
32. Pinheiro, B. A., Proctor, M. R., Martinez-Fl[illegible] Prates, J. A. M., Money, V. A., Davies, G. J., Bayer, E. A., Fontesm, C. M., Fierobe, H. P., and Gilbert, H. J. (2008) The *Clostridium cellulolyticum* dockerin displays a dual binding mode for its cohesin partner, *J. Biol. Chem.*, **283**, 18422-18430.
33. Colovos, C., and Yeates, T. O. (1993) Verification of protein structures: patterns of nonbonded atomic interactions, *Prot. Sci.*, **2**, 1511-1519.
34. Carvalho, A. L., Goyal, A., Prates, J. A. M., Bolam, D. N., Gilbert, H. J., Pires, V. M. R., Ferreira, L. M. A., Planas, A., Romao, M. J., and Fontes, C. M. G. A. (2004) The family 11 carbohydrate-binding module of *Clostridium thermocellum* Lic26ACel5E accommodates β-1,4- and β-1,3-1,4-mixed linked glucans at a single binding site, *J. Biol. Chem.*, **279**, 34785-34793.
35. Bowie, J. U., Luthy, R., and Eisenberg, D. (1991) A method to identify protein sequences that fold into a known three-dimensional structure, *Science*, **5019**, 164-170.
36. Fanutti, C., Ponyi, T., Black, G. W., Hazlewood, G. P., and Gilbert, H. J. (1995) The conserved noncatalytic 40-residue sequence in cellulases and hemicellulases from anaerobic fungi functions as a protein docking domain, *J. Biol. Chem.*, **270**, 29314-29322.

OPEN ACCESS Freely available online

Deciphering Ligand Specificity of a *Clostridium thermocellum* Family 35 Carbohydrate Binding Module (*Ct*CBM35) for Gluco- and Galacto- Substituted Mannans and Its Calcium Induced Stability

Arabinda Ghosh[1], Ana Sofia Luís[2], Joana L. A. Brás[2], Neeta Pathaw[3], Nikhil K. Chrungoo[3], Carlos M. G. A. Fontes[2], Arun Goyal[1]*

1 Department of Biotechnology, Indian Institute of Technology Guwahati, Guwahati, Assam, India, **2** CIISA-Faculdade de Medicina Veterinaria, Avenida da Universidade Técnica, Lisbon, Portugal, **3** North Eastern Hill University, Shillong, Meghalaya, India

Abstract

This study investigated the role of CBM35 from *Clostridium thermocellum* (*Ct*CBM35) in polysaccharide recognition. *Ct*CBM35 was cloned into pET28a (+) vector with an engineered His_6 tag and expressed in *Escherichia coli* BL21 (DE3) cells. A homogenous 15 kDa protein was purified by immobilized metal ion chromatography (IMAC). Ligand binding analysis of *Ct*CBM35 was carried out by affinity electrophoresis using various soluble ligands. *Ct*CBM35 showed a manno-configured ligand specific binding displaying significant association with konjac glucomannan ($K_a = 14.3 \times 10^4\ M^{-1}$), carob galactomannan ($K_a = 12.4 \times 10^4\ M^{-1}$) and negligible association ($K_a = 12\ \mu M^{-1}$) with insoluble mannan. Binding of *Ct*CBM35 with polysaccharides which was calcium dependent exhibited two fold higher association in presence of 10 mM Ca^{2+} ion with konjac glucomannan ($K_a = 41 \times 10^4\ M^{-1}$) and carob galactomannan ($K_a = 30 \times 10^4\ M^{-1}$). The polysaccharide binding was further investigated by fluorescence spectrophotometric studies. On binding with carob galactomannan and konjac glucomannan the conformation of *Ct*CBM35 changed significantly with regular 21 nm peak shifts towards lower quantum yield. The degree of association (K_a) with konjac glucomannan and carob galactomannan, $14.3 \times 10^4\ M^{-1}$ and $11.4 \times 10^4\ M^{-1}$, respectively, corroborated the findings from affinity electrophoresis. The association of *Ct*CBM35with konjac glucomannan led to higher free energy of binding (ΔG) -25 kJ $mole^{-1}$ as compared to carob galactomannan (ΔG) -22 kJ $mole^{-1}$. On binding *Ct*CBM35 with konjac glucomannan and carob galactomannan the hydrodynamic radius (R_H) as analysed by dynamic light scattering (DLS) study, increased to 8 nm and 6 nm, respectively, from 4.25 nm in absence of ligand. The presence of 10 mM Ca^{2+} ions imparted stiffer orientation of *Ct*CBM35 particles with increased R_H of 4.52 nm. Due to such stiffer orientation *Ct*CBM35 became more thermostable and its melting temperature was shifted to 70°C from initial 50°C.

Citation: Ghosh A, Luís AS, Brás JLA, Pathaw N, Chrungoo NK, et al. (2013) Deciphering Ligand Specificity of a *Clostridium thermocellum* Family 35 Carbohydrate Binding Module (*Ct*CBM35) for Gluco- and Galacto- Substituted Mannans and Its Calcium Induced Stability. PLoS ONE 8(12): e80415. doi:10.1371/journal.pone.0080415

Editor: Michael Massiah, George Washington University, United States of America

Received May 9, 2013; **Accepted** October 2, 2013; **Published** December 6, 2013

Funding: Mr. Arabinda Ghosh is supported by a scholarship from University Grants Commission (UGC), New Delhi, India. The funders had no role in study design, data collection and analysis, decision to publish, or preparation of the manuscript.

Competing Interests: The authors have declared that no competing interests exist.

* E-mail: arungoyl@iitg.ernet.in

Introduction

Hydrolytic enzymes and their enhanced polysaccharide specificity often improve by appended non catalytic carbohydrate binding module either at their N or C terminal ends. A major portion of plant carbohydrate reservoir is composed of hemicelluloses such as the polymer and oligomer of xylose, mannose, arabinose etc. apart from celluloses. Polysaccharide recognition, binding and enhanced catalysis of hydrolytic enzymes truly facilitates by non catalytic modular carbohydrate binding modules. Carbohydrate binding modules (CBMs) are classified into 67 distinguished families based on sequence similarity (http://www.cazy.org/Carbohydrate-Binding-Module). CBMs are found in the protein both as appended with hydrolytic enzymes such as cellulase, mannanase, xylanase, as non hydrolytic functions, as scaffoldings and as peptide with non catalytic functions with variety of hydrolytic enzyme complex (cellulosome) [1]. Family 35 carbohydrate binding module is often appended to glycoside hydrolase family 26 (GH26) and GH5 mannanases [2–4], xylanases (GH30) [5] which significantly alter the polysaccharide specificity for plant cell wall polysaccharides such as galactomannan, glucomannan, mannan and glucouronoxylan. Three dimensional structures of CBM35 family generally have the dominance of β-sheet secondary structures with a jelly roll topology [5]. CBM35 usually accommodates the polysaccharides utilizing a planer surface of aromatic side chains which interact with the flat chains of manno-configured carbohydrate residues. This form of conformation is known as type B module [5]. Polysaccharide binding significantly alters the conformation of CBM35 by changing the loop orientation containing amino acid residues which facilitate to create a suitable binding space for polysaccharide accommodation [6]. Since the binding specificity depends on the polysaccharide complexity and side chain interactions of

monosaccharide a variety of diverted binding may be observed. Thus the polysaccharide specificity varies due to chain substitution and orientation of monosaccharides [7]. In earlier study, it was attributed to role of divalent cations in alteration of the domain conformation of CBMs that enhance the higher polysaccharide specificity and thermostability [8]. Thermostability one of the major concern of most of the enzyme stability and activity during industrial process and thus this binding module may restore the potentialities of the hydrolytic enzymes. Moreover, carbohydrate binding modules are used in various analytical processes. Thermostable CBMs were explored to separate cello- and xylo-oligosaccharides based on their affinity towards these carbohydrates [9]. CBM microarray technique is more pronounced that replaced the conventional DNA microarray. This method is simple, effective and an alternative to various conventional microarray technologies [10]. Moreover, substantial rise in effective enzyme catalysis process may induce by this carbohydrate binding module will meet the requirement for carbohydrate fermentation to most demanding biofuel [11].

Our work is focused on the functional and conformational properties of CBM35 from *Clostridium thermocellum* ATCC 27405 (*Ct*CBM35) upon polysaccharide and cation binding. *Ct*CBM35 usually display the specificity towards manno-configured polysaccharides. Mannose has single stereochemical difference from glucose (at 2′-OH site) in the manno-configured polysaccharides which made it less rigid structural conformation. *Ct*BM35 has varying degree of affinity for lesser and higher galactose and glucose substituted polysaccharides. The affinity electrophoresis, fluorescence measurements and dynamic light scattering were employed to analyze both qualitative and quantitative binding of *Ct*BM35 with manno-configured polysaccharides. The structural variations of *Ct*BM35 due to Ca^{2+} ion binding and the alterations of domain conformations were described in this work.

Materials and Methods

Gene amplification and cloning of *Ct*CBM35

The open reading frame (ORF) of *Ct*CBM35 was amplified from the genomic DNA of *Clostridium thermocellum* ATCC 27405 using a forward primer containing *Nhe*I restriction site: CAC**GCTAGC**GCATATTCCCTTCCTG and a reverse primer with *Xho*I restriction site: CAC**CTCGAG**TTAAAGTTCATCCAAGCTG. The PCR conditions were followed as Mg^{2+} ions (2.5 mM), dNTPs (2 mM), primers (1.5 µM), 1.0 µl of Taq DNA polymerase (1 µl of 1Unit μl^{-1}) and 1 µl of genomic DNA of *C. thermocellum*. The PCR amplification cycles used were: denaturation at 94°C for 4 min followed by 30 cycles of denaturation at 94°C for 30 s, annealing at 55°C for 60 s and extension at 72°C for 2 min and final extension at 72°C for 10 min. The amplified products were run on 0.8% agarose gel and further purified by gel extraction (Qiagen kit.) The amplified products were then digested with *Nhe*I-*Xho*I restriction enzymes and cloned into *Nhe*I/*Xho*I restricted pET-28a (+) expression vectors containing kanamycin as resistant marker respectively which resulted in cloned plasmids (pCBM35). Thereafter, *E. coli* DH5α cells were transformed with above cloned plasmids. The transformed cells were grown on LB [12] agar plates supplemented with kanamycin (50 µg ml^{-1}) at 37°C for growth of recombinant clones. Positive clones were selected by restriction digestion analysis of the resulting cloned plasmids.

Protein expression and purification

E. coli BL-21(DE3) (Novagen) cells were used for expressing *Ct*CBM35 as described elsewhere [12]. *E. coli* BL-21 (DE3) cells were transformed with pCBM35. The cells were grown similarly as described in Section 2.1, with incubation at 37°C and shaking at 180 rpm till mid-exponential phase ($A600_{nm} \approx 0.6$). The cells were induced with 1.0 mM isopropyl-1-thio-β-D-galactopyranoside (IPTG) for hyper-expression of recombinant protein at optimized expression conditions of 24°C at 180 rpm for 16 h. The cells were harvested at 9,000 *g* and the resulting pellet was resuspended in Sodium phosphate buffer (50 mM, pH 7.0). Then the cells were sonicated (Vibra cell, Sonics) on ice for 16 min (9 s on/off pulse) with further centrifugation (19,000 g, 30 min, 4°C) to get the crude cell free protein in the supernatant. Hybrid protein containing *Ct*CBM35 appended by His_6 tag were purified in a single step by immobilized metal ion affinity chromatography (IMAC) using Ni-Sepharose columns (HiTrap Chelating, GE Healthcare) as recommended by the manufacturer. The purity and molecular mass of recombinant proteins were verified by SDS-PAGE [13].

Binding assay of family 35 Carbohydrate Binding Module (*Ct*CBM35)

The polysaccharide binding capability of the non-catalytic modules was determined by visualizing the adsorption to soluble polysaccharides using gel retardation in native polyacrylamide gel electrophoresis containing the polysaccharides as described earlier by Takeo, (1990) [14]. Purified *Ct*CBM35 (18 µg) was assayed with soluble polysaccharides such as carob galactomannan, konjac glucomannan, carboxymethyl cellulose, rye arabinoxylan, birchwood xylan, oatspelt xylan and glucouronoxylan. The polysaccharide samples were prepared subsequently by diluting in filtered water from (0.5%, w v^{-1}) polysaccharide stock. Native polyacrylamide gels (7.5%) were prepared containing varying polysaccharide concentrations ranging from 0.0 to 1.5 (%, w v^{-1}). Bovine serum albumin (BSA) sample (1.0 mg ml^{-1}) was run in native gel for non-specific binding interaction. Binding study of *Ct*CBM35 with carob galactomannan and konjac glucomannan was carried out in absence and presence of Ca^{2+} ions. 10 mM Ca^{2+} ion was incorporated in 7.5% native polyacrylamide gel before *Ct*CBM35 electrophoresis. In absence of Ca^{2+} ions 7.5% native gels were prepared as control and the relative mobilities of *Ct*CBM35 were calculated.

Binding analysis of *Ct*CBM35 with insoluble polysaccharides

The quantitative and qualitative assessment of *Ct*CBM35 binding was carried out with insoluble mannan, avicel and wheat arabinoxylan. Thirty microgram of *Ct*CBM35 in 50 mM sodium phosphate buffer, pH 7.0, was mixed with 1 mg of mannan in a final reaction volume of 200 µL. The reaction mixture was incubated for 2 h at 4°C with gentle shaking. After that the insoluble ligand was precipitated by centrifugation at 13000 *g* for 5 min. The supernatant, containing the unbound proteins, was removed and the pellet was washed three times with 200 µl of 50 mM sodium phosphate buffer pH 7.0. The bound protein from the washed pellet was eluted by boiling the polysaccharides in 200 µl of 10% (w v^{-1}) SDS containing 10% (v v^{-1}) β-mercaptoethanol for 10 min. The pellets of bound protein and the supernatant of unbound protein were analysed by 12% SDS-PAGE. A Bovine Serum Albumin (1 mg ml^{-1}) control was set in parallel to check for any non specific binding. All the gels containing protein and no polysaccharide and the electrophoresis were performed in parallel to ensure also that no precipitation of protein occurred. For quantitative analysis the free or unbound protein concentration in un-bound fraction obtained after centrifugation was determined by Bradford method [15] and the

bound protein was estimated by subtracting the free protein from the initial protein concentration. The adsorption parameters were calculated to determine the binding. If we consider [B] the bound protein concentration, [F] the unbound fraction of protein, [N] the number of binding site concentration and K_a is the association constant then at equilibrium adsorption were calculated as described earlier by Gilkes *et al* (1992) [16].

Polysaccharide binding study of *Ct*CBM35 by fluorescence spectroscopy

On binding to polysaccharides, carbohydrate binding modules undergo conformational changes and behave differently than in its unbound native form [17]. To compare the results with affinity electrophoresis, 160 µM of *Ct*CBM35 was incubated with polysaccharides *viz*., carob galactomannan and konjac glucomannan of varying concentrations. Polysaccharide concentrations (0.01%, 0.04%, 0.06%, 0.08%, 0.15% and 0.2%, w v^{-1}) from 0.5% (w v^{-1}) stock solution in 100 µl reaction mixture were prepared in 50 mM sodium phosphate buffer, pH 7.0. The samples were incubated at 4°C for 2 h. The fluorescence measurements were carried out using a fluorimeter (Fluoromax 3, Horiba Scientific, USA). Emission and excitation slits were kept at 3.00 and 1.00, respectively, with 0.5 s integration time. Three scans were taken per sample along with a control to reduce the noise created by buffer and polysaccharide. All the samples were excited at $\lambda_{max} = 295$ nm with observance of emission spectra between $\lambda_{max} = 320$–400 nm. The emission spectra of all the solutions were corrected against buffer and polysaccharide solution without *Ct*CBM35 before setting the interaction study. Relative fluorescence intensities (F_o/F, where F_o is initial fluorescence intensity of *Ct*CBM35 and F is final fluorescence intensity of polysaccharide *Ct*CBM35 conjugate) were plotted against polysaccharide concentration. The association constants $K_a(M^{-1})$ of *Ct*CBM35 complex with carob galactomannan and konjac glucomannan were derived using modified Stern Volmer equation [18] as follows

$$\log\left(\frac{F_0 - F}{F}\right) = \log K_a + n \times \log[Polysaccharide]$$

Study of size of *Ct*CBM35 on binding with polysaccharide and Ca^{2+} by dynamic light scattering

Polysaccharide binding greatly influences the protein conformational changes. These changes may lead to more dispersion in the dynamic environment leading to higher hydrodynamic area. The binding of polysaccharide with *Ct*CBM35 was studied by dynamic light scattering (DLS). In a dynamic environment, the particles of ligand and protein molecules diffuse randomly. DLS essentially measures fluctuation in scattered light intensity due to diffusion of particles, the diffusion coefficient of the particles can be determined. The diffusion coefficient D is then related to the radius R of the particles by means of the Stokes-Einstein Equation [19]:

$$D = \frac{kT}{6\pi R\eta}$$

where, k = Boltzmann-constant, T = temperature and η = viscosity.

The hydrodynamic diameters (R_H) of *Ct*CBM35 in presence of 0.1% (w/v) polysaccharides such as carob galactomannan and konjac glucomannan were measured by Zetasizer Nano ZS (Malvern, UK) spectrophotometer. Refractive index ai of 50 mM sodium phosphate buffer were adjusted to 1.3206 and 8.945×10^{-3} g (cm s)$^{-1}$, respectively by using SEDNTERP tool package (http://www.jphilo.mailway.com). The hydrodynamic radius of *Ct*CBM35 was also studied in presence and absence of 10 mM Ca^{2+} ions. *Ct*CBM35 was incubated at 25°C for 2 h and the extra unbound Ca^{2+} was removed by dialysis against water. The hydrodynamic radius of bound *Ct*CBM35 with Ca^{2+} conjugate was measured and compared against Ca^{2+} free *Ct*CBM35. The instrument was set to measure the absorbance at a fixed angle (θ = 90°). All the measurements were derived by deconvolution of intensity and sample autocorrelation function. Deconvolution of measured intensity was obtained using non negative least square analysis (NNLS) [19,20] algorithm e.g. CONTIN [21], Regularization and Multiple Narrow Mode algorithms [22,23]. These algorithms of fitting the data were included as inbuilt functions of Zetasizer Nano software package.

Protein melting and molecular dynamics study of *Ct*CBM35 in presence of Ca^{2+} ion

Binding assays with soluble polysaccharides showed that an increase in enzyme affinity could be attributed to the presence of family 35 carbohydrate binding module. To investigate whether the presence of Ca^{2+} ion may enhance the stability of *Ct*CBM35, the stabilizing effect was studied by UV spectroscopy. Protein melting curves were generated for recombinant *Ct*CBM35 (pH 7.0, sodium phosphate buffer) by measuring in UV-absorption spectrophotometer (Varian, Cary 100) at 280 nm following the method of Dvortsov *et al.* (2009) [24]. The temperature was varied from 40–100°C using the peltier temperature controller (Cary 100-Bio, Varian) and the solutions were kept at the particular temperature

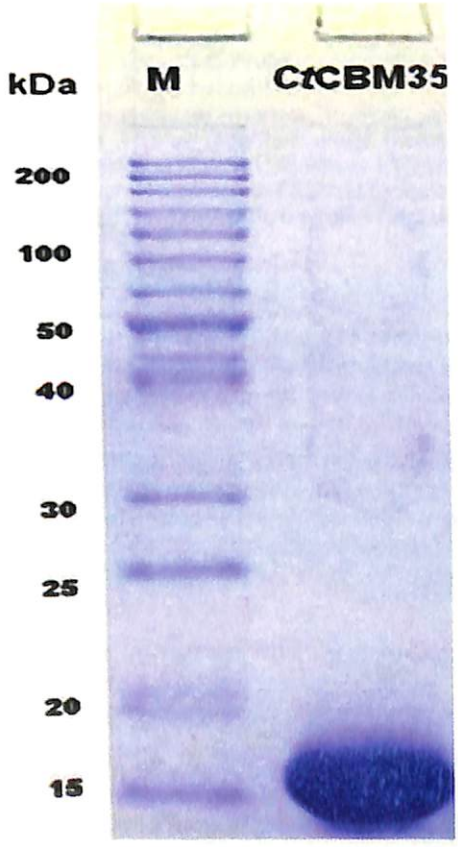

Figure 1. Denaturing SDS-PAGE (12%) of recombinant *Ct*CBM35 purified by IMAC.
doi:10.1371/journal.pone.0080415.g001

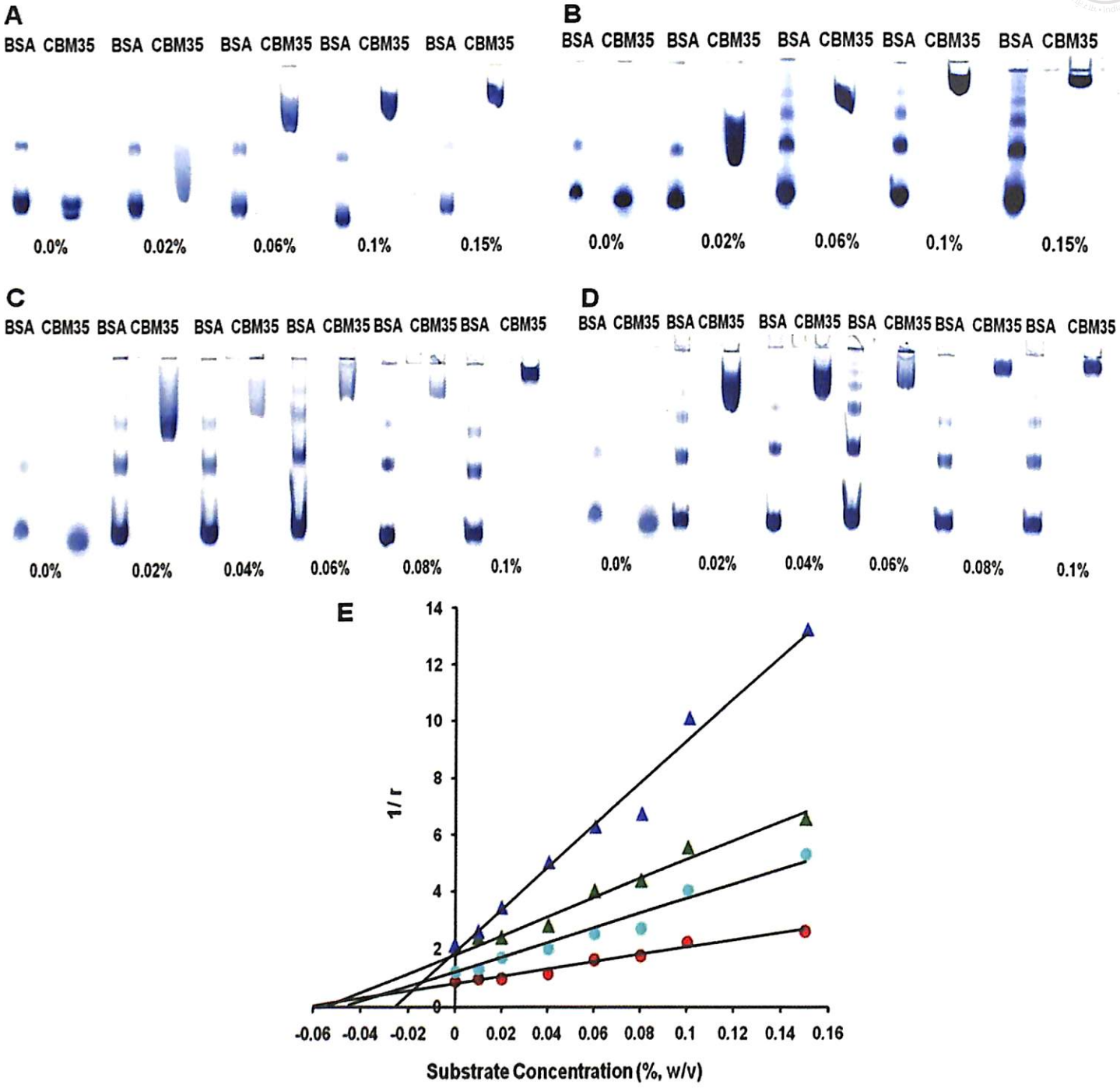

Figure 2. Affinity electrophoresis of *Ct*CBM35 using 7.5% native PAGE in presence of varying concentrations of (A) carob galactomannan (B) konjac glucomannan (C) 10 mM Ca^{2+} incorporated with carob galactomannan (D) 10 mM Ca^{2+} incorporated with konjac glucomannan (E) A non linear regression plot of inverse relative migration of *Ct*CBM35 (1/r) against polysaccharide concentration (%, w v^{-1}), (•) carob galactomannan (in red), (▲) konjac glucomannan (in green) and (•) in presence of 10 mM Ca^{2+} ion with carob galactomannan (in light blue), (▲) in presence of 10 mM Ca^{2+} ion with konjac glucomannan (in dark blue).
doi:10.1371/journal.pone.0080415.g002

Table 1. Association constants (K_a) and free energy of binding of *Ct*CBM35 from affinity electrophoresis and relative fluorescence intensities.

Polysaccharide	K_a from AE (10^4 M^{-1})	K_a from AE (10 mM Ca^{2+}) (10^4 M^{-1})	K_a from fluorescence (10^4 M^{-1})	Binding site (n)	Gibb's free energy (ΔG) (kJ $mole^{-1}$)
Carob galactomannan	12.4	30	11.4	0.79	−22.0
Konjac glucomannan	14.3	41	14.3	0.80	−25.0

AE: Affinity Electrophoresis.
doi:10.1371/journal.pone.0080415.t001

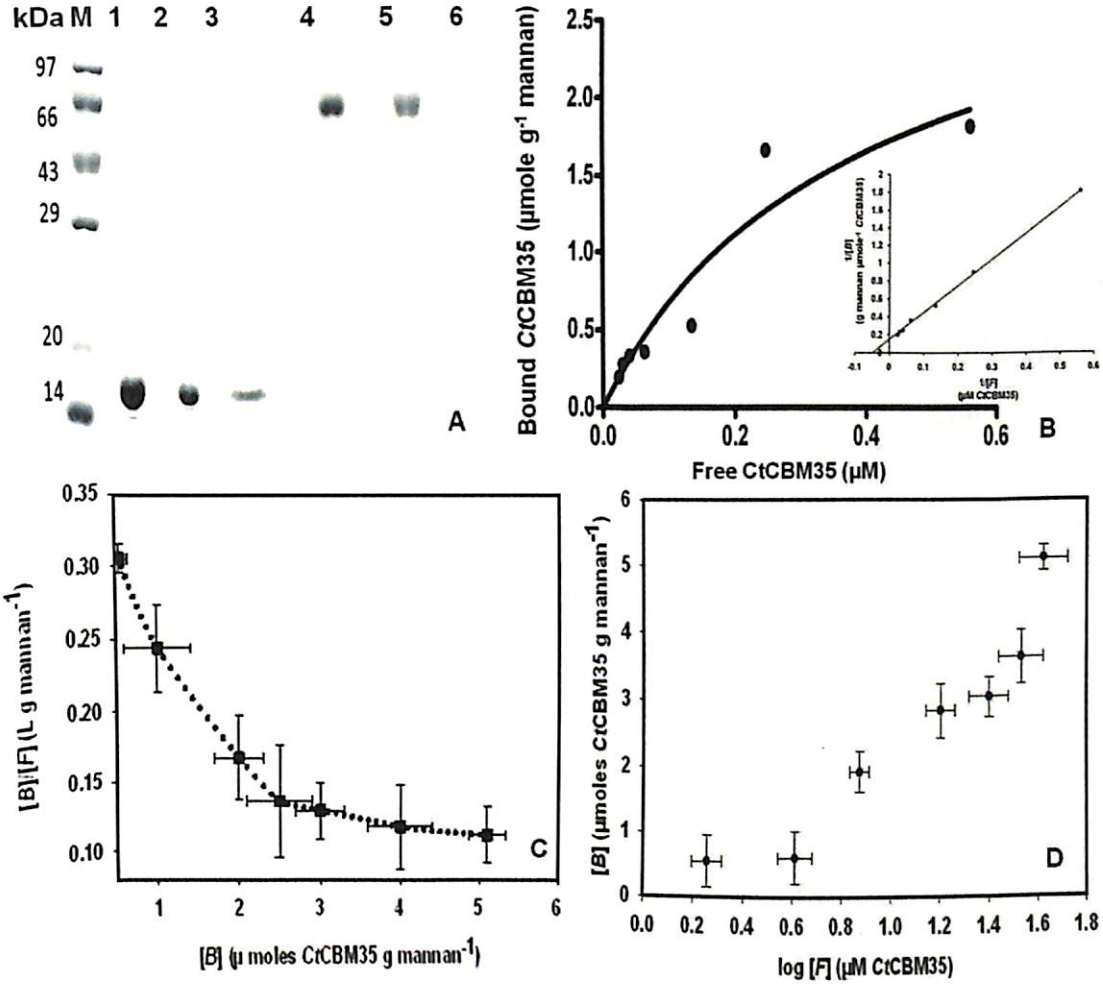

Figure 3. Qualitative binding of *Ct*CBM35 with insoluble mannan (A) using 12% SDS-PAGE. Lane 1: High range unstained molecular weight marker (200 kDa - 10 kDa), lane 2: Purified *Ct*CBM35, lane 3: unbound *Ct*CBM35, lane 4: bound *Ct*CBM35, lane 5: Bovine serum albumin (BSA) as control, lane 6: unbound BSA, lane 7: bound BSA. (B) Adsorption of *Ct*CBM35 to insoluble mannan. The main panel shows the equilibrium adsorption isotherm ([B] versus [F]) for *Ct*CBM35. Adsorption assay was done at 4°C, as described under methods section. Initial protein concentrations of *Ct*CBM35 were 0.2–19 µM. In the small panel showing a linear regression plot of 1/[B] versus 1/[F] concentrations to derive the association constant (K_a). (C) Scatchard plot of [B]/[F] vs [B]. The curved line was fitted to data points for *Ct*CBM35 by least square regression analysis. (D) a semi-logarithmic plot ([B] vs log [F]) for adsorption data of *Ct*CBM35. In both the plots the standard errors in two dimensions are indicated by vertical and horizontal bars.
doi:10.1371/journal.pone.0080415.g003

for sufficient time (10 min) to attain equilibrium. *Ct*CBM35 was incubated with 10 mM $CaCl_2$ at 25°C for 2 h and dialyzed against water to remove additional Ca^{2+} ion.

To investigate the role of Ca^{2+} ion in altering protein conformations a model of *Ct*CBM35 from *Clostridium thermocellum* was generated in presence of Ca^{2+} ion based on the crystal structure of closest homolog of CBM35 from *Amycolaptosis orientalis* (PDB ID: 2VZPA) by Modeller9v8 program. The homolog was identified using Blast PDB (http://www.ncbi.nlm.nih.gov/blast/Blast.cgi). The structure was energy minimized with GROMACS4.0.7 package (http://www.gromacs.org/) using steepest descent algorithm with GROMOS96 43a1 force field and simple point charge (SPC) water model [25–27]. Molecular dynamics (MD) simulation on the energy minimized *Ct*CBM35 model was carried out with the periodic boundary conditions applied in three dimensions to analyse the stability of the protein model. The net charge of system was neutralized by the addition of eleven sodium ions by replacing water molecules that are at least 3.50 Å from the protein surface [28]. The stable model was further visualized and analyzed in PyMOL tool.

Table 2. Binding parameters of *Ct*CBM35 on binding with insoluble mannan derived from adsorption isotherm analysis.

Polysaccharide	K_r (l g $^{-1}$)*	K_a (µM $^{-1}$)	N_o (µmole g $^{-1}$)*
Mannan	0.49±0.02	12	0.04±0.002

**values are mean ± SD (n = 3).*
doi:10.1371/journal.pone.0080415.t002

Results

Cloning, expression and purification of *Ct*CBM35

The ORF region encoding *Ct*CBM35 was amplified by polymerase chain reaction and successfully ligated to pET28a (+) expression vector and transformed *E. coli* DH5α cells. The colonies appeared in the LB plates supplemented with 50 µg ml^{-1} kanamycin were screened for positive clones by digestion with *Nhe* I and *Xho* I restriction enzymes. Few positive clones with an insert of 420 bp and a vector fragment of 5.4 kb were obtained in

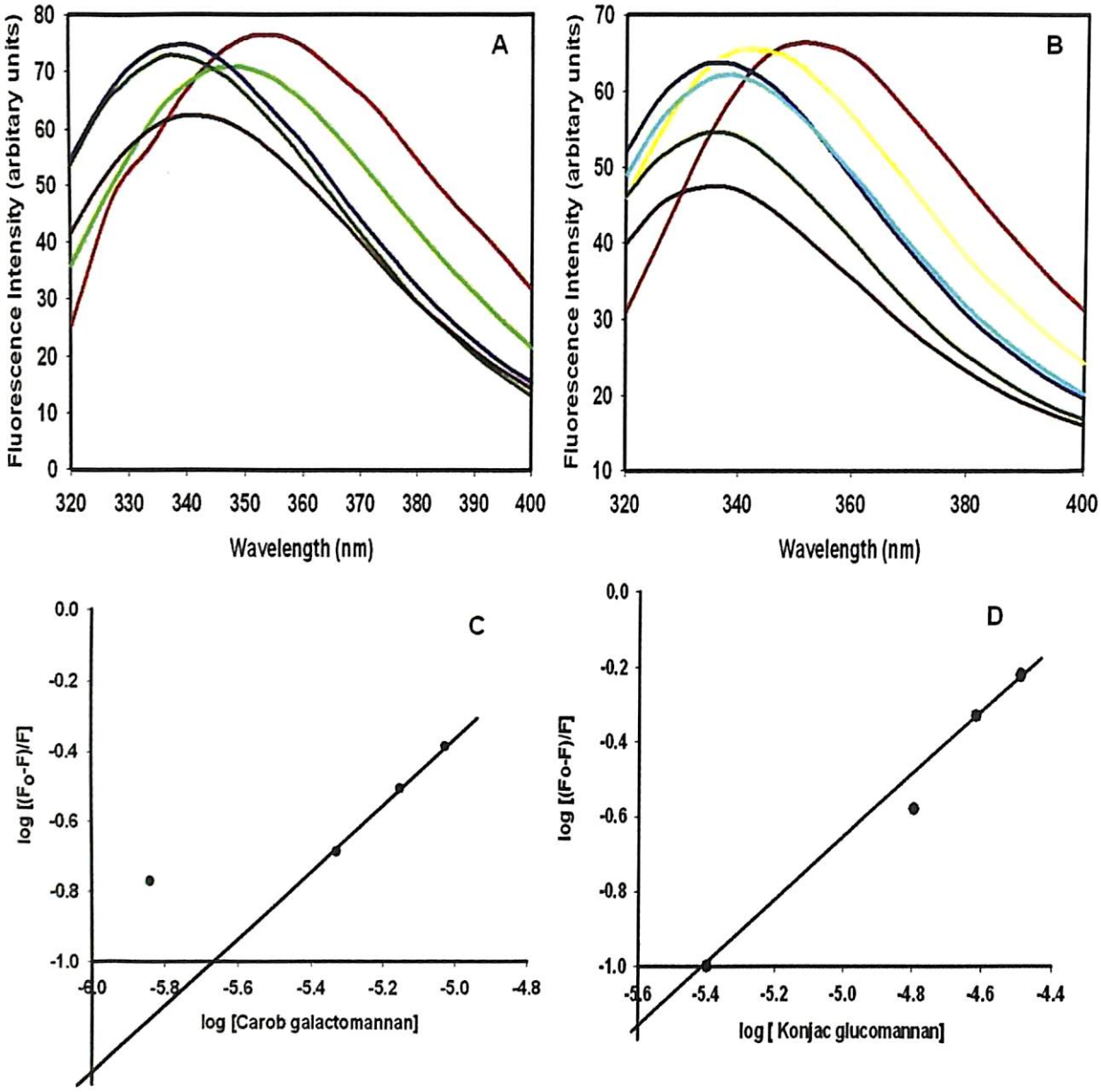

Figure 4. Tryptoptophan fluorescence emission spectrum of *Ct*CBM35 in presence of (A) carob galactomannan (%, w/v), represented in lines: (red) without polysaccharide, (in green) 0.01, (light blue) 0.04, (dark green) 0.06, (dark red) 0.08. (B) konjac glucomannan (red) without polysaccharide, (yellow) 0.01, (deep blue) 0.04, (light blue) 0.06, (dark green) 0.08, (dark red) 0.1. (C) Hill plot of log $[(F_o-F)/F]$ vs log [carob galactomannan] (D) Hill plot of $\log\left(\frac{F_0-F}{F}\right)$ vs log [konjac glucomannan] used to derive association constant (K_a).
doi:10.1371/journal.pone.0080415.g004

1% agarose gel electrophoresis. The transformed *E. coli* BL21 (DE3) cells by recombinant plasmids of positive clones after IPTG induction were screened for expression. The expression of *Ct*CBM35 (15 kDa protein) band was observed on 12% SDS-PAGE by comparing with long range (10–200 kDa) prestained molecular weight marker (Fermentas). The recombinant *Ct*CBM35 was purified by Ni^{2+}-NTA (Immobilized metal ion chromatography) and the elution was accomplished with 300 mM Imidazole. A purified homogenous single band 15 kDa of *Ct*CBM35 appeared on 12% SDS-PAGE (Figure 1).

Binding assay of *Ct*CBM35 with soluble polysaccharides

To investigate the ligand binding specificity of *Ct*CBM35 the protein was expressed and purified to electrophoretic homogeneity. The affinity of *Ct*CBM35 for carob galactomannan, konjac glucomannan, rye-arabinoxylan, oat spelt xylan and lichenan was determined by affinity electrophoresis [14]. The relative mobilities of *Ct*CBM35 in presence of various soluble polysaccharides were calculated against a reference with no ligand in the affinity gel (Figure 2A & 2B). A non linear regression plot was generated between relative migration of *Ct*CBM35 against varying concentrations of ligand to calculate the association constant (K_a) (Figure 2E). The *Ct*CBM35 displayed higher binding affinity with konjac glucomannan as compared to carob galactomannan. The association constants (K_a) were found to be 14.3×10^4 M^{-1} with konjac glucomannan and 12.4×10^4 M^{-1} with carob galactomannan. No association of *Ct*CBM35 was seen with carboxymethyl cellulose, rye arabinoxylan, birchwood xylan, oatspelt xylan, glucouronoxylan (Table 1). To assess the Ca^{2+} induced affinity binding of *Ct*CBM35 with polysaccharides at their varying concentrations a similar approach was carried out by affinity electrophoresis as described earlier (Takeo et al., 1990) [14]. In

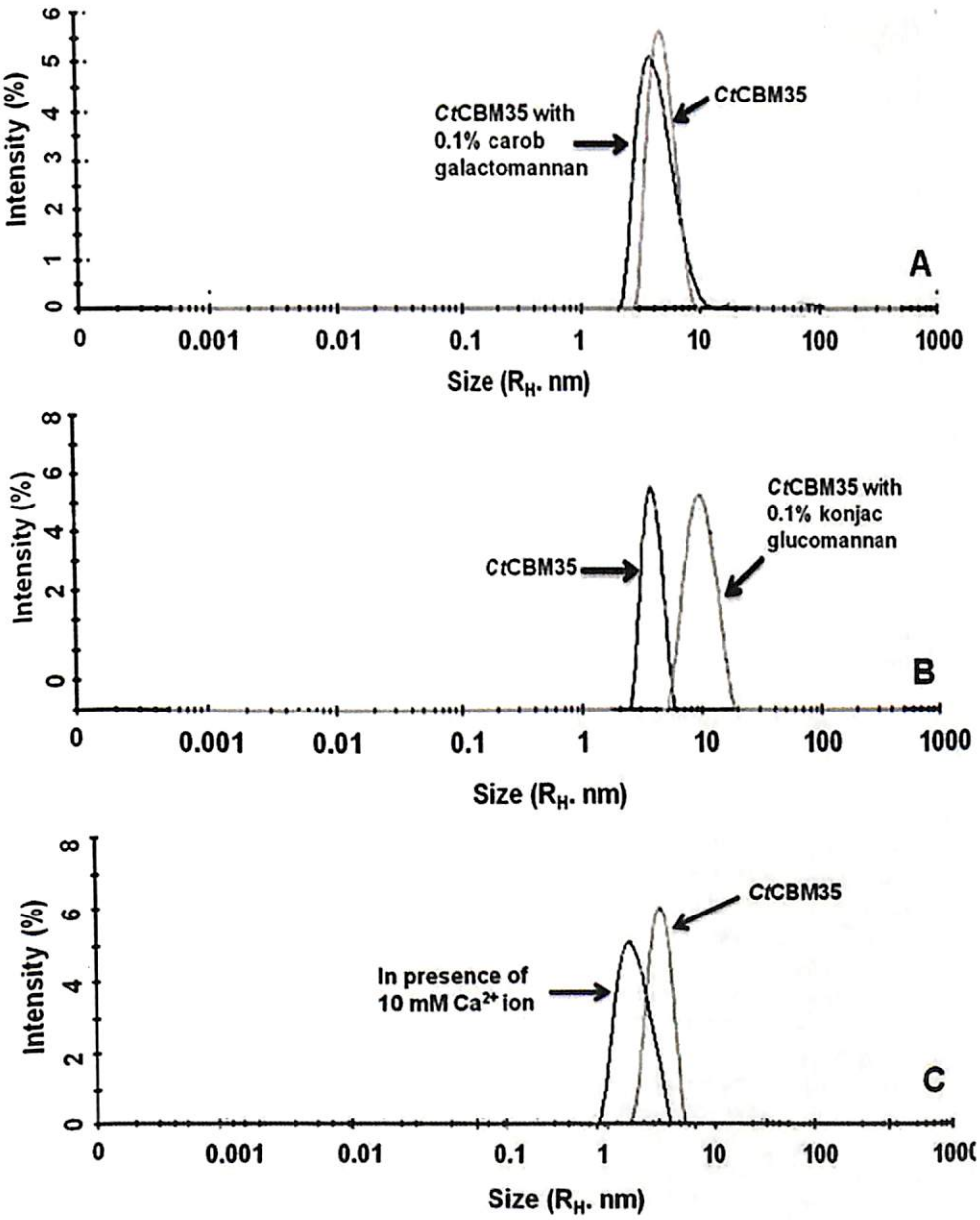

Figure 5. Dynamic light scattering of *Ct*CBM35 in conjugation with 0.1% (w/v) (A) carob galactomannan, (B) konjac glucomannan and (C) 10 mM Ca^{2+} ion.
doi:10.1371/journal.pone.0080415.g005

presence of 10 mM Ca^{2+} ion the affinity of *Ct*CBM35 for carob galactomannan was increased to approximately 2.5 folds and the association constant (K_a) was obtained as 30×10^4 M^{-1} and with konjac glucomannan 41×10^4 M^{-1} (Table 1) (Figure 2C, 2D and 2E).

Binding analysis of *Ct*CBM35 with insoluble polysaccharides

The quantitative and qualitative binding of *Ct*CBM35 with insoluble polysaccharides was assessed by adsorption isotherm analysis. *Ct*CBM35 displayed low binding with insoluble mannan as analysed by SDS-PAGE when compared with the protein in free (unbound to mannan) form and the total purified protein (Figure 3A). *Ct*CBM35 displayed no binding with avicel and wheat arabinoxylan. The saturation of insoluble mannan binding by *Ct*CBM35 was achieved approached but not to the highest protein concentration used (Figure 3B). The failure to reach saturation was detected when the same data was plotted in a semi logarithmic graph between ([B] vs log [F]). Scatchard plot of *Ct*CBM35 (Figure 3C and Figure 3D) indicated the complex binding with insoluble mannan. In this quantitative binding assessment at equilibrium the association constant (K_a) of *Ct*CBM35 with insoluble mannan was 12 μM^{-1} (Table 2). The relative equilibrium association constant K_r and the concentration of binding sites in mannan surface [N_o] were calculated from a non linear regression plot between bound *Ct*CBM35 versus free *Ct*CBM35. The data were analyzed by GraphPad (Prism 2.0.1) software using non-linear regression analysis based on one binding site equation. The estimated values of relative equilibrium constant K_r and concentration of binding sites [N_o] were 0.49 ± 0.2 l g^{-1} and 0.04 ± 0.002 µmole g^{-1}, respectively (Table 2). This result suggested that *Ct*CBM35 bind to insoluble mannan less effectively as the protein binding site on the polysaccharide was less. This may be due to binding of protein to the non reducing end of the polysaccharide.

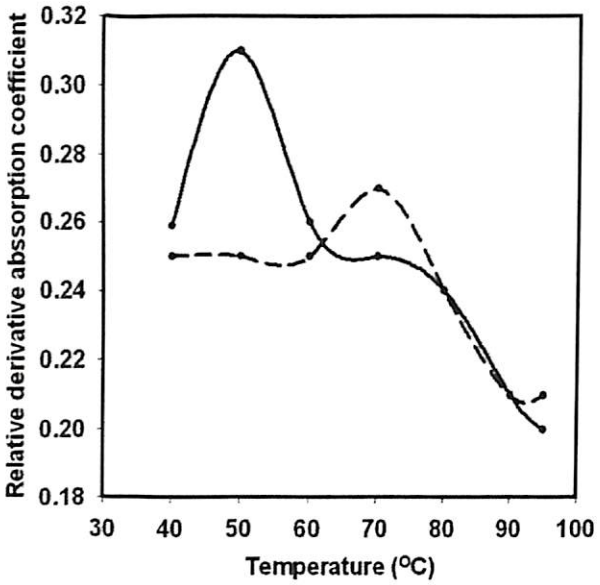

Figure 6. Protein melting curve of *Ct*CBM35 (—) in absence of 10 mM Ca^{2+} ion, (— —) in presence of 10 mM Ca^{2+} ion.
doi:10.1371/journal.pone.0080415.g006

Polysaccharide binding study of *Ct*CBM35 by fluorescence spectroscopy

Among the three aromatic amino acids tryptophan shows highest quantum yield and better stability facilitates its presence to utilize as a probe for fluorescence detection during polysaccharide binding with protein [17]. In presence of polysaccharides such as carob galactomannan and konjac glucomannan with their varying concentration from 0.01%–0.08% (w/v) significant blue shifts were observed. Binding of carob galactomannan and konjac glucomannan with *Ct*CBM35 displayed 21 nm peak shifts towards shorter wavelength of tryptophan emission spectra from λ_{max} 350 nm to 329 nm (Figure 4A and Figure 4B). The association constant (K_a) of *Ct*CBM35 with carob galactomannan and konjac glucomannan were derived from Hill plot (Figure 4C and Figure 4D). From Hill plot and relative fluorescence intensities the values of K_a with carob galactomannan was found to be 11.4×10^4 M^{-1} and with konjac glucomannan 14.3×10^4 M^{-1} (Table 1). It was found that the K_a values approximately similar as derived earlier from affinity electrophoresis. Therefore, the fluorescence studies of polysaccharide binding of *Ct*CBM35 confirmed the results of affinity electrophoresis. The number of binding site concentrations (n) were derived from Stern Volmer equation and with carob galactomannan n = 0.79 and whereas with konjac glucomannan n = 0.80 (Table 1). It means both the polysaccharide has single binding site for *Ct*CBM35. Since *Ct*CBM35 displayed significant affinities for mannose derived polysaccharide in combination of galactose and glucose in their side and main chains, form the derived affinity constants the Gibb's free energy of binding were calculated using the equation:

$$\Delta G = -RTlnK_a$$

where, ΔG = Gibb's free energy, R = gas constant (Joule K^{-1} $mole^{-1}$), T = Temperature in Kelvin, K_a = association constant (M^{-1}). The free energy binding of *Ct*CBM35 with carob galactomannan was −22.0 kJ $mole^{-1}$ and with konjac glucomannan −25.0 kJ $mole^{-1}$ (Table 1). The higher binding affinity and free energy of binding suggested that likely due to the simple molecular architecture of konjac glucomannan made an easy platform for *Ct*CBM35 than carob galactomannan, although both the polysaccharides have similar number of binding sites.

Study of size of *Ct*CBM35 on binding with polysaccharide and Ca^{2+} by DLS

Polysaccharides binding greatly influence the alterations in the dynamic environment of a protein. As measured from dynamic light scattering (DLS) the hydrodynamic radius (R_H) of *Ct*CBM35 was found to be 4.25 nm which was in the acceptable range as this value is higher than theoretical R_H, 2 nm for a 15 kDa protein. The R_H augmentation of *Ct*CBM35 was seen in presence of 0.1% (w v^{-1}) carob galactomannan from 4.25 nm to 6 nm (Figure 5 A). In contrast, konjac glucomannan binding (0.1%, w v^{-1}) exhibited much broader R_H of 8 nm (Figure 5 B). The augmentation of size was due to strong binding with konjac glucomannan leading to a stiffer structure and low random diffusion of the particles of protein and polysaccharides in the dynamic environment. Random diffusion of the particles measured in terms of random diffusion coefficient and is inversely proportional to R_H. In presence of 10 mM Ca^{2+} ion, the hydrodynamic radius of *Ct*CBM35 was changed remarkably from 4.25 nm in absence of Ca^{2+} ion to 4.52 nm (Figure 5 C). In this case Ca^{2+} ion might bind with the amino acid residues of *Ct*CBM35 and imparted a stiffer orientation than the usual. Therefore, random diffusion of the system reduced and as a result the dynamic radius of *Ct*CBM35-Ca^{2+} complex was increased.

Protein melting and molecular dynamics study of *Ct*CBM35 in presence of Ca^{2+} ion

Melting of *Ct*CBM35 was studied in presence of additive Ca^{2+} ion to investigate the protein stability which perhaps, play a major role in polysaccharide recognition at higher temperature and improve the catalytic properties of catalytic modules. The melting of *Ct*CBM35 at λ_{max} 280 nm showed an unfolded peak at 50°C (Figure 6). In the presence of 10 mM $CaCl_2$ as additive, the melting point of *Ct*CBM35 was shifted towards higher temperature at 70°C and the low melting peak at 50°C disappeared completely (Figure 6). Thus, Ca^{2+} ion played a key role in providing better stability of *Ct*CBM35 at higher melting temperature as compared to lack of additive. This analysis was further analyzed using PyMOL tool from the generated model of *Ct*CBM35. There was one Ca^{2+} ion binding pocket interacting with 7 amino acid residues *viz*. Glu 9, Glu 11, Ser 34, Gly 37, Asp 129. It was observed that negatively charged residues were predominant except Ser and Gly which interacted strongly with positively charged Ca^{2+} ions. These amino acid residues made coordinate bonds with Ca^{2+} ion and their orientation was changed remarkably. The comparative study of two *Ct*CBM35 models with unbound and bound Ca^{2+} ion (Figure 7 A and 7 B) displayed orientation of amino acid residues within the binding pocket. When both the models were superimposed (Figure 7 C), it was observed that the residues changed their orientations at their similar positions with Ca^{2+} ion bound state than the unbound structure. The bound state residues have less root mean square deviation (RMSD) value of 1.08 Å as compared to unbound state of 1.8 Å. This reduced RMSD value due to the stiffer binding with Ca^{2+} ion prevented less free movement at their bound state [29].

Discussion

The cloned family 35 Carbohydrate binding module (*Ct*CBM35) from *Clostridium thermocellum* preferred binding with manno-configured polysaccharides. *Ct*CBM35 discriminated during carbohydrate selection showing its affinity only with manno-

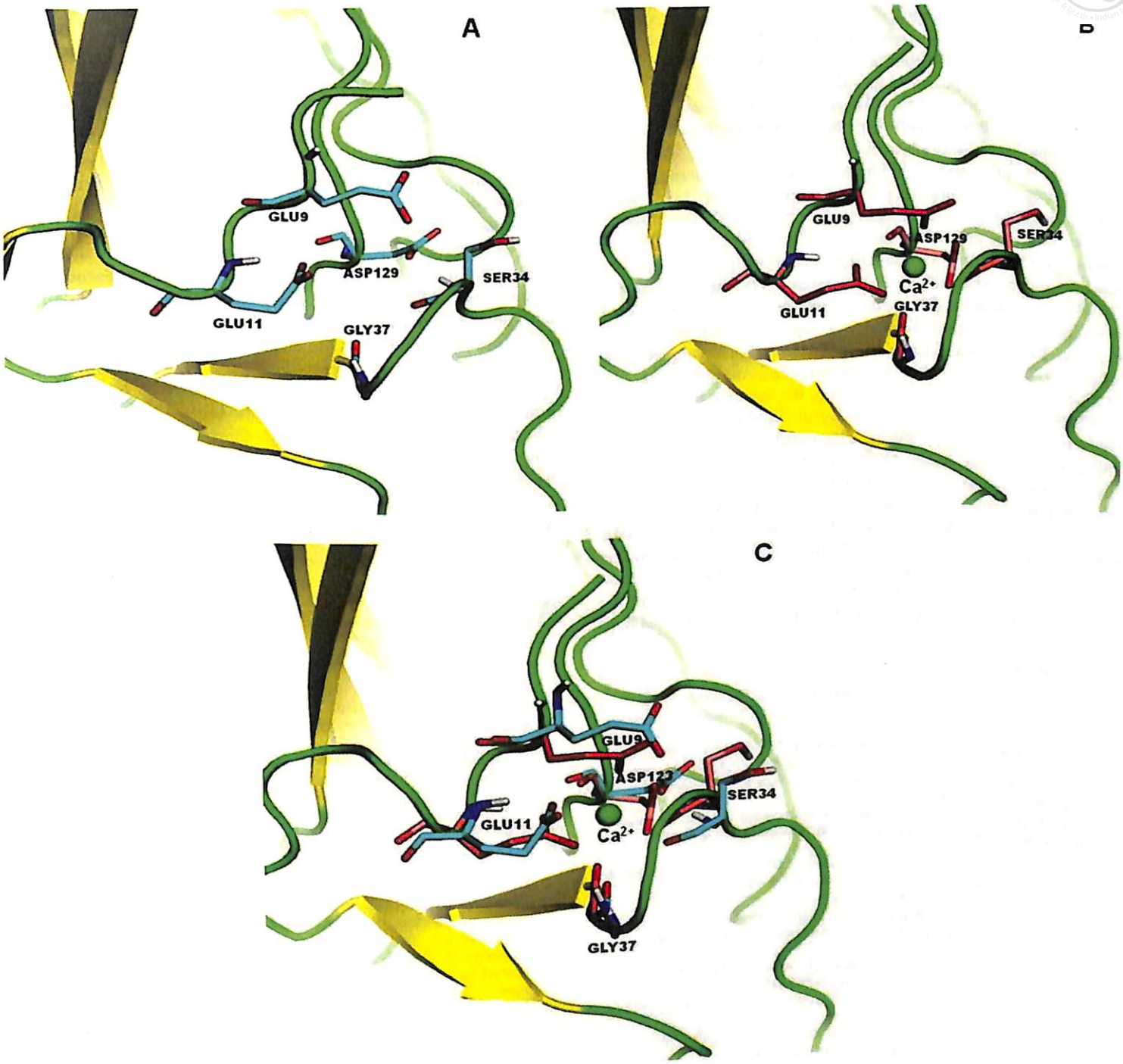

Figure 7. Amino acid residues of *Ct*CBM35 in the modeled structure (A) without Ca^{2+} ion (B) with Ca^{2+} ion (C) superimposed structure of both (A) and (B) showing the Ca^{2+} ion binding pocket to compare the altered positions of the amino acid residues in absence and presence of Ca^{2+} ion.
doi:10.1371/journal.pone.0080415.g007

configured ligands among the manno and xylo-configured polysaccharides. Instead of β-1,4-mannose chain affinity the variance of ligand selection within the manno-configured polysaccharides was often observed. *Ct*CBM35 has higher affinity with konjac glucomannan than carob galactomannan. Rationale behind this selective affinity was due to the galactose unit in carob galactomannan likely interferes with the *Ct*CBM35 binding. Carob galactomannan is composed of a 1,4-β-linked D-mannan backbone to which single D-galactosyl units are attached to C-6 of D-mannosyl residues. Whereas glucomannan is a linear polysaccharide comprising 1,4-β-linked D-glucosyl and D-mannosyl residues. Therefore, *Ct*CBM35 was more glucomannan specific than galactomannan. This finding gained a new insight into the CBM35 family when compared with other mannan specific CBM35 from *Clostridium thermocellum* and *Cellvibrio japonicas* [30,31] which were exo and endo acting to D-mannan chain of galactomannan only. However, the binding of *Ct*CBM35 with insoluble polysaccharides was quite insignificant. Low affinity against insoluble mannan was due to the inability of trans (as a discrete fold) form of *Ct*CBM35 to disrupt the inter chain interactions in mannan. This in contrast to some CBMs has the ability to disintegrate the surface of crystalline insoluble

polysaccharides that potentiates higher binding to some soluble fractions of insoluble polysaccharides [32,33]. Polysaccharide specificity by CBM35 family is probably due to the conserved hydrophobic aromatic residues that play a major role in polysaccharide binding [30]. Tryptophan being one of such residues has indole ring with intrinsic fluorescence property with higher quantum yield, displays fluorescence emission at 320 nm to 400 nm [17]. Polysaccharide binding changes the microenvironment of tryptophan due to conformational changes in protein. Usually in CBMs, the aromatic residues responsible for polysaccharide binding are lying in the hydrophobic core. Due to polysaccharide binding and direct interaction with tryptophan, the fluorescence emission is gradually decreased. The higher affinity of *Ct*CBM35 for konjac glucomannan masks the available tryptophan for fluorescence emission as compared to carob galactomannan. Thus, gradual fall in peak intensities were coupled with peak shifts (~21 nm) due to altered conformation of native *Ct*CBM35. In dynamic light scattering, the larger particle size of *Ct*CBM35 is due to the polysaccharide binding. The cationic interaction of aromatic residues with carob galactomannan and konjac glucomannan insists *Ct*CBM35 domain alteration to more compact form reducing the random diffusion of the particles between polysaccharide and amino acid residues. Due to simpler structure of konjac glucomannan, the interaction with aromatic residues in the binding pocket of *Ct*CBM35 uphold strong binding as compared to carob galactomannan with substituted galactose side chain. The structure of *Ct*CBM35 gains its particle size in the conjunction with polysaccharide and the Brownian motion of light measured between the larger particles and ends up ... hydrodynamic area. Melting of a protein module is a cooperative process [34–36]. CBM acts as an independent subunit from the catalytic module at higher temperature. But divalent cation like Ca^{2+} ion makes polar contact with the amino acid residues away from the polysaccharide binding sites. This imparts stiffer orientation of the residues dragging more towards the ion and holding into a proper position of the residues even at varying physical parameters such as higher temperature, pH change etc with reduced RMSD value. Ca^{2+} ion attacks on the negatively charged amino acid side chains and do not allow their mobility at harsh environmental conditions due to which the protein folding remain intact [29]. Thus a recombinant thermostable glucomannan and galactomannan specific CBM35 from *Clostridium thermocellum* may be useful to enhance the activity by appended to a mannanase for higher degree of hydrolysis of complex manno-configured polysaccharides into simple sugars. Moreover, these findings might lead to comprehend both glucomannan and galactomanan specific CBM35 from *Clostridium thermocellum* which may play a potential role in biofuel production in conjunction with mannanase from mannan rich polysaccharides in future.

Author Contributions

Conceived and designed the experiments: AGh AG NP NKC ASL JB CF. Performed the experiments: AGh AG NP NKC ASL JB CF. Analyzed the data: AGh AG NP NKC CF. Contributed reagents/materials/analysis tools: AG NKC CF. Wrote the paper: AGh AG.

References

1. Cai S, Zheng X, Dong X (2011) CBM3d, a novel subfamily of family 3 carbohydrate-binding modules identified in cel48a exoglucanase of *Cellulosilyticum ruminicola*. J Bacteriol 193(19): 5199–5206.
2. Taylor EJ, Goyal A, Guerreiro CIPD, Prates JAM, Money VA, et al. (2005) How family 26 glycoside hydrolases orchestrate catalysis on different polysaccharides structure and activity of a *Clostridium thermocellum* lichenase. J Biol Chem 280(38): 32761–3276.
3. Sunna A (2010) Modular organisation and functional analysis of dissected modular β-mannanase CsMan26 from *Caldicellulosiruptor* Rt8B.4. Appl Microbiol Biotechnol 86(1): 189–200.
4. Bolam DN, Xie H, Pell G, Hogg D, Galbraith G, et al. (2004) ×4 modules represent a new family of carbohydrate-binding modules that display novel properties. J Biol Chem 279: 22953–22963.
5. Valenzuela SV, Diaz P, Pastor FI (2012) Modular glucuronoxylan-specific xylanase with a family CBM35 carbohydrate-binding module. Appl Environ Microbiol 78(11): 3923–31.
6. Tunnicliffe RB, Bolam DN, Pell G, Gilbert HJ, Williamson MP (2005) Structure of a mannan-specific family 35 carbohydrate-binding module: evidence for significant conformational changes upon ligand binding. J Mol Biol 347: 287–296.
7. Mizutani K, Fernandes VO, Karita S, Luís AS, Sakka, et al. (2012) Influence of a mannan binding family 32 carbohydrate binding module on the activity of the appended mannanase. Appl Environ Microbiol 78(14): 4781–4787
8. Hachem MA, Karlsson EN, Simpson PJ, Linse S, Sellers P, et al. (2002) Calcium binding and thermostability of carbohydrate binding module cbm4-2 of xyn10a from *Rhodothermus marinus*. Biochemistry 41: 5720–5729.
9. Johansson R, Gunnarsson LC, Ohlin M, Ohlson S (2006) Thermostable carbohydrate-binding modules in affinity chromatography. J Mol Recognit 19(4): 275–281.
10. Ofir K, Berdichevsky Y, Benhar I, Azriel-Rosenfeld R, Lamed R, et al. (2005) Versatile protein microarray based on carbohydrate-binding modules. Proteomics 5(7): 1806–1814.
11. Jorgensen H, Sanadi AR, Felby C, Lange NE, Fischer M, et al. (2010) Production of ethanol and feed by high dry matter hydrolysis and fermentation of palm kernel press cake. Appl Biochem Biotechnol 161(1–8): 318–332.
12. Sambrook JF, Russell DW (1989) Molecular cloning: A laboratory manual. 3rd ed. Cold Spring Harbor Laboratory Press. 213 p.
13. Laemmli UK (1970) Cleavage of structural proteins during the assembly of the head of Bacteriophage T4. Nature 227: 680–685.
14. Takeo K (1984) Affinity electrophoresis: Principles and applications. Electrophoresis 5: 187 195.
15. Bradford MM (1976) Rapid and sensitive method for the quantitation of microgram quantities of protein utilizing the principle of protein-dye binding. Anal Biochem 72: 248 254
16. Gilkes NR, Eric JS, Henrissat B, Tekant B, Miller RC Jr, et al. (1992) The adsorption of a bacterial cellulase to crystalline cellulose. J Biol Chem 267(10): 6743–6749.
17. Royer CA (2006) Probing protein folding and conformational transitions with fluorescence. Chem Rev 106:1769–1784.
18. Belatik A, Hotchandani S, Carpentier R, Tajmir-Riahi HA (2012) Locating the binding sites of pb (ii) ion with human and bovine serum albumins. Plos One 7(5): 1–9.
19. Morrison JD, Corcoran JD, Lewis KE (1992) The determination of particle size distributions in small-angle scattering using the maximum-entropy method. Appl Crystallogr 25: 504–513.
20. Provencher SW (1979) Inverse problems in polymer characterization: Direct analysis of polydispersity with photon correlation spectroscopy. Macromol Chem 180: 201–209.
21. Ostrowsky N, Sornette D, Parker P, Pike ER (1981) Exponential sampling method for light scattering polydispersity analysis. Optica Acta 28(8): 1059–1070.
22. Provencher SW (1982) Contin: a general purpose constrained regularization program for inverting noisy linear algebraic and integral equations. Comput Phys Commun 27(3): 213–227.
23. Shiba K, Niidome T, Katoh E, Xiang H (2010) Polydispersity as a parameter for indicating the thermal stability of proteins by dynamic light scattering. Analyt Sci 26: 659–663.
24. Dvortsov IA, Lunina NA, Chekanovskaya LA, Schwarz WH, Zverlov VV, et al. (2009) Carbohydrate-binding properties of a separately folding protein module from β-1,3-glucanase Lic16A of *Clostridium thermocellum*. Microbiology 155: 2442–2449.
25. Berendsen HJC, Van der Spoel D, Drunen RV (1995) GROMACS: a message passing parallel molecular dynamics implementation. Comput Phys Commun 91: 43–56.
26. Van der Spoel D, Lindahl E, Hess B, Groenhof G, Mark AE, et al. (2005) GROMACS: fast, flexible, and free. J Comput Chem 26:1701–1718.
27. Hess B, Kutzner C, Van der Spoel D, Lindahl E (2008) GROMACS 4: algorithms for highly efficient, load-balanced and scalable molecular simulation. J Chem. Theory Comput 4: 435–447.
28. Saravanan P, Avinash H, Dubey VK, Patra S (2012) Targeting essential cell wall lipase Rv3802c for potential therapeutics against tuberculosis. J Molr Graph Mod 38: 235–242.
29. Noorbatcha IA, Sultan AM, Azura A, Salleh HM (2012) Molecular dynamics study of the effect of calcium ions on the thermostability of *Bacillus Amyloliquefaciens* phytase. Aust J Basic App Sci 6(1): 109–116.
30. Tunnicliffe RB, Bolam DN, Pell G, Gilbert HJ, Williamson MP (2005) Structure of a mannan-specific family 35 carbohydrate-binding module: evidence for

significant conformational changes upon ligand binding. J Mol Bio 347(2): 287–296.
31. Correia MAS, Abbott DW, Gloster TM, Fernandes VO (2010) Signature active site architectures illuminate the molecular basis for ligand specificity in family 35 carbohydrate binding module. Biochemistry 49: 6193–6205.
32. Din N, Damude HG, Gilkes NR, Miller Jr RC, Warren RA, et al. (1994) C1-Cx revisited: intramolecular synergism in a cellulose. PNAS 91(24): 11383–11387.
33. Din N, Gilkes NR, Tekant B, Miller Jr RC, Anthony RJ, et al. hydrolytic disruption of cellulose fibres by the binding domain cellulase. Nat Biotechnol 9: 1096–1099.
34. Branden K, Tooze J (1999) Introduction to Protein Structure, 2nd edn. New York: Garland Publishing.
35. Dobson CM, Evans PA, Radsford SE (1994). Understanding protein folding: the lysozyme story so far. Trends Biochem Sci 19:31–37.
36. Finkelstein AV, Galzitskaya OV (2004) Physics of protein folding. Physic of Life Reviews 1: 23–56.

JOURNAL OF AGRICULTURAL AND FOOD CHEMISTRY

Article

pubs.acs.org/JAFC

Thermostable Recombinant β-(1→4)-Mannanase from *C. thermocellum*: Biochemical Characterization and Manno-Oligosaccharides Production

Arabinda Ghosh,[†] Ana Sofia Luís,[‡] Joana L. A. Brás,[‡] Carlos M. G. A. Fontes,[‡] and Arun Goyal*[,†]

[†]Department of Biotechnology, Indian Institute of Technology Guwahati, Guwahati-781 039, Assam, India

[‡]CIISA-Faculdade de Medicina Veterinaria, Avenida da Universidade Técnica, 1300-477 Lisbon, Portugal

Supporting Information

ABSTRACT: Functional attributes of a thermostable β-(1→4)-mannanase were investigated from *Clostridium thermocellum* ATCC 27405. Its sequence comparison the exhibited highest similarity with Man26B of *C. thermocellum* F1. The full length *Ct*Manf and truncated *Ct*ManT were cloned in the pET28a(+) vector and expressed in *E. coli* BL21(DE3) cells, exhibiting 53 kDa and 38 kDa proteins, respectively. On the basis of the substrate specificity and hydrolyzed product profile, *Ct*Manf and *Ct*ManT were classified as β-(1→4)-mannanase. A 1.5 fold higher activity of both enzymes was observed by Ca^{2+} and Mg^{2+} salts. Plausible mannanase activity of *Ct*Manf was revealed by the classical hydrolysis pattern of carob galactomannan and the release of manno-oligosaccharides. Notably highest protein concentrations of *Ct*Manf and *Ct*ManT were achieved in tryptone yeast extract (TY) medium, as compared with other defined media. Both *Ct*Manf and *Ct*ManT displayed stability at 60 and 50 °C, respectively, and Ca^{2+} ions imparted higher thermostability, resisting their melting up to 100 °C.

KEYWORDS: *Man26B, carob galactomannan, manno-oligosaccharides, thermostability*

INTRODUCTION

Plant cell wall is mainly composed of complex structural polysaccharides like celluloses and hemicelluloses. Polysaccharides of the primary cell wall are cellulose, hemicelluloses such as xyloglucans, mannans, galactomannans, glucomannans, laminarin, glucuronoarabinoxylans, and arabinoxylan, etc. Mannans are the polysaccharides with a backbone chain of β-(1 → 4)-linked mannose units. They constitute a major portion of hemicelluloses in hardwoods. The major distribution of mannan in combination with galactose and glucose units in plant hemicellulose reservoir is abundant in nature. Carob galactomannan (from the *Ceratonia siliqua* plant) contain β-(1→4)-D-mannan backbone (78%) and galactose as α-(1→6)-linked (22%) single units, where as guar gum (from endosperm of guar seeds) backbone is a linear chain of β-(1→4)-linked mannose residues to which galactose residues are (1→6)-linked at every second mannose, forming short side-branches.[1] Glucomannan (from *Amorphophallus konjac*) is a water-soluble polysaccharide that is considered a dietary fiber. The component sugars in konjac glucomannan are β-(1→4)-linked D-mannose and D-glucose residues in a molar ratio of 1.6:1 and branched chain composed of β-(1→6)-linked D-glucosyl units.[2]

β-D-Mannanase [endo β-(1→4)-mannan mannohydrolase, E.C. 3.2.1.78] hydrolyzes β-(1→4)-D-mannopyranosyl linkages within the main chain of mannans, glucomannans, galactomannans, and galactoglucomannans.[3] Mannanases have been listed within glycoside hydrolase (GH) families viz. GH26, GH5, and GH113 in carbohydrate-active enzyme database (http://www.cazy.org/Glycoside-Hydrolases.html) based on sequence similarity.[4] β-D-Mannanases belong to families GH5, GH26, GH113 and display a $(\beta/\alpha)_8$ barrel-shaped protein folding pattern, and the acid−base-assisted catalysis via a double displacement mechanism involving a covalent glycosyl-enzyme intermediate.[5,6] The mechanism of glycosidic bond cleavage is found conserved within these families. These are the characteristic patterns of clan GH-A protein families and helped β-D-mannanases of families GH5, GH26, and GH113 to group into this clan.[5,6] Due to the retaining double-displacement mechanism, these enzymes can perform transglycosylation. Transglycosylation may lead to the synthesis of new glycosides or oligosaccharides longer than the original substrate. GH5 and GH113 mannanases have been described as able to catalyze transglycosylation reactions,[5,6] while to date no evidence of transglycosylation has been reported for GH26 mannanases.[7]

The benefit of employing novel enzymes for specific industrial processes is well-recognized with the discovery of β-mannanases. β-Mannanases (EC 3.2.1.78) hydrolyze mannan-based hemicelluloses and liberate short β-(1→4)-manno-oligosaccharides, which can be further hydrolyzed to mannose by β-mannosidases (EC 3.2.1.25). There are currently around 50 β-mannanase gene sequences in families 5 and 26 GHs from various microbial origins. The family 26 Glycoside Hydrolase (GH26) mannanase has narrow substrate specificity hydrolyzing (1→4)-β-D-linkages in mannans, galacto-mannans, glucomannans, and galactoglucomannans but does not show activity against β-glycan chain of soluble cellulose derivatives.[8] Several studies exhibited the presence of distinct types of mannanases (GH5A, GH5B, GH5C, GH26A, GH26B, and GH26C) expressed on the cell surface of *Cellvibrio japonicas*[9]

Received: July 16, 2013
Revised: November 13, 2013
Accepted: November 13, 2013
Published: November 13, 2013

having different substrate specificity. GH5 mannanase exhibits some activity for cellulosic substrates.[10] By contrast, Man26B displays canonical endomannanase activity and linked to the cell membrane via ~70 residue linker sequence of *C. japonicas*.[10] Thus, Man26B gets enough space via the linker sequence to adsorb on the natural substrates galactomannan and glucomannan than other surface-expressed mannanases. Man26B rapidly generates large amounts of mannose, even in the early stages of galactomannan or manno-oligosaccharide hydrolysis. But Man26A displayed a typical endo-β-(1→4)-bond cleavage activity against small manno-oligosaccharides, hydrolyzing mannotriose approximately, 10000 times more efficiently than Man26B.[10] There are distinct differences in topology of the substrate-binding cleft and substrate specificity among the mannnases (Man26A, Man26B, and Man26C) within GH26 family.[5]

There are several reports of manno-oligosaccharides synthesis by the utilization of mannanases from manno-configured substrates.[10,11] Though the manno-oligosaccharides are indigestible inside the human gut, their potential role as dietary fiber and prebiotics were attributed in various studies.[12] It was evident from earlier reports that the efficient prebiotics role of manno-oligosaccharides that supports the growth of human intestinal beneficial microflora viz. Bifidobacteria and *Lactobacilli*.[13,14] In addition, manno-oligosaccharides can prevent the probability of high blood pressure and higher intestinal absorption of fatty acid substance from a high fat diet.[15]

Clostridium thermocellum expresses a large number of hemicellulases in its multienzyme complex, targeting various hemicellulosic components such as mannans and xylans, removes the hemicellulosic polysaccharides exposing the cellulose microfibrils and uses it as primary carbon and energy sources and releases soluble sugars.[16] The carbohydrate binding modules (CBMs) are the noncatalytic modules known to help or bring the catalytic modules in close proximity to its substrates, and also some CBMs are known to stabilize the enzyme (catalytic module) structure and increase its thermostability.[17,18] The majority of *C. thermocellum* cellulosomal enzymes display rather complex multimodular architectures containing CBMs either at the N- or C- terminal domain. These CBMs potentiate the interaction of the multifunctional complex with the diversity of polysaccharides in the plant cell wall by directing the appended catalytic domains to their target substrates.[16] The CBMs may be found to contain up to 200 amino acids and can be found attached as single, double, or triple domains in one protein, located at both the C- or N-terminal within the parental protein.[19] A family 35 carbohydrate binding module (CBM35) often appended with mannanase that binds to the galactose-decorated mannanas and facilitates their efficient hydrolysis.[20] There are few reports of Man26B functions explored earlier from *Paenibacillus* sp. BME14,[21] *C. japonicas*,[22] *C. thermocellum* strain F1,[23] and *Bacillus licheniformis* DSM13.[24] In the present report, we studied the molecular and biochemical characterization of family 26 glycoside hydrolase (GH26) mannanase B (Man26B) from *C. thermocellum* ATCC 27405. Its potential in manno-oligosaccharide production by the hydrolysis of the manno-configured substrate was analyzed.

■ MATERIALS AND METHODS

Bacterial Strains and Plasmid. The genomic DNA of *C. thermocellum* ATCC 27405 was a gift from Professor Carlos Fontes, Faculdade de Medicina Veterinaria, Lisbon, Portugal. *Escherichia coli* DH5α cells were used for cloning, and *E. coli* BL21 (DE3) was used as the expression host. The plasmids used for cloning and expression were pET-28a (+). All the above-mentioned items were procured from Novagen (Madison, WI).

Fine Chemicals and Natural and Synthetic Substrates for Enzyme Assay. Mannose, xylose, glucose, galactose, EDTA, and NaOH solution (50%, w/v), lichenan (from *Cetraria islandica*) were procured from Sigma Chemical Company (St. Louis, MO). Carob galactomannan, konjac glucomannan, locust bean galactomannan, guar galactomannan, ivory nut mannan, β-(1→4)-mannnan, barley β-glucan, rye arabinoxylan, xyloglucan, mannobiose, and mannotriose were procured from Megazyme International, Ireland. Carboxy methylcellulose (CMC), hydroxyethyl cellulose, Avicel (microcrystalline cellulose) and synthetic *p*NP-glycosides like *p*NP-β-mannopyranoside, *p*NP-α-mannopyranoside, glucuronoxylan, and polygalactouronic acid were purchased from Sigma Chemical Company.

Sequence Analysis. Two mannanase genes (locus name: Cthe_0032 and Cthe_2811) (http://www.cazy.org/GH26_bacteria.html) belonging to family 26 glycoside hydrolase (GH26), were identified in the native host *C. thermocellum* ATCC 27405 (16S rDNA sequence ID: CP000568, http://www.straininfo.net/strainPassport.action?page=34&cultureId=40680). Mannanase encoding ORF region was identified using the protein sequence (gene bank protein accession ABN51273.1, locus name: Cthe_0032) of *C. thermocellum* ATCC 27405 in tBLASTn (http://blast.ncbi.nlm.nih.gov/Blast.cgi) tool. This sequence was used to design the desired oligonucleotide primers for amplification of full length *Ct*Manf (CBM35-*Ct*ManT) and truncated catalytic module *Ct*ManT (nucleotide accession: CP000568.1). The sequence for amplification was devoid of signal peptide and dockerin (Doc I). The protein sequence of *Ct*ManT was analyzed for the type of enzyme synthesized using multiple sequence alignment using MULTALIN (http://multalin.toulouse.inra.fr/multalin/cgi-bin/multalin.pl) and viewed in the ESPript (http://espript.ibcp.fr/ESPript/ESPript/) tool. Multiple sequence alignment was performed using the different types of mannanase (Man26A and Man26B) sequences of glycoside hydrolase family 26 (GH26) from *Paenibacillus* sp BME14,[21] *Cellvibrio japonicas*,[22] *Clostridium thermocellum* strain F1,[23] *Bacillus licheniformis* DSM13,[24] *Cellulomonas fimi*,[25] *Rhodothermus marinus*,[26] *Bacillus* sp JAMB750,[27] *Paenibacillus polymyxa* GS01.[28] Evaluation of the functional property of this protein sequence was performed using InterProScan (http://www.ebi.ac.uk/Tools/pfa/iprscan/), and the molecular architecture of the entire protein sequence to be cloned was drawn.

Gene Amplification and Cloning. The ORF region encoding full length *Ct*Manf (CBM35-*Ct*ManT) containing family 35 carbohydrate binding module (nucleotide accession: CP000568.1) at the N-terminal and the family 26 glycoside hydrolase (GH26), a mannanase B (Man26B) catalytic module, *Ct*ManT (nucleotide accession: CP000568.1) were amplified from the genomic DNA of *C. thermocellum* ATCC 27405, using two oligonucleotide primers having *Nhe*I and *Xho*I restriction sites. The 50 μL PCR reaction mixture contained Mg^{2+} ions (2.5 mM), dNTPs (0.2 mM), primers (1.5 μM), 1.0 μL of Taq DNA polymerase (1 μL of 1 Unit/μL), and 1 μL of genomic DNA (10 ng) of *C. thermocellum* ATCC 27405 and PCR-grade water (Sigma Chemical Company). The oligonucleotide primers used for amplifying *Ct*ManT were forward 5′-cacgctagcgcatattcccttcctg-3′ and reverse 5′-cacctcgagttagctaaagtatattttg-3′. The oligonucleotide primers for *Ct*Manf used were: forward 5′-cacgctagcgcatattcccttcctg-3′ and 5′-cacctcgagttaaagttcatccaagctgc-3′. The PCR amplification cycles used were denaturation at 94 °C for 4 min followed by 30 cycles of denaturation at 94 °C for 30 s, annealing at 55 °C for 60 s and extension at 72 °C for 2 min, and final extension at 72 °C for 10 min. The amplified products were run on 0.8% agarose gel and purified by a gel extraction kit (Qiagen). The PCR-amplified *Ct*Manf and catalytic *Ct*ManT were cloned into *Nhe*I/*Xho*I digested pET-28a (+) expression vector containing kanamycin as a resistant marker, resulting in cloned plasmids pMan*f* and pManGH26, respectively. The *E. coli* DH5α cells were transformed with above recombinant plasmids. These transformed cells were grown on LB agar plates,[29] supplemented with kanamycin (50 μg mL^{-1}) at 37 °C

for growth of recombinant clones. The positive clones were selected by restriction digestion analysis of the recombinant plasmids.

Expression and Purification of *Ct*Manf and *Ct*ManT. *E. coli* BL-21(DE3) (Novagen) cells were transformed for expression of *Ct*Manf and *Ct*ManT as described elsewhere.[29] The cells were grown in LB medium containing kanamycin (50 μg mL^{-1}) at 37 °C with 180 rpm to the midexponential phase ($A_{600\ nm} \approx 0.6$). Then the cells were induced with 1.0 mM isopropyl-1-thio-β-D-galactopyranoside (IPTG) and incubated at 24 °C with 180 rpm for 24 h for the hyper-expression of recombinant proteins. The cells were harvested at 9000*g*, and the resulting pellet was resuspended in 50 mM sodium phosphate buffer pH 7.0, containing 1 mM phenylmethanesulfonyl fluoride (PMSF). Then the cells were sonicated (Sonics, Vibra cell) on ice for 16 min (9 s on/9 s off pulse, 30% amplitude) and again centrifuged using the centrifuge (Sigma, 4K15) at 19000*g* at 4 °C for 20 min. The cell free supernatant containing the soluble protein was purified by immobilized metal ion chromatography (IMAC).[29] The recombinant proteins containing *Ct*Manf and *Ct*ManT appended by the His_6 tag were purified in a single step using 1 mL HiTrap chelating columns (GE Healthcare) as recommended by the manufacturer. The purity and molecular mass of recombinant *Ct*Manf and *Ct*ManT were verified by SDS–PAGE.[30]

Enzyme Assays of *Ct*Manf and *Ct*Mant with Natural and Synthetic Substrates. The enzyme activity of *Ct*Manf and *Ct*ManT was determined by using natural substrates, such as carob galactomannan, locust bean galactomannan, konjac glucomannan, guar galactomannan, ivory nut mannan, β-(1→4)-mannan (an insoluble polysaccharide prepared from carob galactomannan pretreated with *Aspergillus niger* mannanase and subsequently debranched to a high extent containing mannose (97%) and galactose (3%), according to the manufacturer Megazyme International, Ireland), barley β-glucan, lichenan, carboxymethyl cellulose, hydroxyethyl cellulose, Avicel, rye arabinoxylan, glucuronoxylan, arabinogalactan, and polygalactouronic acid (PGA) at (1%, w v^{-1}) in 50 mM sodium phosphate buffer (pH 7.0) and by measuring the reducing sugar released, as described previously.[31,32] In both cases, 100 μL of reaction mixture contained 1.0 (%, w v^{-1}) substrate, 10 μL of enzyme (*Ct*Manf, 0.16 mg mL^{-1} and *Ct*ManT, 0.15 mg mL^{-1}). One-hundred microliter reaction mixtures for both the enzymes were incubated at 50 °C for 10 min separately with separate polysaccharides. In the case of Avicel, the reaction mixture was incubated for 60 min under shaking conditions. The resulting reducing sugars viz. mannose, xylose, glucose, and galactose concentrations were measured by the absorbance at A_{500nm}, using a spectrophotometer (Varian, Cary 100 Bio), and standard curves were prepared from standard mannose, xylose, glucose, and galactose (Sigma Chemical Company). The assays were carried out in triplicate.

A wide range of pH was chosen, ranging from pH 3.0 to 8.0 as β-mannanse displays optimum range within this range.[33] For studying the optimum pH profile of *Ct*Manf and *Ct*ManT, 50 mM sodium phosphate buffer, pH 3.0–8.0, was used for the enzyme assays that employed 1.0 (%, w v^{-1}) carob galactomannan at 50 °C. The optimum temperature study was carried out within the range from 10 to 100 °C at their respective optimum pH, using 1.0 (%, w v^{-1}) carob galactomannan.

After the verification of substrate specificity, the enzyme assays for *Ct*Manf and *Ct*ManT were performed using 50 mM sodium phosphate buffer at their optimum pH and temperature to analyze the kinetic parameters viz. K_m, V_{max}, k_{cat}, and k_{cat}/K_m. One unit of enzyme activity was determined as the release of 1 μmole of mannose per minute. The assays involving synthetic substrates *p*NP-β-D-mannopyranoside and *p*NP-α-D-mannopyranoside were performed as reported earlier by Bey et al. (2011).[34]

Zymogram Study and Activity Staining. Zymogram study of recombinant *Ct*Manf and *Ct*ManT were investigated by using 0.5% (w v^{-1}) carob galactomannan as the substrate incorporated in 12% (w v^{-1}) SDS–PAGE. Ten micrograms of each of purified *Ct*Manf and *Ct*ManT by IMAC was mixed with 1× the sample buffer (62.5 mM Tris-Cl, pH 6.8, 20% v v^{-1} glycerol, 2% w v^{-1} SDS, and 0.005% w v^{-1} bromophenol blue)[30] without β-mercaptoethanol[35] were loaded on the gel. After the completion of electrophoresis, the gels were incubated in 2.5% (v v^{-1}) of TritonX 100 at 25 °C for 1 h followed by 1 h incubation in 50 mM sodium phosphate buffer, pH 7.0. Then the gels were incubated in preheated 50 mM sodium phosphate buffer (pH 6.5) at 55 °C for 30 min and then stained with 0.1% (w v^{-1}) congo red for 45 min, as described by Aboul-Enein et al. (2010).[35] After congo red staining, the gels were counter-stained with 1 N HCl, as described elsewhere.[36]

Effect of Metal Ions, Chaotropic Agents, And Detergent on Enzyme Activity. The effects of different metal cations, chaotropic agents, and detergent on the activity of *Ct*Manf and *Ct*ManT were determined. The enzyme activity of both *Ct*Manf and *Ct*ManT was determined in the presence of various metal salts, such as Ni^{2+} ($NiSO_4 \cdot 6H_2O$), Zn^{2+} ($ZnSO_4 \cdot 7H_2O$), Cu^{2+} ($CuSO_4 \cdot 5H_2O$), Co^{2+} ($CoCl_2 \cdot 6H_2O$), Mn^{2+} ($MnCl_2 \cdot 4H_2O$), Al^{3+} ($AlCl_3 \cdot 6H_2O$), or Ca^{2+} ($CaCl_2 \cdot 2H_2O$), chaotropic agents like disodium EDTA, EGTA, urea, or guanidine hydrochloride and detergent such as SDS. The assays of *Ct*Manf and *Ct*ManT were performed at 60 and 50 °C, respectively, using 50 mM sodium phosphate buffer, of pH 6.9 and pH 6.5, respectively. One-hundred microliters of the reaction mixture containing carob galactomannan (1%, w v^{-1}) and metal salt at concentrations (up to 80 mM) or SDS (up to 20 mM) were incubated for 10 min, and a control sample in the absence of the additive was also run. The assays were performed in triplicates. Both enzymes were incubated with EDTA and urea for 1 h, before measuring the residual activity. The enzyme activity was determined, as described earlier.

Thin-Layer Chromatography of Hydrolyzed Products by *Ct*Manf. The qualitative analysis of hydrolyzed products by the reaction of *Ct*Manf on carob galactomannan was performed by thin-layer chromatography (TLC) on silica gel-coated aluminum foil (TLC Silica gel 60 F_{254} 20 × 20 cm, Merck) for detecting sugars. The enzyme *Ct*Manf (10 μL and 0.16 mg mL^{-1}) with 1% (w v^{-1}) carob galactomannan in 100 μL reaction mixtures were incubated at optimized temperature 60 °C and optimized pH 6.9, for time intervals of 1, 4, 8, 16, and 24 h. The reaction products were boiled for 2 min to stop enzymatic hydrolysis and then centrifuged at 13000*g* for 5 min.[6] Then 0.2 μL of sample as well as of standard solutions (1.0 mg mL^{-1}) were loaded on the TLC plate and kept in the developing chamber saturated with the developing solution (mobile phase), which consisted of acetic acid–*n*-propanol–water–acetonitrile (4:10:11:14).[37] Mannose and oligosaccharides (mannobiose and mannotriose) were used as standards. At the end of the run, migrated sugars were visualized by immersing the TLC plate in a visualizing solution (sulphuric acid/methanol 5:95, v v^{-1}; α-napthol 5.0%, w v^{-1}). The TLC plates were then dried at 80 °C for 20 min. The migrated reaction products (sugars) appeared as spots on the TLC plate.

HPAEC Analysis of Polysaccharide Hydrolysis by *Ct*Manf. *Ct*Manf (10 μL and 0.16 mg mL^{-1}) with 1% (w v^{-1}) carob galactomannan in 100 μL of reaction mixtures were incubated, at optimal conditions of 60 °C, and pH 6.9 for 1, 4, 8, 16 and 24 h. These reaction mixtures were treated with 2 volumes (200 μL) of absolute ethanol to precipitate the remaining nonreacted polysaccharides (substrates) and then centrifuged at 13000*g* at 4 °C for 10 min. The supernatant containing the liberated sugar was transferred to another microcentrifuge tube, and the ethanol was removed by evaporation. The supernatant (50 μL) was diluted to 500 μL by adding ultrapure (Milli-Q, Millipore) water and filtered through a syringe filter using a 0.2 μm membrane. The liberated sugars were analyzed by high-pressure anion-exchange chromatography (HPAEC), using an ion chromatography system (Dionex, ICS-3000). From the filtered 500 μL, 25 μL of sample (liberated sugars) was run on CARBOPACK PA-200 column (150 × 3 mm, Dionex), attached with CarboPac PA200 guard column (30 × 3 mm, Dionex) with borate and amino trap columns which removed impurities and provided high resolution. The instrument (Dionex, ICS-3000) was kept at a constant temperature of 30 °C during the analysis, and the flow rate was maintained at 0.3 mL min^{-1}. The elution of liberated sugars released due to enzyme reaction was carried out with 100 mM sodium hydroxide using a pulsed amperometric detector (PAD). Ten micrograms per milliliter of D-mannose, mannobiose, and mannotriose

dx.doi.org/10.1021/jf403111g | J. Agric. Food Chem. 2013, 61, 12333–12344

were used as standards. The solutions of standards were also filtered through a 0.2 μm membrane before loading onto the column. A standard curve was prepared by using a mixture of standards (mannose, mannobiose, and mannotriose) from 10 mg mL^{-1} stock solutions. Quantitative analysis enzyme-catalyzed hydrolysis products were determined from the peak intensity of the released products.

Production of *Ct*Manf and *Ct*ManT in Different Media. Media screening was performed in order to obtain higher production of recombinant *Ct*Manf and *Ct*ManT. Four different media were screened, as listed in Table 4. All four media LB, 5xLB, Terrific Broth (TB), and TY media were prepared, as previously described by Tripathi et al. (2009).[38] LB medium (100 mL) was prepared in a 250 mL flask by weighing constitutents in (%, w/v) were tryptone, 1.0; yeast extract, 0.5; and NaCl, 1.0.[38] A 100 mL 5xLB medium was prepared by using (%, w/v) tryptone, 5.0; yeast extract, 2.5; NaCl, 2.5; glycerol, 1.0.[38] Terrific broth (TB) 100 mL was composed of constituents in (%, w/v) pancreatic digest of casein, 1.2; yeast extract, 2.4; dipotassium phosphate, 0.94; monopotassium phosphate, 0.22; and glycerol, 0.4.[38] The components of 100 mL TY medium used in (%, w/v) were tryptone, 2.68; yeast extract, 2.14; monopotassium phosphate, 0.54; diammonium hydrogen phosphate, 0.16; magnesium sulfate, 0.12; NaCl, 0.85; and glycerol, 0.1.[38] Initially, the seed culture was prepared by inoculating respective *E. coli* BL21 cells, harboring recombinant plasmids *Ct*Manf and *Ct*ManT in 5 mL LB medium supplemented with 50 μg mL^{-1} kanamycin and incubated at 37 °C and 180 rpm for overnight. Each 250 mL culture flasks of four media containing 100 mL medium supplemented with 50 μg mL^{-1} kanamycin were inoculated with 1 mL of seed culture. The cells were grown at 37 °C, 180 rpm up to the mid exponential phase ($A_{600\ nm} \approx 0.6$) followed by induction with 1.0 mM isopropyl-1-thio-β-D-galactopyranoside (IPTG) for hyper-expression of recombinant proteins at 24 °C with 200 rpm for 24 h. Dry cell weight of the bacterial cell was measured, as described by Black (1996).[39] The 10 mL culture broth was centrifuged at 9000*g* for 15 min and the supernatant discarded. The resulting pellet washed with distilled water 3 times followed by centrifugation at 9000*g* for 15 min in each wash. The cell pellet was dried at 60 °C for 16 h, and the dry cell weight was measured by weighing.[39] The cells were harvested by centrifuging at 9000*g* at 4 °C for 20 min, and the resulting cell pellet was resuspended in 50 mM sodium phosphate buffer pH 7.0 containing 1 mM phenylmethanesulfonyl fluoride (PMSF). The cell suspensions were sonicated (Vibra cell, Sonics) on ice for 16 min (9 s on/9 s off pulse, 30% amplitude) and then centrifuged at 19000*g* at 4 °C for 20 min. The recombinant proteins were purified by a single step, using immobilized metal ion affinity chromatography (IMAC) on HiTrap chelating columns (GE Healthcare), as mentioned earlier.[29] The concentration of IMAC-purified recombinant proteins were determined by the Bradford method.[40]

Thermostability study and protein melting analysis of *Ct*Manf and *Ct*ManT. The ability of *Ct*Manf and *Ct*ManT to retain its enzymatic activity at a higher temperature was studied. Both *Ct*Manf and *Ct*ManT (30 μL each from the stock of 0.16 mg mL^{-1} and 0.15 mg mL^{-1}, respectively) were incubated at temperatures from 10 to 110 °C for 1 h. After the incubation, the enzyme activity was determined by taking 10 μL of *Ct*Manf and *Ct*ManT separately in a 100 μL reaction mixture containing 1% (w v^{-1}) carob galactomannan in 50 mM sodium phosphate buffer of pH 6.9 and pH 6.5, respectively. The protein melting curves were generated by subjecting *Ct*Manf and *Ct*ManT to various temperatures and measuring the change in the absorbance at 280 nm by a UV–visible spectrophotometer (Varian, Cary 100-Bio), following the method of Dvortsov et al.[18] The purified *Ct*Manf and *Ct*ManT at protein concentration of 0.3 mg mL^{-1} in 50 mM MES [2-(*N*-morpholino) ethanesulfonic acid] buffer, pH 7.0, were used. The absorbance at 280 nm was measured at different temperatures, varying from 40 to 100 °C using a peltier temperature controller. The protein solutions (1 mL, 0.3 mg mL^{-1}) of *Ct*Manf and *Ct*ManT were kept at the particular temperature for 10 min to attain the equilibrium. A similar experiment was carried out with the addition of 10 mM $CaCl_2$ in the 1 mL enzyme (0.3 mg mL^{-1}) solution, and the temperature was then varied. The experiment was repeated with the addition of $CaCl_2$ and EDTA to 1 mL of enzyme solution (0.3 mg mL^{-1}) containing equimolar concentrations of 10 mM, and finally the change in absorbance at 280 nm was measured. A curve of relative derivative absorption coefficient (first derivative coefficient) versus temperature was plotted, as described earlier by Dvortsov et al. (2009).[18]

RESULTS

Sequence Analysis of *Ct*Manf. The molecular architecture of full length derivative of mannanase *Ct*Manf displayed an appended family 35 carbohydrate binding module (*Ct*CBM35) at its N-terminal end and catalytic *Ct*ManT (Man26B) at its C terminal end (Figure S1of the Supporting Information). Amino acid sequence analysis using InterProScan revealed that *Ct*Manf has two distinct modules: from regions 1 to 134, a noncatalytic carbohydrate binding module family 35 (CBM35) and from 135 to 478, a glycoside hydrolase family 26 (GH26). *Ct*ManT found the most similar 50% sequence homology, (UniProt id: Q9F1T9) to mannanase 26B of *C. thermocellum* strain F1 (*CtF1*Man26B), *Bacillus licheniformis* DSM13 (*Bl*Man26B) (33.080%, UniProt id: Q65MP4), *Paenibacillus* sp. BME-14 (*Ps*Man26B) (37%, UniProt id: C6KL35), and *Cellvibrio japonicas* (*Cj*Man26B) (35%, UniProt id: Q840B9). Sequence homology was found less pronounced, while comparing with mannanase 26A of *Cellulomonas fimi* (*Cf*Man26A) (28%, UniProt id: Q9XCV5), and *Bacillus* sp. JAMB750 (*Bs*Man26A) (26%, UniProt id: Q2ACI1). These results were similarly analyzed from the phylogenetic tree where *Ct*ManT was most closely related with Man26B of the *C. thermocellum* strain F1 (Figure 1). Multiple sequence alignment of *Ct*ManT displayed

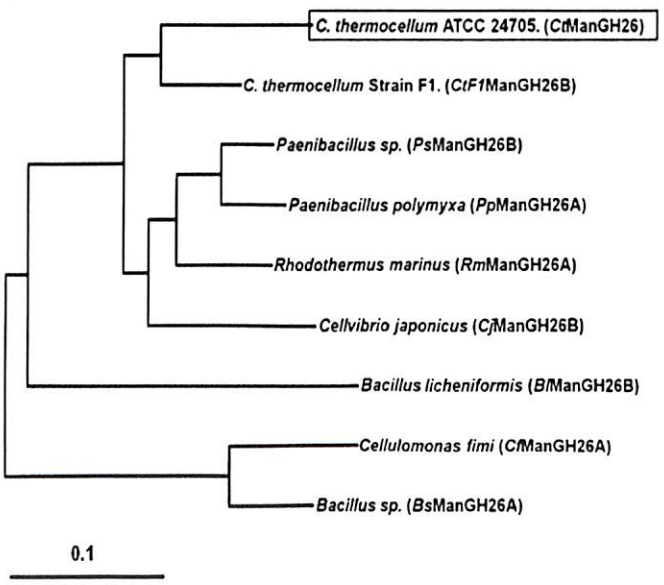

Figure 1. Phylogenetic tree showing the comparative study of our query *Ct*ManT (highlighted in red box) with two different types of GH26 mannanase (Man26A and Man26B) of representative members and their appearance during evolution based on sequence similarity.

a unique identifier sequence that was a highly conserved aromatic amino-acid-rich region with the consensus sequence WFWWG within all the ManGH26 family (Figure S2 of the Supporting Information, highlighted in the box), as also similarly stated by Xiaoyu et al. (2010).[21]

Cloning and Expression of *Ct*Manf and *Ct*ManT. The open-reading frames of *Ct*ManT and *Ct*Manf amplified by

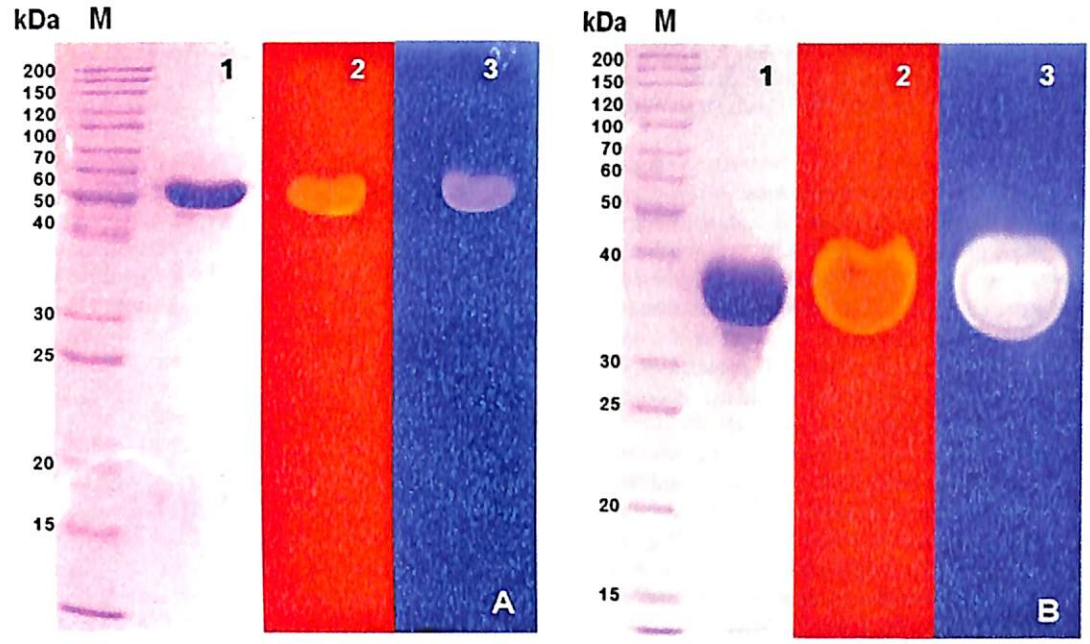

Figure 2. Zymogram study using 12% SDS–PAGE (A) *Ct*Manf (panel 1: purified protein, 2: congo red staining, and 3: 1 N HCl counter staining) and (B) *Ct*ManT (panel 1: purified protein, 2: congo red staining, and 3: 1 N HCl counter staining).

polymerase chain reaction resulted in 1449 bp and 1029 bp sequences, respectively. The amplified DNAs were cloned into the pET-28a (+) expression vector and then transformed the *E. coli* DH5α cells using the cloned plasmids. The positive clones of *Ct*Manf and *Ct*ManT were identified by digestion of resulted recombinant plasmids with *Nhe*I-*Xho*I restriction enzymes. The *E. coli* BL-21 (DE3) cells were transformed with recombinant plasmids, harboring *Ct*Manf and *Ct*ManT. The positive clones were screened by growing individual colonies in LB medium and after, inducing with 1 mM IPTG and further incubating at 24 °C for 24 h. The expressed proteins were analyzed by SDS–PAGE. The two *Clostridial* recombinant His_6-tagged proteins were purified by immobilized metal ion affinity chromatography (IMAC) from the cell-free extracts to homogeneity. The SDS–PAGE analysis of purified *Ct*Manf and *Ct*ManT displayed molecular sizes of 53 kDa and 38 kDa, respectively (Figure 2, panels A and B). Both the recombinant proteins expressed as soluble proteins.

Specificity and Kinetic Parameters of *Ct*Manf and *Ct*ManT with Natural Substrates. The optimum pH and temperature for *Ct*Manf were 6.9 and 60 °C, respectively, and for *Ct*ManT were 6.5 and 50 °C, respectively. The substrate specificities of *Ct*Manf and *Ct*ManT with natural substrates were determined at optimized pH and temperature. The enzyme activities with natural substrates are displayed in Table 1. It is conspicuous from the Table 1 that both *Ct*Manf and *Ct*ManT have specificity for galactomannan, and the highest enzyme activity was achieved with carob galactomannan 97.0 ± 5.0 units mg^{-1} and 91.0 ± 4.0 units mg^{-1}, respectively. Both displayed activity in decreasing order with locust bean galactomannan, konjac glucomannan, and guar galactomannan. Both *Ct*Manf and *Ct*ManT with insoluble polysaccharide ivory nut mannan displayed a biphasic hydrolysis pattern (Figure S3 of the Supporting Information), where rapid hydrolysis of the substrate occurred up to 15 min of incubation followed by slower hydrolysis (Figure S3 of the Supporting Information). These enzymes perhaps acted on the amorphous sites

Table 1. Substrate Specificity of *Ct*Manf and *Ct*ManT from *C. thermocellum*

substrate (1%, w v^{-1})	specific activity *Ct*Manf (units mg^{-1})	specific activity *Ct*ManT (units mg^{-1})
carob galactomannan	97.0 ± 5.0	91.0 ± 4.0
locust bean galactomannan	85.4 ± 6.0	83.1 ± 5.0
konjac glucomannan	81.0 ± 3.0	79.8 ± 4.0
guar galactomannan	47.6 ± 3.0	38.7 ± 4.0
ivory nut mannan	50.0 ± 2.0	26.5 ± 0.9
mannan	40.0 ± 1.0	21.2 ± 2.0
barley-β-glucan	2.94 ± 0.2	1.74 ± 0.1
lichnan	1.92 ± 0.8	1.22 ± 0.2
carboxymethyl cellulose	1.09 ± 0.5	0.9 ± 0.05
hydroxyethyl cellulose	0.87 ± 0.03	0.47 ± 0.03
Avicel	0.39 ± 0.02	0.26 ± 0.03
xyloglucan	1.5 ± 0.5	1.0 ± 0.3
rye arabinoxylan	NA	NA
glucuronoxylan	NA	NA
arabinogalactan	NA	NA
polygalactouronic acid	NA	NA

Values are in mean ± SD (n = 3). NA = no activity was determined.

(hydrolyzable region) of the substrate during rapid hydrolysis in the first phase and then accessed the crystalline sites (tougher region) in the second phase. Similar results were reported by Mizutani et al. (2012).[41] The enzyme activities of both enzymes with insoluble ivory nut mannan and β-(1→4)-mannan from the first phase were calculated (Table 1). *Ct*Manf displayed approximately, two times higher activity than *Ct*ManT with both the substrates (Table 1). The specific activity of *Ct*Manf was 50.0 units mg^{-1}, whereas *Ct*ManT was 26.5 units mg^{-1} with ivory nut mannan and with β-(1→4)-

dx.doi.org/10.1021/jf403111g | J. Agric. Food Chem. 2013, 61, 12333–12344

Table 2. Kinetic Properties and Catalytic Efficiencies of *Ct*Manf and *Ct*ManT from *C. thermocellum* ATCC 27405

substrate	K_m (mg mL^{-1})		k_{cat} (min^{-1})		k_{cat}/K_m (min^{-1} mg^{-1} mL)	
	*Ct*Manf	*Ct*Man T	*Ct*Manf	*Ct*Man T	*Ct*Manf	*Ct*Man T
natural substrates						
carob galactromannan	1.8 ± 0.2	1.6 ± 0.2	737	634	4.1×10^2	3.9×10^2
locust bean galactomannan	1.5 ± 0.1	1.4 ± 0.4	590	520	3.9×10^2	3.7×10^2
konjac glucomannan	1.5 ± 0.3	1.4 ± 0.2	510	462	3.4×10^2	3.3×10^2
guar galactomannan	1.2 ± 0.2	1.1 ± 0.2	320	283	2.6×10^2	2.5×10^2
ivory nut mannan	0.9 ± 0.1	0.8 ± 0.2	310	199	3.4×10^2	2.4×10^2
mannanan	0.9 ± 0.2	0.7 ± 0.1	283	159	3.1×10^2	2.2×10^2
synthetic substrates						
*p*NP-*β*-D-manno- pyranoside	ND	ND	ND	ND	ND	ND
*p*NP-*α*-D-manno- pyranoside	ND	ND	ND	ND	ND	ND

Values are in mean ± SD (n = 3). ND = not detected.

mannan the enzyme activities were 40.0 units mg^{-1} and 21.2 units mg^{-1}, respectively (Table 1). Therefore, the above results indicated that *Ct*CBM35 plays a role in potentiating the enzyme activity of the full length enzyme *Ct*Manf in hydrolyzing the insoluble substrates. A similar comment was stated earlier by Mizutani et al. (2012) for CBM32 appended to GH5 mannanase from *C. thermocellum*.[41]

Both *Ct*Manf and *Ct*ManT displayed low but significant activity against barley *β*-glucan, lichenan, carboxymethyl cellulose, hydroxyethyl cellulose, Avicel and xyloglucan, whereas no activity was observed with arabinogalactan, rye arabinoxylan, glucuronoxylan, and polygalactouronic acid (Table 1). The kinetic properties and catalytic efficiency of both the enzymes were determined with the natural substrates (Table 2). *Ct*Manf and *Ct*ManT displayed turnover numbers (k_{cat}) of 698 and 684 min^{-1}, respectively, and catalytic efficiencies (k_{cat}/K_m) of 4.1×10^2 and 3.9×10^2 min^{-1} mg^{-1} mL, respectively, with carob galactomannan. Both the enzymes *Ct*Manf and *Ct*ManT efficiently acted on insoluble ivory nut mannan, showing catalytic efficiencies (k_{cat}/K_m) of 3.4×10^2 and 2.4×10^2 min^{-1} mg^{-1} mL and with *β*-(1→4)-mannan, 3.1×10^2 and 2.2×10^2 min^{-1} mg^{-1} mL, respectively (Table 2).

The present results showed that *Ct*Manf gave approximately 1.1-fold higher activity against carob galactomannan and approximately 2-fold higher activity against insoluble ivory nut mannan and *β*-(1→4)-mannan than the catalytic *Ct*ManT. Similar results were reported earlier, where enhanced activity in the presence of a carbohydrate binding domain (CBD) in Man26A (mannanase A from family GH26) was observed by Halstead et al. (1999).[8] The presence of CBD at the N-terminal of Man26A enhanced turnover of carob galactomannan by 1.1-fold and 2-fold against insoluble ivory nut mannan.[8]

Specificity and Kinetic Parameters *Ct*Manf and *Ct*ManT with Synthetic Substrates. Both *Ct*Manf and *Ct*ManT did not show any activity against *p*NP-*β*-D-mannopyranoside and with *p*NP-*α*-D-mannopyranoside. On the basis of the enzyme activity of *Ct*Manf and *Ct*ManT against natural as well as synthetic substrates, it was evident that both these enzymes are predominantly endo-*β*-D-mannanase. The enzymes specifically cleaved the *β*-(1→4)-glycosidic linkages between mannopyranosyl residues.

Zymogram Study of *Ct*Manf and *Ct*ManT. Separate SDS–PAGE gels were used in the zymogram study to show the active bands of *Ct*Manf and *Ct*ManT against carob galactomannan (Figure 2, panels A and B). *Ct*Manf displayed an active band around 53 kDa and *Ct*ManT around 38 kDa, congo red staining, and counter staining with 1 N HCl (Figure 2, panels A and B). Both the enzymes displayed homogeneous bands and a clear zone of activity with carob galactomannan. Mannan endo-*β*-(1→4)-mannanase activity was detected as clear zones against red (after staining with Congo red) and blue background (after counter stained with 1 N HCl). The results clearly indicated that both of these enzymes have manno-configured substrate specificity.

Effects of Metal Ions and Chemical Agents on *Ct*Manf and *Ct*ManT. The enzymatic activity of *Ct*Manf and *Ct*ManT significantly increased by 1.5-fold in the presence of low concentrations of Ca^{2+} (10 mM) and Mg^{2+} (15 mM) (Table 3).

Table 3. Effects of Metal Ions and Other Agents on *Ct*Manf and *Ct*ManT from *C. thermocellum* ATCC 27405

ions/reagents	concentration (mm)	relative activity (%)	
		*Ct*Manf	*Ct*ManT
control[a]	–	100	100
Ca^{2+}	10	150	150
Mg^{2+}	15	150	150
Mn^{2+}	10	80	60
Ni^{2+}	8	80	80
Co^{+}	30	70	70
Zn^{2+}	10	70	60
Cu^{2+}	5	20	10
Al^{3+}	6	20	10
EDTA	8	20	20
EGTA	10	20	20
SDS	8	6	2
urea	4×10^3 (4 M)	10	5
GnHCl	100	2	1

[a]No additives were added in the control, and the activity was taken as 100%.

Both *Ct*Manf and *Ct*ManT retained moderate activities in the presence of 10 mM Mn^{2+} (80% and 60%), 8 mM Ni^{2+} (80% and 80%), 30 mM Co^{2+} (70% and 70%), and 10 mM Zn^{2+} (70% and 60%) salts, respectively. The enzyme activities were adversely affected by low concentrations of Cu^{2+} (5 mM) or Al^{3+} (6 mM) salts, and *Ct*Manf lost 80% and *Ct*ManT lost 90% of the activity at the mentioned concentrations of Cu^{2+} and Al^{3+} salts (Table 3). The enzyme activity of both the catalytic modules decreased to more than 80% in the presence of EDTA (8 mM) or 10 mM EGTA (Table 3). The presence of SDS (10 mM) *Ct*Manf lost 94% enzyme activity, while *Ct*ManT almost completely lost the activity. The decrease in activity in the presence of EDTA indicated that Ca^{2+} ions may be essential for

enzyme activity as EDTA and specifically binds and chelates the calcium ions in a 1:1 molar ratio.[36] The enzyme activity drastically reduced with chaotropic agents such as guanidine hydrochloride (GnHCl) and urea at higher concentrations. The enzymatic activity of *Ct*Manf decreased by 90% at 100 mM GnHCl, whereas *Ct*ManT lost 95% activity at the same concentration of GnHCl. In contrast, much higher concentration of urea (4 M) was required for complete diminution (98%−99%) of enzyme activities of *Ct*Manf and *Ct*ManT.

Analysis of Polysaccharide Hydrolysis Products by TLC. The analysis of recombinant *Ct*Manf hydrolyzed products of carob galactomannan by TLC is displayed in Figure 3A.

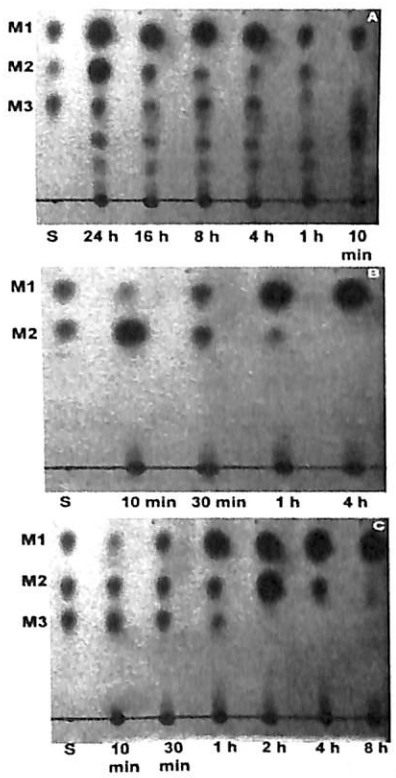

Figure 3. Thin layer chromatography analysis of hydrolysis products from (A) carob galactomannan, (B) mannobiose, and (C) mannotriose by *Ct*Manf. (A) Carob galactoniannan (1%, w v^{-1}) was incubated with *Ct*Manf for 10 min to 24 h, (B) mannobiose (1 mg mL^{-1}) was incubated with *Ct*Manf for 10 min to 4 h, and (C) mannotriose (1 mg mL^{-1}) was incubated with *Ct*Manf for 10 min to 8 h. Samples were taken in intervals, and hydrolysates were analyzed by TLC (standards used M1: mannose, M2: mannobiose, and M3: mannotriose).

Time-dependent hydrolysis of carob galactomannan after 10 min of reaction displayed the release of mannose (dp 1), but after 1 h of consecutive hydrolysis there was a little release of mannobiose (dp 2) and mannotriose (dp 3) (Figure 3 A). Standards of mono and oligosaccharides (M1: mannose, M2: mannobiose, and M3: mannotriose) were run in parallel to compare the released sugars (Figure 3A). Up to 8 h of incubation with *Ct*Manf, carob galactomannan was not completely hydrolyzed, but after 16 h, a large amount of mannose and comparable amounts of mannobiose and mannotriose were released (Figure 3A). Complete hydrolysis of carob galactomannan was achieved after 24 h of incubation, where the maximum amount of mannose, mannobiose, and mannotriose were produced (Figure 3A). Apart from the appearance of dp 1, dp 2, and dp 3, there were two other higher oligosaccharide (dp 4 and dp 5) spots observed and displayed similar appearance throughout the hydrolysis process (Figure 3A). *Ct*Manf displayed a typical endoacting bond cleavage during mannobiose and mannotriose hydrolysis, releasing principally mannose and mannobiose (Figure 3, panels B and C, respectively). *Ct*Manf was unable to hydrolyze mannobiose up to 1 h, but after 4 h, complete hydrolysis of mannobiose occurred, leaving only a mannose spot on the TLC plate (Figure 3B). Whereas, the hydrolysis mannotriose by *Ct*Manf after 4 h released predominantly mannose and a trace amount of mannobiose. The mannobiose spot disappeared completely after 8 h, leaving only the mannose spot (Figure 3C). Thus *Ct*Manf cleaved β-(1→4) bonds of these manno-oligosaccharides elegantly. Therefore, based on the significant role in specifically cleaving the β-(1→4) bond, this enzyme was classified and named as endo-β-(1→4)-mannanase.

HPAEC Analysis of Enzyme Reaction Products. Qualitative and quantitative analysis of *Ct*Manf hydrolyzed products of carob galactomannan were monitored by HPAEC-PAD. Time-dependent hydrolysis of carob galactomannan by *Ct*Manf is displayed in Figure 4. The peak intensities of standards are displayed in Figure 4A. After 1 h of *Ct*Manf treatment of carob galactomannan, the prominent peaks of mannose at 3.4 min, mannobiose at 4.06 min, and mannotriose at 4.96 min were observed with concentrations 2.12, 0.73, and 0.76 mg mL^{-1}, respectively (Figure 4B). Mannobiose peak was more prominent than mannotriose after 4 h of carob galactomannan hydrolysis, while the mannose intensity increased continuously (Figure 4C). The concentrations were determined as 2.23 mg mL^{-1} mannose, 1.12 mg mL^{-1} mannobiose, and 0.80 mg mL^{-1} mannotriose after 4 h of incubation. *Ct*Manf was able to hydrolyze carob galactomannan to a greater extent after 8 h, and the products obtained were mannose (3.16 mg mL^{-1}), mannobiose (1.81 mg mL^{-1}), and mannotriose (0.90 mg mL^{-1}), with much higher peak intensities (Figure 4D). After a 16 h incubation, the mannobiose and mannotriose concentrations increased to 2.1 mg mL^{-1} and 1.1 mg mL^{-1}, respectively. This increase was approximately 1.17 fold and 1.3 fold, respectively, for mannobiose and mannotriose (Figure 4E), as compared with that obtained after 8 h hydrolysis of carob galactomannan. The complete hydrolysis of carob galactomannan by *Ct*Manf was observed after 24 h of enzymatic reaction, where mannose, mannobiose, and mannotriose concentrations of 3.6 mg mL^{-1}, 2.3 mg mL^{-1}, and 1.4 mg mL^{-1}, respectively, were obtained (Figure 4F). All the concentrations were determined from the regression equation of mannose, mannobiose, and mannotriose standard curves. Therefore, *Ct*Manf quite effectively hydrolyzed 10 mg mL^{-1} (1%, w v^{-1}) carob galactomannan and released a maximum after 24 h, yielding 36% mannose, 23% mannobiose, and 14% mannotriose. The overall results quite interestingly described the performance of *Ct*Manf in the releasing of manno-oligosaccharides from carob galactomannan, which can be scaled up for commercial production.

Production of Enzymes (*Ct*Manf and *Ct*ManT) in Different Media. The highest concentration of recombinant proteins were obtained from a 100 mL flask containing TY and TB media, followed by LB and 5xLB media after 24 h of incubation. TY medium achieved the highest cell densities of 31 and 30 g L^{-1} dry cell weight, respectively, for *Ct*Manf and *Ct*ManT. The protein concentration of *Ct*Manf and *Ct*ManT

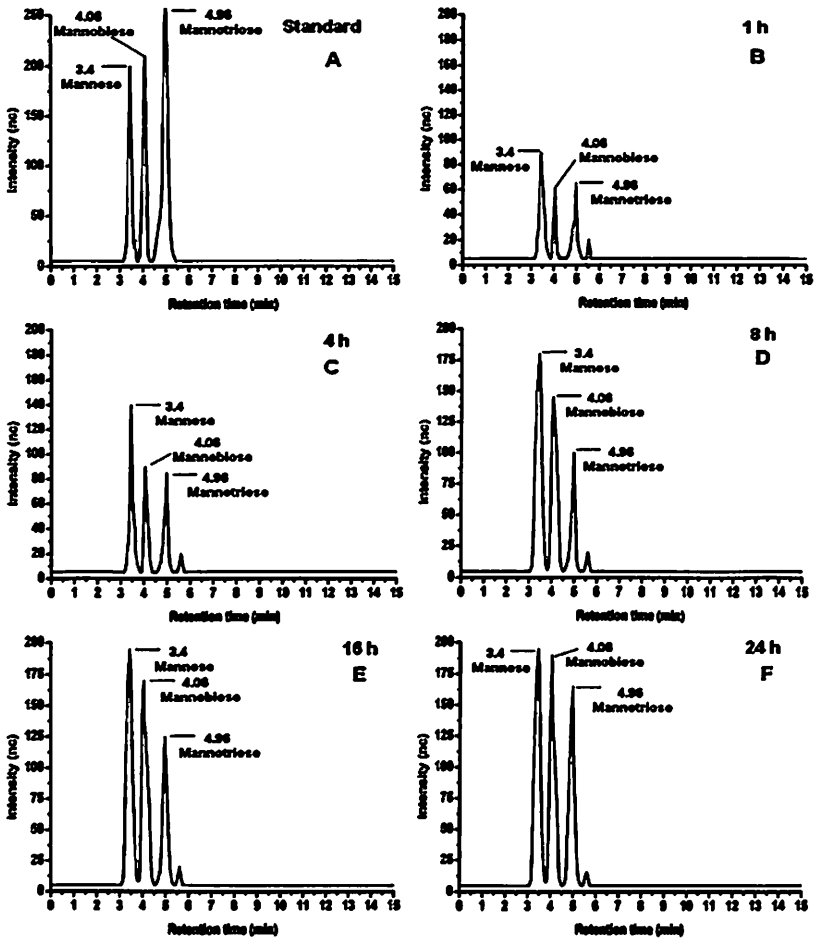

Figure 4. HPAEC-PAD analysis of hydrolyzed products of carob galactomannan by *Ct*Manf. (A) Elution patterns of standards used mannose (3.4 min), mannobiose (4.06 min), and mannotriose (4.96 min). Elution pattern of mannose, mannobiose, and mannotriose from carob galactomannan (1%, w v^{-1}) treated by *Ct*Manf after (B) 1, (C) 4, (D) 8, (E) 16, and (F) 24 h.

after sonication and purification by IMAC obtained was 910 and 880 mg L^{-1}, respectively. Similar results were reported by Tripathi et al. (2009),[38] where TY medium gave the highest cell density of *E. coli* cells achieved, 1.12 g L^{-1}, and the recombinant dengue protein was expressed at a concentration of 10.37 mg L^{-1}.[38] *Ct*Manf and *Ct*ManT gave less DCW with TB medium 28 g L^{-1} and 26.9 g L^{-1}, respectively, as compared with TY medium. The purified protein concentrations from TB medium obtained were 500 mg L^{-1} and 410 mg L^{-1}, respectively, for *Ct*Manf and *Ct*ManT. The dry cell weight (DCW) from 100 mL LB medium obtained 21 and 20 g L^{-1} for *Ct*Manf and *Ct*ManT, respectively. The concentrations of purified protein obtained from LB medium were 160 mg L^{-1} for *Ct*Manf and 150 mg L^{-1} for *Ct*ManT. These results are similar to those of the earlier report of Tripathi et al. (2009).[37] The lowest growth of cell mass of *E. coli* BL21 (DE3) cells were observed for both enzymes in 5xLB medium. The cell densities obtained were 12.0 and 10 g L^{-1}, respectively, for *Ct*Manf and *Ct*ManT. The recombinant *Ct*Manf and *Ct*ManT proteins after purification obtained were 300 mg L^{-1} and 280 mg L^{-1} in 5xLB medium, respectively. Therefore, it can be suggested that productivity of recombinant mannanase and cell mass can be improved by altering and optimizing media components.

Thermostability Study and Protein Melting Analysis of *Ct*Manf and *Ct*ManT. Thermostability study displayed stability of *Ct*Manf and *Ct*ManT at higher temperatures (Figure 5 A). *Ct*Manf remained stable up to 60 °C, retaining 100% activity for 1 h. The enzyme activity of *Ct*Manf decreased after 60 °C and left with 20% at 100 °C. *Ct*Manf and *Ct*ManT retained more than 55% and 30% enzyme activity at 80 °C. *Ct*ManT was stable up to 50 °C and lost 90% at 100 °C. Therefore, *Ct*Manf was more thermostable than *Ct*ManT. The results indicated that the higher thermostability of *Ct*Manf could be due to the presence of the carbohydrate binding module, *Ct*CBM35. Protein stability was also observed with protein melting curve analysis. The full-length *Ct*Manf showed two separate melting peaks at 50 and 80 °C (Figure 5 B), whereas *Ct*ManT displayed a single melting peak at around 80 °C (Figure 5C). This suggested that the peak at 50 °C corresponded to noncatalytic *Ct*CBM35 and the peak at 80 °C to the catalytic module *Ct*ManT and that the two modules are melting independently (Figure 5B). The presence of Ca^{2+} ions (10 mM) caused significant changes in *Ct*Manf, as well as in *Ct*ManT protein-melting profiles. The peak for *Ct*ManT shifted toward higher a temperature (i.e., from 80 to 100 °C), but the peak corresponding to *Ct*CBM35 in *Ct*Manf was masked in the presence of Ca^{2+} ions (Figure 5, panels B and C). On addition of EDTA (10 mM) to the enzyme–substrate reaction mixture containing Ca^{2+} (10 mM), the melting peaks shifted back to the original temperature of 80 °C of catalytic *Ct*ManT and *Ct*CBM35 (Figure 5, panels B and C, small dotted lines). Therefore, from both thermostability and protein melting study

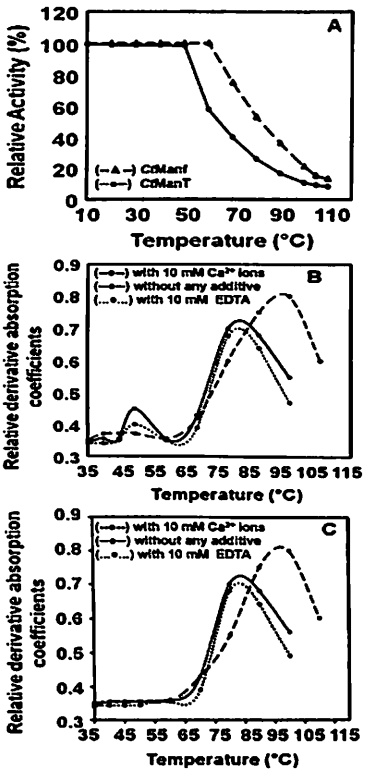

Figure 5. Thermal stability analysis of (A) *Ct*Manf and *Ct*ManT from 10 to 110 °C. Protein-melting analysis of displaying normal melting curve without any additives, in the presence of 10 mM Ca^{2+} ions and in the presence of 10 mM Ca^{2+} ions and 10 mM EDTA of (B) *Ct*Manf and (C) *Ct*ManT.

of *Ct*Manf and *Ct*ManT, it could be concluded that both these enzymes are thermostable and Ca^{2+} ions provide significant thermal stability.

■ DISCUSSION

The molecular architecture of full length *Ct*Manf from *C. thermocellum* ATCC 27405 displayed a modular structure. Sequence homology of the catalytic module *Ct*ManT identified as Man26B, showed highest similarity with that of the *C. thermocellum* F1 strain.[21] The Man26B enzymes have subtle differences with Man26A enzymes in topology of substrate binding and functional property of substrate hydrolysis as previously described by Hogg et al. (2003) in a study of Man26A and Man26B from *C. japonicas*.[22] Both *Ct*Manf and *Ct*ManT preferred higher degrees of catalysis against carob galactomannan than locust bean galactomannan and konjac glucomannan, while similar observations were stated earlier by Xiaoyu et al. (2010) and Kurokawa et al. (2001) for Man26B isolated from *Paenibacillus* sp. BME-14 and *C. thermocellum* strain F1, respectively.[21,23] It is worth mentioning here about the wide range of substrate specificity of both *Ct*Manf and *Ct*ManT. Both these enzymes were able to hydrolyze β-(1→4)-gluco based substrates viz. barley β-glucan, lichenan, carboxymethyl cellulose, hydroxyethyl cellulose, Avicel, and xyloglucan. ManA from *Thermoanaerobacterium polysaccharolyticum* similarly showed both mannanase and endoglucanase activities.[42] Low activities of *Ct*Manf and *Ct*ManT against ivory nut mannan and β-(1→4) may be attributed to the crystalline nature of the substrate, which greatly inhibits the access of enzymes for catalysis. Interestingly, *Ct*Manf exhibited 2-fold higher activities against insoluble ivory nut mannan and β-(1→4)-mannan, as compared to *Ct*ManT. By comparing the hydrolyzing capacity of *Ct*Manf and *Ct*ManT against different mannans, it was concluded that the *Ct*CBM35 of *C. thermocellum* ATCC 27405 GH26 mannanase played an important role in the degradation of insoluble ivory nut mannan and β-(1→4) (Table 2). The apparent biphasic action of *Ct*Manf and *Ct*ManT against ivory nut mannan and β-(1→4)-mannan was quite distinguishable and thus suggested that both these enzymes preferred to attack the amorphous region of the substrate in the early reaction stage and the crystalline region later. This might give a lucid idea about the substrates that consist of two distinct regions, which was more resistant toward *Ct*ManT action. Similar, types of observations were reported by Mizutani et al. (2012),[41] while comparing the role of Man26A from *C. thermocellum* against insoluble substrate hydrolysis. Higher degree of hydrolyzing capacity of *Ct*Manf than *Ct*ManT was attributed to the appended N-terminal *Ct*CBM35 domain which facilitated the increased catalysis by concentrating the catalytic module in the vicinity of the substrate. *Ct*CBM35 helped in prolonged binding of the substrate and decreased its resistance to the catalytic attack by *Ct*ManT. As an instance CBM32 from *C. thermocellum* ATCC 27405 has recently been shown to improve hydrolysis of insoluble substrates by mannanase of GH5.[38] Moreover, higher activity of *Ct*Manf at a higher temperature was attributed to the presence of N-terminal carbohydrate binding domain (*Ct*CBM35) than catalytic *Ct*ManT. Similarly in an earlier report, it was suggested by Xiaoyu et al. (2009),[21] the appended carbohydrate binding domain in Man26B of *Paenibacillus* sp. BME-14 potentiated in higher activity against locust bean gum than the lone catalytic module.[21] The presence of *Ct*CBM35 in *Ct*Manf played a unique role in higher hydrolysis of soluble carob galactomannan as compared with the catalytic *Ct*ManT. Both enzymes exhibited significant turn over against other soluble as well as insoluble substrates. It was reported previously that carob galactomannan composed of 78% mannose formed the β-(1→4)-mannan backbone, while galactose contributes 22%.[1] Each β-(1→4)-mannan is substituted by the α-(1→6)-galactose side chain. The enzymes randomly hydrolyze β-(1→4)-linkages in diverse substrates, such as galactomannans and glucomannan. Both *Ct*Manf and *Ct*ManT did not show any activity against synthetic substrates *p*NP-β-mannopyranoside and *p*NP-α-mannopyranoside. Therefore, it is evident that both *Ct*Manf and *Ct*ManT are endo-acting enzymes and are endo-β-(1→4)-mannanases (endo-Man26B) from *C. thermocellum* ATCC 27405. The performances of *Ct*Manf and *Ct*ManT were investigated under the influence of salts, chaotropic agents, and detergent. Both *Ct*Manf and *Ct*ManT are metalloenzymes, and Ca^{2+} and Mg^{2+} ions act as cofactors for these enzymes. The enzyme activities of *Ct*Manf and *Ct*ManT increased significantly by 1.5-fold in the presence of Ca^{2+} and Mg^{2+} salts, which suggested that these ions are required as cofactors. However, the enzyme activity was unaffected by lower concentrations of Mn^{2+}, Ni^{2+}, Co^{+}, and Zn^{2+} and were able to retain their moderate activities. The enzyme activities of *Ct*Manf and *Ct*ManT were completely inhibited by lower concentrations of Cu^{2+} and Al^{3+}. Similar observation was reported earlier by Yoshikawa et al. (2009), where a noncompetitive type of inhibition imposed by Cu^{2+} ions by binding at different sites other than the α-glucosidase active center or enzyme–substrate complex.[43] In the presence of a low concentration of chelating agents such as EDTA or

dx.doi.org/10.1021/jf403111g | J. Agric. Food Chem. 2013, 61, 12333–12344

EGTA, the enzyme activity sharply decreased. The enzyme activity of *Ct*Manf and *Ct*ManT was adversely affected at the low concentration of SDS. The higher concentration urea and lower concentration of guanidine hydrochloride was required to inactivate the enzymes.

*Ct*Manf-catalyzed substrate hydrolysis products were analyzed by TLC and HPAEC. It was apparent from TLC that *Ct*Manf released mannotriose, mannobiose, and mannose in prolonged hydrolysis of carob galactomannan. But, in the earlier stages, the amount of mannobiose was less, as compared to mannotriose and mannose. After complete hydrolysis of carob galactomannan, *Ct*Manf was able to release mannose, mannobiose, and mannotriose. The salient feature of *Ct*Manf catalysis involved only β-(1→4)-bond cleavage, when mannobiose and mannotriose were used as substrates and liberated mainly mannose as the main product. The release of large amounts of mannose at early stages of enzymatic reaction by *Ct*Manf was commonly seen against carob galactomannan and manno-oligosaccharides. In an earlier report by Hogg et al. (2003), the release of mannose at the early stage of hydrolysis of manno-configured substrates and oligosaccharides is characteristic of a typical Man26B mannanase.[22] HPAEC analysis corroborated the results of TLC analysis of hydrolysis of carob galactomannan products released by *Ct*Manf. The results of HPAEC showed that *Ct*Manf exclusively cleaves carob galactomannan into mannotriose, mannobiose, and mannose. It was apparent from TLC and HPAEC analyses that *Ct*Manf was able to hydrolyze only the β-(1→4) bond cleavage and had potential to produce manno-oligosaccharides from carob galactomannan. Thus effective β-(1→4)-mannanase from *C. thermocellum* ATCC 27405 may be exploited for higher production of manno-oligosaccharides, especially for the controlled synthesis of mannobiose and mannotriose. Kurakake et al. (2006) reported the synthesis of manno-oligosaccharides from guar gum by utilizing of β-mannanase from *Penicillium oxalicum* SO.[44]

Media composition plays a significant role in production of recombinant proteins.[38] Use of chemically defined medium is a common practice in producing recombinant proteins.[45−47] The recombinant *Ct*Manf and *Ct*ManT showed the highest cell density and concentration of protein in TY medium. In TB medium, moderate cell densities and protein production were observed. In LB medium, moderate cell density was achieved with low protein concentration. The 5xLB medium did not support the growth due to higher concentrations of yeast extract, tryptone, and sodium chloride, and as a result, the lowest protein concentration was achieved. Similar effects of media were stated earlier, while producing recombinant dengue protein in *E. coli*.[38] The rich source of tryptone, yeast extract, and phosphate salts facilitated to achieve highest cell densities in TY media as compared to other chemically defined media used. Yeast extract is a known source of trace components and can relieve cellular stress responses such as the production of proteases during synthesis of recombinant protein in *E. coli*.[38] Higher concentration of phosphate is important for attaining high cell densities of *E. coli*, as the lower concentrations of phosphate limits the growth.[37] The phosphate salts in the medium provided buffering capacity against pH fluctuations, which adversely affects the metabolic activity of cells.[38] The low cell densities and lower production of recombinant proteins in LB and 5xLB medium were due to a lack of buffering capacity.

Protein stability while functioning at higher temperature is a major concern in industry. A temperature stability study of *Ct*Manf and *Ct*ManT showed that after 1 h of incubation at 60 and 50 °C, respectively, 100% activity was retained. But they have retained around 10% of enzymatic activity at 100 °C. When compared with recombinant ManB from *Bacillus licheniforms* DSM13,[24] the recombinant Man26B from *C. thermocellum* ATCC 27405 was thermally more stable at higher temperatures. The protein melting phenomenon of recombinant *Ct*Manf and *Ct*ManT was analyzed to study their thermostability. Protein-melting curves of full length *Ct*Manf showed that the catalytic module *Ct*ManT and carbohydrate binding module *Ct*CBM35 melt independently of each other. The protein-melting peaks of *Ct*ManT and *Ct*CBM35 shifted to higher temperature in the presence of Ca^{2+} ions. However, on addition of equimolar concentration of EDTA to the solutions of *Ct*Manf and *Ct*ManT, the melting temperature peaks shifted back to the original positions. The shift of peak to a higher temperature in the presence of Ca^{2+} ions might be due to the reason that Ca^{2+} ions provide stability to the protein structure by inducing electrostatic interactions with amino acids, as reported by Noorbatcha et al. (2012).[48] The electrostatic interactions imparted by Ca^{2+} ions in bound protein resulted in less hydrogen bonds and higher number of salt bridges as compared to nonbonded proteins.[48] Because of the higher fluctuations in the backbone of protein at higher temperature, the number of hydrogen bonds will be destabilized, which allowed residues in close proximity to calcium ions to form more numbers of salt bridges in the Ca^{2+} ion-bound state as compared with the Ca^{2+} ion-free state.[48] Thus, the binding by Ca^{2+} ion makes protein more conformationally stable at higher temperature.[47] The shifting back of melting peaks in the presence of EDTA was due to chelation of calcium ions, making them unavailable for the enzyme. This is the first report of cloning and biochemical characterization of a thermostable Man26B form *C. thermocellum* ATCC 27405 and its potential role in manno-oligosaccharide production from manno-configured substrates.

■ ASSOCIATED CONTENT

Supporting Information

Molecular architecture of full length *Ct*Manf of *C. thermocellum* ATCC 27405; multiple sequence alignment of *Ct*ManT with Man26A from *Cellulomonas fimi*; and biphasic hydrolysis pattern of insoluble ivory nut mannan. This material is available free of charge via the Internet at http://pubs.acs.org.

■ AUTHOR INFORMATION

Corresponding Author

*E-mail: arungoyl@iitg.ernet.in. Tel: (361) 258 2208. Fax: (361) 269 0762.

Notes

The authors declare no competing financial interest.

■ ACKNOWLEDGMENTS

A.G. is supported by a scholarship from University Grants Commission (UGC), New Delhi, India. The research work in part was supported by a Cutting-edge Research Enhancement and Scientific Training (CREST) Fellowship from the Department of Biotechnology, Ministry of Science and Technology to Arun Goyal.

REFERENCES

(1) Hirst, E. L.; Jones, J. K. N. The galactomannan of carob-seed gum (gum gatto). *J. Chem. Soc.* **1948**, 1278−1282.

(2) Katsuraya, K.; Okuyamab, K.; Hatanakab, K.; Oshimab, R.; Satoc, T.; Matsuzakic, K. Constitution of konjac glucomannan: Chemical analysis and ^{13}C NMR spectroscopy. *Carbohydr. Polym.* **2003**, *53*, 183−189.

(3) Dumitriu, S. In *Polysaccharides: Structural diversity and functional versatility*, 2nd ed.; CRC Press: Boca Raton, FL, 2010; pp 1020.

(4) Henrissat, B. A classification of glycosyl hydrolases based on amino acid sequence similarities. *Biochem. J.* **1991**, *280*, 309−316.

(5) Bolam, D. N.; Hughes, N.; Virden, R.; Lakey, J. H.; Hazlewood, G. P.; Henrissat, B.; Braithwaite, K. L.; Gilbert, H. J. Mannanase A from *Pseudomonas fluorescens* ssp. *cellulosa* is a retaining glycosyl hydrolase in which E212 and E320 are the putative catalytic residues. *Biochemistry* **1996**, *35*, 16195−16204.

(6) Zhang, Y.; Ju, J.; Peng, H.; Gao, F.; Zhou, C.; Zeng, Y.; Xue, Y.; Li, Y.; Henrissat, B.; Gao, G. F.; Ma, Y. Biochemical and structural characterization of the intracellular mannanase AaManA of *Alicyclobacillus acidocaldarius* reveals a novel glycoside hydrolase family belonging to clan GH-A. *J. Biol. Chem.* **2008**, *14*, 31551−31558.

(7) Couturier, M.; Roussel, A.; Rosengren, A.; Leone, P.; Stålbrand, H.; Berrin, J. G. Structural and biochemical analyses of glycoside hydrolase families 5 and 26 beta-(1,4)-mannanases from *Podospora anserina* reveal differences upon manno-oligosaccharides catalysis. *J. Biol. Chem.* **2013**, DOI: 10.1074/jbc.M113.459438.

(8) Halstead, J. R.; Vercoe, P. E.; Gilbert, H. J.; Davidson, K.; Hazlewood, G. P. A family 26 mannanase produced by *C. thermocellum* as a component of the cellulosome contains a domain which is conserved in mannanases from anaerobic fungi. *Microbiology* **1999**, *145*, 3101−3108.

(9) Hogg, D.; Woo, E. J.; Bolam, D. N.; McKie, V. A.; Gilbert, H. J.; Pickersgill, R. W. Crystal structure of mannanase 26A from *Pseudomonas cellulosa* and analysis of residues involved in substrate binding. *J. Biol. Chem.* **2001**, *276*, 31186−31192.

(10) Cartmell, A.; Topakas, E.; Ducros, M. A. V.; Suits, M. D. L.; Davis, G. J.; Gilbert, H. J. The *Cellvibrio japonicus* mannanase CjMan26C displays a unique exo-mode of action that is conferred by subtle changes to the distal region of the active site. *J. Biol. Chem.* **2008**, *283*, 34403−34413.

(11) Fontes, C. M. G. A.; Gilbert, H. J. Cellulosomes: Highly efficient nanomachines designed to deconstruct plant cell wall complex carbohydrates. *Annu. Rev. Biochem.* **2010**, *79*, 655−681.

(12) Asano, I.; Hamaguchi, K.; Fujii, S.; Iino, H. In vitro digestibility and fermentation of mannooligosaccharides from coffee mannan. *Food. Sci. Technol. Res.* **2003**, *9* (1), 62−66.

(13) Asano, I.; Ikeda, Y.; Fujii, S.; Iino, H. Effects of mannooligosaccharides from coffee on microbiota and short chain fatty acids in rat cecum. *Food. Sci. Technol. Res.* **2004**, *10*, 273−277.

(14) Kim, Y. J.; Park, G. G. Identification and growth activity to *Bifidobacterium spp.* of locust bean gum hydrolysates by *Trichoderma harzianum* β-mannanase. *J. Korean Soc. Appl. Biol. Chem.* **2005**, *48*, 364−369.

(15) Hoshino-Takao, U.; Fujii, S.; Ishii, A.; Han, L. K.; Okuda, H.; Kumao, T. Effects of mannooligosaccharides from coffee mannan on blood pressure in dahl salt-sensitive rats. *J. Nutr. Sci. Vitaminol.* **2008**, *54*, 181−184.

(16) Fierobe, H. P.; Mingardon, F.; Mechaly, A.; Belaich, A.; Rincon, M. T; Pagès, S.; Lamed, R.; Tardif, C.; Bélaïch, J. P.; Bayer, E. A. Action of designer cellulosomes on homogeneous versus complex substrates: Controlled incorporation of three distinct enzymes into a defined trifunctional scaffoldin. *J. Biol. Chem.* **2005**, *280*, 1625−1634.

(17) Boraston, A. B.; Bolam, D. N.; Gilbert, H. J.; Davies, G. J. Carbohydrate-binding modules: Fine-tuning polysaccharide recognition. *Biochem. J.* **2004**, *382*, 769−781.

(18) Dvortsov, I. A.; Lunina, N. A.; Chekanovskaya, L. A.; Schwarz, W. H.; Zverlov, V. V.; Velikodvorskaya, G. A. Carbohydrate-binding properties of a separately folding protein module from beta-1,3-glucanase Lic16A of *C. thermocellum*. *Microbiology* **2009**, *155*, 2442−2449.

(19) Shoseyov, O.; Shani, Z.; Levy, I. Carbohydrate binding modules: Biochemical properties and novel applications. *Microbiol. Mol. Biol. Rev.* **2006**, *70*, 283−295.

(20) Couturier, M.; Roussel, A.; Rosengren, A.; Leone, P.; Stålbrand, H.; Berrin, J. G. Glycoside hydrolase families 5 and 26 β-(1,4)-mannanases from *Podospora anserina* reveal differences upon manno-oligosaccharide catalysis. *J. Biol. Chem.* **2013**, *288*, 14624−14635.

(21) Xiaoyu, F.; Huang, X.; Liu, P.; Lin, L.; Wu, G.; Li, C.; Feng, C.; Hong, Y. Cloning and characterization of a novel mannanase from *Paenibacillus sp.* BME-14. *J. Microbiol. Biotechnol.* **2010**, *20*, 518−524.

(22) Hogg, D.; Pell, G.; Dupree, P.; Goubet, F.; Martin-Oru, S. M.; Armand, S.; Gilbert, H. J. The modular architecture of *Cellvibrio japonicus* mannanases in glycoside hydrolase families 5 and 26 points to differences in their role in mannan degradation. *Biochem. J.* **2003**, *371*, 1027−1043.

(23) Kurokawa, J.; Hemjinda, E.; Arai, T.; Karita, S.; Kimura, T.; Sakka, K.; Ohmiya, K. Sequence of the *C. thermocellum* mannanase gene man26B and characterization of the translated product. *Biosci. Biotechnol. Biochem.* **2001**, *65*, 548−554.

(24) Songsiriritthigul, C.; Buranabanyat, B.; Haltrich, D.; Yamabhai, M. Efficient recombinant expression and secretion of a thermostable GH26 mannan endo-1,4-β-mannosidase from *Bacillus licheniformis* in *Escherichia coli*. *Microb. Cell Fact.* **2010**, *9* (20), 1−13.

(25) Stoll, D.; Boraston, A.; Stålbrand, H.; Warren, R. A. Mannan-degrading enzymes from *Cellulomonas fimi*. *Appl. Environ. Microbiol.* **1999**, *65*, 2598−2605.

(26) Politz, O.; Krah, M.; Thomsen, K. K.; Borriss, R. A highly thermostable endo-(1,4)-beta-mannanase from the marine bacterium *Rhodothermus marinus*. *Appl. Microbiol. Biotechnol.* **2000**, *53*, 715−721.

(27) Hatada, Y.; Takeda, N.; Hirasawa, K.; Ohta, Y.; Usami, R.; Yoshida, Y.; Grant, W. D.; Ito, S.; Horikoshi, K. Sequence of the gene for a high-alkaline mannanase from an alkaliphilic *Bacillus sp.* strain JAMB-750, its expression in *Bacillus subtilis* and characterization of the recombinant enzyme. *Extremophiles* **2005**, *9*, 497−500.

(28) Cho, K. M.; Hong, S. Y.; Lee, S. M.; Kim, Y. H.; Kahng, G. G; Kim, H.; Yun, H. D. A cel44C-man26A gene of endophytic *Paenibacillus polymyxa* GS01 has multi-glycosyl hydrolases in two catalytic domains. *Appl. Microbiol. Biotechnol.* **2006**, *73*, 618−630.

(29) Das, S. P.; Ravindran, R.; Ahmed, S.; Das, D.; Goyal, D.; Fontes, C. M. G. A.; Goyal, A. Bioethanol production involving recombinant *C. thermocellum* hydrolytic hemicellulase and fermentative microbes. *Appl. Biochem. Biotechnol.* **2012**, *127*, 1475−1488.

(30) Laemmli, U. K. Cleavage of structural proteins during the assembly of the head of Bacteriophage T4. *Nature* **1970**, *227*, 680−685.

(31) Nelson, N. A photometric adaptation of the Somogyi method for the determination of glucose. *J. Biol. Chem.* **1944**, *153*, 375−380.

(32) Somogyi, M. A new reagent for the determination of sugars. *J. Biol. Chem.* **1945**, *160*, 61−68.

(33) Huang, J. L.; Bao, L. X.; Zou, H. Y.; Che, S. G.; Wang, G. X. High-level production of a cold-active B-mannanase from Bacillus subtilis BS5 and its molecular cloning and expression. *Mol. Genet., Mikrobiol. Virusol.* **2012**, *4*, 14−27.

(34) Bey, M.; Berrin, J. G.; Poidevin, L.; Sigoillot, J. C. Heterologous expression of *Pycnoporus cinnabarinus* cellobiose dehydrogenase in *Pichia pastoris* and involvement in saccharification processes. *Microb. Cell Fact.* **2011**, *10*, 1−15.

(35) Aboul-Enein, A.; Abouelalla, F.; Serour, E.; Hussien, T. Purification and characterization of a novel thermoactive cellulase from thermophilic actinomycetes isolated from soil sample of Egypt. *J. Int. Acad. Res* **2010**, *2*, 81−86.

(36) Ruijssennars, H. J.; Hartmans, S. Plate screening method for the detection of polysaccharide- producing microorganisms. *Appl. Microbiol. Biotechnol.* **2001**, *55*, 143−149.

(37) Cote, G. L.; Leathers, T. D. A method for surveying and classifying *Leuconostocs* pp Glucansucrases according to strain-

dependent acceptor product patterns. *J. Ind. Microbiol. Biotechnol.* **2005**, *32*, 53−60.
(38) Tripathi, N. K.; Shrivastva, A.; Biswal, K. C.; Rao, P. V. L. Optimization of culture medium for production of recombinant dengue protein in *Escherichia coli*. *Ind. Biotechnol.* **2009**, *5*, 179−183.
(39) Black, J. G. *Microbiology Principles and Applications*, 3rd ed.; Prentice Hall: Upper Saddle River, NJ, 1996; pp. 140−144.
(40) Bradford, M. M. Rapid and sensitive method for the quantitation of microgram quantities of protein utilizing the principle of protein-dye binding. *Anal. Biochem.* **1976**, *72*, 248−254.
(41) Mizutani, K.; Fernandes, V. O.; Karita, S.; Luís, A. S.; Sakka, M.; Kimura, T.; Jackson, A.; Zhang, X.; Fontes, C. M.; Gilbert, H. J.; Sakka, K. Influence of a mannan binding family 32 carbohydrate binding module on the activity of the appended mannanase. *Appl. Environ. Microbiol.* **2012**, *78*, 4781−4787.
(42) Cann, I. K. O.; Kocherginskaya, S.; King, M. R.; White, B. A.; Mackie, R. I. Molecular cloning, sequencing and expression of a novel multidomain mannanase gene from *Thermoanaerobacterium polysaccharolyticum*. *J. Bacteriol.* **1999**, *181*, 1643−1651.
(43) Yoshikawa, Y.; Hirata, R.; Yasui, H.; Hattorib, M.; Sakurai, H. Inhibitory effect of $CuSO_4$ on a-glucosidase activity in ddY mice. *Metalomics* **2009**, *2*, 67−73.
(44) Kurakake, M.; Sumida, T.; Masuda, D.; Oonishi, S.; Komaki, T. Production of galacto-manno-oligosaccharides from guar gum by α-mannanase from *Penicillium oxalicum* SO. *J. Agric. Food. Chem.* **2006**, *54*, 7885−7889.
(45) Lim, H. K.; Jung, K. H. Improvement of heterologous protein productivity by controlling post induction specific growth rate in recombinant *Escherichia coli* under control of the PL promoter. *Biotechnol. Prog.* **1998**, *14*, 548−553.
(46) Cserjan-Puschmann, M.; Kramer, W.; Duerrschmid, E.; Striedner, G.; Bayer, K. Metabolic approaches for the optimization of recombinant fermentation processes. *Appl. Microbiol. Biotechnol.* **1999**, *53*, 43−50.
(47) Zhang, J.; Greasham, R. Chemically defined media for commercial fermentations. *Appl. Microbiol. Biotechnol.* **1999**, *51*, 407−421.
(48) Noorbatcha, I. A.; Sultan, A. M.; Azura, A.; Salleh, H. M. Molecular dynamics study of the effect of calcium ions on the thermostability of *Bacillus Amyloliquefaciens* phytase. *Aust. J. Basic Appl. Sci.* **2012**, *6*, 109−116.